MAX-PLANCK-INSTITUT FÜR PLASMAPHYSIK
GARCHING BEI MÜNCHEN

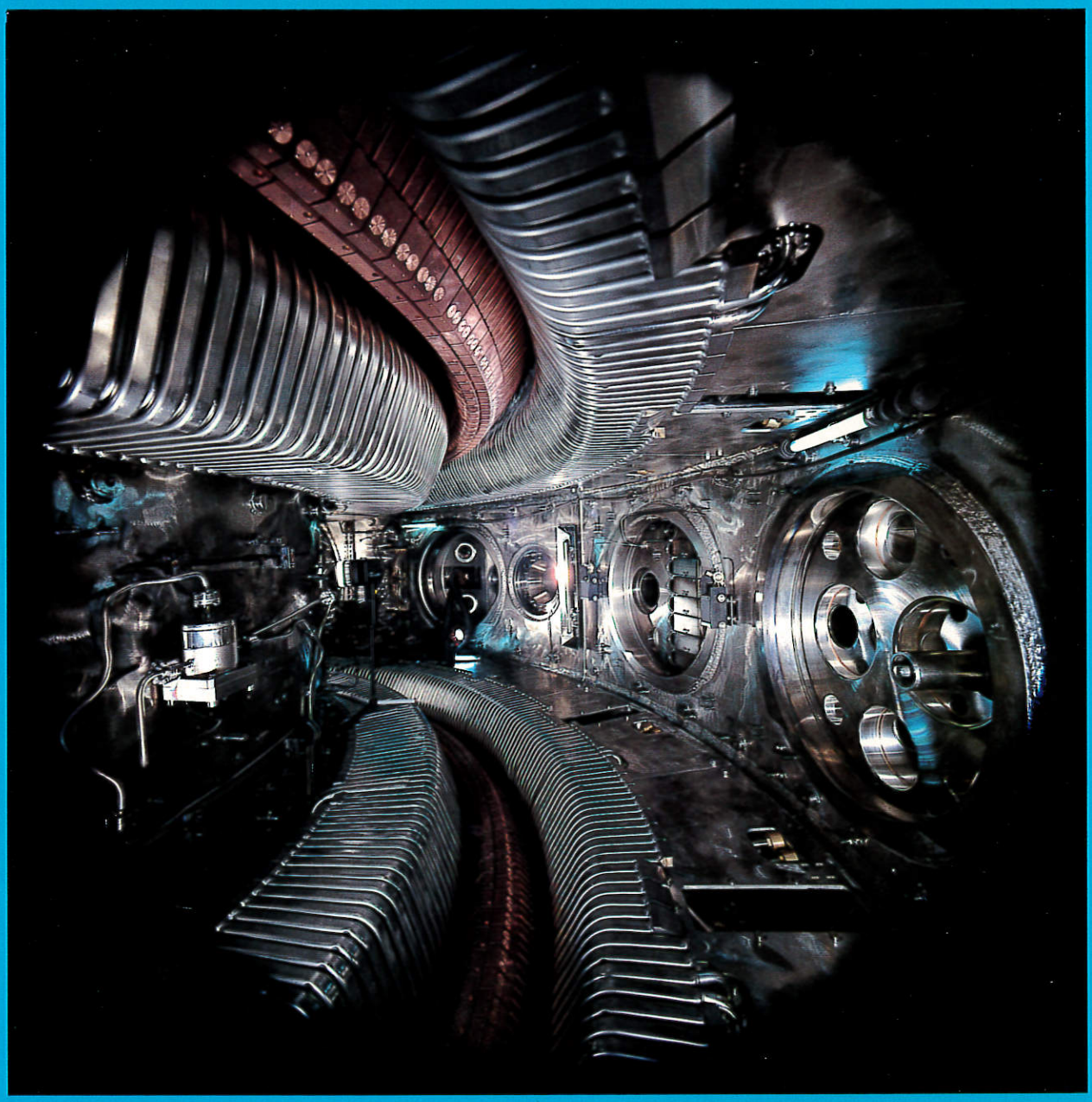

IPP

ANNUAL REPORT 1986

IPP AR/1986

COVER ILLUSTRATION

Interior of the vacuum vessel of the ASDEX fusion experiment: The divertor coils and divertor plates are fitted with water-cooled shielding to "harden" the ASDEX vessel for the long-pulse heating experiments scheduled to start in April 1987. These heating experiments will have a pulse length of 10 seconds. They will allow high-temperature plasmas to be investigated while the plasma current, plasma density and impurity concentration are under steady-state conditions.

MAX-PLANCK-INSTITUT FÜR PLASMAPHYSIK
GARCHING BEI MÜNCHEN

Annual Report 1986

C O N T E N T S

Preface

A. PROJECTS 1

I. Tokamaks 3

ASDEX PROJECT 5

1. Experimental Results and Comparison with Theorectical Studies 5
2. Development of Diagnostics and Data Analysis 39
3. Data Acquisition and Electronics 44
4. Operation of ASDEX and the Preparation for Long-pulse Heating 45
5. Continuation of the Lower Hybrid Programme in ASDEX 48

ASDEX Upgrade Project 49

1. Summary and Status of the Project 49
2. Considerations on Physical and Technical Problems 50
3. The ASDEX Upgrade Tokamak System 51
4. Peripheral Installations 56
5. Diagnostics for ASDEX Upgrade 56
6. Additional Plasma Heating 57

IEA Implementing Agreement 59

JET Cooperation Project 61

1. Contributions of the JET Diagnostic and Pellet Injection Group (JDP) 62
2. Contributions of the Plasma Wall Interaction Group 63
3. Task Agreement No. 1 63
4. Task Agreement No. 2 66
5. Contributions of Various Groups of IPP 66

NET Cooperation Project 69

1. Development of a Pellet Injection Model for Implementation in the NET Tokamak Transport Code 69
2. Improvement of the SUPERCOIL Design Code 69
3. INTOR Contribution 70

II. Stellarators 71

WENDELSTEIN VII-AS Project 73

1. Introduction 73
2. Heating 74
3. Technological Status 76
4. Diagnostics 78
5. Data Processing 80
6. Experimental Results from W VII-A 83

WENDELSTEIN VII-X Project 90

1. WENDELSTEIN VII-X Studies 90
2. Contributions of the Stellarator Physics Group 94

Contents

B. DIVISIONS AND GROUPS 99

The Scientific Divisions of IPP 100
Experimental Plasma Physics Division 1 101
Experimental Plasma Physics Division 2 (Stellarators) 102
Experimental Plasma Physics Division 3 (ASDEX) 103
Theory Division 1 104
Theory Division 2 108
Theory Division 3 109
Surface Physics Division 115
Computer Science Division 122
Technology Division 124

C. PUBLICATIONS, CONFERENCE REPORTS AND AUTHOR INDEX 129

Publications 131
Lectures 143
Laboratory Reports 156
Author Index 159

D. UNIVERSITY CONTRIBUTIONS TO IPP PROGRAMME 167

Institut für Plasmaforschung (IPF) at Stuttgart University 169
Physikdepartment at the Technical University of Munich 186
Institut für Angewandte Physik II at Heidelberg University 188
Institut für Kernphysik, Strahlenzentrum, at Giessen University 190
Surface Science Group at Osnabrück University 192

SITE PLAN OF MAX-PLANCK-INSTITUT FÜR PLASMAPHYSIK 194

Preface

Much of the work at IPP in 1986 was devoted to constructing the ASDEX Upgrade and WENDELSTEIN VII-AS experiments and to modifying the ASDEX experiment. The latter was shut down in April to alter it for the long-pulse heating experiments planned for 1987. Thus the time for experiments was short, but even then ASDEX yielded significant results: It was the first experiment ever to enter the H-regime by means of ion cyclotron heating alone without the support of neutral injection. A new confinement regime characterized, like the H-regime, by high density and long energy confinement time was achieved with ohmic heating assisted by pellet injection. These good properties derive from the fact that the plasmas transport behaviour is distinctly improved by the use of pellets compared with that in previous purely ohmic discharges. Also noteworthy are experiments on current drive by lower hybrid waves. The resulting possible decoupling of the temperature profile and current density distribution allows effective suppression of sawtooth instabilities, i.e. the confinement is improved.

In addition to the construction of the WENDELSTEIN VII-AS advanced stellarator, which will start operation in 1987, work in the field of stellarator physics was particularly noteworthy with respect to the development of the Helias concept. This magnetic field configuration promises highly favourable stability and confinement properties. Thus, four configuration proposals are now available for the planned WENDELSTEIN VII-X reactor-relevant stellarator, which affords a good basis for selection of the final concept, scheduled for 1987.

On a national level, IPP coordinate their research effort with Kernforschungszentrum Karlsruhe within the "Entwicklungsgemeinschaft Kernfusion" and also in close liaison with the other members of the Association of National Research Centres (AGF) who are also involved in fusion research. IPP also maintain a number of cooperative ties with German universities. Their collaboration with the University of Stuttgart in the field of electron cyclotron resonanace heating has been especially successful.

The subjects of research performed at IPP are also an integral part of the European fusion programme. They contribute in two ways: Firstly, IPP are directly involved in JET, the joint European experiment. In 1986 IPP provided JET with a pellet injection system and two crystal spectrometers for observing the JET plasma by means of soft X-radiation. Secondly, the ASDEX and ASDEX Upgrade tokamaks and the alternative stellarator concept as embodied in the WENDELSTEIN VII-AS advanced stellarator and the planned WENDELSTEIN VII-X give essential information for preparing the next steps in the overall European programme.

Coordination of IPPs research activities also extends to the international level. Two Implementing Agreements have been concluded with the USA. One regulates the cooperation in the joint stellarator programme, to which the WENDELSTEIN experiments make a major contribution. The other one refers to the cooperation in the ASDEX and ASDEX Upgrade divertor tokamak experiments. This implements a new lower hybrid current drive experiment in ASDEX which will also involve ENEA Frascati, Italy, and PPL, Princeton.

Klaus Pinkau

Projects

Tokamaks

Most of the capacity at IPP is devoted to investigating magnetic confinement in the tokamak configuration, this line still being the furthest advanced towards application in a fusion reactor. With the tokamaks ASDEX and ASDEX Upgrade, the latter being under construction, IPP have concentrated their tokamak research on the divertor principle.

Meanwhile, the divertor has proved successful both for solving problems characteristic of the edge plasma and - connected to that - for improving the central plasma confinement. The discovery of H-regime by ASDEX in 1982, in a period when general results concerning the energy confinement in strongly heated tokamak devices were rather negative, has focussed the world-wide attention on the possibilities to influence the global transport behaviour by manipulating the plasma-wall interaction. Still the most promising way for this are separatrix-bound plasma configurations, and the past year was highlighted by the attainment of the H-regime on JET with a new record value for the fusion product $n_{Do} \cdot \tau_E \cdot T_{io}$ (2×10^{20} keV $\cdot$ m^{-3}). ICRH-experiments on ASDEX have shown for the first time that this regime can also be reached with heating methods other than neutral beam injection, although problems relating to antenna coupling and impurity production afflict at present still the duration of this phase.

Although primary emphasis is now on discharges with strong additional heating, purely Ohmically heated experiments are still of interest to understand the physics of transport processes and to investigate operational limits on plasma parameters not a priori directly connected to the heating power. Outstanding developments on ASDEX in 1986 regarded the confinement improvement with pellet injection, and operation at low q_a-values and high density. A regime with peaked density profiles and extremely high central density and confinement times of up to twice the standard ohmic values (up to 160 ms) was obtained in ASDEX with pellet injection. The experiments made it clear that the regime is not simply the result of a particle source near the centre but of favourably modified transport properties induced by pellet injection.
The coming experimental campaign will concentrate on an attempt to realise this good confinement regime in discharges with strong auxiliary heating. Limits on the plasma density n_e and the safety factor q_a independently place important restrictions on the operating regime of tokamaks. A pleasant surprise resulting from ASDEX investigations in the past year was the fact that a successful way to enlarge this range is the simultaneous optimisation of both, leading to the lowest q_a and the highest $\bar{n}_e$ values ever achieved on ASDEX in the same discharge with gas-puffing and ohmic heating.

ASDEX has been shut down in April 1986 until approximately April 1987 to allow for the installation of water-cooled divertor inserts and target plates ("hardening"). These, together with modifications of the heating systems, should allow auxiliary heating up to 10 s pulse length.

A critical item in the understanding of tokamak transport is the role of the plasma currents and their spatial distribution. The strong coupling in quasi-stationary equilibrium between the electron temperature profile, and the rotational transform profile $\iota(r)$ have been partly blamed for anomalous transport behaviour of tokamaks. Current drive by lower hybrid waves has been demonstrated to be able to break this relation but would require higher frequencies and larger total powers than previously available to ASDEX to be applicable in plasma density and current regimes of relevance to confinement studies. The importance of such experiments was, however, so stronlgy felt in the tokamak community that ENEA Frascati and PPL Princeton have agreed to pool their existing LH equipment and to join IPP in the construction and operation of a LHCD experiment on ASDEX (2.45 GHz, 3 MW transmitted power). The PPL participation takes place in the frame of the DOE-EURATOM Implementing agreement on Poloidal Divertors.

In the present phase of tokamak research, where future planning is based on empirical extrapolation and where theoretical concepts can be verified only through elaborate statistical procedures, an integrated system for data analysis and interpretation (AIDA) is being built up. This system is centered around the repetitive 60 Hz T_e- and n_e-profile measurements.

Experimental success with ASDEX and other divertor experiments and increasing know-how have made the poloidal field divertor the first option for solving plasma boundary problems in NET. For technical reasons, however, the magnetic configuration of the divertor will have to be modified - in relation to that in the ASDEX device. To ensure proper functioning of such an "open" divertor in NET and allow experiments in which the values of major parameters are equivalent to those in the boundary layer of a reactor, an upgraded version of ASDEX was needed to provide NET with definitive solutions of plasma boundary layer problems. IPP are constructing such an experiment, ASDEX Upgrade. Besides having a reactor-relevant divertor, ASDEX Upgrade is characterized by a strongly enhanced plasma current which should provide access to much improved plasma parameters. As its magnetic field configuration is very similar to that of NET, ASDEX Upgrade will contribute in addition to the study of reactor plasma control.

The efforts being made in the construction of ASDEX Upgrade encompass several areas of engineering and physics work. The physics work during 1986 concerned refined plasma equilibrium and poloidal field coil current calculations, stability calculations of divertor configurations, and the problem of plasma configuration description suited to plasma shape and position control.

The engineering work was concerned, in part, with the tokamak system and its components and, to an increasing extent, with the installation in the periphery of the tokamak system, which comprises energy supply circuits, cooling facilities, control system and heating systems. Experts of the computing science division were concerned with the construction of the data acquisition system in hardware and software. Progress with the tokamak system in 1986 was determined by the fabrication of all major components, some of which have already been delivered. After delay, manufacture of the toroidal field coils and toroidal field coil support structure is now proceeding.

Besides conducting their own tokamak experiments, IPP have been involved in JET, the joint European large-scale project at Culham (U.K.), since the planning phase. IPP have constructed and put into operation a large fraction of the JET diagnostics and participate in the exploitation of the JET experiment.

IPP host the NET Team, an internationally composed group of scientists and engineers called together to define the objectives of NET, the Next European Torus, and to prepare its design. NET is conceived as the next major step in the European fusion programme and many of its objectives are in the technology field. IPP contribute to NET activities both by direct secondment of personnel to the NET Team and by performing supporting work mainly via NET study contracts.

ASDEX Project

Head of Project: F. Wagner

1. EXPERIMENTAL RESULTS AND COMPARISON WITH THEORETICAL STUDIES

G. Becker, B. Bomba[1], H.S. Bosch[2], H. Brocken[3], A. Carlson[5], A. Eberhagen, G. Dodel[4], H.-U. Fahrbach[5], G. Fussmann, O. Gehre, J. Gernhardt, G. v.Gierke, E. Glock, O. Gruber[10], G. Haas, W. Herrmann[5], J. Hofmann[2], A. Izvozchikov[7], E. Holzhauer[4], K. Hübner[8], G. Janeschitz, F. Kaesdorf[9], F. Karger, M. Kaufmann[5], O. Klüber, M. Kornherr, K. Lackner[10], M. Lenoci[11], G. Lisitano, F. Mast[5], H. M. Mayer, K. McCormick, D.Meisel, V. Mertens[5], E. R. Müller[12], H. Murmann, J. Neuhauser[10], H. Niedermeyer, A. Pietrzyk[13], W. Poschenrieder[17], H. Rapp, H. Riedler[6], A. Rudy[14], F. Schneider, C. Setzensack, G. Siller, E. Speth[6], F. Söldner, A. Stäbler[6], K.-H. Steuer, U. Stroth[9], S. Ugniewski[15], O. Vollmer[6], K.L. Wong[16], H. Wurz[8], D. Zasche[5]

1.1 Overview

ASDEX was in operation from January until March. During the main part of 1986, however, the experiment was shut down to allow installation of water-cooled divertor inserts and target plates and water-cooled ICRH antenna screens. Parallel to these activities, extraction grids of the neutral injection sources were replaced by water-cooled ones. These modifications provide the technical means for long-pulse auxiliary heating up to 10 s pulse lengths. This allows us to address the still unexplored areas of impurity and recycling control, current profile relaxation and true steady-state conditions with auxiliary heating. Additionally, long-pulse heating increases the instrumentation on ASDEX for experiments which are not possible with short heating pulses.

In spite of the short operation time in 1986, important results were obtained: By pellet injection the ohmic energy confinement time could be increased from 90 ms to 160 ms; the H-mode transition was achieved with ICRH alone; the operational limits of ASDEX were extended to higher densities and, most important to low q: q-values as low as 1.9 were attained with the divertor configuration. Another success of ASDEX in 1986 was not achieved at the machine itself but outside IPP: Attainment of the H-mode at JFT2-M, BIG-D and, in particular, JET. It is gratifying that, owing to the results of ASDEX, more experiments are able now to operate in the H-mode and contribute to its understanding.

A regime with peaked density profiles and extremely high central density and confinement times of up to twice the standard ohmic values was obtained in ASDEX with pellet injection. This regime seems to correspond to that found in ALCATOR C with single-pellet injection. A thorough evaluation of our results made it clear that the regime is not simply the result of a particle source near the centre due to deep pellet penetration but of favourably modified transport properties induced by pellet injection. A relation between edge conditions (governed by recycling and gas puffing) and the central density was found. The deeper understanding of the mechanisms provided by deep pellet

---

1 Doctoral fellow, since September 1986
2 Doctoral fellow
3 Up to July 1986
4 University of Stuttgart, FRG
5 Experimental Plasma Physics Division 1
6 Technology Division
7 Ioffe Institute, up to April 1986
8 University of Heidelberg, FRG
9 Post-Doc since November 1986
10 Theory Division 3
11 Up to July 1986
12 Assigned to Jet up to November 1986
13 University of Washington, Seattle, USA
14 Undergraduate, since August 1985
15 Inst. for Nuclear Research, Swierk, Poland
16 Texas Tech. University, since November 1986
17 Plasma-Wall Interaction group

refuelling in contrast to gas-puffing may help us to realise this good confinement regime in discharges with strong auxiliary heating.

During density limit investigations it was found that a low-q regime exists in ASDEX at very high densities. q_a-values (in cyclindrical approximation) of 1.9 were achieved in divertor discharges with and without beam heating. Confinement times are high. With sufficient heating power the H-mode could be reached. It seems that the edge conditions of these high-density discharges are able to stabilize the m=2 MHD mode on the q=2 surface, which is localized very close to the separatrix at q_a-values of around 2. This success has two aspects: On the one hand, it is demonstrated that the H-mode is compatible with very low q_a-values, and, on the other, low-q_a operation is not being paid for by a reduced density limit but rather by the highest absolute values obtained so far in ohmic gas-puff-refuelled discharges.

Concerning the problem of plasma current profile shaping by lower hybrid waves, not only sawteeth suppression was demonstrated, but, thanks to the Li-beam diagnostic for plasma current distribution measurement, it was also possible to show the interrelations between the $N_{\parallel}$-wave spectrum, current profile and sawteeth behaviour. The sawteeth are suppressed when, by profile broadening, the central q-value increases above one. It was shown that the radial LH power deposition profile can be controlled by shaping the launched $N_{\parallel}$-wave spectrum. Stronger broadening of the current profile is observed by gradually increasing the RF power at high $N_{\parallel}$.

ICRH experiments were made in the minority D(H) heating mode up to a launched power of 1.8 MW. The heating efficiency and - at high power - the energy confinement time, too, were found to be quite comparable to the second-harmonic heating mode ($2\Omega_{CH}$). In both modes the confinement follows an L-mode scaling slightly better than in the case of neutral injection. The H-mode was achieved with ICRH alone in the D(H) regime at an absorbed power of 1.1 MW.

1.2 Pellet Injection

(in collaboration with K. Büchl, R.S. Lang, W. Sandmann (JET Diagnostic- and Pellet Group))

1.2.1 Introduction

An intensive campaign to study the consequences of pellet injection was carried out on ASDEX. It was possible by pellet injection to improve the plasma performance considerably compared with earlier investigations. In addition, greatly improved understanding of the relevant mechnisms was obtained. The dominant difference between earlier and recent experimentation was different recycling in the plasma boundary and the divertor. While the earlier campaign aimed at low-recycling pellet injection (LRP) to study genuine pellet fuelling, the second campaign aimed at improvement of the density limit. Therefore, pellet injection started typically later in the discharge at higher starting densities, and gas puff was used in addition (high recycling pellet-injection HRP). As a characteristic and quantitative difference the measured neutral gas flow density in the divertor was a factor of about 5 to 10 larger for HRP discharges than for the LRP cases.

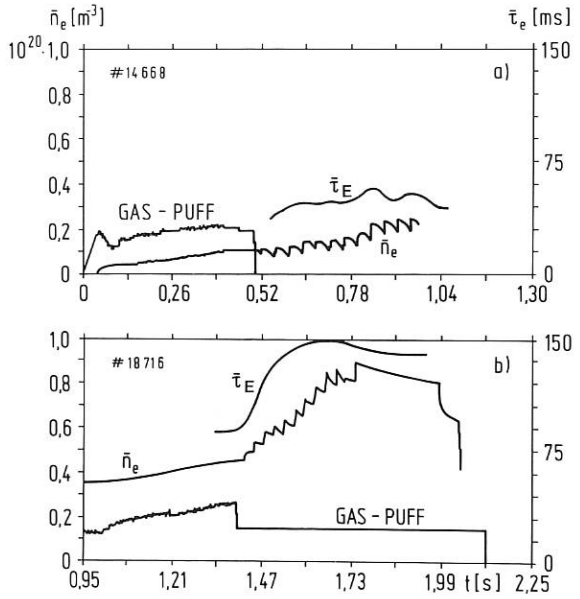

Fig. 1: Averaged density $\bar{n}_e(t)$ in a LRP (1a) and a HRP discharge (1b). In the first case, gas-puff is switched-off during pellet injection. A much more successful density build-up can be observed in the second case, when τ_E rises parallel to $\bar{n}_e$ in time.

The immediate consequence for the density build-up in LRP and HRP discharges can be seen in Fig. 1. In the LRP case nearly all the injected mass leaves the plasma in between two pellets, while in HRP discharges a remarkable density build-up of the central value up to 2.5×10^{20} m^{-3} was obtained. This high density with its peaked profile remained nearly stationary for times up to 230 ms after pellet injection. A considerable increase in the energy confinement time was found in these HRP discharges in parallel.

Pellets were injected by a centrifuge[1] which could produce up to 80 pellets with about 4×10^{19} deuterium atoms each and a velocity of 620 m/s. The typical penetration depth of the pellets was half the plasma radius (15 to 25 cm). In a limited series of discharges pellets with a velocity of only 200 m/s were used, penetrating less than 10 cm into the plasma.

In the following we report the energy confinement and the particle behaviour in more detail (Sect. 1.2.2). We describe the property of the late phase of HRP discharges with strong central radiation

[1] W. Amenda, R.S. Lang, J. Phys. E: Sci. Instrum. 19 (1986) 970

(Sect.1.2.3) and then continue with specific information about slow pellets (Sect. 1.2.4), cases with additional heating (Sect. 1.2.5) and measurements at the plasma boundary (Sect. 1.2.6), which show distinct differences between LRP and HRP discharges. The discussion (Sect. 1.2.7) reveals the importance of particle transport and its variation for a better understanding of the transport properties. In Sect. 1.5.1 the increase of the density limit achieved with pellet along with gas-puff refuelling is reported.

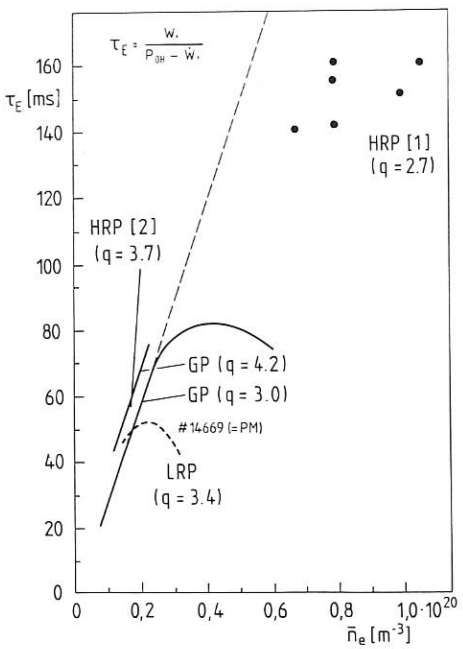

Fig. 2. Energy confinement time τ_E as a function of line-averaged density $\bar{n}_e$ for ohmic LRP and HRP discharges compared with discharges with gas-puff fuelling only (GP).

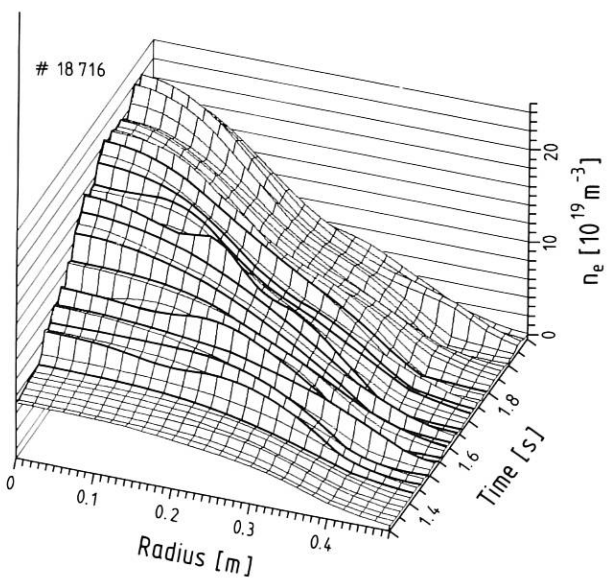

Fig. 3: Density profile n(r,t) before, during and after pellet injection for a typical HRP-discharge.

1.2.2 Energy confinement and particle transport

In OH-heated HRP discharges with successful density build-up, the energy confinement time τ_E could be improved by a factor of about 2 compared with the gas-puff (GP) cases under the same conditions. Figure 2 compares τ_E as a function of the line-averaged density $\bar{n}_e$ between HRP [1] and GP discharges. In the region of confinement saturation an improvement of τ_E up to 160 ms can be found. The increase of τ_E is accompanied by very little change in the T_e profile and a remarkable increase and peaking of the density profile (see Fig. 3). The density shows a strong increase especially in the centre region, while the pellet travels only to about half the radius. An analysis of the mass flow shows a strong inward drift of particles. From the nearly stationary and source-free density profiles before and after injection one can deduce the ratio of an inward drift V_D to a diffusion term D:

$$V_D/D = n'/n.$$

Figure 4 compares $V_D(r)/D(r)$ before and after injection demonstrating the strong change in transport especially around half the plasma radius. In the nearly stationary phase after injection the sawtooth activity has disappeared.

1.2.3 The "late" phase

The period of central density peaking and improved energy confinement finally ends in a situation with strong central radiation and an internal disruption. It is important to note that the "late" phase is well separated - typically by some 100 ms - from the time where τ_E is already at its high value.

In the late phase the central radiation increases typically within 100 ms from low values to about 100 % of the local ohmic heating power. The relative T_e profile flattens at the high radiation level. Spectroscopic analyses indicate iron to be responsible for the radiation.

The peaked pressure profile and the flattening of $T_e(r)$ in the centre lead one to assume that the internal disruption is caused by a violation of the ballooning criterion.

1.2.4 Slow pellets

A few pellets with a velocity of only 200 m/s were injected into the discharges as an additional experimental programme after lower hybrid heating or neutral injection. The pellets penetrated less than 10 cm into the discharge. They were partly ablated outside the bulk plasma by non-thermal electrons left over from the preceding lower hybrid heating period. One can clearly see from Fig. 5 that the density in the centre rises as with the high-velocity pellets as a result of an inward drift of

the material ablated in the boundary. A final peaking of the relation density profile seemed to be prevented by the respective broadening due to the next pellet.

Also in the case of slow pellet (see Fig. 2, HRP [2]) τ_E increases beyond the GP curve. The increase in the linear part of $\tau_E(\bar{n}_e)$ should be noted.

1.2.5 Neutral-injection-heated discharges

A limited number of discharges was carried out with pellet injection and neutral beam heating at the same time. The results can be summarized as follows:

1. Typical HRP discharges with improved energy confinement could be obtained with co- and counter injection and with a heating power staying below a level of 0.5 to 1 MW.

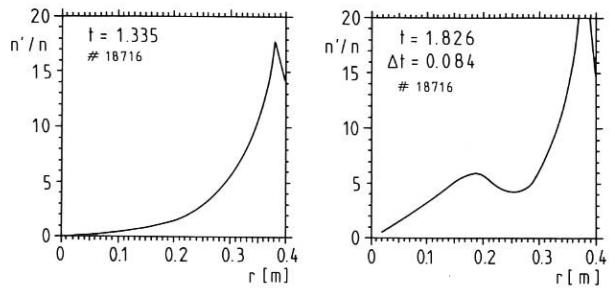

Fig. 4: $V_D/D=n'/n$ before and after pellet injection for an HRP-discharge.

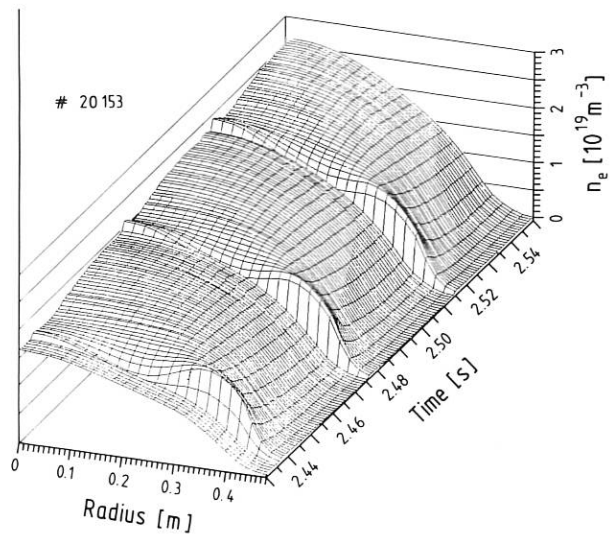

Fig. 5: The density profile development in a discharge with 3 slow (200 m/s) pellets. An inward drift of particles can be clearly seen.

2. Beyond that level successful density build-up was usually not possible. This does not seem to be partly caused by continuous mass outflow even with high recycling but in addition by internal disruptions enhanced by the auxiliary heating. After a pellet particles are lost by a single sawtooth, accompanied by m=1 activity in the centre but also high m-mode activity in the boundary.

1.2.6 Plasma boundary phenomena

Recycling condition: The analysis of the particle balance (external gas-puff and pellet refuelling and recycling from the divertor chambers) shows that pellet injection improves the global particle confinement over GP discharges both for HRP and LRP conditions. In LRP-shots this may be a consequence of deep fuel deposition; in the HRP cases, however, of the modified transport as described above. A crucial difference between LRP and HRP discharges is the much increased neutral gas flow density in the divertor chambers for the latter case. High-recycling conditions seem to be a prerequisite for the good confinement properties requiring gas-puff refuelling in addition to the pellets to provide and maintain it. On the contrary, extreme LRP conditions are established by recycling control via titanium gettering in the divertor chamber.

Edge density: A Li-beam diagnostic enables us to measure the density in the region of the separatrix. In GP discharges the density at the separatrix n_s is proportional to the line-averaged density $\bar{n}_e$ with a factor close to 0.3 only weakly depending on $\bar{n}_e$ and q. In typical HRP discharges this factor decreases in line with the central peaking, while n_s shows little variation in time during the pellet cycle. On the contrary, in LRP discharges $n_s(r)$ shows distinct changes with the pellet cycle: after pellet injection the density gradient in the boundary initially steepens declining continuously toward the end of the cycle.

1.2.7 Summary and discussion

At present the phenomenology and the understanding of pellet injection in ASDEX can be summarized as follows:

a) There is a clear difference between LRP and HRP discharges, this being made particularly evident by the neutral gas flow density in the divertor. In LRP discharges the particle density in the boundary does not seem to be in equilibrium with the bulk density, on the one hand, and the recycling process in the divertor, on the other. This lack of equilibrium leads to a continuous outflow of the injected particles.

b) HRP discharges are successful in the sense that they show a remaining density build-up (beyond the GP density limit) after pellet injection with a strongly peaked profile. They show in parallel for OH discharges a remarkable improvement of energy confinement by a factor of about 2. The peaked density profile, as the primary cause for improved energy confinement, originates from an increased inward drift (or reduced diffusion). Reduced outward flow of

particles during a sawtooth disruption - compared with GP discharges - might be responsible for the peaking. This is supported by GP discharges without sawtooth showing a similar peaking.

c) The unsuccessful density build-up at higher neutral injection heating power seems to be correlated with a specific MHD activity triggered by the pellets.

1.3 Confinement of Auxiliary Heated Plasmas

1.3.1 Confinement results from the different heating methods

The results from various investigations on plasmas heated by different methods - neutral injection (NI), ion cyclotron resonance heating (ICRH) in various heating schemes (hydrogen second-harmonic heating ($2\Omega_{CH}$ at 67 MHz) in pure hydrogen and hydrogen/deuterium mixtures, hydrogen minority heating in deuterium (D(H), 33.5 MHz, $n_H/n_e \approx 5$ %)) and lower hybrid heating (LH) allowed a broader view of confinement physics. In particular, the discovery of the H-mode with pure ICRH heating demonstrated that the global confinement pattern - degraded L or improved H mode confinement - does not depend on the microscopic details of the heating method but is an intrinsic plasma characteristic.

The H-mode was realized - for the first time - with ICRH alone in the D(H)-minority scheme at an absorbed power of about 1.1 MW. Thus it appears that the dominant confinement regimes of auxiliary heated plasmas are found to be independent of the heating method. The H-mode, which has so far just marginally been achieved , develops out of an L-phase with sawteeth (Fig. 6) and shows all the characteristic features, such as a distinct drop in the H_α-signal in the divertor chamber, enhanced plasma energy content, the existence of the typical edge MHD phenomena, called ELMs, and a significantly enhanced edge electron temperature (rising from about 50 eV to about 250 eV close to the separatrix).

In the other heating scenarios or at lower power, ICRH operated in the L-regime like NI. The study of ICRH-heated plasmas without NI assistance was found to be possible after wall carbonization (See Sect. 1.5.3). Wall carbonization prevented disruptions otherwise caused by excessive impurity radiation and allowed the ICRH to work up to maximum RF power ($P_{IC} \approx 15 P'_{OH}$) without NI assistance. At high power in standard (double-null) configurations, both RF scenarios follow essentially an L-type scaling. Figure 7 summarizes the energy confinement times normalized to the values of the ohmic phases (which eliminates isotope effects on τ_E).

Also scaling studies of τ_E indicated rather similar behaviour of NI- and ICRH-heated plasmas. In the L-mode, τ_E degrades with increasing power. The confinement degradation of both RF schemes seems, however, slightly less severe than with beam heating. This is supported by the observation that, with ICRH, the particle confinement only weakly degrades with respect to the ohmic phase. It is not yet clear whether the improved particle confinement (with respect to NI) or the absence of plasma rotation during ICRH has any influence on the degree of energy confinement degradation. Both NI and ICRH yield $\tau_E \alpha I_p$ and no density scaling. It is well known that already under ohmic conditions τ_E is independent of density in the so-called saturation regime. Owing to this similarity in scaling, we have reconsidered the role of heating power and plasma current for confinement.

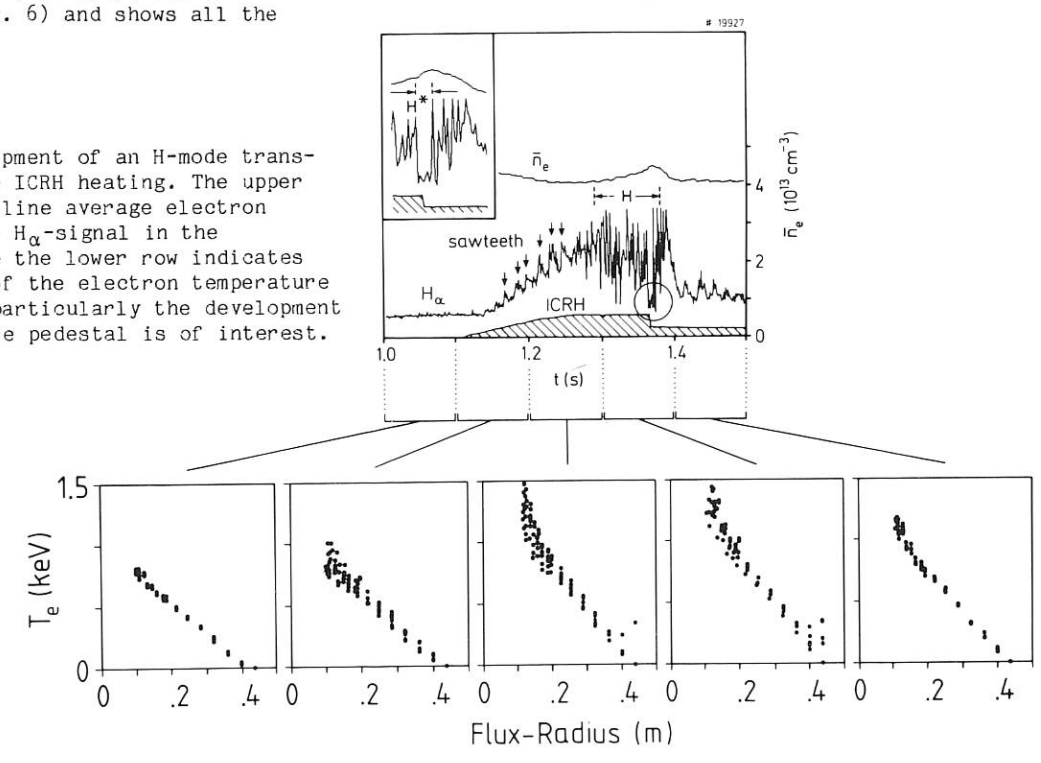

Fig. 6: Temporal development of an H-mode transition with pure ICRH heating. The upper plot shows the line average electron density and the H_α-signal in the divertor, while the lower row indicates the evolution of the electron temperature profile where particularly the development of a temperature pedestal is of interest.

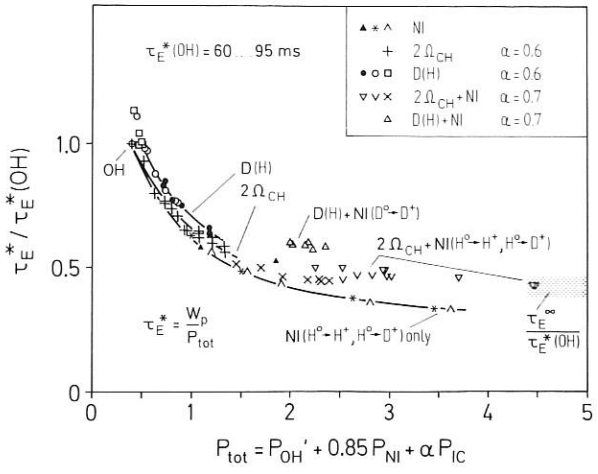

Fig. 7: Energy confinement times (normalized to the value of the ohmic phases) versus total absorbed heating power.

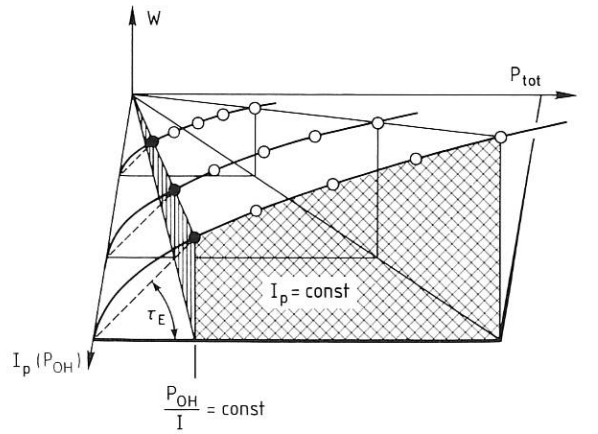

Fig. 8: 3-dim. plot which schematically shows the expected nonlinear relation between W and P at constant I_P and the different paths of ohmic and auxiliary heating power scans.

We conclude that there is no difference in the basic confinement principles of the ohmic saturation and the L-regime. The intrinsic degradation in confinement with increasing power which is already present in the ohmic saturation regime continues into the L-regime with auxiliary heating. The confinement of both the OH- and L-regimes is affected by a fundamental nonlinear relation between the energy content and heating power. This non-linear dependence becomes obvious with auxiliary heating in the L-mode.

The other important parameter for confinement, the poloidal magnetic field, affects ohmic and auxiliary heated plasmas differently. At given toroidal field B_T, the plasma temperature and density profiles broaden with rising I_P, causing the energy content to rise. At constant heating power (with auxiliary heating) this principle leads to the $\tau_E \propto I_P$ scaling; with OH heating when $P_{OH} \propto I_P$, the effects of P_{OH} and I_P cancel each other, leading to high (because P_{OH} is low), but power- and current-independent confinement.
Figure 8 shows schematically the nonlinear variation of the energy content W with heating power at various plasma current values and indicates the operational planes for ohmically and auxiliary heated plasmas. An ohmic power scan occurs in a plane where I_P/P=const, an auxiliary heated one generally in a plane I_P=const. This change in "operational direction" gives rise to a discontinuity of W versus P at the transition from ohmic to auxiliary heating, which leads to the mistaken view that ohmic heating has a special quality.

The operational space below the ohmic power level where good confinement is expected is only made accessible by an auxiliary heating method which couples energy preferentially to suprathermal electrons. Thereby the electric resistivity is decreased and the ohmic power input can be reduced with the plasma current being kept constant. This may be achieved by Lower Hybrid heating or current drive.

The energy confinement was studied for LH heating and current drive up to powers of $P_{LH} \approx 1$ MW. The LH power absorbed in the plasma is determined from the power balance at the beginning and at the end of the RF pulse. The absorption coefficient α is obtained from

$$\alpha = (-\Delta P_{OH} + \dot{W}_P + \Delta P_{rad})/P_{LH},$$

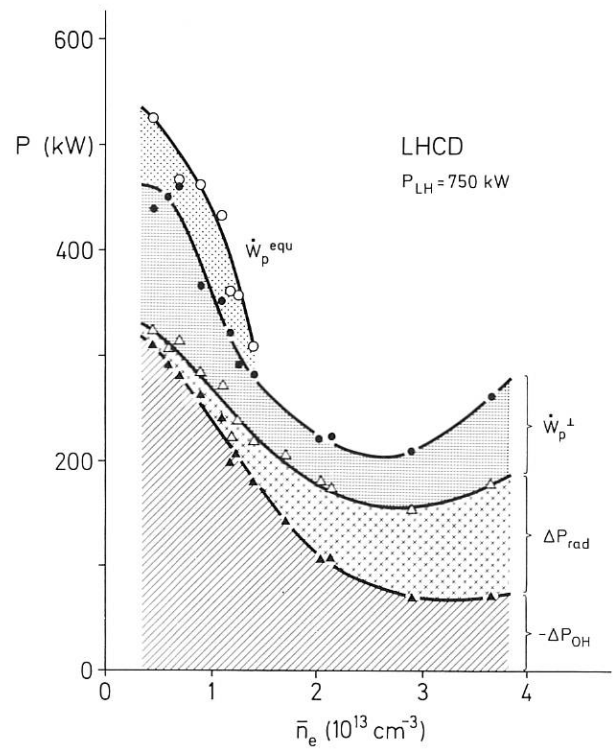

Fig. 9: Density dependence of the different terms in the power balance for LH current drive. $\alpha P_{LH} = -\Delta P_{OH} + \dot{W}_P + \Delta P_{rad}$.

where $-\Delta P_{OH}$ is the reduction in OH power input, $\dot{W}_p$ the rate of change of the total plasma energy content, ΔP_{rad} the increase in radiation losses and P_{LH} the net RF power transmitted. The density dependence of the different terms of the power balance is shown in Fig. 9 for LH current drive with P_{LH} = 750 kW. The drop of the total absorbed power with increasing density can be explained by a diminishing of the accessible part of the RF power launched. The absorption coefficient also decreases with increasing power, thus indicating saturation effects.

The power dependence of the plasma energy content W_p, as determined from diamagnetic measurements, is shown in Fig. 10 for LH current drive at $\bar{n}_e \approx 0.6 \times 10^{13}$ cm^{-3}. The evaluation is made in two ways by assuming that all RF power is absorbed (α=1) and by taking the experimentally determined absorption coefficient α . This shows that the energy confinement time during LH application is indeed increased above the ohmic value at low plasma density ($\bar{n}_e \lesssim 1 \times 10^{13}$ cm^{-3}) under conditions where the total power input is smaller than or comparable with the power input during ohmic heating.
The results are similar, both for LH heating and current drive mode.

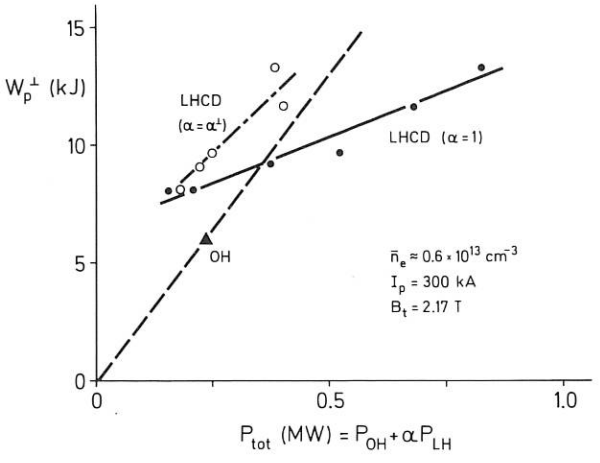

Fig. 10: Power dependence of the plasma energy content $W_p^{\perp}$.

1.3.2 Combination of different heating methods

The combination of ICRH with NI has some obvious technical advantages. With NI preheating, it is possible to apply the full ICRH power up to P_{IC}=2.3 MW (0.8 MW of NI preheating is sufficient). In the case of an ohmic target plasma the ICRH power is limited to P_{IC}=1.2 MW owing to excessive impurity radiation caused by ICRH. With NI, the power flux in the discharge is sufficiently increased so that high radiation levels can be tolerated without causing disruptions.

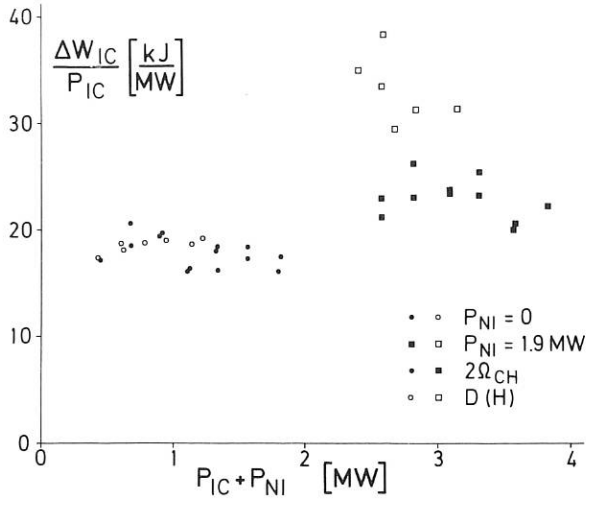

Fig. 11: Change in plasma energy content ΔW_{IC} normalized to ICRH power launched by the antennae P_{IC} versus total power. The ICRH-power scans without NI preheating were obtained under carbonized wall conditions.

In the application of ICRH to an ohmic plasma, the power launched by the antennae P_{IC} is ~80 % of the generator power. In the case of an NI-preheated plasma 90 % of the generator power can be launched. Also the fraction of the launched power which is actually absorbed by the bulk plasma improves from a maximum of ~60 % in the OH case to a maximum of ~70 % with NI preheating.

The improved application of ICRH power in a beam-heated discharge is demonstrated in Fig. 11. Plotted is the rise in plasma energy content ΔW_{IC} due to ICRH, normalized to the launched ICRH power P_{IC} versus the total power $P_{IC}+P_{NI}$. Two cases are considered: (1) ICRH is applied to an ohmic target plasma and (2) ICRH is applied to a beam-heated plasma. Figure 11 shows that ICRH power is more efficiently used in a plasma which is preheated by NI. The difference in $\Delta W_{IC}/P_{IC}$ cannot be fully explained by the trivial reasons of a reduction of a) the ohmic power input as soon as ICRH heats the plasma and b) of the impurity radiation losses.

The possibility of favourable coupling of the ICRH wave ($2\Omega_{CH}$) to the beam ions was studied in a case where first the ICRH power was applied to a deuterium plasma preheated by hydrogen beams. The results were compared with a case where deuterium was injected into a deuterium plasma where no beam ion-ICRH wave interaction could be expected. Though a favourable beam-ion-wave interaction has been observed in the beam ion distribution when hydrogen is injected, it was found to be insufficient to give rise to synergetic improvements in the plasma energy content. The rise in $\Delta W_{IC}/P_{IC}$ with beam heating might be due to better RF coupling at modified plasma parameters in the scrape-off layer in front of the antennae.

The combination of LH and NI concentrates on the effects of different current distributions (OH or

LHCD) on global confinement when NI is additionally applied. Another aspect is that, in the OH-case thermal electrons and, with LH, suprathermal electrons carry the current. Low density ohmic discharges with mostly suprathermal current carriers showed improved energy confinement.

Figure 12 summarizes the results obtained when either ICRH or LH is combined with NI. Plotted is the energy content of the discharge versus the total heating power. The results of combined heating are compared with those when NI or ICRH alone is applied. (The vessel wall was carbonized for these cases.) This diagram shows that ICRH and NI power can be superimposed linearly and that the heating results are also independent of the method of current drive. The improvement of ICRF-heating when simultaneously applied together with NI may give rise to a rather linear dependence of W_p on P_{tot} without the slight saturation in W_p with pure NI-heating at high power generally observed in the L-mode. This result indicates favourable aspects when a high auxiliary heating power is split up into ICRH and NI.
Further results of combining LH and NI are presented in Sect. 1.7.

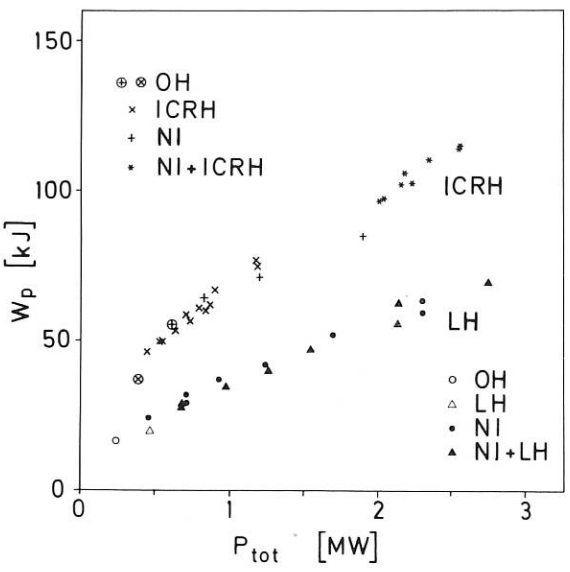

Fig. 12: Variation of the plasma energy content with total heating power for NI (400 kA, 2.2 T, $\bar{n}_e=5\times10^{13}$ cm^{-3}), ICRH (380 kA, 2.3 T, 3.5×10^{13} cm^{-3}) and LH (current drive conditions, 280 kA, 2.2 T, 1.2×10^{13}) and ICRH and LH in combination with NI. In case of ICRH $P_{NI}=1.9$ MW is added and P_{IC} is varied; in case of LH $P_{LH}=0.45$ MW is added to a beam power scan. W_p of the ohmic (or LH) target plasma is also shown.

1.3.3 Deposition experiments and the study of plasma profiles

1.3.3.1 "Consistency" of electron temperature profile

The shapes of T_e profiles exhibit a remarkable invariance when very different heating methods are compared, such as ohmic heating or combined ohmic and additional neutral beam heating, even under extremely different injection conditions, peaked or off-axis power deposition. The same profile invariance is observed for discharges with neon added as impurity, and those with and without sawtooth activity.

When high-frequency additional heating is applied to ASDEX discharges, the T_e profiles do change, however, and take an axially peaked shape. Generally, this peaked central region is enclosed within the q=1 flux surface. This inner zone obviously represents a confinement region of its own and is governed by processes that are not representative of the global plasma confinement. Well outside the influence of the q=1 surface (in general at a radius $r_1=\sqrt{2}\ r(q=1)$), the shapes of the relative T_e profiles coincide again, which becomes evident when the functions $T_e(r)$ are normalized at r_1; this is demonstrated in Fig. 13, where a variety of discharges with very different heating and refuelling methods are compared. The normalization radius of 18 cm corresponds to $\sqrt{2}\ r(q=1)$ for a total q_a of 2.5.

It is, on the other hand, well known that the T_e profile shape is clearly influenced by the safety factor q_a. An example is given in Fig. 14, which shows $T_e(r)$ profiles of 5 discharges during ohmic

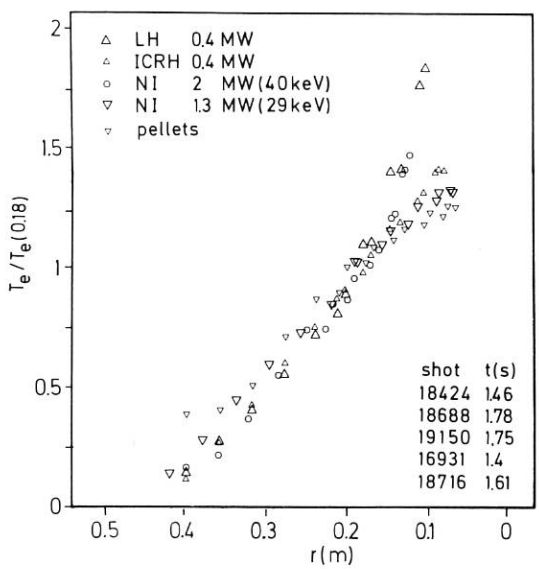

Fig. 13: Normalized T_e profiles achieved with various heating and refuelling methods: lower hybrid (LH), ion cyclotron heating (ICRH), neutral injection heating (NI), and ohmic heating with pellet injection. The abscissa represents the radius of the flux tube on which T_e is measured.

and neutral beam heating with different values for q_a at the boundary; the profiles are normalized again at r=18 cm. The surprising result is an astonishing coincidence of the normalized profile slopes outside r_1. The influence of q_a on the profile shape seems to be totally restricted to the zone within the q=1 surface, no matter whether the plasma is heated by neutral beams or by the plasma current alone. For radii > r_1 all T_e profiles (Fig. 13 and Fig. 14) exhibit a constant relative slope (within the accuracy of the measurement):

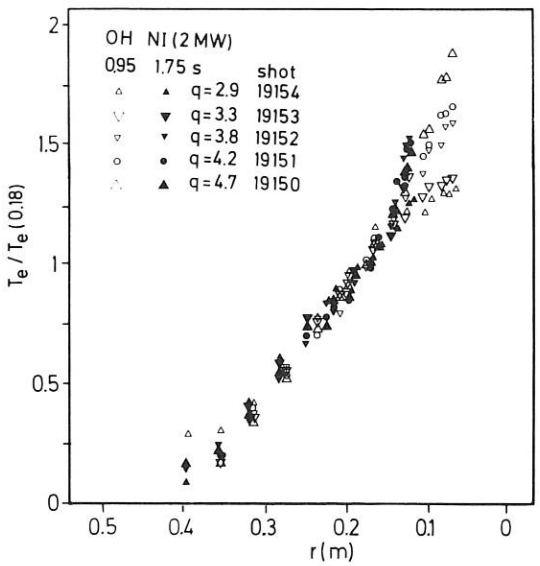

Fig. 14: Normalized T_e profiles vs. flux tube radius r. Ohmic heating (OH) and neutral injection (NI) for various values of the safety factor q_a.

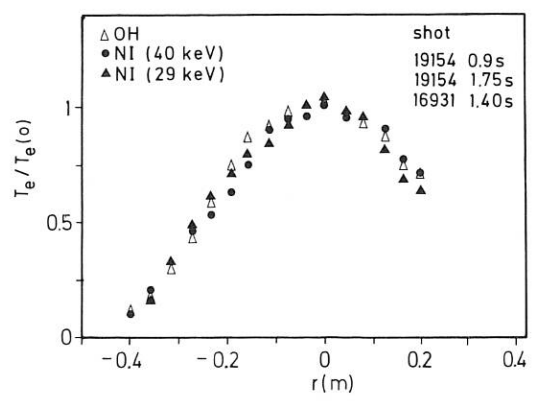

Fig. 15: Normalized T_e profiles.
Δ ohmic heating (OH): q=2.9
$T_e(0)$=0.9 keV

• neutral injection (NI): q=2.9,
$T_e(0)$=1.68 keV, $\bar{n}_e$= 2.9x10^{13} cm^{-3},
D^o(40 keV)→D^+

▲ neutral injection: q=2.6, $T_e(0)$= 1.1 keV, $\bar{n}_e$=5.6x10^{13} cm^{-3}, D^o(29 keV)→H^+

$1/T_e(0.18\ m) \times dT_e/dr = (4\pm0.3)m^{-1}$ for $r>\sqrt{2}\ r(q=1)$.

In order to substantiate the concept of "profile consistency" (the electron thermal diffusivity $\chi_e(r)$ depends directly on the electron thermal conductive loss $P_{cond,e}$ across a magnetic surface), the development of the T_e profile was studied for different power deposition profiles. Figure 15 compares normalized T_e profiles for peaked NI power deposition (40 keV/D^o→D^+) into a low-density plasma and off-axis power deposition (29 keV D^o→H^+) into a high-density discharge.

An attempt to explore the extent of T_e profile shaping was also made by varying the ICRF power deposition either by 1) shifting the $2\Omega_{CH}$ resonance layer radially or 2) working with two $2\Omega_{CH}$ resonance layer positions of variable power simultaneously (67 MHz for $r_{res}\approx0$ cm, and 61.92 MHz for $r_{res}\approx a/2=20$ cm), combined with a small amount of NI power (≈0.4 MW).

Studies with P_{IC}=1.4 MW on top of P_{NI}=0.8 MW did not exhibit any significant alteration of the electron temperature profiles, as shown in Fig. 16, when the $2\Omega_{CH}$ resonance was shifted radially from r_{res} = 0 cm to r_{res} = 21 cm by varying the toroidal magnetic field (B_t = 2.27 T to 2.55 T) and the plasma current (I_p = 333 kA to 370 kA) in such a way as to keep q_a=3.3=const.

Investigations with two $2\Omega_{CH}$ resonances simultaneously in the plasma cross-section (the RF power at each resonance layer was varied in such a way that the total RF power was kept constant) did not cause strong profile modification either: With mainly off-axis deposition ($P_{IC}(0)$=0.27 MW; $P_{IC}(a/2)$=0.63 MW) neither a significant variation of the $T_e(r)$ and the $p_e(r)$ profiles outside q=1 nor a change of the global energy confinement time was found in relation to mainly on-axis deposition.

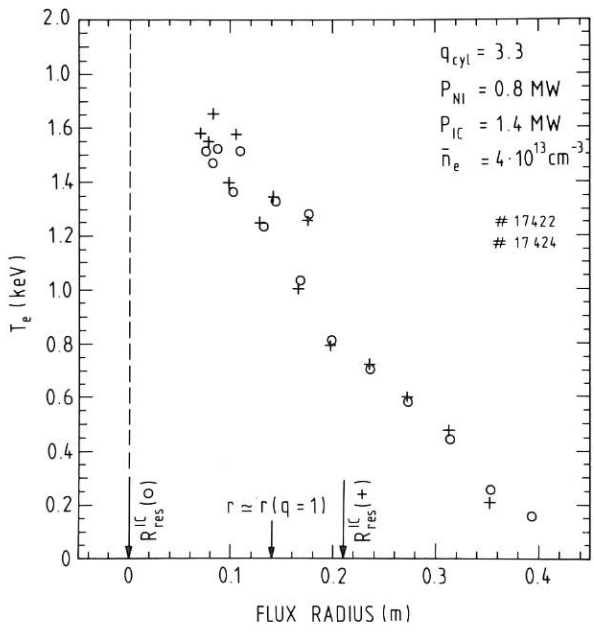

Fig. 16: Electron temperature profiles relating to ICRH on-axis and off-axis resonance layer position at constant q_a.

Transport analysis of the cases with various deposition profiles support the concept of "profile consistency". The transport analysis is done by means of the TRANSP 2 transport analysis code of PPPL[1] and measured radial plasma profiles. The definition of a local χ_e which only depends linearly on local plasma parameters does not seem to be appropriate.

In nearly steady-state ohmic discharges χ_e can be described by a local parameter dependence $\chi_e(OH)=\chi_{CMG}\cdot(B_t a/R)/(n_e^2\cdot^8 T_e q)$, too. But in ohmically heated pellet discharges only the χ_e values averaged over one pellet cycle agree with χ_{CMG}, whereas a description in agreement with "profile consistency" also depicts the time-resolved χ_e measurements and yields an explanation for the scaling given by χ_{CMG}.

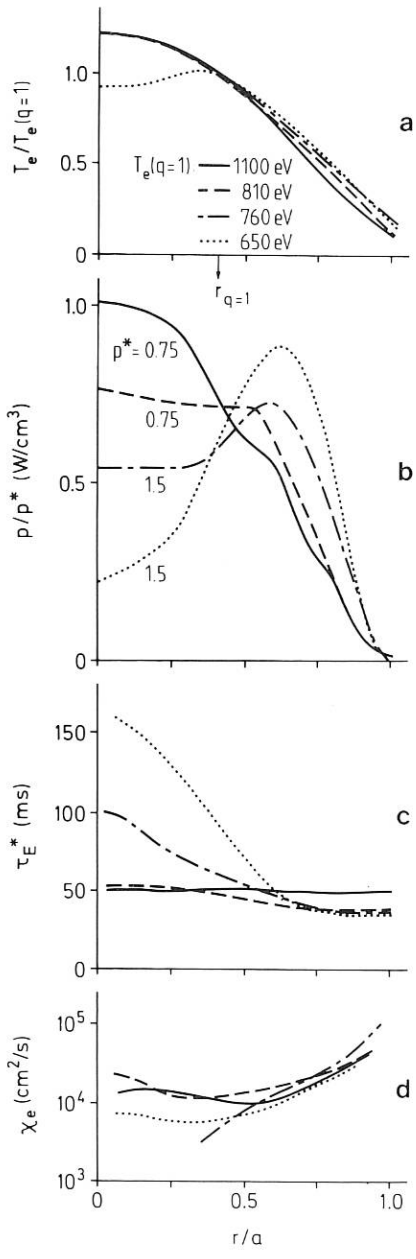

Fig. 17: Normalized T_e, heating power density p, energy confinement time τ_E^* and χ_e radial profiles of L-mode discharges with q(a)=2.6.

L-mode discharges at q(a)≈2.6 with strongly varying deposition profiles were studied by means of $H^0\rightarrow D^+$, $D^0\rightarrow H^+$, $D^0\rightarrow D^+$ injection by varying the injection energy from 14.5-40 keV maximum energy/nucleon. About the same normalized T_e profiles are obtained despite quite different heat deposition profiles (see Fig. 17), total heating powers ($P_h=P_{bi}+P_{be}+P_{OH}$)=1.5-4.1 MW) and densities ($\bar{n}_e=4\times10^{19}\div11.3\times10^{19}$ m^{-3}). The electron heating ($P_{be}+P_{OH}$) slightly exceeds the ion heating (P_{bi}) and $T_i\gtrsim T_e$ is obtained.

The central confinement times $\tau_E=W_p/(P_h-\dot{W}_p)$ distinctly increase with off-axis heating deposition, whereas the global confinement times are about the same. The deduced $\chi_e(r)$ values given in Fig. 17 are accordingly reduced in the plasma centre with off-axis heating and can be well described by $\chi_e\sim P_{cond,e}/(n_e T_e r^2)$ for $r_{q=1}<r<0.8a$ for individual discharges. At a fixed radius of r=2a/3 the relation $(\chi_e n_e T_e)/2a/3\sim P_{cond,e}(2a/3)$ holds for different discharges, too. At that radius $P_{cond,e}$ is about $(0.5\div0.65)P_h$, displaying the dominance of electron thermal transport in the L-mode over the entire density range.

1.3.3.2. Analysis of density profiles

Parameter dependence: Anomalous diffusion and inward drift in ohmically heated (double-null divertor) discharges with sawteeth were investigated in extensive parameter studies. For deuterium and hydrogen plasmas the variation of the density profile with plasma current I_p, toroidal magnetic field B_t and line-averaged density $\bar{n}_e$ was explored. Several series of discharges were studied in which only one of these parameters was scanned. In all cases, data measured during long current and density plateaus are analyzed.

The electron density n_e is measured by a multichannel HCN laser interferometer (λ = 337 µm). The electron density profile is constructed by a fit procedure for the measured line densities of the horizontal channels. A modified parabola of the form $n_e(r)=n_e(0)(1-(r/a)^\beta)^\alpha$ describes the profile inside the separatrix, while an exponential function with a typical decay length of 2 cm is used outside. The measured profile shapes are characterized by $n_e(0)/\langle n_e\rangle$, i.e. the ratio of the central density to the volume-averaged density.

The dependence of $n_e(0)/\langle n_e\rangle$ on the plasma current (expressed by q_a) is shown in Fig. 18. With increasing q_a a peaking of the density profile is observed which is stronger for deuterium than for hydrogen plasmas. Raising q_a in a B_t scan (see Fig. 19), however, gives rise to much weaker profile peaking both for deuterium and for hydrogen which is attributed to the shrinking of the q = 1 radius. The variation of $n_e(0)/\langle n_e\rangle$ with $\bar{n}_e$ is presented in Fig. 20. Slightly broader profiles are found at higher densities.

[1] R. Hawryluk, in Physics of Plasmas Close to Thermonuclear Conditions, Vol. 1, Varenna (1979) (EUR-FU-BRU/XII/476/80).

Particle transport analysis: The experiments are simulated with a modified version of the BALDUR transport code. For deuterium and hydrogen plasmas the computations fit the measured $n_e(r)$ and $T_e(r)$, the central ion temperature $T_i(0)$ from CX diagnostics and the poloidal beta β_p from the diamagnetic loop. The following expressions for the electron heat diffusivity χ_e and the diffusion coefficient D are to be used for best fits in ohmically heated plasmas:

$$\chi_e(r) = 1.61\times10^{16} A_i^{-1/2} B_t n_e(r)^{-1} T_e(r)^{-1} q(r)^{-1} \text{cm}^2\text{s}^{-1} \quad (1)$$

$$D(r) = 0.2\ \chi_e(r), \quad (2)$$

where B_t is in kG, n_e is in cm^{-3} and T_e is in keV. A_i denotes the ion mass number. Note that the ion mass dependence given holds under pure deuterium and hydrogen plasma conditions after glow-discharge cleaning. The ion heat diffusivity χ_i used is one time the neoclassical values according to Chang and Hinton. For the anomalous inward drift velocity $v_{in} = \gamma(r/r_w)^2$ is applied instead of the Ware pinch. γ is a factor whose parameter dependences are investigated by scanning I_p and $\bar{n}_e$, and r_w is the wall radius (r_w = 49cm). As illustrated in Fig. 18, this model yields the measured profile variation with I_p. For deuterium $v_{in} = -550\ (r/r_w)^2$ cm s^{-1} is used, while for hydrogen $v_{in} = -710\ (r/r_w)^2$ cm s^{-1} is applied. The inward drift velocity is found to be independent of the plasma current. Results from modelling the density scan are presented in Fig. 20. For a given electron temperature the inward drift exhibits an inverse $\bar{n}_e$ scaling. On the basis of all scans, it is concluded that v_{in} depends inversely on n_e and T_e, but it is independent of the poloidal magnetic field B_p, B_t and A_i. With $B_t/q = R_o B_p/r$ one obtains

$$v_{in}(r)/D(r) = -A_i^{1/2}\ B_p(r)^{-1} f(r) \quad (3)$$

independently of B_t, n_e and T_e. Smaller currents and larger ion mass correspond to higher $|v_{in}|/D$, i.e. more peaked density profiles, in agreement with the measurements. The v_{in} scaling given by eq.(3) differs from the previously used relation $v_{in}/D = -2\alpha r/a^2$, with α being a constant. An explicit dependence of χ_e, D and v_{in} on Z_{eff} was not identified in the scans.
For ohmically heated and injection-heated discharges of the L and H types it is shown that the anomalous inward particle flux can be described by a thermoelectric-type effect yielding $v_{in}/D = 0.5 T_e^{-1} \partial T_e/\partial r$.

Owing to this process the density profiles are found to adjust to the electron temperature profiles in the different confinement regimes and with the different heating schemes.

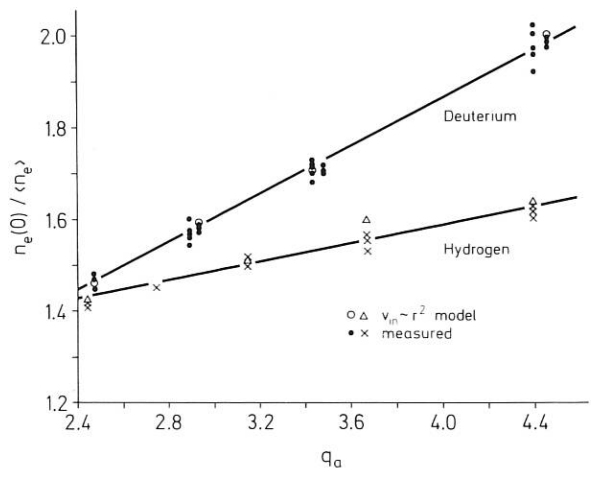

Fig. 18: $n_e(0)/\langle n_e\rangle$ versus q_a by scanning the plasma current between 250 and 450 kA (B_t = 2.25 T, $\bar{n}_e$ = 2.7 x 10^{13} cm^{-3}).

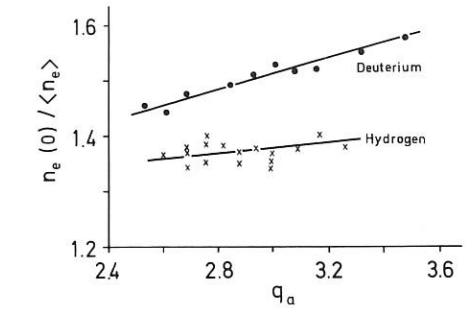

Fig. 19: Measured $n_e(0)/\langle n_e\rangle$ versus q_a by scanning the toroidal magnetic field (I_p=380 kA).

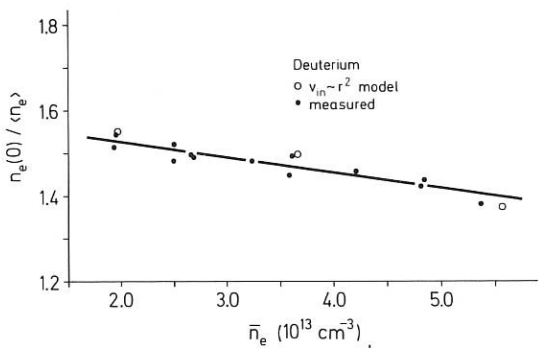

Fig. 20: Measured and computed $n_e(0)/\langle n_e\rangle$ versus $\bar{n}_e$ (I_p = 420 kA, B_t = 2.18 T).

1.3.4 Fluctuation measurements (in collaboration with G. Dodel, E. Holzhauer, Universität Stuttgart)

Turbulent fluctuations are considered to be the most likely reason for the anomalous transport in tokamaks. For this reason fluctuation measurements by different methods were continued or started.

1.3.4.1 Measurement of low-frequency density turbulence by collective far-infrared scattering

Broad-band low-frequency (100 kHz<f<2 MHz) density fluctuations were observed under various operational conditions of ASDEX using the 119 µm scattering system described in the Annual Report

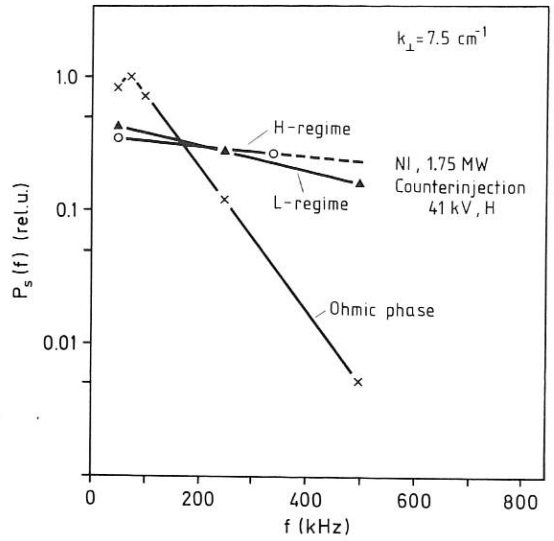

Fig. 21: Frequency spectra of scattered power during different phases of a divertor discharge. D_2, B_t = 2.17 T, I_p = 320 kA, $\bar{n}_e$ = 2.4 x 10^{19} m^{-3}, P_{NI} = 1.75 MW, H^o Counterinjection.

1985. The results can be briefly summarized as follows:

a) Ohmic heating. The frequency spectra peak around 100 kHz. The wave number ($k_\perp$) spectra decrease as $k_\perp^{-4}$ in the accessible range of 5 cm^{-1}<$k_\perp$<20 cm^{-1}. The rms scattered power scales linearly with the mean electron density $\bar{n}_e$, indicating constancy of the relative fluctuation level $\tilde{n}_e/\bar{n}_e$.

b) Neutral beam injection heating. The frequency spectra become broader with increasing heating power. In the majority of L-discharges the scattered power increases above the ohmic level. A decrease of the scattered signals is observed at the transition from the L- into an ELM-free H-mode. (Figure 21 shows frequency spectra of different discharge phases.)

c) Ion cylotron resonance heating. The scattering signals increase above the ohmic level for $k_\perp$< ~5 cm^{-1}. Density fluctuations with $k_\perp$ > ~7.5 cm^{-1} are observed at the heating frequency (33.5 or 67 MHz).

d) Lower hybrid heating and current drive. No significant change in the low-frequency density fluctuations with respect to the ohmic phase is seen.

e) Sawtooth activity. Precursors to the sawtooth crash in the SX signals are observed in the frequency range >500 kHz. There is experimental evidence that they are only localized inside the q=1 surface.

f) Pellet injection. The scattering signals increase with beginning ablation of the pellets and decrease with relaxation of the radial density profile.

A conclusive statement concerning the nature of the density turbulence and possible correlations to anomalous transport requires more experiments and access to the range $k_\perp$ < 5 cm^{-1}. The scattering system is being modified to meet these requirements.

1.3.4.2 Measurement of broad-band magnetic fluctuations

Mirnov coils in the limiter shadow of ASDEX were used to demonstrate the existence of broad-band magnetic fluctuations with radial and poloidal components. Above about 70 kHz the temporal evolution of these spectra is distinctly different from the coherent Mirnov oscillations and their harmonics.

To obtain an estimate of the poloidal mode number m it was assumed that the field due to current disturbances decays like a vacuum field outside the plasma boundary in a cylindrical geometry. For L-mode discharges with NI the plasma position, and thus the distance to the Mirnov coil, was varied. From the observed decay length a value of m≥10 is deduced. Typical fluctuation levels at the probe position were $B_r/B_T \approx 10^{-5}$. Using the vacuum field decay model, the fluctuation level at the plasma boundary would be $\geq 10^{-4}$. Between 70 kHz and 200 kHz the spectral power density drops by a factor of 10.

No qualitative difference was seen in the temporal development of the radial and poloidal field components. The power spectra of the magnetic fluctuations are not correlated with those of density fluctuations obtained with collective laser scattering (see above). In an ohmic discharge a linear density ramp was produced. Within a fixed frequency range (85-115 kHz), the signal power of the magnetic fluctuations decreased slightly in contrast to the scattered signal.
The fluctuations increase for all three types of additional heating and lower hybrid current drive.

Contrary to expectation, the transition into the H-phase produces a further increase in the fluctuation level which can be strongly modulated in the presence of ELMs. In addition, the frequency spectrum is significantly broadened.

In the presence of sawteeth the fluctuations suddenly increase at the time of the sawtooth

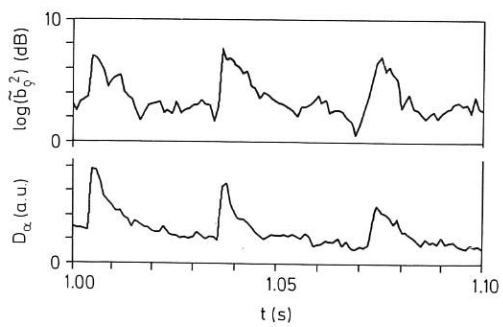

Fig. 22: Power of magnetic fluctuations (85 ÷ 115 kHz) and D_α light (upper divertor chamber) showing the sawtooth activity.

crash, similarly to the D_α signal observed in the divertor chamber (see Fig. 22). The signal power seems to depend on conditions in the plasma boundary, as can be seen in the case of gas puffing.

Further experiments will be needed before a comparison with proposed theoretical models for magnetic fluctuations and their propagation mechanism inside the plasma can be made. A new probe which can measure all three field components will be mounted on a manipulator which allows a fast radial scan of the plasma boundary region.

1.3.4.3 Visible edge turbulence

Eight fibre bundles connected to photomultiplier tubes were imaged onto the separatrix region of the plasma. Hydrogen gas puffing close to the place of observation provides sufficient light intensity for a good signal-to-noise ratio and a time resolution of several 100 kHz. The array of observation points is flexible and was oriented in the poloidal and toroidal direction at the low field and high-field sides of the plasma boundary. Correlation functions, auto and cross power spectra and coherence functions were calculated with up to 32,000 samples per channel. As the light emission depends on density and electron temperature, this diagnostic is only able to provide general information on the fluctuations, such as correlation lengths, frequency range, propagation velocity, poloidal distribution. Since this method excludes radial resolution, the emission of the Li-beam (see Sect. 1.6.2) penetrating in the radial direction was analyzed by the same methods.

It was found that the fluctuations are well correlated along the magnetic field. The correlation length in perpendicular direction is of the order of 1 cm in ohmic discharges. The fluctuations are localized outside the separatrix and originate at the low-field side of the torus (see Fig. 23).

1.3.5 Transport analysis of injection-heated plasmas

At present, reliable instability-based electron heat diffusivities χ_e are not available for tokamaks with ohmic and auxiliary heating, so that preference is given to empirical scalings determined by means of transport modelling of many series of discharges. The flux-surface-averaged χ_e exhibits a scaling in injection-heated plasmas as $\chi_e^I \simeq B_p^{-1}$, which greatly differs from that with ohmic heating as $\chi_e^{OH} \simeq n_e^{-1} T_e^{-1} B_p$, where B_p is the poloidal magnetic field. It was demonstrated that the ohmic transport scaling is not a universal plasma quality which is independent of the heating method. The electron heat diffusivity is investigated by transport simulations of a power scan of the injection heating and of the time evolution of L-discharges.

The confinement in the intermediate range between OH and L scaling is studied by simulating a series of discharges at $\bar{n}_e = 2.5 \times 10^{13}$ cm^{-3}, $I_p = 380$ kA, $Z_{eff} = 1.5$ and $P_{OH} = 0.52$ MW with various absorbed beam powers P_{abs}. At small powers equal to 0.3 and 0.6 MW the χ_e values clearly exceed the ohmic result in the middle of the confinement zone at $r = 2a/3$ in agreement with the observed decrease of the global energy confinement time τ_E. Special attention is paid to the local ratio of the beam

Fig. 23: Light signals from 8 observation points separated 7.5 mm in the poloidal direction. Left: part of signals recorded during a stationary ohmic phase. Right: correlation functions with channel No. 1 computed from these signals.

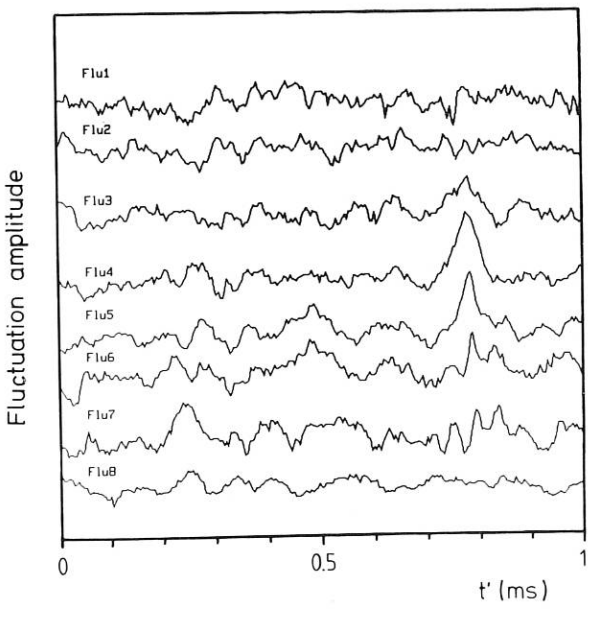

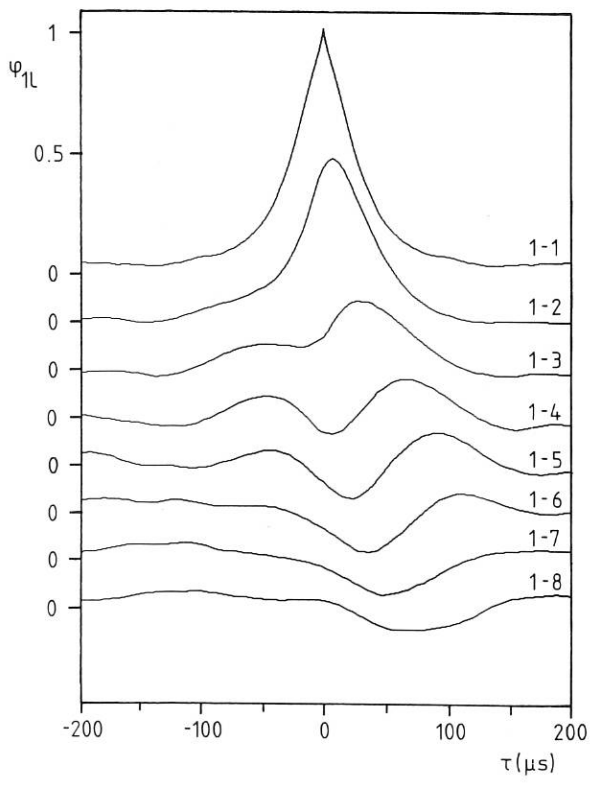

power density P_b and the ohmic power density ηj_t^2. Results for various absorbed beam powers are shown in Fig. 24. It is obvious that $P_b/(\eta j_t^2) \approx 0.3$, where the influence of beam heating should become important, is already exceeded with $P_{abs} \approx 0.3$ MW. As mentioned, the corresponding χ_e and τ_E values are indeed found to deviate from the ohmic scaling. With P_{abs} = 0.6 and 0.9 MW, neutral injection becomes dominant in the confinement zone. This explains the observed fast transition of τ_E to the L scaling. For $P_{abs} \gtrsim 1.2$ MW the beam power density is large compared with ηj_t^2, which agrees with the essentially pure L confinement found. The power scan shows that the transition to the L regime correlates with the ratio $P_b/(\eta j_t^2)$. Both the deviation from the ohmic scaling and the approach to the L confinement occur at power density ratios which agree with the expected values. The change in confinement suggests that the χ_e scaling responds to the auxiliary heating. The fact that the coupling between the ohmic heating profile and $T_e(r)$ is broken up with neutral injection should play an important role. As the smallest injection power scarcely modifies the plasma parameters, such as density and temperature gradients and poloidal beta, a transition to other instabilities and/or saturation effects is unlikely.

A characteristic time development of the χ_e in L discharges was found by means of transport simulations. It was shown that the L phase persists for about 100 ms after the end of injection. As the slowing-down time of the fast beam ions is only about 10 ms, the injection power rapidly decays. It is thus concluded that the L transport does not require the presence of injection heating, beam fuelling and direct ion heating. Simulations of many L discharges revealed that the phase with the ion-electron energy transfer rate $P_{ie}>0$ also lasts for a time span of about 100 ms. Only close to the end of the L phase is the ratio $P_{ie}/(\eta j_t^2)$ found to be so small that the scaling becomes almost purely ohmic. It is concluded that deviations from the ohmic scaling occur if the non-ohmic electron heating (due to neutral injection or ion-electron energy transfer) locally exceeds the ohmic power density.

The steady-state electron and ion energy equations and measured T_e profile shapes are used to derive constraints on χ_e. In the stationary ohmic and neutral-beam-heated phases characteristic shapes of $T_e(r)$ are observed. Gaussian shapes are found during the ohmic phase, while triangular shapes are present during the injection period in the confinement zone $r_{q=1} \leq r \leq 0.9$ a. If the ion heat conduction is neglected , the steady-state electron and ion energy equations yield

$$1/r\ d/dr(rn\chi_e\ dT_e/dr)+\eta jt^2+P_b \approx 0 \qquad (1)$$

with $\eta j_t^2 = E_t j_t$. The power density of the neutral injection system can be approximated by $P_b(r)=\alpha_b/r$ with $\alpha_b = P_{abs}/(4\pi^2 R_0 a)$ and major radius R_0. After integration it follows that

$$\chi_e(r) = c/4\pi\ E_t\ B_p(r) + \alpha_b\ \times$$
$$n(r)^{-1}\,|dT_e/dr|^{-1}. \qquad (2)$$

With $P_b=0$ and $T_e(r)=T_e(0)\ \exp(-\alpha r^2/a^2)$ one obtains the constraint

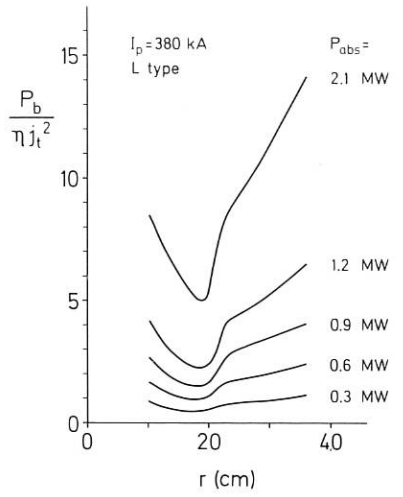

Fig. 24: Ratio of the beam and ohmic power densities versus radius from simulations of a power scan.

$$\chi_e^{OH}(r)=c/8\pi\ a^2/\alpha\ E_t\ B_p(r)/(rn(r)T_e(r)). \qquad (3)$$

Large injection power and $T_e(r) \approx T_e(0)(1-r/a)$ yield the constraint

$$\chi_e^{L}(r) \approx a\ \alpha_b\ T_e(0)^{-1}\ n(r)^{-1}. \qquad (4)$$

Comparing the constraints shows that the χ_e scalings depend on the heating method and its variation with the plasma parameters. Neutral injection does not introduce a $B_p(r)$ dependence in contrast to ηj_t^2. Owing to $j_t(r) \sim T_e(r)^{3/2}$ the ohmic heating and electron temperature profiles are strongly coupled, whereas $P_b(r)$ depends on the target density and injection energy. It is obvious from eq. (2) that the transport in the intermediate range cannot simply be represented by superposing the ohmic and L scalings, but that rather complex, mixed χ_e scalings occur because beam heating and ohmic contribution mutually affect each other.

1.4 Beta Limit

1.4.1 Observations

Owing to the good confinement in the H-mode of ASDEX, neutral-beam-heated discharges allow the β limits to be tested over a large range of magnetic fields ($1.2<B_t<2.7$ T) and plasma currents ($0.2<I_p<0.48$ MA) with the modest beam powers of up to 4.5 MW available. A clear "operational" beta limit at $\beta_C = 2.8\ I_p/(aB_t)$ (%, MA, m, T) is observed in agreement with theoretical predictions (see Annual Reports 1984 and 1985).

In the L-mode even combined neutral beam and ion cyclotron resonance heating with powers of up to 5 MW allowed values of $\beta_{max} \lesssim 0.85\ \beta_C$ - possibly as a result of the limited heating time. H discharges with a maximum beta value β_{max} below $0.75\ \beta_C$ display a nearly constant time behaviour of beta after reaching β_{max}. Their normalized beta β/β_C is

found to be proportional to the normalized heating power $P_N=3P/(bR_oB_t)$ (MW, m, T), where P is the total heating power (absorbed beam plus ohmic heating power), 2b is the vertical plasma diameter (b/a≈1) and R_o is the toroidal major radius. The resulting energy replacement time τ_E^* depends only on the plasma current. Various combinations of P, I_p, and B_t produce no gradual reduction of confinement when β is increased, but a "hard β saturation limit" when β_C is approached. Such a hard saturation is also seen in the time evolution of discharges with $\beta_{max}>0.8\ \beta_C$, which also exhibit only a small confinement deterioration before β_{max}. After attainment of β_{max} the beta values of these discharges decay to about 0.7 β_C and often reach a new stationary state at this level (see Annual Report 1985). This saturation near the β_C limit without disruption is a peculiarity of ASDEX discharges. Disruptions may occur, however, both during the rise and the fall of beta, especially at values of the cylindrical q_a near or below three.

The β decrease after transiently reaching β_C happens on a time scale of about 30 to 50 ms. An explanation for this behaviour consisted in a reduction of the ballooning mode limited beta due to broadening of the toroidal current density profile with time. In fact, integration of the ideal ballooning mode equation in the approximation for circular, concentric magnetic surfaces:

$$\alpha_M = -\frac{2\mu_o R_o q^{*2}}{B_t^2}\left(\frac{dp}{dr}\right)_M = \alpha(s) \qquad (1)$$

(where (s) is a known function of the shear $s=(r/q^*)dq^*/dr$, p is the total pressure, $q^*=5B_tr^2/(2\pi R_o\int j_t r\,dr)$ (T, m, MA), and j_t is the toroidal plasma current density) over the whole cross-section yields a maximum attainable value of $\beta q_a^*/\varepsilon$ increasing with q_a^*/q_o or the internal inductance l_i (see Fig. 25) but depending only weakly on the finer details of the current density distribution (here $\varepsilon=a/R_o$). Indeed during the high-beta phase, an increase of q_o is indicated by the disappearance of sawteeth, and an l_i decrease can be deduced from magnetic measurements, although the characteristic time for current diffusion due to neoclassical resistivity significantly exceeds the time scale of the β changes.

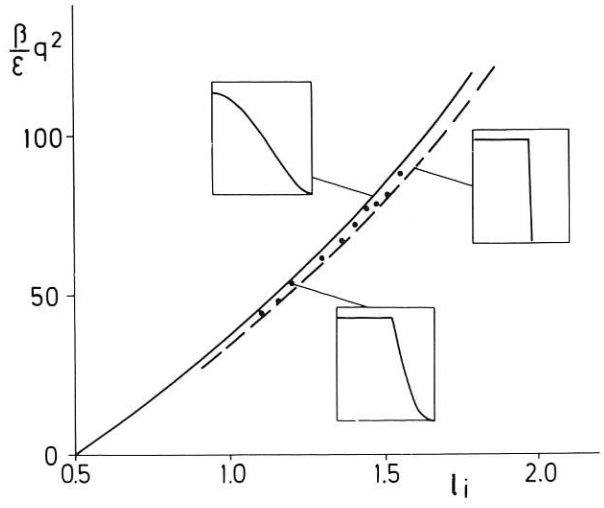

Fig. 25: Dependence of ballooning-mode-limited $<\beta_T>$ on the internal inductance l_i for different current distributions from the α(s) criterion (eq. 1).

There are two possibilities for reducing this apparent discrepancy of time scales. First, the instability which causes the β limit might also give rise to an anomalously fast current flattening. Measurements suggest an additional, more classical explanation. In H mode discharges with improved energy and particle confinement a central accumulation of metal impurities takes place leading to strongly peaked radiation power densities p_r. Although the central p_r values become comparable to the local beam heating of the electrons, the globally radiated power rises at most by about 25 % and always remains less than one third of the total heating power. This implies that radiation itself is not responsible for the beta limitation. But central Z_{eff} values of above 4 are easily deduced if iron is assumed to cause the central radiation losses. This increase in Z_{eff} at r < 15 cm can explain an enhanced and accelerated broadening of j_t: TRANSP calculations in this case predict during the β decay of the $D^0 \rightarrow D^+$ discharge an increase of 1.1 to 1.4 (rather than to only 1.2, as would result for a fixed $Z_{eff}(r,t)=1.5$) and an l_i decrease from 1.2 to 1.04.

In summary, the β time behaviour is consistent with the conjecture that the plasma stays at a marginal stability limit governed by the broadening current density profiles.

1.4.2 Transport analysis

On the basis of measured plasma profiles, plasma transport properties were investigated by means of the TRANSP analysis code of PPPL[1] and of a modified version of the BALDUR predictive transport code[2]. The pressure and current profiles obtained from transport computations were then used to calculate consistent MHD equilibria, which were in turn subjected to stability analysis by the 3D CART code[3] and by an exact solution of the ballooning mode equation. By comparison with measured Mirnov and soft XR signals we then tried to identify the instabilities responsible for the β limit.

Beam-heated H-mode discharges staying well below β_C show energy replacement times comparable in magnitude to the ohmic ones with a rough scaling $\tau_E^*=0.1\ I_pA_i$ (s, MA, A_i=ion mass number) independent of the heating power. For these high confinement times and consequently high plasma

---

[1] Hawryluk, R., in Phys. of Plasmas Close to Thermonuclear Conditions, Vol. 1, Varenna (1979) (EUR-FU-BRU/XII/476/80).

[2] D.E. Post, C.E. Singer, A.M. McKenney, BALDUR: A One-dimensional Plasma Transport Code, PPPL Transport Group, TFTR Physics Group, Report 33 (1981).

[3] J.K. Lee, Nucl. Fusion 26 (1986) 955.

energies the convective losses $P_{conv}/P \approx 5/2k(T_e+T_i)/\langle E\rangle$ (with $\langle E\rangle$ being the medium energy of the injected neutrals) and the ion conduction losses become comparable to the electron conduction losses. The ion heat diffusivity χ_i is taken as 3 times the neoclassical value calculated by C. Chang and F. Hinton for all discharge phases (OH, L, H), which gives the best fit to the T_i measurements. For these discharges the ion heating by the beams, P_{bi}, exceeds the electron heating, P_{be} ($P_{bi} \leq 3P_{be}$) and the beam contributes up to 25 % to the total β during the rise phase.

In discharges coming close to β_C transport analyses confirm that additional energy losses set in just after β_{max} has been reached, which results in a strong degradation of the energy confinement times by a factor of up to two. These additional losses have to be attributed to enhanced electron heat conduction and partly to the convection associated with the density decrease. The radial profiles of the electron heat diffusivity χ_e are therefore found to be nearly time-independent in the H-mode during the β rise phase, but are increased over the whole plasma during the β decrease. Transport simulations by the predictive BALDUR code reproduce the measured evolution of the n_e, T_e and T_i profiles and of β_P up to the β limit if transport scalings derived from H-regime discharges well below β_C are applied: $\chi_e^H(r)=1.3\ a^2/(R_o r_n I_P)$ (m, s, MA), particle diffusivity $D^H(r)= 0.4 \times \chi_e^H(r)$ and anomalous pinch velocity $v_{in}^H(r)= -0.5 x D^H(r)\ r_{Te}^{-1}$ (m/s, m) (with $r_n=-n/(\partial n/\partial r)$ and $r_{Te}= -T_e/(\partial T_e/\partial r)$). After the attainment of β_{max} also here the electron heat diffusivity has to be enhanced by a factor of 4 to simulate the measurements.

1.4.3 Low-m-mode stability

Our investigations of low m MHD activity are based on results from Mirnov probe measurements and two-dimensional soft-XR tomography and on their comparison with stability calculations.

The measurements show that the observed modes always have a toroidal mode number n=1. During the L phase of beam-heated ASDEX discharges a "continuous" mode develops, whose amplitude decreases to a low level after the L to H transition. Both an m=1 (detected by soft XR) and an m=3 component (from Mirnov signals) are present at the same frequency in the range of 10 to 20 kHz (see Fig. 26). During the H phase ELM's occur and additionally MHD bursts with a "fishbone-like" character are observed. The fishbone amplitudes are much smaller than those of the continuous mode and exhibit an m=3 to 4 structure at lower β_P values ($\beta/\beta_C<0.6$) and an m≈6 structure near the β limits (from Mirnov signals). This poloidal mode number is above the value of q at the boundary of an equivalent circular discharge at finite β $q_a \approx q_a^*(1+\varepsilon^2(1+.5 x (\beta_P+l_i/2)^2))$, so that the resonant surfaces m=q should lie close to , but inside the separatrix. The frequency of the mode is observed to increase with heating power and β_P up to ≈25 kHz. Both the continuous and the fishbone-like mode show an amplitude ratio of up to 20 between the torus outside and inside and propagate with the central toroidal rotation velocity. Sometimes, during β decay, a strong m=2 to 3 mode with f=5-10 kHz develops (seen in soft XR and Mirnov coils, (see Fig. 26), being triggered by an ELM, which frequently leads to a disruption especially at low q values.

The low-m MHD activity observed seems to be mainly due to resistive modes. Linear results of CART calculations for the resistivity dependence of the growth rate predict a change from tearing to pressure driven mode scaling when β_p is increased from ~1 to ~2. In addition, we find external kink

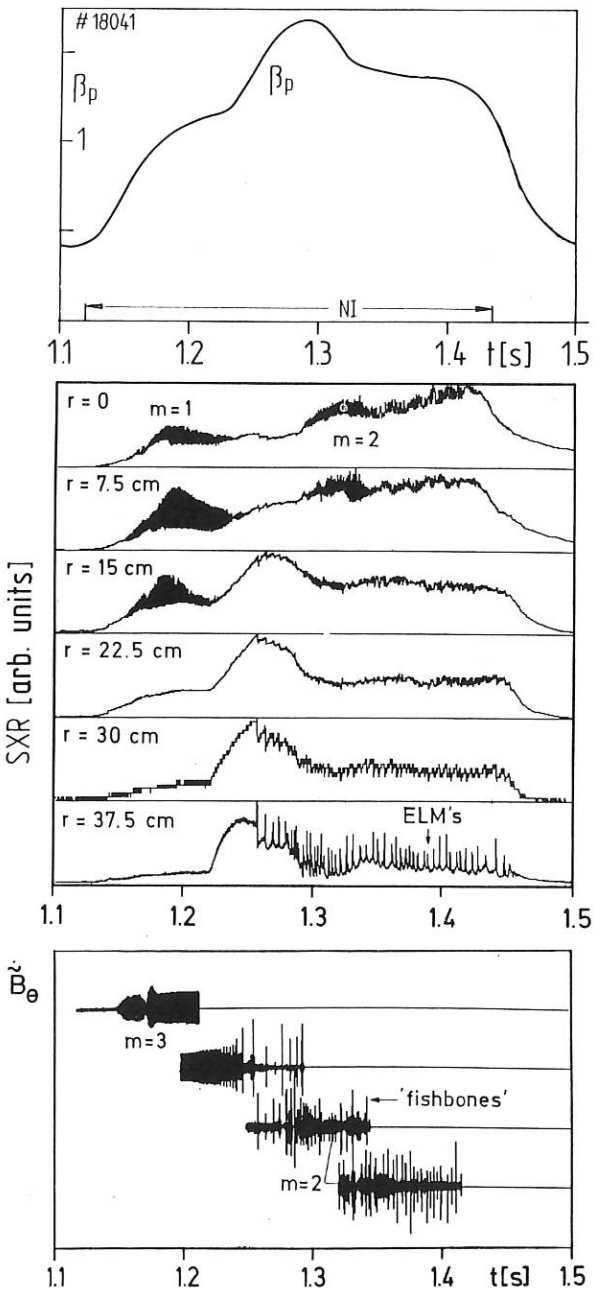

Fig. 26: Time behaviour of diamagnetic poloidal beta, line-averaged soft XR radiation at various tangential radii and Mirnov signals at the torus outside.

contributions to be negligible in all cases. CART results for the perturbed magnetic field are compared with Mirnov probe data. We find that amplitudes as well as phases agree very closely with measurements. Finally, the large poloidal mode number m≲6, as well as the observed poloidal inside-outside mode asymmetry, can be reproduced if one assumes a radially increasing vacuum resistivity.

However, no clear correlation between the observed n=1 mode activity and the β_C limit or the β decrease can be detected in the experiments. The strong m=2 to 3 mode sometimes observed during β decay does not seem to be a necessary prerequisite for it, but may be produced by the increase of q_o during the high-β phase. The contribution of this mode - if present - to the β decrease is hard to state.

1.4.4. Ballooning mode stability
(in collaboration with P. Zehrfeld (Theory Division 3))

A ballooning mode stability analysis of true ASDEX equilibria was done by solving the full ideal-MHD ballooning equation (see also Theory Division 3). The attainable marginal value for a given equilibrium configuration was obtained by modifying the local β_p until a marginal solution with a β_p value β_M was reached.

Besides the general evaluation of the ballooning equation we also performed a large-aspect-ratio expansion taking into account the correct differential displacement of the magnetic surfaces due to toroidal curvature. Except for the neighbourhood of the magnetic axis, we find the results of our large aspect ratio expansion in good agreement with those of the complete treatment. Both these refined approaches yield, however, p'/p'_M values about 20-30 % lower than given by the simple $\alpha=f(s)$ criterion when p' is in the vicinity of the marginal limit.

The time development of the ideal ballooning stability for a $D^o \rightarrow D^+$ discharge is illustrated in Fig. 27. At the time of maximum beta (≈1.26 s) the discharge reaches a normalized pressure gradient $p'/p'_M=0.8$ in the region $0.4<r/a<0.9$. This is also the region where the enhanced plasma losses start according to the TRANSP analysis. During the β decrease between 1.28 to 1.38 s, the $p'/p'_M=0.8$ region shrinks only slightly but for $0.20<r/a<0.85$ a region with p'/p'_M values between 0.7 and 0.85 remains. The pressure gradient decreases in fact, but so does p'_M owing to the broadening of the current density profile (the latter being calculated using classical resistivity and the increase in the central Z_{eff} described in Sect. 1.4.1). For discharges with $\beta_{max}<0.8\ \beta_C$ the p'/p'_M values remain significantly below unity.

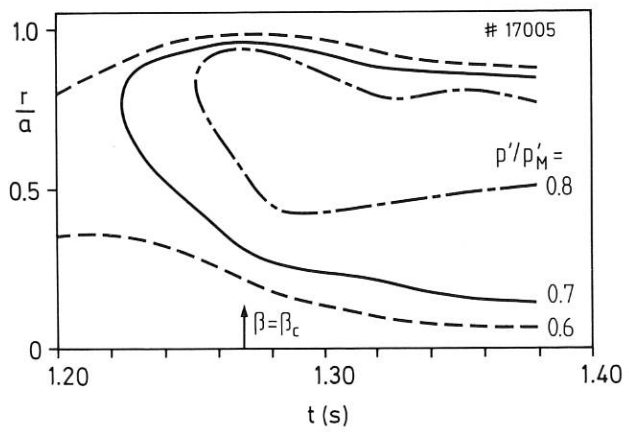

Fig. 27: Time evolution of pressure gradient p' profile normalized to the marginally stable one p'_M due to ideal ballooning modes for a $D^o \rightarrow D^+$ discharge.

In the ASDEX discharges close to the β limit the resistivity is very small but finite, so that, strictly speaking, the modes to be studied are resistive ballooning instabilities. The influence of these modes and resistive interchange modes on the β limit was investigated near the plasma axis ($r \lesssim 0.1a$)[4].

For r=0.1a and mode numbers $20<n<40$ that are not yet stabilized by the finite ion Larmor radius effects, the critical beta due to resistive ballooning modes is 25 to 40 % below the ideal MHD limit. We conclude that the β limit discharges are ideal ballooning stable but may be marginal with respect to resistive ballooning modes with high wave numbers. This would also explain the near-invariance of the p'/p'_M profiles during the β decrease.

1.5 Extension of the Operating Range

1.5.1 Density limit
(in collaboration with K. Büchl, R.S. Lang, W. Sandmann, (JET Diagnostic and Pellet Group)

After the results of 1985 had yielded a substantial increase of the density limit by pellet injection, attempts were made to optimize the method on the basis of improved knowledge of the underlying limiting mechanisms.

Pellet injection is able to generate strongly peaked density profiles even with pellet penetration to half the minor radius or less. This effect has been attributed to a change of the particle transport properties of the discharge, especially to an increase of the ratio of inward drift velocity to diffusion constant (see Sect. 1.2). Thermal edge losses increasing with edge density are normally responsible for the density limit. The maximum average density or peak density may be achieved if peaked profiles are produced by pellet injection and the absolute value of the density is increased by simultaneous gas puffing.

[4] D. Correa-Restrepo, Plasma Phys. and Contr. Fusion 27 (1985) 565.

Peaking of the density profiles, unfortunately, is accompanied by accumulation of impurities in the plasma centre. Central radiation often increases on a 100 ms time scale and finally causes disruptive termination of the discharge, thus representing another density-limiting mechanism. Optimized gas puffing is essential for controlling this effect. A further improvement is possible with wall carbonization. As metal radiation from the centre is of concern in ASDEX, the reduction of the metal content of the discharge even at the cost of a slightly increased carbon concentration is favourable.

Murakami parameters ($M=\bar{n}_e \cdot R/B_t$) of up to 9 were achieved both in ohmic discharges and with weak beam heating.

With strong neutral beam injection in the co-direction strong profile peaking was not yet possible and no improvement of the density limit could be achieved. First experiments with counter-injection were encouraging. Experiments with ICRH suffered from the technical problem of a sudden mismatch of the wave coupling properties with pellet injection. These experiments will be continued.

An increase of the density limit with only gas puffing was found at very low q-values (see next section).

1.5.2 q-limit

The operating limits in the low-q high-density corner of the Hugill diagram was carefully investigated for ohmic deuterium discharges with gettered divertor chambers. Previously a smooth drop of the density limit when approaching q=2 was experienced. Now it became clear that the drop starting with $q < 2.7$ indicates only a dip similar to that observed in other tokamaks close to q=3. At a q-value of 2.1 (defined as $a^2B_t/2IR$) the density limit jumps to a value higher than that at the first maximum at q=2.7. A Murakami parameter of 7.5 has been reached. The density limit decays again with decreasing q. It was possible to achieve q=1.88 at a Murakami parameter of above 6.

At q-values between 2.7 and 2.1 a stable m=2 mode develops during the discharge the amplitude of which increases with rising density until a disruption determines the density limit. At $q < 2.1$ the mode also develops initially but then disappears with rising density and appears again at much higher densities. The developments of the plasma current, density and m=2 mode for the two cases are shown in Fig. 28. The stability of the m=2 mode at the q=2 surface, which is located very close to the separatrix at these low q-values, is obviously directly affected by gas-puffing or by the edge density.

While disruptions are very hard when the q-limit is reached at low densities simply by ramping up the plasma current, it is rather soft at very high densities. At low densities a q-limit of 2.0 was previously found, i.e. a higher value than at high densities. It is not yet clear, however, whether this value is absolute or depends on edge plasma conditions, e.g. edge radiation.

Energy confinement of low-q high-density discharges corresponds to the values in the saturation regime (80 ms). It was possible to heat these discharges with high-power neutral injection and to reach the H-mode for short periods. These discharges are particularly attractive, not only because of the good parameters already achieved but also because of the obvious possibility to improve mode stability by simple external means to the extent of an increased operational range.

Figure 29 plots the operational boundary for high-density discharges (Hugill diagram) for pellet-refuelled and low-q discharges and compares it with these of ohmic, gettered and non-gettered plasmas.

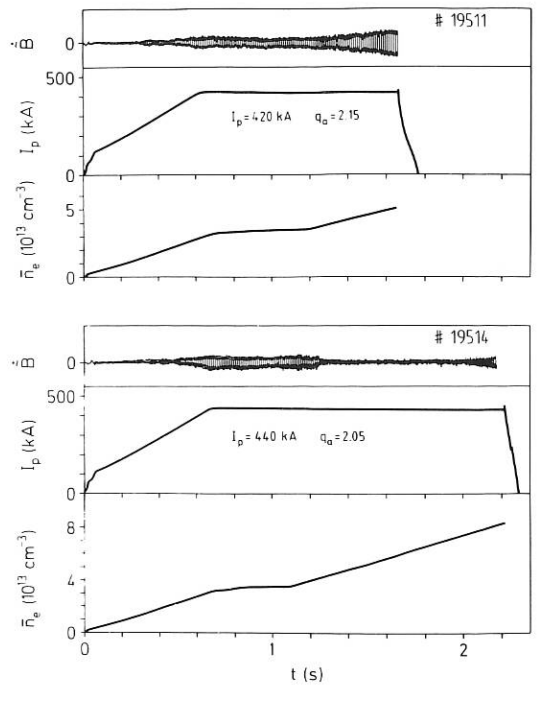

Fig. 28: Time evolution of the plasma current, the mean density and the MHD-activity during discharges at q_a = 2.15 (top) and 2.05.

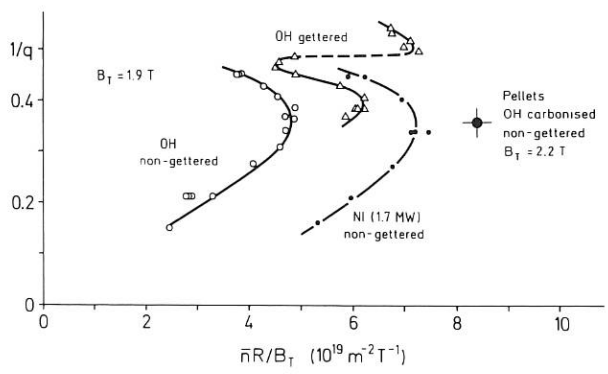

Fig. 29: Maximum achievable densities for different types of divertor discharges plotted in the Hugill-diagram.

1.5.3 Wall carbonization and its effects on plasma behaviour

The following summarizes the results obtained in experiments with carbonized walls, which are described in more detail in separate sections of this report. Most characteristic and significant was an order-of-magnitude reduction in Fe radiation. Global radiation, however, was much less reduced owing to a strong increase of C-radiation at the plasma boundary, but as the amount of central radiation was reduced (Fig. 30), the global energy confinement generally improved. The most dramatic gain resulted for ICRH, which had been much impeded by a strong increase of central Fe radiation with uncarbonized walls. Instead of 1 MW the full power of 2.4 MW could now be launched without disruptions. Even the attainment of the H-regime with ICRH could now be demonstrated.

The power limits for reaching the H-regime with NI were hardly affected, but the quality of the H-regime appeared somewhat degraded and also the maximum β_{pol} was not as high. The differences seem to be linked to the increased boundary radiation of C. Also LH heating has profited from carbonization, extending the working range to $n_e = 5 \times 10^{19}$ m^{-3}. Previously, the strong influx of Fe caused by generated fast ions had led to disruptions at $n_e = 3.5 \times 10^{19}$ m^{-3}. Pellet injection now leads to extremely high central densities of 2.2×10^{20} m^{-3} since the reduced influx of Fe eliminated the thermal collapse observed without carbonization. This was accompanied by unusually long energy and particle confinement times with the Murakami parameter increased from 6 to 8.5 for q=2.7.

The carbonization was achieved by adding about 20 % CH_4 to the standard conditioning DC glow discharge in H_2 or D_2. In contrast to the procedures in TEXTOR and JET, which work at elevated (> 150°) wall temperatures, carbonization in ASDEX was executed at room temperature without any obvious disadvantage. Figure 31 depicts the behaviour of the partial pressures of D_2, H_2, HD and CH_4 when the discharge is switched on and off. Strong

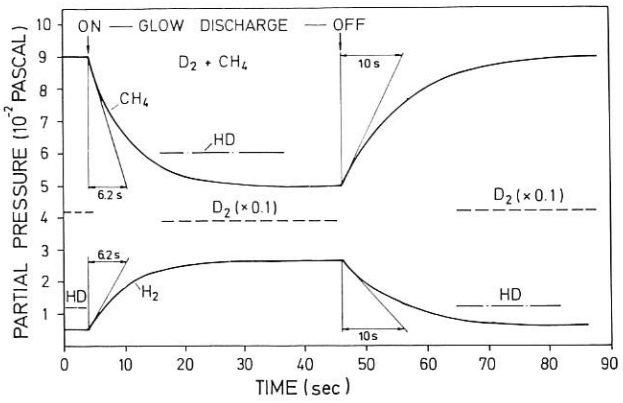

Fig. 31: Change of partial pressures in a mixture of D_2 and CH_4 when the carbonizing glow discharge is switched on.

cracking of CH_4 with concomitant production of H_2 is clearly seen. From the time constants in Fig. 31 a cracking rate of 3.5×10^{19} CH_4 molecules/s is derived, while the discharge current to the walls of 2A corresponds to only 1.2×10^{19} ions/s. Time-of-flight spectroscopy shows mostly CH_4^+, which is consistent with the observed carbon deposition rates. The discrepancy between cracking rate and current is explained by the observed formation of higher gaseous hydrocarbons. These typical discharge conditions with a cathode fall potential of about 300 V are known to lead to deposition of amorphous a-C:H layers. Owing to geometric effects, however, the deposition was not homogeneous and varied between 500 and 1500 Å, as judged from the interference colours. Decarbonization with pure H_2 in the same type of discharge took several days. The use of a mixture of He and O_2 reduced this time to several hours but led to less favourable conditions for the following plasma discharges.

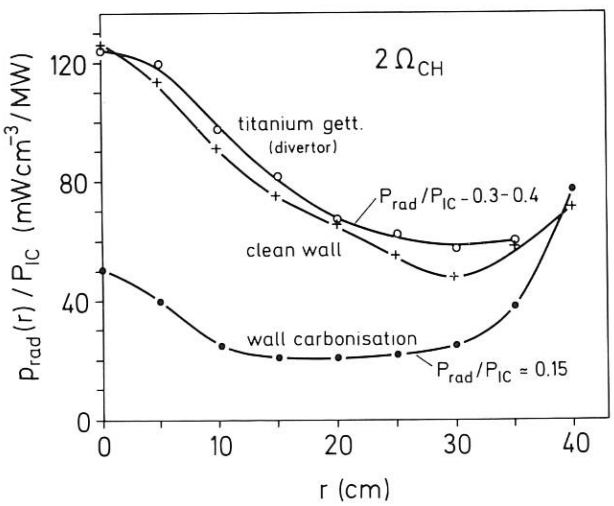

Fig. 30: Total radiation profiles before and after carbonization.

1.6 Scrape-off Layer and Divertor Plasma Studies and Plasma Wall Interaction

1.6.1 Exact location of the separatrix

The proper location of the separatrix is one of the crucial questions in the discussion of plasma edge measurements and their application to scrape-off models. The difficulty in determining the position is due to the fact that most parameters, such as n_e and T_e, do not show a discontinuity or any abrupt change at the separatrix.

So far the position of the separatrix has been determined only in an indirect way by using the magnetic probe measurements outside the scrape-off region as input data to an equilibrium code. The separatrix position calculated in this way is estimated to be correct within ± 1 cm in the equatorial plane.

In 1986 efforts were made to get further independent information from measurements based on a

completely different method. The principle of these measurements is related to the extremely low collisionality of runaway electrons. When diffusing out of the bulk region, these particles are rapidly lost after passing through the separatrix. Thus, their density should exhibit a step-like discontinuity at the separatrix. In order to keep the shift of the runaway electron drift separatrix below 0.15 cm, only low-energy electrons (E<100 keV, so-called slide-aways) can be used. We have consequently attempted to produce slideaway electrons in the range 20 keV $\lesssim$E $\lesssim$50 keV by applying LH heating to low-density discharges. An X-ray detector measures the X-ray flux being produced by the Mo tip of a Langmuir probe, which can be shot into the outer plasma region by a fast driving mechanism.

A typical measurement is shown in Fig. 32. The probe is injected twice during a low density discharge ($\bar{n}_e = 1.4\times10^{13}$ cm^{-3}) with additional LH-heating (500 kW). Only at the second time, when the slideaway density is strongly enhanced by LH heating, is a sharp X-ray emission peak observed. In Fig. 33 the peak intensity is shown as a function of the maximum penetration depth of the probe, with d being the distance with respect to the calculated separatrix position. According to these preliminary measurements the magnetic separatrix would be inferred about 0.7 cm further out. The uncertainty is approximately $\pm$ 0.5 cm, which is larger than expected. One cause of this relatively large uncertainty are fluctuations in the background intensity (Fig. 32). In addition, however, high-energy runaways may also contribute to the broadening of the intensity step function on account of low-energy bremsstrahlung and stray light.

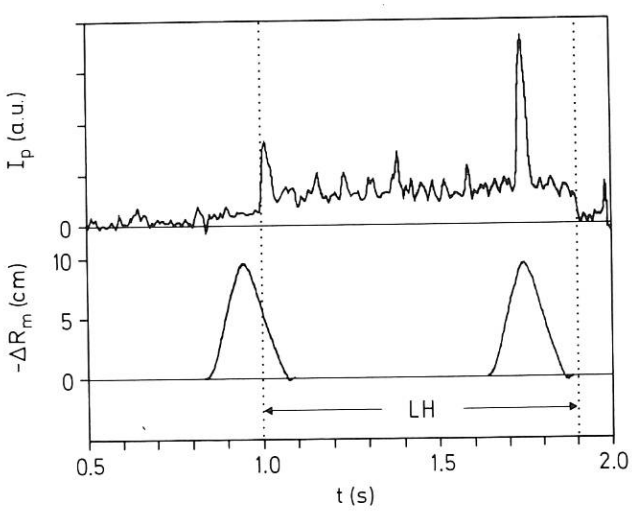

Fig. 32: Probe shift (bottom) and X-ray response (top) as a function of time for two probe strokes; the first stroke occurs prior to LH heating the second during this period.

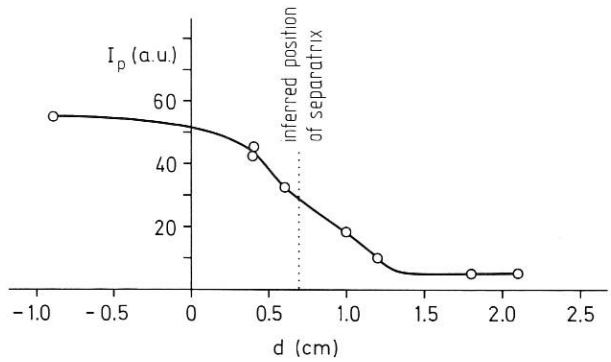

Fig. 33: X-ray peak intensity vs. probe distance d, with d being determined from magnetic measurements.

1.6.2 Parametric description of the scrape-off layer density profile

Systematic investigations of the scrape-off layer (SOL) density profile in the outer midplane of stationary, double-null, diverted, ohmic discharges fuelled by gas puffing have revealed a scaling for the density n_s at the separatrix and for the exponential density decay length λ_n of the SOL within two cm of the separatrix.

For $\bar{n}_e \geq 1.5\times10^{13}$ cm^{-3}, λ_n is found to depend only on the cylindrical safety factor q as $\lambda_{ni}=k_i q^{\alpha i}$ (i=H, D, He), in the fashion illustrated in Fig. 34, where variations in $\bar{n}_e$~1.4-4.7x10^{13} cm^{-3}, I_P~200-450 kA and B_T~16-23 kG are encompassed. No explicit dependence on any of these quantities nor on the ohmic power input P_{OH} is observed. To place the above scaling in context, note that a value α=0.5 corresponds to the change expected in λ_n purely as a consequence of the varying midplane-divertor plate distance L (proportional to q), given that λ_n can be described by $\lambda_n=(D_\perp L/v_\parallel)^{0.5}$, $D_\perp$ being the perpendicular diffusion coefficient and $v_\parallel$ the global streaming velocity along field lines in the SOL. Below $\bar{n}_e$~1.5x10^{13} cm^{-3}, λ_n increases, reaching values greater than 3 cm at, for example, $\bar{n}_e$~0.5x10^{13} cm^{-3}.

n_s appears to be principally a function of $\bar{n}_e$, as n_s~0.29 $\bar{n}_e$. Again, no significant dependence on I_P, B_T or P_{OH} is evident. For example, with respect to Fig. 34, there is absolutely no variation in n_s for shot #14919 (H_2), about $\pm$5 % in #14548 and $\pm$2 % for #14550 (both D_2) over the q-range indicated. P_{OH} at q=3 for #14548 is about 30 % higher than for #14550 (~330 vs 250 kW) leading to only a 6 % increase in $n_s/\bar{n}_e$. Even for non-stationary phases of a discharge, n_s remains proportional to $\bar{n}_e$ to within ~$\pm$10 %. However, successful deep refuelling by pellets radically changes this behaviour, generally clamping n_s to its pre-pellet-injection value (see Sect. 1.2). Finally, it should be pointed out that statements about n_s are inherently a function of the exact position of the separatrix, which at present is only deduced from magnetic signals. In addition, the exact constant of proportionality between n_s and $\bar{n}_e$ may yet undergo slight revision as more statistics are compiled.

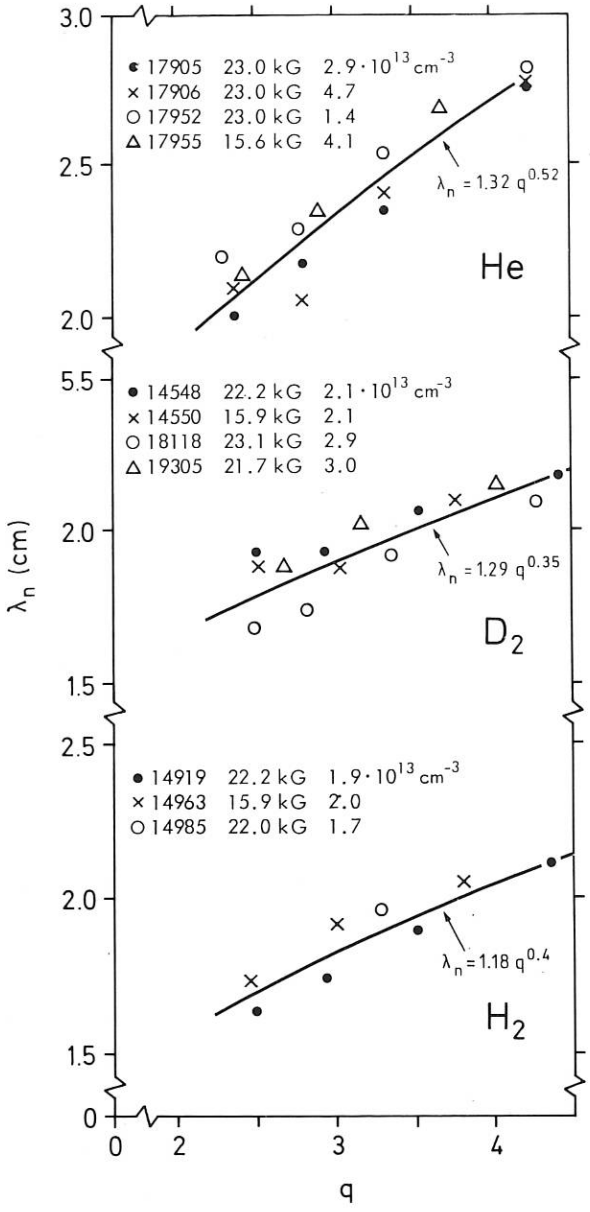

Fig. 34: Dependence of λ_n on q for the filling gases He, D_2, H_2 under stationary conditions. The solid lines give an approximate fit to the points. The shot number, toroidal field and line density are indicated for each point. For each set of conditions, the q-scan was realized by stepping I_p during a single discharge.

1.6.3 Langmuir probe measurements in ASDEX divertor plasma
(in collaboration with N. Tsois, Democritos, Athens)

The plasma parameters in the upper outer divertor of ASDEX were studied by means of a fast moving Langmuir probe system. A triple-probe arrangement was mainly used so that radial profiles of electron temperature, T_e, ion saturation current, I_i^{sat}, and floating potential, V_{fl}, were obtained. Two fast sweeping movements with a speed of 1 m/s and 10 cm amplitude were possible during each shot. This allows up to four radial profiles to be obtained at the desirable time intervals. Since triple probe operation is very sensitive to differences of the plasma parameters seen by the three tips, we chose an optimum inclination of the probe arm for which all tips are as close as possible to the same flux surface.

The divertor Langmuir probe system was able to work in all operation regimes of ASDEX (OH, NI, LH, ICRH, NI+ICRH, NI+LH) and some new features were obtained.

Strong positive charging of the divertor plasma and high radial gradients were observed at low densities ($n_e \lesssim 2 \times 10^{13}$ cm^{-3}), suggesting a local non-ambipolar transport to divertor plates.

Very close (4-7 mm) to the calculated position of the separatrix a narrow negative dip in the floating potential profile developed, being very likely due to a group of nearly collisionless fast electrons originating from the main plasma edge. Important amounts of energy can be deposited in a narrow region of divertor plates by this group of electrons. This fact could explain the discrepancy in half-width of power loading profiles calculated from probe data (without fast electrons) and measured thermographically.

During RF heating (LH and ICRH) the SOL plasma parameters are strongly affected. The disturbance extends to the divertor chamber and is easily measured there. Specific structures with high gradients in the floating potential and density profiles have been observed. Their origin and implications are not yet well understood.

1.6.4 Impurity production during auxiliary heating
(in collaboration with J. Roth, G. Staudenmaier, E. Taglauer, H. Verbeek (Surface Physics Division))

The main impurity source in ohmic discharges is CX neutral sputtering at the walls of the main plasma chamber, as was previously shown (see Annual Report 1985). During auxiliary heating by NI or ICRH increased impurity concentrations of Fe in the main plasma are observed, which are especially large during ICRH heating. The investigations of the plasma-wall interaction group focused in 1986 on the question whether additional sources of impurities have to be considered in these cases. We measured neutral particle fluxes using the low energy neutral particle analyzer (LENA) and carbon resistance probes (CRP), and the Fe fluxes, which reach the divertor target plates by the divertor collector probe. These diagnostic methods differ in some fundamental respects: The time resolution during an ASDEX shot is good for the LENA, moderate for the collector probe, and is restricted to a whole shot for the CRP. LENA delivers energy distributions of the neutral flux in the range of 20-2000 eV (for D^0), while the CRP determines neutral fluxes and their mean energy. With the energy-dependent sputtering yields known, it is

possible to calculate impurity fluxes from the walls. The divertor collector probe directly measures the Fe divertor fluxes, which, in steady state, can be directly related to the Fe concentrations in the bulk plasma. The LENA only sees a small solid-angle interval and its results are therefore highly specific to the particular toroidal and poloidal location, while the CRP sees the whole 2π solid angle and is more representative of the tokamak as a whole. The divertor collection probe sees a small part of the entire divertor plate surface, and toroidal and poloidal symmetry of the scrape-off-layer has to be assumed.

The combination of these three plasma-wall diagnostics together with the results of other boundary diagnostics (Langmuir probes, Li-beam) delivers a fairly consistent picture of the impurity production at the walls during auxiliary heating.

An increase of the neutral flux to the walls is observed with all auxiliary heating modes . In Fig. 35 results from the LENA show the increase of the neutral flux, its mean energy and the corresponding increase of the Fe production due to CX sputtering at the walls during 2.6 MW NI heating. In Fig. 36 the Fe flux from the walls, calculated from the neutral fluxes measured with CRP and LENA and the Fe fluxes directly measured by the divertor probe

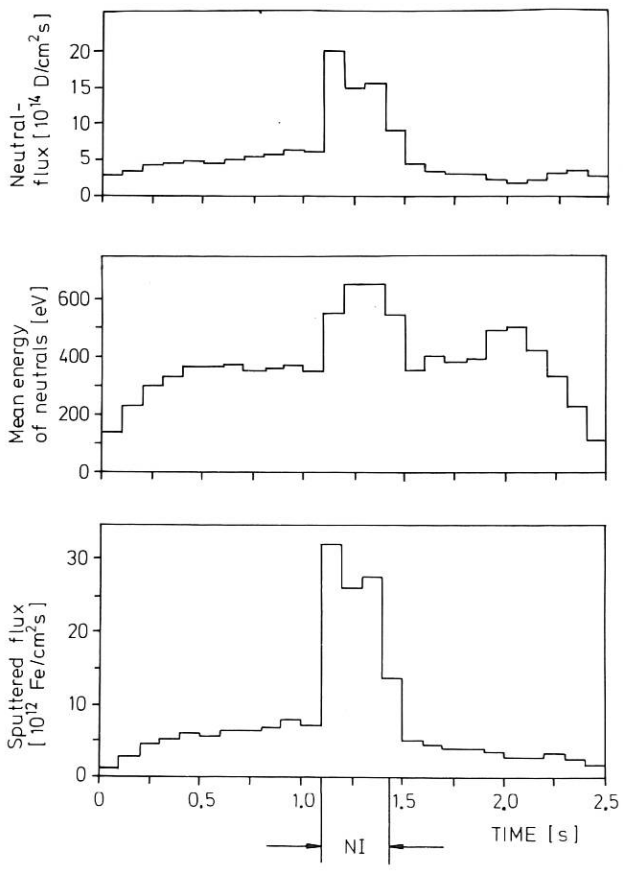

Fig. 35: Neutral particle flux, its mean energy, and the Fe influx due to sputtering by the neutrals during an ASDEX shot with 2.5 MW NI heating.

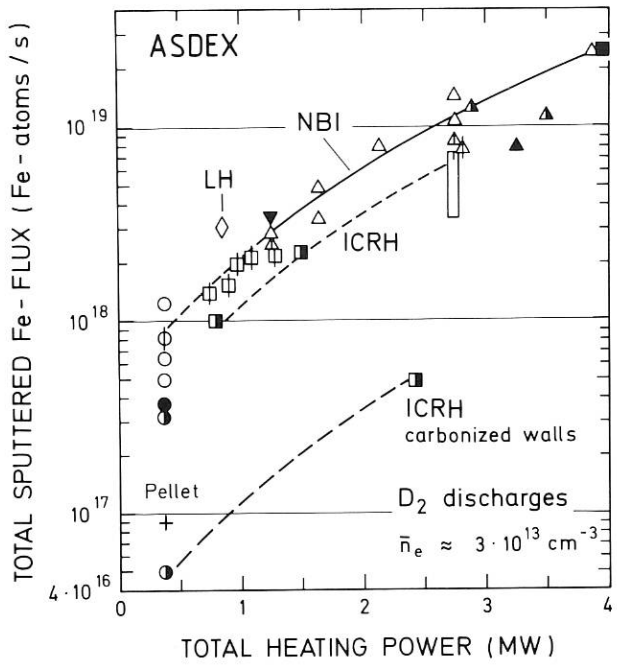

Fig. 36: Total Fe fluxes generated at the wall as evaluated from various diagnostics:
CRP (o OH, Δ NBI, □ ICRH, ◇ LH, + Pellet)
LENA (ϕ OH, ⍋ NBI, ⊕ ICRH)
Divertor probe (◑ OH, ▲ NBI, ◨ ICRH)
Spectroscopy (● OH, △ NBI, ■ NBI+ICRH)
NPA (▼ NBI)

are plotted versus the total heating power. In the case of OH and NI heating good agreement is found between the results of the 3 diagnostics and the data evaluated from spectroscopic measurements. During ICRH it is observed that the Fe flux produced increases approximately by the same amount as during NI heating. This is in contrast to the dramatic increase of the Fe content in the bulk plasma as observed spectroscopically for non-carbonized walls, while for carbonized walls the increase of sputtered and collected fluxes is equivalent to the spectroscopic density measurements. The question whether the dramatic increase for non-carbonized walls is caused by some additional source of impurities which is not seen by LENA and CRP - sputtering by fast ions for instance - must be denied since the divertor probe does not see a large increase of the Fe flux as compared with NI heating.
Therefore, only a drastic change of the plasma parameter in the boundary during ICRH or improved particle confinement as discussed in Sect. 1.8.3 can account for the large Fe increase in the bulk, rather than additional sources.

1.6.5 Deuterium and metal deposition on the divertor channels

(in collaboration with R. Behrisch , J. Roth, M. N. Wang (Surface Physics Division))

The stainless steel-plates of the divertor slits were partly covered with carbon ribs for the last year of operation before shutdown in April 1986. The surface layer composition of the carbon ribs was investigated by accelerator analysis. Besides deuterium, the major impurities found were Fe, Ni, Cr, O, Ti, Cu, K, Ca, Cl, S and Zn. All materials are nearly uniformly distributed in the toroidal direction, but definite variations in the poloidal direction are found. The deuterium and the metal deposition on the inside ribs are larger at the top than at the bottom, on the outside ribs the opposite is the case.

Measured deposits: The amount of deuterium found on the carbon ribs is about $3 \times 10^{17}/cm^2$ with toroidal and poloidal variations smaller than a factor of two (see Fig. 37).

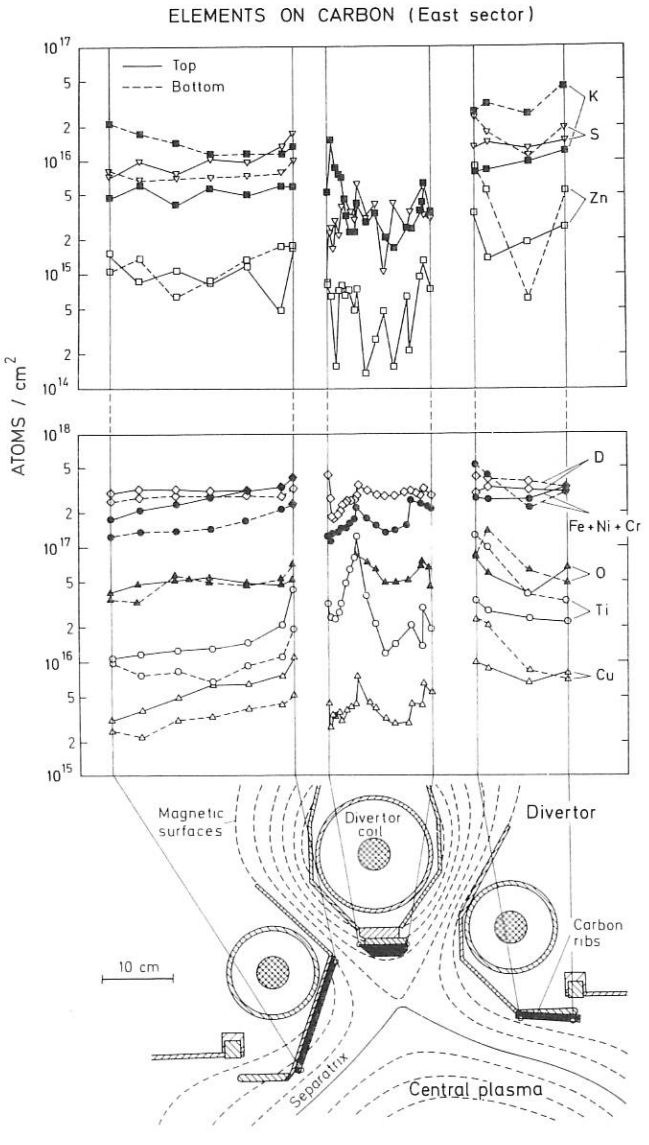

Fig. 37: Impurity deposition onto carbon ribs.

The amount of deposited Fe+Cr+Ni is 1 to $5 \times 10^{17}/cm^2$ corresponding to an equivalent of 50 to 200 monolayers. The relative concentrations of Fe:Cr:Ni were found to be 69:21:10 on the inside ribs and 68:22:10 on the outside ribs. They are very constant along the toroidal direction and nearly equal to the concentrations in the wall material except for a systematic enhancement in Cr of 4 to 5 %.

There are relatively large depositions of Ti and Cu, and the ratio of Ti:Cu is between 3 and 8 but mostly around 4. The metal deposition increases toward the divertor entrance and peaks are observed at all edges of the central tiles.

The amount of the additional elements found correspond to about one to 20 monolayers. The deposition of K, Ca and Cl are very similar, their concentrations at the bottom are a factor of about 2 to 5 larger than those on the top tiles.

Interpretation: The very uniform toroidal distribution of nearly all elements found on the carbon ribs shows the good toroidal symmetry of the ASDEX divertor experiment.

The amount of trapped deuterium being 2 to 3 $10^{17}/cm^2$ can be attributed to implantation into carbon at a deuterium temperature of 200 to 300 eV if the fluences are of the order of 10^{19} to $10^{20}/cm^2$. The fluxes of CX neutral particles are of this order of magnitude and can represent the major source for the collected deuterium. For implantation with ions, the distribution of the deuterium is expected to be less uniform. There is no major carbon deposition expected which would exclude a large contribution of deuterium trapping by codeposition with carbon.

The large amount of Fe+Ni+Cr corresponding to about 100 monolayers on the carbon ribs shows that the surface composition is dominated by deposition. The slightly larger Cr concentration than in the steel of the vessel can be explained by Cr segregation and preferential Cr erosion probably caused by sputtering at the vessel walls. Local heating as occurring in erosion by electrical arcs can further increase the Cr erosion.

The Ti and Cu deposition on the carbon ribs must originate from the divertor plates: the ratio of Ti:Cu of 3 to 8 represents about the fraction of the divertor plates covered initially with Ti and Cu, mulitiplied by the sputtering yields. Cu is found in equal amounts also on the carbon ribs from the top divertor entrance, while it was initially present only on the bottom divertor plates. This is in agreement with the conclusions of the spectroscopic and probe measurements on the large impurity transport in the scrape-off layer (see Annual Report 1985).

The increase of the deposition on the carbon ribs toward the divertor entrance and at edges indicates that a fraction of the impurities leaving the divertor plates is directly deposited on the sides of the slits.

Finally, the K, Ca and Cl (only K is shown in the figure) found on the vessel walls may probably be the residue from dust particles originating from clothes worn in the torus. This is confirmed by the

fact that these elements are more abundant at the bottom than at the top. Zn and S found on the carbon ribs may originate from inherent impurities in the carbon used.

1.6.6 Simulations of the 2D hydrogen flow pattern in the scrape-off layer (J. Neuhauser, R. Wunderlich (Theory 3))

The hydrogen flow pattern in the divertor scrape-off layer strongly depends on the hydrogen recycling near the divertor target. A Monte Carlo description of neutrals is therefore desirable, but requires excessive computer time.

As an intermediate step, a simple but quite realistic recycling model was added to the 2D hydrodynamic edge code of B. Braams. The basic assumption is that neutrals only move along coordinate lines in the poloidal plane, this being equivalent to decomposition of an oblique particle trajectory into a movement along a flux surface and a subsequent step across it. Fast and slow particles (atoms and molecules) are considered and various recycling conditions at the target and chamber walls can be prescribed. The resulting recycling pattern is surprisingly similar to that obtained with a full Monte Carlo code.

When applied to typical ASDEX high-recycling divertor conditions, a quite complicated flow pattern is obtained: Close to the separatrix, the plasma flows forward into the divertor, because of plasma loss in the divertor across the separatrix to the topologically decoupled inner part of the scrape-off layer. Farther away from the separatrix, however, subsonic backflow of hydrogen plasma occurs starting just inside the divertor chamber and extending to the midplane. A few centimetres away from the separatrix, the parallel flow is again forward into the divertor. The backflow is obviously caused by strong, localized target recycling occurring on those field lines.

The hydrogen flow reversal at high divertor recycling together with thermal forces in the same direction could be responsible for the strongly reduced retention of gaseous impurities in the ASDEX divertor for high-recycling conditions.

Until now, a simplified geometry has been used and plasma rotation, neoclassical effects, asymmetric divertor recycling etc. have not been considered. If these are included, an even more complex global and local hydrogen flow pattern in the edge region is to be expected, causing equally complicated impurity transport in that region. The experimentally determined impurity deposition on ASDEX walls seems to support this hypothesis.

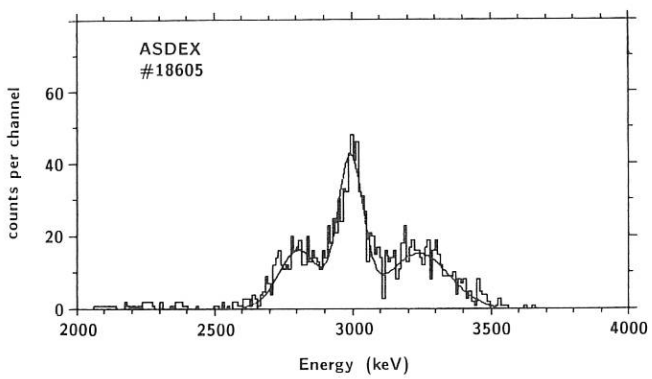

Fig. 38: Example of a proton spectrum from lower hybrid heated discharges indicating the superposition of the double-humped distribution of the two-dimensional high energy ions with the central peak of the thermal ions.

1.7 Lower Hybrid Experiments (in collaboration with F. Leuterer, H. Derfler[1], D. Eckhartt, M. Münich, T. Vien[2], F.v. Woyna[3], M. Zouhar, (Lower Hybrid Group, Techn. Division))

The lower hybrid experiments at 1.3 GHz were continued with power levels of up to 1 MW/1.5 s. Besides the investigations described in the following sections, we mention here briefly some results of X-ray spectroscopy and of charge exchange analysis. With X-ray spectroscopy the fractional density of LH-generated suprathermal electrons was determined. For LH current drive with nearly zero loop voltage, the fast current-carrying electrons were determined to be only about 1 % of all electrons with a fairly flat radial distribution. This percentage agrees with estimates based on the average phase velocity of the applied LH-waves. Applying a symmetric wave spectrum in heating experiments, the number of fast electrons strongly increased very probably owing to the non-zero electric field.[4]

At plasma densities $\bar{n}_e \geq 3 \times 10^{13}$ cm^{-3} suprathermal electrons are no longer generated but fast ions are observed. The toroidal variation of the charge exchange neutral fluxes (angle variation $\pm 8^o$) and the measurement of fusion products indicate that these fast ions mainly originate from the edge region. Since the fast ions, which are created during LH have a two-dimensional energy-distribution (high energy only in the poloidal plane), the spectra of protons and tritons have a double-humped structure. An example of such a proton spectrum is given in Fig. 38. By varying the direction of the collimator it could be proved that the fast ions are created in the outer part of the plasma. The depth of the fast ion population depends on the ion energy. This generation of fast ions is assumed to prevent deep penetration of the LH waves at higher densities.

1.7.1 Coupling measurements

The individual reflection coefficients in the eight waveguide grill antenna were measured and compared

---

[1] Till 31.3.86
[2] Till 30.9.86
[3] Till 30.6.86
[4] R. Bartiromo et al., Nucl. Fus. 26, 1106, 1986

with theory, assuming a non-zero edge density, n_{edge}, and a linear density gradient, ∇n_e, in front of the grill. The measurements were in rather good agreement with theory. Grill phasings, like $0\pi0\pi0\pi0\pi$ or $00\pi\pi00\pi\pi$, which generate symmetric wave spectra also show a symmetric distribution of reflection coefficients. At low densities the edge waveguides show a low reflection coefficient while the centre waveguides show a higher reflection coefficient. At high densities, the opposite distribution is found. In the intermediate density range all reflection coefficients can be low, resulting in $\langle R \rangle \lesssim 0.1$. An example of the case of $0\pi0\pi0\pi0\pi$ phasing is shown in Fig. 39a (theory) and Fig. 39b (experiment).

For a phasing of $\Delta\phi=\pi/2$ between adjacent waveguides, an asymmetric wave spectra as used in the current drive experiments is launched. The calculated reflection patterns are then also found to be asymmetric. They do, however, show the same pronounced density dependence with a minimum average reflection coefficienet $\langle R \rangle < 0.1$ at intermediate edge densities. An example of this situation is shown in Figs. 40a and 40b.

In all cases the best matching of the grill is theoretically found for edge densities in the range 1 to 3×10^{11} cm^{-3}. When extrapolating edge density measurements to the grill position, we arrive at comparable values.

1.7.2 Behaviour of the boundary plasma during LH application

Langmuir probe measurements were made in the boundary plasma outside the separatrix during LH application. With a fast-moving triple probe the radial profiles of density and temperature over a range of 10 cm can be obtained during one discharge. The probe is placed toroidally 1 m away from the grill in a plasma volume directly connected through magnetic field lines to the space around the grill antenna. During injection of LH waves large toroidal and poloidal variations in the floating potential of the three tips of the probe are seen inside the radial position of the grill (see Fig. 41). The electric field vector derived from the floating potentials shows a strong radial variation in amplitude and direction. The main reason are large electron temperature gradients of 15-30 eV/cm. These can be measured by operating the triple probe as two combined double probes. The electron temperatures are derived from the current-voltage characteristics of the probe as shown in Fig. 42 during LH and in Fig. 43 during OH. The electron temperature in the plasma region in front of the grill is strongly increased during LH (65-80 eV) above the OH value (~15 eV). The electron density in this region, on the other hand, is decreased. This is in agreement with former measurements with single Langmuir probes and also with interferometer measurements at low n_e.

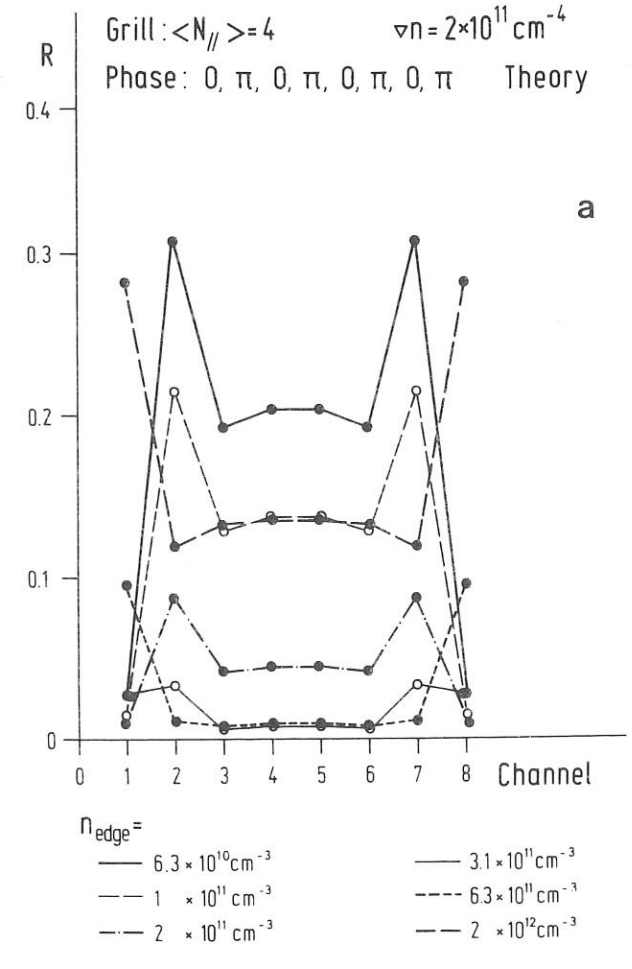

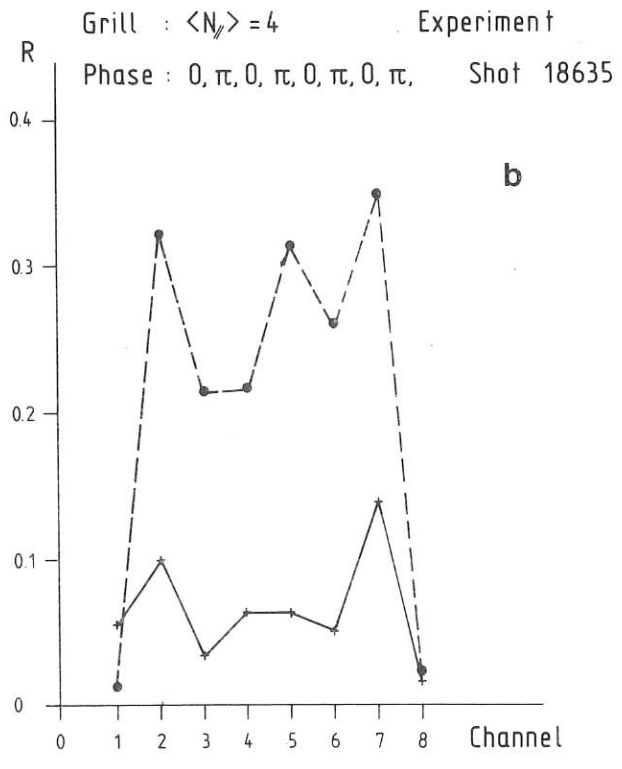

Fig. 39: Power reflection coefficient in each channel of the 8-waveguide grill for a phasing of $\Delta\phi=\pi$.
a) calculation, b) experiment

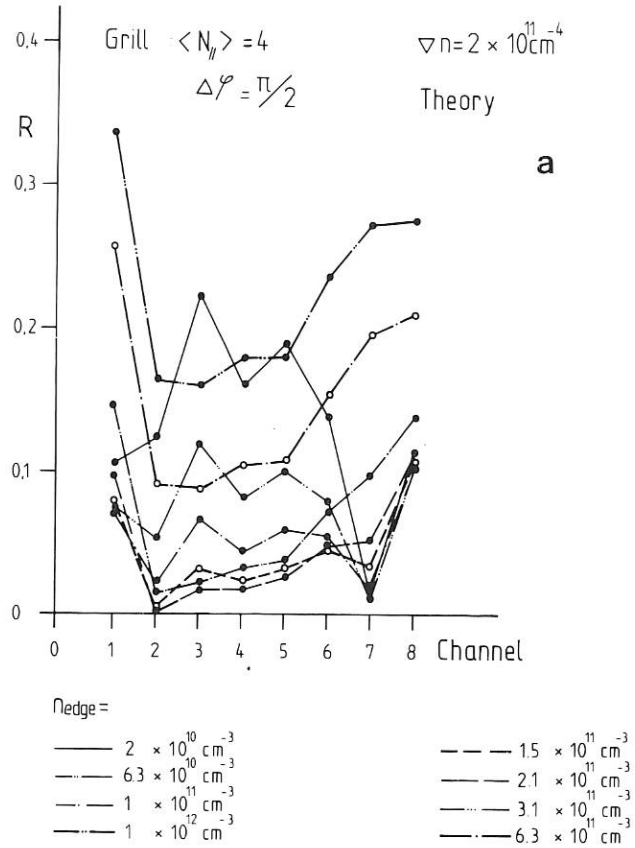

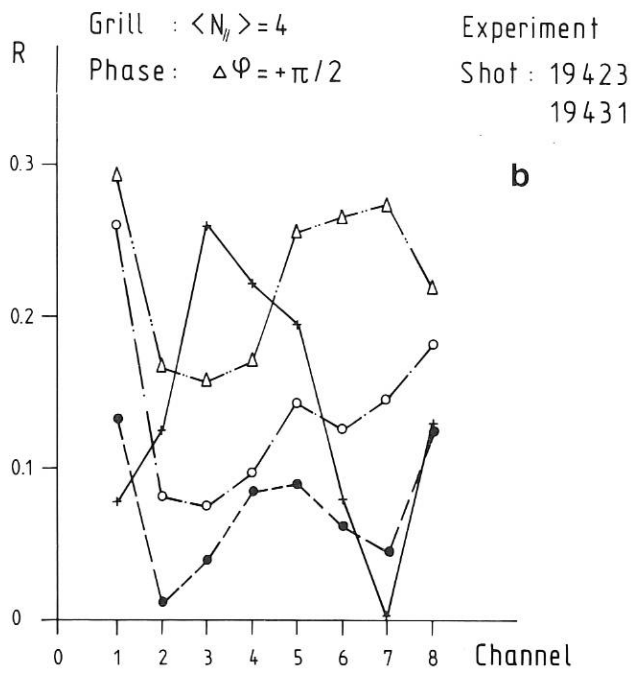

Fig. 40: Power reflection coefficient in each channel of the 8-waveguide grill for a phasing of $\Delta\phi = \pi/2$.
a) calculation, b) experiment

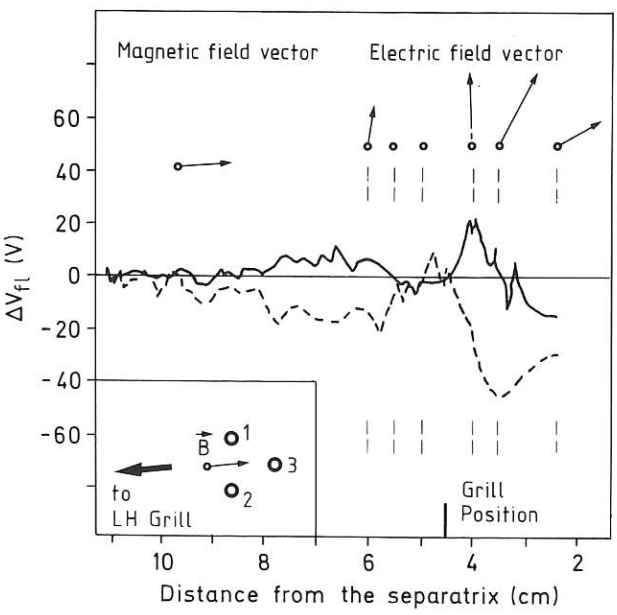

Fig. 41: Radial profiles of floating potential differences between different tips of a triple probe ($\bar{n}_e = 1.4 \times 10^{13}\,cm^{-3}$)
——— tips 1-3
- - - - - tips 2-3

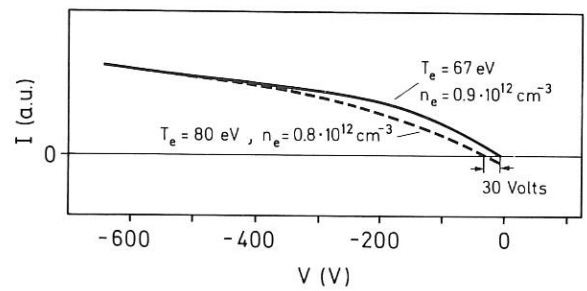

Fig. 42: Current-voltage characteristics during LH, ($\bar{n}_e = 1.4 \times 10^{13}\,cm^{-3}$)
——— tips 1-3
- - - - - tips 2-3

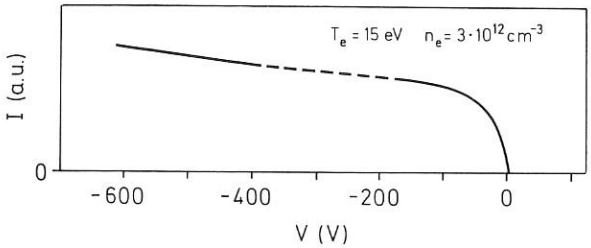

Fig. 43: Current voltage characteristics during OH ($\bar{n}_e = 2.9 \times 10^{13}\,cm^{-3}$).

In addition to the measured local variation of the thermal electron temperature, also inhomogeneous fluxes of suprathermal electrons and gradients in the plasma potential have to be assumed in order to explain observations like the shift in the current-voltage characteristics of two combined pairs of probes (see Fig. 42) and large components of the electric field vector parallel to the magnetic field. During application of LH, the boundary plasma between grill and separatrix therefore seems to be strongly modified, at least close to the grill in the region where the LH waves should propagate after launching from the antenna.

1.7.3 Application of LH current drive to NI -heated plasmas

Two aspects are of major interest for LH current drive in combination with other additional heating methods: the influence of a large variation of the electron temperature on the absorption of LH waves by electrons and the concomitant absorption of part of the wave energy by fast ions. The combined operation of LH current drive and NI was studied in ASDEX up to powers of P_{LH} = 1 MW and P_{NI} = 3.4 MW.

With NI alone the ohmic power required for constant plasma current decreases with increasing beam power in the case of co-injection owing to the increase in electron temperature. With counter-injection, P_{OH} increased because of an increase in Z_{eff} due to accumulation of heavy impurities. With additional LH current drive the ohmic power input is reduced in both cases, but less for counter- than for co-injection. The reduction in P_{OH} by LH current drive is considerably smaller in combination with NI than in an ohmic target plasma. This is seen from Fig. 44 where P_{OH} is plotted versus beam power for the different scenarios. The decrease in the drop of P_{OH} which is shown in Fig. 45 can be partly explained by the increased electrical conductivity in the case of co-injection which reduces the RF-driven current. But additional absorption of LH-power by beam ions certainly plays an important role. This is seen from the charge exchange analysis where fast ions with up to twice the injection energy are observed. The absolute amount of power transferred to these ions could not yet be determined. Orbit calculations for this purpose are under way. Absorption of LH waves on the ions might be avoided in future experiments by a proper choice of the frequency and shaping of the wave spectrum.

1.7.4 Sawtooth suppression

The studies on stabilization of sawtooth oscillations by lower hybrid current drive were continued. Sawteeth are suppressed if the current profile j(r) is broadened so that the central q-value increases above 1. In ohmically heated plasmas this requires about half of the RF power necessary for complete current drive with a wave spectrum at high phase velocities ($\bar{N}_{\parallel} \approx 2$, $\Delta\phi = 90°$). The threshold power P^{*}_{LH} for sawtooth suppression is plotted versus density in Fig. 46 for the range of experiments performed in ASDEX. Also shown is the fraction of RF power accessible in these cases to regions inside r=30 cm or r=10

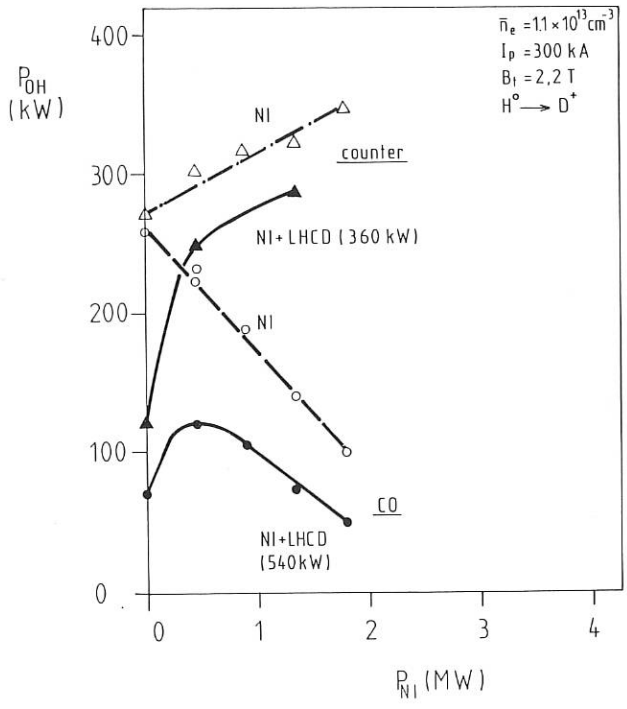

Fig. 44: Ohmic power input at constant plasma current for (co and counter) NBI alone and with superposed LH-current drive.

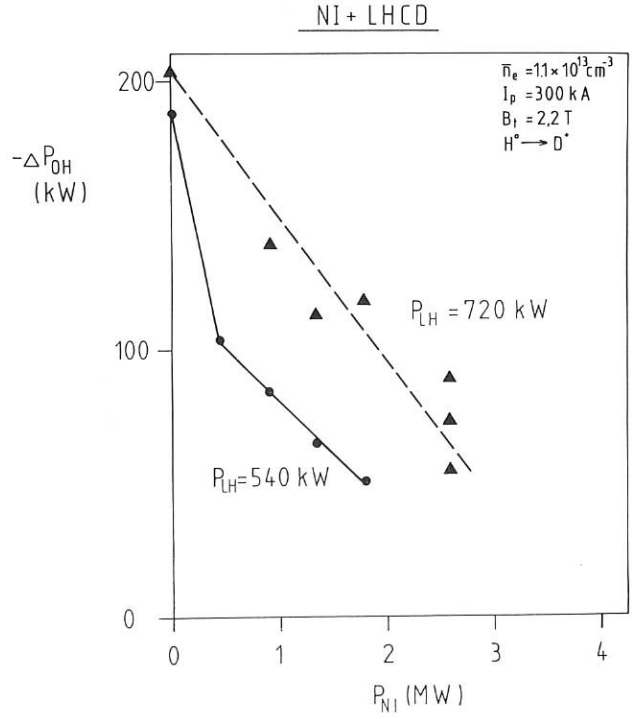

Fig. 45: Reduction in ohmic power by LH current drive in combination with NI heating versus beam power.

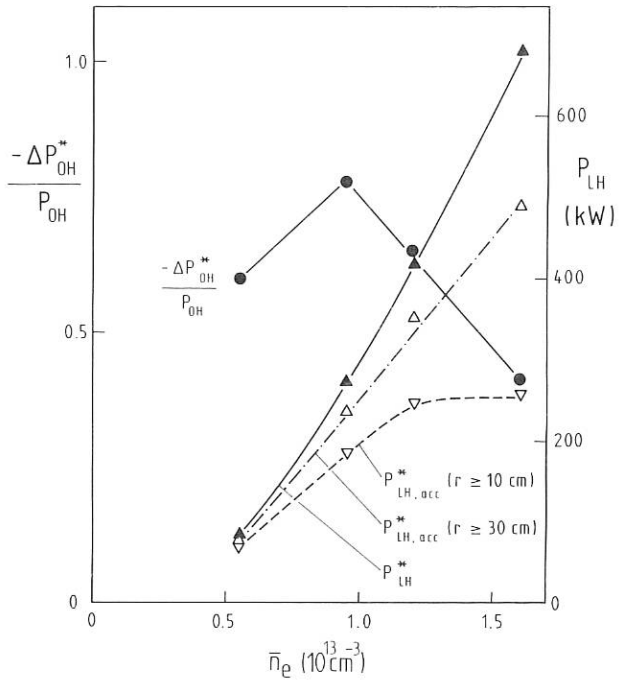

Fig. 46: LH-power P_{LH}^* required for sawtooth stabilization by LHCD together with the fraction P_{LH}^* accessible to regions inside r=30 cm or r=10 cm. Relative drop of OH power $-\Delta P_{LH}^*/P_{OH}$ for LHCD with P_{LH}^* (I_p = 300 kA, B_t = 2.2 T).

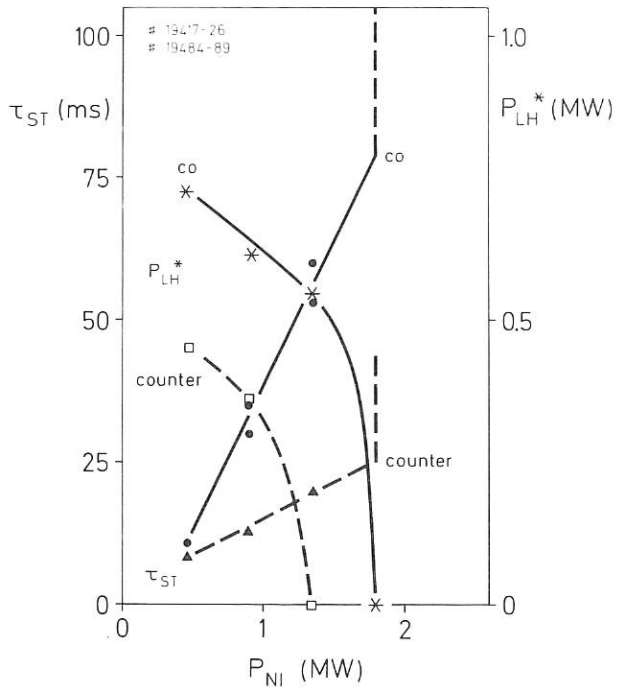

Fig. 47: Sawtooth period τ_{st} for NBI and threshold power P_{LH}^* for sawtooth stabilization by LH during NBI for co- and counter-injection as a function of P_{NI}. $\bar{n}_e$=1.1 x 10^{13} cm^{-3}, I_p =300 kA, B_t = 2.17 T.

cm, as determined by ray tracing calculations. The relative drop in ohmic power input $-\Delta P^*_{OH}/P_{OH}$ (the plasma current being kept constant) is in the range 0.4 - 0.8 under these conditions.

Sawteeth could be suppressed by LH current drive also during NBI heating. The density range was limited to a region where still an appreciable part of the plasma current can be driven with the existing LH system on ASDEX ($\bar{n}_e \lesssim 1.5\times10^{13}$ cm^{-3}). The stabilizing mechanism is again based upon broadening of the current profile as indicated by an observed decrease of the internal inductance l_i during application of the LH. The RF power P^*_{LH} required for sawtooth suppression decreases with increasing NBI power and it is smaller for counter- than for co-injection. For both cases, the threshold power P^*_{LH} is plotted versus NBI power in Fig. 47 for the range where sawteeth are present during NBI. Also shown is the sawtooth period τ_{ST} during beam heating alone. For a given LH power the delay between the start of the RF and disappearance of the sawteeth is shortened for higher beam powers. A possible explanation of the dependence of sawtooth stabilization on NBI power is a flattening of j(r) already during NBI heating. This would then also explain why sawteeth disappear above a certain NBI power in divertor discharges. In limiter discharges no such behaviour is observed, probably because of a more rigid current density profile due to fixed plasma edge conditions.

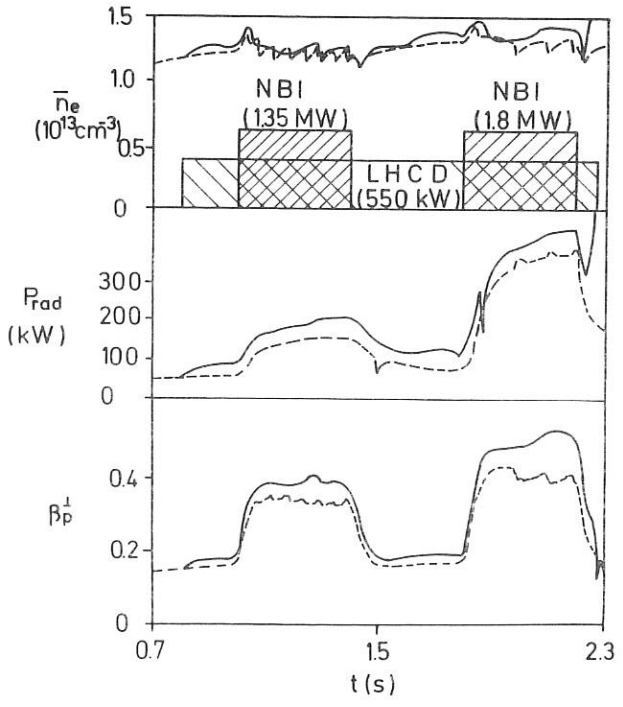

Fig. 48: Temporal evolution of $\bar{n}_e$, P_{rad} and β_p during a sawtoothing discharge with NBI (dashed lines) and a sawtooth-free discharge with LHCD+NBI (solid lines).

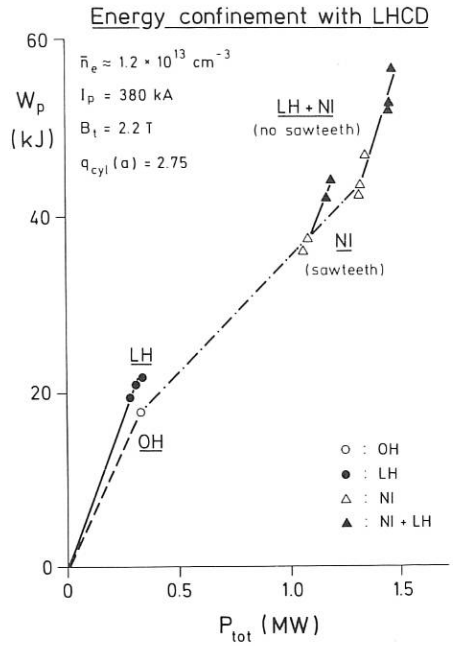

Fig. 49: Total energy content versus total power input in sawtoothing (OH, NI) and non-sawtoothing discharges (LH, LH+NI).

When sawteeth are stabilized during NBI by LH current drive, higher central electron temperatures can be achieved and also the global energy confinement is slightly improved. In Fig. 48, the time behaviour of the electron density (n_e), radiation losses (P_{rad}) and diamagnetic beta (β_p) are shown for a sawtoothing discharge with NBI alone (2 pulses with 1.35 and 1.8 MW) and for a sawtooth-free discharge with superposed LH current drive (P_{LH} = 550 kW). Higher beta-values are obtained in the absence of sawtooth oscillations. No increase of radiation is observed in this case, and therefore no accumulation of impurities seems to occur. The net gain in total energy content can be seen from Fig. 49 where the total plasma energy, as determined from the diamagnetic signal, is plotted versus the total absorbed power for the different types of discharges. It seems that the global scaling of the total energy content with power (L-scaling) is not changed by sawtooth stabilization but just offset by a small additional gain from the increase in central energy content.

1.7.5 Influence of the $N_{\parallel}$-spectrum on LHCD

The LHCD experiments described in the Annual Report 1985 were all performed with a rather narrow $N_{\parallel}$-spectrum of waves which was obtained when the grill was operated with a phase difference of $\Delta\phi=\pi/2$ between successive waveguides. For the following, we will consider this spectrum as a reference spectrum. Since the wave spectrum plays a key role in the current drive theory, we generated spectra which show a definite wing at the high-$N_{\parallel}$ side. The ratio between the power in the low-$N_{\parallel}$ part around $N_{\parallel}$=2 and the power in the high $N_{\parallel}$ part was varied while the total input power was kept constant at 400 kW. Two sets of such spectra are shown in Fig. 50; the spectra called C1 and F1 correspond to the reference spectrum.
At a density of $\bar{n}_e$=6x10^{12} cm^{-3}, we obtained with the reference spectrum a stationary current drive (I_{OH}=I_p=0). With increasing power in the wing we find that I_{OH} during LH decreases (Fig. 51) and therefore the current drive efficiency decreases, too. A comparison of the results with theory, which assumes a rectangular $N_{\parallel}$-spectrum, leads to the conclusion that not only the boundaries of the spectrum but rather its exact shape have to be considered in evaluating the current drive efficiency. Otherwise the high-$N_{\parallel}$ waves are overemphasized with respect to those at low $N_{\parallel}$.

LHCD was also found to change the current density profile. j(r) and T_e(r) are no longer related by the Spitzer conductivity. Changing the shape of the launched spectrum, we find that with increasing power at high $N_{\parallel}$ the drop in l_i (determined from magnetic measurements) increases (Fig. 52) indicating a broadening of j(r) although the current drive efficiency decreases. This result, obtained from magnetic measurements, is corroborated by direct measurements of j(r) and by the disappearance of the sawteeth, as described in Sect. 1.7.4. We also find that with increasing power at high $N_{\parallel}$ the heating of the electrons is considerably reduced near the plasma centre, whereas, in some cases, it is slightly increased near the edge.

From these observations we conclude that the higher $N_{\parallel}$ waves are absorbed nearer the plasma edge and the waves with low $N_{\parallel}$ nearer its centre. This suggests that with proper tailoring of the $N_{\parallel}$-spectrum, one can achieve a control of the current density profile rather independent of the electron temperature profile. Limits of such profile modifications are imposed by the excitation of m=2 modes when $\Delta l_i \lesssim -0.2$ or when q(a) is low.

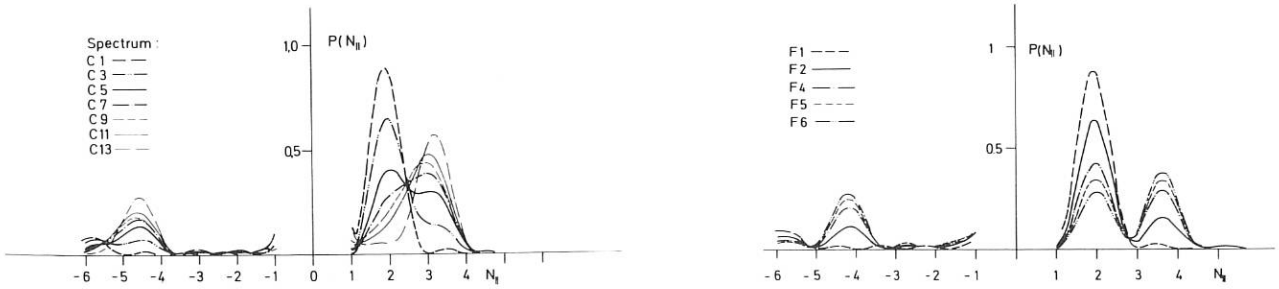

Fig. 50: Two series of power spectra with different shapes, in which the power in the range $1<N_{\parallel}<2.5$ is decreased while the power within $2.5<N_{\parallel}<4$ is increased. The total power in the spectra is constant.

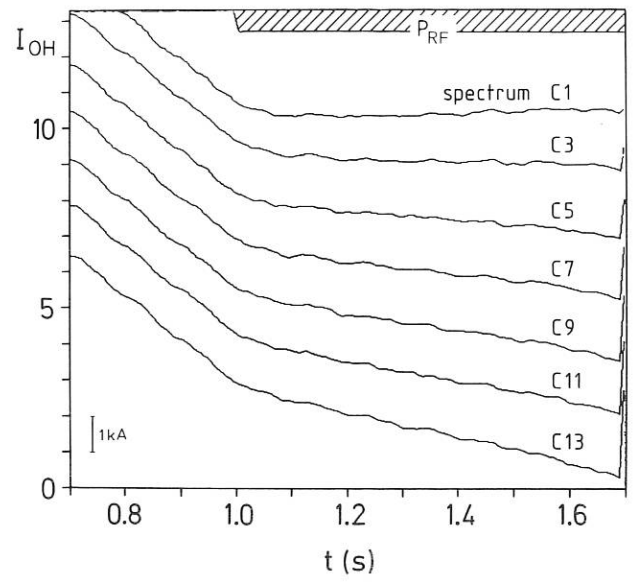

Fig. 51: Time variation of the primary current in the OH transformer after application of LH power with the $N_{\parallel}$-spectra of Fig. 50a.

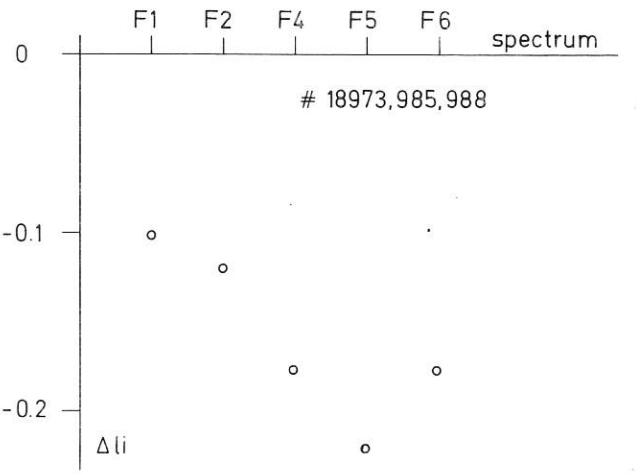

Fig. 52: Change of the internal inductance due to application of LH current drive with the $N_{\parallel}$-spectra shown in Fig. 50b.

1.7.6 Current density measurements during LHCD

Temporal measurements of the poloidal field distribution $B_P(r,t)$ during lower hybrid current drive (LHCD), and the associated OH phase, were continued in 1986 using the Li-beam diagnostic technique (see Annual Reports 1984 and 1985). Only narrow ranges of plasma parameters were studied ($\bar{n}_e$~0.7-1.2x10^{13} cm^{-3}, I_P~300 kA, q_a~3.3-3.5), emphasis being placed on the response of a standard plasma to various levels of RF power and different $N_{\parallel}$-spectra.

Figure 53 illustrates the OH and stationary LHCD B_P profiles for one measurement series with P_{LH}~730 kW, leading to a drop of about 75 % in the loop voltage V_L. In this case, LHCD has caused $B_P(r)$ to decrease over a substantial portion of the radius, indicating that the current profile j(r) has broadened in spite of a peaking electron temperature profile[1]. The change in internal inductance Δl_i is calculated to be ~ -0.16. The slope of the straight line connecting the experimental points for $r \lesssim a/4$ corresponds to $q^{OH}(0)$ ~ 1.03 and $q^{LH}(0)$~1.3.

Table 1 summarizes the results obtained by varying P_{LH} from 180 to 870 kW for $\bar{N}_{\parallel}$=1.9; a case with $\bar{N}_{\parallel}$=1.7 is also included as well as two spectra, designated as C5 and C13 (see Sect. 1.7.5), where $\bar{N}_{\parallel}$>2. For P_{LH}=180 kW, Δl_i is positive, meaning that in contrast to the 730 kW case, j(r) has narrowed. No change, however, is found in the safety factor q in the central region which remains at $q(\lesssim a/4)$ ~1.0. Increasing P_{LH} to 540 kW yields Δl_i =-0.12 and $\Delta q(0)$= +0.16, i.e. the current profile broadens. Finally, application of 870 kW - leading to almost 100 % current drive - produces Δl_i= -0.24 and $\Delta q(0)$~+0.4, with the negative side-effect that strong m/n=2/1 modes are excited, this feature being exacerbated at lower values of q_a than studied here. Interestingly, $\bar{N}_{\parallel}$=1.7 with complete current drive produces only a very small change in l_i, Δl_i ~ -0.04, while at the same time $\Delta q(0)$~ +0.3, this being the consequence of a broadening of j(r) confined to the inner half-radius. C5 and C13 with higher $N_{\parallel}$ are at the other extreme: the current drive efficiency is poor, whereas Δl_i is quite large.

From this data set the general picture emerges that higher $\bar{N}_{\parallel}$ leads to a more pronounced change in j(r) with respect to the ohmic profile. Furthermore, for a given spectrum the extent of current profile broadening is directly related to P_{LH} once the RF power is above a certain level. The effect of different power levels on j(r) for $\bar{N}_{\parallel}$=1.9 is depicted in Figure 54, where a typical OH profile

[1] K. McCormick et al., Phys. Rev. Lett. 58, 491 (1987)

Table 1

$\bar{N}_{\parallel}$	P_{LH} (kW)	$\bar{n}_e$ ($10^{13}cm^{-3}$)	$V_L^{OH}:V_L^{LH}$	$q^{OH}(0)$	$\Delta q(0)$	Δl_i
1.9	180	0.9	0.83:0.22	1.0	0	+0.11
1.7	400	0.7	0.6:0	-	+0.3	-0.04
1.9	540	1.2	0.9:0.3	0.98	+0.16	-0.12
1.9	730	1.0	0.99:0.23	1.03	+0.27	-0.16
1.9	870	1.2	0.83:0.14	-	+0.4	-0.24
C5	360	0.8	1.01:0.29	1.02	+0.27	-0.18
C13	360	0.8	0.75:0.35	1.01	+0.11	-0.16

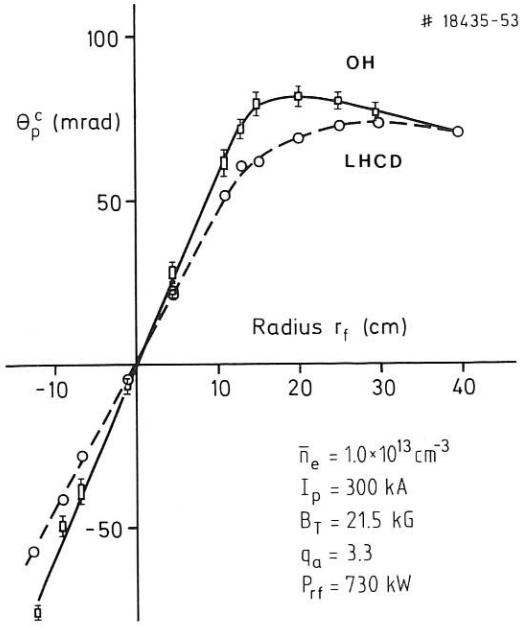

Fig. 53: Experimental pitch angle curves θ_p^c ($B_p = B_T \tan\theta_p^c$), adjusted to cylindrical geometry, for the OH and LHCD discharge phases. The (OH) box height gives the mean standard deviation of θ_p^c over 50 ms, and the error flags indicate the base line uncertainty.

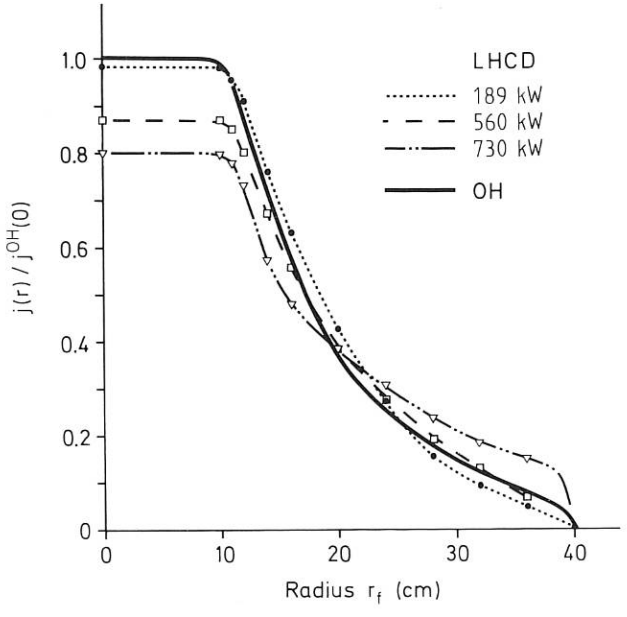

Fig. 54: Current profiles derived from experimental θ_p^c (r) measurements, associated with LHCD at three different power levels in addition to the typical ohmic case. The profiles have been normalized to the corresponding $j^{OH}(0)$ value (~200-210 A/cm^2) in order to account for slight differences in the plasma parameters Ip and B_T.

is also drawn. Evidently, by varying P_{LH} alone, j(r) may be altered over an appreciable range.

The values for $q^{OH}(0)$ in Table 1 all lie around ~1.0, with a typical uncertainty of perhaps 5 %. The lack of measurements for other q_a makes it impossible to ascertain whether q(0) ~1 is generally valid, or only an artifact of q_a~3.4 discharges. One indication that q(0)~1 is a limiting condition comes from the P_{LH}=180 kW series, where current is found to concentrate towards the centre, but no augmentation in j(r) is found inside the q=1 radius. Sawteeth were present during the OH phase for all discharges considered here, with the exception of $\bar{N}_{\parallel}$=1.7, where the presence of suprathermal electrons during OH did not permit determination of sawteeth via ECE.

1.8 ICRH

(in collaboration with F. Wesner, J. Bäumler, W. Becker, F. Braun, R. Fritsch, F. Hofmeister, E. v.Mark, J.-M. Noterdaeme, S. Puri, M. Söll, K. Steinmetz, H. Wedler (Technology Division))

1.8.1 Comparison of $2\Omega_{CH}$ and D(H) heating

Second-harmonic heating has been successfully applied to H/D mixtures at hydrogen concentration levels where conventional hydrogen minority heating at the fundamental frequency no longer works. In these mixtures, where the resonant species (H^+) can be a small fraction of the total particle density, the RF heating efficiency ($\Delta W_p^{IC}/P_{IC}$) is found to be strongly enhanced beyond that of pure hydrogen (Fig. 55) owing to the heating of basically a deuterium plasma favoured by the isotope effect on confinement. Even the lowest hydrogen concentration ($n_H/n_e \approx 0.1$), the heating efficiency of the '$2\Omega_{CH}$ minority' scenario (≈36 kJ/MW) compares well with that of the conventional D(H) minority mode (≈35 kJ/MW) and is well above that of the $2\Omega_{CH}$ heating in pure hydrogen (≈21 kJ/MW). On the basis of these results second-harmonic heating appears as an attractive scenario for a reactor-like DT plasma, where efficient heating is expected to be achieved much more easily in the tritium second-harmonic scheme than in a

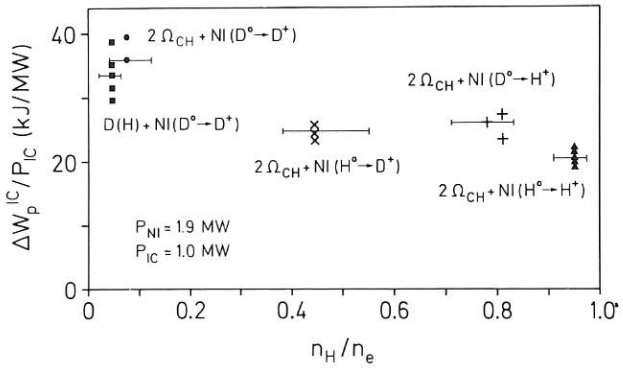

Fig. 55: ICRH heating efficiencies in the $2\Omega_{CH}$ mode for various hydrogen concentrations of the plasma.

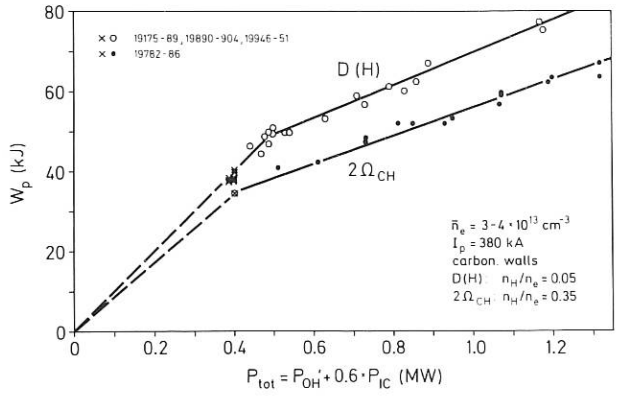

Fig. 56: Scaling of plasma energy content versus absorbed total heating power in the $2\Omega_{CH}$ and the D(H) minority mode.

The electron temperature profiles during ICRH compared with NI and ohmic heating are illustrated in Fig. 58. The T_e profiles are normalized to a radius $r \approx a/2$, which is outside the sawtooth reconnection region. Obviously the shape of the profiles is rather invariant outside $r=r(q=1)\sqrt{2}$ with respect to the heating method. Inside the q=1 surface the electron temperature profiles are more strongly peaked during ICRH than with NI or ohmic heating, whereas D(H) minority heating gives rise to even more peaked profiles than $2\Omega_{CH}$-heating.

A particularly interesting feature occurs in case of off-axis RF ($2\Omega_{CH}$) power deposition (see Sect. 1.3.3.1). A significantly enhanced direct electron heating (Fig. 59) close to the $2\Omega_{CH}$ resonance at $r \approx a/2$, and a remaining power transfer to the electrons near the plasma axis is observed indicating 1) the existence of (weak) electron heating by Ion Bernstein waves (IBW) as predicted by theory and 2) a finite, still notable damping of the IBW when propagating towards the plasma centre.

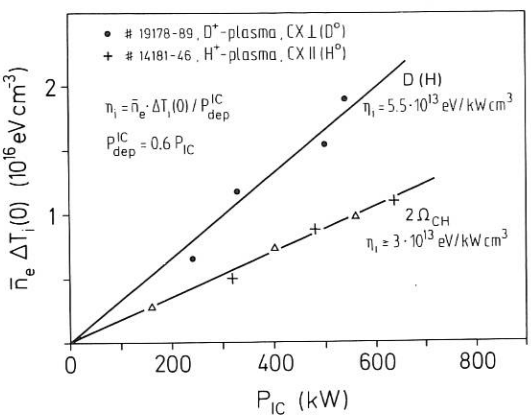

Fig. 57: a) Comparison of central ion heating in the $2\Omega_{CH}$ and the D(H) scenarios.

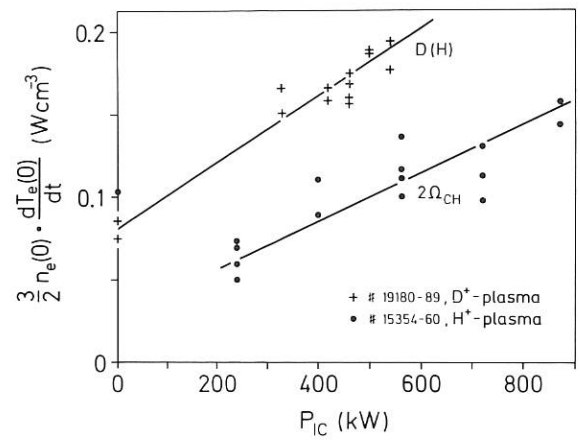

b) Direct central electron heating of both ICRH heating regimes.

three-species minority scenario (e.g. D(H) in a DT mixture) owing to the difficult control of the minority concentration within a narrow range.

Another important feature concerning the comparison of $2\Omega_{CH}$ and D(H) heating is shown in Fig. 56, where the plasma energy content W_p is plotted versus the total absorbed heating power. At low ICRF power ($P_{IC}<0.7$ MW), the D(H) minority scheme clearly exhibits no degradation of confinement, while the $2\Omega_{CH}$ secenario immediately follows an L-mode scaling. The non-degraded confinement of the D(H) scenario at low ICRF power ($P_{IC}<0.7$ MW) is manifested in enhanced ion heating (Fig. 57a) and an increased direct power deposition to the electrons (Fig. 57b), measured via the time derivative of the electron temperature just after a sawtooth crash. At higher RF power, both the $2\Omega_{CH}$ and the D(H) scheme show an offset-linear behaviour of W_p vs P_{tot} with almost equal heating efficiencies (i.e. incremental confinement times $\Delta W_p^{IC}/\Delta P_{tot} = \tau_{E,inc} \approx 35$ to 40 ms).

1.8.2 Probe measurements

(in collaboration with R. van Nieuwenhove and G. van Oost, LPP-Association "Euratom-Belgian State"-ERM/KMS, Brussels

Measurements with electric and magnetic probes performed on ASDEX during ICRH are being analyzed. Strong harmonics of the transmitter frequency were observed and the correlation with the RF absorption in the plasma is being investigated. The results are compared with theoretical calculations and with measurements made on TEXTOR.
The aims of this research work are to study effects of ICRH on the plasma edge and investigate the propagation of plasma waves in the boundary.

For further investigation of radial dependencies a set of moveable probes has been prepared which will allow measurement of the electric and magnetic field components of waves in the boundary of ASDEX.

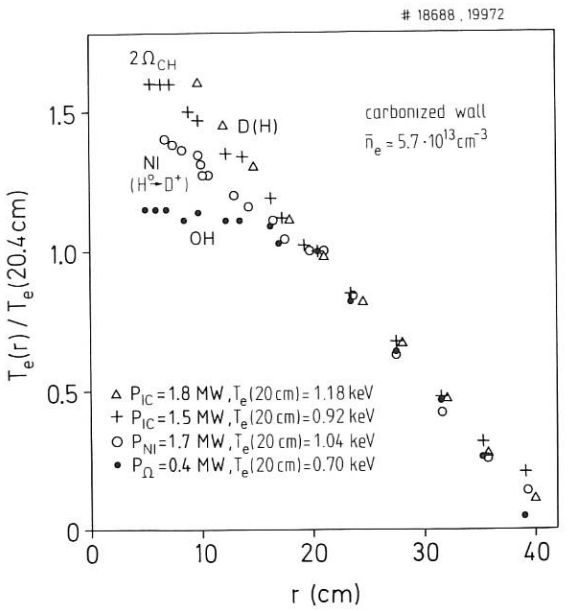

Fig. 58: Electron temperature profiles (normalized to a radius outside the sawtooth reconnection region, here r≈a/2) of ohmic heating and with auxiliary NI and ICRH ($2\Omega_{CH}$ and D(H)) heating.

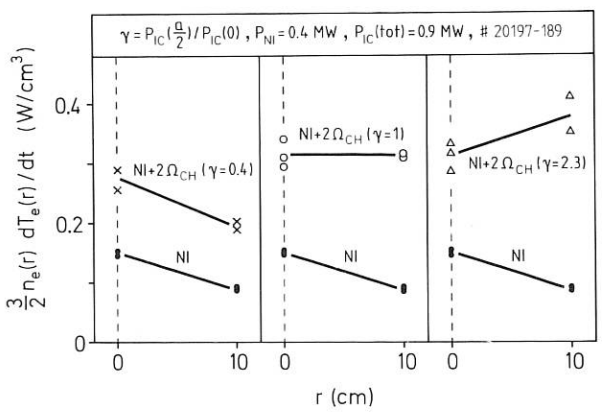

Fig. 59: Variation of local direct electron heating with increasing local ICRH off-axis heating in the $2\Omega_{CH}$ mode.

1.8.3 Impurity studies

The ICRH-related reduction of particle and impurity transport with respect to NI is shown in Fig. 60, where the decay times of TiXX injected into the plasma by laser blow-off are illustrated, indicating similar trends for impurity/particle transport and confinement. The transport analysis suggests an enhancement of the inward drift velocity rather than a reduction of the diffusion coefficient with respect to NI. The reduction of the impurity transport during ICRH leads to, besides additional ICRH-specific mechanisms of impurity release, an enhanced impurity level which is dominated by iron released from the torus walls. The radiated power of about 35 % mainly originating from the plasma centre (Fig. 30), limits high-power ICRH operation to $P_{IC}<1.5$ MW if no wall carbonization or NI preheating is provided. Carbonization of the torus wall allowed an almost iron-free plasma with a radiation level of about 15 % (Fig. 30) where the residual peaking sometimes observed in the radiation profile results from an imperfect carbon coating. The impurity content of the plasma and the magnitude of the fast ion fluxes at the plasma boundary have been found to be related to wave absorption: Conditions of poor absorption (as verified at e.g. $2\Omega_{CH}$ launching in helium or pure deuterium discharges) have always been accompanied by a particular large central radiation and a significantly increased flux of high energetic ions at the plasma edge.

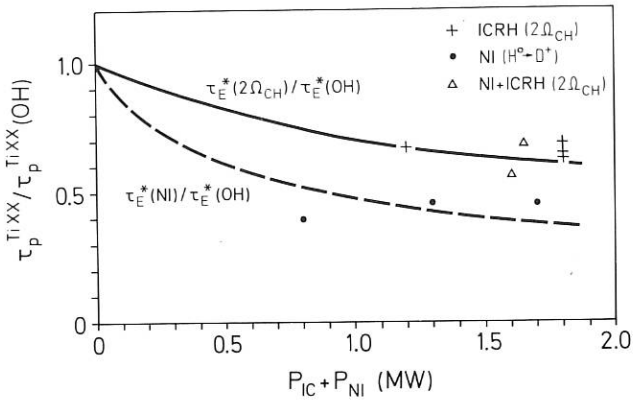

Fig. 60: Transport times of TiXX (deduced from laser blow-off measurements), compared to global energy confinement.

1.8.4 Deposition and erosion at the ICRH antennae (in collaboration with R. Behrisch, M. Wielenski, E. Taglauer (Surface Physics Division))

After the ASDEX torus was opened in April 1986, the two ICRH antennae were removed and the carbon protection limiters, the TiC-coated rods of the Faraday shield and the silver-plated current-carrying conductor behind the open Faraday shield were analyzed in respect of their surface layer composition. Generally, a deposition of D, Fe+Ni+Cr, Ti, Cu, and Ag at intensities corresponding to values of 1 to a few 100 monolayers was measured. On a few areas small amounts of Ta and W deposition were found. The measurements indicate erosion at the Faraday screen by D bombardment and Fe+Cr+Ni deposition due to erosion around the antenna. Figure 61 shows the measured depositions of D, Fe+Ni+Cr, Ti, Cu and Ag on the carbon limiter blocks.

On the TiC-coated rods of the open Faraday screen the D deposition is 0.3 to $2.5\times10^{17}/cm^2$ with a

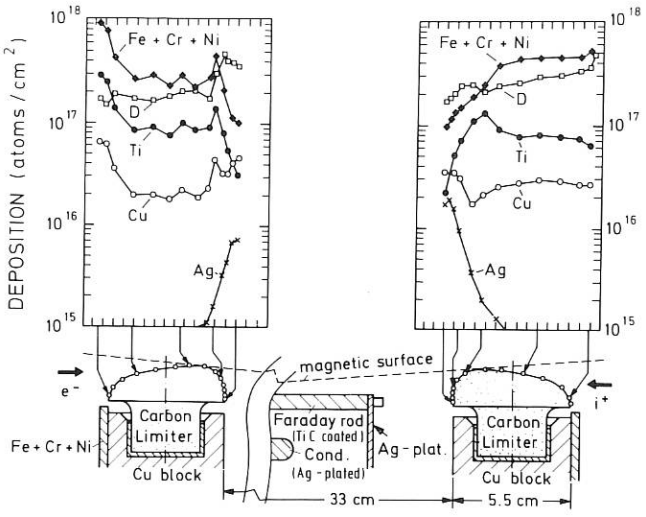

Fig. 61: D and metal deposition on the carbon limiters of the ICRH antenna.

maximum on those areas which face the plasma. This is similar to the D deposition on graphite surfaces throughout the torus. The Fe+Cr+Ni deposition was 1 to $8 \times 10^{16}/cm^2$ with maxima toward the sides between the rods, while the Ag deposition reaches up to $5 \times 10^{17}/cm^2$ and shows a maximum at the inner side facing the silver-plated conductor.

On the closed Faraday screen hardly any Ag deposition ($<2 \times 10^{15}/cm^2$) was found on the areas facing the Ag-plated conductor and none on the area facing the plasma. D and Fe+Cr+Ni are present in quantities similar to those on the open Faraday screen.

For the antenna with the open Faraday screen the silver-plated conductor showed bright and dark stripes. Viewed from the plasma, the dark areas were in the shadow of the rods, while the areas between the rods were bright. Surface analysis showed that the bright areas had a D concentration of about $2 \times 10^{16}/cm^2$, while the value was only half on dark areas. The dark areas had a factor of 20 higher deposition of iron, which was contained within a depth of 10 to 30 monolayers.

Interpretation: The elements found on the different areas of the ICRH antenna are the result of deposition, implantation, and erosion by ions and neutrals. While the neutral flux is independent on minor radius, the ion flux decreases with increasing distance from the separatrix.

Most of the deuterium is likely to be deposited during plasma discharges by implantation of CX neutrals up to saturation. The maxima at the ion drift side indicate an additional ion implantation.

The larger Fe+Cr+Ni deposition on the carbon limiters compared with other wall areas, such as the carbon ribs at the divertor slits, indicates a source near the antenna, possibly the steel sheet protecting the Cu blocks or the surrounding vessel walls. The Fe+Cr+Ni may arrive as ions, which would explain the generally lower deposition on the Faraday rods being in the shadow of the limiter and more distant from the separatrix than the limiter. On the areas of the rods facing the plasma, erosion by deuterium bombardment overcompensates the deposition of metals, while at the sides metal deposition dominates.

On the dark areas of the Ag-plated conductor behind the open Faraday screen, Fe+Cr+Ni deposition has probably occurred during glow discharge cleaning, while it was again removed on the bright areas owing to the ion bombardment. This may indicate that the interior of the antenna with the open Faraday screen is not much affected by the main plasma discharges, in agreement with the operational experience.
Ti and Cu are found in larger amounts on the carbon limiters than on other areas of the torus, such as the divertor ribs, which also indicates an additional source for these elements near the antenna. While Ti can originate from the TiC coating of the antenna rods, the Cu originates from the Cu blocks on which the carbon limiters are mounted (see Fig. 61). This is confirmed by the increase of Cu towards the side facing the screen. Finally, the Ag deposition on the carbon limiters probably originates from the Ag-plating of the steel structure supporting the antenna rods.

The results of these investigations gave rise to some modifications in the immediate vicinity of the antennae.

1.8.5 Measurements of the antenna radiation resistance

Based on input power and standing-wave voltage measurements in the antenna feeder lines, calculations were made to evaluate the antenna radiation resistance as a function of the ICRF heating regime and of the plasma properties. It increases with the plasma density and with decreasing distance between the separatrix and antenna in fair agreement with the theoretical predictions. As an example, the radiation resistance of one antenna amounts to 4.8 Ω at a line density of $4 \times 10^{19}\ m^{-3}$, a distance of 5 cm between the Faraday screen and separatrix and a heating power of 2 MW ICRH, second harmonic, and 1.6 MW NI.

2. DEVELOPMENT OF DIAGNOSTICS AND DATA ANALYSIS

2.1 Diagnostic Development

2.1.1 T_i measurements (overview of results from different diagnostics including contributions from H.S. Bosch, H.J.B.M. Brocken[1], H.U. Fahrbach, G. Fussmann, W. Herrmann, J. Hofmann, K. Hübner[2], A. Izvozchikov[3], G. Janeschitz, H.M. Mayer, H. Rapp, F. Ryter[4], U. Schumacher)

The methods used to determine the ion temperature in ASDEX are based on the analysis of i) photons ii) plasma atoms and iii) fusion products leaving the discharge. The plasma may emit i) and ii) without additional measures (passive diagnostics) or when stimulated by an atomic "doping beam" which, by intersection with the detector's cone of acceptance, localizes the measurement in space (active diagnostics).

Methods used for T_i-measurements:

X-ray spectroscopy (passive): The occurrance of heavy-metal impurities with a sufficiently high degree of ionization in only a narrow region around the plasma centre offers the possibility to determine $T_i(0)$ from the Doppler widths of the corresponding X-ray lines.

Charge exchange recombination spectroscopy CXRS (active): The broadening of visible CXR lines excited by one of the NI beams and examined by two grating monochromators give additional information on T_i in regions between 15 and 25 cm off axis.

Neutral particle analysis (NPA) (passive): This diagnostic makes use of the fact that the high energy tail of the energy distribution of atoms emitted is dominated by the Maxwellian ion distribution of the hottest zone along the line of sight. In practice, the fluxes at the appropriate energies may either fall below the noise level owing to reabsorption or become masked by a small minority of non-thermal particles.

NPA (active): The recently installed diagnostic injector offers at the same time the possibility to increase the charge exchange source well inside the plasma and to locate its origin on the line of sight of the analyzer. Together with information on plasma profiles coming from other diagnostics, an interpretation code can therefore approximately re-establish the original Maxwellian ion distribution, which markedly reduces ambiguities in the evaluation.

Neutron yield: In deuterium plasmas the production of neutrons varies approximately as $n^2(D^+)xT_i^5$, sensitively reflecting the central ion temperature. Nevertheless the influence of profiles and the dilution of the D^+ ion density by H^+ from NI and by impurities must be accounted for. (See also Sect. 2.1.2)

Proton and triton spectra: A Si diode placed not far from the plasma edge measures the fusion products from DD reactions. In ASDEX the protons and tritons can leave the plasma without collisions. The width of their energy distribution reflects the distribution function of the reaction partners and thus the ion temperature in the plasma centre.

Comparison of T_i-measurements:
The absence of discharges where all T_i diagnostics have been working simultaneously limits us to comparing methods in selected cases.

Figure 62 presents $T_i(0)$ values derived by passive NPA, from neutron yields and X-ray spectroscopy. Within its estimated uncertainty, NPA overlaps the higher X-ray as well as the lower neutron values. The reliability of the latter is affected by assumptions on the D^+/H^+ ratio suggested by numerical simulation as well as by NPA measurements. In similar plasmas with B_T=2.18 T X-ray values are distinctly above NPA values, a discrepancy which remains unexplained but may possibly be caused by fluctuations.

Figure 63 compares a profile obtained by active NPA with measurements based on neutron yield and on CXR lines excited by one of the NI beams. With the exception of the C^{6+} line the agreement is good. The excellent agreement with neutron measurements may partly be fortuitous in view of the uncertainty in the D^+/H^+ ratio.

This uncertainty is absent in ohmic D^+ discharges and good agreement between neutron and NPA measurements exists up to medium densities. Neutron-derived ion temperatures could be most convincingly verified in pellet-refuelled high-density plasmas where the expected relation $T_i(0) \approx T_e(0)$ was remarkably well confirmed.

In Fig. 64 measurements during 1.25 MW H^0 injection into a D_2 discharge are shown. The low background allowed evaluation of both the proton and the

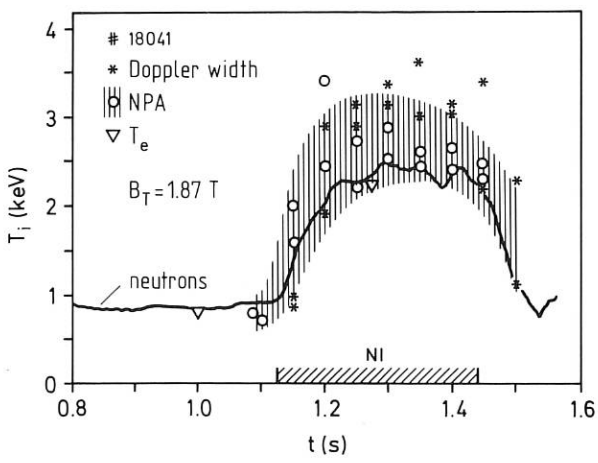

Fig. 62: $T_i(0)$ from Doppler effect of the 2.61 Å line of Ti XXI compared with NPA (passive) and neutron diagnostics (H-mode discharge with 3.5 MW NI).

[1] Datawell Corp., the Netherlands
[2] Universität Heidelberg
[3] Ioffe Institute, Leningrad
[4] CRP, Lausanne

triton spectra. The results agree with those of passive NPA within the error bars. The slight systematic difference is presumably attributable to the passive NPA method, which easily runs the risk of underestimating the central temperature. But it should be noticed that the fusion product spectra give particularly strong weight to the highest temperatures.

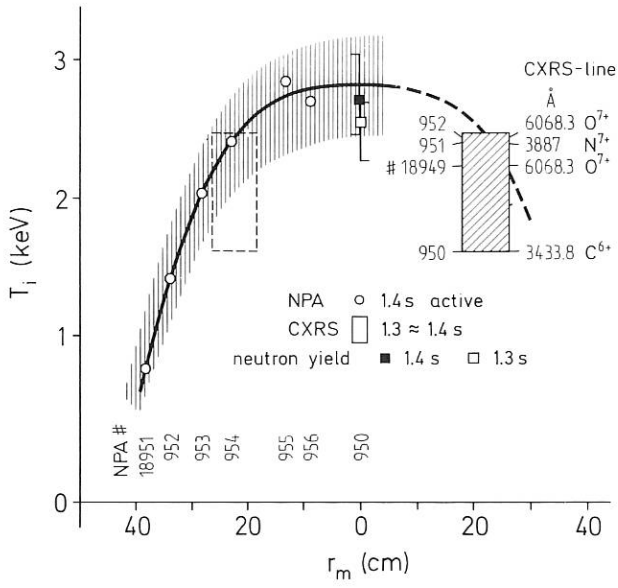

Fig. 63: $T_i(r_m)$ (r_m= magnetic radius) from NPA (active) compared with CXRS and neutron diagnostics (H-mode discharge with 3.5 MW NI).

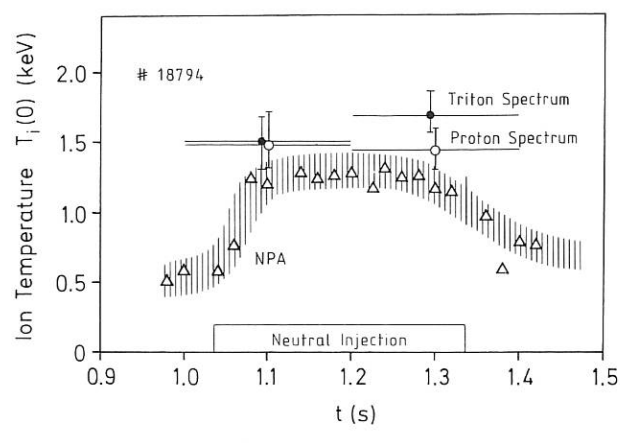

Fig. 64: Comparison of central ion temperature in a D_2 discharge with 1.25 MW H^0 neutral injection (L-mode) deduced from fusion product spectra and passive charge exchange diagnostic. The horizontal error bars indicate the integration intervals.

2.1.2 Measurement of the toroidal plasma rotation during H^0 injection in D plasmas using nuclear emulsion neutron diagnostics
(K. Hübner, H. Hinsch, R. Bätzner (University of Heidelberg))

During a series of discharges (≒16744-49) with H^0 injection in deuterium we measured neutron energy spectra by observing the plasma both in the co- and counter-directions with respect to the injection. The spectra (Fig. 65) show an energy shift which is related to plasma rotation. The total shift between the two spectra is 120 ±20 keV and from this we get a plasma rotation velocity in the direction of injection of 2.6×10^7 cm/s ±15 %, in good agreement with Doppler measurements or the rotation frequency of the m=1 n=1 mode.

The FWHM of the two lines is 190 ± 10 keV. Deconvoluting the broadening caused by counting the number of neutrons in 100 keV intervals, this value is reduced to 176 keV. The energy resolution ΔE/E of our measurement is (4.8 ±0.35) %. Thus we get from the spectral width an ion temperature of 2.5 keV. Owing to the fact that the temperature broadening (131 keV) is of the same order as the energy resolution (118 keV), the error in the temperature is large and not easy to determine. It is about 30 %.

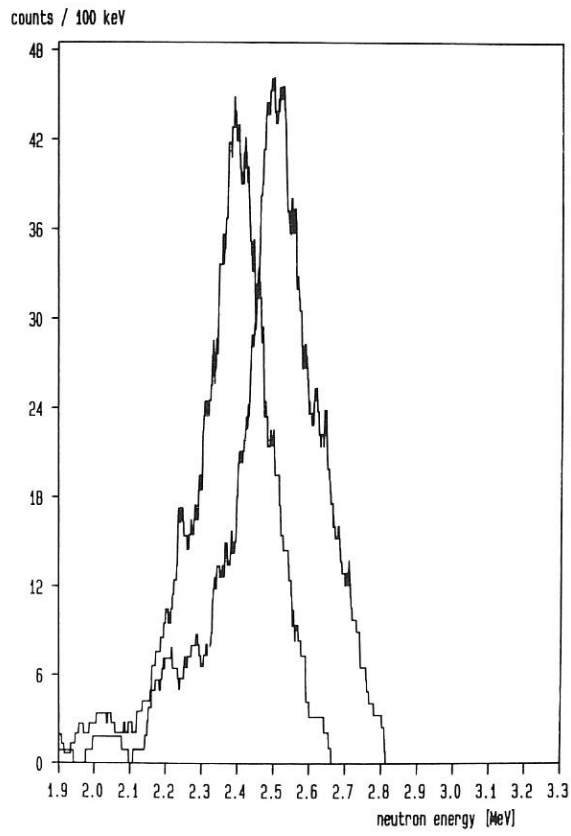

Fig. 65: Neutron energy spectra measured tangentially in co- and counter directions.

2.1.3 ASDEX SPRED spectrometer (G. Janeschitz)

A VUV survey spectrometer dubbed SPRED has been developed in cooperation with B+M Spektronik and was delivered to ASDEX at the end of 1985. The instrument is a flat field spectrograph, equipped with three readily interchangeable gratings, which cover three distinct wavelength ranges with different resolution capability. The detector is an intensified (microchannelplate) 1000-channel self-scanning photodiode array (Reticon).

The spectrometer can be operated in two modes:

- the full spectrum mode, where a 1000-channel spectrum is archived every 27 ms (minimum time resolution).
- the pixel grouping mode, where up to 12 spectral areas of interest (impurity lines) are archived: in this case, the time resolution depends on the number of groups to be read (~4 ms).

The instrument is additionally equipped with two gold-coated mirrors situated in the flange on which SPRED is mounted. This equipment allows poloidal and toroidal scans on a shot-to-shot basis. However, with a time resolution of ≥ 200 ms for a full scan, space-resolved measurements are also possible within one shot.

First experience with this spectrometer was made during the last three months of ASDEX operation. The wide spectral range (up to 1500 Å) not only gives a lot of detailed information about the impurity behaviour within different operational regimes (NI, ICRH, pellets), but also facilitates interpretation of the monochromator signals (see Fig. 66).

From June till December 1986 the instrument was on loan to the D III-D tokamak at GA in San Diego, California. The information obtained there was especially useful in clarifying impurity behaviour during the inital clean-up phase and of H-mode discharges with and without ELMs.

2.1.4 Development of the bolometer diagnostic on ASDEX (H.-F. Mast and R. Müller)

Poloidal asymmetries of bolometrically measured local radiation density were detected in ASDEX. The present array of 19 bolometers, arranged symmetrically to the horizontal midplane in one horizontally directed pinhole camera, detected

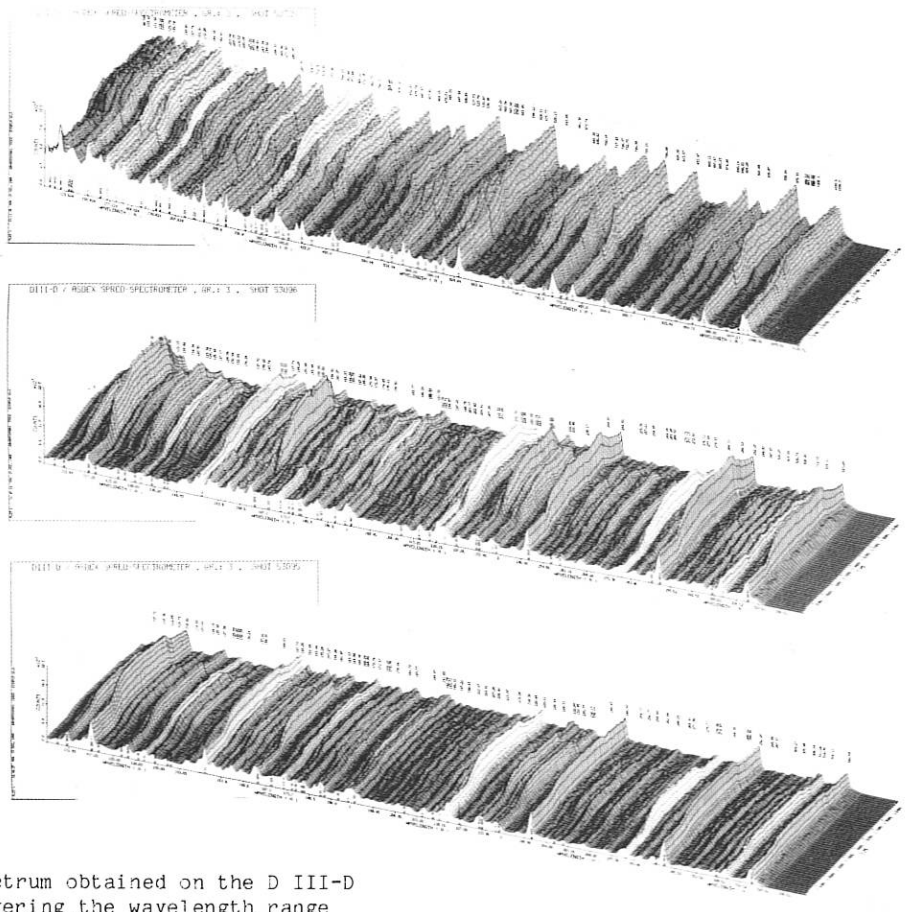

Fig. 66: Typical spectrum obtained on the D III-D tokamak, covering the wavelength range from 100 to 1100 Å.

vertical up-down asymmetries of emissivity and strong radiation from the two X-points. During neutral beam injection inward-outward asymmetries of emissivity are expected from neoclassical impurity transport and from density variation on flux surfaces owing to plasma rotation. Correlated density and temperature asymmetries are observed near the density limit.

In order to separate the various phenomena, additional bolometers with lines of sight mainly in the vertical direction have to be included. Owing to the limited access to the vacuum vessel, a new miniaturized 4-bolometer module was developed on the basis of ASDEX and JET bolometer design. Each "bolometer" comprises 4 identical bolometers, two measuring and two reference bolometers, which are arranged in one full Wheatstone bridge. Four such bridges are evaporated on one Kapton foil with an area of 2.0 x 3.3 cm^2. The reference bolometers are shielded against the radiation to be measured.

Low temperature drift and small electrical interferences were observed. The thermal cross-talk is $\leq$ 0.3 %, the bridge symmetry is 1 %, the sensitivity is $\Delta V/\Delta P$ = 0.5 V/W and the time constant is T = 0.2 s. The bolometer can either be operated with DC electronics or with a carrier frequency of 50 KHz.

Two modules are installed in the main plasma chamber which allow not only the separation of the X-point radiation but also the detection of inward-outward asymmetries, which are mainly localized near the plasma boundary. Two arrays allow spatially resolved measurement of the radiation in an outer divertor chamber.

2.1.5 Z_{eff} measurements
(H. Röhr, K.-H. Steuer)

The Nd:YAG Thomson scattering system was used to determine the continuum radiation along 16 chords in a poloidal plane of ASDEX. For high electron temperatures and line-radiation-free wavelength regions, $Z_{eff}(r,t)$ can now be inferred from these radiation profiles.

The Thomson system offers the possibility to measure within three spectral ranges simultaneously: 780-880 nm, 900-970 nm and 985-1020 nm. As the electronics of the scattering system only allows measurement of high-frequency signals (AC coupling), the plasma radiation must be calculated from the shot noise signal which is detected during each Thomson measurement. This method yields averaged results during selectable time intervals of the order of a few 100 ms or more. The relative calibration of the noise signals is done by illuminating the avalanche diodes by LED's with different intensities. The absolute calibration of the plasma radiation can be done by using Thomson scattered signals and the known laser pulse power. The electron temperature and density profiles measured by Thomson scattering allow comparison with actual bremsstrahlung profiles.
As an example, we discuss the brightness and Z_{eff} profiles before and after pellet injection in ASDEX. During the injection of 12 pellets into an ohmic plasma with $n_o = 5x10^{13}$ cm^{-3}, the density on axis rises to $2x10^{14}$ cm^{-3} and keeps constant for about 0.3 s without any gas puffing.

The Abel-inverted radiation profile averaged over the 3 spectral channels in the ohmic phase and the profile in the high-density phase are similar in shape. The radiation increases by a factor of more than 20 and scales as n^2/ T_e (bremsstrahlung). This scaling indicates that there is no essential change of Z_{eff} due to pellet injection.

2.1.6 New microwave interferometer for the divertor throats
(G. Siller)

A non-modulated 35 GHz microwave interferometer has been used so far to measure the electron density of the scrape-off plasma in the four divertor throats. The interferometer often failed, particularly during discharges with strong additional heating, where the divertor density normally rises beyond the fairly low cut-off density. The problem was most severe with both outer channels, because a much higher density than in the inner channels is observed there during double-null discharges. Another disadvantage arose from the simple technique of a non-modulated interferometer. The signal-to-noise ratio is small and fast fluctuations could not be resolved. It was thus necessary to develop a new interferometer working at a high enough frequency to avoid cut-off during most of the discharges. At the same time it had to provide a very large signal to noise ratio to give sufficient resolution even at very low densities and to permit a time resolution in the MHz range. A schematic outline is shown in Fig. 67.

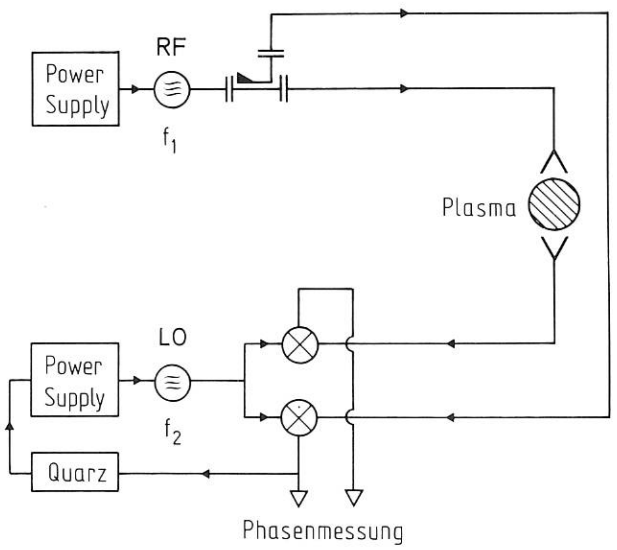

Fig. 67: Schematic outline of one channel of the new divertor interferometer.

The frequency of 89 GHz allows measurements up to local peak densities of nearly 1×10^{20} m^{-3}. A superheterodyne technique with an intermediate frequency of 10 MHz is the prerequisite for a time resolution in the MHz range. A relatively powerful klystron is being used as the main power source, while a Gunn oscillator serves as a local oscillator. It was not possible for financial reasons to phase-lock both oscillators to a stable reference source. To compensate phase shifts resulting from frequency fluctuations of the klystron, the dispersion of the reference path had to be made equal to that of the plasma path. A feedback loop stabilizes the intermediate frequency. A special phase detector had to be developed (see Sect. 3.2). Since the system contains components sensitive to magnetic fields, it is located in the control room at a fairly large distance from the experiment. Oversized waveguides are being used wherever possible to minimize losses. The sensitivity of the system is high enough to cope with unavoidable losses. Mode filters close to the horns were found to be necessary for accurate measurements.

A first test of one interferometer channel equipped with the new system was sucessfuly performed during the very end of the experimental period in March 1986. Both outer channels will be ready for operation in early 1987.

2.1.7 Measurement of atomic charge exchange cross-sections

(G. Fußmann and P.G. Carolan[1])

The investigations on CX recombination lines were continued in 1986. In particular, the $\Delta n=1$ transitions of He, C, and O were measured on absolute scale and a comparison with predictions based on various theoretical CX cross-sections was performed. Applying the cross-sections given by Ryufuku [2], we deduced concentrations of 0.6-1.4 % for carbon and about 3 % for oxygen. These values are in rough agreement with other spectroscopic determinations yielding for oxygen typically $n_O/n_e \lesssim 1$ %. A detailed description of these investigations and of previous VUV-CX recombination studies is presented by Carolan[3].

Measurements in pure helium discharges allow a more precise comparison between theory and experiment. Quite satisfactory agreement (± 30 %) for a number of HeII lines in the visible range was found.

Another study during 1986 was devoted to the CX recombination processes from the Ne-like to Na-like states. These processes are of particular importance for heavier elements (e.g. Fe, Ni) which concentrate in the Ne-like state. Adding Kr to the discharges, we could substantiate all seven $\Delta n=1$ Rydberg transitions ($n = 22 \rightarrow 21$ to $16 \rightarrow 15$) in the wavelength range 2500 Å $\leq \lambda \leq$ 6700 Å. The relative intensities of these lines as a function of the main quantum number n can be regarded as a valuable check of the theory (results still under discussion).

[1] Culham Laboratories
[2] Ryufuku H., Japan Atomic Research Institute Report, JAERI-P2-031 (1982)
[3] Carolan, P.G. et al., Phys. Rev. 30 (to be published)

2.2 Development of Data Analysis Packages

(K. Grassie[1], O. Gruber[1], K. Lackner[1], P. Martin[1], F. Mast[2], V. Mertens[2], P. McCarthy[1], R. Wunderlich[1])

Profile handling and mapping: A code package is currently being developed to facilitate the comparison of measured data with models for plasma transport and tokamak stability limits. The final aim is the construction of a comprehensive data bank, including both global quantities and plasma profiles. The content of these data banks was defined last year, in a way compatible with the future more detailed data storage needs of ASDEX Upgrade. The necessary data input and output routines have been written.

The determination of profiles of quantities which to lowest order are expected to be constant on magnetic flux surfaces first requires identification of the latter's structure. This is done in ASDEX by applying the method of function parametrization (FP) to magnetic measurements as described in previous annual reports. The further profile fitting proceeds via two parallel routes.

In the first (MULTIPRO), spline fits are applied to the line-integrated (interferometry) or pointwise (laser Thomson scattering, ECE) measured data. These profile fits are typically carried out with a sample frequency corresponding to that of the pulsed Thomson scattering system (60 Hz). They are stored in a data bank together with information that can be directly derived at any time point from these fitted profiles and the results of magnetic measurements. Data of a complete shot are then checked in another routine (ZANA) for the consistency of the energy content as given by kinetic and magnetic data, and used to derive further parameters, such as the energy confinement time, including corrections for non-stationary energy content. These results are then again stored in a data bank.

The second profile production code, FPYAG, performs simultaneous FP recovery of electron temperature and density profiles from Thomson scattering spatial point measurements and poloidal flux, poloidal field and multipole current raw data. For specified discharges, all YAG spectra in a specified time window are processed and the following information is stored on disk: (a) the raw spectra with experimental error bars (b) flux radii for each channel (c) summary geometrical information (d) FP-recovered temperature and density profiles with error bars. The code may be run in batch mode to process as many shots as disk space limitations allow.

Analysis of Mirnov probe measurements: In ASDEX, where Mirnov probes cover a limited angular region of 102° at the outer side and 45° at the inner side of the torus only, it is of special importance to compare experimental results with model calculations.

[1] Theory Division 3
[2] Experimental Division 1

On the basis of a previous theoretical paper[1] the magnetic field code PROBE was developed, destined for the calculation of the magnetic field of given helical surface currents flowing on a rational magnetic surface parallel to the magnetic field of a plasma in equilibrium.

The code predicts a strong outside-inside asymmetry if toroidal effects are taken into account. In particular, the mode structure is distorted to the inner side of the torus, whereas the poloidal wavelengths on the torus outside remain approximately constant for $2 \leq m \leq 4$. It turns out that even the combination of several low m-modes with adjustable phases and amplitudes are not able to explain the observations in "fishbone-like" events of H-mode discharges. Thus, in the framework of this model, "fishbone-like" instabilities are subject to $m > 4$ (see also Sect. 1.4.3).

[1] G. Fussmann, B.J. Green, H.P. Zehrfeld, 8th Int. Conference on Plasma Physics and Contr. Nucl. Fus. Research, Brussels 1980, paper IAEA-CN-38/M-1-3

3. DATA ACQUISITION AND ELECTRONICS

3.1 Data Acquisition

(N. Ruhs, H. Hohenöcker, D. Zimmermann, H. Bauer, H. Blank, M. Harnau, A. Kus, J.G. Müller, T. Wendt)

There were no major changes to the ASDEX Data Acquisition System configuration up to the end of the experimental phase in March 1986. The system was designed to acquire the data for plasma discharges with a duration of up to 3.5 s. Up to 8 Mbyte of data are collected per discharge.

After the hardening phase of the experiment, the duration of plasma discharges will increase up to 5 s. The design work for the required extensions to the data acquisition system as well as for some new diagnostics has been done. Hardware installation is on the way.

The local area network (based on Ethernet hardware) has been upgraded. Experimental data on all the subsystems are now transparently accessible from any user program. Furthermore, the W VII and NET computers have been connected to this network and a better bidirectional link (RSCS with 4800 bit/s) to the Computer Centre and to other IBM-type computers was included in addition to the existing special 2 Mbit/s unidirectional link.

Furthermore, the ASDEX computer has been connected to the Public Switched Data Network (PSDN), which allows, in particular, better cooperation with TEXTOR at Jülich and with experiments in the USA.

Since the amount of experimental data has been growing steadily in the past and will further expand after hardening of ASDEX, online storage of data is a bottleneck. Experimental data will in future be stored on optical disks. Tests have been performed with different disk drives. On the basis of these tests, a storage system with three drives and a capacity of 1 GByte per removable disk was bought at the end of the year. A GKS standard (Graphic Kernel System) software package was implemented in order to reduce the programming effort required for various graphic terminals and various graphic systems on different computers.

3.2 Electronics Development

(F. Schneider, H. Czich, K. Stockinger)

In order to increase the flexibility which has been achieved by standardization of electronic components and systems, a system of distributed microprocessors was designed and partly tested. This is very useful for complicated control tasks and much wiring can be eliminated. For many purposes, however, and particularly for closed loop control, the digital processors are too slow or the programming is too complicated. We therefore designed an analogue processor which can be "programmed" with the screwdriver for any arithmetic function up to the fifth polynominal degree. The response time is about 0.005 ms.

Other design work was done on a new phase demodulator for interferometer signals. It determines the phase information from a 10 MHz signal reliably and linearly over a range of many periods. For fast fluctuation measurements two other outputs are available to show with high resolution the phase within the range of one period up to 1 MHz bandwidth.

For computer control of mechanical movements a stepping motor system was developed and manufactured in many units. These systems are able to operate in a closed loop mode with absolute multiturn position decoders, which eliminates the reference problems coming from mechanical or electrical disturbances.

4. OPERATION OF ASDEX AND THE PREPARATION FOR LONG-PULSE HEATING

4.1 Operation of the Experiment

(H. Rapp, J. Gernhardt, F. Gresser, G. Herppich, G. Klement, P. Krüger, F. Schneider)

In 1986 experiments were limited to the period from January to the end of March owing to the plasma shutdown for the modification of ASDEX for long pulse heating. 1716 discharges were carried out on 36 days, most of them with NI, ICRH or LH. No technical difficulties hampered experimental operation until the last few days when the planned shutdown and a fault at the multipole current feeds coincided.

4.2 The Long-pulse Heating Programme

4.2.1 The need for new target plates

(H. Niedermeyer, H. Rapp, R. Allgeyer, F. Finkelmeyer, H. Hartz, G. Herppich, P. Krüger, B. Quiel, S. Schraub, ASDEX assembly group, Central Technical Services)

The investigation of many plasma physics problems, such as beta limit or current drive studies, needs heating pulses much longer than the characteristic time for current profile changes, which is of the order of 1 s. Plasma-wall processes, which are especially important for impurity and divertor studies, have an even longer time scale. A long-pulse heating programme was therefore initiated in 1981. The heating methods will involve NI and ICRH with a pulse length of 10 s and powers of 3 and 4 MW, respectively. A new LH system just under construction will contribute another 3 MW of heating power for 1 s (see Sect. 5).

As a result, the total energy supplied to the plasma can reach a value of about 60 MJ. Already in 1981 it was clear that the titanium target plates of the divertor would not withstand this load, which exceeds the design value by a factor of more than 30. Moreover, the protection plates for the multipole coils in the vacuum chamber were not adequate. Both the target plates and the protection plates were radiatively cooled. Their heat storage capabilities were highly insufficient to protect the mutipole coils from damage due to high temperature.

Experimental proof of this statement was provided very early during the ASDEX experiments when fixing bolts of the target plates broke owing to high thermal heat flux and mechanical shrinking afterwards. The target plates were deformed, resulting in severe damage. In 1984 and 1985 melting at the edges of the target plates was also observed (Fig. 68). The total energy input therefore had to be limited to approximately 2 MJ which severely hampered the experimental program during the latter period.
When the vacuum vessel was vented in March 1986, a new type of damage was observed: at the inner side of the lower divertor many target plates were partially cut through by a focused beam of fast electrons all around the torus (Fig. 68b)[1]. The width was only 2 to 3 mm and the power density reached values of up to 2 kW/cm^2 for about 1 s. The mechanism is not yet clear but there is some evidence that suprathermal electrons were generated during experiments with lower hybrid waves at low densities.

For the new target and coil protection plates a solution based on a water-cooled structure was chosen. It is a distinct advantage of actively cooled target plates that a steady-state temperature can be reached on a short time scale, which eases the study of plasma wall interaction. The protection for the smaller multipole coils consists of stainless-steel tubes, whereas the target plates at the inner big multipole coils consist of copper and include the coil protection. The water-cooled copper bars are brazed on steel backings for mechanical support. All structures are meander-like to keep eddy currents and mechanical stresses as low as possible (Fig. 69). The choice of copper as the target surface material is a result of balancing technological and physics arguments. Meanwhile, we learned from preliminary experiments with copper-coated titanium plates that the sputtered impurity flux in the medium electron density range is very low. Heat flux tests at Sandia Laboratories confirmed our calculations that the copper surface temperature stays below a

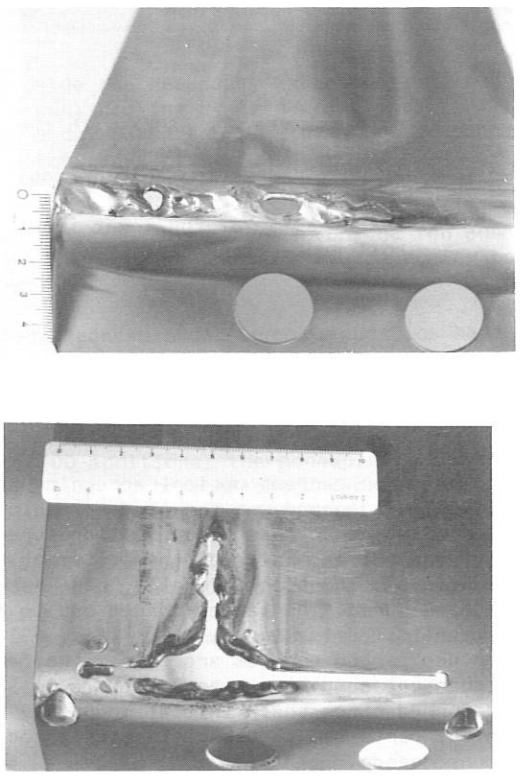

Fig. 68: Damage of the ASDEX titanium target plates. a. thermal overload at the edges, b. cutting by fast electrons.

[1] H. Rapp, H. Niedermeyer, et al., 12th Symp. Fus. Techn., Avignon 1986

tolerable level of 200° C for peak power densities of up to 330 W/cm^2, as derived from ASDEX experiments. Even power densities of 1 kW/cm^2 did not cause surface damage. More refined calculations simulating focused heat fluxes, as mentioned above, yielded surface temperatures which are below critical values.

a

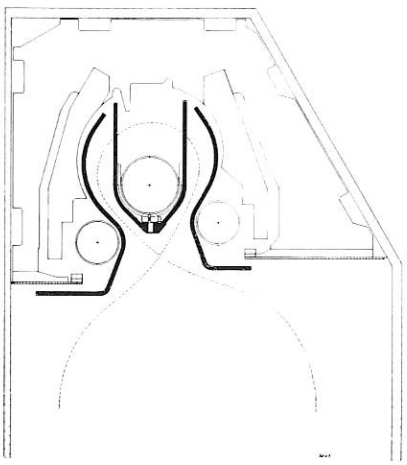

b

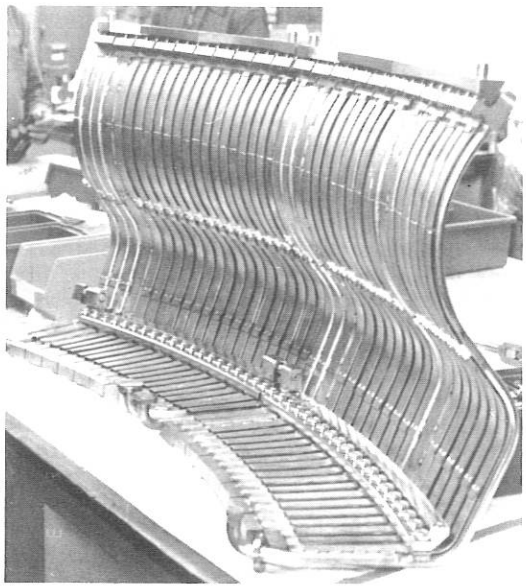

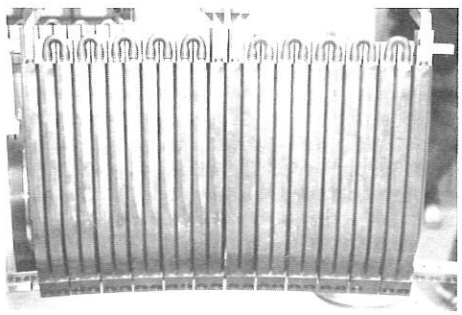

c

Fig. 69: a) poloidal view of ASDEX with the new divertor target plates.
b) 1. coil protection shield (top) and 2. target plate (bottom).
c) installation of the lower inner coil coil protection shield.

4.2.2 Repair Work and Installation of New Protective and Target Plates

Prior to the installation of the new integrated target and divertor plates difficult repair work at the casings of the multipole current leads had to be carried out. These Inconel casings with rigid sections alternating with bellows of 0.2 mm thickness have become a serious problem during he last few years, causing many shutdowns due to vacuum leakage. Also the contacts of the current feeds for the multipole coils had to be renewed. Furthermore, a broken current lead to the OH transformer had to be repaired.
Construction of the new protective shields and target plates had to meet several conditions. The first was the tight space around the divertor coils and the need for perfect optical screening against the plasma. The second was the need to avoid high eddy currents and to take the resulting forces. Thirdly, thermal expansion of the equipment had to be taken into account and, finally, easy assembly had to be assured. The latter turned out to be a severe problem during installation (Fig. 69). Another unexpected problem arose from the fact that the mechanical support of the multipole coils had been deformed since their initial mounting. Many mechanical parts had to be substantially modified as a consequence.

The four toroidal target plates consist of 32 meander segments. Target plates and protection shields together with the water pipes have a surface area of about 130 m^2 and a mass of 1300 kg

copper and 4100 kg steel. The need for active cooling during plasma heating caused parallel feeding of the water to the neutralizer plate segments. It was therefore necessary to install 256 water feedthroughs in the vacuum vessel. The topological design of the cooling circuits was governed by the need for quick and precise vacuum leakage testing. There are 10 separate cooling circuits for the different protection shields and target plates in the upper and lower divertor.

By the end of 1986 the new upper divertor was completed and the extremely difficult installation of the inner protection plate in the lower divertor was successfully finished. The cooling systems for the target plates and for the long-pulse NB systems have been commissioned. The piping is proceeding on time. The diagnostic equipment is being reinstalled, as also are the NB boxes. ASDEX is expected to be in operation again at the end of March 1987.

4.2.3 Long-pulse Beam System
(E. Speth, J.H. Feist, K. Freudenberger, S. Götz, J. Kolos, R.C. Kunze, H. Lohnert, W. Melkus, W. Ott, F.P. Penningsfeld, H. Riedler, J. Sielanko, A. Stäbler, O. Vollmer, K. Wittenbecher, Neutral Injection Group (Technology Division))

During shutdown of ASDEX, the NI system has been prepared for long-pulse operation. The grids of the ion sources and the beam dumping elements of the beam line are now actively water-cooled and allow pulse lengths of up to 10 s. Besides these modifications, many changes within the supporting system have been required by the increased pulse length.

- To provide the necessary water cooling, two additional cooling systems were installed.
- Light decel power supplies have replaced the capacitor banks hitherto used.
- The deflection magnets need more powerful supplies.
- A newly designed gas supply for the ion sources allows a change of the working gas during tokamak operation.

Additional controls and beam diagnostics have been implemented for the long pulses

- Two programmable controllers (S5-Simatic) are used to extend the existing system.
- About 100 additional thermocouples allow the power flows to be monitored. Overheating of critical components by the beams will result in beam switch-off.
- H_α measurements will be performed in the duct region to estimate the pressure rise during the beam.
- The species ratio can be measured by Doppler shift spectroscopy.
- A Micro PDP for NI data acquisition is in operation.

The NW beam line is already completely connected and the modified supporting systems have been tested for short-pulse operation with one ion source. Long-pulse operation with four ion sources will be possible by the end of March 1987.

4.2.4 Long-pulse ICRH System
(F. Wesner, J. Bäumler, W. Becker, F. Braun, R. Fritsch, F. Hofmeister, E. van Mark, J.-M. Noterdaeme, S. Puri, M. Söll, K. Steinmetz, H. Wedler (Tech. Division)

Since the major components of the ICRH system for ASDEX and W VII had already been designed for 10 s pulses right from the very beginning, only parts of the antenna had to be exchanged for long-pulse heating by water-cooled elements. But further improvements have been developed and installed in the RF generators and in the coaxial transmission lines in order to increase the power capability.

Concerning the antennae, the largest effort was the development of water-cooled Faraday screens. This development, already described in the Annual Report 1985, and the fabrication of the screens have been completed. The centre conductors have also been replaced by coolable ones, while the return conductors remain largely unchanged, but being cooled, too, by the water manifolds of the screens. The antenna protecting limiters were already designed for water-cooled operation (see Technology Division, Sect. 2.1).

Tests had shown the capability of the high-power tetrodes used in the RF generators to provide an output power of 2 MW each. So the generators could be upgraded by modifications of the control, power supply and cooling units. Modifications in the high voltage supply system and separate supply units for the driver amplifier, which have been prepared and ordered, will allow an output of 2 MW even under mismatched conditions with a VSWR (voltage standing wave ratio) of up to 1.5 in the second half of 1987.

Long-pulse investigations at the test bed showed that the coaxial transmission lines need not be actively cooled for long-pulse heating and do not have to be varied owing to the longer pulses. But since the heating power was often limited by the voltage strength of the lines, all vacuum feedthroughs and ceramic insulators in the vacuum- and pressurized line segments have been replaced by elements with a larger voltage strength, developed at the ICRH test bed (see Technology Div., Sect. 2.3).

These improvements of the system should not only allow heating with long pulses of up to 10 s, but also extend the power capability of the ICRH system and improve its insensitivity to changes of the antenna coupling, e.g. at H-mode transitions.

In collaboration with Ecole Polytechnique Fédérale de Lausanne an Alfvén wave heating experiment is under preparation and should be performed in 1987.

5. CONTINUATION OF THE LOWER HYBRID PROGRAMME IN ASDEX

(in collaboration with F. Leuterer, M. Münich, H. Zouhar, LH-group Techn. Division)

As the current density distribution due to lower hybrid current drive (LHCD) will be determined by the absorption of the waves and the local current drive efficiency, its profile will be decoupled from that of the electrical resistivity. This leads to significant deviations from the steady-state ohmic current distributions. Proof of this has been obtained in ASDEX from the observed stabilization of the sawtooth oscillations, but in particular also from direct determination of the current density distribution. The latter was carried out by means of Zeemann splitting measurements using a neutral lithium beam probe and is in agreement with the observed reduction in the internal inductance l_i as determined from magnetic measurements. Both these direct measurements as well as the indications from MHD activity changes show a broadening of the current density distribution upon application of LHCD.
The current profile modifications do not depend on the fraction of RF-driven current, but also on the shape of the launched wave spectrum. Waves with higher $N_{\parallel}$ are absorbed radially further outward. Corresponding measurements are described in Sect. 1.7.

With the 1.3 GHz LH system these phenomena could, however, be studied in ASDEX at only relatively low densities, $\bar{n}_e \lesssim 1.6 \times 10^{13}$ cm^{-3}. In order to improve our understanding of phenomena linked to the current density profile, especially in combination with strong plasma heating, we have to operate at higher densities for ICRH and NI.
For this purpose, a 2.45 GHz/3 MW/1 s lower hybrid system will be built in collaboration with ENEA-Frascati and PPL-Princeton (see Technology Division, Sect. 1). At this frequency the critical density for the beginning interaction with ions is above 10^{14} cm^{-3}, and we expect that, with a power of 3 MW, we can achieve sawtooth stabilization and significant current profile modification up to densities of $\bar{n}_e = 4 \times 10^{13}$ cm^{-3}. The grill will consist of two horizontal rows of 24 waveguides each with a nominal $\langle N_{\parallel} \rangle$ of 4.4 at $\Delta\phi = \pi$. It will be fed by 6 klystrons. External power splitting and mechanical phase shifters allow one to launch a wide variety of $N_{\parallel}$-spectra, such as symmetric spectra, current drive spectra and opposite current drive spectra. $\langle N_{\parallel} \rangle$ can be varied from low values satisfying the accessibility condition up to 4.4. Different $N_{\parallel}$-spectra at equal or different power levels can be launched with the top and bottom grills. In this way we expect that the current density profile can be locally modified over a wide range.

The principle aim of the experiments planned in ASDEX is the study of synergetic effects of LH current profile modification and high-power additional heating and energy confinement with dominant LH heating. Major subjects are:

(1) to study scaling of sawtooth suppression in the presence of strong ICRH and NI in particular to explore lower limits on power thresholds by using $N_{\parallel}$ shaping,

(2) to understand the mechanism responsible for profile consistency and the associated confinement behaviour by decoupling the electron temperature from current density profiles,

(3) to study the effects of the current profile on β-limits:
a) to verify the present interpretation of the observed reduction of the β-values during the pulse (see Sect. 1.4) as a consequence of flattening current profiles; LH provides the means of high-power heating into discharges with different current density profiles,
b) to test predictions of the possibility of access to a mixed 1st/2nd stability regime by impressing a flattened current density profile with a central q-value significantly above 1 (≈1.5),

(4) to study the effect of current profiles on the access and the properties of H-mode confinement.

The experiment is planned to be operating at full power level in autumn 1988. It will be performed in cooperation with scientists from ENEA-Frascati and PPL-Princeton.

ASDEX Upgrade Project

Head of Project: W. Köppendörfer

ASDEX Upgrade Project Group:

M. Blaumoser, S. Cha, K. Ennen, J. Gernhardt, J. Gruber, D. Jacobi, H. Kollotzek, E. Lackner, V. Mertens, M. Pillsticker, H. Preis, W. Reese[1], G. Reichert, K. Schindler, H. Schneider[2], G. Schrembs, S. Schweizer, U. Seidel, B. Streibl, M. Troppmann, H. Vernickel, F. Werner, A. Wieczorek

Tokamak Theory Group:

R. Chodura, K. Grassie, O. Gruber, S.C. Jardin[3], K. Lackner, J. Neuhauser, R. Weiner

Central Technical Services:

H. Gillhuber, H. Goss, R. Hadersbeck, A. Hasenmiller, W. Jakobus, S. Kamm, M. Kluger, H. Kosniowski, M. Kottmair, H.J. Kutsch, E.M. Maier, R. Mathis, S. Mukherjee, B. Sombach, E. Trcka

JET Diagnostik Group:

C. Andelfinger, E. Buchelt, Ch. Dorn, K.F. Mast, E.R. Müller, D. Pohl, H. Röhr, G. Schramm, J. Sommer, M. Ulrich, G. Weber, D. Zasche

Neutral Injection Group:

J.H. Feist, K. Freudenberger, S. Götz, J. Kolos, R.C. Kunze, H. Lohnert, W. Melkus, W. Ott, F.P. Penningsfeld, E. Speth, H. Riedler, J. Sielanko, A. Stäbler, O. Vollmer, K. Wittenbecher

Ion Cyclotron Resonance Heating Group:

J. Bäumler, F. Braun, R. Fritsch, F. Hofmeister, E. v.Mark, J.M. Noterdaeme, S. Puri, M. Söll, K. Steinmetz, H. Wedler, F. Wesner,

Other Groups:

M. Mahl, G. Mannhardt, G. Venus

1) Noell, Würzburg
2) Interatom, Bensberg
3) PPPL, Princeton

1. SUMMARY AND STATUS OF THE PROJECT

The efforts being made in the construction of ASDEX Upgrade encompass several areas of engineering and physics work /309/. The physics work during 1986 concerned refined plasma equilibrium and poloidal field coil current calculations, stability calculations of divertor configurations, the development of measurement interpretation codes of general validity and applicability, and the problem of plasma configuration description suited to plasma shape and position control.

The engineering work was concerned, in part, with the tokamak system and its components and, to an increasing extent, with the installation in the periphery of the tokamak system, which comprises energy supply circuits, cooling facilities, control system and heating systems. Experts of the computing science division were concerned with the construction of the data acquisition system in hardware and software.

Progress with the tokamak system in 1986 was determined by the fabrication of all major components, some of which have already been delivered. After some delay, manufacture of the toroidal field coils and toroidal field coil support structure is now proceeding smoothly. All poloidal field coils are in fabrication, some being completed and already delivered. The poloidal field coil support structure was delivered in summer 1986 and assembly of the bottom part has started. Production of the vacuum vessel is now making fast progress after assembly of the phototype octant and testing of insulation flange. The contract for fabrication of the holding fixtures for the poloidal field coils was signed in December 1986 with a French producer.

All auxiliary gear for the torus octant assembly was delivered during 1986, and assembly has begun.

In the periphery, construction of the energy supply circuits and cable connections is well under way. The cooling systems for all coils and the cooling and heating system for the vacuum vessel were ordered.

In the following, the progress and achievement of this work are described in detail.

At present, the construction time schedule of ASDEX Upgrade is one year behind time. This is because the start of production of the TF coil and the overturning force support structures has been delayed. Other components seem to be uncritical in this respect. Several alternatives for the torus and poloidal field system assembly have been worked out and the necessary auxiliary equipment provided. A rail system, for example, allows the TF magnet with vacuum vessel to be moved away so that the lower PF coils can be put in place after TF magnet assembly. This was done in order to compensate possible delay of certain components. Commissioning of the ASDEX Upgrade tokamak system is therefore anticipated early in 1989.

2. CONSIDERATIONS ON PHYSICAL AND TECHNICAL PROBLEMS

2.1 Numerical Simulation of the Dynamical Plasma Evolution at ASDEX Upgrade

The dynamical behaviour of plasma equilibria in ASDEX Upgrade is studied using the Princeton tokamak-simulation-code (TSC). This free boundary axisymmetric simulation code models the resistive time scale evolution of a toroidal plasma, including its interaction with poloidal field coils and other nearby conductors. The circuit equations for the ohmic heating, equilibrium fields and poloidal field systems are solved simultaneously with the plasma equations.

We apply the code to study the passive and active feedback system of ASDEX Upgrade needed to control axisymmetric instabilities of the vertically elongated plasma with single- and double-null configurations. Passive plates are needed to slow down the growth rates from the Alfvén-time scale to moderate one's and have a L/R-time of 400 ms. The residual growth time (τ_r) of double-null-equilibria at low β_p ($\beta_p \approx 0.1$) was found to be: $\tau_r \leq 50$ ms, so that the ratio of the stabilizing force, due to the passive elements, to the destabilizing force is given by: $F_{stab}/F_{instab} \approx 1.125$, which is in reasonable agreement with the result of quasistatic calculations with fixed plasma shape. For single-null-low-β_p-equilibria the residual growth time is somewhat larger.

At present we are investigating the vertical instability of high-β_p-equilibria. The effect of active control coils inside and outside the toroidal field coil, which are used to feedback the radial and vertical position of the plasma and to control the residual resistive instability is also studied.

Finally, calculations showing the plasma evolution during the start-up phase, where the plasma evolves from an inside limiter bounded circular plasma to the final divertor configuration have been performed (see: Anual Report 1985).

2.2 The Poloidal Stray Field Outside the Tokamak System

The PF coils positioned outside the TF magnet produce in the reference single-null (SN) divertor discharge (I_p = 1.6 MA) a poloidal return flux of up to 14 Vs in the horizontal midplane at $R \geq 5$ m. At R = 5 m the value is B_{ps} (R = 5) $\lesssim$ 0.1 T, decaying approximately as R^{-3} to the outside. Certain installations, such as the neutral injector, the turbomolecular pumps and diagnostic apparatus, need to be shielded. Individual shielding by iron casings would result in an iron distribution around the torus which would distort the toroidal symmetry of the poloidal field. Dangerous magnetic islands with an n = 1, 2 structure would result. A 3D computer code (PROFI) was therefore used to calculate the stray field reduction in space by means of large iron columns periodically distributed around the torus. Sixteen vertical iron beams 3.5 m long and a cross-section of 0.4 m² produce a "shadow" zone in the stray field in which the field is strongly reduced a few metres outside the columns, but by only 20 % farther out. The columns are dimensioned such that the induction in the iron just fails to saturate. Since the ion deflection magnet of the neutral injector has about the same iron mass as one shielding column, the deflection magnet and shielding concept is at present being investigated in cooperation with the Neutral Injection Group. The object is to integrate the deflection magnet iron into the shielding iron mass and to minimize the amount of iron required.

2.3 Numerical Analysis of Eddy Currents and Magnetic Forces in the Vacuum Vessel

The magnetic field diffusion through the toroidal vacuum vessel and the resulting eddy current distribution of the ASDEX Upgrade tokamak that occurs on sudden disruption of the plasma current was numerically investigated. The ring-shaped plasma in the single-null configuration considered here occupies an asymmetric position in the vessel.

The diffusion process was calculated by an approximation method, the finite-element network method (FEN). The basic idea of the FEN is that the field-permeated structure, i.e. in the present case the vacuum vessel, is subdivided into finite elements, according to distinct rules[1]. These elements can be regarded as longitudinal or transverse branches of a passive three-dimensional electric RL network. Besides the conductive connections which the branches have in the nodes of the network, all branches are inductively coupled with one another and with the external circuits, which generate the diffusing field. The external circuit in this investigation is the loop current of the plasma, which, when varying in time, excites the passive RL network. The eddy currents are then calculated as transient branch currents of the network. The only constraint of the FEN is the requirement that the current density be constant within a finite element. This condition is satisfied in good approximation when the cross-sectional dimensions of the finite elements are chosen smaller than the penetration depth $\delta = (\mu\kappa\omega)^{-1/2}$. The FEN was incorporated in the FEDIFF computer code, with which the following individual calculation steps were performed:

[1] H.Preis, Die Finite-Element-Netzwerkmethode für dreidimensionale Wirbelstromberechnungen in Experimenten zur kontrollierten Kernfusion, Archiv für Elektrotechnik 65 (1982) 233-239.

- subdivision of the vessel into finite elements and calculation of their inductances and ohmic resistances
- calculation of the mutual inductances between the finite elements and the field-producing circuits
- development of the electric network with allowance for topological links
- solution of the network differential equation and calculation of the eddy currents
- calculation of the eddy current fields
- calculation of the magnetic forces.

Due to the single-null divertor configuration the eddy current and force distribution had no top-bottom symmetry to the torus midplane. The originally symmetric FEDIFF computer code had to be extended and adjusted to this situation. The results are discribed in detail in /IPP 1/229/.

3. THE ASDEX UPGRADE TOKAMAK SYSTEM

3.1 Toroidal Field (TF) Magnet

3.1.1 TF coils

3.1.1.1 Status of work

When the last manufacturing test had demonstrated the feasibility of simultaneously assembling the upper and lower pancakes of a coil, assembly of the prototype coil (spare coil) was started in the middle of the year. At the end of 1986 two coils were assembled (Fig. 1) and the prototype coil cured.

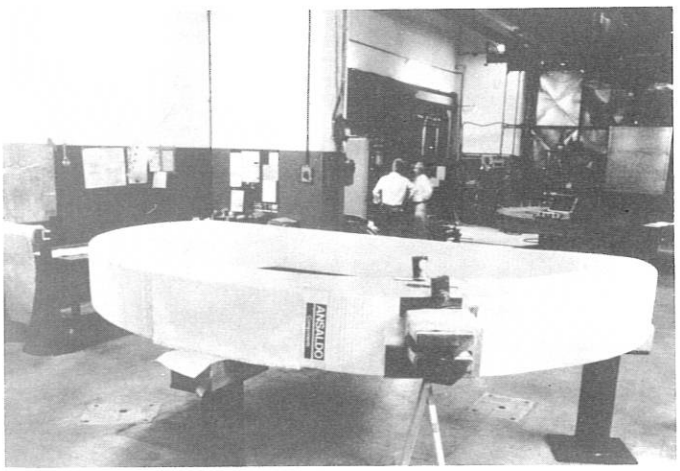

Fig. 1: The TF prototype coil with ground insulation at ANSALDO.

3.1.1.2 Inductive brazing

The brazing cycle was feedback-controlled. The butt joint pressure and the generator power are now switched by the voltage of a thermocouple near the joint location. A safety timer limits the brazing temperature to below 850° C in case the feedback system fails.

3.1.1.3 Resin for coil impregnation

The flexibilizer content of the resin was optimized by means of fatigue tests with a tubular torsion specimen. The results showed that a flexibilizer content of 5 parts of weight (POW) is too low for the combination of ARALDIT F with the hardener HT 907. With 10 and 15 POW an almost identical improvement resulted and the envisaged target with a shear strength of above 20 Mpa for more than 20,000 cycles could be safely verified at 60° C /437/. As a consequence the flexibilizer content was finally fixed at 12.5 POW.

3.1.2 Turnover structure (TOS)

3.1.2.1 Status of work

In 1986 four octants of the TOS were cast and the first octant was rough machined (Fig. 2). After tests with the pilot casting had achieved a high machining accuracy for the main flanges, the final machining of the first octant was started at the end of the year.

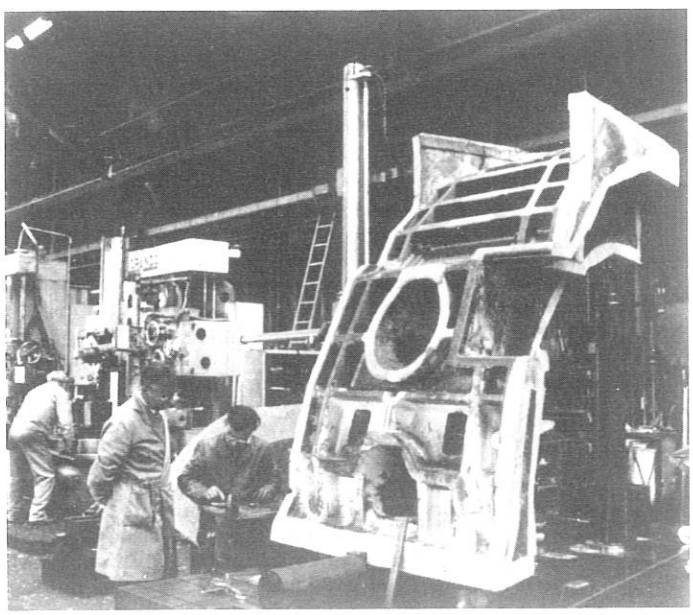

Fig. 2: A turnover force support sector on the measuring stand.

3.2 Poloidal Field (PF) Coils

3.2.1 Status of work

The PF coils OH2 and V2 have been produced and already delivered to IPP by BBC Neusäss. They have passed the preliminary but fundamental tests for insulation and leakage. The outer PF coils V2, OH3, CoOH, CoA and OH1 are still being manufactured

by BBC Mannheim and Neusäss and the V3 coils by Laborde et Kupfer in Lyon. The two CoI coils will be manufactured by BBC Neusäss. This contract was signed in December 1986. The concept, the manufacturing and tests are described in /463/.

3.2.2 Problems of manufacturing

Investigations with an OH1 prototype coil show that the production method proposed has to be changed. The pressure of the internal ground insulation must be reduced in order to avoid damage when impregnating the coil. Special tests with improved tools were successful.

The procedure for manufacturing the CoI coil was exactly defined in detail. These coils are divided into two halves each and will raise new and difficult manufacturing problems not encountered with the other coils. We decided to form the profiles of the joints combining the half rings to a coil after the insulation is completed. This ensures an accurate fit. The insulation system within the joint region was tested for function and mounting. The current terminals will consist of a three-conductor system, so that the resulting forces to the terminal will be minimized.

3.2.3 Poloidal field coil holding fixtures

The coil holding fixtures mechanically connect the PF support structure and the PF coils. They allow different movements of the support and coils, thus preventing overstressing of the coils.

The coil movements are permitted by a slide mechanism or swing joints. The holdings will be manufactured from stainless, non-magnetic steel, in some parts extremely high strength is needed. The contract for manufacturing was conducted in December 1986 with Jeumont-Schneider. All the critical components, such as axial and swinging joints and variable spacers, will be produced by industrial companies having special experience.

3.2.4 Connections for power and cooling systems

The principles of the connections between the PF coils and their electrical power supplies and between the coils and the cooling system were defined and some of the components have already been tested. A current connection element has elastic coupling links to the transmission lines from the power supply and to the coil leadings. These elements also include insulating tubes from the transmission lines and the coil cooling loops to the cooling system. All the other cooling loops of the coils are connected to the cooling system just with insulation tubes. The quality of flow within the different cooling loops will be adjusted by orifice plates. The usability of different flowmeters within magnetic fields still has to be checked.

3.2.5 Experimental coil control

The concept for controlling the coils under experimental conditions was defined and some details have already been developed. To ensure precise cooling of the coils, the flow of each cooling loop has to be controlled. Besides permanent control of the current and voltage, high-voltage pulse control by an overload safety switch is obviously needed for protecting the coil insulation.

The ratio of the coil currents under experimental condition is variable and is so far imprecisely defined. This means that the stress of the coils cannot be exactly predetermined. Therefore we have to control the coil stresses permanently during a current pulse by measuring time-dependent values giving the input for computer-supported stress calculations at critical points within the coils and comparing with permissible stress values.

Moreover, we have to control movements of the coils within the tokamak system.

3.3 The Poloidal Field Coil Support Structure

The PF coil support structure was completed in 1986 after two years of construction at DWE (Deggendorfer Werft und Eisenbau). It was delivered to IPP after test assembly and quality control at the factory. Two kinds of austenitic steel materials were used. The central shaft consists of a modular cast GGG Ni Mn 13.7 produced by Buderus (Fig. 3). The outer framework was made from welded double T-bars using an austenitic CrNi steel (X2 CrNiN 1810) of the type 304 LN (DIN 1.4311) (Fig. 4).

The annealed cast steel of the central shaft shows excellent quality with regard to ductility, ductile yield and impact value (Table I). These features, the low permeability and the low electrical conductivity determined the choice of this material. The latter reduces induced eddy currents.

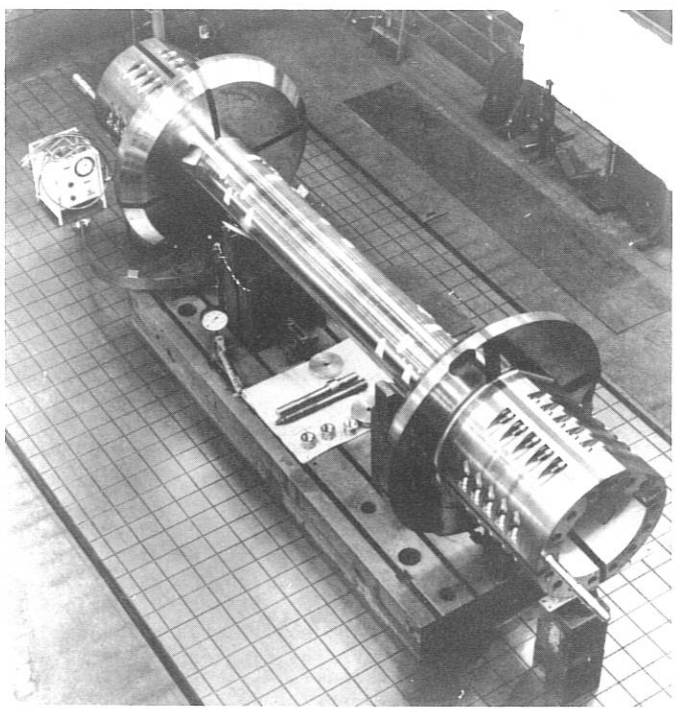

Fig. 3: The central shaft of the PF coil support structure.

The nitrogen dosed SS 304 LN exibits increased strength with a negligible reduction of ductility. Other elements, such as Mo, Nb, Ti, Ta, which usually improve corrosion resistance turned out to be of no importance for the present application. High strength and low permeability were only obtained with the elements Cr, Ni, N, C (Table II). The low permeability could also be preserved after machining and welding. Each manufacturing step, however, required care and strict welding material selection. The low heat conductivity required careful design of welding seams and a programmed welding sequence. Deformations caused by welding were flame-corrected but temperature-limited to $\leq$ 650° C.

As welding material nitrogen dosed austenitic steel X2 CrNiMnMoN 2016 (DIN 1.4455) was used throughout.

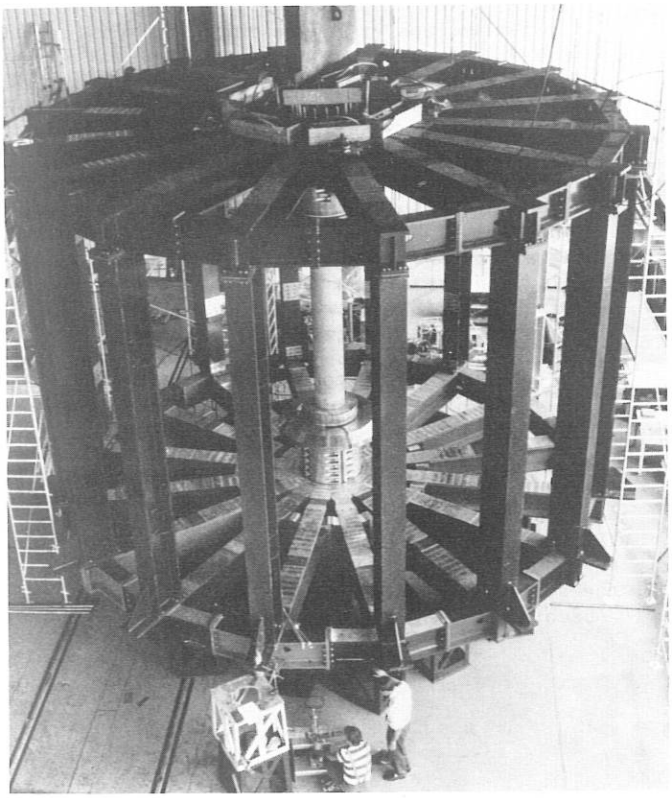

Fig. 4: The PF coil support structure at preassembly.

Table I: Physical and mechanical properties of GGG NiMn 13 7 at ambient temperature.

Spec. weight	$7.3 \cdot 10^3$ kg m^{-3}
Modulus of elasticity	$145 - 154 \cdot 10^3$ N mm^{-2}
Tensile strength	456 - 545 N mm^{-2}
$\sigma_{0.2}$-limit	250 - 303 N mm^{-2}
Ductile yield A_5	22 - 41 %
Notching resistance	$\sim$ 23 J
Electric conductivity	1.0 mΩ^{-1} mm^{-2}
Heat conductivity	12.6 W m^{-1} K^{-1}
Magn. permeability	1.03 - 1.2

Table II: Physical and mechanical properties of X2 CrNiN 1810 at ambient temperatures.

Spec. weight	$7.9 \cdot 10^3$ kg m^{-3}
Modulus of elasticity	$195 - 198 \cdot 10^3$ N mm^{-2}
Modulus of shearing stress	$75 \cdot 10^3$ N mm^{-2}
Tensile strength	605 - 658 N mm^{-2}
$\sigma_{0.2}$-limit	306 - 382 N mm^{-2}
Ductile yield A_5	> 46 %
Notching resistance	270 J
Electric conductivity	1.37 mΩ^{-1} mm^{-2}
Heat conductivity	15 W m^{-1} K^{-1}
Magn. permeability	1.01 - 1.02

3.4 The Vacuum Vessel

As described previously, the vacuum vessel is a rigid, self-supporting structure. The main forces acting on the vessel are the atmospheric pressure and the electromagnetic forces during a plasma disruption. The vessel octant is the unit of fabrication and delivery. At the assembly site the octants will be equipped with 2 toroidal field coils and the corresponding shear structure, and these units will then be assembled to form the torus. The octants will be connected by welding. Figure 5 shows a CAD representation of the vessel, obtained by combining the octants in their state of delivery, the external tubing and thermal insulation being ommited.

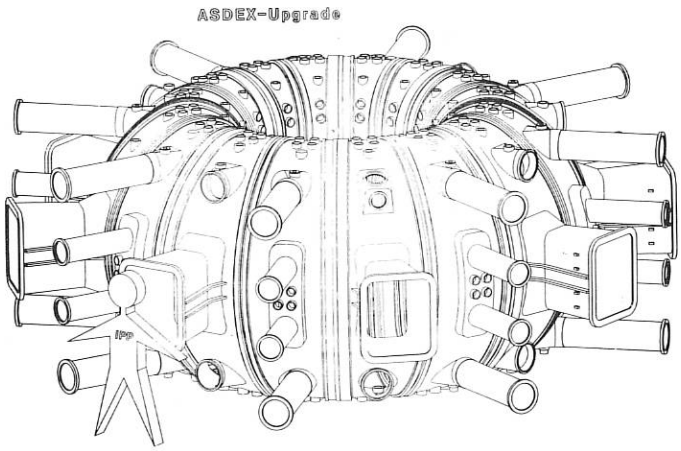

Fig. 5: A CAD drawing of the ASDEX Upgrade vacuum vessel consisting of eight equal octants.

In order to get sufficient toroidal electrical resistivity, each octant contains an electrically insulated screw and shear bolt connection. Vacuum integrity is ensured by bellows which also defines the toroidal electrical resistivity. The vessel is stiffened by flanges at the insulation joint as well as close to the welding position.

3.4.1 Construction

Construction of the vessel octants is well advanced. Most individual parts have been manufactured. Assembly and final machining of the octants are under way. The various octants are in different stages of assembly. The prototype octant is finished, the final vacuum test successfully performed in mid-December. The first regular octant will be delivered around April 1987.

After some additional testing at IPP it will then be ready for torus assembly. Two details of the vessel construction are described in the following.

3.4.2 Insulating joint

The mechancial load on the insulating joint is complex. The atmospheric pressure, causes primarily a pressure between the flanges and tension on the inside of the vessel. To prevent gaping, the tension bolts have to be prestressed. The saddle currents that are caused by plasma disruption flow primarily in the flanges on both sides of the insulator in opposite directions. In combination with the toroidal magnetic field they cause shear forces that have to be absorbed by shear bolts. The insulation between the flanges is 1 mm thick glass-fibre tissue with phenolether resin, and the shear bolt cavities are filled with resin. Several bake-out cycles with intermittent re-strengthening of the tension bolts ensure that lateron no setting of the insulation occurs that would lead to loss of prestress. The technical details and the prefabrication testing of the insulating flange connection are described in detail in /311/.

3.4.3 Mechanical test of bellows

The bellows were loaded by atmospheric pressure. In case of disruption the toroidal components of the induced currents flow through the bellows. Their interaction with the external magnetic fields gives rise to a complicated force distribution. Experimental simulation of these forces is not practicable. One therefore has to rely on finite-element stress analysis. In order to test the calculations the FE-model was also used to calculate the mechanical (elastic) deformation of the bellows under external pressure and this was compared with measurements performed in the prototype bellows. In accordance with expectations the maximum deformation was found at position B (Fig. 6). The deflection was 0.65 mm/bar as compared with a calculated value of 0.47 mm/bar. Similarly, the deformation at position F is 0.18 mm/bar, that calculated 0.14 mm/bar. This agreement is satisfactory. (The calculated results are from a report by W. Stohler of the firm of Sulzer.) The test pressure was raised to 3 bar without buckling of the bellows. We conclude that the mechanical performance of the bellows is satisfactory.

3.4.4 In-vessel components

No major changes occured in the design of the divertor plates and heat shield. The call for tender for the metal parts was sent out for some of them and will soon be distributed for the rest.

Hydrogen, neutralized at the divertor plates, will

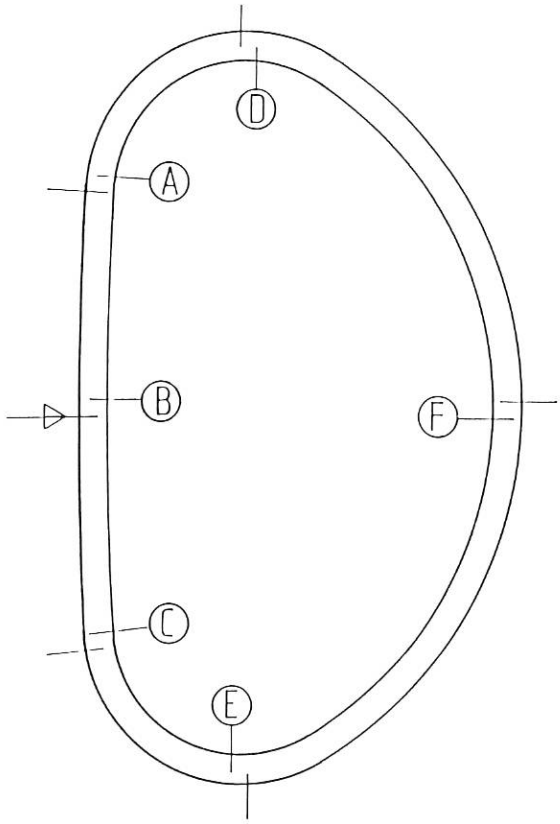

Fig. 6: Bellow cross-section with measuring positions.

largely be re-ionized in the plasma in front of the plates. Neutral hydrogen escaping will either enter the pumping ducts or escape the divertor area and be ionized in the main plasma chamber. The latter is undesirable and therefore the bypasses will be closed by the shielding plate and the separating plate as indicated in Fig. 7 (see "Abschirmblech" and "Trennbleche".

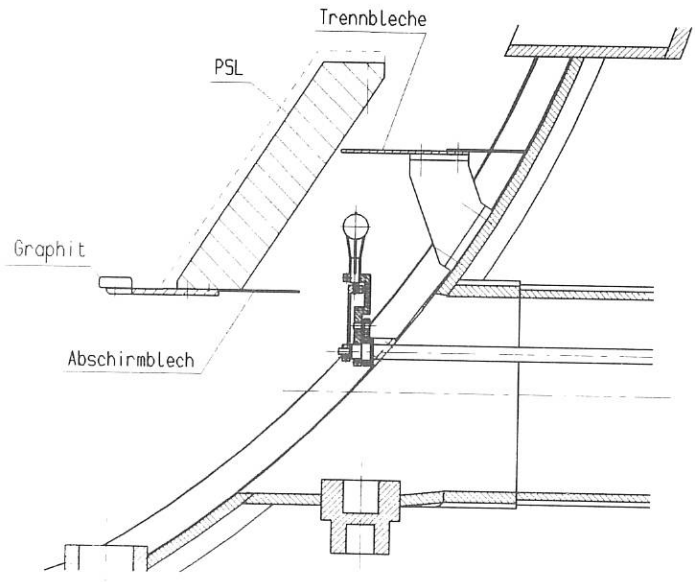

Fig. 7: Divertor chamber with closed bypass and Ti-evaporators.

In case the walls are saturated during high-density long-pulse (~ 10 s) shots, density control would depend on external pumping. Calculations indicate that the external pumps will remove all the gas introduced by neutral injection but there is no large safety margin. Four titanium evaporators are therefore being installed (Fig. 7). Increased pumping speed may be obtained by evaporating titanium on the walls of the divertor chamber.

3.4.5 Torus pumping system (TPS)

Construction of the TPS by industry has begun. The TPS power supply system and control electronics were defined and ordered.

3.5 The Tokamak System Assembly

During 1986 all major auxiliary equipment for assembly was delivered, put together, and is now being tested. The octant assembly mechanism was already installed in spring 1986. It serves to slide the TF coils over the vacuum vessel octants and to insert the sectors of the turnover force support structure. This octant assembly stand was tested by using a dummy TF coil of the actual size and weight. The torus assembly framework was delivered and erected in summer. It includes a two-rail system on which first one torus half and later the whole torus (400 tons) have to be moved. Sliding foils cover the raisl, which provide a friction coefficient of $\mu = 0.04$. During commissioning the system was tested in the factory with a dummy load of 200 tons. Before erection of this framework, the torus support columns had been put in place and a screw lifting mechanism installed its purpose being to lift the bottom spoke-wheel of the PF coil support structure during assembly (Fig. 8). This spoke-wheel was also put into place. In preparation for assembly, scaffolding was arranged around the assembly installations.

The above described work required fixing of all important axes and planes and setting of the measuring marks.

3.6 Plasma Control

A first design of a feedback system for the control of plasma position (vertical and horizontal) was completed in the context of our collaboration with the Institut für Steuerungs- und Regelungstechnik, TU München. It is based on a lumped-parameter model of rigid global plasma movements and employs the principle of decoupling to achieve multivariable control.

Considerations on the integration of such a positional feedback system into a more general concept of experimental control has led to the identification of additional control tasks, which must be taken care of by a special "discharge control system" with real time capacity. One of its coordinating and supervising functions should be the systematic generation, correction and automatic control of all currents relevant to plasma shaping.

The numerical basis for this function can be provided by an extended utilization of function parametrization (FP). Applied to a corresponding ASDEX

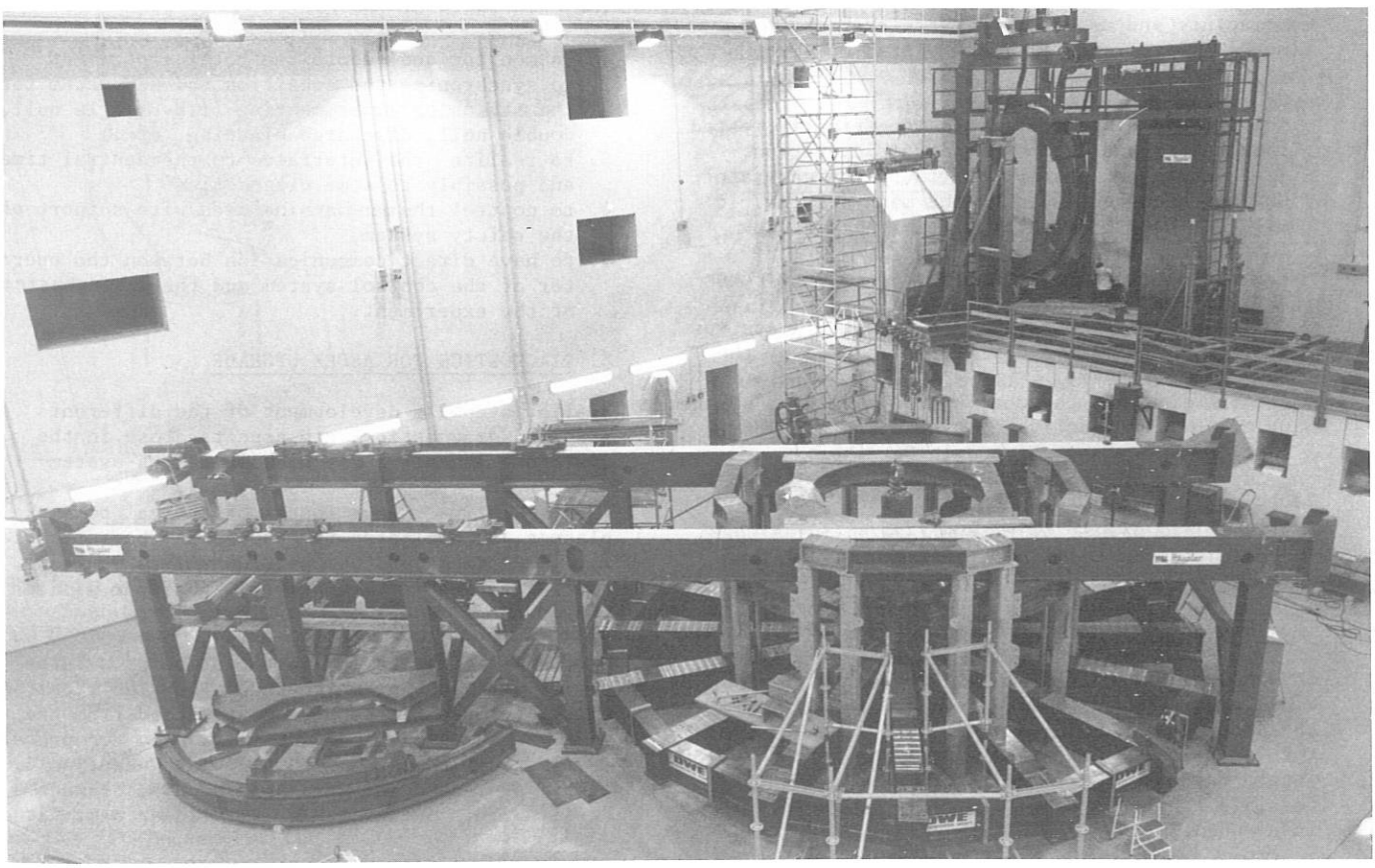

Fig. 8: The torus assembly installation with the octant assembly stand (background).

Upgrade data base, FP has been so far employed to verify the feasibility of reconstructing the plasma shape parameter from simulated measurements gathered by a model of the real magnetic probe configuration of ASDEX Upgrade (see also Theory 3). For extended control purposes FP will now possibly also be applied for modelling the nonlinear relation between the currents and plasma shape parameters.

With the final aim to provide a powerful tool for detailed studies of all questions related to the control of plasma equilibrium the latest version of the Princeton-Plasma-Equilibrium-Code ("Jardin-Code") was procured and implemented (see also section 2.1).

The detailed design and the preparation for fabrication and assembling of the magnetic flux and field measuring devices located on the outside of the vessel have been concluded.

Investigations for determining the final position and mechanical set-up of the probes inside the vessel are still going on.

The four raw half-rings for the passive stabilization loop system were forged from a single 62-ton copper casting and are now being prepared for final machining.

4. PERIPHERAL INSTALLATIONS

4.1 Power Supply Systems

After contract placement for the main components of the ASDEX Upgrade power supply systems in 1985, manufacture and assembly of these systems was continued, started,and partly completed in 1986, according to schedule.

- The 160 MVA diode rectifiers were finally tested in December and are now ready for operation.
- Manufacture and assembly of the pulse generator EZ4 has been concluded by the manufacturer. It will be installed at IPP within the next few month.
- The 150 MVA thyristor rectifiers are under construction at the manufacturer.
- Installation of power lines and switch gears was started in October and will be finished by the end of April 1987.
- The breakers and the commutation capacitor of the OH circuit were delivered by the end of 1986. Final assembly was started in December.

Technical details of the ASDEX Upgrade power supply systems are given in /214/ and /215/.

4.2 Control System of ASDEX Upgrade

The concept of the control system for ASDEX Upgrade is to be realized with PLC's (Programmable Logic Controllers), type SIMATIC S5-150U, supplied by Siemens AG. The COROS SP visual display systems from the same manufacturer acts as monitoring and operator communication with the experiment. The COROS SP incorporates a signalling system which makes it possible to display and record events and faults independently.

The concept itself is to have a central unit for operating, monitoring and recording the total experiment in its essential values and parameters. Assigned to the central unit are the subsystems, such as the vacuum system, the energy supply system, etc., which are fitted with their own visual display systems, and which should be monstly autonomous. The monitoring and operation are intended to afford much greater detail than the central unit. Local operation should only be possible at the level of the subsystems.

All systems, central unit and the subsystems,are connected by a communication bus system based on the ethernet principle and built up with fibre optics ground loops.

An insulation level is introduced to all signals coming directly from the experiment or its surrounding to have protection against voltages induced by the magnetic and electric fields during the shot. Safety loops were realized redundantly by software and hardware.

The software is programmed by flow charts as far as possible and with symbolic addresses. The reason for this is that technicians have experience in reading flow charts rather than in reading statement lists.

The central unit and the safety system are located in the ASDEX Upgrade control room, the other systems being housed near their own subsystems assembled in a separate room.

The main tasks of the central unit are:

1. to monitor and record the total experiment
2. to synchronize and condition the subsystem for the status of experimenting (i.e. single null, double null, discharge cleaning, etc.)
3. to realize the interfaces to the central timer and possibly to some diagnostics
4. to control the man-machine area with support of the safety system
5. to have direct communication between the operator of the control system and the head physicist of the experiment.

5. DIAGNOSTICS FOR ASDEX UPGRADE

Beside stepwise development of the different standard diagnostics, new aspects arose in the field of the soft-X-ray pinhole camera system:

Bulk radiative energy losses of typical tokamak plasmas are dominated by photons in the soft-X-ray (SXR) range of the spectrum which are easy to be measured as photocurrent in simple silicon photodiodes.

This simplicity permits installation of a large number of channels, which then allow the local SXR emissivity profile to be reconstructed from the measured chord-averaged intensities by the process of numerical tomography. A rapid and numerically stable procedure has been used by R.S. Granetz et al[1]. This method achieves a linear best-fit of

[1] R.S.Granetz, J.F.Camacho, "Soft-X-ray Tomography on Alcator C", Nuclear Fusion 25, 727 (1985).

standard poloidal harmonics the radial dependences which are given by an expansion in Zernicke polynomials for the measured chord averages. Because of the special radial functions chosen, one gets an analytic formula which then yields coefficients describing the unknown local emissivity in poloidal harmonics.

The method has been used to optimize the layout of pinhole cameras for ASDEX Upgrade using reasonable guesses for the plasma emissivity. Figure 9 shows the set of five cameras with a total of 123 channels. This arrangement balances the need for high radial resolution, which is determined by the number of channels in each camera with the need for high poloidal resolution which in turn, is determined by the number of cameras distributed around the plasma. The set-up has been shown to allow stable analysis up to a radial resolution given by a parameter L = 10 and a poloidal resolution of up to M = 3, thus yielding 77 best-fit coefficients.

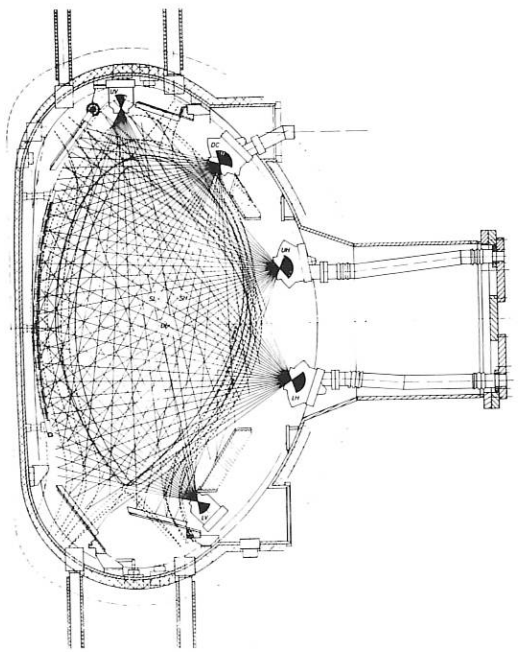

Fig. 9: The five SXR cameras proposed for ASDEX Upgrade.

The test also showed the need to change the code to accommodate the strongly noncircular shape of the ASDEX Upgrade plasma. A suggestion for maintaining the inherent rapidity and stability of the original program can be made.

SXR radiation is measured at ASDEX with two pinhole cameras and 58 channels. Figure 10 gives results from the code showing SXR emissivity before, during, and after a sawtooth crash at a radial resolution of L = 10. Because of the small number of cameras the poloidal resolution had to be restricted to M = 1.

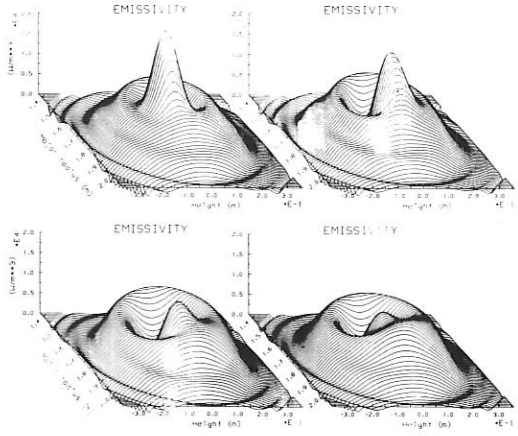

Fig. 10: SXR emissivity for an ASDEX sawtooth crash in steps of 100 microseconds.

A very similar chord distribution as for the soft-X-ray diagnostics was chosen for the bolometer diagnostic (80 channels for the bulk plasma, 8 for divertor plate observation). New 4-channel modules were developed and will be tested in ASDEX. See contribution in the ASDEX report.

The diagnostics system included the diagnostics of charged fusion particles: Under AUG conditions investigation of the high-energy particles of the D-He^3 reaction allows measurement of the ion temperature and confinement behaviour of He^3. In addition, beam-target protons can be separated from thermal protons.

6. ADDITIONAL PLASMA HEATING

6.1 Ion Cyclotron Resonance Heating

The ICRH system for ASDEX Upgrade has already been described in the annual report 1985. It will allow the choice of different heating scenarios (He_3 minority, H minority, D second harmonic and H second harmonic) with an RF power of 8 MW between 30 - 80 MHz and steadily decreasing to 4.8 MW in the range 80 - 120 MHz.

6.1.1 RF generators and lines

Manufacturing of the four RF generators and of the special high voltage power supplies is in progress. The first generator will be delivered by the middle of 1987.

The layout of the transmission lines in the experimental hall and to the generators was finalized. The long transmission lines from each generator will be 50 Ω , 6 1/8", the matching system which will be situated near the experiment consists of two 9" tuners, with the possibility to change the length between them.

At the second tuner, the line splits in two to feed the different parts of the antenna array. In

those sections a third stub used for introduction of coolant will also allow a first reduction of the VSWR.

The antenna feeder is limited to 6 1/8" in ASDEX and WVII-AS. So similar solutions can be used (see section Technology, chapter 2.3).

6.1.2 Antenna

The design of the antenna was further defined. The concept is sufficiently flexible that new experimental results can be taken into account. A recent development that points to the need to cover the components in the antenna neighbourhood with carbon is already incorporated in ASDEX Upgrade because of the presence of the passive stabilizing conductor and its structure which are covered with graphite.

Since optimal use of the available space requires a varying distance between central conductors and return conductor, and even in some cases an asymmetric antenna (SN configuration), and because such variations are presently beyond the capabilities of even numerical evaluation, a 1/2 scale flat model (neglecting curvature, but including varying distances, and asymmetries) was built.

Electrical measurements will allow the choice of the optimal shape for the different operating frequencies and for the different plasma configurations(SN, DN, limiter).

6.2 Neutral Injection into ASDEX Upgrade

The neutral beam system for ASDEX Upgrade is designed to provide an additional heating power of 6 MW for $\tau_p < 10$ s when injecting hydrogen. By running the sources with deuterium this value may be increased to around 9 MW. This power will be delievered by one injector box equipped with four ion sources operating at 55 kV/65 KV (H_2 operation, D_2 operation).

Apart from the plasma generator, all parts for these ion sources have now been ordered. The water-cooled extraction grids, designed in collaboration with KFA Jülich, will be manufactured by electrodepositing copper onto a copper substrate with the cooling channels machined in. After delivery they will be installed in the PINI structures and the first complete system should be available in autumn 1987. For the plasma generator the use of an RF ion source instead of a standard bucket source is still being discussed.

Detailed design work on the beam line and its various components was started during the year. The height, width and length of the vacuum box will be around 4.4 m, 2.4 m, and 3.6 m, respectively. Concerning the beam line assembly concept, it is intended to mount the main components, fixed to their individual flanges, vertically from above into an aligned position. Simple and fast mounting is essential especially for the Ti pumps since the Ti filaments have to be routinely replaced after some period of operation. The four individually alignable ion sources will be attached to the box via a common flange.

The calorimeter is designed to handle the neutral power only in the case of 9 MW D° injection. This means for H° injection that beams of neutrals plus ions may be stopped for voltages of up to 50 kV. The power will be absorbed on actively cooled panels similar to those developed for the long-pulse injection into ASDEX. Detailed calculations of power density profiles on various panel arrangements have been done in order to determine the input for the panel layout and the requirements for cooling water. Since it is intended to use the same panels for the ion dumps as well, the final panel design has to wait for the outcome of the calculations concerning the ion removal system.

These calculations started by adapting the available codes (3D iron magnet code: PROFI, ion trajectory code based on Gourdon code) to the case of ASDEX Upgrade. Different magnet configurations and their optimization are being studied.

The magnet design is strongly connected with the problem of shielding the ion trajectories against the rather high stray magnetic field from ASDEX Upgrade. Provided that this stray field is reduced by some shielding measures around the tokamak to about 150 G in the magnet region, a relatively simple additional shielding built inside the vaccum box together with the rather large amount of iron from the magnet is sufficient to reduce the field further to tolerable values of about 5 G between the neutralizer and magnet. In addition, the neutralizers will be individually shielded, resulting in magnetic field values below 1 G, and the ion sources are surrounded by a common shielding house (remaining field on source level: < 1.5 G) which also acts as a HV cage for the sources.

The vacuum box will be connected to the large ASDEX Upgrade port via a vacuum valve, bellows, an electrically insulating ring,and an adapter flange. Owing to lack of space and the beam crossovers in this region the power loadings in this duct area are rather high. Various protection elements (watercooled graphite elements, inertially cooled Cu plates) have been designed on the basis of detailed power density calculations. Power densities of up to 600 W/cm² have to be handled for the 10 s beam pulse. The geometrical losses will be between 5 % and 10 %, depending on beam divergence. These tight conditions inside the duct region call for precise beam alignment which must not be affected by the tokamak stray field.

The test stand for the neutral injection experiment into ASDEX Upgrade, and for further developments, will be a full-size vacuum box with a full-size magnet but otherwise with only one quadrant of the beam line equipped. To accommodate this test stand, together with a target tank for the duct simulation, a new area will be used close to the ASDEX Upgrade torus hall and to the assembly site for the beam line. It is envisaged to test the critical parts of the beam line with a full-power beam before injection into ASDEX Upgrade.

IEA IMPLEMENTING AGREEMENT
for the joint work on the investigation of toroidal physics and plasma technologies in ASDEX and ASDEX Upgrade
EUROPEAN ATOMIC ENERGY COMMUNITY/US DEPARTMENT OF ENERGY

1. OBJECTIVES OF THE AGREEMENT

The general objective of the agreement is to investigate toroidal physics and plasma technologies in ASDEX and ASDEX Upgrade. The programme of this agreement is implemented by undertaking a task. This specifies the objective as the investigation of toroidal physics and plasma technologies in tokamaks with poloidal field divertor(s) as a means of optimizing plasma performance and preparing a common data base in these areas. The agreement has been concluded between EURATOM and US-DOE to regulate the cooperative work between IPP and US laboratories.

The following means of implementation have been agreed upon:

(a) Exchange of information between the participants on boundary theory and modelling, experimental operation, and development and testing of components.
(b) Assignment of scientists, engineers, and other technical experts to work at the facilities of the participants.
(c) Workshops, seminars, and symposia.
(d) Establishment of a communication link for terminal traffic and file transfer between the laboratories of the participants in support of cooperative projects when the need arises.
(e) Exchanges and joint development of relevant nonproprietary computer codes.
(f) Transfer of equipment and material between the facilities of the participants.

2. STATUS OF THE AGREEMENT

Cooperation between the partners, IPP and US laboratories, continued along the lines described in the objectives and detailed in the annex to the agreement. The Executive Committee met in Tokyo after the IAEA Conference, discussed the cooperative work in 1986, and agreed on a programme for 1987 in which Lower Hybrid Heating will be a focal point.

3. REPORT ON THE 1986 ACTIVITIES

3.1 Theory

H. St.John (GA) and P. McCarthy (IPP) are developing in collaboration a fast and generally valid algorithm for determination of tokamak equilibrium parameters (position, shape, β_{pol}, l_i, etc.) from magnetic signals using function parametrization. This method was introduced into tokamak physics by B. Braams and has been proved to work on ASDEX. It should be particularly useful for non-circular plasma cross-sections and GA and IPP are working together to establish it for Big-D and ASDEX Upgrade.

ASDEX Upgrade will work with near-perpendicular injection and (at least at low magnetic fields) could be affected by fishbones. R. White (PPPL) conducted studies on ASDEX Upgrade parameters. His visit to IPP served to make the results known to ASDEX Upgrade physicists and to reach agreement on realistic and important ASDEX Upgrade parameter combinations for further studies.

The CART code for MHD mode identification in ASDEX was installed at IPP during a visit of J.K. Lee (GA). It has meanwhile been applied to simulation of MHD oscillations and a study of theoretical ß-limits given by large-scale resitive and ideal MHD modes, using measured ASDEX parameter profiles. A later visit of K. Grassie to GA served to clarify questions arising during initial operation and the continuation of joint scientific work.

Neoclassical transport of impurities was the subject of discussions between D. Sigmar and R. Isler from ORNL with physicists from IPP.

N. Pomphrey (PPPL) visited IPP Garching, to familiarize himself with the specific problems of position control in ASDEX Upgrade and pick up the necessary technical specifications for its modelling with the TSC (Tokamak Simulation Code) package.

S. Jardin (PPPL) was in Garching twice during

1986; his visits were dedicated to installing the TSC Code at IPP and to discussing the optimum performance and usage of the package.

W. Schneider (IPP) was at PPPL for one year (5/85 - 6/86); he was involved in code development for BALDUR Upgrade ($1\frac{1}{2}$D version), made initial test runs with the TSC code for ASDEX Upgrade, and did some calculations of the propagation of ablated pellet material along field lines for comparison with experimental measurements in TFTR.

U. Schneider (IPP) was primarily engaged in software development for the new data acquisition of the CHERS diagnostic in TFTR; in addition, she developed a user interface for comparing BALDUR simulation results with experimental data.

P. Diamond (Univ. Texas) analyzed the confinement of runaway electrons to elucidate the role of electromagnetic turbulence for the energy transport in ohmic, L- and H-phases of ASDEX.

K.S. Riedel (Courant Institute) used the propagation of the heat pulse caused by the sawtooth crash to determine the electron heat conductivity χ_e by fitting a solution of a forced initial value problem for the heat transport equation to the temperature variations, measured by ECE.

3.2 Experimental Cooperation

G. Janeschitz spent 6 months at GA. He brought the ASDEX SPRED spectrometer with him and installed it on the D III-D tokamak. His work was concentrated on spectroscopy but he was also involved in the H-mode investigations. The extremely good quality of the H-mode, found in a totally open divertor configuration, is an important result for the tokamak community.

F. Wagner took part in the confinement studies of TFTR in the supermode regime and investigated especially the effects of plasma rotation on confinement, caused by different mixtures of co- and counter-injection of the neutral beams.

3.3 Ion Cyclotron Resonance Heating

The main topic in the collaboration with PPPL was the physics of ion cyclotron heating. In addition, the collaboration led to an exchange of information on technological questions. The main concern in the collaboration with ORNL was the technology of ion cyclotron heating, particularly the development of vacuum feedthroughs at Oak Ridge with power tests at Garching, load tests on cooled Faraday shields for ASDEX and Oak Ridge and planning of joint experiments for waveguide antennae.

This collaboration included visits by F.W. Baity and T.C. Owens from ORNL and J.R. Wilson from PPPL to IPP and visits by H. Wedler and F. Braun to PPPL, ORNL and GA.

3.4 Lower Hybrid Heating

Two visits by F. Söldner, IPP, to PPPL and MIT served mainly for the preparation of the envisaged collaboration of PPPL, Frascati and IPP in the future LH programme on ASDEX. This included the preparation of technical solutions, discussions and agreement with the PPPL Programme Committee and drafting of contractual arrangements. Both sides used Söldner's visit to PPPL for a thorough discussion of the lower hybrid results on PLT and ASDEX. Söldner contributed to the experiments on lower hybrid current drive on PLT. Further technical details of the common experiment on ASDEX were clarified during a visit by M. Münich and F. Gresser to PPPL.

3.5 Surface Material Testing, Plasma Wall Interaction

During a visit by W. Eckstein to PPPL a data base for light ion backscattering to be used in the DEGAS plasma simulation code was prepared in collaboration with D. Heifetz.

Discussions with W.B. Kunkel of Berkeley University related to the study of an intense low-energy ion source for plasma simulation measurements (ion backscattering, ion trapping and diffusion).

J. Bohdansky took part in experiments at SANDIA, Albuquerque. Graphite plates to be used in ASDEX Upgrade were tested under high heat load with a pulsed electron beam. The erosion of graphite during ion bombardment was studied at very high current densities. The collaboration included work of K. Wilson, SANDIA, Livermore, and R.W. Conn, UCLA.

J. Roth collaborated with J. Roberto, ORNL, on the radiation damage and erosion mechanisms of graphits.

3.6 Pellets

Z.A. Petrzyk from the University of Washington contributed during his one-year stay at IPP to the ASDEX experiment. He was mainly concerned with measuring the density of the scrape-off layer using McCormick's Li beam diagnostics for various discharge phases, particularly during pellet refuelling phases.

Joint experiments with pellet injection into the ZT-40M reversed field pinch were prepared and performed during a 3-month visit by K. Büchl, IPP, to LANL.

3.7 Resonant Helical Divertor, Pump Limiter

G. Haas (2 months), F. Karger (1 week), IPP, participated in experiments with the resonant helical divertor in TEXT at UTA and in experiments with the pump limiter and the divertor of DIII-D at GA. The contributions consist in both cases in installing and operating special fast ion gauges and in interpreting their results in terms of the performance of the divertor or pump limiter arrangements.

JET COOPERATION PROJECT

Head of Project: M. Kaufmann

The tokamak experiment JET (Joint European Torus) is the world's largest fusion experiment. IPP is a member of this Joint European Undertaking and contributes funds and personnel to JET. The JET experiment at Culham (U.K.) went into operation in 1983 and has since been conducting a major experimentation programme.

IPP involvement in the joint European experiment takes various forms. Several IPP employees have been seconded to JET for long terms and are integrated in the JET team. IPP also continued to develop and build diagnostics essential for investigating the JET plasma. Now IPP have supplied JET with five bolometer cameras, a soft-X-ray system, a casette probe system for investigating surface samples, a surface analysis station,and in 1986 a pellet injection system for diagnostic purposes,and two crystal spectrometers for the X-ray region.

Besides having taken part in the construction of JET and providing diagnostics for it IPP are also participating in the experiments. For this purpose IPP have concluded task agreements with JET which define the cooperation of IPP in certain areas and are concerned with, in particular, the operation of IPP-built diagnostics. Under the terms of these task agreements IPP assign personnel to JET. Two task agreements are now in force. The first provides for investigations in impurity physics; the second is concerned with plasma-wall interaction. In 1986 several staff members of IPP were active with JET in the context of these task agreements.

Apart from this work on diagnostics and assignments under the task agreements IPP also supported JET with theoretical work and numerical calculations in various fields.

JET operated continuously throughout 1986 until the end of November with only small breaks for commissioning, maintenance,and repair. The most important new system put into operation during this period was the first neutral injection box. The neutral beam system was rapidly put into operation with deuterium injection at the design voltage of 80 kV, at which voltage it is capable of injecting up to 10 MW of power into the torus.

The injection of particles creates a fuelling effect in the plasma, which in combination with the increased power input is found to raise the critical density for disruption by a factor of two. Neutral beam injection does not lead to an increase of impurities. Indeed, if the density is allowed to rise, the value of Z_{eff} falls significantly. At low density, ion temperatures of about 12 keV are reached in the so-called hot ion mode, the electron temperature in the same discharge being about 6 keV.

The simultaneous operation of neutral beam injection and ion cyclotron resonance heating proved to be straightforward. The maximum combined power input including ohmic power was 18 MW into a 5 MA discharge. The global energy confinement time was about 0.4 s and the plasma energy content about 7 MJ. With relatively high average density (4×10^{19} m^{-3}), the electron and ion temperatures of about 4 keV were modest.

After considerable research the H-mode (high mode) of confinement, which was first discovered in the ASDEX divertor tokamak of IPP was achieved in JET at plasma currents of up to 3 MA. This was done with a single X-point near the upper wall of the vacuum vessel. The overall performance of the discharge at 3 MA in this mode is substantially better than that of a 5 MA limiter-bounded discharge and gives the best value for the fusion product, i.e. the product of central deuteron density, central deuteron temperature, and global energy confinement time (2×10^{20} m^{-3} keV s). The individual values are central deuteron density 5×10^{19} m^{-3}, ion temperature 7 keV, and global energy confinement time 0.4 s. A significant thermonuclear yield in D-T requires a fusion product of 10^{21} m^{-3} keV s. Further developments in the JET programme are designed to reach this figure.

1. CONTRIBUTIONS OF THE JET DIAGNOSTIC AND PELLET INJECTION GROUP (JDP)

C. Andelfinger[1], K. Büchl[1], C. Dorn, H.U. Fahrbach, J. Fink[1], H. Frischmuth, H. Morsi[1], E. Oberlander, H. Röhr, G. Rupprecht[1], H.B. Schilling[1], G. Schramm, U. Schumacher, A. Stimmelmayr, H. Weichselgartner, D. Zasche

In 1986 the bolometer and soft-X-ray diagnostics and the pellet launcher were regularly operated as JET Standard Systems. The very positive experience gained with the soft-X-ray system led JET to enlarge it with 5 small cameras distributed in the toroidal direction. IPP contributed by delivering electronics and supervising contracts with industry. The two crystal spectrometers are being commissioned and will be in operation when JET resumes operation after the present shutdown.

The bolometer diagnostic measures the total radiation power loss of JET discharges in the entire relevant spectral region with moderate time and space resolution. In the case of discharges with X-point it was possible to separate the radiation emitted from the plasma inside the separatrix and that from the edge plasma. The essential features of the soft-X-ray diode array are high time and space resolution in conjunction with high sensitivity. This diagnostic started operation in December 1985 and proved to be a most valuable tool affording an insight into various phenomena connected with sawteeth, disruptions, H-mode, impurities, and pellet injection. The two double cystal monochromators yield high spectral resolution and serve for measuring soft-X-ray emssion lines, thus identifying impurity atoms and determining their concentrations. One monochromator is mounted on a vertical port and can scan spatial profiles. The other, which is placed outside the torus hall and is capable of operating during the deuterium-tritium phase of JET, as well, surveys the X-ray emission along a line-of-sight in the midplane of the torus. The progress made and results obtained with these systems are described in the following sections.

The main objectives of pellet injection experiments in JET with the IPP injection system are (i) to explore whether pellet fuelling gives access to regimes of higher plasma density, increased plasma purity, improved confinement characteristics, and improved ICRF and NI heating, (ii) to diagnose plasma behaviour, and to model the measured response in order to develop predictive methods. Pellet fuelling experiments were already performed in 1986 with pellets 3.6 and 4.6 mm in diameter (2.2 and 4.5 x 10^{21} D atoms) with velocities between 0.8 and 1.2 km/s. The pellets were fired into a wide variety of discharges and the pellet penetration was found to agree well with a theoretical model of ablation. Penetration was found to depend only on plasma parameters with no additional effects due to neutral beam or ICHR heating. With pellets, the density limit for disruption could be increased by a factor of about two, even with ohmic heating alone. As expected, the influx of pellet particles dilutes the impurities to give post-pellet Z_{eff} values close to unity.

1.1 Single-shot Pneumatic Pellet Launcher

The single-shot pneumatic pellet launcher was installed in June 1986 and yielded interesting results in the remaining operation phase of 1986. The injector is able to accelerate D_2 and H_2 pellets providing 20, 50 or 100 % of the plasma fuel.

The acceptance tests yielded the following results:
- velocities: H pellets 1200 - 1600 m/s
  D pellets 1100 - 1500 m/s
- liquid helium consumption 3 l/h (1 tank of 250 l/week)
- propulsion gas flux into the torus $\prec$ 1 % of pellet mass
- stray angle $\prec \pm 0.3$ degrees
- jitter in pellet mass $\prec$ -10 %
- reliability in acceptance tests 100 %.

First physical results in JET operation are
- increase of density limit
- increase of particle confinement in limiter discharges
- decrease of Z_{eff}.

1.2 Soft-X-Ray Double-crystal Monochromators

KS1 and KS2 were completed and acceptance tests were satisfactorily carried out. These two double-crystal monochromators for identifying impurities and clarifying their transport by soft-X-ray spectroscopy in hot plasmas were built for JET. Both are characterized by high mechanical accuracy enabling fast wavelength scan or continuous spatial scan together with flexibility in wavelength range and spectral resolution.

The KS1 double-crystal monochromator device was installed at JET in a concrete shielding housing behind the shielding wall at JET in October 1986. Connected to a horizontal port of the JET vessel via a long beam line, the instrument will scan a large spectral range of a rate of a few cycles/s on one line of sight through the midplane of the JET plasma.

Prior to its installation, the mechanical accuracy of the various components of the instrument was measured and its operation was tested by optical and X-ray methods. The angular correction for the rotation units carrying the crystal tables, which is necessitated by the nonlinearity of the linear displacement units, was found to be reproducible being in the range of about ± 10 seconds of arc. The X-ray tests were performed using the X-ray source (with Cu and Cr anodes), the gridded collimator (with a resolution of 600) and the large-area multi-wire detector. Figure 1 gives an example of the CuK_α spectrum obtained with KS1, the count rate of the detector being plotted versus the Bragg angle. The results of the CuK_α, CuK_β and CrK_α spectra measured with LiF (220) and topaz (303) crystals were in good agreement with expectations.

The KS2 double-crystal monochromator device built to allow a continuous scan with up to 5 Hz over more than the half-axis of the JET plasma was installed on top of vertical port 3 of JET in Sep-

[1] part-time assigned to JET

tember 1986. However, as failures occurred during commissioning in October and November results from JET plasmas have not yet been obtained. The extensive optical and X-ray tests and adjustments prior to shipment of the instrument to JET showed that the operation of KS2 for X-rays works according to specification.

Some components, such as the crystals for swivelled positioning, the high-resolution collimator, and the large-area X-ray calibration source, are still undergoing test and development work.

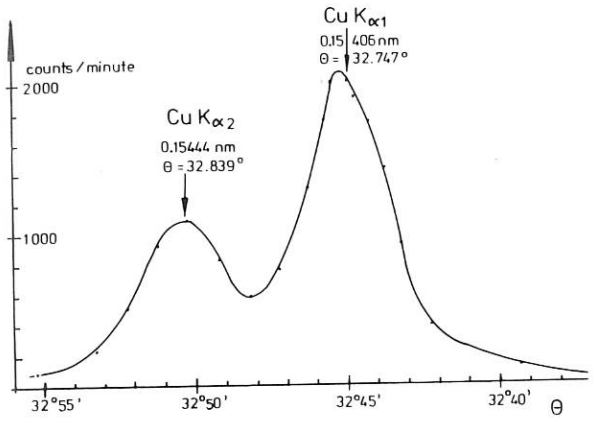

Fig. 1: The CuK$_\alpha$ spectrum measured with the KS1 double-crystal monochromator by scanning the Bragg angle.

1.3 Tritium Technology

1.3.1 Decontamination of metallic surfaces

Development of a strippable decontamination foil was continued. The efficacy of the degreasing, etching, and decontaminating chemicals used was tested on foils produced in a single stage. This yielded decontamination factors in the region of DF = 10, P = 90 %. These decontamination foils can thus be assigned to class 2 (in accordance with NFT 30-901, "Peintrues pour l'industrie nucléaire, essai de décontamination"). Difficulties are still being encountered in depositing the foil material on the surfaces to be decontaminated, particularly by the airless spraying method preferred in nuclear power plants.

1.3.2 Isotope separation by preparative gas chromatography

The improved column filler was also tested in large separation columns. With several separation columns, 100 mm in diameter and approx. 2.4 m long, arranged in succession it was possible to separate up to 4000 Nml of an equimolar mixture of H_2/HD/D_2 in about 140 min. The purity of the individual species exceeds 98 %. With respect to the method of filling the separation columns numerous tests have been conducted with the objective of optimizing the packing homogeneity.

1.3.3 Tritium removal and tritium waste

In 1986 the TROC pilot rig was converted for solid organic getters. Elimination of the liquid phase essentially simplifies the process: the tritiated gases are blown across catalyst-coated Al_2O_3 balls impregnated with organic getter substances the tritium being chemically bonded to the getters.

For detritiation of all pump exhaust gases a further rig with a capacity of 1000 Nl was installed and tested.

The two rigs now produce only solid waste, thus dispensing with the need for further facilities for solidifying liquid waste. The waste volume, however, is probably of the same order of magnitude as the solid TROC waste products.

2. CONTRIBUTIONS OF THE PLASMA WALL INTERACTION GROUP

2.1 Surface Analysis System (SAS)

(Ch. Dorn, W. Möller)

The JET surface analysis system is part of an on-line system for automatic exposure and analysis of boundary layer probes. It has passed the acceptance tests for its mechanical and vacuum components. First manual probe exchange procedures have been performed with the fast transfer system which connects the surface analysis station to the JET torus. The analytical equipment at one of the two analysis chambers has been installed being set up for high-energy ion beam analysis (Phase II, contract No. JE2/0687).

3. TASK AGREEMENT No. 1

3.1 JET Bolometry

(H.J. Jäckel[1], R. Müller[1], K. Behringer[2], W. Engelhardt[2], N. Gottardi[2], G. Magyar[2], K. Scheidt[2])

The main emphasis in the JET operation programme for 1986 was placed on auxiliary heating with NB injection (NI) and ICRH (RF). Different operation schemes were performed, the plasma being attached to the outer limiter or to the inner wall or with a modified magnetic field configuration having the separatrix inside the vacuum vessel (x-point). In the latter case the magnetic stagnation points could be kept inside the vessel for plasma currents of up to 3 MA.

The two JET bolometer camera systems look into the confinement region from the side and from the bottom[3]. Depending upon the operation scheme, the radial distribution of the radiation power was rather different for the above-mentioned cases. With the plasma attached to the inner wall or to the outer limiter, enhanced radiation was observed at the inside or the outside of the plasma cross-section, respectively. The asymmetry at the outside is due to the interaction of the plasma with two RF antennae in the immediate vicinity of the bolometer cameras and is toroidally localized. In

1) Part-time assigned to JET
2) JET Joint Undertaking, Abingdon, U.K.
3) K.F.Mast et al., Rev. Sci. Instr. 56 (5), 969 (1985).

x-point discharges two ("double-null", DN) or one ("single-null", SN) bright spots were observed at the bottom and/or the top of the plasma cross-section.

3.1.1 Local emissivities

By means of tomography it is in principle possible to calculate local emissivities for distorted radiation distributions. Two computer programs with slightly different mathematical approaches[1,2] can be applied to the bolometer data. Owing to the geometry of the two bolometer camera systems poloidal asymmetries up to m=2 can be reconstructed. This means that physically very localized and narrow asymmetries are spread out poloidally over about a quadrant by the reconstruction method. In these cases the local emissivity has to be evaluated by a simple Abel inversion neglecting the distorted channels. But in many other cases tomography is a powerful tool for showing local sources of emission in the plasma. In particular, it demonstrates that the surfaces of constant emissivity generally do not coincide with surfaces of constant pressure.

3.1.2 Total radiation

The error in the calculation of the total radiated power due to local effects is up to about 10 %. The power loss in JET discharges measured by bolometry is typically between 40 and 80 % of the input power with a tendency to be higher during RF heating than during NI and to increase as the density.

3.1.3 X-point discharges

In X-point discharges it is of particular interest which fractions of the total radiated power are emitted from the confined plasma inside the separatrix and from the X-point regions. A method has been devised to distinguish between these two portions. It can be applied particularly well to SN discharges, where in many cases a transition from L to H-mode was observed. Figure 2 shows the time evolution of bulk plasma and X-point radiation when a transition from L to H-mode occurs. Typical during the H-mode is a strong increase of the radiation from the bulk plasma due to the steadily growing plasma density, whereas the radiation power from the X-point region becomes stationary.

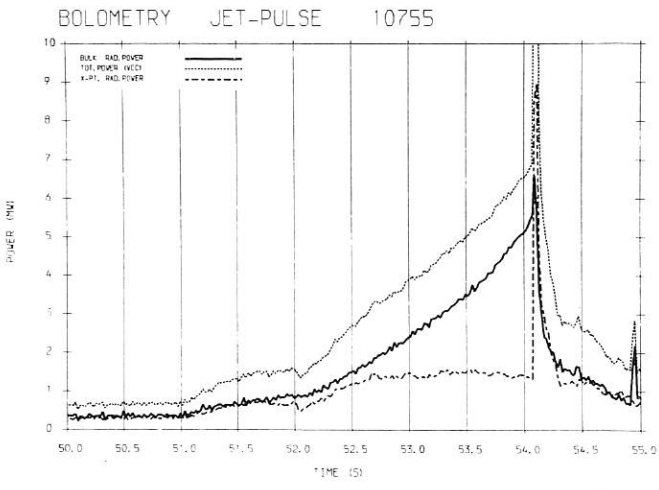

Fig. 2: Time evolution of the radiation power from the total plasma cross-section (dotted), the confined plasma (solid) and the X-point region (dashed-dotted). The steep increase in the radiation power marks an H-mode phase and is due to a strong increase in the plasma density.

3.2 JET Soft-X-Ray Cameras

(A.W. Edwards[1], R.D. Gill[1], R.S. Granetz[2], and A. Weller[3])

In 1986 the soft-X-ray system[4] delivered quite remarkable data, in particular details of the sawtooth collapse, MHD activity before and during major disruptions, H-mode-related phenomena, pellet ablation, and pellet-induced density perturbations associated with rational q-surfaces, and finally impurity radiation losses.

3.2.1 Sawtooth collapse

A wide variety of sawteeth has been observed[5,6] in JET including giant, partial, and monster sawteeth in addition to normal sawteeth. The partial sawteeth are accompanied by MHD activity, but the other sawteeth are often seen without precursors although successor oscillations are frequently seen.

1) J.F. Camache, R.S. Granetz, Rev. Sci. Instr. 57 (3), 417 (1986).
2) P. Smeulders, Nucl. Fus. 25 (3), 267 (1986).

1) JET Joint Undertaking, Abingdon, U.K.
2) MIT, Cambridge, Mass., USA
3) Part-time assigned to JET
4) A.W. Edwards et al., Rev. Sci. Instr. 57 (8), 2142 (1986).
5) A.W. Edwards et al., Phys. Rev. Lett. 57 (2), 210 (1986).
6) D.J. Campbell et al., Proc. 11th Int. Conf. on Plasma Phys. and Contr. Nucl. Fusion Research, Kyoto, IAEA-CN-47/A-VII-5, (1986).

The sawtooth collapse occurs on a very rapid time scale ($\sim$ 100 µs). In the first phase the central hot spot rapidly moves outwards until it stops at about the sawtooth inversion radius. This phase has a strong m=1 component. Secondly the hot spot collapses, leading to a symmetric final state. The observations are in disagreement with models of the sawtooth collapse which require magnetic island structures on the q = 1 surface, but are in good agreement with calculations of Wesson[1] in which the collapse is caused by an ideal instability.

3.2.2 H-mode phenomena

During the H-mode in JET very substantial profile broadening of the soft-X-ray emission is seen, which implies enhancement of the plasma edge temperature. The tomography plots of Figure 3 show that during the H-mode the profiles become much more triangular in shape and that the volume of plasma emitting X-rays increases to nearly the full torus aperture.

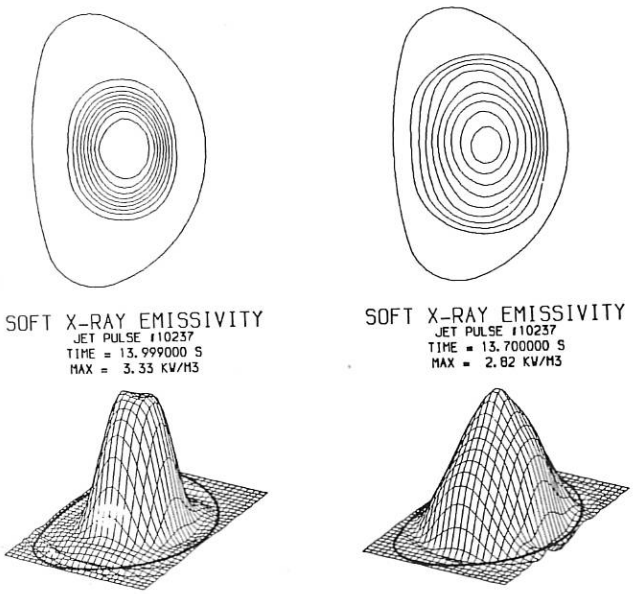

Fig. 3 : Local soft-X-ray emissivity during L-mode (left) and H-mode (right).

Edge-localized modes (ELMS) have been regularly observed in H-mode discharges. These disruptive-like instabilities generally occur when there is an L → H or H → L transition, but not during the H-mode itself. A sawtooth collapse frequently triggers the onset of an ELM-free phase. Correlations with signals of H_α and of MHD coils were found.

1) J.A. Wesson et al., Proc. 11th Int. Conf. on Plasma Phys. and Contr. Nucl. Fusion Research, Kyoto, IAEA-CN-47/E-I-1-1, (1986).

3.2.3 Pellet effects

The ablation of injected pellets in JET produces a pronounced resonance effect when the pellets reach surfaces with q-values 1 and 3/2. Subsequently m = 1, n = 1 and m = 3, n = 2 structures are observed as compact snake-like perturbations by the soft-X-ray cameras. Figure 4 shows the soft-X-ray emission as seen from the vertical camera during 10 ms intervals around pellet injection (horizontally in the same octant). The intense emission peak is caused by bremsstrahlung from the pellet material and is used to measure the pellet penetration. After ablation the snake modulation is seen. These structures, caused by the trapping of ablated particles in flux tubes with q = 1 and 3/2, can persist for $\geq$ 2 s indicating good confinement properties. Local cooling along the flux tube implies a current perturbation and magnetic island formation. The radial position of the structure gives the radius of the q = 1 and 3/2 surfaces. The structures can persist through several sawtooth collapses and therefore can give information on plasma sawtooth behaviour.

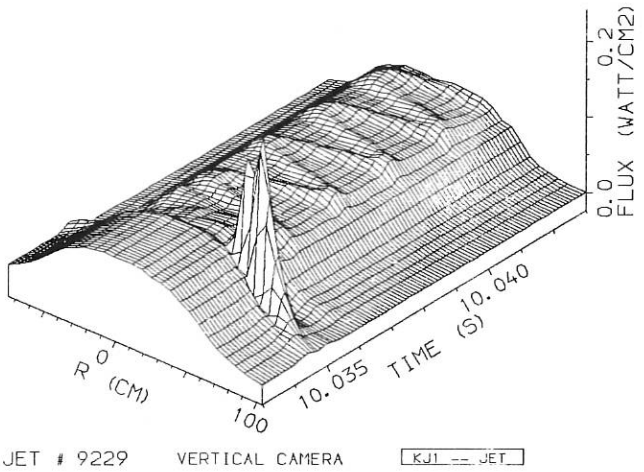

Fig. 4 : Snake modulation of the soft-X-ray emission after pellet injection. The pellet ablation is seen as a high intensity peak.

3.2.4 Impurity radiation modelling

The soft-X-ray intensities and the radial profiles, as measured by the cameras, are interpreted in terms of radiation from individual impurity species. The required input data, i.e. the concentrations of metals and light impurities, are derived from fitting the JET pulse-height-analysis (PHA) spectra with the same code[1] /462/ which also calculates the emission profiles. In this way, a consistent picture of the total impurity content in the plasma centre is obtained.

1) C.D. Pasini et al., Proc. of the Int. School of Plasma Physics, Varenna, Italy, September 1986.

4. TASK AGREEMENT No. 2

(R.Behrisch, J.Ehrenberg[1], A.P. Martinelli, J. Roth, M. Wielunski[2], W. Wenmin[3])

4.1 Erosion and Deposition Processes at the Limiters and Walls of JET

Analysis of the limiters and samples from the first wall of JET, together with information from Langmuir probes and impurity spectroscopy, indicates that metallic impurites enter the plasma predominantly via contamination of the carbon limiter surface caused by disruptive discharges and/or wall conditioning during glow discharge cleaning. Removal of metals from the limiter surfaces occurs by two different processes. At the central part of the limiter erosion dominates and both carbon and the deposited metals are removed. At the sides of the limiter more distant from the plasma, deposition dominates and metal deposits are finally covered up by carbon layers. In collaboration with JET and Culham a quantitative model was developed for these processes which allows one to describe the main features observed.

4.2 Hydrogen Recycling

On the limiters the deuterium is low at the central erosion-dominated area, while it reaches values of 2×10^{18} D/cm² at the deposition-dominated side areas. Thus limiters represent a continuous sink for deuterium (and hydrogen). At the vessel wall long-term samples of both carbon and Inconel show a similar amount of trapped deuterium which closely correlates with the carbon deposition on the Inconel probes, the ratio D:C being 0.3 to 0.4. This indicates that also on a carbon wall the major effect of long-term D retention is codeposition with carbon.

5. CONTRIBUTIONS OF VARIOUS GROUPS OF IPP

5.1 Electron Density Transport in JET after Pellet Injection

(V. Mertens[1], W. Engelhardt[4], A. Gondhalekar[4], N. Gottardi[4], J. O'Rourke[4])

Because of the markedly hollow electron density profile after pellet injection a direct estimation of inward pinch velocities V at specific radii can be made without any assumption about the diffusion coefficient D. This fact was used to determine the electron density transport properties directly after pellet injection in limiter discharges.

Investigations were concentrated on limiter discharges in deuterium with medium target density plasmas ($n_{av} \sim 1.7 \times 10^{19}$ m^{-3}, I_p = 3 MA, B (tor) = 2.1 tesla and 3.1 tesla and D_2-pellets with 2.2×10^{21} atoms. The penetration depth at the injection velocity of approx. 1000 m/s is roughly a/2 (a: minor radius). The injection changes the density profile from centrally peaked to extremly hollow with $n_{max}/n(o) \sim 2$ (Fig. 5). The plasma inventory nearly doubles. Typically 85 % of the pellet mass is accounted for by integration of the density profile. Electron density profile information was obtained from FIR interferometer data by converting the line integrals into local densities by Abel inversion.

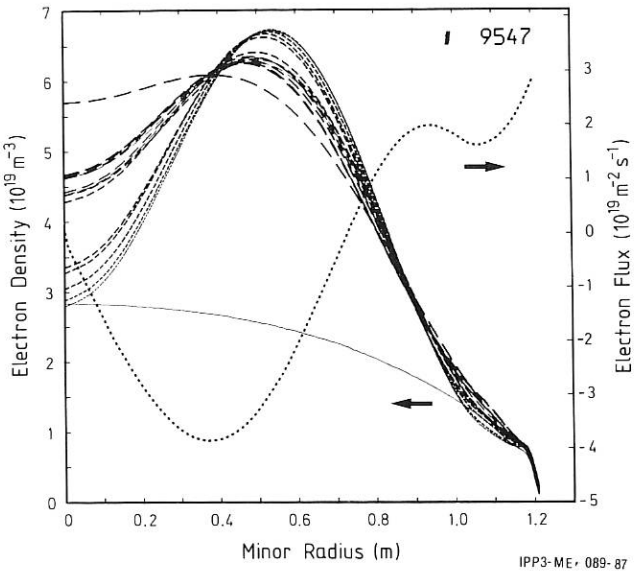

Fig. 5: Abel-inverted electron density profiles before (centrally peaked) and after (hollow) pellet injection at subsequent equidistant times. The density jumps, which flatten the profiles, quickly happen approx. 0.02 s and 0.09 s after pellet injection. The dotted curve represents the electron flux calculated from measured electron density profiles and calculated electron sources (eq. 1) approx. 0.01 s (averaged over 0.015 s) after pellet injection.

After injection the maximum density decays via diffusive and convective transport and the central density increases. Typically after 0.02 to 0.10 s small density jumps concurring with sawtooth-like temperature drops fill up the central density and successively flatten the profile. Sometimes only one density jump changes the electron profile from centrally hollow to centrally peaked. Nearly no particles are lost by these density jumps.

Electron fluxes in cylindrical geometry are calculated:

$$\Gamma(r) = 1/r * \int_0^r (S(r') - \partial n/\partial t)\, r'\, dr' \qquad (1)$$

These electron fluxes can be interpreted in terms of a model of electron transport consisting of diffusive and convective driving terms:

$$\Gamma(r) = -(D(r) * \partial n/\partial r + V(r) * n(r)). \qquad (2)$$

Investigation of the radial flux (eq. 1) after pellet injection shows finite inward flux at radii where the density reaches a maximum ($\rightarrow \partial n/\partial r = 0$) (Fig. 5). Equation (2) then allows one to estimate

---

1) Part-time assigned to JET
2) Institute of Nuclear Research, Warsaw, Poland
3) Institute of Nuclear Research, Shanghai, People's Republic of China
4) JET Joint Undertaking, Abingdon, U.K.

the inward pinch velocity at one particular radius without any assumption about the diffusion coefficient. By assuming a linear radial V dependence it is possible to deduce the diffusion coefficient.

These data indicate that the electron transport in JET limiter discharges is not changed by the highly perturbed density profiles caused by pellet injection. The deduced inward pinch velocities and diffusion coefficients agree with those determined in ohmically and additionally heated JET plasmas.

5.2 A Neoclassical Transport Model of the Tokamak Scrape-off Layer

(W. Feneberg[1], R. Simonini[2])

The description of the neoclassical particle transport has been completed in deriving expressions for the radial electric field and the electric currents flowing in the scrape-off layer which will be worked out numerically in the 2-d code of Simonini, Taroni.

The radial electric field leads to a plasma rotation in poloidal direction in the order of 10^3 m/s which can compete with the parallel flow at low mach numbers. Especially near the X-point, where the parallel flow is directed only toroidally, the $\vec{E} \times \vec{B}$ motion is dominant and can be responsible for the impurity transport from the divertor into the main plasma region. Therefore a self-consistent calculation of the electric field is important for the boundary codes.

The electric currents consists besides the usual Pfirsch/Schlüter return current of a part which is due to a temperature difference between the two positions, where a field line hits the wall. This temperature difference which can be estimated to be of the order of 10 eV according to code results obtained up to now is connected with a difference in the electric potential and drives a thermoelectric current parallel to the field lines of about 10 A/cm² in the JET case.

In the momentum equation which describes the motion of the fluid parallel to field lines the classical gyro-viscosity is being included which allows us to study the influence of a plasma rotation of the bulk plasma as induced with neutral injection on the flow velocity in the scrape-off layer: Plasma rotation would change completely the flow pattern and could be responsible for the impurity motion in the scrape-off layer as observed in the ASDEX experiment.

5.3 Effects on Doppler Profiles in the case of NI heating

(W. Feneberg[1], G. Fussmann[1])

With respect to the systematic differences found in the ion temperature measurements in JET from Doppler broadening of light impurities (CXRS = charge exchange resonance spectroscopy) and metallic impurities (XCS = X-ray crystal spectroscopy), we investigated several effects that may influence these measurements. The differences are observed in the case of NI heating when T_i exceeds about 3 keV. For a typical case of P_{NI} = 5 MW, $n_{e0} = 2.5 \times 10^{19}$ m^{-3} the central ion temperatures obtained from CXRS-CVI (λ = 5294 Å, n = 8 → 7) and He-like Ni XXVII (λ = 1.59 Å) Doppler profiles are T_c = 6 keV and T_{Ni} = 10 keV, respectively.

In the case of the XCS measurements it has to be noted that owing to the tangential observations the toroidal rotation of the plasma can result in additional broadening of the line profiles. This effect cancels exactly if the plasma rotates as a rigid body with constant angular velocity. Since the actual motion of the plasma is unknown, however, we studied the possible influence of a rotational shear by assuming velocity profiles of the type $v_\varphi = v_{\varphi 0} (1 - r^2/a^2)^m$. From these numerical calculations we learned that this effect can lead to errors not larger than ± 10 % for moderately peaked velocity profiles ($m \leq 2$). Only in the case of unrealistically high rotational shear ($m \gtrsim 5$) would significantly increased temperatures ($\geq$ 30 %) be deduced from the XCS measurements.

In addition to this macroscopic effect we analyzed various microscopic effects which may cause changes in the velocity distribution functions. The matter of concern in this context is the preferential energy and momentum input into the impurity ions. Three effects were distinguished: 1) Enhanced temperature of the impurities with respect to the background ions. 2) Deviations from a Maxwellian for an otherwise isotropic distribution. 3) Shifts and anisotropic distortions of the impurity velocity distribution.

From a discussion of the corresponding rate equations and from a more profound treatment of the Fokker-Planck equation we conclude that under the cited conditions all three effects are small. The largest effect is obtained for the first process. Here we estimate excess temperatures of $(T_{bulk} - T_{imp})/T_{bulk} \lesssim$ 5 - 10 %. Moreover, these excess temperatures are found to be independent of the mass and charge of the impurities insofar as $m_{imp} \gg m_{bulk}$. The temperatures measured from carbon and nickel lines should therefore be equal.

Apart from hidden systematic errors in the diagnostics, no good explanation has so far been put forward for the discrepancies in the measurements. There is, however, one further possibility, namely plasma turbulence, that should be taken into consideration. In particular, if the turbulent velocity v_t is caused by $\vec{E}_t \times \vec{B}$-drifts, v_t would be equal for all particles, and a constant turbulent line broadening $\Delta\lambda_t^2/\lambda^2 = \langle v_t^2 \rangle / c^2$ is then added to the Doppler broadening part $\Delta\lambda_D^2/\lambda^2 = 2\ T/m\ c^2$. Since the latter effect decreases with increasing mass, too high temperatures would be inferred from the total line width $\Delta\lambda = \sqrt{\Delta\lambda_D^2 + \Delta\lambda_t^2}$, especially from that of the heavy ions. At the moment, this effect is difficult to assess on a quantitative basis and line profile measurements of ions with intermediate mass ($m \gtrsim 30$) would be needed.

---

1) Part-time assigned to JET
2) JET Joint Undertaking, Abingdon, U.K.

5.4 Study of profile control in JET

(F. Söldner, M. Brambilla, F. Leuterer, H. Münich)

A study of profile control in JET with lower hybrid waves was made in the frame of an Article 14 contract. The main interest was to stabilize the large-amplitude sawteeth during ICRH. Experimental results from ASDEX, Petula and PLT show that about half of the total plasma current had to be driven by the LH in order to accomplish this stabilization. The RF power required for LH current drive in JET was determined on the basis of ASDEX results and comparison with Fisch's theory. The scaling with density and magnetic field is given in Fig. 6 for an emitter frequency of 2.45 GHz. All calculations were made for three possible frequencies: f_o = 2.45, 3.7 and 4.6 GHz. Ray-tracing calculations show that for the envisaged density range of $n_{eo} \gtrsim 5x10^{13}$ cm^{-3} the central plasma region ($r/a \lesssim 0.5$) is not accessible to LH waves at these frequencies if they are launched from the low-field side (see Fig. 7). Toroidal effects lead to a strong variation of the wave indices $N_{\parallel}$ and $N_{\perp}$ during propagation. All rays encounter the whispering gallery effect and are reflected back to the plasma surface. The innermost flux surface to which waves (with f_o = 2.45 GHz) can penetrate depends on antenna phasing and density. At 2.45 GHz, $\Delta\phi = 90°$ and $n_{eo} = 5 \times 10^{13}$ cm^{-3} the rays reach only r/a = 0.67. For higher frequencies the penetration is somewhat improved. Absorption of LH waves on the electrons might be reduced by damping on energetic ions when the LH is operated together with ICRH and NI. In fact, the wave energy is strongly depleted by interaction with fast ions in the central plasma for higher $N_{\parallel}$.

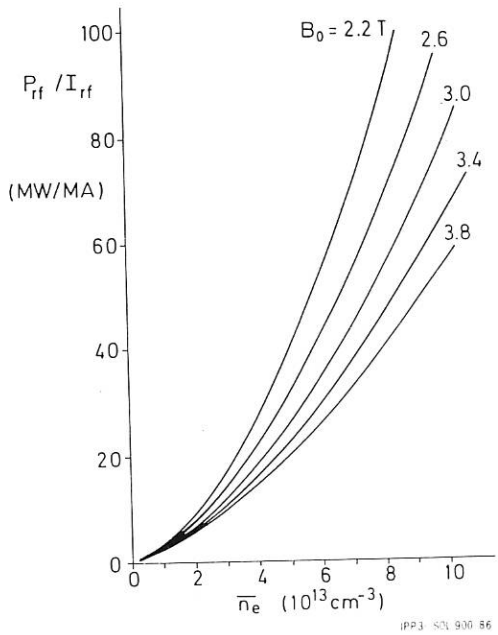

Fig. 6: Calculated power required for complete current drive in JET. $P_{rf}/I_{rf} = (n_e \cdot R \cdot \gamma)/(\eta \cdot \mu \cdot g)$. (MW, MA, 10^{13} cm^{-3}, m) with η = 2.75, μ = 0.7, γ = 1.25, R = 3 m, f = 2.45 GHz, $\Delta N_{\parallel}$ = 0.6, D_2, plane wave accessibility.

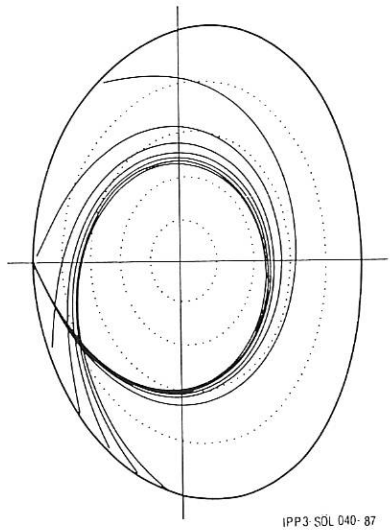

Fig. 7: Ray tracing results on LH wave propagation in JET for I_p = 3.5 MA, B_{to} = 3.4 T, $n_{eo} = 4x10^{13}$ cm^{-3}, with f_o = 2.45 GHz, side launch.

As a consequence of the poor penetration and also of the large power requirements for LH current drive at high density, only scenarios are envisaged where the radial profiles are controlled by LH current drive in the low-density edge region. There is also electron interaction dominating in all cases, and the lowest frequency of 2.45 GHz, which offers some technical advantages, can be chosen for the RF emitter. Flexibility in the profile control requires fine tuning of the wave spectrum. Therefore, a scheme with independent phasings of various rows in the grill antenna array is proposed. The main parameters of the proposed LH system are given in Table 1. The study is reported in /IPP III/111/.

Table 1: Parameters of a LH system for JET

Frequency	f_o = 2.45 GHz
Number of klystrons	N_K = 30
Power per klystron	P_k = 600 kW
Total power	P_{tot} = 18 MW
Total power radiated	P_t = 12.8 MW
Pulse length	τ = 20 s
Number of waveguides	N_{tot} = 216
Radiating surface	S_{tot} = 2376 cm²
Mean $\bar{N}_{\parallel}$	$\bar{N}_{\parallel}(\angle\phi = \pi) = 4.4$
Width of spectrum	$\Delta N_{\parallel}$ = 0.6

NET COOPERATION PROJECT

Head of project: G. Grieger

IPP host the NET Team, an internationally composed group of scientists and engineers called together to define the objectives of NET, the Next European Torus, and to prepare its design. NET is conceived as the next major step in the European fusion programme and a considerable fraction of its objectives are in the technology area. IPP contribute to the NET activities both by direct secondment of personnel to the NET Team and by performing NET supporting work mainly via NET study contracts. In addition there has been established a rather close correlation between those activities of the IPP which have particular relevance to NET, i.e. the ASDEX experimental programme and the related theoretical investigations which also include ASDEX upgrade. These contacts are not formally channeled but work by a person-to-person relation as one would expect with the NET team localized at IPP. Together with additional work directly related to the INTOR (INternational TOkamak Reactor) activities this work also serves as input to the INTOR Workshop. In the following the essence of two NET study contracts and of some INTOR related work will be described.

In this connection it should be noted that the INTOR terms of reference were modified for 1987 in order to make the INTOR work most useful for the discussions about the potential collaborative project ETR. The INTOR workshop of December 1986 was used to prepare this new activity.

1. DEVELOPMENT OF A PELLET INJECTION MODEL FOR IMPLEMENTATION IN THE NET TOKAMAK TRANSPORT CODE

L.L. Lengyel

A recent assessment of the potential of pellet injection for NET confirmed the necessity of developing improved pellet ablation models for thermonuclear plasmas. The existing spherically symmetric neutral gas shielding models yield results that agree, within tolerable limits, with the majority of measurements performed in ohmically heated plasmas at low and intermediate plasma temperatures. Experiments performed in high-temperature thermal plasmas yield ablation rates notably lower and those performed in plasmas with non-thermal particles present yield ablation rates considerably higher than those predicted by theory.

The physical model considered and the associated numerical code take the following effects into account: (a) The basically multi-dimensional nature of the expansion of the ablated substance in a magnetic field; (b) The ionization dynamics and its influence on the shielding and particle deposition characteristics; (c) The possible synergetic action of different thermal and non-thermal plasma particles affecting the pellet.

The expansion of the ablated substance along the magnetic field lines as well as the energy transport to the pellet by the plasma particles are followed-up with the help of a 1-d numerical code incorporating non-local heat conduction and stopping length calculations. The dynamics of the transverse expansion in a magnetic field is calculated on the basis of a semi-analytical model developed for this purpose. The temporal variations of the shielding characteristics and of the energy fluxes associated with the traversing motion of a pellet in a plasma of given temperature and density distributions are also taken into account.

2. Improvement of the SUPERCOIL design code

H. Söll

The extension of the SUPERCOIL computer program with respect to the superconducting magnet system has been completed. The areas investigated were: cooling of the superconducting toroidal magnet system by force flowing supercritical helium, and

life time calculations of the toroidal magnets on the basis of the crack growth rate concept.

The force cooling model includes cable-in-conduit conductors and hollow conductors with rectangular and circular cooling channels. Material properties of the superconductor NbTi and Nb_3Sn, for the stabilizer Cu and Al and for the supercritical helium are self-consistently taken into account.

For the lifetime calculations of the toroidal magnets, an analytical model was developed to calculate the maximum tolerable number of cycles induced in the toroidal magnets by the changes of the poloidal magnetic field.3.

INTOR Contribution

A.F. Knobloch

In continuation of previous work, the accessible data range for INTOR-like conceptual designs was studied, simplified scaling relations again being used and the guidelines commonly defined at the INTOR workshop being applied. On this basis the following results were found:

- A plasma elongation of somewhat above 2 would be needed for attaining reactor parameters not too far in outlay from the INTOR data point as of Phase Two A Part II /91/, when assuming Goldston τ_E-scaling (L-mode, x2) with continous τ_E-degradation from alpha heating power and an ignition margin of one or alternatively ASDEX H-mode scaling and a correspondingly larger ignition margin. The Troyon factor is 3.5. Engineering and nuclear layout were assumed as in Phase Two A Part II.

- The plasma current can be kept at or somewhat below 10 MA under such conditions.

- If, starting from a certain design point that is satisfactory in the above sense, the design data are consistently modified so that the initial values of the ignition margin according to the two scalings are maintained, the common range of accessible data sets is a rather narrow domain in the parameter space of plasma dimensions, current and maximum toroidal field. The tentative application of two sufficiently different τ_E-scalings reflects the present lack of one universal relation.

The findings allow the conclusion that the INTOR data point as described in /91/ can still be adapted to Troyon β-scaling with only small changes in dimensions, provided the elongation and plasma current are increased as mentioned above /IPP 4/224/. Preparatory studies dealt with the cumulative impact of improvements in input assumptions on possible reactor data /87/ and with the balanced selection of alternative enhanced parameters for INTOR design points /92/.

Stellarators

The Stellarator line of magnetic confinement uses external electric currents to produce the magnetic field in which a ring of plasma is passively contained. This line has been pursued since the foundation of IPP and during the 10 years of operation of the WENDELSTEIN VII-A this device has been the centre of the experimental activity. Successful operation of this device - in spite of its relatively small plasma cross-section - and of a few other machines in other countries has made the Stellarator line the most serious contender with the Tokamak for the future fusion reactor principle. The most important obvious difficulties with the Stellarator concept have been greatly reduced by the results of the last few years. The predicted poor containment of ions in "classical" Stellarators (such as W VII-A) was found to be drastically improved by the action of the electrical polarization of the confined plasma. The progress in the construction of the "Advanced Stellarator" upgrade of the present W VII-A, called W VII-AS, demonstrates that the technical difficulties in producing the complicated external magnetic fields can be overcome in a way which should be applicable to full-size fusion reactors. Theoretical work is continuing to tackle the greatest single remaining problem of Stellarators, namely to increase its effective confinement power, as expressed by the value of β, and has now led to impressive results. It seems likely that the stability limit to β of acceptable Stellarator configurations might exceed that of Tokamaks.

On 15 November 1985 the experiments with W VII-A were terminated, the machine was dismantled, and its upgrading into the W VII-AS started. Fortunately, none of the components foreseen for further use in W VII-AS showed major damage and need for repair. During 1986 all the necessary modifications of the base machine were finished and nearly all the new components were delivered by industry. The few remaining ones are expected to arrive early in 1987. The final assembly of W VII-AS was started in late autumn of 1986. This activity, however, still requires considerable effort to assure accurate relative positioning of all the various components, which is a consequence of the chosen time and cost saving method of constructing the individual components (coils, parts of the vessel etc.) with high internal accuracy but with flexible interfaces between them. During the assembly procedure the various components will then be adjusted by careful measurements to their proper position and this position be fixed by means of cushions filled with epoxy resin. Their thermal expansion remains possible by the introduction of sliding areas. It is hoped that the machine will be ready for measuring its magnetic surfaces by mid 1987 so that the start of plasma physics experiments could be expected for autumn 1987.

The Advanced Stellarator W VII-AS incorporates important new physical properties: By proper shaping of the magnetic field the Pfirsch-Schlüter currents are reduced in comparison to an axisymmetric configuration together with an optimization of the particle drift orbits. This leads to the expectation of higher equilibrium betas (by reduction of the Shafranov shift) and of improved confinement properties. The request of being compatible with the geometry of the W VII-structrure has allowed only moderate optimization of W VII-AS but it is large enough to demonstrate the underlying physics which is the aim of the W VII-AS experiment.

ECRH (1 GHz, 1 MW) will be used for plasma initiation, first plasma heating, and for studies in the regime of low collisionality. NI will be available at 45 keV energy and 1.5 MW power with the possibility of a later increase of the power by a factor of 1.8. Heating by ICF will be possible at frequencies between 30 and 110 MHz and with powers up to 3 MW. In 1986 large progress has been made with the installation of these heating systems, with ECF and NI in particular. These two systems will be available when the plasma experiments will start.

Even after shutdown of the W VII-A experiment the evaluation of the experimental results continued. This work was concentrated on the investigation of the heating efficiency during ECF-heating and comparison with ray-tracing calculations, on the evaluation of the local electron transport by means of a power modulation technique, the study of the impurity sources and transport, the clarification of the importance of radial electric fields for the confinement, and on the description of how the magnetic field configuration, in particular its twist and shear, influences the plasma confinement.

The experimental results on the relation of the energy confinement on the detailed structure of the magnetic configuration were compared with theoretical investigations on the same subject. This work again led to a strong support of the Garching hypothesis that optimum confinement requires the avoidance of major magnetic resonances all over the confinement region and thus also a strong limitation of shear. This result is of importance for the definition of W VII-X where this condition is used as one of the optimization criteria.

A major achievement of Theory Division 2 was the identification of the Helias configuration as a candidate for a next generation stellarator. Helias configurations appear to have favourable MHD properties, a stability limit above $\langle\beta\rangle \geq 0.05$ at an acceptable aspect ratio, as well as low neoclassical energy loss if an electric potential of the order the particle energy is present. In addition, significant progress with respect to the computation of 3D equilibria was made with the implementation of a free-boundary code (NEMEC) and a code for computing coils for given stellarator configurations (NESCOIL).

There are now four configuration classes considered for W VII-X upon which the attention is concentrated, an upgrade version of W VII-AS, several Helias versions, a modular Heliac and a bean-shaped Advanced Stellarator. During 1986 extensive numerical studies were aimed at establishing the data base needed for concept selection for W VII-X which is expected for 1987. At least some of the configurations considered seem now to possess most of the properties needed for a convincing Stellarator reactor concept.

Studies on reactor properties of Advanced Stellarators were continued in close collaboration with KfK and with the University of Wisconsin via KfK. This work complements the optimization activities in physics and introduces all those elements which need to be considered in addition when working towards a convincing reactor concept. To allow investigations in more detail these activities had started from an extrapolation of the W VII-AS configuration to reactor dimensions and has now been extended to include also those configurations which are considered for concept selection for W VII-X. It is expected that the report on these comparative studies will be finished in spring 1987.

On 31 July 1985 the IEA Implementing Agreement for Cooperation in Development of the Stellarator Concept was concluded between the US Department of Energy and EURATOM with the IPP being the Operating Agent. It is still hoped that in the near future also Japan will join this Agreement. The objective of the co-operation is to improve the physics base of the Stellarator concept and to enhance the effectiveness and productivity of research and development efforts related to the Stellarator concept by strengthening co-operation among Agency member countries. In this connection, the term "Stellarator" refers generally to all toroidal concepts based on external confinement of fusion plasmas, including Stellarators, Heliotrons and Torsatrons. Apart from an exchange of scientists and regular workshops aiming at joint evaluation of experimental and theoretical results, high value is attributed to the up-dating of the Joint US-EURATOM Report on Stellarators, Status and Future Directions (July 1981) on which task the first cooperative activity was concentrated. It is expected that also this report will be ready for publication in spring 1987.

WENDELSTEIN VII-AS

H. Renner (Physics), J. Sapper (Engineering)

W VII-AS

G. Cattanei, D. Dorst, A. Elsner, K. Engelhardt, V. Erckmann, R. Fowler[1], U. Gasparino, G. Grieger, P. Grigull, H. Hacker, H.J. Hartfuß, H. Jäckel, R. Jaenicke, J. Junker, M. Kick, H. Kroiss, G. Kuehner, H. Maaßberg, C. Mahn, R. Mathis[2], G. Müller, H. Münch, W. Ohlendorf, F. Rau, H. Renner, H. Ringler, J. Sapper, F. Sardei, I. Schoenewolf, M. Tutter, A. Weller, H. Wobig, E. Würsching, M. Zippe.

Neutral Injection

J.H. Feist, K. Freudenberger, K. Hanatani[3], J. Kolos, W. Ott, F.-P. Penningsfeld, E. Speth (Technology Division).

ECRH (Electr. Cycl. Resonance Heating)
IPF Stuttgart)

H. Barkley, W. Kasparek, H. Kumrić, G.A. Müller, E. Räuchle, P.G. Schüller, K. Schwörer, M. Thumm, R. Wilhelm.

ICRH (Ion Cyclotron Resonance Heating)

J. Bäumler, W. Becker, F. Braun, R. Fritsch, F. Hofmeister, E. v. Mark, J.M. Noterdaeme, S. Puri, K. Steinmetz, H. Wedler, F. Wesner (Technology Division).

Pellet Injection

R. Lang, K. Büchl
(Division 1)

Computer Centre

K. Behler, J. Gassmann, J. Steuerwald, I. Weidl.

1. INTRODUCTION

Assembly of the W VII-AS advanced stellarator is in progress. First experiments will start in fall 1987.

The most important new properties of the W VII-AS are the reduction of the Pfirsch-Schlüter currents $j_{\parallel}/j_{\perp}$ and the optimization of the particle drift orbits. For this purpose the magnetic surfaces are shaped to reduce the effective geodesic curvature of the field lines. It will be possible to reduce the Shafranov shift for a higher equilibrium-limit of the plasma pressure and achieve smaller collisional losses in the Pfirsch-Schlüter and plateau regimes. A system of modular field coils has been realized[4] for the optimized magnetic configuration.
The combined heating by ECF, ICF and NI will extend the parameter range of the plasma to $\beta > 1$ % and low collisionality. For this purpose a 70 GHz heating system with high power and long pulse duration ($P_N \approx 1$ MW, $\Delta t \approx 3$ s) is available to build up the plasma and heat the electrons at densities of up to $6 \cdot 10^{13}$ cm^{-3}. The advanced launching system, irradiating the polarized HE_{11} mode, provides flexibility for shaping the power deposition profiles and allows modification of the angle of incidence for current drive[5]. Further heating by NI (first stage: 1.5 MW at an accelerating voltage of 45 kV for a pulse duration of 3 s) becomes effective owing to the long interaction length of L = 2 m even at low densities ($n \geq 10^{13}$ cm^{-3}). A fast density increase can be achieved by means of pellet injectors. Different heating scenarios by application of ICF ($P_N \approx 3$ MW at frequencies 30 - 110 MHz, $\Delta t \approx 3$ s) will be tested.

---

1) Guest from ORNL, Oak Ridge
2) ZTE
3) Guest from Kyoto University
4) V. Brossmann, et al., Plasma Physics and Contr. Nuclear Fusion Baltimore (1982), IAEA Vienna (1983), Vol. 3, p. 141;
5) M. Thumm, et al. Proc. 4th Int. Symp. on Heating in tor. Plasmas, Rome (1984), Vol. 2, p. 1462;

Energy replacement times τ_E = 5 - 30 ms may be expected on the basis of TEMPL code calculations /171/ for investigations at low collisionality ($n_e < 5 \cdot 10^{13}$ cm^{-3}, $T_e, T_i \approx$ 2-3 keV) and high β ($n \approx 3 \cdot 10^{14}$ cm^{-3}, $T_e, T_i \approx$ 1 keV).

In addition a toroidal field and a vertical field allow variation of the rotational transform ι, the shear $\Delta\iota/\iota$ and the magnetic well $\Delta V'/V'$. By proper shaping of the ι-profiles the stability conditions will be investigated as a function of the plasma pressure. The main goals of the experiment are:

(1) demonstration of the optimization principle for a magnetic configuration generated by a system of modular coils,
(2) analysis of transport influenced by magnetic ripple and radial electric fields,
(3) investigation of impurity sources and impurity transport in long pulse operation,
(4) description of equilibrium and MHD stability as functions of the magnetic configurations,
(5) provision of a data base for further development of the advanced stellarator concept.

Improved instrumentation for diagnostics will be applied (Fig.1). A data acquisition system based on 12 Micro-VAX-II subunits and 2 VAX 750 units has been partly installed and tested.

2. HEATING

2.1 ECRH for W VII-AS

2.1.1 RF sources

The activities in 1986 were concentrated on upgrading the existing ECRH system (0.2 MW, 0.1 s, 70 GHz) to the full performance of 1 MW RF power, by adding four 3s, 200 kW gyrotrons. Three long pulse gyrotrons were ordered in 1984 from VARIAN, Palo Alto, US, and one from VALVO, Hamburg. The additional microwave tubes are located in the experimental hall L3. The necessary reconstruction of this hall was completed at the beginning of the year and is ready for installation of all four long pulse gyrotrons. The previous short-pulse gyrotron remains at its original site in hall L3E. All peripheral systems, such as the automatic cryogenic refill system for the superconducting magnets, the water-cooling circuits, the FC-75 RF window cooling circuits, the high voltage (80 kV) installation, the gyrotron gun-anode modulators as well as the control-room were established in L3 and completed before the delivery of each gyrotron. Due to the particular requirements of high reliability (plasma build-up) for the ECRH system, the basic philosophy in the technical realization was to make each gyrotron completely independent (except for the high-voltage supply) by providing separate

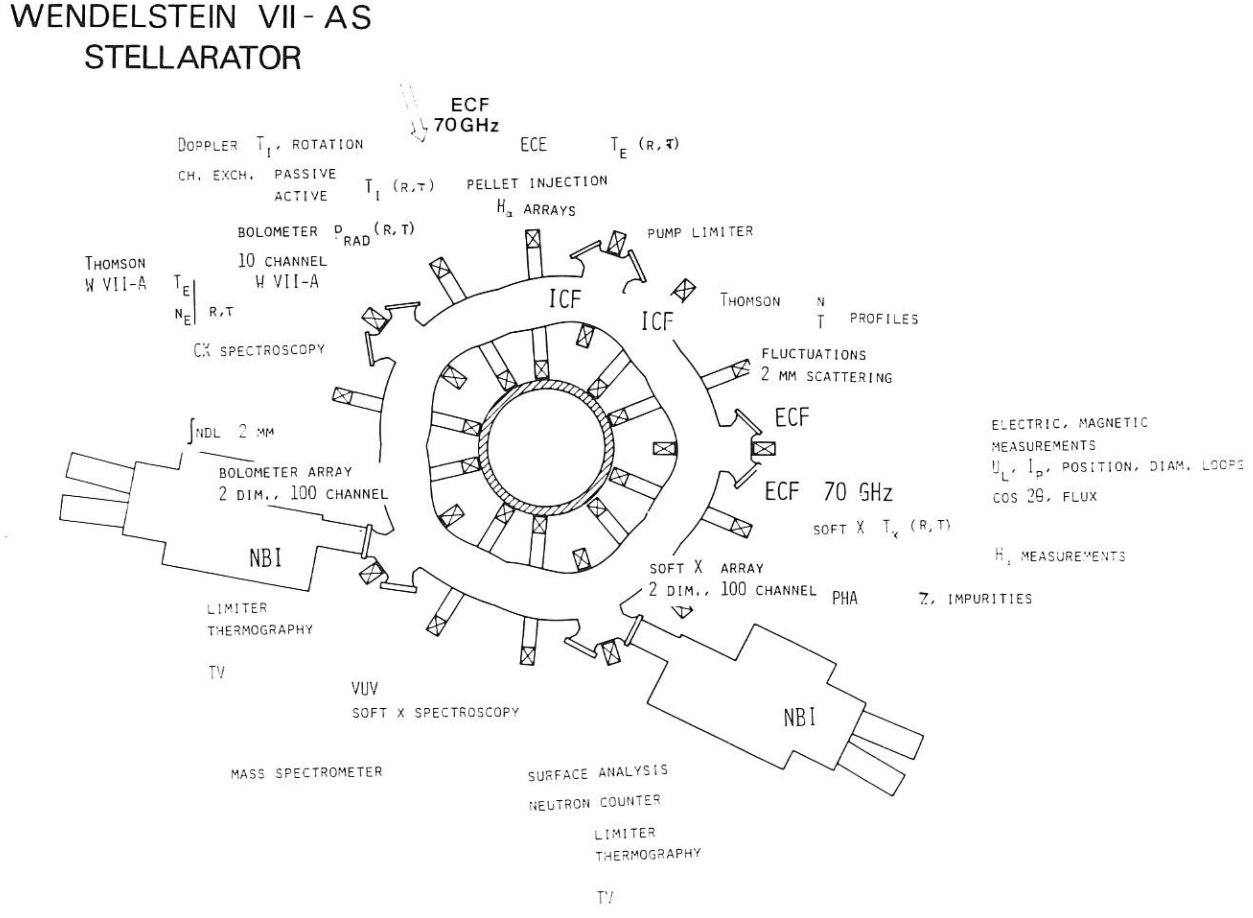

Fig.1: Schematic of W VII-AS (heating and diagnostics)

peripheral systems. The failure or repair of one gyrotron will therefore not affect the operation of the remaining system. The first VARIAN gyrotron was delivered in July, the second in September, and the third in December. The tests of three tubes together with the superconducting magnets showed the full specified performance with respect to RF output power (both exceeding the 200 kW level), pulse width (≥ 3s) and mode purity (= 95 % in the desired TE_{02}-mode) and were accepted by the IPP. The VALVO tube showed promising results at the factory test set and there is confidence that the remaining problems in meeting the final specifications can be solved by the manufacturer. Delivery of this gyrotron is expected in mid-1987.

2.1.2 Transmission lines

The microwaves will be transmitted from hall L3 to hall L7 through four overmoded waveguide systems 50 m in length. The highly sophisticated transmission lines were designed and most of the components also manufactured by the "Institut für Plasmaforschung", Universität Stuttgart. The main goal of the design was conversion of the gyrotron's TE_{02} output mode into a linearly polarized, narrow Gaussian-like HE_{11} mode, while simultaneously minimizing mode conversion to unwanted modes and transmission losses. Each transmission line consists of three bends, three mode converters, mode filters, and several up and down tapers. All waveguide components are available and tested under low-power conditions, showing experimental data close to those theoretically predicted (for details see Annual Report IPF Stuttgart, in this volume).

2.1.3 Antenna system and RF diagnostics

In order to satisfy the various requirements for ECRH and to make optimum use of the advantages of narrow power deposition, a flexible antenna system was designed and is ready for installation at the torus ports. The antenna system gives access to:

a) wave-physics studies and heating with variable power deposition,
b) EC current-drive.

Four out of five beams (long pulse) are fed in one poloidal plane using two large tangential ports, each port being equipped with two waveguides. Each beam hits a separate movable mirror mounted inside the vacuum vessel. An outline drawing of the EC wave-launcher is shown in Fig.2a, the assembly in Fig.2b.
By proper adjustment of the mirrors, the injection angle of the beams can be varied from parallel to perpendicular with respect to the direction of the magnetic axis. Balanced (co and counter) parallel injection is also possible. This degree of freedom may be of particular use for EC current-drive.

Access to wave absorption studies will be given by the ability to vary the power density in the absorption region up to 20 kW/cm² by combining all four beams in one focal spot. An array of 35 pick up horns at the inner torus wall opposite to the launching mirrors will allow control of the beam quality (divergence, polarization) and positioning. It will provide a direct measurement of single pass absorption, too.

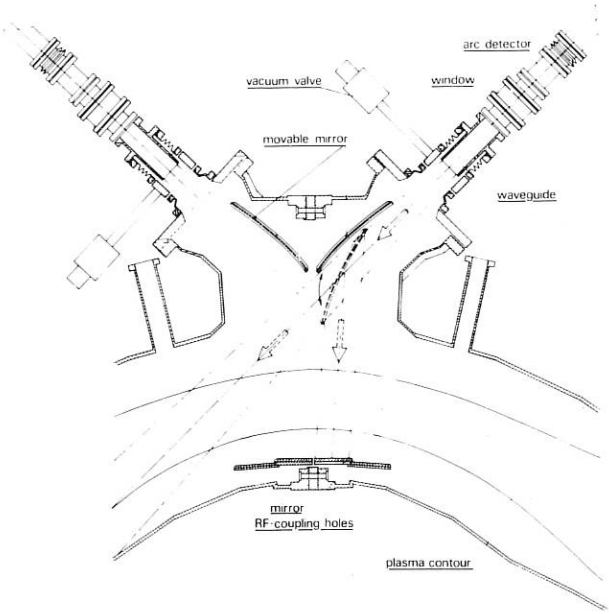

Fig.2: a) Outline drawing of the ECRH antenna, which combines four beams by means of focussing mirrors (0.8 MW source power).

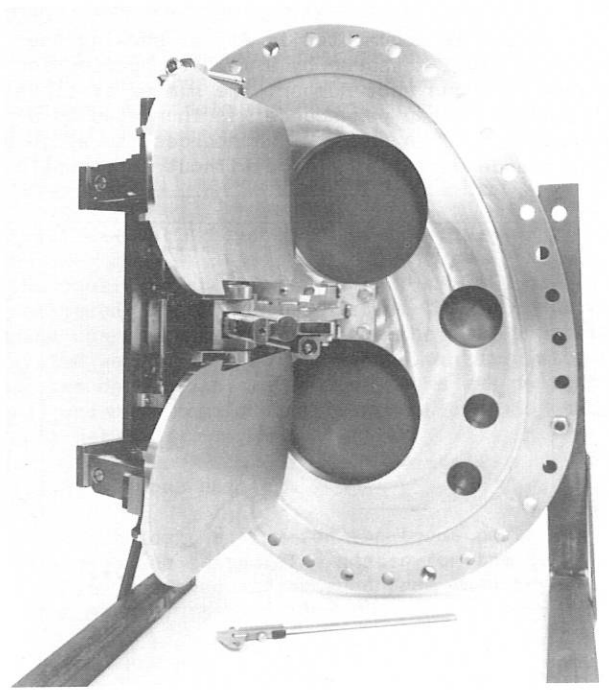

Fig.2: b) Assembly of the mirror system.

2.2 Neutral Injection Heating for W VII-AS

2.2.1 Status

Nearly all mechanical parts for the W VII-AS injection are delivered. The UHV-valve components consisting of insolation flange, entrance scraper, valve, and duct shielding as well as the supporting rails for the two boxes will follow early in 1987.

The box of the 'EAST'-beamline is preassembled. The 'WEST'-beamline is being used as a testing facility at present. The installations of the power supplies and transformer circuitry are under way after some major modifications and extensions. Two programmable control systems (S5-135U) were assembled with specially designed operating panels, one for each beamline. The corresponding software was developed and partially tested by simulating the response of single peripheral subsystems. All other electronic components needed for beamline operation and data acquisition are available and will now be tested step by step.

2.2.2 Beam impurities

The beam impurities were again analyzed in connection with our capability of gettering the internal surfaces of the W VII-AS ion sources. Using a conditioned source, the first pulses in the morning began with a level of about 3% of carbon and oxygen impurities. This level decreased from pulse to pulse until it became constant at about 1%. The same behaviour was observed earlier (see Annual Report 1984). The activation of the newly installed titanium getter filaments at first increased the impurity level again by outgassing of the filaments. But finally the getter effect dominated and reduced the impurity content of the beam to about 0.25%. This is a factor of 4 better than without gettering and still a factor of 2 better than for the W VII-A sources.

This effect is documented in Fig.3, showing the impurity level measured by a magnetic deflection analyzer versus shot number. The number of titanium filaments mounted per source was increased to 8 (compared to 2 in the W VII-A sources) to allow a long source operation period without interruption.

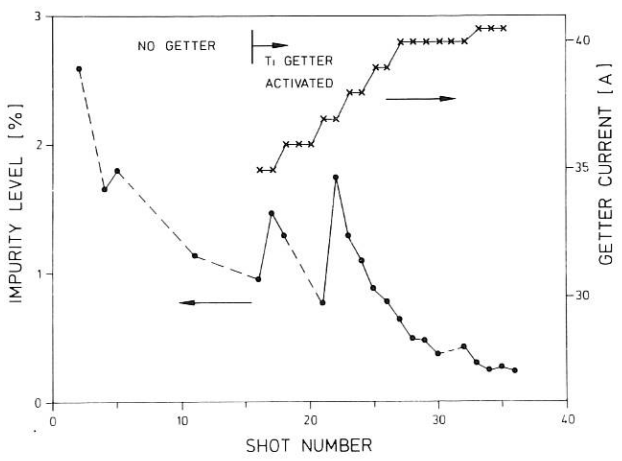

Fig.3

2.3 ICRH for W VII-AS

W VII-AS will be equipped with two ICRH antennae, installed at a distance of only about 35 cm at a position where the magnetic field has a radial gradient. Local power deposition can thus be achieved and the spectra of the radiated waves can easily be varied by adjusting the phase difference between the antennae.

The design of the antennae and feeding lines has been largely completed. The antennae are planned to be installed before the first plasma operation. A second, different antenna type for a later operation phase, has been prepared for model measurements.

2.4 Pellets

Construction of the pellet centrifuge for the W VII-AS is proceeding. This accelerator for quasi-continuous pellet-injection will be an extended version of the pellet-centrifuge which is installed at Asdex (IPP Ann. Rep. 1985, p. 66). It is planned that the new centrifuge will accelerate single pellets or series of square-shaped D_2-pellets (1x1x1.2 mm^3) up to a velocity of about 1000 m/s. Series of up to 80 pellets with a pellet frequency of up to 50 Hz can be injected into W VII-AS. In addition a single shot gun injector with variable pellet size will be used.

3. TECHNOLOGICAL STATUS

3.1 Introduction

The delivery of all essential machine components of W VII-AS, ordered from industry, was made in 1986, except for the last 8 coils of the modular field system. These coils will be delivered to IPP in the first two months of 1987, so that all parts for the assembly of the confinement system will be in the institute at the end of February 1987.

After shutdown of W VII-A in November 1985 this device was dismantled in the experimental hall up to the end of March 1986. Only the concrete basement, the lower supporting ring and the central supporting cylinder remained in place as starting equipment for W VII-AS. A lot of civil engineering work was done during the following months in- and outside the experimental hall: The new building for the ECRH transmission line, transformer basements, NI-beam chamber basements, the additional control room and alterations of the laboratory floor and doors were finished up to late autumn 1986. The final assembly of W VII-AS started in detail at that time.

3.2 Engineering

3.2.1 Modular field system

All delivered series coils for the MF-System have been tested at IPP with nominal current and pulse length. The coil deflection in two representative diameter axes has been recorded. Comparison of the measured data shows that for all coils the electrical, thermal, and mechanical qualities are within a narrow tolerance band and meet the specifications. At the time of this report the coils are prepared for final assembly into the structure shells with the radial and lateral pads and sliding areas.

3.2.2 Structure

The central supporting cylinder and the upper and lower supporting rings of the machine were prepared

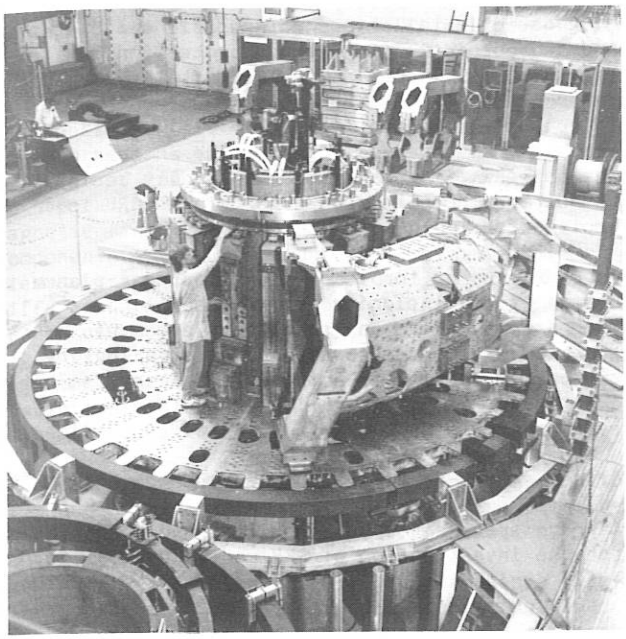

Fig.4: Partially mounted structure shells on the central supporting structure of W VII-AS, Nov. 1986.

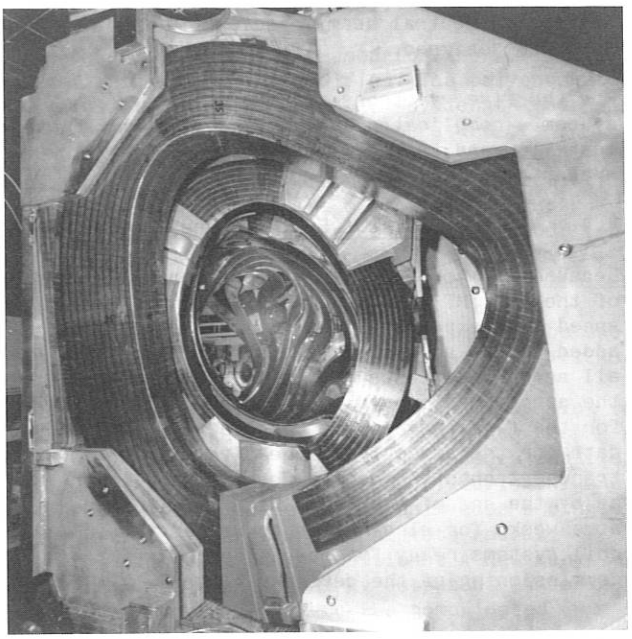

Fig.5: Preassembled module, view into the bore in the direction of the plasma axis.

with new cutouts and bores for the new port hole positions of W VII-AS. All structural parts and supporting elements have been delivered with the specified quality to IPP. A preassembly test of the total structure was made, so that all tolerances of the radial and circumferential dimensions could be checked. The status of the assembly with partially mounted structure shells is shown in Fig.4.

3.2.3 Module assembly

The modules will be assembled as follows:

- insertion of MF-coils into the half-shells with provisional bedding by local spacers for the purpose of final and detailed adaption of the supporting elements and the current bridges
- after dismantling, final machining and correction of the supporting elements
- treatment of supporting elements in the area of the coil terminals with insulation coating
- application of resin casting in the gap between the cast steel supporting elements and the milled sheet steel surface of the structure shells. This ensures a homogeneous mechanical performance of the coil structure
- final reassembly of the modules with final embedding of the coils by resin casting of the tolerance gaps between coils and supporting elements.

In Fig.5 a preassembled module together with a preassembled enlarged coil in its separate housing is shown. At the time of this report the preparatory work for three complete modules had been finished and final assembly of the first module has started.

An additional assembly test established how to insert the torus parts into the bore of the modules. All tools and devices for the final assembly have been improved in this respect.

3.3. Auxiliaries and Power Supplies

3.3.1 Cooling system

The cooling system for the W VII-AS coil sets was delivered, installed, and tested. The water-flow pick-ups and thermocouples for the coil protection system were developed and tested. An acquisition system on the basis of data-loggers was designed and ordered from industry for protection of the coil set.

3.3.2 Torus heating

The electrical heating for the torus ports was developed and tested. The heater for the torus wall area was designed and ordered from industry (hot water system, 15 bar, 180° C).

3.3.3 Power supplies

An additional gyrotron HV-power supply (110 kV, 40 A dc, 3 s) was installed and prepared for commissioning. In future five gyrotrons can thus be supplied in parallel from this power supply which is connected to one of the flywheel generators. A new power supply for NI (50 Hz, 2.2 MW, 10 s) was installed. A separate air cooled indoor transformer is used for decoupling the other mains from ripples which are generated by the thyristor rectifiers for the beam-shaping coils.

A new HV-power supply and installation for the diagnostic neutral beam injector (50 kV, 40 A dc, 3 s) was designed.

For the five gyrotrons and their voltage regulation system a complicated interlock system was designed, installed and tested with a programmable control system.

3.4 Time Scale of Delivery and Assembly

Because of another delay of four months in delivery of the last MF-coil, caused by a lower fabrication speed than expected, an additional delay has to be added to the scheduled data of the past year. Since all acceptance tests of the delivered material meet the specifications, a surer schedule can be made for the final assembly of the machine. The earliest date for the assembly of the five modules and their transport onto the central structure will therefore be by the end of May 1987. With an allowance of some weeks for closing the torus and getting the coil systems ready for operation the start of commissioning of the device will be July 1987.

4. DIAGNOSTICS

4.1 Magnetic Diagnostics

Besides the standard magnetic field diagnostics (loop voltage, Rogowski coil, diamagnetic coil, Mirnov coils) two additional magnetic diagnostics are being prepared for W VII-AS which are especially designed for use in an almost net-current-free stellarator.

The first ($B_{P\zeta}$-coils) is intended to measure the small poloidal field components of pressure driven currents in the plasma (Pfirsch-Schlüter currents). Information can be gained on the average plasma pressure together with the integral magnetic field geometry. Second-order terms of this field depend on the plasma position. The main problem will be to distinguish between these small field components and the vacuum field or the field produced by a net plasma current.

The second additional diagnostics is an approximated $\cos 2\theta$-coil. Used at a position with strongly elliptical magnetic surfaces the signal of a $\cos 2\theta$-coil depends on the current density distribution of a net plasma current. It is anticipated that in the case of small residual currents (no external loop voltage) as observed in W VII-A it will be possible to discriminate between a centred current density distribution and a hollow one expected, for example, with a bootstrap current.

4.2 Plasma-wall Interaction Control System

Completion of the rail-type primary limiter cooling and support structures is expected to be on time with respect to the assembly of the machine. Main components of the limiter cooling system were installed. The TiC-coated graphite tiles of the limiter front sides were finally specified and ordered.

The concept of secondary limiters and graphite shielding was completed with certain NI aperture-limiting wall protections, shieldings of some diagnostic installations (diagnostic coils etc.) and two poloidal ICRH antenna protection limiters. The latter will consist of horizontally moveable water-cooled support structures (SS) covered by TiC-coated graphite tiles. They will be placed close to the toroidal edges of the antenna modules. The antenna limiters are being finally designed now and will be completed on time before ICRH is implemented.

In order to monitor temperatures of near-plasma installations including primary as well as secondary limiters and shieldings a set of thermocouples and a corresponding data-logging system was specified. A thermographic system has been defined to monitor limiter surface temperatures and is now finally being specified.

4.3 Soft-X-ray and VUV Spectroscopy

A Bragg spectrometer was designed and constructed for the investigation of SXR radiation (0.1 to 4 nm) during the start-up phase of W VII-AS. The small instrument is completely metal-sealed, the crystals (KAP, stearates etc.) are easily interchangeable and it can be equipped with different detectors, i.e. MCPs and proportional counters. The resolving power (~ 1000) is kept moderate to enhance radiant flux to the detector. Special efforts were made to reduce long-wave-length stray light and fluorescence radiation.

In order to calibrate SXR spectrometers, a 1.5 kW X-ray tube with large-area air-cooled anode was designed and will now be constructed. It will operate in two modes: as a high-power X-ray tube with different anode materials and as a fluorescence tube. The tube will be attached to the spectrometer and can easily be withdrawn for the spectrometer viewing at the plasma.

Conceptional studies have been performed for the VUV space-resolving diagnostic using two rotating mirrors, similar to the W VII-A system. Detailed design work has begun. The two mirror systems (optical axes at right angle to each other) provide spatial scans of the full minor cross-section in the spectral region 40 to 120 nm with $\Delta t \leq 20$ ms.

4.4 Diagnostic Injector

The diagnostic injector on W VII-AS serves as a tool for active and thus spatially resolved measurements of CX-particles and CXR-photons in order to gain information on the radial ion temperature profile of the plasma.

The W VII-A diagnostic injector had to be changed to fit the W VII-AS conditions. For the benefit of the CXRS measurements the beam energy was increased to 36 keV. The whole beamline had to be redesigned for geometrical reasons. The electrical supplies and controls as well as the vacuum system were redesigned, too.

The beam of neutral hydrogen particles will be vertically injected into the plasma in a plane of elliptical plasma cross section. It will intersect the plasma column with an area of about 4 cm x 10 cm. This results in optimum spatial resolution and intensities for the intersecting lines of sight of

the CX analyzers or the CXR spectrometers (see sect. 4.5 and 4.6).

4.5 Ion Temperature and Plasma Rotation

Charge Exchange Recombination Spectroscopy (CXRS) will serve in W VII-AS as a means to obtain radial profiles of ion temperature and plasma velocity, in both parallel and poloidal directions to the magnetic field. In order to separate the two components a volume element is simultaneously viewed by two identical spectrometers but at different angles of observation. The volume element is defined by the intersection of the lines of sight with the neutral beam of the diagnostic injector (see sect. 4.4), thereby allowing a radial resolution of about 2 cm or better. The radial scan is achieved by turnable mirrors.

In addition, a third spectrometer serves as monitor of the central ion temperature and of the relative change of the central impurity concentration.

All three spectrometers will view the plasma via mirror optics, thus allowing changes of wavelengths without realignment of the optics.

Each spectrometer will be provided with a 15-channel photomultiplier-equipped quartz fibre-optic as detector system allowing single-shot measurements.
The results of these measurements will also provide a possibility to determine the relative radial distribution of oxygen and carbon, and, with more detailed knowledge of the diagnostic beam, their absolute radial distribution, too.

The monitoring spectrometer will be the first to go into operation. It is scheduled for August 1987. The other two will follow by the end of 1987.

4.6 Neutral Particle Energy Analysis

The ion temperature profile will be measured by analyzing the CX-particle flux arising from four different points along the vertical beam of the diagnostic injector. Two 10-channel and two 5-channel analyzers are arranged along a vertical line and the whole set can be moved up and down to scan the plasma diameter. The access to the diagnostic beam will be provided through a tangential port. The line of sight intersects the magnetic axis at an angle of 36°, the radial resolution is 4 cm in the horizontal direction. This allows the temperature profile to be measured with a resolution of 2 cm or better provided the diagnostic beam (see sect. 4.4) is properly adjusted to the axis of the almost elliptical plasma cross section.

The mechanical structure for supporting and moving the four analyzers has been designed and construction is under way.

4.7 Thomson Scattering at W VII-AS

For measuring the electron temperature and density distributions by laser light scattering, two systems are under construction which will be used at different cross-sections of the plasma, a) elliptical and b) triangular.

a) In this case the system used for the W VII-A stellarator is being modified. The polychromator system will be upgraded to 7 wavelength channels to cover also an electron temperature of 2-3 keV. Profiles will be taken shot by shot along the large axis of the ellipse (vertical) for the radial scan. The optics with counter-rotating prisms had to be considerably modified for the W VII-AS geometry. It now allows positions even 2.5 cm behind the maximum limiter aperture to be observed.
The system will be completed in time, to be used during the first experimental phase of W VII-AS.

b) At the triangular cross-section the laser is focussed through a horizontal port into the plasma. This allows changes in pressure profiles (induced by high plasma pressure) during high-β operation to be detected. In this case a single laser shot will deliver a complete radial profile from 20 radial positions. A new ruby laser system with an energy output of 15 Joules has been bought. Owing to the complicated geometry for Thomson scattering a small section of the torus was manufactured separately to allow tests of optical components and experiments to reduce parasitic light. The detection of the scattered light has to take place through 2 observation ports at 121° and 143° with respect to the laser beam. Two special composite objectives had to be developed and are already completed. The laser beam is focussed onto an array of 20 light guides, which transmit the scattered light to 20 interference filter polychromators of that type which already was successfully used on W VII-A.

   This system requires considerable effort and time and will therefore be ready for operation in a later experimental phase of W VII-AS.

4.8 ECE Instrumentation at W VII-AS

A new multichannel radiometer system for W VII-AS was designed and partly constructed. Diagnostic aims are to determine $T_e(r_i,t)$, the electron temperature as a function of time for 12 different radii r_i and to gain information about the suprathermal electron content from the electron cyclotron emission spectrum recorded at the 1st, 2nd, and 3rd ECE harmonics.

The system is designed for 2.5 T on the axis, which is the W VII-AS standard case. The main plane for ECE offers an almost elliptical plasma cross-section. Here three fixed antennae for the different harmonics are placed in the horizontal symmetry plane together with two toroidally revolvable ones. In addition two 2nd harmonic horns are mounted in two planes above and two planes below the symmetry plane, so it will be possible to obtain the full spatial dependence of the electron temperature in the poloidal cross-section. ECE measurements will be carried out in two further planes, parallel to B = constant lines in the region where electron cyclotron heating power is fed into W VII-AS. In this observation geometry suprathermal population can be detected most significantly. The other observation plane is of

triangular plasma shape. In this plane no 1/R dependence exists, B is almost constant in the plasma center region, resulting in a narrow emission line. Again the suprathermal electron content and finite plasma pressure should clearly affect both width and center frequency of the spectrum. Altogether 13 antennae will be used alternatively. They are designed as optimum-gain circular horns each including polarization and high pass filters formed by fundamental-mode rectangular waveguide pieces. Torus feed-through is accomplished by newly developed quartz windows optically matched with PTFE layers on both sides. Signal transmission is in TE_{11} mode in overmoded circular copper wave-guides to the receiver station. The full system can be absolutely calibrated. Calibration can be controlled and a number of functions checked without any disconnection of individual parts for optimum reproducibility.

4.9 Bolometry at Wendelstein VII-AS

The integral energy loss by radiation at the W VII-AS stellarator will be measured by means of Ge-bolometers. Two 32-channel pinhole cameras will be employed for two-dimensional profile analysis. Furtheron a 10-channel turnable bolometer probe and a number of single uncollimated bolometers (2π geometry) are expected to give information on radiation sources with toroidally asymmetric distribution.
The 10-channel system is an advanced version of the one described in the Annual Report 1984, p.100. It has been redesigned to allow its use at different ports of the torus, especially at those positions, where the plasma is elliptical or nearly triangular.

A technical problem arose during the manufacturing process of the Ge-bolometer detectors, as the insulation layer could not be reasonably reproduced. Thus a series of tests became necessary which are still underway.

4.10 Probe Diagnostics in Preparation for the Stellarator W VII-AS

A probe array of 32 probes placed on well-defined positions outside but aligned to the outermost magnetic flux surface is under construction. All probes of the array will be arranged equally spaced in the poloidal direction in one toroidal plane. Ion fluxes I_{pr} as well as floating potentials U_{pr} both vs. time, can be measured with the probes of the array. The probes will be sensitive to the +/- toroidal components of the signals. The array will be movable in radial direction and adjustable to the outermost magnetic flux surface (at a triangular plasma cross-section). The probes and the covering of the probe housing will be made from high-density graphite to prevent new impurity materials being introduced into the plasma. A second probe array to be build in at a different poloidal position is intended to be constructed later.

Single RF-Probes,, coaxially built-up, dc up to 1 GHz and radially movable are planned for the W VII-AS stellarator. One application of these probes will be to measure low-frequency plasma fluctuations in the plasma edge region, where edge oscillations of high amplitudes are expected.

Dynamic AC double probes, for measuring of n_+ and T_e vs. time, with a time resolution of $\Delta t \leq 1$ ms, again radially movable, are also planned for W VII-AS stellarator. Electronic hardware has been developed in part.

Triple Langmuir probes for measurements of n_+ and T_e vs. time, also radially movable, are to be prepared.

4.11 Electron Density Diagnostics

The design of a 337 µm interferometer for line electron density measurements has been completed. For reasons of restricted access to the W VII-AS only three parallel probing beams, spaced at 70 mm, are operated. The reference beams are modulated within a frequency range from 10 to 100 kHz by the rotating grating technique. To avoid errors in the plasma density measurement due to the mechanical stress during a shot, the optical elements, i.e. beamsplitters and mirrors, are supported on a frame independent of the machine. The 337 µm HCN laser and the optical components have been tested and are pre-aligned. The supporting structure is under construction.

5. DATA PROCESSING

5.1 Data Acquisition

5.1.1 The UDAS concept

In 1983 development of a new "Universal Data Acquisition System" (UDAS) was initiated. Implementation of the most essential functions of the system was completed in 1986. A more detailed description of the UDAS concept is being written and will be published in the near future.
A significant advantage of the UDAS data acquisition system is its flexibility in the following respects:

- The range of possible application of the UDAS concept extends from an autonomous, single-user system to a distributed multicomputer network that is organized in several levels.
- A large selection of interfacing for data acquisition hardware is available (CAMAC, IEEE488, IEEE802, Parallel, V24 etc.).
- The data acquisition software is to a large degree independent of the operating system and the processor type since it is written in high-level languages (PASCAL and FORTRAN).
- The number of computer systems as well as the data acquisition hardware can be extended without software modifications.
- The data acquisition sequence is almost completely automatic.

The following passages give a short description of the history and the current state of the develop-

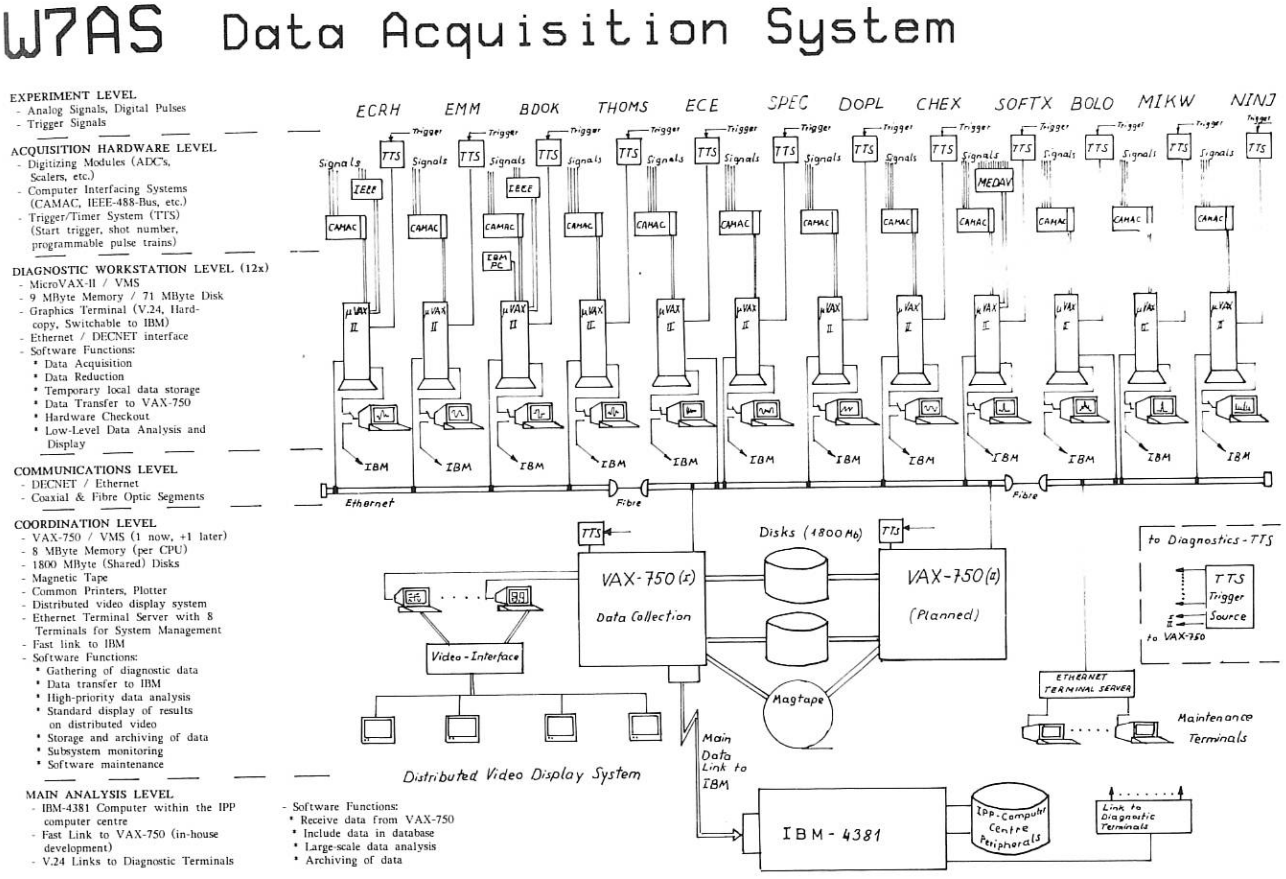

Fig.6

ment of UDAS.

5.1.2 Developments up to 1986

The W VII Data Acquisition Group began the planning of a new data acquisition system for W VII-AS in early 1983. The first step was the definition of the data structure of the acquired experimental data based on experience with data acquisition systems previously used at IPP and on discussions with members of other experimental groups and the Computer Centre. This stage was completed by June 1983.

In the next phase, a first working version of a single diagnostic subsystem was implemented to run on a LSI microcomputer (PDP-11/23). The software was for the most part written in the PASCAL programming language. Only those routines directly controlling the experiment hardware - a small fraction of the entire code - were written in PDP-11 Assembler. A simple trigger device to start the data acquisition process was developed; a prototype was operational by 1985.
At this point, the decision was made to implement the ultimate version of the diagnostic subsystem on Micro-VAX microcomputers, to overcome the narrow limits on program size inherent in PDP computers (a maximum of 64 K-Bytes virtual address space).

Furthermore, ETHERNET was chosen as a hardware network standard for the interconnection of the subsystems among each other and to a central archiving and control computer (a VAX 11/750). This choice was made because of the high throughput possible with ETHERNET and because ETHERNET-compatible hardware is available from many manufacturers.

The conversion of the diagnostic software to run on the Micro-VAX was made without major difficulties. Only the assembler routines had to be rewritten. The adaptation of the PASCAL programs to the VAX compiler was completed with only minor changes in a very short time. An initial version was operational in November 1985.

5.1.3 Developments in 1986

5.1.3.1 Planning

The final structure of the overall data acquisition system was defined in early 1986 (see Fig. 6). One Micro-VAX computer is dedicated to each of the 12 experiment diagnostics. Each Micro-VAX is configured as a work station allowing the diagnostic owner to acquire experimental data, perform a preliminary analysis, and display the results independently of the rest of the experiment.
The diagnostic computers are connected via an

ETHERNET channel. DECNET - a standard software product of the computer manufacturer DIGITAL - was chosen as the transmission protocol in all computers.
Also connected to ETHERNET/DECNET is the central computer, a VAX 11/750. This machine handles the tasks of collecting the data from the individual diagnostics and integrating them into a single data set, storing them on magnetic disk, and immediately passing them on to the W VII-AS main analysis computer, an IBM 4381, in the IPP Computer Centre. Also to be run on the VAX 11/750 are programs to do a standard analysis and display of data immediately following each shot.

Transmission of the data to the Computer Centre is handled by a fast interconnect between the VAX 11/750 and the IBM 4381 being developed at this institute.

In case of failure of the central computer or the ETHERNET channel, the diagnostic computers can continue operating on their own. The storage capacity of the disk at each diagnostic is dimensioned to hold all data acquired in one day of operation.

All computers run under the VAX/VMS or Micro/VMS operating systems.

5.1.3.2 Software

The programs for the diagnostic subsystems were extensively tested and have been completed. In particular, additional device-specific driver programs for new data acquisition modules were created. Handy dandy module test programs and an auto-configuration program (automatic detection of which data acquisition hardware modules are actually connected) were implemented. The handling of the trigger-timer system (see below) was incorporated into the control program (CP).

A subroutine package to handle devices connected to an IEC Bus (IEEE-488) - to be used within future module driver programs - was developed.

In the area of computer networking, timing measurements confirmed that the data transfer rates (throughput) achievable with ETHERNET/DECNET are sufficient by far to meet the time limit of under 30 seconds from the beginning of a shot to the availability of the data on the central computer, assuming a total data amount of 2 megabytes. A general software package for DECNET communication between PASCAL programs was developed.

To support the programmers of data analysis software, a set of FORTRAN-callable data access routines for UDAS data sets was written. The GKS library (basic terminal-independent graphic functions) was installed and checked out.

5.1.3.3 Hardware

A prototype of the trigger-timer system was built and tested. The plans are ready for series production by an external firm.

Each TTS unit has a master controller (MC), which synchronizes the computer operations with trigger pulses received from the experiment control hardware. The MC also receives system-wide information items, such as trigger times, current date, shot number, etc. and passes them on to the connected computer.
Additionally, TTS units on the diagnostic computers have timer modules (TM), which generate programmable pulse trains to control the sampling of the data acquisition modules.

A digital input/output module was developed to provide economical transmission of quasistatic digital signals between galvanically decoupled areas. Up to 256 binary signals may be tested or set using this device. The input signals are encoded into hexadecimal ASCII digits and sent via a fibre optic cable (in V24 standard) to the computer. In the other direction, output signals from the computer are sent via the fibre, decoded, and placed on the individual output lines.

5.1.4 Outlook for 1987

Development for the diagnostic subsystems is largely completed as far as autonomous operation is concerned. Two systems are ready to be handed over to the physicists for hardware development and testing. A training workshop for users is planned for April 1987.

By this time demonstration programs for data analysis and graphic display will be available.

The software for transferring diagnostic data to the central computer is under development and a preliminary version will be available in April.

The connection between the VAX 11/750 and the IBM 4381 is being developed by the Computer Centre Division. The work is well under way and will be completed by July 1987, so that all major functions of the data acquisition system will be available by the time W VII-AS goes into operation.

5.2 Data Base System for W VII-AS

To obtain a quick overview of the essential results of the W VII-AS experiment for the SPIRES data base manager three subfiles have been developed which povide information on the physical objectives, particulars of the discharges, and evaluation of the data.

5.2.1 SPIRES data base manager

The SPIRES data base management system (DBMS) is running in the VM/CMS environment.

SPIRES is a multi-user system with a flexible file structure, i.e. a subfile can be relational or hierarchical in structure.

SPIRES provides a high-level retrieval language; there is also an easy-to-use interface for end-users.

SPIRES is suitable for unstructured data and any input/output formatting is possible. Data security and integrity are guaranteed.

5.2.2 Subfiles in SPIRES for W VII-A and W VII-AS

5.2.2.1 INFOPP subfile

The characteristic data of the machine configurations for one day of operation are specified in the INFOPP subfile. During interactive work at the terminal the physicist can use a menu control to obtain a quick overview of essential parameters such as plasma current, magnetic field, target gas, heating methods etc. By means of the Fortran interface these parameters can be used in evaluation programs as selection criteria for single discharges and sequences of discharges (shots).

5.2.2.2 INFOSHOT subfile

The INFOSHOT subfile contains the relevant information for the single shots and shot sequences. This includes data on the diagnostics installed, the presence of evaluated data, the quality of (preliminary or validated) data, and evaluated single measurements and radial profiles of plasma parameters.

5.2.2.3 INFOFRAME subfile

This subfile contains the descriptions of the diagnostics and of the physical quantities measured.

Figure 7 shows how the three subfiles are organized and how they are interlinked.

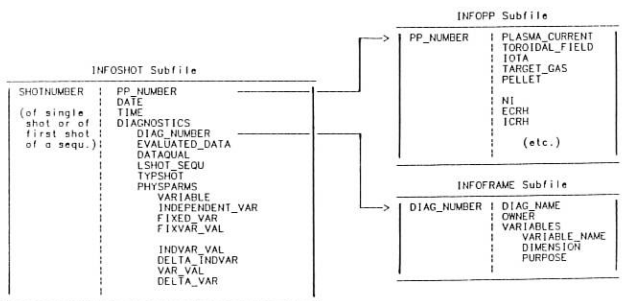

Fig.7: Organization of the subfiles for W VII-AS

The three subfiles contain some of the results of the W VII-A experiment dating from 1985. Further completion of the data sets is under progress.

Data of the W VII-AS discharges will be kept from the start of the experiment and will then be available for analyzing.

6. EXPRIMENTAL RESULTS FROM W VII-A

After shutdown of W VII-A in November 1985 analysis of experimental data was continued. The main lines of research in W VII-A were investigation of the heating efficiency during ECF-heating and comparison with ray-tracing calculations /41/, evaluation of the local electr. transport by means of a power modulation technique /58/, study of the impurity sources and transport /387/, clarification of the importance of radial electric fields for the confinement /466/, and description of how the magnetic field configuration, on which the rotational transform and shear depend, influences the plasma confinement /51/.
Optimal confinement was achieved (1) far from "resonances" at rational values of the rotational transform ι = m/n at the boundary and (2) with low shear, which excluded resonant surfaces in the entire plasma. The results of a detailed analysis of the electron transport in the centre are found to be in reasonable agreement with predictions of the neoclassical model including helical ripple. In the edge region an anomalous transport coefficient assumed to be the same as derived from ohmically heated discharges becomes important.

For ECF-generated discharges ambipolar electric fields have been calculated on the basis of a neoclassical transport model and correlated to experimental density and temperature profiles under the condition $\Gamma_e = \Gamma_i$. A comparison with electric fields derived from measurements of the poloidal rotation by means of the Doppler shift of spectral lines from oxygen and carbon shows good agreement. Under the conditions of W VII-A ($\iota \sim 0.5$, aspect ratio A = 20) the ion heat conduction is significantly reduced by the observed electric fields ($E_r \sim 100 - 200$ V/cm). Even higher electric fields are observed to be generated by the fast ion losses during NI.

Particle transport in the centre seems comparable with neoclassical descriptions. However, it has to be concluded that there are strongly enhanced losses in the boundary region. For NI -sustained discharges, the impurity transport in the case of Al trace-impurities injected by laser blow-off and of intrinsic impurities is found to be in good agreement with neoclassical models. In contrast, fast loss of impurities is observed in pure ECF discharges.
Presumably, impurity accumulation could be reduced by means of gas-puffing pellet injection and power deposition for proper shaping of the boundary conditions, density profile and temperature profile and by means of ergodization of the magnetic surfaces.

The plasma confinement exhibits a strong dependence on the rotational transform and on the shear of the magnetic field configurations. Extended studies involving variation of the rotational transform and shear by both, internal (pressure, I_p) and external measures (torsatron configuration), indicate favourable confinement properties for configurations with small positive shear to exclude "resonant" surfaces. The influence of the pressure profile and pressure-driven currents (bootstrap currents) has to be taken in account. So far, perturbations due to island formation and ergodization as evaluated by numerical studies of the configuration fit the observations rather than being due to MHD instabilities.

6.1 Structure of Magnetic Surfaces in W VII-A

The structure of magnetic surfaces in W VII-A has been investigated using the mapping technique. Field line integration is thereby replaced by an

area preserving map which allows the structure of magnetic surfaces perturbed by various external error fields to be studied. The various Fourier harmonics in the spectrum of the error field create primary islands on resonant rational magnetic surfaces. Close to $\iota = 1/2$ or $\iota = 1/3$ only high-order rational surfaces exist and islands can only be generated by higher harmonics of the error field. The size of islands has been computed when varying the amplitude of the error field, its Fourier spectrum and the external rotational transform. The region occupied by islands is found to be smallest if ι_0 is close to $\iota = 1/2$ or $\iota = 1/3$. With the perturbation and the shear kept fixed the effective plasma radius (geometric radius minus island width) is shown in Fig.8. These results confirm the idea that islands generated by symmetry-breaking perturbations are responsible for the deterioration of confinement in W VII-A. An increase of the shear leads to a rapid overlap of the primary islands and to the onset of stochasticity. It is found that high shear stellarators exhibit stochasticity of field lines at smaller error fields than low shear systems.

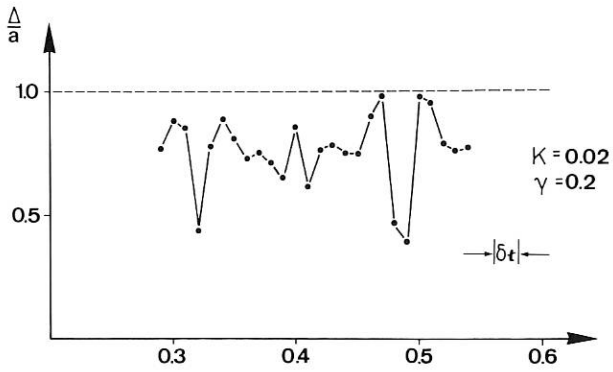

Fig.8: Effective plasma radius vs. boundary value of ι, with a as plasma radius.

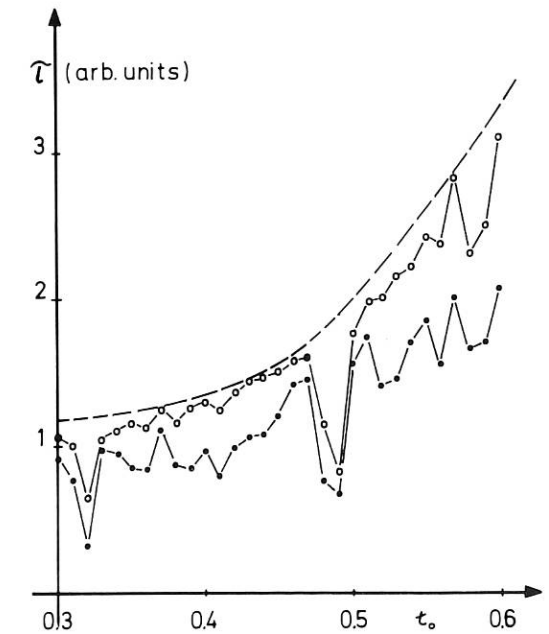

Fig.9: Confinement time vs. rotational transform, Effect of external field perturbation.

6.2 Diffusion in Partly Destroyed Magnetic Surfaces

The mapping technique which has been useful in studying the structure of magnetic surfaces has been extended to describe diffusion of circulating particles in magnetic fields with islands and ergodic layers. The theory starts from the Hamiltonian formalism of drifting particles and calculates the generating function of the map from an approximate solution of the Hamilton-Jacobi equation. The map T_μ contains the magnetic moment μ of the particles. A numerical code has been developed which follows a sample of 1000 particles by iterating the map T_μ. Either the diffusion coefficient or the confinement time of the test particles can be computed. In applying the method to W VII-A it is of interest to keep the external perturbation fixed and to vary the external rotational transform. As expected, the islands on rational surfaces enhance the test particle transport and reduce the confinement time. The normalized confinement time of test particles is shown in Fig.9. The effect depends on the Fourier spectrum of the external perturbation, as expected. Close to $\iota = 1/2$ or $\iota = 1/3$ where only high order rational surfaces exist reduction of confinement is small. The dashed line indicates the confinement time without external perturbation.

6.3 Impurity Confinement for NBI-sustained Discharges with Additional EC Heating

Extensive simulation studies were carried out in order to analyze the transport behaviour of both the injected Al trace impurities and intrinsic impurities for W VII-A discharges, heated jointly by NI and ECR. During the 150 kW, 50 ms ECRH pulse a flattening of the density evolution is typically observed (see Fig.13). This flattening may be explained by deterioration of the particle confinement during the ECRH pulse or by reduced penetration of recycled neutrals due to edge deposition of ECRH power. The interpretation of reduced particle confinement is supported by the observed evolution of the Al radiation from soft-X and single-line radiation measurements which indicate a fast loss of Al from the plasma center contradiction to neoclassical theory. The time-scale for the decay of the radiation and the values of D_{anom} required to simulate it with the code were about the same as for pure ECRH discharges.

The soft X-radiation from the intrinsic impurities for this discharge type is shown in Fig.10a. In a previous paper /84/ it was shown that the increase of the central radiation could be reproduced reasonably well by pure neoclassical transport with oxygen impurities from 1 % beam contamination and from wall-influx rising from 2×10^{18} to 5×10^{18} s^{-1} during the discharge. However, if the same anomalous behaviour is assumed for the intrinsic impurities as for the ablated Al during its escaping phase from the plasma center, i.e. if the same D_{anom} is added while keeping the wall influx unaltered, then the central oxygen radiation drops to unacceptably small intensities. In this case, the measured radiation (Fig.10b) could only be reproduced if the oxygen influx at the plasma edge was raised by almost an order of magnitude with respect to the values assumed for the neoclassical simulations. However, only about 10 % of this

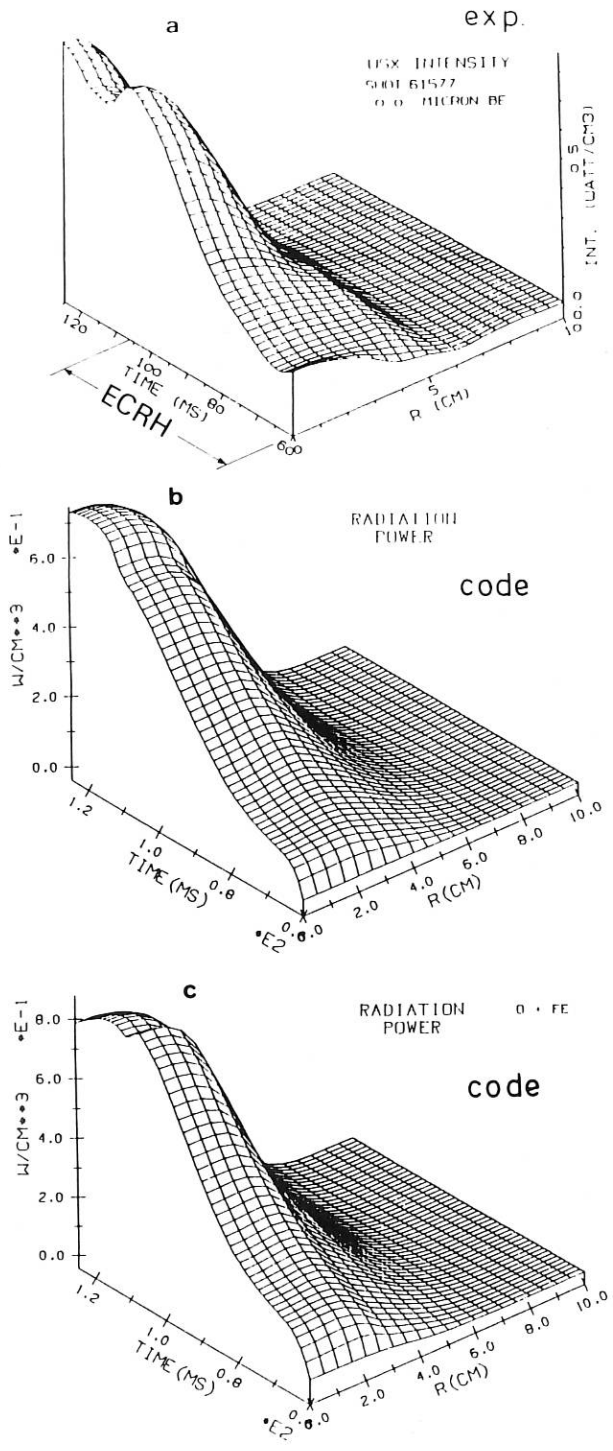

Fig.10: a) Evolution of soft X-radiation for a NBI + EC-heated discharge.
b) Code simulation of OVII and OVIII radiation with neoclassical + anomalous transport.
c) Same as b), but with additional Fe impurities.

---

impurity influx contributes to the increase of the central oxygen density. The remaining 90 % circulates, after ionization, back to the wall, thus keeping the impurity gradients at the plasma edge higher than in the neoclassical case.

In this picture of enhanced transport the typical neoclassical impurity accumulation is strongly reduced. That is, for a given central radiation level the impurity density at the edge can be maintained at a substantially higher level than in the neoclassical picture. This may facilitate impurity removal from the plasma edge.

In order to improve the code results during the late stage of the discharge, additional high-Z material was included in the simulations (Fig.10c). Such impurities could originate, for example, from sputtering of plasma ions at the vacuum vessel wall (Fe, Cr) and sputtering at the limiter and NI beam dump plates (Mo)[1) 2) 3)]. By assuming an Fe influx from the wall of 4 % of the oxygen influx, the measured central radiation could be qualitatively reproduced.
For the same discharge type, the evolution of the O^{8+} density has been measured by CX recombination spectroscopy (active signal) /84/. On the other hand, the passive signal obtained with the diagnostic beam off yields a flux which is proportional to the O^{7+} density /84/. The time histories of both signals are reproduced reasonably well by the simulations (Figs. 11,12). In particular, the decrease of the O^{8+} density relating to the T_e drop observed after switching off the ECRH pulse is clearly confirmed by the CX recombination measurements (ΔT_e = 140 eV within 10 ms).

Electron confinement: Starting from ECRH target plasmas NI leads to density increases of $N_e \approx 0.5 - 2 \times 10^{20}$ s^{-1}, as in NI discharges starting from OH target plasmas, which can be explained by the total particle influx from the

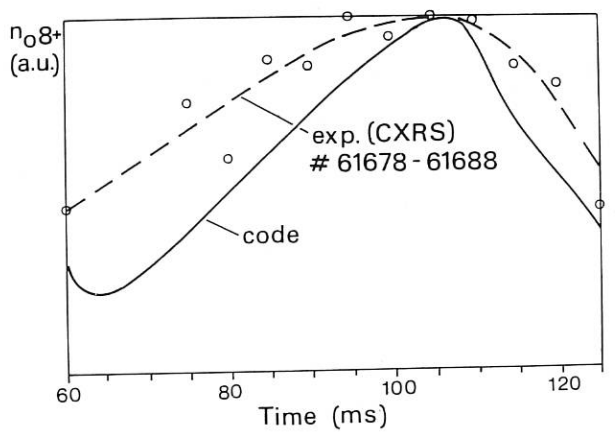

Fig.11: Central O^{8+} density (a.u.) vs. time from active CXRS measurements in comparison with code calculations.

---

1) W VII-A Team, NI Group, 5th Int. Workshop on Stellarators, Vol . 1, CEC Brussels (1984) 259.
2) P. Bogen and B. Schweer, H. Ringler and W. Ott, J. Nucl. Mat. 111 + 112, (1982) p.67-70.
3) A. Weller, Measurements of the Radiation Energy Distribution in the Soft X-ray Region in the Wendelstein VII-A Stellarator, IPP 2/277 (1985).

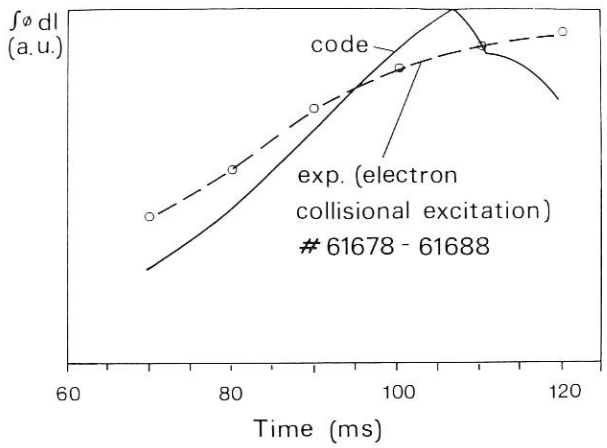

Fig.12: Flux of OVIII (2976 A) line intensity (a.u.) vs. time from electron excitation in comparison with code calculations.
W VII A ECRH 70 GHz + NBI
O-Mode B_o = 2.5 T
61364 - 61385

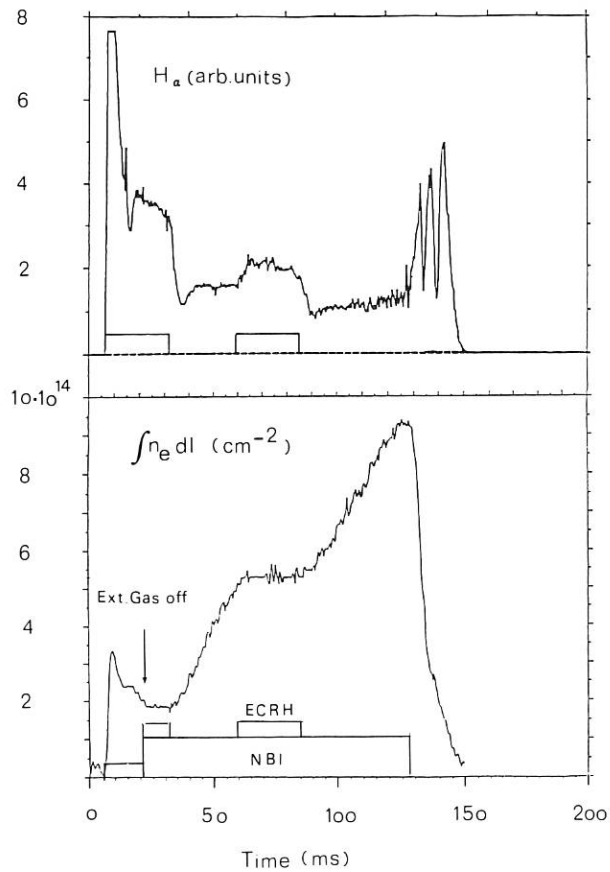

Fig.13: H_α signal and line-integrated electron density vs. time. H_α signal taken at the position of the ICRH antenna.

neutral beams (ECRH switched off after transition phase). There is no saturation of the density increase during the injection phase, which leads to particle confinement times in the $\tau_p \approx 100$ ms range. Impurity transport and particle confinement show no difference from those measured earlier[1].

With an additional ECRH pulse during NI, however, the line density increase levels off and stays constant, with a significant increase in the H_α-signal (see Fig. 13). An influence of ECRH on the time evolution of the density has also been observed in tokamaks[2) 3)]. At electron densities n_{eo} well below $n_{e,crit}$ core heating is observed while for n_{eo} approaching $n_{e,crit}$, edge heating is seen from ECE /41/. But even for $n_{eo} > n_{e,crit}$ during ECRH $\int n_e dl$ stays constant. Two possible explanations for this behaviour have been given /41/:

a) In addition to impurity confinement the electron confinement is also decreased or
b) the gas flux from the walls is ionized by ECRH power outside the last closed flux surface reducing the gas flux penetrating through the scrape-off layer and thus allowing constant density with electron confinement still unchanged.

So far no clear-cut experimental proof for either one of these explanations can be given. A more detailed discussion of these two possibilities is given in /387/ which led to the following conclusions:

The technique of an additional ECRH pulse applied to a NI sustained discharge has some very interesting aspects:

- Stationary discharges can be maintained with good energy confinement at tolerable radiation levels, whereas without additional ECRH pulse the density increases linearly with time along with high radiation losses due to impurity accumulation.
- For the ablated Al a faster loss of impurities from the central region is observed.
- There is experimental evidence that the electron particle confinement is also deteriorated.

6.4 Neutral Gas Transport Code for W VII-AS

Plasma particle and power balance and edge plasma behaviour were strongly affected by neutral gas transport in W VII-A. This is expected to be the case for W VII-AS as well. Transport modelling of neutral gas for W VII-AS by a 3D version of the DEGAS code[4)] has been started to obtain, for example, neutral density and energy distributions, neutral/plasma reaction rates as well as neutral-particle-, momentum- and energy fluxes to the

1) W VII-A Team, NI Group, Nuclear Fusion 25 (1985) p.1593.
2) V.V. Alikaev et al. Proc. 10th Int. Conf. on Plasma Phys. and Contr. Nucl. Fus. Res. London (1984) Vol. 1, p.419.
3) FOM ECRH Team and TFR Group, 12th ECCFPP, Budapest EPS, Vol. 12, (1985), p.60.
4) D.B. Heifetz et al., J. Comput. Phys. 46, (1982), p.309.

walls. A 3D plasma grid and a 2D wall grid, which will be used as "geometric input" to the DEGAS code, have been developed to give a realistic description of W VII-AS flux surfaces and internal wall structures. The grid can easily be adjusted to take into account possible variations of the magnetic configuration due to changes of the rotational transform and to shifts of the magnetic axis associated with the superposition of a vertical field.

Figure 14 gives a perspective view of the modelled inner wall surface of W VII-AS at the position of the module connecting flanges and the large injection portholes ($20^o \leq \phi \leq 52^o$). A vertical cross-section of the plasma grid at $\phi = 36^o$ and a horizontal cross-section at $z = 0$, including the wall, the flux surfaces and one of the limiters, are shown in Figs.15a and b, respectively. In this region around the limiter high neutral fluxes and strong deviations from toroidal and poloidal symmetries are expected.

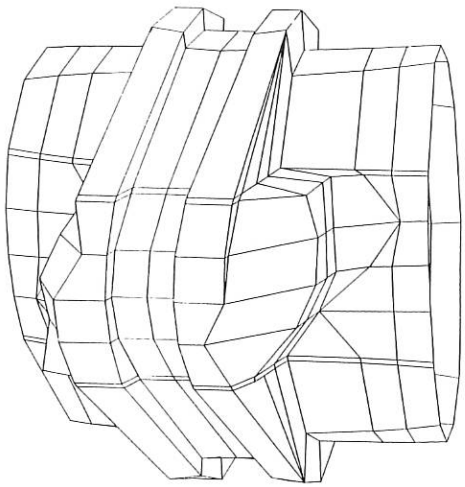

Fig.14: Grid of the W VII-AS wall surface at the position of the module-connecting flanges.

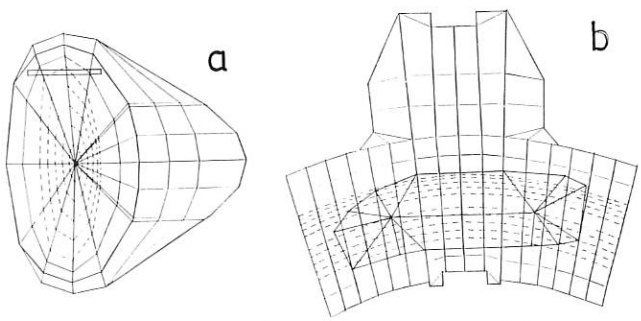

Fig.15a,b: Vertical (a) and horizontal (b) cross sections of the 3D plasma-grid at $\phi = 36^\circ$ and $z = 0$, respectively, including the wall, a sample of flux surfaces and one of the limiters.

6.5 Electron Cyclotron Emission (ECE) Diagnostic

6.5.1 Simulation of electron cyclotron phenomena

The 3-dimensional ray-tracing code for calculation of electron cyclotron waves in W VII-stellarators has been improved. The ray trajectories are now evaluated by integrating the geometrical optics equations in their Hamiltonian form the cold plasma Appleton-Hartree dispersion relation being used. The magnetic field strength and plasma density and temperature are obtained by means of a linear interpolation between the corresponding values given at equidistant planes in the toroidal direction. Diamagnetic effects on the magnetic field as well as wall reflections are considered. The absorption coefficient, needed for simulating electron cyclotron diagnostics (ECE) and heating (ECRH), is evaluated on the hypothesis of a weakly relativistic Maxwellian electron distribution function by means of the Shkarofsky functions. For the purpose of studying effects relating to the presence of more general distribution functions, e.g. to simulate a suprathermal plasma component, or a temperature anisotropy, or distortions due to quasi-linear effects, the absorption and the emission coefficients (no longer linked by the usual Kirchhoff law) can be numerically estimated by means of an alternative approach.

6.5.2 Measurement of electron heat conductivity

After successfully demonstrating the experimental determination of the local electron heat conductivity coefficient $\chi_e(r)$, applying power-modulated EC heating and diagnosing the propagation of the generated heat wave /58/, we investigated six different types of discharges in a wide parameter range of electron densities $(1...5)\cdot 10^{19}/m^3$ and temperatures (450...1300) eV together with the corresponding radial profiles in order to define the necessary experimental conditions of the method. In agreement with earlier intuitive requirements, three conditions have to be fulfilled to assure clear separation between the source and the propagation observation regime of the heat wave:

1. Flat, sufficiently broad temperature profiles assuring that the gradient region is clearly outside the deposition zone.
2. Density profiles as broad as possible to meet the requirements of the simplified theoretical model (all transport processes not related to the electron temperature gradient are neglected).
3. Temperature and density both high enough - considering the restrictions of the cut-off density - to assure high single-pass absorption of the ECH beam and to avoid wall reflections and boundary layer absorption /60/.

6.6 Scattering of CO_2 Laser Radiation from Fluctuations

Evaluation of the multi-channel detector system (nine or five elements) for the far forward scattering showed: the resulting profiles (frequency-selected scattering signals versus diameter of the laser beam) cannot be interpreted by means of a simple model for the density modulation (e.g. just one longitudinal wave traversing the laser beam). A more sophisticated model was attempted that may explain the results obtained, but not in a unique manner. Only supporting information from other diagnostics might restore uniqueness.

6.7 Shinethrough of the W VII-A NI

The energy E_{exp} deposited on the torus calorimeter of the W VII-A injectors is a measure of the time varying shinethrough of the neutral beams during a plasma discharge. For a reliable power balance of NI-heated plasmas, these shinethrough losses must be known precisely as well as the orbit losses and the power deposition profile. These quantities are usually calculated for W VII-A by the ODIN code. By a subsequently performed data analysis reported shinethrough losses computed by the ODIN code[1] could be verified (see data points in Fig.16 without error bars; the plotted value is the sum over all active injectors). Furthermore the newly developed NEUDEN code /IPP 4/229/ was modified to calculate this shinethrough, too. The results obtained [2] are also in good agreement with the experimental data improving confidence in this program for further applications.

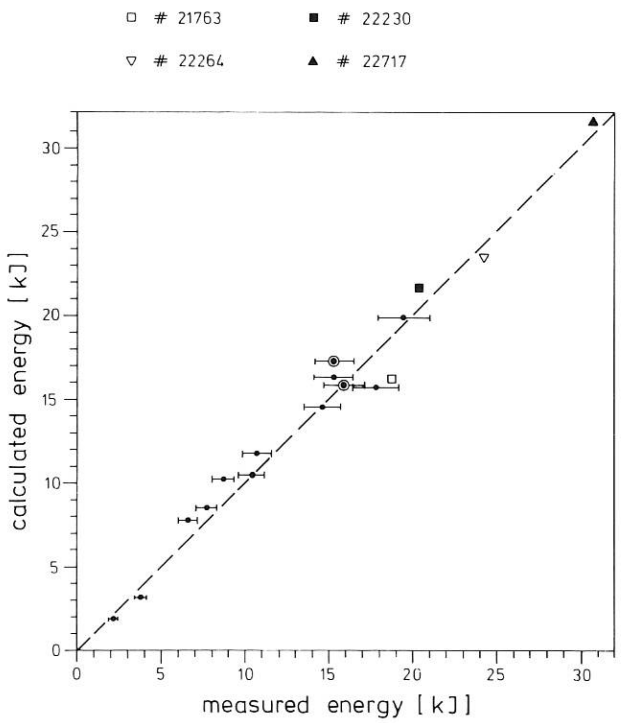

Fig.16: Correlation between the measured energy E_{exp} on the torus calorimeter and the energy E_{cal} calculated by the NEUDEN code. The points without error bars show the results of older shine through computations correlated with subsequently evaluated shot data.

6.8 Confinement Study of Fast Injected Ions in W VII-A

A new three-dimensional orbit-following code based on the axisymmetric field approximation developed by Hanatani et al.[1] has been benchmarked against the ODIN code[2] by comparing the behaviour of single-ion trajectories in the W-VII A magnetic field configuration for different radial electric fields. The two codes calculated nearly identical ion trajectories for a wide variety of start parameters despite the differences in the approximations used for the magnetic and electric field configurations. It was shown that fat banana orbits of toroidally trapped injected ions, which are strongly affected by the radial electric field, dominate the fast orbit losses. Furthermore, a simplified neutral beam heating-efficiency was derived, only accounting for shinethrough and fast orbit losses, in order to allow the two codes to be compared. This was done because the new code had no slowing-down part at this time. The results of both codes are summarized in Fig.17. They compare very well.

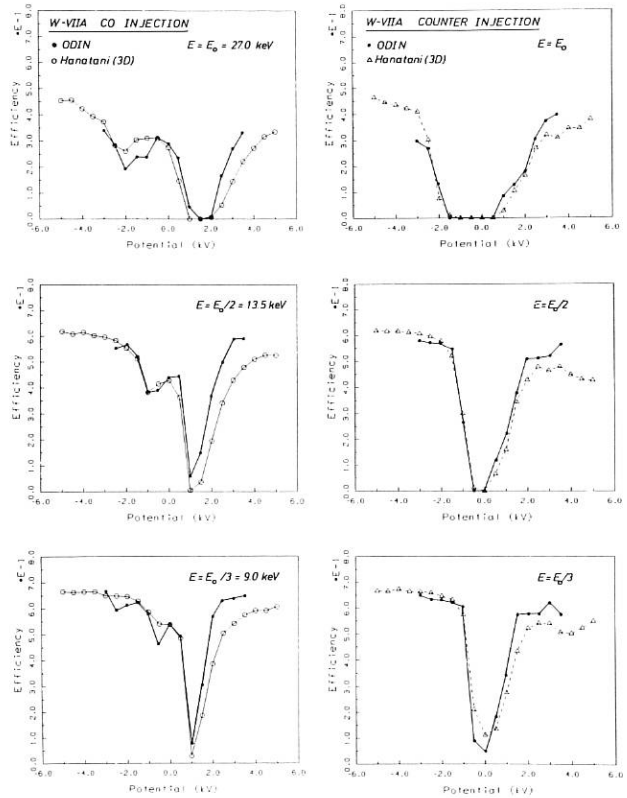

Fig.17 Estimation of the heating efficiency of the W-VII A injection by a simplified model without slowing-down. The abscissa denotes the on-axis values $\Phi(0)$ of the assumed parabolic potential.
The resonance condition $\ell\, v_{\parallel}/R + \Omega_E = 0$, where the drifts caused by rotational transform and radial electric field cancel each other, is clearly reproduced by both codes.

1) W VII-A Team, NI Team:
Neutral Beam Heating in the W VII-A Stellarator
Proc. 2nd Int. Symp. on Heating in Toroidal Plasmas, Vol.II, 789, (1980).
2) F.-P. Penningsfeld:
IPP report, to be published (1987).

1) K. Hanatani, K. Uo: Proc. US-Japan workshop on 3D MHD studies (Oak Ridge, Tennessee) (1984).
2) F.-P. Penningsfeld, W. Ott, E. Speth:
Proc. 12th Eur. Conf. Contr. Fus. and Plasma Phys. 9F(I), p.397.

The new 3D code works in real space coordinates and uses a 'field splitting' algorithm to compute the magnetic field values and the gradients needed for the orbit calculations. The direction of the radial electric field can be obtained consistently from the gradient of the corresponding magnetic flux. In this way the code is able to fit the real magnetic field configurations of W VII-A closer than could be realized in ODIN. Even an application to the more complicated field configuration of W VII-AS, which is excluded for ODIN, should be possible.

WENDELSTEIN VII-X PROJECT

Head of project: H. Wobig

The investigation of vacuum field configurations with reduced Pfirsch–Schlüter currents has been continued in order to find an appropriate configuration for the W VII–X experiment. Besides an upgrade version of Wendelstein VII–AS, described as W VII–X1 in the Annual Report 1985, several Helias configurations and a 5–period modular Heliac with helical magnetic axis have been studied. Since for the Helias configuration a maximum average $< \beta >$ of 9 % stable against resistive interchange modes has been predicted, enhanced effort to find feasible modular coils for this case has been made. A further modification of the W VII–AS configuration with a plane magnetic axis led to the concept of the Bean–shaped Advanced Stellarator. Compared with W VII–AS this configuration has smaller Pfirsch–Schlüter currents and therefore a higher equilibrium limit of β . During the year 1987 a selection among these various options will be made.

Stellarator reactor studies have been continued in cooperation with the Kernforschungszentrum Karlsruhe and Fusion Power Associates, Madison (USA). A final report on the modular Advanced Stellarator reactor ASRA6C will be published in 1987.

1. WENDELSTEIN VII-X STUDIES

E. Harmeyer, J. Kisslinger, F. Rau, H. Wobig,
and F. Herrnegger (Theory 2).

1.1 W VII–X1D

As described in the Annual Report 1985 the coil system of W VII–X1D is an upgrade version of Wendelstein VII–AS with $R_o = 5\,m$, $B = 4\,T$, and a rotational transform $\iota_o = 0.39$ on the axis.

For experimental purposes, however, a variation of the rotational transform is necessary, which can be achieved by double layer modular coils with separate current feeders to the lower and upper layer. The achievable ι–regime is determined by the maximum current density in the coils which was $40\,MA/m^2$. By varying the currents in the coil halves separately, the rotational transform can be changed from $\iota = 0.3$ to $\iota = 0.6$. However, the maximum magnetic field of $4\,T$ is only possible in the regime $\iota = 0.3 - 0.45$; at a maximum rotational transform $\iota = 0.6$ the magnetic field has to be reduced to $2.6\,T$.

This method of ι–variation can be applied to any modular stellarator, thus giving the experiment a very useful flexibility.

1.2 Bean–shaped Advanced Stellarators (BSX)

A modification of the Advanced Stellarator (AS) configuration is a Bean–shaped Advanced Stellarator magnetic field given by Dommaschk potentials. The magnetic axis is nearly planar and undulates radially. Starting from surface currents on a given analytic torus, modular coils have also been found. Initially, the coil bores were shaped to the magnetic surfaces / 65/ , in the further development their cross sections were chosen toroidally invariant, see Figure 1. In systems with 5 field periods at least 9 coils per period are required for a magnetic well ($\approx -0.1\%$) in the vacuum field. The well deepens with a larger number of coils or with a value of $\iota_o \leq 0.5$ on

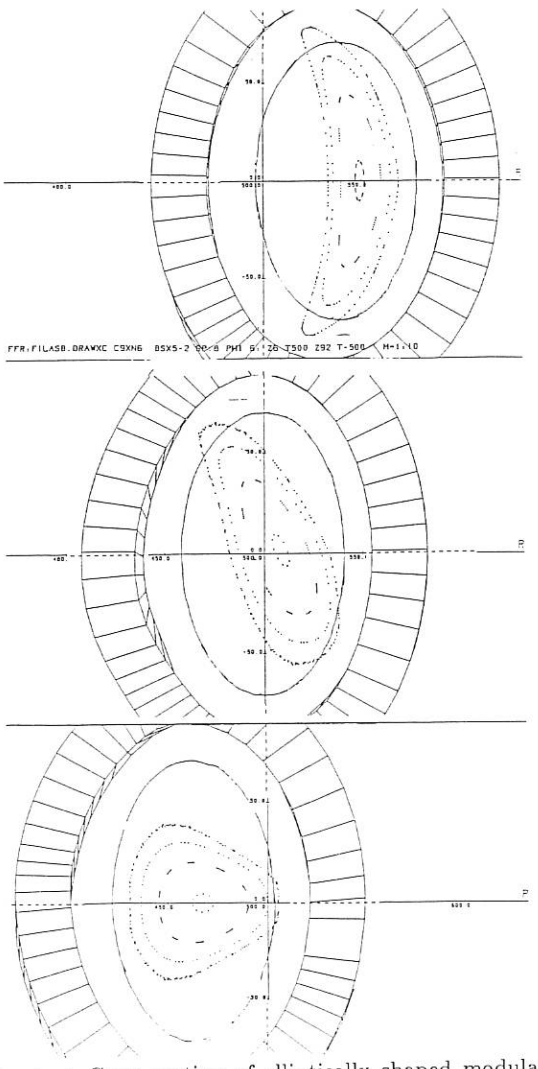

Fig. 1 : Cross section of elliptically shaped modular coils for BSX5–2 , magnetic vacuum field with $\iota_o = 0.49$ on axis shown for 3 toroidal positions, and contours of a preliminary elliptical vacuum tank.

the axis. Compared with W VII–AS the Pfirsch–Schlüter currents (secondary currents) are significantly reduced. A higher equilibrium limit with $\beta_o = 9.6\,\%$ on the magnetic axis was calculated / 65 / for a parabolic pressure profile in the configuration FZH298 at an aspect ratio $A = 11.1$. This data set is characterized by 44 Dommaschk potentials and has a rotational transform of $\iota_o = 0.39$ on the magnetic axis of the vacuum field.

1.3 Modular Helias Configurations

The Helias configuration, as proposed by J. Nührenberg et al.[1] promises the highest stability limit against resistive interchange modes, with a value of $< \beta_{st} > \leq 9\%$ found so far. In these configurations the magnetic axis is slightly helical with the vertical excursion being roughly 50 % of the horizontal excursion. Modular coils were investigated which produce a vacuum field of the Helias type. The procedure starts from a toroidal surface adjusted to the outer magnetic surface of a finite–β equilibrium. A vacuum field tangential to this surface and the corresponding surface currents are calculated by the method of P. Merkel [2] . The surface currents are then described in a Fourier series. With this torus as basis the central current filaments of the coils were constructed and described in an analytic form. The period number was varied between 4 and 6 . The aspect ratio of the last magnetic surface increases with the period number. The shear is small in these configurations. By proper choice of the coil parameters and the period number, however, it is possible to find ι in the neighbourhood of 0.5 or 1.0 where, according to experiments in W VII–A and theory, magnetic surfaces are less vulnerable to error fields. Pfirsch–Schlüter currents show a strong reduction with $< j_{||}/j_{\perp} > = 0.75$ for five field periods. Guiding center orbits of circulating particles are close to the magnetic surfaces ($\Delta/\rho \leq 0.5$, Δ = radial offset, ρ = Larmor radius), so that a strong reduction of Pfirsch–Schlüter diffusion and plateau diffusion is expected. With $B_o = 4\,T$ on the magnetic axis the maximum field at the coils is only $6.3\,T$, which is less than in the configuration W VII–X1D . As example the modular coils and the magnetic field of the system HS4–8 (4 field periods, 12 coils per field period) are shown in Figures 2 to 4 .

1) : J. Nührenberg, et al., see / 69 /.

2) : P. Merkel, et al., see / 110 /.

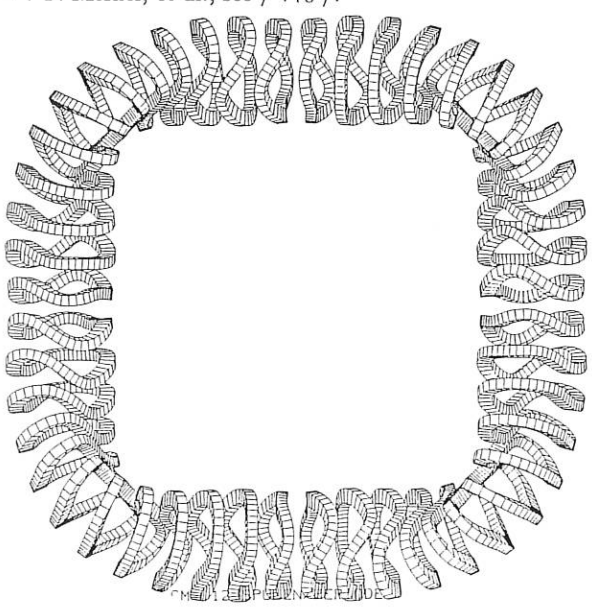

Fig. 2 : Top view on a Helias coil set, 4 field periods.

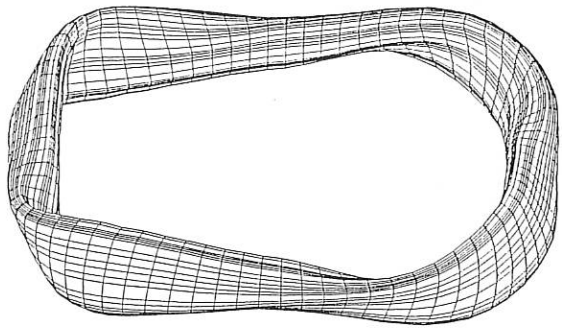

Fig. 3 : Perspective view on an outer flux surface.

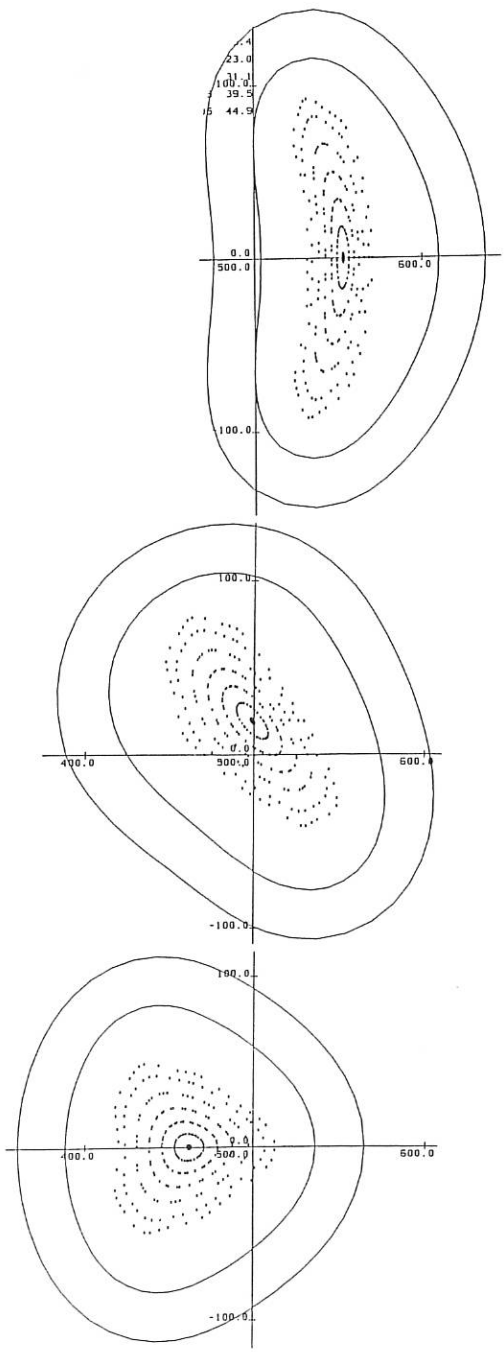

Fig. 4 : Cross section of shaped modular coils for HS4–8 and magnetic vacuum field in 3 toroidal positions.

1.4 Modular Heliac Systems

A fourth category of magnetic fields under study are modular Heliac systems with different periodicities. Coil sets for modular Heliacs were already described in the Annual Report 1984 . Here an improved version is used for comparison with the Helias configuration. The standard case with five field periods and ι close to 2.0 has a slightly smaller plasma aspect ratio than the Helias configuration ($A = 11.1$ *vs* $A = 12.5$). In these modular Heliac configurations the reduction of the Pfirsch–Schlüter currents is mainly due to the high value of the rotational transform. Particle orbits are less optimised than in the Helias case, therefore a higher plateau diffusion has to be expected.

1.5 Comparison between these options

The decision between these options will be made on the basis of MDH equilibrium and stability limits, transport properties, and the feasibility of the coil system. Concerning MHD–equilibrium, small Pfirsch–Schlüter currents are favourable. As a figure of merit the value $J^* = < B_o^2/B^2\,(1 + j_{||}^2/j_{\perp}^2) >$ is used, where the average $< \cdots >$ is taken over the magnetic surface. A small number of J^* is also favourable with respect to resistive interchange stability. In Figure 5 a comparison of the different options listed above is made. The smallest value of $J^* = 1.3$ could be achieved with a 6–period Helias configuration. However, a smaller number of field periods leads to a smaller plasma aspect ratio, and the 4–period Helias shown in Figures 2 to 4 offers more space for coils and vacuum tank.

In the configurations described above the drift surfaces of circulating particles differ less from magnetic surfaces than in standard stellarators. Therefore smaller diffusion rates are expected. Evaluation of the plateau diffusion coefficient for general nonaxisymmetric devices [3] showed that in Helias and BSX configurations the plateau diffusion rate is reduced by a factor of 3 compared with standard stellarators.

[3] : E. R. Solano and K.C. Shaing, submitted to Phys. Fluids.

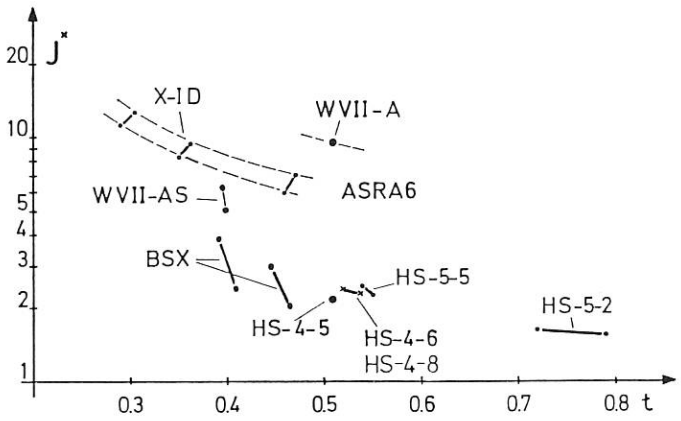

Fig. 5 :
Dependence of the stability parameter J^* on the rotational transform ι for several systems with reduced secondary currents.

1.6 Magnetic forces and stresses

The coil configuration W VII-X1D consists of $n = 30$ coils, see Figure 6 , with a mean coil radius of $r_c = 1.2\,m$. The stored magnetic energy at an axis field $B_0 = 4\,T$ amounts to $W \approx 1\,GJ$. At an average winding pack volume $V_c \approx 1\,m^3$ the virial stress $\sigma_V = W/(n \cdot V_c)$ reaches $35.8\,MPa$, a value about three times higher than in W VII-AS . This calls for a strong reinforcement of the coils by a coil housing of stainless steel.

A local maximum of $F'_m = 295\,MN/m^3$ was calculated for the magnetic force density in an operating case with an average coil current density $j_c = 40\,MA/m^2$ in the outer and $20\,MA/m^2$ in the inner part of the coils. Each coil of the assembly envisages a net force of about 6 MN per coil in the direction towards the torus centre in the same operating case.

A scheme of mutual coil support was applied. Each coil was surrounded by a suitably shaped housing with lateral reinforcement in regions of high curvature of the coils. The coil housing has a lateral and radial inside width of $5\,cm$, and a radial outside width of $8\,cm$. Rigid boundary elements were provided on the outer rings of the arrangement in the region towards the torus center. The finite-element computations were based on isotropic material data of the coils. The results apply for the load case of equal current densities of $j_c = 30\,MA/m^2$ in the coil parts. With the data of copper one obtains in / 285 / maximum values of the equivalent stress (von Mises stress) of about $\sigma_{vM} = 95\,MPa$ at a maximum tangential strain ϵ_T of about 0.1 %. The maximum shear stress is $\sigma_{ST} \approx 40\,MPa$.

A similar stress investigation was performed for the coils of the reactor–sized system ASRA6C also, comparing several load cases.

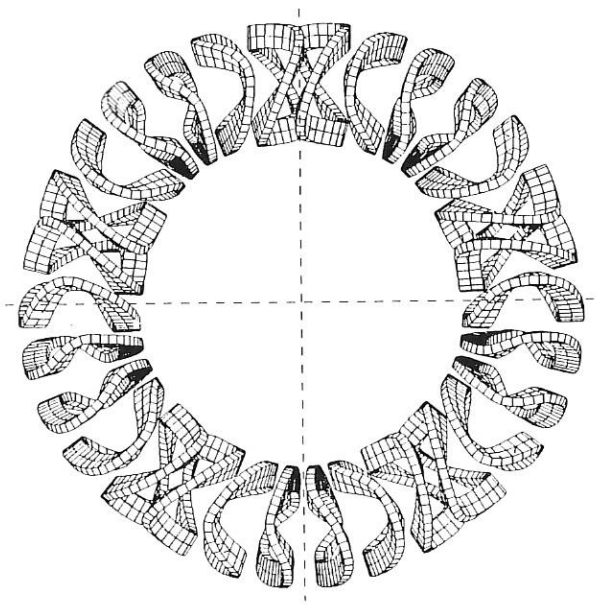

Fig. 6 :
Top view on the coil configuration W VII–X1D , 6 coils per field period.

2. ASR–Studies

The studies of critical issues of an Advanced Stellarator Reactor were brought to an end. This work was performed in collaboration with groups at the Kernforschungszentrum Karlsruhe and at the University of Wisconsin, Madison (USA). A common final report is being prepared. The tasks were shared in the following way :

IPP : Coil configurations and magnetic field studies; plasma physics with emphasis on scenarios for heating and steady state burn; magnetic forces and their support, finite element calculations of stresses and strains of the coils.

KfK : questions of coil development for the superconducting magnets, conductor concept, principles of coil construction, helium transfer, safety discharge of magnets; general layout of the system; maintenance studies; radiation limits.

University of Wisconsin : Blanket and shield studies, neutronics calculations, general layout of the system, principles of plasma edge control.

This report concentrates on the reference configuration ASRA6C. It is expected that such a system will reflect the general reactor properties of an Advanced Stellarator . Some information on ASRA6C was given in the Annual Report 1985, page 131. The major results are summarized in / 275 /; details of the IPP contribution to the ASRA6C study are given in / 286 /, / 287 /, / 288 /, and / 56 /.

2.1 New configurations

The search for new Advanced Stellarator Reactor configurations is stimulated by the desire to improve their stability behavior beyond the comparatively low values envisaged for systems of the WENDELSTEIN VII–AS type. An average $\beta \approx 5\,\%$ is typical for the operation regime of the reactor. Regarding the critical value for stability, β_{st} , theory predicts lower numbers for this type of configurations. Bean–shaped Advanced Stellarators with a nearly planar magnetic axis and their modular coil systems are described in / 63 / .

A preliminary version of a Bean–shaped system in reactor dimensions, called BSR, uses 9 coils per field period, see Figure 7, with an aspect ratio of about 5.5, a larger value than that ot 4.4 in the ASRA6C data set. Therefore it is not yet clear wether the required space for blanket and shield is available in the present BSR system. The coils have differently shaped bores and are placed at radially undulating positions. The coil current density amounts to $j_{eff} = 20\,MA/m^2$. The reduction of the secondary plasma currents is shown in Figure 8 . The bold symbols apply for ASRA6C and for the preliminary BSR configuration. Characteristic data of the Bean–shaped system BSR are compared to those of ASRA6C as well as to those of previous reactor and burner systems in Table I.

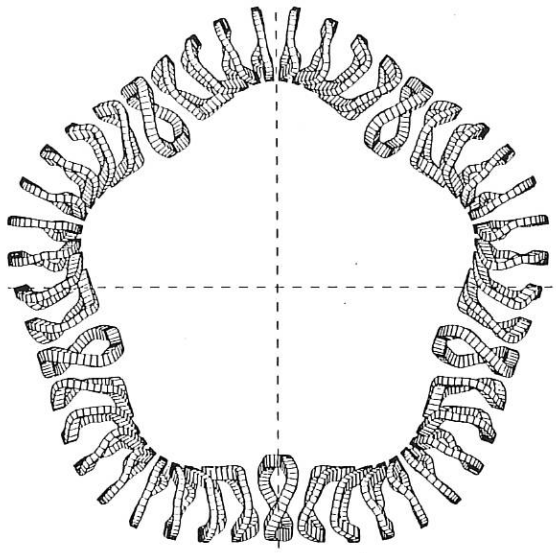

Fig. 7 : Top view on the BSR coil system.

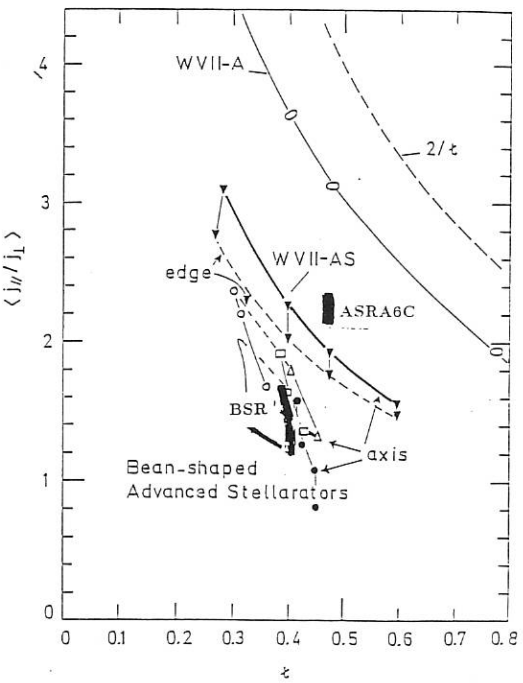

Fig. 8 : Average values of $< j_{||}/j_{\perp} >$ versus the rotational transform ι for ASRA6C and a preliminary BSR configuration, compared to data for WVII–A , WVII–AS , and other Bean–shaped Advanced Stellarators.

Advanced Stellarator			Burner ASB06E	Reactor ASR25T7	Reactor ASRA6C	Reactor BSR *preliminary*
Av. major radius	R_o	$[m]$	15.2	25.5	20.	20.
Av. coil radius	r_c	$[m]$	3.24	5.24	4.57	3.6
Coils/F.P.			6	10	6	9
Conductor			Nb_3Sn	NbTi	Nb_3Sn	Nb_3Sn
Eff. current density	j_{eff}	$[MA/m^2]$	18.	9.8	15.	20.
Max. induction coil	B_m	$[T]$	12.6	8.7	10.4	11.7
Magnetic energy	W_m	$[GJ]$	67	170	117	78
Induction on axis	B_o	$[T]$	7.0	5.3	5.3	5.7
Rot. transform	ι_o		0.53	0.58	0.47	0.41
Av. plasma radius	r_p	$[m]$	0.9	1.75	1.6	1.6
Distance to coils	Δ	$[m]$	1.2	>1.8	1.2	
Average β	$<\beta>$	$[\%]$	2.5	5	5	
Fusion power	P_f	$[GW]$	0.42	3.8	3.9	

Table I

Characteristics of Advanced Stellarator Burner and Reactor Systems

CONTRIBUTIONS OF THE

STELLARATOR PHYSICS GROUP

W. Dommaschk, F. Herrnegger, G.G. Lister, W. Lotz, P. Merkel, J. Nührenberg, A. Schlüter, U. Schwenn

Guests: S.P. Hirshman [1], A. Varias [2]

Major achievements in 1986 were: an increase of β in Helias configurations to $\langle\beta\rangle \approx 0.1$ by admitting a somewhat larger $\ell = 2$ content, as verified by β iteration towards marginal stability with respect to resistive interchanges, the development of a code for free-boundary 3D equilibria, and a method of computing coils for stellarator configurations by means of a boundary value problem. Four new codes extend Table 1 of the Annual Report 1983: the VMEC 3D MHD code (Hirshman, ORNL), the NEMEC free-boundary 3D code, the NESCOIL code (*NE*umann *S*olver for fields produced by external *COIL*s) and FAFNER 2, a code for simulating neutral injection into stellarators of general geometry in the presence of an electric field.

1. β-values in Helias and in Heliac

In continuation of Helias stability studies /166/, a configuration with five periods and aspect ratio 11.5 was identified in which a β-value of $\langle\beta\rangle \approx 0.09$ is marginally stable against resistive interchange modes and is obtained by β iteration towards marginal stability /69/ [3]. Figure 1 shows the flux surface geometry of this configuration. The finite-β shift of the magnetic axis is negligible.

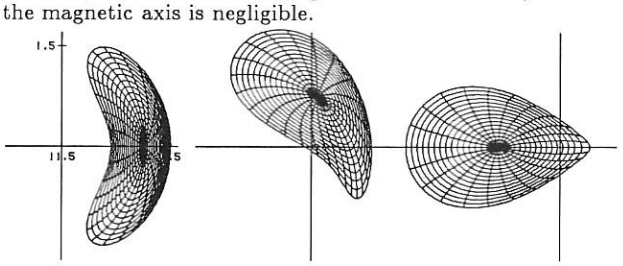

Fig.1: Flux surface cross-sections at $V = 0, \frac{\pi}{2}, \pi$ of a Helias equilibrium with $N = 5$, $A = 11.5$, $R_{0,1} = 0.8$, $Z_{0,1} = 0.4$, $\Delta_{1,0} = 0.1$, $\Delta_0 = 0.07$, $\Delta_{2,0} = 0.05$, $\Delta_{1,-1} = 0.39$, $\Delta_{2,-1} = 0.24$, $\Delta_{2,-2} = 0.07$.

Figure 2 (left) shows the rotational transform profile of the vacuum and the finite-β case. Note the small change in rotational transform and the virtually unchanged shear. Figure 2 (right) shows the corresponding pressure profile, $-dp/ds$, which exhibits the flattening around the $\iota_p = \frac{1}{6}$ resonance, resulting in a β-value which is about 10% smaller than it would be without taking this resonance into account.

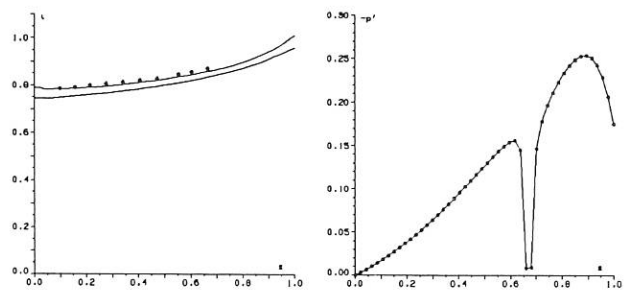

Fig.2: Figure 2 (left) shows three ι-profiles: the circles are obtained from the result of Fig.3a, the upper line is the result obtained with MOMCON [4] for the $\beta = 0$ case, the lower line the result for $\langle\beta\rangle \approx 0.09$. Figure 2 (right) shows the corresponding profile $-p'(s)$. The radial label s is the square root of the normalized toroidal flux.

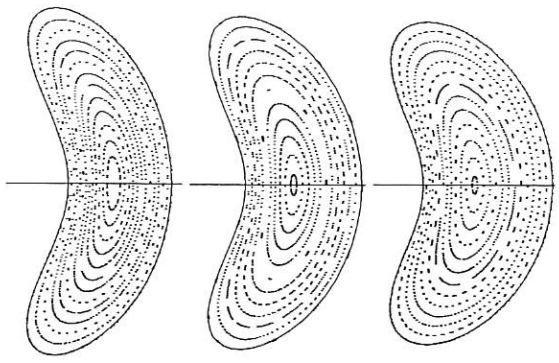

Fig.3: Poincaré plots of Helias vacuum fields with the surface parameters as given in Fig.1, except $\Delta_{1,-1} = 0.39$, 0.3336, 0.284.

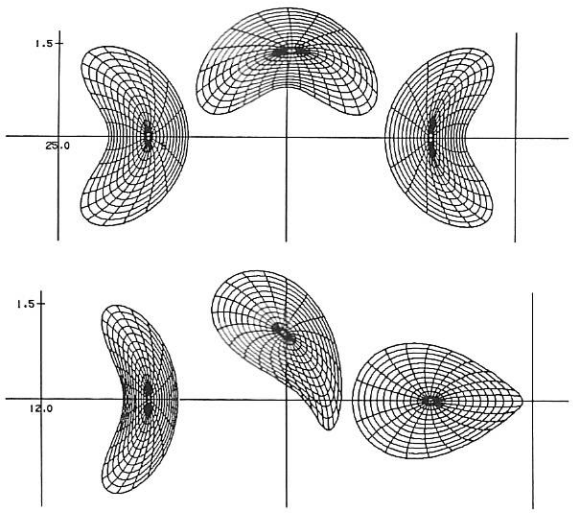

Fig.4: Figure 4 shows flux surface cross-sections at $V = 0, \frac{\pi}{2}, \pi, \frac{3\pi}{2}$ of Heliac (4a) and Helias (4b) equilibria. In the notation of /119/ the values of the boundary parameters are given by: (1a) $A = 25$, $N = 10$, $R_{0,1} = 0.96$, $Z_{0,1} = 0.96$, $\Delta_{1,-2} = 0.36$, $\Delta_{2,-1} = 0.38$, $\Delta_{2,-3} = 0.11$. The Heliac sequence is given by $0.14 \leq \Delta_{1,-2} \leq 0.36$; (1b) $A = 12$, $N = 5$, $R_{0,1} = 1.4$, $Z_{0,1} = 0.7$, $\Delta_{1,0} = 0.1$, $\Delta_0 = 0.07$, $\Delta_{2,0} = 0.05$, $\Delta_{1,-1} = 0.39$, $\Delta_{2,-1} = 0.24$, $\Delta_{2,-2} = 0.07$. The whole sequence is given by $0.8 \leq R_{0,1} \leq 1.4$, $0.4 \leq Z_{0,1} \leq 0.7$, $0.29 \leq \Delta_{1,-1} \leq 0.39$.

Figure 3a shows the vacuum field solution obtained with the NESCOIL code /110,111/; see also Sect.5. Comparison of the negligible island thickness in the vacuum field and the sizeable width of the pressure profile flattening clearly shows the need for refined 3D codes which can compute the island size as a function of β. Given this lack of knowledge, one would prefer configurations in which both the size of the vacuum

---

1) Visiting scientist from ORNL

2) Visiting scientist from JEN, Madrid

3) W. Dommaschk, F. Herrnegger, W. Lotz, P. Merkel, J. Nührenberg, A. Schlüter, U. Schwenn, R. Zille, 11th Int.Conf.on Plasma Physics and Contr.Nuclear Fusion Res., Kyoto 1986, IAEA-CN-47/D-I-3

4) Hirshman, S.P., Lee, D.K., Comput. Phys. Comm.**39** (1986) 161

field islands and the width of the pressure profile flattening are small. This is the case for Helias configurations which stay below $\iota_p = \frac{1}{7}$, as is shown in Fig.3. An alternative to these moderate-shear cases would be to avoid resonances of this order by considering finite-β equilibria with sufficiently small shear. Such Helias equilibria have also been found [1].

Considering two sequences of Helias and Heliac equilibria (see Fig.4) by means of β iteration towards marginal stability, one can clearly exhibit the effects of resonances as the rotational transform passes through low-order rational values (see Fig.5). Note the strong depression of β near $\iota \approx \frac{1}{3}$ in the Heliac sequence although $N = 10$ and $A = 25$.

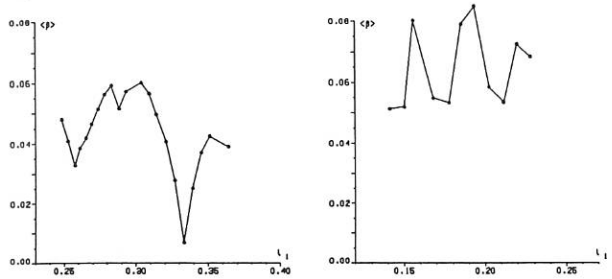

Fig.5: $\langle\beta\rangle$ as a function of $\iota_1 = \iota(s = 1)$ for the Heliac (5a) and the Helias (5b) sequences.

2. β-values in TJ-2 and Vintotron

Vacuum field calculations reproducing specific cases of two Heliac designs, TJ-2 [2] and Vintotron [3], were used to obtain boundary representations of these configurations for the finite-β analysis analogous to Section 1; preliminary results indicating $\langle\beta\rangle \approx 0.015$ and $\langle\beta\rangle \approx 0.005$, respectively, have been obtained. Figure 6 shows flux surface cross-sections.

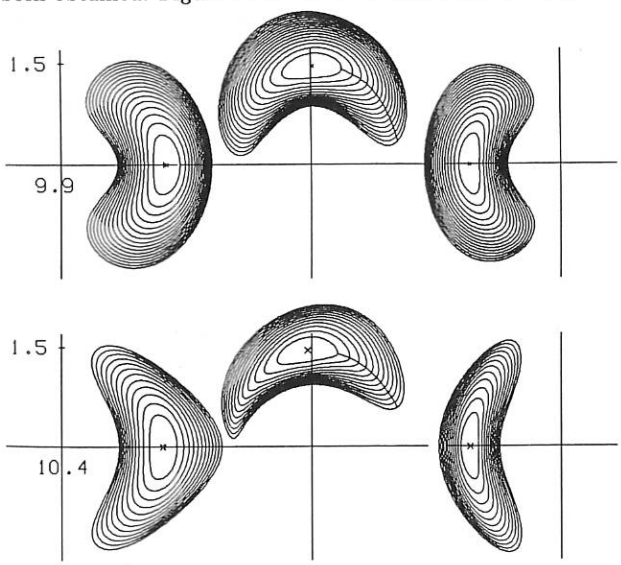

Fig.6: Flux surface cross-sections of TJ-2 (6a) and Vintotron (6b).

3. Free-boundary Equilibria

Two codes, the VMEC 3D MHD fixed-boundary code /110/ and the NESTOR code /111/, which solves the Neumann problem at the plasma boundary for the vacuum field in the outer region, were coupled /70/ to obtain the NEMEC free-boundary code. Figure 7 shows the convergence of an $\ell = 2$ stellarator free-boundary equilibrium with axisymmetric circular flux surfaces as initial condition. Figures 8 and 9 show case studies for W VII-AS and ATF with applied vertical fields which eliminate the outward shift at $V = 0$ (the position of the vertically elongated cross-section). Without these vertical fields shifts $\Delta R/R_0 \approx 0.4\langle\beta\rangle$ and $\Delta R/R_0 \approx 0.4\langle\beta\rangle$ are found for W VII-AS and ATF, respectively.

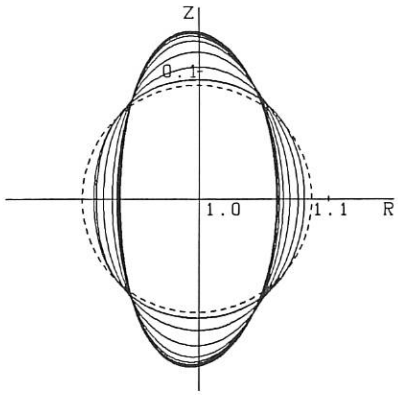

Fig.7: Evolution of initially circular plasma (dashed line) into stellarator ellipse (at $V = 0$). Curves are drawn at every fifty equilibrium iterations.

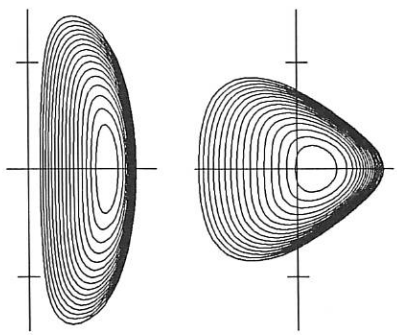

Fig.8: Flux surfaces of free-boundary W VII-AS equilibrium with $\langle\beta\rangle = 0.015$ and $B_v/B_0 = 0.01$.

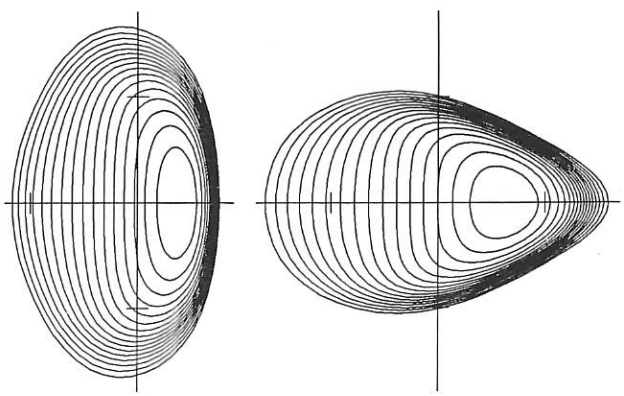

Fig.9: Flux surfaces of free-boundary ATF equilibrium with $\langle\beta\rangle = 0.02$ and $B_v/B_0 = 0.015$.

1) W. Dommaschk, F. Herrnegger, W. Lotz, P. Merkel, J. Nührenberg, A. Schlüter, U. Schwenn, R. Zille Kyoto Stellarator Workshop

2) J. Guasp, J.L. Alvarez-Rivas et al., 12th EPS Conf., Budapest 1985, Eur. Conf. Abstracts, Vol.**9f**, Part I, 441

3) S. Nagao, Y. Abe, Nucl. Fusion **26** (1986) 671

4. Non-local Modes

Non-local ideal modes resonant for $\iota = \frac{1}{2}$ were investigated in $\ell = 2$ stellarators with rotational transform per period $\iota_p \approx 0.1$ and small to moderate shear.

Extension of previous work / 64/with STEP to moderate m-number modes ($m \leq 6$) /66/ leads to the conclusion that only free-boundary modes may be used for a realistic assessment of ideal MHD stability. Figure 10 shows the structure of such a mode, Figure 11 eigenvalues obtained for these modes.

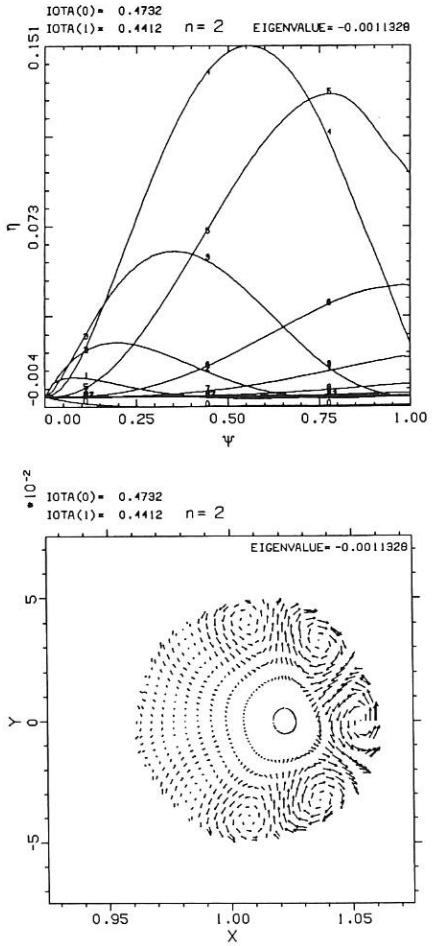

Fig.10: Mode structure of an $n = 2$, $m = 4$ free-boundary mode in a toroidal $\ell = 2$ configuration. Figure 10a shows the harmonic content, Figure 10b the poloidal projection of the displacement vector.

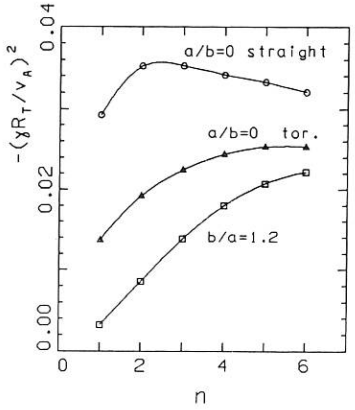

Fig.11: Normalized eigenvalues as functions of the toroidal mode number n in straight and toroidal $\ell = 2$ stellarators, a: plasma radius, b: wall radius.

Direct secondary minimization to find unstable modes was pursued further with the help of the FIT code and led to a significant improvement / 141/ in the physical parameters for which the instability can still be detected: for $A = 9$, $N = 12$, $\langle\beta\rangle = 0.1$, $\Delta W < 0$ was shown; for $A = N = 20$, $\langle\beta\rangle = 0.12$, for example, $\Delta W/W = -10^{-5}$ was obtained with 12 Fourier amplitudes for the equilibrium and 25 additional Fourier amplitudes for the stability calculation. Figure 12 shows the 6 largest Fourier amplitudes in the nonlinear saturated final state. An estimate of an approximate Rayleigh quotient is $\Delta W / \int \xi^2 \mathrm{d}^3\tau = -3.8 \times 10^{-3}$.

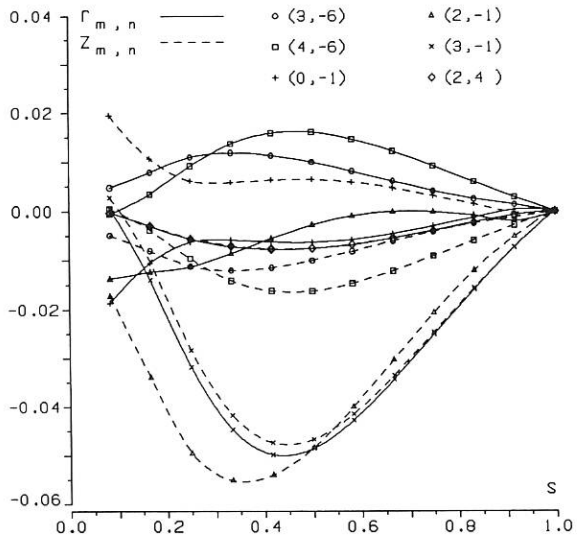

Fig.12: Fourier amplitudes of a saturated $m = 2$, $n = 1$ instability in a toroidal $\ell = 2$ stellarator.

5. Coils for Stellarators

With respect to finding coils for given stellarator fields four different approaches were pursued.

Solution of the boundary value problem $\vec{B} \cdot \vec{n} = 0$ with NESTOR yields the structure of coils at the plasma boundary [1] and provides a start for a heuristic modular coil finding procedure, which was applied to Helias by the W VII-X group. Results are described in the W VII-X project section.

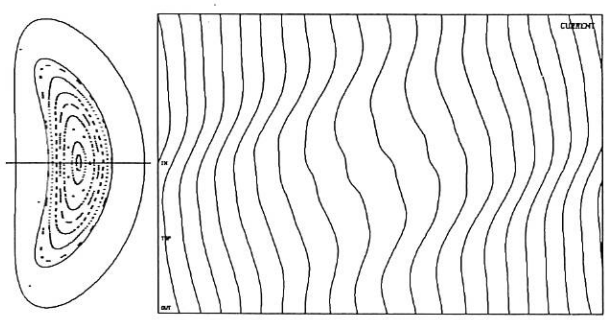

Fig.13: Figure 13a shows (at $V = 0$) a Helias boundary with parameters of Fig.1, except $A = 12$, $\Delta_{2,-1} = 0.12$, $\Delta_{2,-2} = 0.1$, the magnetic surfaces of the approximate solution of the boundary value problem with Dommaschk potentials, and the outer surface on which the modular coils are calculated. Line currents are shown in Fig.13b, the ordinate being the poloidal parameter, the abscissa $0 < V < 2\pi$.

[1] IPP Annual Report 1985, p.138

Solution of the same boundary value problem with Dommaschk potentials of arbitrary order /26/ [1] allows the computation of modular coils on a surrounding surface at a finite distance. Figure 13 shows an example which gave the first proof of feasibility of coils for Helias.

Searching the stellarator configurational space with a relatively small number of low-order Dommaschk potentials avoids the occurrence of infeasible coils in a qualitative way. Configurations with nearly plane magnetic axis – bean-shaped advanced stellarators /65/, which interpolate between W VII-AS and Helias – and configurations approximating Helias parameters were obtained in this way and coil configurations were studied /63/ [2] [3].

Solution of the Neumann boundary value problem with the external currents as variables to be determined appears to be the most successful approach. The NESCOIL code [4] [1] solves this problem. Figure 14 shows coils and magnetic surfaces obtained with NESCOIL for the configuration described in Fig.1.

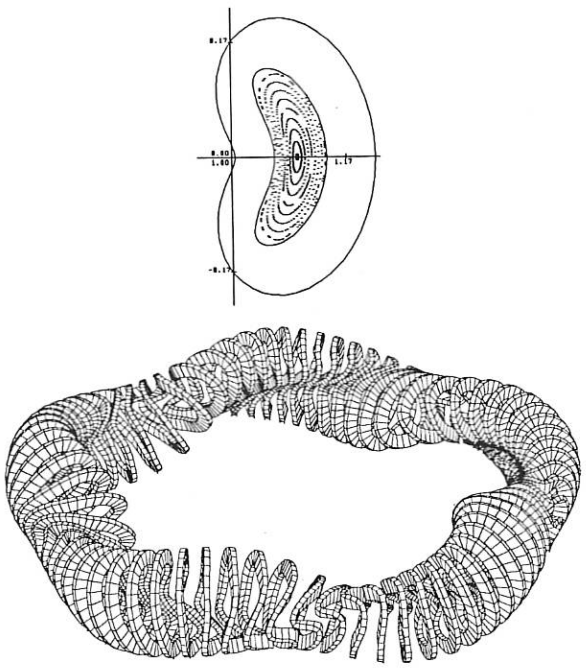

Fig.14: Helias boundary, magnetic surfaces of the NESCOIL solution, modular coil surface contour and modular coils (right part) for the configuration of Fig.1.

6. Monte Carlo Studies of Neoclassical Transport

Previous studies with monoenergetic test distribution functions of kinetic energy E showed that, in the lmfp regime, stellarators assumed to exhibit no electric field are dominated by a loss belt at small $v_{\|}/v$ in the distribution function causing a confinement time close to the collision time [5],[6]. With an assumed electric field F in the form of a potential ϕ constant on magnetic surfaces and of the order of the particle energy, this loss belt behaviour is relieved and the loss rates $S(E)$ in the lmfp regime decrease by more than an order of magnitude. For these cases a local diffusion coefficient $D_F(E)$ can be obtained for all mean free paths Λ, turns out to be independent of the sign of the electric field, and obeys the ordering relation [6] /106/

$$S_-^* < D_F^* < S_+^* ,$$

where the $\pm$ signs indicate the cases with electrostatically inward pulling ($-$, called attracting) and outward pushing ($+$, called repelling) potential ϕ, respectively, and * indicates quantities normalized to the appropriate plateau values. Figure 15 shows these results for an $\ell = 2$ stellarator.

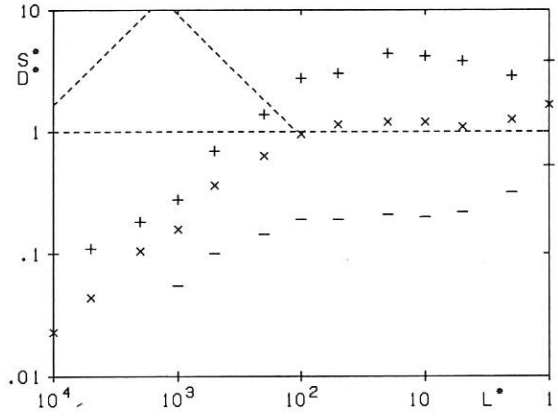

Fig.15: Normalized loss rates S^* $(+,-)$ in an $\ell = 2$ stellarator with $e\phi_0/E = \pm 2$; $Q_\rho = 500$ (Q_ρ plasma- to deuteron gyroradius ratio), $R_0/a = 8.6$, $N = 5$, $\iota = 0.5$, $\delta_e \approx 0.02$ (at aspect ratio $A = 17$). In addition, the corresponding normalized transport coefficient D^* $(\times)$ (which does not depend on the sign of the electric field) is shown; $Q_\rho = 500$, $A = 12.5$, $N = 5$, $\iota = 0.5$, $\delta_e \approx 0.03$, $H = 14$. The L^* and L^{*-1} regimes are also indicated.

For a given potential the diffusion coefficient $D_F(E, \Lambda)$ can be calculated as a function of E and then be convoluted with a Maxwellian energy distribution to yield estimates of the coefficients for thermal particle ($\propto \int D(E, \Lambda(E)) \mathrm{e}^{-E} E^{\frac{1}{2}} \mathrm{d}E$) and energy ($\propto \int D(E, \Lambda(E)) \mathrm{e}^{-E} E^{\frac{3}{2}} \mathrm{d}E$) diffusion. Figures 16 and 17 show these results for ions and electrons in W VII-AS and ATF.

---

1) W. Dommaschk, F. Herrnegger, W. Lotz, P. Merkel, J. Nührenberg, A. Schlüter, U. Schwenn, R. Zille, 11th Int.Conf.on Plasma Physics and Contr.Nuclear Fusion Res., Kyoto 1986, IAEA-CN-47/D-I-3

2) E. Harmeyer, F. Herrnegger, J. Kisslinger, F. Rau, H. Wobig, 4th Technical Comm. Meeting and Workshop of Fusion Reactor Design and Technology, Yalta 1986

3) E. Harmeyer, F. Herrnegger, J. Kisslinger, F. Rau, H. Wobig, Kyoto Stellarator Workshop 1986

4) P. Merkel, submitted for publication

5) IPP Annual Report 1985, p.140

6) W. Lotz, J. Nührenberg, A. Schlüter, J.of Comp. Phys., in print

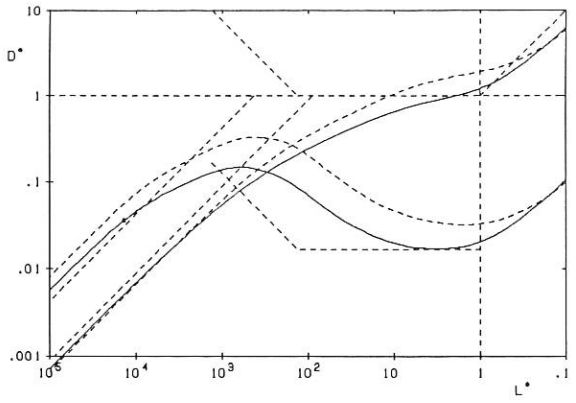

Fig.16: Local transport coefficients normalized to the ion plateau value for ion and electron particle (—) and energy (- - -) transport as functions of the thermal mean free path normalized to half the connection length. Shown are results for W VII-AS obtained at $A = 20$ with a plasma to thermal deuteron gyroradius ratio of 100 and an electric field corresponding to $e\phi/\langle E\rangle = 1$. Additional lines shown represent diffusion coefficients corresponding to the ν-regime without electric field, to tokamak banana diffusion, the ion and electron ripple diffusion, and the electron plateau value.

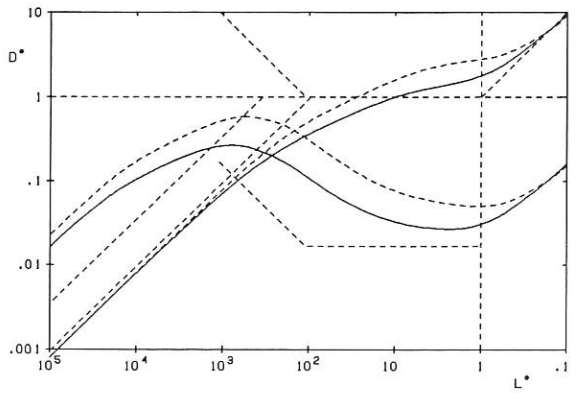

Fig.17: Same representation as Fig.16, but for ATF.

7. Monte Carlo Simulation of Neutral Injection

A modification of the FAFNER code [1] simulating neutral injection heating in stellarators was developed. This new code, FAFNER 2, is formulated in Boozer's coordinates and is therefore suitable for including an electric field in the form of a potential constant on magnetic surfaces of general geometry.

The code was applied to W VII-AS and the following qualitative trends were verified. For perpendicular neutral injection, an electric potential small compared with the neutral particle energy already significantly reduces the orbit losses; in particular, the electrostatically confining potential easily eliminates the orbit losses. For parallel neutral injection, the notations co- and counter-injection are used to define $v_{\|} = \vec{v}\cdot\vec{B}/|B| > 0$ and $v_{\|} < 0$, respectively. For the case of W VII-AS, a stellarator with left-handed-screw-like field lines, neutral injection with a pencil beam and with a radius of tangency and the plasma density chosen such that the deposition mainly occurs on the inboard side of the magnetic axis (i.e. between magnetic axis and main axis of the torus), the following qualitative result was verified. For co-injection as well as for counter-injection the electrostatically confining potential is beneficial, while the repelling potential increases the orbit losses.

---

[1] G.G. Lister, IPP Report 1985, IPP 4/222

Divisions and Groups

THE SCIENTIFIC DIVISIONS OF IPP

Experimental Plasma Physics Division 1

Director: Dr. M. Kaufmann

ASDEX Upgrade
- construction and preparation of the experiments of the follow-up to the ASDEX experiment for investigating the NET divertor and a reactor-relevant plasma boundary

JET diagnostics and pellet injection
- construction and operation of diagnostics and pellet injection for JET and IPP

Experimental Plasma Physics Division 2 (Stellarators)

Director: Dr. G. Grieger

Wendelstein VII-AS (Advanced Stellarator)
- Stellarator with improved confinement conditions
- toroidal plasma confinement in the Stellarator
- net-current-free plasmas, plasma production and heating by neutral injection, and high-frequency
- plasma stability and impurity effects

Wendelstein VII-X
- basic investigations and definition

Contributions to stellarator reactor systems studies

Contributions to NET studies

Experimental Plasma Physics Division 3 (ASDEX)

Director: Dr. G. von Gierke

ASDEX
- tokamak experiment with axisymmetric divertor and auxiliary heating pulses up to 10s in detail: energy confinement, impurity production and transport, ß-, density-, and q-limits with neutral injection, ion cyclotron and lower hybrid heating
- comparative studies of different heating and refuelling techniques
- current drive with lower hybrid waves

Computer Science Division

Director: Prof. F. Hertweck

Development of the AMOS/2 operating system

Development of data acquisition systems for experiments at IPP

Studies in parallel computer architectures

Theory Division 1

Director: Prof. D. Pfirsch

Theoretical basis of plasma physics
- analytical and numerical MHD computations
- models for anomalous transport
- high-frequency current drive
- turbulence theory

Theory Division 2

Director: Prof. A. Schlüter

Stellarators physics
- numerical and analytical methods of investigating equilibrium, stability and transport in three-dimensional toroidal configurations

Theory Division 3

Director: Dr. K. Lackner

Tokamak physics
- experiment-oriented theoretical work for interpretating and designing tokamak experiments such as ASDEX, ASDEX Upgrade, JET and NET

Surface Physics Division

Director: Prof. V. Dose

Surface Physics
- atomistic characterization of surfaces

Plasma Wall Interaction
- interactions of ions and electrons with solid surfaces
- wall fluxes in the boundary layer of plasma devices
- limiter and wall analyses

Technology Division

Acting Director: Dr. K. Lackner

Neutral Injection
- development and construction of the injection systems for W VII-AS, ASDEX and ASDEX Upgrade
- implementation of injection experiments

Lower hybrid heating
- preparation and implementation of LH heating and current drive experiments for ASDEX

Ion cyclotron resonance heating
- preparation and implementation of ICRH experiments for W VII-AS, ASDEX and ASDEX Upgrade

Contributions to INTOR studies

EXPERIMENTAL PLASMA PHYSICS DIVISION 1

(Dr. Michael Kaufmann)

Division E1 comprises two groups:

1. JET DIAGNOSTICS AND PELLET INJECTION (JDP)

Head: C. Andelfinger

Deputy Head: H. Röhr

Team: E. Buchelt, K. Büchl, C. Dorn, A. El-Sharnouby[1], H.U. Fahrbach, J. Fink, H. Frischmuth, H. Krause, R.S. Lang, F. Mast, E. Oberlander, D. Pohl, G. Prausner, G. Rupprecht, W. Sandmann, H.B. Schilling, G. Schramm, U. Schumacher, J. Sommer, A. Stimmelmayr, M. Ulrich, G. Weber, H. Weichselgartner, D. Zasche

This group is responsible for designing and producing plasma diagnostics and a pellet injector for JET and is also involved in a Task Agreement on the investigation of impurities in the JET plasma. These activities are detailed under the JET Cooperation Project. Other work is concerned with the development and operation of pellet injectors for ASDEX, WVII-A and ASDEX Upgrade

1) Guest, Nuclear Research Centre, Cairo, Egypt

2. ASDEX Upgrade

Head: W. Köppendörfer

Deputy Head: M. Blaumoser

Team: S. Cha, K. Ennen, J. Gruber, D. Jacobi, H. Kollotzek, E. Lackner, V. Mertens, M. Pillsticker, H. Preis, W. Reese[1], G. Reichert, K. Schindler, H. Schneider[2], U. Seidel, B. Streibl, M. Troppmann, H. Vernickel, F. Werner, A. Wieczorek

This group is concerned with the construction of the tokamak experiment ASDEX Upgrade and its peripheral installation. ASDEX Upgrade is the follow up experiment of ASDEX. This work is described under the ASDEX Upgrade project.

1) Noell, Würzburg

2) INTERATOM, Bensberg

EXPERIMENTAL PLASMA PHYSICS DIVISION 2 (Stellarators)
(Dr. Günter Grieger)

IPP activity in the field of Stellarator physics is mainly done in Experimental Plasma Physics Division 2 and Theory Division 2 (see there).

The relevant teams are:

W VII-AS

G. Cattanei, D. Dorst, A. Elsner, K. Engelhardt, V. Erckmann, R. Fowler[1], U. Gasparino, G. Grieger, P. Grigull, H. Hacker, H.J. Hartfuß, H. Jäckel, R. Jaenicke, J. Junker, M. Kick, H. Kroiss, G. Kuehner, H. Maaßberg, C. Mahn, R. Mathis[2], G. Müller, H. Münch, W. Ohlendorf, F. Rau, H. Renner, H. Ringler, J. Sapper, F. Sardei, I. Schoenewolf, M. Tutter, A. Weller, H. Wobig, E. Würsching, M. Zippe.

W VII-X

E. Harmeyer, J. Kisslinger, F. Rau, H. Wobig, F. Herrnegger[4]

The contributions of these teams are described in Part A of this Report in the sections on W VII-AS and W VII-X.

1) Guest from ORNL, Oak Ridge
2) ZTE
3) Guest from Kyoto University
4) Theory 2

EXPERIMENTAL PLASMA PHYSICS DIVISION 3 (ASDEX)

(Dr. Gerhart von Gierke)

Experimental Plasma Physics Division 3 comprises the ASDEX group, the work of which is fully reported in the section "ASDEX Project". The members of this group are as follows:

Head: F. Wagner
Deputy Head: H. Niedermeyer

G. Becker, B. Bomba[1], H.S. Bosch[2], H. Brocken[3], G. Dodel[4], A. Eberhagen, G. Fussmann, O. Gehre, J. Gernhardt, G. v.Gierke, E. Glock, G. Haas, J. Hofmann[2], E. Holzhauer[4], A. Izvozchikov[7], K. Hübner[8], G. Janeschitz, F. Kaesdorf[7], F. Karger, O. Klüber, M. Kornherr, M. Lenoci[8], G. Lisitano, H. M. Mayer, K. McCormick, D.Meisel, E. R. Müller[9], H. Murmann, H. Niedermeyer, A. Pietrzyk[10], H. Rapp, A. Rudy[11], F. Schneider, C. Setzensack, G. Siller, F. Söldner, K.-H. Steuer, U. Stroth[7], S. Ugniewski[12], K.L. Wong[13], H. Wurz[6],

---

1 Doctoral fellow, since September 1986
2 Doctoral fellow
3 Up to July 1986
4 University of Stuttgart, FRG
5 Ioffe Institute, up to April 1986
6 University of Heidelberg, FRG
7 Post-Doc since November 1986
8 Up to July 1986
9 Assigned to Jet up to November 1986
10 University of Washington, Seattle, USA
11 Undergraduate, since August 1985
12 Inst. for Nuclear Research, Swierk, Poland
13 Texas Tech. University, since November 1986

THEORY DIVISION 1

(Prof. Dr. Dieter Pfirsch)

Besides the most critical problems in fusion plasma physics, viz. β-limits and anomalous losses, Theory 1 were also concerned with questions relating to the phenomenon of profile consistency in tokamaks, sawtooth dynamics, HF current drive, and some problems of a more fundamental nature. An example of the latter: Exactly treatable 1-dimensional models of turbulent velocity fields with realistic spatial and time correlations were constructed and shown to lead to average square distances covered by a particle in such a velocity field which are asymptotically proportional to powers of the time between 0 and 2. The linear time dependence usually assumed, which is also obtained by a Eulerian approximation, is not a necessary feature. Anomalous transport might therefore not be describable in terms of a diffusion constant. - Important progress was made in 2D linear codes for resistive instabilities and 3D nonlinear codes for non-ideal MHD. Localized resistive modes which seem to be responsible for the β-limits observed in ASDEX are being evaluated for INTOR configurations, the consequences so far being similar to those for ASDEX.

1. ON THE THEORY OF THE SAWTOOTH DISRUPTION

(D. Biskamp, H. Welter, M. Walter)

Numerical studies of the MHD processes relating to the sawtooth oscillation were conducted in cylindrical as well as in toroidal geometry by using the full non-ideal MHD equations. Linear mode properties were investigated for q-profiles consisting of a flat central part $q = q_o \cong 1$, a shallow well (or skin current), and a subsequent parabolic rise. For small transport coefficients eigenmodes are essentially ideal modes with a sharp upper boundary of the unstable q_o-region. For q_o close to unity many modes are unstable, not only m = 1 as in the case of a peaked current profile with $q_o < 1$. In the cylindrical case maximum growth rates scale as $\gamma \propto \sqrt{mp_o'}$, as expected for interchange-type modes. In the toroidal case, too, no instability threshold in the pressure gradient is found, but for small p_o' growth rates are significantly reduced, scaling linearly as p_o'. Nonlinear computations have thus far been restricted to cylindrical geometry. The nonlinear evolution of an unstable m = 1 mode occurs on the time scale of the linear growth rate, the final state consisting of a completely inverted p_o-profile. It is only in a very narrow transition region close to the marginal points that saturation at a finite helical amplitude is found.

Simulations of the complete sawtooth cycle evolving self-consistently under the effects of ohmic heating and heat conduction were performed. Steady amplitude sawtooth oscillations are found in a broad range of the transport parameters. This is by no means self-evident, since for flat q-profiles any negative average pressure gradient leads to a rapid interchange motion, so that a stationary convective cell appears to be the most likely final state. The cylindrical model cannot, however, give a quantitative description of the sawtooth phenomenon in tokamaks. Because of the inherent inefficiency of energy storage the sawtooth amplitudes are far too small for small η, $\Delta T_e/T_e \propto \eta^{1/2}$. More appropriate modelling requires toroidal effects to be taken into account. The properties of the linear growth rates indicate how a more efficient way of energy storage is achieved in toroidal geometry.

2. NATURAL CURRENT PROFILES IN TOKAMAKS

(D. Biskamp)

While the perpendicular current density in a plasma configuration is fixed by the pressure distribution, the parallel current distribution is a priori undetermined, since only the total current I can be controlled directly. It is

therefore proposed that in the presence of an effective magnetic reconnection process the current density relaxes to a state of minimum magnetic energy under the constraint of constant I. Performing the variation in a particular way, one obtains a class of current profiles depending on a free parameter q_o for given q_a (i.e. I) which is determined by the sawtooth process through the experimental relationship $r_1 = a/q_a$, $q(r_1) = 1$, so that the "natural" current profile becomes

$$j(r) = \frac{j_o}{(1+q_a \frac{r^2}{a^2})^2}$$

Using the equilibrium equation and the condition for resistive equilibrium with Spitzer resistivity one finds that the pressure distribution is proportional to j(r) and that the density profile is broader than the electron temperature profile $n(r) \propto (T_e(r))^{1/2}$. Since tokamaks are externally driven systems, complete relaxation cannot take place. One expects the closest agreement in the ohmic regime, while for strong additional heating profiles are probably determined by different effects.

3. ENTROPY PRINCIPLE FOR TOKAMAK PROFILES

(D. Pfirsch, F. Pohl)

It was shown that experimental temperature and density profiles are consistent with the assumption that they relax towards profiles related by $T(\underline{x})/T_o = (n(\underline{x})/n_o)^{2/3} \exp(\alpha(1-n(\underline{x})/n_o))$, with $\alpha \geq 0$ independent of $\underline{x}$. $\alpha = 0$ means an isentropic plasma which appears to be the better realized the larger the machine size is and the less additional heating is applied. The relation follows from an "entropy principle" proposed by D. Pfirsch. Combination with Coppi's T-n-r relation yields explicit temperature and density profiles for almost circular plasma cross-sections: $n(r)/n_o = \hat{n}(\alpha, Q r^2)$; $T(r)/T_o = \hat{T}(\alpha, Q r^2)$. Q: function of q_a/q_o and minor plasma radius a, q: safety factor, r: distance from magnetic axis. These "combination profiles" also agree reasonably well with experimental ones. On the other hand, it is shown that Coppi's relation follows approximately from our relation if one assumes Spitzer conductivity for the parallel current density.

4. NATURAL CURRENT PROFILES AND CONVECTION

(D. Biskamp)

The conditions under which actual tokamak profiles relax to the "natural" shape are investigated. Since conventional tokamak transport computations do not yield simple self-similar profiles, while natural profiles are set up in convection-sustained current sheets, it appears that convection plays an important role in the relaxation process. On the basis of the observation that 2D toroidal convection being essentially incompressible does not transport the main field, a cylindrical mock-up is constructed which by eliminating the convective transport of the potential field allows much larger convective flows, $v_r \propto \eta p'/B_\theta^2$. The model equations contain several free parameters, the exponent ν in a Spitzer-type resistivity $\eta \propto T^{-\nu}$, the adiabaticity coefficient, an ohmic heating efficiency factor σ, and thermal conductivity. Solving the equations in time, steady-state solutions are obtained which over a broad range of these parameters yield current profiles very close to the natural shape. Only if heat diffusion dominates over convective heat transport substantially different profiles are set up.

5. NUMERICAL STUDIES OF LOCALIZED RESISTIVE MODES IN TOKAMAKS

(D. Correa-Restrepo)

The analytical investigation of localized resistive modes in tokamaks is being complemented by numerical calculations which are relevant to realistic plasma configurations. In particular, the stability of INTOR equilibria with respect to localized resistive modes is being investigated. The calculations include computation of numerical equilibria, investigation of both Mercier and ideal ballooning stability, and computation of all the surface-averaged quantities which are necessary to evaluate previously derived resistive stability criteria.

6. COLLISIONAL MODEL FOR TOKAMAK TRANSPORT

(W. Kerner, H. Weitzner[+])

The temporal evolution of a tokamak up to the transport time scale is studied with the two-fluid Braginskii model where the flows are consistently treated. The system evolves through a sequence of equilibria in the usual 1 1/2D transport model. The scaling parameter is the ratio of electron to ion mass, $\varepsilon = \sqrt{m_e/m_i}$. The large and dominant transport coefficients are the parallel heat conductivity and the parallel viscosity; compared with the usual plateau forms, our coefficients could be regarded as anomalous.
The system has to be subjected to special profile constraints and for experiment-relevant parameters the energy confinement time is of the order of 100 ms. If, however, these profile constraints are not matched, energy is released at a rate of 1 to 10 ms.
The stationary state yields equilibria with flows where the temperature is a flux function, $T=T(\psi)$, but the density has poloidal dependence, $n=n(\psi,\theta)$. It is aimed to adapt this model to neoclassical transport.

7. PLASMA HEATING AND CURRENT DRIVE

(E. Canobbio, R. Croci)

It has already been shown (see Annual Report 1985) that the ponderomotive decay of LH waves can explain the observed power absorption without intro-

[+] Courant Institute, New York

ducing ad hoc "spectrum upshifts". Numerical evaluation of the analytical results which make use of the quasi-linear expression for electron Landau damping and ion Karney damping has shown that the absorption essentially takes place in the neighbourhood of singular surfaces where $|\text{grad } \underline{E}| \to \infty$, beyond which the solution is no longer single-valued. For consistency we had to introduce explicitly the possibility of localized absorption in the nonlinear differential equation for the electric field. This has led to a new set of singular surfaces and to a solution that is single-valued everywhere. The power absorption has thus been consistently explained. The evaluation of the power distribution between ions and electrons would require numerical calculations. Besides the power absorption a problem of current drive still open was the presence of a "density limit". We have shown that the polarization induced in the plasma by a LH ray interacts with the ray itself when it propagates in the plasma for more than a toroidal turn. This interaction destroys the singular surfaces. Since the penetration angle of the ray depends on the density, a larger and larger part of the ray does not give rise to appreciable power absorption when the density increases. If the frequency is large enough (the important parameter being the product of frequency and mass number divided by the magnetic field strength) this phenomenon does not occur. The comparison of the value of the density limit, when it occurs, and of the value of the parameters for which it does not occur (i.e. for which $I \propto P/n$, as given by Fisher's formula), with the theoretical predictions shows surprisingly good agreement. We note that the theoretical formulae only depend on frequency, magnetic field, aspect ratio and mass number without adjustable parameters.

8. PHASE SPACE AND STATISTICS OF CONTINUA

(H. Tasso)

Problems in introducing suitable phase space for continua are discussed. Euler variables lead to degeneracy, Clebsch variables to redundancy, and Lagrange variables to an implicit Hamiltonian which is of no use for purposes of phase space integration and statistical mechanics.
These difficulties can be solved for evolution equations such as the Korteweg-de Vries equation, for which the k-spectrum was previously obtained by the author. The classical removal of the ultraviolet catastrophe in this case is contrasted with Planck's black-body radiation spectrum.

9. LYAPUNOV STABILITY AND ATTRACTORS

(H. Tasso)

Lyapunov functions valid in the greater part of phase space were found for a system of nonlinear oscillators of an extended Van der Pol type. They yield a good estimate of the location of attractors. High-dimensional limit cycles are produced under certain conditions. For a particular single oscillator the appropriately modified Van der Pol equation delivers an ellipse as limit cycle.

The general attracting system in the case of two oscillators can be completely integrated via complex plane representation and elliptic integrals. The solutions of this system are highly nontrivial and they deliver the key to the solution of a more general second-order complex differential equation.
The extended Van der Pol system has some relationship with resistive MHD up to the sign of resistivity. It is, however, too early to consider it as a possible model for resistive MHD phenomena such as sawteeth in tokamaks.

10. EXACT EULERIAN TREATMENT OF TURBULENT DIFFUSION

(D. Pfirsch, P. Gräff, F. Pohl)

On the basis of a previous paper (P. Gräff, D. Pfirsch Z. Naturforsch. 37a, 804 (1982)) we constructed a class of one-dimensional turbulent velocity fields with vanishing average and decaying correlations in space and time for which the transition probabilities can be found exactly. This was possible in a purely Eulerian framework, i.e. avoiding a Lagrangian description of the turbulent motion. The result is that

$$\langle x^2 \rangle = g(t) = \int_{-\infty}^{\infty} D(\omega) \, \frac{1-\cos\omega t}{\omega^2} \, d\omega \quad ,$$

with $D(\omega)$ being any spectral function. This allows a large variety of diffusion processes with asymptotic behaviour of $g(t)$ for large values of t between $g = \text{const}$ and $g \sim t^2$. In a plasma diffusion might be related to a stochastic $\underline{E} \times \underline{B}$ velocity field. Our examples show that the ordinary type of diffusion described by $g(t) \sim t$, as usually assumed even for the anomalous case, may be an exception.

11. TOPOLOGY OF MAGNETIC SURFACES

(D. Lortz, A. Salat)

Very little is known about the existence of nested toroidal magnetic surfaces $\psi(\underline{r})$ without symmetry, as solutions of the MHD equations.
As a first step in the hope of obtaining exact results, the behaviour of ψ was studied by series expansion in $\varepsilon \ll 1$ (perturbation parameter, e.g. wall indentation) or $\xi \ll 1$ (distance from initial surface). For vacuum fields a formula for the shear on a surface was derived which only contains quantities on the surface itself.
In contradiction to suggestions (H. Grad) vanishing of the shear is not a necessary condition for the existence of 3D MHD equilibria.

12. MHD NORMAL MODE COMPUTATION

(W. Kerner, K. Lerbinger, E. Schwarz und J. Steuerwald)

The non-ideal MHD equations with resistivity and heat conductivity as dissipative effects are

numerically solved by applying the finite-element method. This leads to a large-scale complex eigenvalue problem $A\underline{x} = \lambda B\underline{x}$ with A a non-Hermitian matrix. The calculations for 1D equilibria in cylindrical geometry are continued for various applications. First accurate results for 2D configurations were recently obtained.
Further progress has been achieved for the eigenvalue solver based on inverse vector iteration. For matrices with block-tridiagonal band structure the system of equations is solved by a LU factorization with only four sub-blocks kept simultaneously in the fast memory and with access to other blocks through I/O from disk. Optimization of the overall CPU and I/O operations is performed. Matrices with large dimensions, i.e. d ≈ 100,000, can be treated. This algorithm will be further tuned to the use of two and four processors.

13. A PARAMETER-DEPENDENT NONLINEAR EIGENVALUE PROBLEM

(R. Meyer-Spasche, M. Wagner[+])

The following mathematical problem was treated: "Given a parameter-dependent nonlinear system of partial differential equations, how do the number of solutions and the spatial structures of these solutions depend on the parameters?" We investigated this question for a special example (Taylor problem), using the TAYPERIO code written earlier [1]. Some of the patterns which were found [2,3] are non-generic (i.e. not typical) in the sense of Catastrophe Theory. They seem to describe, however, situations often encountered in practice (fluid dynamics, chemical engineering, phase transitions).

1. R. Meyer-Spasche and H.B. Keller, Phys. Fluids 28, 1248-1252 (1985)
2. R. Meyer-Spasche and M. Wagner, Proc. "Bifurcation", Dortmund 1986. (ed. Küpper, Seydel, Troger), Birkhäuser Verlag, in press
3. R. Meyer-Spasche and M. Wagner, Proc. "The Physics of Structure Formation", Tübingen 1986. (ed. Güttinger, Dangelmayr), Springer Series in Synergetics, to appear.

[+] Freie Universität, Berlin

THEORY DIVISION 2

(Prof. Dr. Arnulf Schlüter)

Theory Division 2 mainly comprises the Stellarator Physics Group, the work of which is reported in the section "W VII-X Project".

The members of the Stellarator Physics Group are W. Dommaschk, F. Herrnegger, W. Lotz, P. Merkel, J. Nührenberg, A. Schlüter, U. Schwenn.

THEORY DIVISION 3

(Dr. Karl Lackner)

The primary task of this division is to provide theory support for the present and future tokamak experiments of the institute. Most of the investigations carried out are therefore described in the respective sections of the ASDEX, ASDEX Upgrade, JET and NET projects. The work described in detail in the following thus concerns only the more basic investigations and the development of physical models and mathematical tools for future application to different experiments.

Team: A. Blobel, B. Braams[1], M. Brambilla, R. Chodura, W. Feneberg, K. Grassie, O. Gruber, O. Kardaun, T. Krücken, L. Lengyel, P. Martin, P. McCarthy[2], J. Neuhauser, K. Riedel[3], W. Schneider, R. Weiner, R. Wunderlich, G. Zavala, H.P. Zehrfeld

1. MHD EQUILIBRIUM AND STABILITY

This topic covers equilibrium studies for choosing tokamak plasma configurations and identifying the actually assumed plasma shapes on the basis of measured magnetic signals, simulations of the axisymmetric stability and the control of the plasma configuration, and investigations of the expected and observed MHD activity in ASDEX. Most of the respective work is therefore described under the ASDEX and ASDEX Upgrade projects.

1.1 Flow Equilibria for ASDEX and ASDEX Upgrade

(H.P. Zehrfeld)

Neutral beam injection into magnetically confined plasmas is accompanied by plasma flow and a corresponding alteration of the equilibrium characteristics of the discharge. We considered the combined action of toroidal and poloidal plasma rotation by calculating the corresponding two-dimensional MHD flow equilibria for separatrix-bounded plasma configurations of ASDEX and ASDEX Upgrade /175/. A specific feature of such equilibria is the appearence of radial components of the plasma current density and the formation of corresponding current surfaces which in analogy to the magnetic ones are defined as level surfaces of solutions of $j \cdot \nabla \Omega = 0$ for Ω. The existence of distinct magnetic and current surfaces is due to the fact that both poloidal and toroidal flows are present: The finite rotational transform of the flow field lines together with the effect of toroidal curvature produces accelerating forces in the toroidal direction, which must be balanced by corresponding $j \times B$ forces. This requires plasma currents across and - together with the strong component of the magnetic induction in the toroidal direction - balancing pressure gradients in magnetic surfaces. The latter effect - for Mach numbers of the poloidal flow < 0.3 - leads to density variations on magnetic surfaces of ≈ 20 % (ASDEX).

---

1) PPPL, Princeton, USA

2) University of Cork, Ireland

3) Permanent address: New York University, New York, USA

1.2 Compact Torus Flow Equilibria

(H. Bruhns, H.P. Zehrfeld)

While equilibria of compact toroidal (spheromak) configurations are easy to obtain analytically for the case of force-free current or a linear dependence of the pressure on the poloidal flux function, numerical procedures must be invoked if more complex equilibria are to be determined. We addressed the free boundary equilibrium of a spheromak, including a parallel flow in the force balance. The calculation is applied to the HSE configuration with a major radius of 0.08 m and a toroidal (poloidal) plasma current of 0.2 (0.24) MA. While two or four discrete coils generate the vertical field in the experiment the numerical studies use an idealized meridional field pattern. Comparing the results with the experiment for a modest average beta (6.5 %) and for flow speeds of up to several tens of per cent of the sound speed reasonable agreement is found for the flux pattern. However, there are deviations in the poloidal current profile which at present impede quantitative evaluation of, for example, flow properties.

1.3 Equilibria for Specified Profiles of Pressure and Toroidal Current

(H.P. Zehrfeld)

The calculation of static axisymmetric MHD equilibria - proceeding from the usual equilibrium partial differential equation - is mostly performed for specified distributions of the poloidal current J and the pressure p over the poloidal flux Ψ. For given pressure distribution, a desired toroidal current profile $I(\Psi)$ can be achieved only by appropriate variation of J as a function of Ψ. For the purpose of data generation for stability investigations (CART code and ballooning calculations) we modified the static version of the NIVA flow equilibrium code so that, instead of $J(\Psi)$, a toroidal current profile can be prescribed from the very beginning. This means that we solve the equation

$$\mathrm{div}(\nabla\Psi/R^2) + 4\pi^2\mu_0(1/R^2\langle 1/R^2\rangle^{-1} + \beta_p(1 - 1/R^2\langle 1/R^2\rangle^{-1})\frac{dI}{dV} = 0$$

where $\beta_p = (dp/d\Psi)(dV/dI)$, R is the distance from the axis of symmetry, V is the volume enclosed by the magnetic surface considered, and $\langle \ldots \rangle$ is the usual flux surface average.

1.4 Ballooning Stability of High-beta ASDEX Equilibrium

(K. Grassie, O. Gruber, H.P. Zehrfeld)

The high-n stability of two-dimensional MHD ASDEX equilibria was considered by solving the corresponding Sturm-Liouville problem for ideal ballooning modes /279/. In order to make the investigations relevant to the problem of the experimentally maximum attainable ß-value, TRANSP code interpreted ASDEX data were used to determine radial equilibrium profiles for toroidal current and pressure. On the basis of such profiles MHD equilibria were calculated and subjected to a detailed ballooning stability analysis (see Sect. 1.3).

Further to the evaluation of the general ideal ballooning equation, we considered that of a large-aspect-ratio expansion for the corresponding equilibrium and stability relations. Although assuming circular flux surfaces, we took into account here the correct differential displacement of the magnetic surfaces due to toroidal curvature, β_p, and the inductance coefficient l_i. Except in the neighbourhood of the magnetic axis, we find the results for the large-aspect-ratio expansion in good agreement with those of the general one (see also Sect. 1.4.4 of the ASDEX project).

1.5 MHD Analysis with the CART Code

(K. Grassie, O. Gruber, O. Klüber, K. Lackner, H.P. Zehrfeld)

In summer 1986 the CART-3D stability code of GA was installed at IPP. CART is based on the large aspect ratio expanded resistive MHD equations in high ß-ordering, which in contrast to other stability codes are solved in Cartesian coordinates. This is of considerable importance for the analysis of realistic ASDEX and ASDEX Upgrade discharges, since here divertor configurations and/or large plasma elongation require an increased spatial resolution in the poloidal plane.

In our simulations we assume the radial dependence of the resistivity $\eta(r)$ to vary as $\eta \sim \eta_0/j_{tor}(r)$ throughout the plasma region. However, the experimental observation of large poloidal mode numbers above the corresponding values for q_a (=q(r=0.95a)), which is connected with the MHD activity during H-mode discharges (see Sect. 1.4.3 of the ASDEX project), can be reproduced only if the vacuum resistivity is also varied from its value at the plasma boundary by three orders of magnitude to its value near the inner wall. Furthermore, this radial dependence of η_v is necessary to obtain the correct poloidal in-out mode asymmetry in high-ß discharges, i.e. the poloidal wavelength of the mode structure decreases if one moves from the outer side of the torus to its inner side.

In order to achieve saturation in the non linear phase, we tried to reduce the numerical steepening of the perturbed pressure by introducing some specific terms of third order in the inverse aspect ratio. These additional contributions guarantee the correct treatment of the sound wave, i.e. its finite velocity, and lead to equilibration of the perturbed pressure along lines of constant flux. However, in the ASDEX parameter regime these terms turn out to be insignificant. We thus enforce nonlinear saturation by adding a diffusive damping term for the perturbed pressure with a factor linearly dependent on p_{max} ($p(x,y)$. The pressure evolution equation is thus replaced by

$$\frac{\partial p}{\partial t} = - v_\perp \cdot \nabla_\perp p + C p_{max} \nabla_\perp^2 p \ .$$

The constant C is chosen such that the corresponding saturated value for $\tilde{B}$ matches the experimental level. Typically, we find $\tilde{B} \sim C^{-1}$. Subsequently results for the perturbed magnetic field can be confronted with Mirnov-probe data. More sensitive to non-linear effects are soft X-ray measurements. Traces of these might be compared with corresponding calculations of the line-integrated squared pressure.

1.6 Stabilization of Tearing Modes

(K. Grassie)

A simple model has been constructed where temperature and current density profiles are determined by tearing mode stability considerations. The basic idea is the coupling of the heat conduction equation to a Δ'-code. The heat conduction coefficient $\chi_{\parallel}$ is strongly increased throughout the island region, which forms if $\Delta' > 0$, and allows a large radial heat transport along magnetic field lines. Clearly, this coupling results in a flattening of the current density profile and subsequently stabilizes the tearing modes. Usually only very few unstable modes exist and since these have small saturated island sizes this simple mechanism is not able to explain profile consistency. However, this model can be used to study several confinement scenarios, e.g. by testing different assumptions for the radial dependence of the heat conduction coefficient.

The time-dependent version allows calculation of the time evolution of the island width. This requires additional assumptions concerning the relation of current density and temperature profiles on a short time scale, as well as a model for island formation. In this context, effects of local additional heating on tearing mode stability are investigated.

2. PLASMA TRANSPORT

Our work in this area is concerned with deriving the numerical values of the energy and particle transport coefficients from experimental data on ASDEX. The main tool used at present is the TRANSP transport analysis code of Princeton, the applications of which are described in the ASDEX section.

2.1 ASDEX Heat Pulse Propagation as a Forced Boundary Value Problem

(K.S. Riedel[1])

The electron heat conductivity $\chi_{e\perp}$ immediately after a sawtooth crash is investigated for a variety of different parameters. To determine χ_e, we solve a forced initial value problem outside the mixing radius. The forcing parameter is the temperature evolution at the inner boundary point. The experimentally measured ECE signal at the first point outside the mixing radius is used as the input. χ_e is then determined by fitting the temperature evolution of the other electron cyclotron emission channels outside the input channel.

This approach has several important advantages over the standard method of fitting the arrival time of the peak of the pulse to a theoretically initialized perturbation. The region inside the mixing surface where the conductivity may be anomalously large is excluded from consideration. The arrival of the peak depends primarily on the conductivity between the input radius and the output radius. Local values of χ_e are thus determined. No assumptions on the position of the q = 1 surface or the radial redistribution of energy are necessary. The conversion of magnetic energy into heat is automatically taken into account. Finally, the ECE measurements give a time history of the heat pulse at a few spatial locations and the method makes effective use of this information.

The method is tested on a standard ohmic discharge with the following parameters, $q(a) = 3.3$, $T(0) = 1075$ eV, $n = 2.4 \times 10^{13}$, $Z_{eff} = 1.3$. The input channel is at 18.1 cm and the fit channel at 25.6 cm. Ten sawteeth are averaged over the sawtooth period. The period is 13 ms, the crash time is 1 ms, the amplitude is 90 eV, and the peak of the pulse arrives at r = 18.1 cm in 1.65 ms and at 25.5 cm in 2.65 ms. In practise, the pulse has four characteristic parameters, the arrival of the peak, the amplitude of the peak and slope of the temperature rise and the slope of the decay. We are able to fit the first three parameters with a constant χ_e of 70 cm²/ms. A radially increasing χ_e gives a slightly better fit. The decay of the pulse depends on both the radial variation of χ_e and the boundary condition. The corresponding power balance χ_e is 12 cm²/ms at 18 cm and 17 cm²/ms at 25 cm.

The standard calculation for a Kadomtsev initialization gives $\chi_e = 38$ cm²/ms, but the amplitude is significantly smaller, the exact amount depending sensitively on the position of the mixing radius, and the shape being greatly distorted. A possible explanation is that immediately after the crash the heat conductivity is greatly enhanced in the centre and that the plasma is in thermal equilibrium with the new flat profile.

2.2 Mapping of Equilibrium Flux Surfaces

(G. Bateman[1], W. Schneider)

Representing the surfaces of constant magnetic flux in the poloidal cross-section of a tokamak by a harmonic description is a compact formulation. In most cases a few Fourier components suffice to describe the contours adequately. Such a description is also used in the 1 1/2 D versions of the TRANSP and BALDUR transport analysis and simulation codes of Princeton to be used for ASDEX Upgrade. On the other hand, the very effective free boundary equilibrium codes developed at IPP in Garching, different versions of which will be also used for identifying the plasma equilibria in this device, are based on a rectangular grid. A new effective mapping algorithm has therefore been developed as interface between the two descriptions.

---

1) Permanent address: New York University, New York, USA.

1) PPPL, Princeton, USA.

3. PHYSICS OF THE SCRAPE-OFF LAYER

The emphasis on this topic stems from IPP's decision to follow the divertor line for controlling the plasma-wall interaction in tokamaks and from the realization that aspects of the plasma-wall contact have a large effect on bulk plasma parameters in addition to that trivially expected via the impurity behaviour.

Simulation code studies in this area are included in the ASDEX section. The derivation of a consistent model for neoclassical transport in the scrape-off layer and its inclusion in a 2D simulation code were carried out in collaboration with JET and is described there.

3.1 Fokker-Planck Model of the Scrape-off Layer

(A. Blobel, R. Chodura)

The particle and energy flow in a scrape-off layer of arbitrary mean free path length for Coulomb collisions is studied by a 1D particle model with the Fokker-Planck collision term. The flow starts from a particle and energy source, passes through the collisional presheath and the nearly collisionless electrostatic sheath, and is absorbed at a target plate. The physical processes in the sheath require an electron energy influx at the sheath entrance of $Q_{es} = \delta\, T_{es} \Gamma$ (with Γ the electron flux, T_{es} the electron temperature, and $\delta = 4 \ldots 4.8$) which is larger than the convective flux $\gamma_e/(\gamma_e-1) T_{es} \Gamma$, $\gamma_e = 5/3$. An additional electron heat flux must thus be transported through the presheath region. For large collisionality in the presheath, i.e. small mean free path length, the heat flux is macroscopically coupled to the local temperature gradient by the Braginskii heat conductivity. Microscopically the heat flux is carried by an overpopulation of the downstream wing of the velocity distribution function. For low collisionality, i.e. long mean free path length, on the other hand, the heat flux is caused by a truncation of the velocity distribution due to particle absorption at the target plate and is decoupled from the local temperature gradient.

Comparison of the results of the kinetic Fokker-Planck model with those of a fluid model yields the limits of applicability of the latter. Within these limits the Fokker-Planck model serves to derive the appropriate boundary conditions of the fluid equations at the sheath edge.

In addition to the particle code, a method of direct solution of the Fokker-Planck equation was tested. The distribution function is expanded in a set of orthogonal Burnett functions in velocity space with space and time-dependent coefficients which are related to the moments of the distribution. These coefficients are determined by numerically solving a set of coupled partial differential equations. The method is used for a systematic investigation of transport in a plasma with smooth distribution function but arbitrary ratio of mean free path to gradient lengths.

3.2 A Divertor Scrape-off Layer Model for Radial Tokamak Transport Codes

(J. Neuhauser, R. Wunderlich)

The radially continuous two-chamber model of a high-recycling divertor tokamak edge layer (described in the Annual Report 1985) was reformulated to include the time dependence. The combined continuity equations of plasma and divertor neutrals was then rearranged in such a way that all the divertor recycling physics just appears in the form of effective radial diffusion and drift coefficients in a simple radial plasma transport equation.

When applied to a standard tokamak transport code these coefficients must be recalculated for each time step in a subroutine which contains all the divertor physics leaving the transport code otherwise practically unchanged. The highly nonlinear physics hidden in the transport coefficients, however, can easily influence the time stepping in the main code. In addition, it has been shown that physically relevant, radial instabilities are to be expected for certain edge parameters, in which case the code run would usually fail, unless other provisions are made, e.g. enhancement of the anomalous part of the radial diffusion coefficient.

3.3 Inhomogeneous Time Transformation in Computations on a Highly Non-equidistant Grid

(R. Zanino[1], K. Lackner, W. Schneider)

The description of phenomena in the scrape-off layer encounters severe numerical problems near the target plates where most physical parameters undergo significant changes over a short distance. More generally, similar problems arise in the solution of differential equations, in which the highest-order term has a small coefficient and is thus unimportant in the interior of the system, but is necessary to satisfy the boundary conditions and therefore dominates in a boundary layer zone. To resolve the strong, localized gradients in numerical calculations, a refined mesh is required in the latter and will dominate the permissible time step in an explicit formulation of a time-dependent problem. If only the asymptotic, steady-state solution is of interest this can be resolved by an appropriate space-dependent time transformation.

4. Wave Heating

4.1 Theory of Ion Cyclotron Heating of Tokamak Plasmas

(M. Brambilla, T. Krücken)

The "ballistic" model for describing HF wave propagation and absorption in the ion cyclotron frequency range in an axisymmetrically confined plasma /IPP 5/10/ takes into account the full geometry of the static magnetic field configuration, finite Larmor radius effects, and kinetic absorption

[1] University of Turin, Italy.

for both ions (fundamental and first-harmonic cyclotron damping) and electrons (Landau and transit time damping). It has been completed by a new formulation of the energy balance equation which explicitly shows that a Maxwellian plasma is always locally dissipative and is easy to be implemented numerically.

The resulting system of two partial integro-differential equations was solved numerically for plasmas with circular cross-sections, using a spectral ansatz in the poloidal (and toroidal) directions and a finite-element discretization with Hermitian cubic interpolation in the radial direction. The first successful runs show that the method converges satisfactorily; with the help of a solver developed by W. Kerner and E. Schwarz it is possible to deal with plasmas at least up to the size of ASDEX.

4.2 Theory of Bernstein Wave Launching

(M. Brambilla)

Coupling to Bernstein waves from an external antenna is described in a fully 3D plane layered approximation. To solve the sixth-order ordinary differential equations for the field in the plasma a finite-element discretisation with cubic Hermitian interpolation is used. The code evaluates the radiation resistance of the antenna and the field distribution in the near-field region. The former is found to be quite sensitive to the density profile: a region of low ß ($\ll m_e/m_i$) or a thin vacuum layer ($d \lesssim 1$ cm) near the antenna are necessary for effective coupling.

The code can also be used to investigate parasitic effects which might affect coupling of the fast wave in conventional IC heating experiments. These are found to be particularly strong if the density near the Faraday shield becomes so low that the lower hybrid resonance exists in the scrape-off plasma.

4.3 Numerical Simulation of Reflectometry Density Measurements in a Reversed Pinch

(M. Brambilla, M. Moresco[1])

Two codes were written to help with the interpretation of density measurement by reflection of the ordinary wave from the density cut-off in a reversed field pinch configuration. A ray-tracing code (adapted from a tokamak version) can be used to investigate the effects of beam divergence and refraction. A full-wave finite-element code describing the propagation of nearly equatorial waves investigates mixing between ordinary and extraordinary polarization, which is very strong in a RFP because of the large shear. It is found that this effect imposes additional constraints on the design of the diagnostic system, but the interpretation of the measurements should remain possible.

5. DATA ANALYSIS AND INTERPRETATION

Our activities in this field aim at obtaining an integrated package of codes and data bank files starting with identification of the plasma configuration and fitting of profiles of plasma parameters to the experimental data and ending with multivariant regression analyses of the derived and stored transport properties. The parts of this package which are already in operational use are described in the section of ASDEX.

5.1 Fast Processing of Diagnostic Raw Data

(P.J. McCarthy[1])

The processing of plasma diagnostic raw data frequently entails the iterative fitting of physical models to obtain best estimates of relevant plasma parameters, a task whose time requirements may well relegate it to the realm of off-line analysis. A separate problem may exist where a large number of raw measurements are analyzed: if some data are highly correlated the results will be prone to numerical instabilities unless steps are taken to detect such interdependences.

Despite the large number of inherent degrees of freedom in a plasma, the behaviour of many physically interesting quantities in a given experimental configuration seems to be characterized by a relatively modest dimensionality. A statistical analysis of the dependence of desired plasma parameters on diagnostic raw measurements accordingly suggests itself.

In a two-pronged approach to this problem, linear dependences in the raw data are detected by a principal component analysis and the multilinear regression method of function parameterization (FP) is then applied to permit very fast recovery of plasma information directly from linearly independent combinations of the raw data.

The first plasma physics application of the technique to the recovery of some characteristic MHD equilibrium parameters of the ASDEX experiment from external magnetic signals was reported here /IPP 5/3/. The technique has since been successfully applied to the recovery of electron temperature and density profiles from a combination of external magnetic signals and Thomson scattering electron density and temperature measurements from the ND:YAG 60 Hz repeating laser diagnostic on ASDEX /IPP 5/12/.

The recovery of plasma information from simulated ASDEX Upgrade equilibria, where FP is expected to be an integral part of both the real-time feedback control system and between-shot analysis, has also been demonstrated. Critical quantities like the plasma position may be recovered with a sub-centimetre uncertainty with some 1000 floating point operations. More detailed information, such as the equilibrium flux structure, space-to-flux coordinate transformation of spatially localized measurements or the unfolding of chordal arrays of line-integrated measurements will be recoverable in a time compatible with between-shot analysis.

---

[1] University of Padua, Italy

[1] Permanent address: University of Cork, Ireland

6. PELLET ABLATION MODELLING

Part of our work in this field aims at creating an advanced pellet ablation model useable in transport simulation codes. It is covered by a NET contract and described in the respective section.

6.1 Two-dimensional Calculations on the Expansion of High-density Cold Plasma Substance in Magnetically Confined Plasmas

(G. Zavala[1], L. Lengyel)

A cryogenic pellet injected into a hot plasma becomes ablated and ionized, thus producing rather significant local temperature and density perturbations in the recipient plasma. It is of interest to gain information on the temporal development of the cold, high-density cloud surrounding the pellet under different pellet and plasma parameter conditions.

For this purpose, a three-fluid (neutral, ion, and electron components), two-velocity (neutrals, ions) and two-temperature (heavy particles, electrons), cylindrically symmetric model has been developed within the framework of a doctoral dissertation[2].

Since a cryogenic pellet is of rather low temperature and comparatively high density ($\sim 10^{\circ}$ K and $\sim 10^{28}$ m^{-3}), it is rather difficult to follow up numerically its interaction with the recipient plasma (typical plasma parameters: 10^{6} to $10^{8\circ}$ K, 10^{20} m^{-3}) within the framework of a hydrodynamic code because of the large gradients present.

For this reason, the pellet is replaced by a given source of cold neutral particles which is of finite extent in space and whose strength is a prescribed function of time. The expansion and ionization dynamics of the gas cloud evolving from the source region is computed by assuming cylindrical symmetry and solving the respective initial-boundary value problem.

The cloud particles are heated by the thermal and non-thermal particles that may be present in the recipient plasma. In the absence of non-thermal particles, the dominant energy transfer mechanism is the electron thermal conduction along the magnetic field lines, which is computed by taking non-local energy transfer phenomena into account as well. Energy transfer in the direction perpendicular to the magnetic field is modelled in an optional way by prescribing a conductivity (anomalous if desired) mechanism. Various scenarios are envisaged and considered, these corresponding to different combinations of neutral particle source strengths and plasma parameters.

---

1) Permanent address: University of Michigan

2) In cooperation with the University of Michigan

SURFACE PHYSICS DIVISION

(Prof. Dr. Volker Dose)

The activities of the surface physics division fall into two main categories. Substantial activities take place in collaboration with the plasma machine groups and reports on this work are included in the respective project reports. This chapter deals therefore only with auxialiary laboratory research on plasma-wall interaction and basic surface science. A main objective of plasma-wall interaction is the impurity production by sputtering. Experiments on physical and chemical sputtering of graphite were combined and in particular new mechanisms of chemical sputtering e.g. CH_4 formation were further elucidated. Preferential sputtering and sputtering of segregating layers address the problem of material tailoring for first wall materials. Apart from wall erosion, hydrogen recycling from the wall is of major importance for the total particle balance. Calculations relating to this problems were continued and supplemented by new measurements on the energy distribution of reflected and sputtered particles. Further experiments address the problem of hydrogen trapping, permeation, and reemission. Surface analysis of machine samples has again been a substantial activity. The available analytical tools mainly based on high energy ion scattering have been supplemented to electron-induced x-ray emission and are presently extended to x-ray fluorescence and secondary ion mass spectroscopic depth profiling. Basic surface science projects, which where in the past mainly limited to low energy ion scattering for the analysis of surface structure and composition have been supplemented in 1986 by an inverse photoemission activity addressing the electronic structure of clean and adsorbate covered surfaces.

Surface Physics Division

Head: V. Dose; Deputy Head: E. Taglauer
W. Altmann[1], R. Aratari[2], A. Bähr[1],
B. Baretzky[1], R. Behrisch, E. Bertel,
J. Bohdansky, P. Børgesen[2], T. Brodbeck[2]
K. Desinger[1], M. Donath[1], R. Drube[1],
H. Dürr[1], W. Eckstein, J. Ehrenberg[3],
G. Engelmann, W. Englert, K. Ertl, Th. Fauster[2]
A. Goldmann[4], M. Hashmi, W. Jacob[1], U. Kolac[1],
H. Liebl, R. Margraf[1], A.P. Martinelli, N. Memmel,
W. Möller, W. Poschenrieder, J. Roth,
A. Santaniello[2], B. Senftinger[1], B. Söder[1],
B.M.U. Scherzer, R. Schneider[1], G. Staudenmaier,
G. Venus, H. Verbeek, W. Wang[5], J.-H. Wang[6],
M. Wielunski[7], G. van Wyk[8].

---

1) Doctoral candidate
2) Post Doc
3) Assigned to JET since June 1984
4) Guest, Universität Duisburg,
5) Guest, Institute of Nuclear Studies, Shanghai, P.R. of China
6) Guest from Tsinghua University, Peking, P.R. of China
7) Guest, Institute of Nuclear Studies, Warsaw, Poland
8) Guest, University of Orange Free State, South Africa

1. RECYCLING

The limited magnetic confinement of plasma particles in tokamak discharges leads to multiple exchange of hydrogen between the plasma and wall. The major wall processes concerned are reflection, trapping, permeation and re-emission which decisively govern the particle balance.

1.1 Particle Reflection

1.1.1 Reflection of heavy ions

Reflection of heavy ions (heavier than helium) was investigated with the TRSP1CN Monte Carlo program. The dependence of the particles and energy reflection coefficients on the incident energy and angle of incidence was determined. So, too, were the angular and energy distributions of the reflected atoms. The agreement with the few experimental data available is good; the same applies to the agreement with results of the analytical theory. Furthermore, it was shown that the reflection coefficients scale as the mass ratio (target mass to projectile mass) and the reduced energy ε, if $\varepsilon > 0.02$.
(W. Eckstein)

1.1.2 Energy dependence of reflected and sputtered atoms

For measurements of the energy distributions of reflected and sputtered atoms (and ions) a time-of-flight spectrometer was tested and improved. First energy spectra of reflected hydrogen atoms have been recorded with this spectrometer. For heavy atoms time-of-flight measurements can be made with the electrostatic energy spectrometer previously used. Keeping the pass energy of the spectrometer constant it is thus possible to determine the masses of the atoms passing through the spectrometer. This allows energy and mass-resolved distributions of reflected and sputtered atoms to be determined.
(R. Aratari, W. Eckstein)

1.2 Trapping, Permeation and Re-emission

1.2.1 Molecular diffusion of hydrogen implanted into graphite

High fluence implantations of keV hydrogen ions into graphite at temperatures below 800 K form a saturated hydrogen-rich surface layer with an atomic concentration of e.g. 0.4 H/C at around room temperature. In order to study the mechanisms of saturation and the corresponding re-emission of excess hydrogen atoms experiments were performed on saturated protium/deuterium bilayers in sintered graphite. Results obtained from both gas re-emission during bombardment and from thermal release, strongly suggest local recombination of hydrogen atoms in the damaged material and molecular outdiffusion to the surface. This model can also explain the energy dependence of chemical sputtering yields found during hydrogen bombardment of graphite (see Sect. 2.1.2).
(W. Möller, B.M.U. Scherzer, P. Børgesen)

1.2.2 Dynamic measurements of deuterium concentrations in nickel during ion bombardment

The experimental setup for simultaneous implantation and analysis of deuterium was combined with the equipment for elastic recoil detection (ERD) measurements at a scattering angle of 30°. Beam-limiting diaphragms of elliptical cross-sections ensure sufficient overlap of the implantation spot over the analyzing spot. ERD yields deuterium depth profiles at analyzing doses more than one order of magnitude smaller than those with nuclear reaction analysis. The problem of damage induced by the analyzing beam is thus significantly reduced. The depth profiles of D in Ni obtained by ERD extend far beyond the kinetic range of the implanted ions (Fig. 1) and cannot be explained by the common diffusion and trapping model.
(B.M.U. Scherzer, W. Möller, T. Brodbeck)

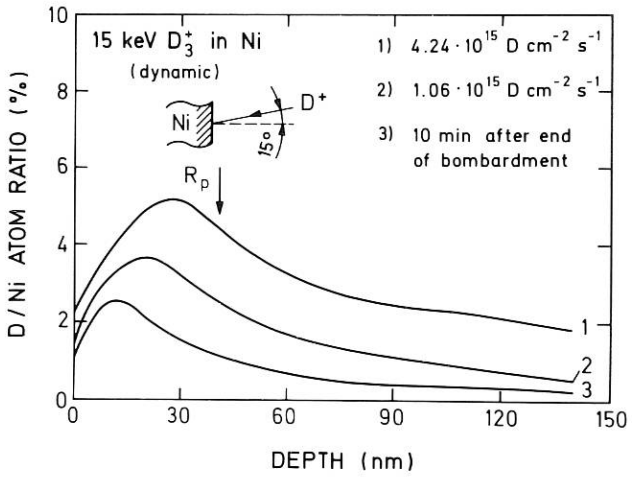

Fig. 1: Depth profiles of implanted D in Ni measured dynamically, i.e. during implantation, at two different fluxes and 10 min after bombardment is terminated. Rp is the mean range of the ions as obtained from the TRIM code. The scale of the D/Ni atom ratio is uncertain by a factor of 2.

2. IMPURITY PRODUCTION

Impurities are produced by non-confined energetic plasma particles. The most important processes leading to the emission of impurity atoms are sputtering and radiation-induced desorption. In the case of graphite the sputtering process is enhanced by chemical reactions (chemical sputtering) and radiation-enhanced sublimation.

2.1 Sputtering of Graphite

2.1.1 Sputtering of graphite by hydrogen ions

Chemical sputtering of graphite by hydrogen ions is a function of the ion energy and the graphite temperature. At elevated graphite temperatures ($\sim$550°C) chemical sputtering occurs in the whole ion energy range (20 eV - 6 keV) which was investigated in the experiment. At room temperature chemical sputtering is restricted to low ion energies ($\sim$ 200 eV) leading to a constant sputtering yield between 20 eV and 100 eV (see Fig. 2). In this energy regime the expected yield for physical sputtering (dashed-dotted line in Fig. 2) is significantly smaller. Methane production was observed in the range of elevated sputtering yield. (J. Roth, J. Bohdansky).

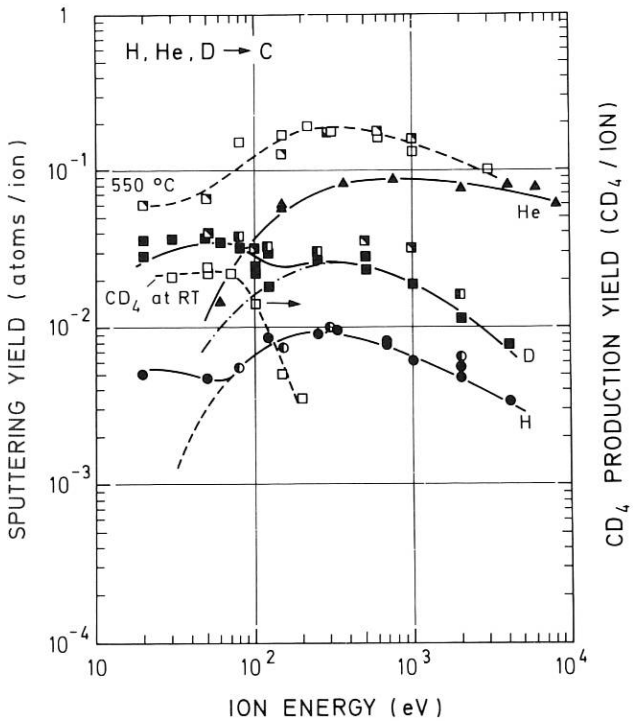

Fig. 2: Energy dependence of the total sputtering yield of graphite at room temperature. For deuterium, the energy dependence at 550° C and the CD_4 production yield at room temperature are also given,
● ▲ ■ pyrolytic graphite, c axis ∥ to surface normal,
◐ ◧ pyrolytic graphite, c axis ⊥ to surface normal,
◪ fine-grain isotropic graphite, EK 98.
□ CD_4 production yield.

2.1.2 Methane formation

In order to localize the origin of methane formation, graphite samples were prepared with a ^{13}C overlayer of about 200 Å. The samples kept at a temperature of 530°C were irradiated with D^+ ions of 50 eV and 1 keV. At the lower energy the ions cannot penetrate through the ^{13}C overlayer. At the higher energy the ions penetrate the ^{13}C layer and are stopped in the ^{12}C bulk material. During irradiation $^{12}CD_4$ and $^{13}CD_4$ were observed. At lower ion energy the $^{13}CD_4$ signal was dominant, whereas at high energy it was mainly $^{12}CD_4$ that was observed. It is concluded from this result that methane is formed in the bulk (implantation depth). The outdiffusion must occur in the molecular state, similar to the finding for recombined H_2 molecules (see Sect. 1.2.1).

2.2 Preferential Sputtering

2.2.1 Preferential sputtering of Ta_2O_5 by He^+ ions

The work on preferential sputtering was continued by measuring the surface composition of Ta_2O_5 subjected to 1.5 keV He^+ bombardment as a function of the angle of incidence by AES (Auger electron spectroscopy) and ISS (ion scattering spectroscopy) and simulating it with computations based on the TRIDYN binary collision code. The two measuring methods and the calculations show good agreement with respect to the steady-state surface composition, the characteristic fluence, and the depth profiles of the altered layer.

This confirms that the preferential sputtering at room temperature and in certain ranges of mass and energy is governed by collision processes rather than diffusive processes (e.g. segregation) or the surface binding energy. In addition, for the surface composition we found a quantitative relation containing only the assumption that the sputtering of a surface atom is independent of its chemical environment.
(B. Baretzky, W. Möller, E. Taglauer)

2.3 Sputtering of Segregated Layer

2.3.1 Sputtering of CuLi alloys

Li segregation at the surface of a CuLi alloy is considered as an effective low-Z protective layer and should reduce the Cu sputtering yield. Alloys with 4, 10 and 16 at % Li were bombarded with 100 eV and 1 keV D^+ ions and the Cu sputtering yield was measured by the catcher foil technique. Only in the case of 16 at % Li was a significant reduction of the Cu sputtering yield observed. This reduction occurred only in the temperature range between 450°C and 600°C. A repetition of the experiment six months later gave different results and it is presumed that the residual gas may influence the result.
(J. Bohdansky, J. Roth)

2.3.2 Ion-induced C segregation and sputtering of thin Fe layers

Iron films of different thicknesses evaporated on pyrolytic graphite were bombarded with deuterium ions in the temperature range from 300 K to 800 K. Both orientations of the pyrolytic graphite substrate were investigated at different ion energies and film thicknesses. The Fe sputtering yield was measured by means of laser-induced fluorescence (LIF) and the depth distribution of Fe and C on top of the graphite substrate was determined by Rutherford backscattering spectroscopy (RBS). The LIF results show that at room temperature the Fe sputtering yield corresponds to the yield of pure Fe. This yield can be drastically reduced in the temperature range between 700 and 800 K if the ions have a sufficiently high energy to reach the Fe-C interface. In situ RBS measurements show the segregation of C on top of the iron film for these conditions. The thickness of the C layer is strongly dependent on the orientation of the graphite substrate. The segregated C layer can exceed 1000 Å for a graphite substrate cut perpendicularly to the basal planes.
(A. Santaniello, J. Roth, J. Bohdansky)

3. SPECIAL ANALYSIS

Special analysis techniques are necessary in order to improve understanding of surface processes and the surface structure. Such techniques are of great help for analyzing processes occurring at the first wall of fusion devices during operation.

3.1 Ion Scattering

3.1.1 Surface structure

Ion scattering experiments with a large scattering angle of 164° are used to study the geometrical structure of solid surfaces. The relative position of neighbouring atoms can be determined by observing the angle of incidence where the atom disappears in its neighbour's shadow. The technique can be calibrated on known surfaces and can then be applied to unknown systems. A study of the sulphur adsorption on three different nickel single-crystal planes gives equal nearest-neighbour distances between sulphur and nickel atoms of 2.20 ± 0.05 Å. Sulphur is adsorbed into the hollow site in all cases studied. The data analysis is done by triangulation requiring only simple geometry.

The scattering of neon ions (1.5 - 4.0 keV) from metal surfaces (Cr, Fe, Ni and Cu) shows discrete energy losses and an increase of the scattered ion intensities above definite projectile energies. The observation of doubly charged scattered ions confirms the importance of ionization and excitation processes during the hard collision between the neon projectile and the target atom.
(Th. Fauster, H. Dürr, D. Hartwig, R. Schneider)

3.1.2 Adsorption of water on stainless steel

The adsorption of water on wall surfaces in fusion machines and its particle-induced release during a plasma discharge are considered to be relevant mechanisms for the appearance of oxygen impurities in the plasma. The adsorption of water on polycrystalline stainless steel was therefore investigated by low-energy (1 keV) ion scattering at varying sample temperatures between 140 K and 500 K. The H^+ recoil signal as well as the Ne^+ and He^+ scattering signals from Fe and O could be measured. Figure 3 shows the corresponding intensities for equilibrium adsorption. At temperatures below 180 K monolayer coverage was obtained after an exposure of 150 Langmuirs; additional exposure (1500 L) results in multilayer adsorption. Above 180 K complete coverage of the substrate was not observed. The increase of the O signal together with decreasing H^+ recoil intensity indicates dissociation of the H_2O molecule on the surface at elevated temperatures. Ion-induced desorption using 1 keV Ne^+ and He^+ was also studied.
(G. van Wyk, W. Englert, E. Taglauer)

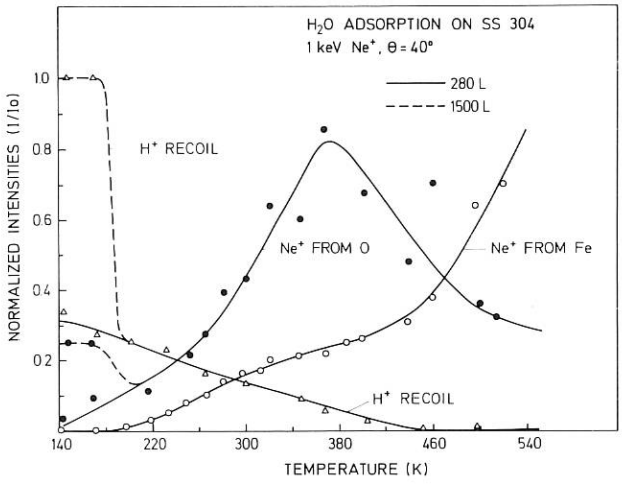

Fig. 3: Temperature dependence of the Ne^+ scattering signals from Fe and O and the H^+ recoil signal for two different H_2O exposures. For temperatures above 200 K both exposures yield identical results.

3.1.3 Catalysts

With the preparation of supported catalysts in mind, we investigated the distribution of catalyst material (MoO_3) on a substrate (Al_2O_3, TiO_2) by means of ion scattering. The catalysts were produced by thermally treating the appropriate mixture, e.g. MoO_3-Al_2O_3, for various lengths of time with and without the influence of water. In the first case with a calcination temperature of 720 K the ion scattering showed a maximum

distribution of the molybdate after approx. 10 h of treatment; in Raman spectroscopy complete development of the polymolybdate phase is found after approx. 30 h. This demonstrated that the spreading of the molybdenum is a different process to the formation of the polymolybdate phase.
(R. Margraf, E. Taglauer in cooperation with the University of Munich through H. Knözinger)

3.2 Inverse Photoemission

Inverse photoemission spectroscopy (IPE) is used to probe empty electronic states in solids and on clean and adsorbate-covered surfaces by analyzing the radiation emitted from the probe on bombardment with a well-defined low-energy electron beam. This radiation is due to transitions of electrons from an initial state above the vacuum level into an unoccupied state above the Fermi level (Fig. 4). Two different techniques are applied in our experiments:

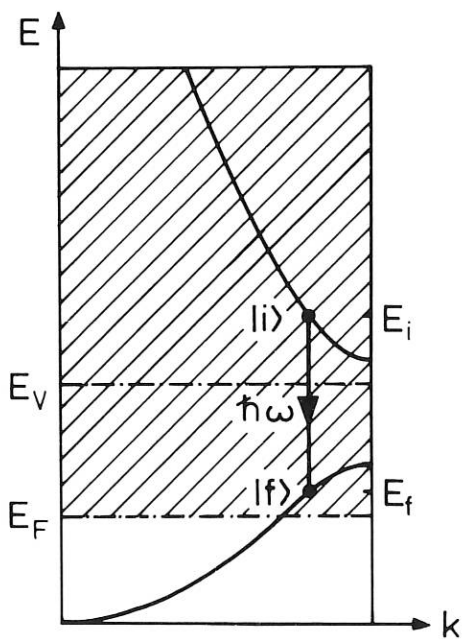

Fig. 4: Schematic of direct transition in inverse photoemission

The "isochromat" mode, i.e. recording of the emitted photon intensity at a fixed photon energy during a scan of the electron energy, offers simple design and excellent sensitivity.
IPE with tunable photon energy allow complete determination of the energy-momentum relation of the unoccupied electronic states.

3.2.1 Spin-dependent inverse photoemission

IPE with polarized electrons is a useful technique to differentiate between empty minority and majority bands of ferromagnetic materials. In 1986 two separately mounted and tested experimental arrangements, the polarized electron source (negative-electron-affinity GaAsP photoemitter) and the apparatus for the isochromat spectroscopy, were coupled via a high-transmission electron optics (Fig. 5).

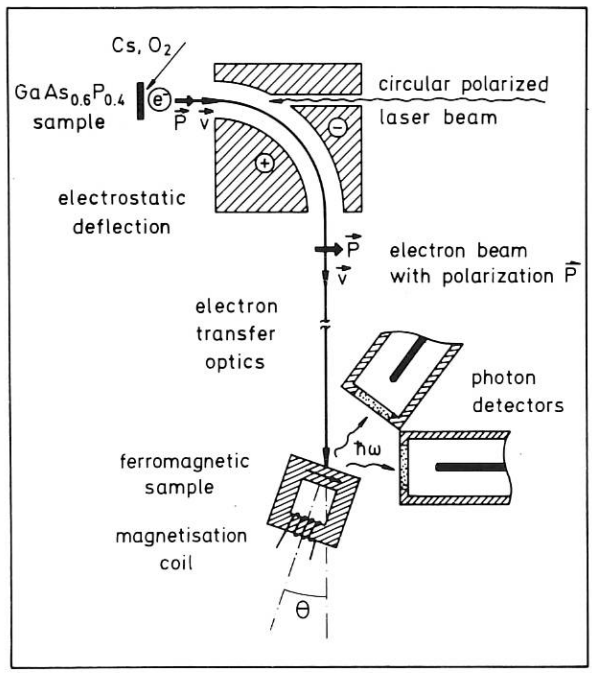

Fig. 5: Experimental arrangement for spin-dependent IPE

The arrangement with two Geiger-Müller counters placed at different angles to the probe permits photon polarization effects to be measured. This helps to identify surface states and allows the parity of bulk final states to be determined. First results on Ni(110) showing the spin polarization of the empty d-band could be obtained (Fig. 6).
(M. Donath, K. Ertl, U. Kolac)

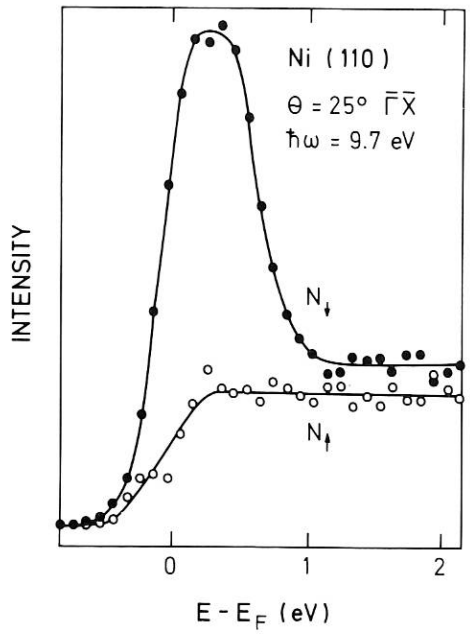

Fig. 6: Inverse photoemission data from Ni(110) showing the spin polarization of the empty d-band.

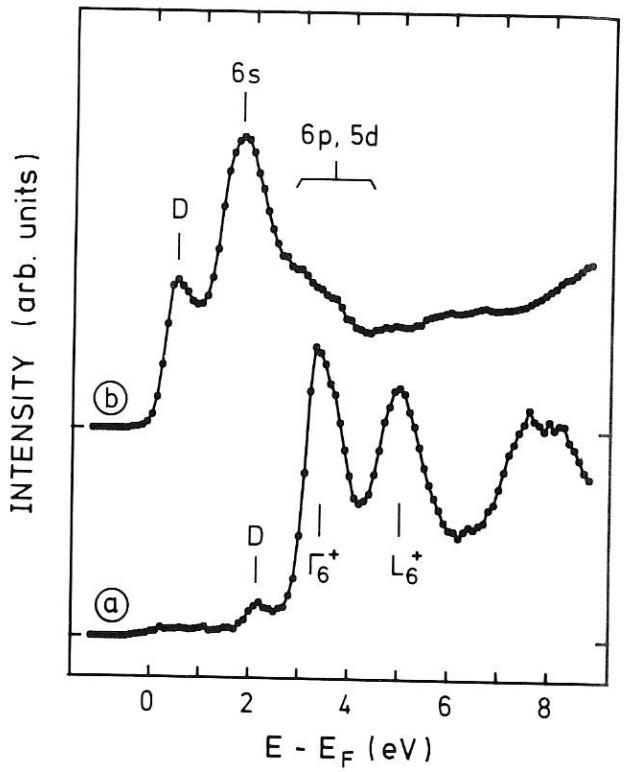

Fig. 7: Inverse photoemission spectra from Xe on Ag(110) (a) characteristic of wetting behaviour. Xe on Ag(110) + 2ML potassium (b): characteristic of non-wetting behaviour.

3.2.2 Isochromat spectroscopy on metals and adsorbates

Owing to the comparatively large spatial extent of unoccupied orbitals, IPE spectra are rather sensitive to structural changes in metal surfaces and adsorbate layers. Surface reconstruction of metal surfaces and phase transitions in adsorbate layers therefore promised to be a rewarding area for IPE studies. In 1986 first results could be obtained for the changes in empty electronic level structure which accompany the reconstruction of the Pt(100)-(1x1) to the Pt(100)-(5x20) surface. Similar experiments on the Au(100) surface are in progress. Studies on phase transitions in adsorbate layers, however, are more advanced. The unoccupied levels in ionic alkali layers have been identified in IPE for the first time. With the K/Ag(110) system it could be demonstrated how these levels drop in energy as the coverage is increased and finally induce the ionic to metallic overlayer transition by merging with the Fermi level. For adsorbed Xe films a wetting to non-wetting transition was dicovered on an Ag(110) surface predosed with potassium (Fig. 7). From the spectacular changes in the corresponding IPE spectra it is possible to derive important information about this kind of phase transition.
(E. Bertel, R. Drube, W. Jacob, N. Memmel)

3.2.3 Inverse photoemission with tunable photon energy

A spectrometer for inverse photoemission with an UV monochromator was tested and calibrated.
(W. Altmann, K. Desinger, T. Fauster)

3.3 ^{13}C-Marker Technique

For erosion and deposition measurements on graphite structures in plasma experiments surfaces are frequently implanted with ^{13}C markers (10 keV to 1.4 MeV) and the marker shift and broadening is measured using ion beam techniques and SIMS. For the interpretation of these data the selfdiffusion of carbon has to be investigated.

3.3.1 Influence of the structure of graphite on radiation-induced selfdiffusion

Due to irradiation damage at ion bombardment the selfdiffusion of carbon atoms in the graphite lattice can be enhanced. To examine the influence of the graphite structure, different graphites - amorphous carbon, sintered isotropic graphite, and pyrolytic graphite cut parallel and perpendicular to the lattice planes - were implanted with a ^{13}C marker. The broadening and shift of this marker has been examined for different fluences of 20 keV D^+ bombardment at temperatures between room

temperature and 1500 K. From the different behaviour of different orientations of pyrolytic graphite it can be concluded that the broadening of the marker profile is due to the production of interstitials and vacancies during irradiation. Interstitials diffuse rapidly parallel to the lattice planes already at room temperature until they recombine with immobile vacancies. For amorphous carbon the marker broadening is drastically reduced compared to graphites. (B. Söder, J. Roth, W. Möller).

3.4 Other Methods

3.4.1 COALA apparatus for SIMS

In order to analyze samples not only by Cs^+ bombardment and mass spectrometry of the negative secondary ions, but also by Ar^+ or D_2^+ bombardment and mass spectrometry of the positive secondary ions, the apparatus is being modified so that the two modes can be alternatively applied without mechanical changes. In addition, the primary beam intensity will be increased at the expense of lateral resolution to improve the signal-to-noise ratio and the speed of erosion in depth analyses. Several elements will be measured quasi-simultaneously by programming the mass spectrometer. (H. Liebl)

3.4.2 Surface analysis by electron-induced X-rays (EIX)

The topography and composition of surfaces are being routinely analyzed in a scanning electron microscope. The investigations are focussed on graphite samples originating from the ASDEX and JET tokamak experiments. Metal deposits on the carbon surfaces are frequently not homogenous layers but droplets with diameters in the range of micrometers. Knowledge of the droplet size is of importance for a quantitative understanding of the amount of the metal deposit measured by other methods, e.g. Rutherford backscattering.

Quantiative analyses by EIX are being performed in a separate experiment. The detection limit of metals on carbon is about 10^{-2} monolayers. Such high sensitivities are required for erosion experiments performed at the wall of the ASDEX tokamak since the erosion rates are of the order of 10^{-3} monolayers per second.

Recently, we performed first experiments using X-ray fluorescent analysis (XRF) in order to investigate larger graphite tiles without cutting them into pieces. An additional advantage of XRF is that the analysis is performed in air or in a helium atmosphere.
(G. Staudenmaier)

COMPUTER SCIENCE DIVISION

(Prof.Dr.Friedrich Hertweck)

The main activities are at present the design and implementation of the AMOS/D Data Acquisition System for ASDEX Upgrade. It will be a "distributed system" of autonomous diagnostic computers, a large central computer, and a powerful communications subsystem connecting the diagnostic computers to the central system. A preliminary version of the system has been demonstrated on ASDEX.

(F. Hertweck, H. Fisser, H. Friedrich, K.-H. Goihl, A. Hackl, P. Heimann, J. Maier, I. Precht, H. Richter,[1] U. Schneider, D. Stolz, R. Tisma, R. Wang, M. Zilker)

The new concept for data acquisition and analysis for ASDEX Upgrade was already presented in earlier reports.
Two diagnostics were demonstrated on the ASDEX experiment.

1. The Central System (CDAS)

The IBM 4381 was commissioned during the first quarter so that it was available for the demonstration of two diagnostics on ASDEX (see sect. 2 below). The AMOS/2 system was enhanced to include the full capability to run FORTRAN jobs (computing, loading, executing). The IBM I/O interface was replaced by our own design whichs shows superior robustness against user input errors. The normal OS/360 SVCs used by a typical user job were emulated by the corresponding AMOS/2 supervisor functions. Thus it is possible to execute load modules obtained from elsewhere. The diagnostic programs were capable of fully utilizing the novel virtual I/O feature of AMOS/2. The plot output of the diagnostics was transmitted as a metafile via the standard message links of our communications network to the AD work stations.

2. The Autonomous Subsystems (AD)

While the ASDEX experiment was still in operation two diagnostics have been demonstrated (ECE and THOMSON). Both used a Qbus Computer with UNIX. For the THOMSON diagnostic a standard colour graphics display was used, for the ECE diagnostic a fast monochrome bit-map display. Because of its speed and high resolution (1280 x 1024 pixels) the bit-map display seems preferable. Both computers were coupled via fiber glass lines to a node at the experimental site. From there, data was transmitted with a rate of 100 KByte/sec to a node near the CDAS machine. A 40 KByte/sec prototype of the IBM channel interface (developed by the computing centre) was used to transmit the data into the CDAS system where the diagnostic programs were run. In this setup, the local AD computers were in fact work stations of the CDAS system. It was also shown that the diagnostics could run off-line on the AD computers alone.

3. The Communications Subsystem

The HSCC (high speed communications

[1] Doctoral candidate

controller) was available in two copies so that a transmission line between two nodes could be implemented and tested. The transmission speed for file transfers was shown to be 1.1 MByte/sec thus utilizing about 90 % of the bandwidth. The design of the IBM channel interface was completed by the Computer Centre; two prototype versions were available towards the end of the year which could transmit well over 1 MByte/sec data (using the AMOS/2 software).

4. Parallel Processing

A study was made to investigate the possibilities of using multiprocessor systems for the fast analysis of experimental data. The prototype of such a system built with four Transputer T414 microprocessors and incorporating a reconfigurable interconnection network was successfully demonstrated. It is expected that such a (low-cost) system will permit large amounts of data to be analysed in a very short time.

TECHNOLOGY DIVISION

ACTING DIVISION HEAD: Dr. Karl Lackner

The main objective of the technology division is to provide heating for the stellarator and tokamak programme of the IPP. The efforts are concentrated on the design, development, construction, operation of, and participation in heating experiments in the field of neutral beam heating, ion cyclotron heating and lower hybrid heating and current drive. As in the preceeding years the main results referring to the individual experiments W VII-AS, ASDEX and ASDEX Upgrade are being reported there. Within the specific tasks for the different experiments a considerable amount of basic development and general studies had to be performed. For neutral injection this included the development of long-pulse beamlines for W VII-AS and ASDEX. The testing of the prototype beamline was continued and was completed successfully. For ICRH distinct advances in the development of antennas, of transmission elements, and the theory of Alfvén wave heating have been reached. In the field of lower hybrid current drive a new project (2.45 GHz, 3 MW) was established in collaboration with ENEA-Frascati and PPPL-Princeton, aiming at the modification of the current density profile in ASDEX in order to improve confinement and stability.

1. LOWER HYBRID CURRENT DRIVE

Group leader: F. Leuterer

D. Eckhartt, M. Münich, M. Zouhar

Field: Plasma wave interactions in the lower hybrid frequency range

Objectives: Lower hybrid heating and/or current drive on ASDEX

See also ASDEX project.

The lower hybrid experiments at a frequency of 1.3 GHz were terminated in April 1986, coinciding with the shutdown of ASDEX for hardening. Experimental results can be found in the report of the ASDEX project (Sect. 1.7).

The 1.3 GHz system has meanwhile been dismantled to prepare the site for construction of a 2.45 GHz lower hybrid system for current profile modification in a density range up to 4×10^{13} cm^{-3}, which was not accessible with the 1.3 GHz system (see ASDEX project, Sect. 5).

The new system will be built in collaboration with ENEA-Frascati. The transmitter, 2.45 GHz/3 MW 1 s, will consist of 6 klystron amplifiers with an output power of 500 kW each. Three of these klystrons were previously in use at the FT tokamak in Frascati; the other three will be available on loan from PPPL-Princeton until April 1989. A block diagram of the system is shown in Fig. 1. Each group of 3 klystrons will be fed by one high-voltage power supply (0 - 70 kV/50 A) and will be protected by a fast crowbar system in case of arcing in a tube. Nevertheless, high voltage switches allow independent selection of each klystron for operation or grounding. The auxiliary power supplies and control units of the previous 1.3 GHz transmitter will be modified and adjusted for use in the new 2.45 GHz transmitter.

The six klystrons will be driven from one frequency-stabilized master oscillator. A pin diode switch between the oscillator and the low-power divider provides protection in the event of RF arcs or excessive reflection. Phase and amplitude feedback loops will allow the output of each klystron to be electronically controlled in the range of 360° and 20 dB, respectively. On the high-power side each klystron is connected to a four-port differential phase shift circulator providing good matching for the klystron. Six WR 430 transmission lines then lead to the ASDEX device.

The experimental programme to be performed is described in the ASDEX report (Section 5). This requires an antenna which allows the $N_{\parallel}$ spectrum

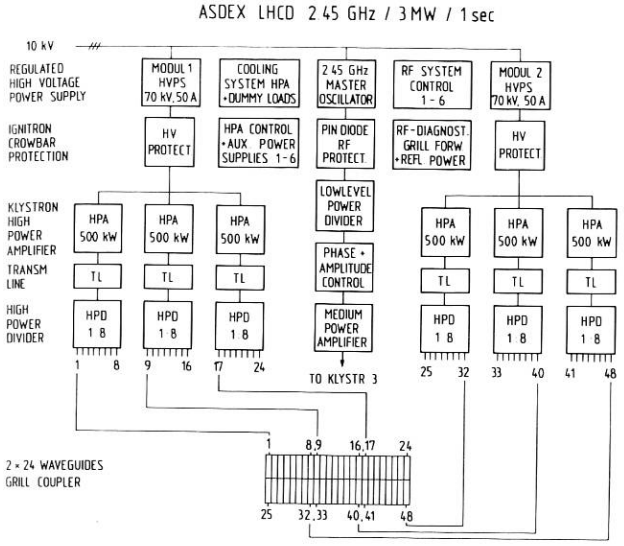

Fig. 1: Block diagram of the 2.45 GHz/3 MW/1 s lower hybrid transmitter for ASDEX.

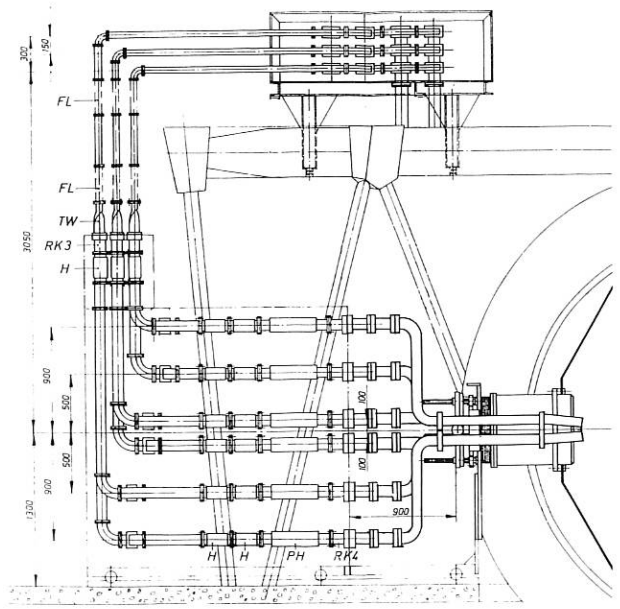

Fig. 2: Sketch of the 2.45 GHz grill and power splitter system.

of the lower hybrid waves to be varied over a wide range, both with respect to the average phase velocity of the waves and to the shape of the power spectrum. In addition, safe operation requires that an average power density of 4.5 kW/cm² at the antenna (as reached in the FT and PLT tokamaks) should not be exceeded. This led to the design of a grill antenna consisting of 2 x 24 waveguides with inner dimensions of 10 x 109 mm and with a wall thickness of 4 mm. The front end is made of stainless steel and is to be chemically coated with the antimultipactor coating already used for the 1.3 GHz experiments. Immediately behind the front end, two 24-waveguide front window sections (Princeton design) will be installed so that the ω_{ce} transition occurs in the narrow waveguides at atmospheric pressure. The 2 x 24 narrow waveguides made of copper tubes lead out of the ASDEX vacuum chamber to the outside of the main support structure of ASDEX. A fanning structure of narrow waveguides and step transformers then provide 48 standard-size WR 430 inputs for the grill. A high-power divider system constructed of a sequence of 3 dB E-plane hybrids allows the output power of the six transmission lines to be distributed to six groups of 8 waveguides of the grill (Fig. 2). Adjustable mechanical phase shifters at the outputs of the power divider provide high flexibility in the wave spectrum. The total loss between the klystrons and grill is estimated to be 0.93 dB.

The laboratories involved will contribute to the construction of this system as follows:

ENEA:	2 x 24 waveguide grill transmission line components vacuum windows (to be constructed at PPPL) three complete klystrons amplifier
PPPL:	three klystrons with magnets construction of front windows
IPP:	transmitter assembly power supplies, cooling low-power systems high-power splitter system circulators system assembly data acquisition.

Full-power operation is planned to begin in autumn 1988.

2. ION CYCLOTRON RESONANCE HEATING

Group leader: F. Wesner
Deputy: F. Hofmeister

J. Bäumler, W. Becker, F. Braun, R. Fritsch, E. van Mark, J.-M. Noterdaeme, S. Puri, M. Söll[1], K. Steinmetz, H. Wedler

Field: Plasma-wave interaction in the ion gyroresonance frequency range

Objectives: Ion cyclotron frequency heating in ASDEX, ASDEX Upgrade, and WENDELSTEIN VII-AS

See also ASDEX, ASDEX Upgrade and W VII-AS project

Ion cyclotron resonance heating is applied to the ASDEX tokamak and is being prepared for application to the W VII-AS and ASDEX Upgrade experiments. Besides the special efforts made for the experiments, the results of which are reported in the sections on these projects, some general work has been done in the field of antenna development, matching and further development of RF components for ICRH, and on the theory of Alfvén wave heating.

1) Until 28.2.1986

2.1 ICRH Antenna Development (J.-M. Noterdaeme)

The first cooled Faraday screen developed for the ASDEX long-pulse heating has been completed and tested [1]. It is optically closed (the design decision had to be made before the experimental results of open antennae were available) and has chevron-shaped stainless-steel tubes vacuum-brazed in the header and collector. The tubes are copper-plated and coated with titanium carbide by chemical vapour deposition before brazing.

Finite-element calculations gave as maximum stress due to plasma disruption and thermal loading 128 N/mm², about 20 % below the yield strength. The loading was simulated on a test piece for 10,000 cycles without its vacuum tightness being impaired. Thermal load tests were made at Oak Ridge National Laboratory (USA). Unconstrained rods were able to withstand a thermal load of 1000 W/cm² for 700 cycles (water velocity 1.6 m/s), constrained rods withstood 10,000 cycles at the design value of 100 W/cm² and 1 m/s without damage.

The uncooled antennae were analysed after their removal from ASDEX. Surface investigations of Faraday screen rods and pieces of the protecting limiters (see ASDEX, Sect.1.8.4) showed that the surface of the screen elements facing the plasma is not predominantly coated with wall material. These results, together with the JET observation that part of the impurities comes from the antenna surface, underline the importance of the titanium carbide coating. Surface analysis of the interior of an open antenna shows that it is not much affected by the plasma discharges as also found experimentally [2].

2.2 Matching Proposal for Ease of Control (F. Hofmeister)

Calculations show that it is possible with a proper choice of ICRH power coupling network to rely fully on frequency control alone for matching the plasma-dependent antenna resistance. In feeder line configurations, where the relative phase is of no concern, a matching network may be optimized such that a relatively small frequency variation leads to a large change in the real part of the network's output impedance.

A technically feasible matching network was proposed which covers an antenna resistance range of 1:10 with a frequency variation of 1 % and matches to the generator output with a VSWR within 1.5. A major advantage of such a matching method would be the possible speed and ease of control.

These matching considerations should be taken into account for future devices no longer devoted to heating investigations.
For flexible systems with large frequency ranges and different antenna parts fed by one generator, a conventional double-stub tuner system remains a good choice.

[1] J.-M. Noterdaeme, SOFT 86
[2] J.-M. Noterdaeme, EPS Schliersee 1986

2.3 Development of High-power RF Components (H. Wedler)

The voltage strength of coaxial lines is one of the high power limitations of an ICRF heating system. In ASDEX 35 kV and 17 kV peaks were the limits of safe operation for pressurized and vacuum insulated lines respectively, due to breakdown at the ceramic insulators. The development work at the ICRH test bed [1] now led to modifications of all coaxial line elements for areas with large VSWR.

2.3.1 Pressurized lines

Figure 3 shows the modification of the insulator geometry in pressurized lines. At high voltage tests with a pulse length of 100 ms no breakdown occured below 90 kV peak indicating a safe operating range up to about 70 kV. High power tests showed that the resistance against heat shocks due to RF losses at long (10 s) pulses is improved, too. All insulators of the 9" pressurized coaxial lines at ASDEX and W VII-AS are replaced by parts with this geometry, the first vacuum feedthrough included.

2.3.2 Vacuum feeding lines

Owing to the geometrical constraints in ASDEX the antenna vacuum feeder line is limited to a diameter of 6 1/8" and has a complicated geometry. The following insulator and feedthrough elements, which were developed for an improved electrical strength, are now used in the ASDEX and W VII-AS feeding lines:

- First vacuum feedthrough: The previous double T-insulator is to be replaced by a T-insulator with Helicoflex sealing.
- Second vacuum feedthrough: The previous TFR feedthrough is to be replaced by a disc feedthrough with Helicoflex sealing.
- The previous three-rod insulator is to be replaced by a disc insulator with slotted holes.
- The antenna insulator will be replaced by a disc insulator similar to the disc feedthrough and elastically supported with Helicoflex rings.

All these components are based on a uniform design concept and were tested on the test bed with peak voltages of up to 34 kV and peak currents of 1360 A at pulse lengths of 10 s.

Al_2O_3 insulators can break at 10 s high-voltage pulses due to dielectric losses if not properly shaped. So finite-element calculations of the electric field, temperature and mechanical stress distributions have been started in order to optimize the insulator design.

The testbed investigations also included surface coating, heating and pumping methods for minimizing the gas release from the line walls due to temperature and multipactor effects, which is the reason for glow and arc discharges.

[1] H. Wedler, 14 SOFT, Avignon 1986

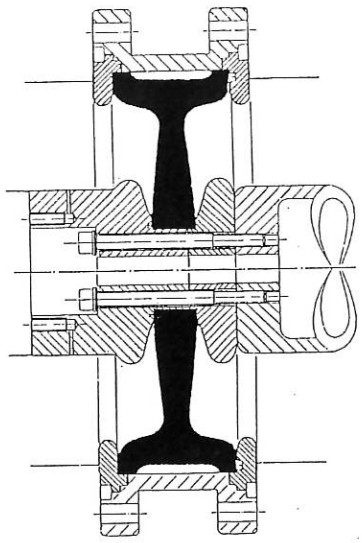

Fig. 3 : New T-insulator with 70 kV breakdown threshold for the ASDEX and W VII-AS a"-50 Ω pressurized transmission-line.

2.4 Role of Plasma Equilibrium Current in Alfvén Wave Antenna Optimization
(S. Puri)

The modifications in the antenna loading produced by the plasma equilibrium current, the Faraday shield, and the finite electron temperature for coupling to the Alfvén waves are studied with a self-consistent, three-dimensional, fully analytic periodic-loop-antenna model. The only significant changes are found to occur as a result of the plasma current and consist of an improved coupling (by a factor of about 2.5) at low toroidal wave-numbers (n = 1 - 3). Despite this gain, however, the coupling to low n continues to be poor with an antenna radiation resistance R = 0.03 Ω and a quality factor of Q = 180 for n = 2. Optimum coupling with R = 0.71 Ω and Q = 16.8 occurs for n = 8, as was also the case in the absence of the plasma current. For the large n values, mode splitting due to the removal of the poloidal degeneracy combined with the finite electron temperature effects lead to significant broadening of the energy absorption profile. Direct antenna coupling to the surface shear wave is small and no special provision, such as Faraday shielding, may be needed for preventing surface losses. The introduction of the Faraday screen, in fact, increases the coupling to the surface shear wave, possibly by acting as an impedance matching transformer between the antenna and the plasma. The finite electron temperature causes the predictable increase in the absorption width without influencing the antenna coupling. Thus the recommendations for antenna design for optimum coupling to the Alfvén wave remain unaffected by the inclusion of the plasma current. Efficient coupling with capabilities for dynamic impedance tracking through purely electronic means may be obtained using a dense-cluster-array antenna with a toroidal configuration of n about 8.

3. NEUTRAL INJECTION HEATING

Group leader: E. Speth
Deputy: W. Ott

J.H. Feist, K. Freudenberger, S. Götz, J. Kolos, R.C. Kunze, H. Lohnert, W. Melkus[1], F.P. Penningsfeld, H. Riedler[2], J. Sielanko[3], A. Stäbler, O. Vollmer, K. Wittenbecher

Field: Plasma neutral beam interaction
Objectives: Neutral injection heating on Wendelstein VII-A, VII-AS, ASDEX and ASDEX Upgrade

See also W VII-A, W VII-AS, ASDEX and ASDEX Upgrade projects.

3.1 Preparation for long-pulse neutral injection (LPNI)

The main activities in 1986 were:
- conditioning of two sources for ASDEX and of one for W VII-AS,
- performance tests with the testbed beam line,
- assembly of two injectors for ASDEX and of one for W VII-AS.

Long-pulse sources
A W VII-AS source, after being modified for Viton ring sealing, was brought up to the full parameters of 45 kV, 24 A. No change in the source behaviour, compared with the original all-metal sealed ones, was observed. Titanium evaporation in the source was also tried showing the known effect of impurity reduction in the beam. Two water-cooled grid sets for ASDEX were also conditioned up to 55 kV, 23 A.

Beam line performance
Various tests of the different beam line components, especially of the ion removal system and the actively cooled calorimeter, have shown their design to be adequate for a full-power beam. The extrapolation of neutral beam power measurements in the newly installed target tank for one source at 50 kV to the design value of 55 kV and eight sources ends up with approx. 3.2 MW. Further improvement is expected by gas flow optimization and better beam quality than at present available.

Beam line assembly
In April the two beam lines from ASDEX were brought into the assembly hall for the necessary modifications. The first beam line was put back to ASDEX in August, the second in October. The first new beam line for W VII-AS is nearly complete.

1) ZTE
2) Fellow of the Friedrich-Schiedel-Stiftung
3) Visiting scientist of the University of Lublin-Poland

3.2 First test of a RF source

For ASDEX Upgrade it is envisaged to use a RF ion source plasma generator instead of the traditional arc ion source. For a first test with this type of source with full beam extraction, a 20 cm-source (RIG 20) was mounted on a standard water-cooled extraction system. After several optimization steps, especially with the geometry of the RF coil, a beam of approx. 17 A at 42 kV was extracted for several seconds. The RF power was approx. 20 kW. The source operation was found to be rather reliable. The main problem occured with the Al_2O_3 coating of the backplate, which was severely melted by the backstreaming electrons. Further tests with this system with a number of modifications are planned for 1987. This is done in close cooperation with the University of Giessen.

Publications, Conference Reports, Author Index

PART C: PUBLICATIONS AND CONFERENCE REPORTS

1 Altmann, W., V.Dose and A.Goldmann[1]: Momentum-resolved bremsstrahlung isochromat spectroscopy of silver surfaces. Z. Phys. B - Condensed Matter 65, 171-180 (1986).

2 Amenda, W. and R.S.Lang: Centrifugal pellet injector with direct solid-deuterium feed. J.Phys.E.: Sci.Instrum. 19, 970-975 (1986).

3 Baretzky, B. und E.Taglauer: Preferential sputtering of tantalum oxide: Reemission of helium and transient effects in the altered layer. In: Erosion and Growth of Solids Stimulated by Atom and Ion Beams. Eds. G.Kiriakidis, G.Carter, J.L.Whitton, Martinus Nijhoff Publishers, Dordrecht, NATO ASI Series E: Appl. Sciences 112, 1986, 146-150.

4 Barth, H.J., E.Mühling and W.Eckstein: Formation of different charge states and the charge state fractions of sputtered Ti and Ni. Surf. Sci. 166, 458-479 (1986).

5 Bartiromo, R.[1], M.Hesse[1], F.X.Söldner, R.Burhenn[1], G.Fussmann, F.Leuterer, H.Murmann, ASDEX-Team[2] and LH-Group[9]: Experimental study of non-thermal electron generation by lower-hybrid waves in the ASDEX tokamak. Nucl. Fus. 26, 1106-1111 (1986).

6 Bartiromo, R.[1], M.Hesse[1], F.X.Söldner, R.Burhenn[1], G.Fussmann, F.Leuterer, H.Murmann, D.Eckhartt, A.Eberhagen, A.Giuliana[1], G.Becker, H.S.Bosch, M.Brambilla, H.Brocken, H.Derfler, O.Gehre, J.Gernhardt, G.v.Gierke, E.Glock, O.Gruber, G.Haas, J.Hofmann, A.Izvozchikov[1], G.Janeschitz, F.Karger, M.Keilhacker , O.Klüber, M.Kornherr, M.Lenoci, G.Lisitano, F.Mast, H.M.Mayer, K.McCormick, D.Meisel, V.Mertens, E.R.Müller, M.Münich, H.Niedermeyer, A.Pietrzyk[1], W.Poschenrieder, H.Rapp, H.Röhr, N.Ruhs, F.Ryter[1], T.Vien, F.Wagner, F.v.Woyna, D.Zasche and M.Zouhar: Measurements of non-thermal electron population during lower-hybrid heating in ASDEX. In: Proc. 13th Europ. Conf. on Contr.Fusion and Plasma Heating, Eds. G. Briffod, M. Kaufmann, EPS, Schliersee 1986, 10 C, Part II, 335-338.

7 Battiston, L.[1] and ASDEX-Team[2]: Dimensionality of fluctuations in ASDEX. In: Proc. 13th Europ. Conf. on Contr. Fus. and Plasma Heating, Eds. G.Briffod, M.Kaufmann, EPS, Schliersee 1986, 10C, Part I, 81-84.

8 Becker, G.: Critical parameters for the L and H confinement in neutral-beam-heated tokamaks. Proc. Course and Workshop on Basic Physical Processes of Toroidal Fusion Plasmas, Int. School of Plasma Physics, Varenna 1985, I, 217-223.

9 Becker, G.: Key parameters for the confinement of neutral-beam-heated tokamaks. Nucl. Fus. 26, 415-424 (1986).

10 Becker, G.: Local transport in tokamaks with ohmic and injection heating. In: Proc. 13th Europ. Conf. on Contr. Fusion and Plasma Heating, Eds. G. Briffod, M. Kaufmann, EPS, Schliersee 1986, 10 C, Part I, 224-227.

11 Behringer, K.[1], A.Edwards[1], H.U.Fahrbach, R.D.Gill[1], R.Granetz[1], N.Gottardi[1], H.Jaeckel, G.Mayar[1], E.R.Müller, A.Weller and D.Zasche: Radiation behaviour during additional heating of JET plasmas. In: Proc. 13th Europ. Conf. on Contr. Fus. and Plasma Heating, Eds. G.Briffod, M.Kaufmann, EPS, Schliersee 1986, 10C, Part I, 180-183.

12 Behrisch, R. and D.R.Harries: Lifetime predictions for the first wall and blanket structure of fusion reactors. Nucl. Fus. 26, 5, 685-687 (1986).

13 Behrisch, R.: Mechanisms of wall erosion in fusion devices. In: Proc. Techn. Comm. Meeting of Lifetime Predictions for the First Wall and Blanket Structure of Fusion Reactors, Karlsruhe 1985, IAEA-TEDOC-393, 1986, 221-231.

14 Biskamp, D.:
Magnetic reconnection via current sheets. Phys.Fluids 29, 1520-1531 (1986).

15 Biskamp, D.:
Natural current profiles in tokamaks. Comments Plasma Phys.Contr.Fus. 10, 165-172 (1986).

16 Børgesen, P., B.M.U.Scherzer and W.Möller:
Surface recombination of deuterium implanted into SS304. Nucl. Instr. & Meth. in Phys. Res. B15, 540-545 (1986).

17 Bosch, H.S., U.Schumacher, G.Becker, H.Brocken, A.Eberhagen, D.Eckhartt, G.Fussmann, O.Gehre, J.Gernhardt, G.v.Gierke, E.Glock, O.Gruber, G.Haas, J.Hofmann, A.Izvozchikov[1)], G.Janeschitz, F.Karger, M.Keilhacker, O.Klüber, M.Kornherr, K.Lackner, M.Lenoci[1)], F.Leuterer, G.Lisitano, F.Mast, H.M.Mayer, K.McCormick, D.Meisel, V.Mertens, E.R.Müller, H.Murmann, H.Niedermeyer, J.N.Noterdaeme, A.Pietrzyk[1)], W.Poschenrieder, H.Rapp, H.Riedler, H.Röhr, J.Roth, R.Ryter[1)], E.Speth, F.Schneider, C.Setzensack, G.Siller, P.Smeulders[1)], F.X.Söldner, K.Steinmetz, K.Steuer, O.Vollmer, F.Wagner, F.Wesner and D.Zasche:
Measurements of charged fusion products in ASDEX. In: Proc. 13th Europ. Conf. on Contr. Fusion and Plasma Heating, Eds. G. Briffod, M. Kaufmann, EPS, Schliersee 1986, 10 C, Part I, 124-127.

18 Braams, B.J., W.Jilge and K.Lackner:
Fast interpretation of magnetic measurements using function parametrization. Nuclear Fus. 26, 699-708 (1986).

19 Brambilla, M. and T.Krücken:
1-d model for propagation and adsorption of HF waves near ion cyclotron resonances in tokamak plasmas. In: Proc. 13th Europ. Conf. on Contr. Fus. and Plasma Heating, Eds. G.Briffod, M.Kaufmann, EPS, Schliersee 1986, 10C, Part II, 89-92.

20 Brambilla, M.:
Ray tracing of lower hybrid and ion cyclotron waves. Comp. Phys. Rep. 4, 71-93 (1986).

21 Chodura, R.:
Particle simulation of the plasma-wall transition. In: Proc. 8th Europhys. Conf. on Comp. Phys., Ed. J.Nührenberg, EPS, Eibsee 1986, 10D, 97-100.

22 Chodura, R.:
Plasma flow in a collisional presheath region. In: Proc. 13th Europ. Conf. on Contr. Fus. and Plasma Phys., Heating, G.Briffod, M.Kaufmann, EPS, Schliersee 1986, 10C, Part I, 411-414.

23 Correa-Restrepo, D., D.Pfirsch and H.K.Sommel:
Combined Maxwell and kinetic guiding-center theory with polarization drift: Regularized variational formulation with local charge and energy conservation. Physica 135A, 453-474 (1986).

24 Correa-Restrepo, D.:
Stability properties of localized resistive modes in a circular tokamak. In: INTOR-Phase IIA, 3rd Part, Critical Issues-European Contrib. to INTOR-Phase IIA Workshop, 13th Session, Physics (Groups B, C and G), EURFUBRU/XII-52/86/EDV10.

25 Croci, R. and E.Canobbio:
Nonlinear concept for lower hybrid wave absorption: model and comparison with experiments. In: Proc. IAEA INTOR-related Specialist's Meeting on Non Inductive Current Drive, Garching, 1986, NET-PM-86-003, 381-388.

26 Dommaschk, W.:
Representations for vacuum potentials in stellarators. Comp. Phys. Comm. 40, 203-218 (1986).

27 Donath, M., M.Glöbl[1)] and B.Senftinger:
Photon polarization effects in inverse photoemission from Cu(001). Solid State Communications 60, 3, 237-240 (1986).

28 Dose, V., R.Drube and A.Härtl:
Empty electronic states in solid and liquid nickel. Solid State Commun. 57, 4, 273-275 (1986).

29 Dose, V., T.Fauster and R.Schneider:
Improved resolution in VUV isochromat spectroscopy. Appl. Phys. A 40, 203-207 (1986).

30 Duesing, G. and JET-Team (from IPP: J.Ehrenberg, H.Jäckel, S.Kissel, U.Küphnapfel, R.Müller, A.Stäbler and A.Weller):
First results from neutral beam heating on JET. Plasma Phys. Contr. Fus. 28, 1429 (1986).

31 Eckstein, W. and J.P.Biersack[1)]:
Reflection of heavy ions. Z. Phys. B - Condensed Matter 63, 471-478 (1986).

32 Eckstein, W. and J.P.Biersack[1)]:
Self-sputtering and reflection. Z. Phys. B - Condensed Matter 63, 109-120 (1986).

33 Eckstein, W., H.J.Barth and E.Mühling:
Charge state fractions of Ni sputtered by Ne and Ne reflected from Ni. Nucl. Instr. & Meth. in Phys. Res. B14, 507-514 (1986).

34 Edwards, A.W.[1)], D.J.Campbell[1)], W.Engelhardt, H.U.Fahrbach, R.D.Gill[1)], R.S.Granetz[1)], S.Tsuji[1)], B.J.D.Tubbing[1)], A.Weller, J.Wesson[1)] and D.Zasche:
Rapid collapse of a plasma sawtooth oscillation in the JET tokamak. Phys.Rev.Lett. 57 (2), 210-213 (1986).

35 Edwards, A.W.[1)], H.U.Fahrbach, R.D.Gill[1)], R.S.Granetz[1)], E.Oord[1)], G.Schramm, S.Tsuji[1)], A.Weller and D.Zasche:

JET Soft X-Ray Diode array Diagnostic. Rev.Sci.Instrum. 57 (8), 2142-2144, (1986).

36 Ehrenberg, J., G.M.McCracken, R.Behrisch, P.E.Stott, J.P.Coad and L.de Kock[1]: Erosion and redeposition of metals and carbon on the JET limiters. In: Proc. 13th Europ. Conf. on Contr. Fusion and Plasma Heating, Eds. G.Brifford, M. Kaufmann, EPS, Schliersee 1986, 10 C, Part I, 391-393.

37 Ehrenberg, J., R.Behrisch, P.E.Stott[1], J.P.Coad[1], L.de Kock[1], and G.M.McCracken[1]: Redistribution of limiter and wall materials in JET. In: Proc. Techn.Comm. Meeting on Lifetime Predictions for the First Wall and Blanket Structure of Fusion Reactors, Karlsruhe 1985, IAEA-TEDOC-393, 1986, 221-231.

38 Engelhardt, W.W. and JET-Team (from IPP: J.Ehrenberg, H.Jäckel, S.Kissel, U.Küphnapfel, R.Müller, A.Stäbler and A.Weller): Impurity behaviour in JET. Plasma Phys. Contr. Fus. 28, 1401 (1986).

39 Engelmann, G., E.Taglauer and D.P.Jackson[1]: Scattering of low-energy Ne^+ and Na^+ from Cu(110): Thermal and neutralization effects. Nucl. Instr. Meth. in Phys. Res. B13, 240-244 (1986).

40 Erckmann, V., R.Wilhelm[1], G.Janzen[1], W.Kasparek[1], G.A.Müller[1], P.G.Schüller[1], M.Thumm[1] and W VII-A Team[3]: Performance of the 70 GHz ECRH system on W VII-A. Proc. 13th Europ. Conf. on Contr. Fus. and Plasma Heating, Eds. G.Brifford, M.Kaufmann, EPS, Schliersee, 1986, 10 C, Part I, 211-214.

41 Erckmann, V., W VII-A Team[3], NI-Team (W VII-A)[5] and ECRH Group (IPF Stuttgart)[7]: Electron cyclotron resonance heating in the Wendelstein VII-A stellarator. Plasma Physics and Controlled Fusion 28, 9A, 1277-1290 (1986).

42 Erckmann, V., W.Kasparek[1], H.Kumric[1], G.A.Müller[1], P.G.Schüller[1], M.Thumm[1], and R.Wilhelm[1]: Very high power mm-wave components in oversized waveguides. Microwave Journal 29, 11, 103-121 (1986).

43 Ertl, K., ASDEX-Team[2] and B.Jüttner[1]: Relevance of plasma-induced arcs for divertor tokamaks. Nuclear Fus. 25, 10, 1413-1419 (1985).

44 Freund, H.J.[1], J.Rogozik, V.Dose and M.Neumann[1]: Bremsstrahlung isochromat spectroscopy study of the system CO/Ni(110): Strong intermolecular interaction. Surf. Sci. 175, 651-658 (1986).

45 Fussmann, G.: Analytical modelling of impurity transport in toroidal devices. Nucl. Fus. 26, 983-1002 (1986).

46 Gehre, O., G.Becker, A.Eberhagen, H.S.Bosch, H.Brocken, G.Fussmann, J.Gernhardt, G.v.Gierke, E.Glock, O.Gruber, G.Haas, J.Hofmann, A.Izvozchikov[1], G.Janeschitz, F.Karger, M.Keilhacker, O.Klüber, M.Kornherr, K.Lackner, M.Lenoci, G.Lisitano, H.M.Mayer, F.Mast, K.McCormick, D.Meisel, V.Mertens, E.R.Müller, H.Murmann, H.Niedermeyer, A.Pietrzyk[1], W.Poschenrieder, H.Rapp, H.Röhr, J.Roth, F.Ryter[1], F.Schneider, C.Setzensack, G.Siller, P.Smeulders[1], F.X.Söldner, K.-H.Steuer, F.Wagner and D.Zasche: Particle confinement in ohmically heated ASDEX plasmas. In: Proc. 13th Europ. Conf. on Contr. Fusion and Plasma Heating, Eds. G. Briffod, M. Kaufmann, EPS, Schliersee 1986, 10 C, Part I, 220-223.

47 Gierke, G.v., G.Becker, H.S.Bosch, H.Brocken, K.Büchl, A.Eberhagen, D.Eckhartt, G.Fussmann, O.Gehre, J.Gernhardt, E.Glock, O.Gruber, G.Haas, J.Hofmann, A.Izvozchikov[1], G.Janeschitz, F.Karger, M.Kaufmann, M.Keilhacker, O.Klüber, M.Kornherr, K.Lackner, R.S.Lang, M.Lenoci[1], F.Leuterer, G.Lisitano, F.Mast, H.M.Mayer, K.McCormick, D.Meisel, V.Mertens, E.R.Müller, H.Murmann, H.Niedermeyer, J.-M.Noterdaeme, A.Pietrzyk[1], W.Poschenrieder, H.Rapp, H.Riedler, H.Röhr, J.Roth, F.Ryter[1], W.Sandmann, F.Schneider, C.Setzensack, G.Siller, P.Smeulders[1], F.X.Söldner, E.Speth, K.Steinmetz, K.-H.Steuer, G.Vlases[1], O.Vollmer, F.Wagner, F.Wesner and D.Zasche: The influence of the current distribution on the achievable ß-values in ASDEX. In: Proc. 13th Europ. Conf. on Contr. Fusion and Plasma Heating, Eds. G. Briffod, M. Kaufmann, EPS, Schliersee 1986, 10 C, Part I, 33-36.

48 Gill, R.D.[1], D.V.Bartlett[1], G.Bracco[1], D.J.Campbell[1], S.Corti[1], A.E.Costley[1], A.W.Edwards[1], W.Engelhardt, H.U.Fahrbach, D.J.Gambier[1], C.W.Gowers[1], R.S.Granetz[1], A.Hubbard[1], S.E.Kissel[1], N.Lopes-Cardozoy[1], G.Magyar[1], J.O'Rourke[1], E.Oord[1], J.A.Wesson[1], V.Zanza and D.Zasche: Sawtooth activity during additional heating in JET. In: Proc. 13th Europ. Conf. on Contr. Fus. and Plasma Heating, Eds. G.Briffod, M.Kaufmann, EPS, Schliersee 1986, 10C, Part I, 21-24.

49 Grieger, G. and H.Wobig: Stellarators for fusion reactors. ENC '86, Fourth Int. ENS/ANS Conf., Geneva 1986, ENC '86 Transactions 3, 23-28.

50 Grieger, G., R.Buende, P.E.Grohnheit[1], W.Gulden[1], G.Kessler[1], H.Klippel[1], J.Pericart[1], P.Rocco[1], J.L.Rouyer[1] and W.R.Spears[1]:

Environmental Impact and Economic Prospects of Nuclear Fusion. CEC, Brussels 1986, EURFU BRU/XII-828/86.

51 Grieger, G., W VII-A Team[3], NI-Team (W VII-A)[5], ECRH Group (IPF Stuttgart)[7] and Pellet Injection Group (K.Büchl and R.Lang):
Confinement of stellarator-plasmas with neutral beam and rf heating in W VII-A. Plasma Phys. and Contr. Fusion 28, 1A, 43 (1986).

52 Gruber, O., W.Jilge, H.S.Bosch, H.Brocken, A.Eberhagen, G.Fussmann, O.Gehre, J.Gernhardt, G.v.Gierke, E.Glock, G.Haas, J.Hofmann, G.Janeschitz, A.Izvozchikov, F.Karger, M.Keilhacker, O.Klüber, M.Kornherr, K.Lackner, M.Lenoci, G.Lisitano, F.Mast, H.M.Mayer, K.McCormick, D.Meisel, V.Mertens, E.R.Müller, H.Murmann, H.Niedermeyer, W.Poschenrieder, H.Rapp, H.Riedler, H.Röhr, J.Roth, F.Ryter, F.Schneider, C.Setzensack, G.Siller, P.Smeulders, F.X.Söldner, E.Speth, K.-H.Steuer, O.Vollmer and F.Wagner:
Transport in beam-heated ASDEX discharges below and in the vicinity of the beta limit. In: Proc. 13th Europ. Conf. on Contr. Fus. and Plasma Heating, Eds. G.Briffod, M.Kaufmann, EPS, Schliersee 1986, 10C, Part I, 228-250.

53 Gruber, O., W.Jilge, V.Mertens, ASDEX-Team[2] and Pellet-Team[10]:
Energy and particle transport in ASDEX-pellet discharges. In: Proc. 13th Europ. Conf. on Contr. Fus. and Plasma Heating, Eds. G.Briffod, M.Kaufmann, EPS, Schliersee 1986, 10C, Part I, 228-231.

54 Gruber, O. and ASDEX Upgrade Project Group (W.Köppendörfer, M.Blaumoser. K.Ennen, J.Gruber, M.Kaufmann, H.Kollotzek, H.Kotzlowski, E.Lackner, K.Lackner, T.v.Larcher, J.Neuhauser, M.Pillsticker, R.Pöhlchen, H.Preis, H.Schneider, U.Seidel, B.Sombach, B.Streibl, F.Werner and A.Wieczorek):
ASDEX Upgrade, start-up and operation. In: Tokamak Start-up, Problems and Scenarios Related to the Transient Phases of a Thermonuclear Fusion Reactor, Ed. H.Knoepfel, Pergamon Press, Oxford 1986, 131-141.

55 Haglund, R.F.[1], R.G.Albridge[1], D.W.Cherry[1], R.K.Cole[1], M.H.Mendenhall[1], W.C.B.Peatman[1], N.H.Tolk[1], D.Niles[1], G.Margaritondo[1], N.G.Stoffel[1] and E.Taglauer:
Mechanisms of electron- and photon-stimulated desorption in alkali halides. Nucl. Instr. & Meth. in Phys. Res. B13, 525-532 (1986).

56 Harmeyer, E., J.Kißlinger, F.Rau and H.Wobig:
Magnetic field studies near separatrix. Proc. 13th Europ. Conf. on Contr. Fus. and Plasma Heating, Eds. G.Brifford, M.Kaufmann, EPS, Schliersee, 1986, 10 C, Part I, 323-326.

57 Harned, D.S.[1] and W.Kerner:
Semi-implicit method for three-dimensional resistive magnetohydrodynamic simulation of fusion plasmas. Nucl.Sc.Eng. 92, 119-125 (1986).

58 Hartfuß, H.J., H.Maassberg, M.Tutter, W VII-A Team[3] and ECRH Group (IPF Stuttgart)[7]:
Evaluation of the local heat conductivity coefficient by power-modulated electron cyclotron heating in the Wendelstein VII-A stellarator. Nucl. Fus. 26, 678-684 (1986).

59 Hartfuß, H.J., H.Maassberg, M.Tutter, W VII-A Team[3] and ECRH Group (IPF Stuttgart)[7]:
Experiments on heat transport applying the modulation and correlation technique to electron heated plasmas in the Wendelstein VII-A stellarator. Proc. 5th Int. Workshop on ECE and ECH, Eds. R.Prater and J.Lohr, San Diego 1986, GA Report No. A 18294, 145.

60 Hartfuß, H.J., H.Maaßberg, M.Tutter, W VII-A Team[3] and ECRH Group (IPF Stuttgart)[7]:
Experimental determination of the local heat conductivity coefficient $\chi_e(r)$ in the W VII-A stellarator. Proc. 13th Europ. Conf. on Contr. Fus. and Plasma Heating, Eds. G.Brifford, M.Kaufmann, EPS, Schliersee, 1986, 10 C, Part I, 315-318.

61 Hartfuß, H.J., M.Tutter, W VII-A Team[3] and ECRH Group (IPF Stuttgart)[7]:
Electron cyclotron emission measurements during electron cyclotron heating in the Wendelstein VII-A stellarator at 1 tesla and 2.5 tesla. Proc. 5th Int. Workshop on ECE and ECH, Eds. R.Prater and J.Lohr, San Diego 1986, GA Report No. A 18294, 37.

62 Hemsworth, R.S., A. Stäbler, H.D.Falter, P.Massmann, G.H.Deschamps and A.P.H.Goede:
Neutralisation measurements for the JET injector. In: Proc. 13th Europ.Conf. on Contr.Fus. and Plasma Heating, Eds. G.Briffod, M.Kaufmann, EPS, Schliersee 1986, 10C, Part II, 297-300.

63 Herrnegger, F. and F.Rau:
Bean-shaped advanced stellarators with modular coil systems. In: Proc. 13th Europ. Conf. on Contr. Fus. and Plasma Phys., Eds. G.Briffod, M.Kaufmann, EPS, Schliersee 1986, Vol.10C, Part I, 307-310.

64 Herrnegger, F., P.Merkel and J.L.Johnson:
Comparison of two-dimensional and three-dimensional MHD equilibrium und stability codes. J. Comput. Phys. 66, 445-457 (1986).

65 Herrnegger, F.:
Bean-shaped advanced stellarator configurations with small shear and

reduced parallel current. In: Proc. 8th Europhys. Conf. on Comp. Physics, Ed. J.Nührenberg, EPS, Eibsee 1986, ECA 10D, 145-148 (1986).

66 Herrnegger, F.:
Free-boundary n = 1,2,3 modes in low-shear $\ell = 2$ stellarators. In: Proc. 8th Europhys. Conf. on Comp. Physics, Ed. J.Nührenberg, EPS, Eibsee 1986, 10D, 153-156 (1986).

67 Hertweck, F.R.:
Les gros ordinateurs. Bull. de Liaison de la Recherche en Informatique et Automatique, INRIA 109, 26-28 (1986).

68 Hertweck, F.R. and J.Maier:
Data structure for the description of tokamak diagnostics. In: Proc. 6th Topical Conf. on High Temperature Plasma Diagnostics, South Carolina, USA. Rev. Scientific Instruments 57, No 8, Part II, 1935-1937 (1986).

69 Hirshman, S.P., J.Nührenberg and R.Zille:
Resistively stable stellarator equilibria by ß iteration. In: Proc. 8th Europhys. Conf. on Comp. Physics, Ed. J.Nührenberg, EPS, Eibsee 1986, 10D, 157-160 (1986).

70 Hirshman, S.P., W.I.van Rij and P.Merkel:
Three-dimensional free boundary calculations using a spectral green's function method. Comp. Phys. Comm.43, 143-155 (1986).

71 Hou, M.[1] and W.Eckstein:
Computer simulation of low energy static single crystal sputtering. Nucl. Instr. & Meth. in Phys. Res. B13, 324-330 (1986).

72 INTOR Group[11]:
International Tokamak Reactor, Phase Two A, Part II. IAEA, Vienna 1986, STI/PUB/714.

73 Jacob, W., V.Dose and A.Goldmann[1]:
Atomic adsorption of oxygen on Cu(111) and Cu(110). Appl.Phys. A41, 145-150 (1986).

74 Jacob, W., V.Dose, U.Kolac, T.Fauster and A.Goldmann[1]:
Bulk, surface and thermal effects in inverse photoemission spectra from Cu(110), Cu(110) and Cu(111). Z. Phys. B - Condensed Matter 63, 459-470 (1986).

75 Janeschitz, G., G.Fussmann, J.-M.Noterdaeme, K.Steinmetz, A.Izvozchikov[1], F.Ryter[1], G.Becker, H.S.Bosch, H.Brocken, A.Eberhagen, O.Gehre, J.Gernhardt, G.v.Gierke, E.Glock, O.Gruber, G.Haas, J.Hofmann, F.Karger, M.Keilhacker, O.Klüber, M.Kornherr, M.Lenoci, G.Lisitano, F.Mast, H.M.Mayer, K.McCormick, D.Meisel, V.Mertens, E.R.Müller, H.Murmann, H.Niedermeyer, W.Poschenrieder, H.Rapp, H.Röhr, F.Schneider, C.Setzensack, G.Siller, P.Smeulders[1], F.X.Söldner, E.Speth, K.-H.Steuer, S.Ugniewski[1], O.Vollmer, F.Wagner, F.Wesner and D.Zasche:
Impurity production during ICRF heating. In: Proc. 13th Europ. Conf. on Contr. Fusion and Plasma Heating, Eds. G. Briffod, M. Kaufmann, EPS, Schliersee 1986, 10 C, Part I, 407-410.

76 Janeschitz, G., G.Fussmann, P.B.Kotzé[1], A.Mahdavi[1], J.Roth, E.Taglauer, R.Bartiromo[1], G.Becker, H.S.Bosch, A.Eberhagen, O.Gehre, J.Gernhardt, G.v.Gierke, E.Glock, O.Gruber, G.Haas, F.Karger, M.Keilhacker, A.Kislyakov[1], O.Klüber, M.Kornherr, M.Lenoci[1], G.Lisitano, H.M.Mayer, K.McCormick, D.Meisel, V.Mertens, E.R.Müller, H.Murmann, H.Niedermeyer, W.Poschenrieder, H.Rapp, F.Ryter[1], F.Schneider, G.Siller, P.Smeulders[1], F.X.Söldner, E.Speth, K.Steinmetz, K.-H.Steuer, O.Vollmer, F.Wagner and F.Wesner:
Retainment of gaseous and target-produced impurities in the ASDEX divertor. 12th Europ. Conf. on Contr. Fus. and Plasma Phys., Budapest, September 1985. Nucl. Fusion 26, 12, 1725-1728 (1986).

77 Kaufmann, M., K.Lackner, L.Lengyel and W.Schneider:
Plasma shielding of hydrogen pellets. Nuclear Fus. 26, 171-178 (1986).

78 Kaufmann, M.:
Review on Pellet Fuelling. Plasma Phys. and Contr. Fusion 28, 9A, 1341-1352 (1986).

79 Keilhacker, M., G.v.Gierke, E.R.Müller, H.Murmann, F.X.Söldner, E.Speth, K.Steinmetz, F.Wagner, R.Bartiromo[1], G.Becker, H.S.Bosch, A.Eberhagen, D.Eckhartt, G.Fussmann, O.Gehre, J.Gernhardt, A.Giuliana[1], E.Glock, O.Gruber, G.Haas, G.Janeschitz, F.Karger, O.Klüber, M.Kornherr, K.Lackner, M.Lenoci[1], F.Leuterer, G.Lisitano, H.M.Mayer, K.McCormick, D.Meisel, V.Mertens, M.Münich, H.Niedermeyer, W.Poschenrieder, H.Rapp, F.Ryter[1], F.Schneider, G.Siller, P.Smeulders, K.-H.Steuer, O.Vollmer, F.Wesner and D.Zasche:
Confinement in ASDEX with neutral beam and RF heating. 12th Europ. Conf. on Contr. Fus. and Plasma Phys., Budapest, September 1985, Plas.Phys.and Contr.Fus. 28, 1,29 (1986).

80 Kerner, W., A.Jakoby and K.Lerbinger:
Finite-element semi-discretization of linearized compressible and resistive MHD. Computational Physics 66 2, 332-355 (1986).

81 Kerner, W., E.Schwarz and J.Steuerwald:
Out-of-core algorithm for the general non-Hermitian eigenvalue problem $\underline{A}\underline{X} = \underline{B}\underline{x}$. In: Proc. 8th Europhysics Conf. on Comp. Physics, Ed. J. Nührenberg, EPS, Eibsee 1986, 10D, 83-85.

82 Kerner, W., K.Lerbinger and K.Riedel[1]: Resistive Alfven spectrum of tokamaklike configurations in straight cylindrical geometry. Phys.Fluids 29, 2975-2987 (1986).

83 Kerner, W.: Computing the complex eigenvalue spectrum for resistive magnetohydrodynamics. In: Large scale eigenvalue problems, Mathematics Studies Series. Eds. J.Cullum and R.A.Willougby, Elsevier Science Publ. B.V. Amstderdam, 1986, 127, 241-265.

84 Kick, M., H.Ringler, F.Sardei, A.Weller, W VII-A Team[3], NI-Team (W VII-A)[5] and ECRH Group (IPF Stuttgart)[7]: CX-recombination spectroscopy during NBI heating of ECRH target plasmas in W VII-A stellarator and comparison with a transport model. Proc. 13th Europ. Conf. on Contr. Fus. and Plasma Heating, Eds. G.Brifford, M.Kaufmann, EPS, Schliersee, 1986, 10 C, Part I, 319-322.

85 Klüber, O., J.Gernhardt, K.Grassie, J.Hofmann, M.Kornherr, R.D.Stambaugh[1], H.P.Zehrfeld, G.Becker, H.S.Bosch, H.Brocken, A.Eberhagen, G.Fussmann, O.Gehre, G.v.Gierke, E.Glock, O.Gruber, G.Haas, A.Izvozchikov[1], G.Janeschitz, F.Karger, M.Keilhacker, K.Lackner, M.Lencoi, G.Lisitano, F.Mast, H.M.Mayer, K.McCormick, D.Meisel, V.Mertens, E.R.Müller, H.Murmann, H.Niedermeyer, A.Pietrzyk[1], W.Poschenrieder, H.Rapp, H.Riedler, H.Röhr, J.Roth, R.Ryter[1], F.Schneider, C.Setzensack, G.Siller, P.Smeulders[1], F.X.Söldner, E.Speth, K.-H.Steuer, O.Vollmer, F.Wagner and D.Zasche: MHD characteristics of ASDEX H-type discharges approaching the ß limit. In: Proc. 13th Europ. Conf. on Contr. Fusion and Plasma Heating, Eds. G. Briffod, M. Kaufmann, EPS, Schliersee 1986, 10 C, Part I, 136-139.

86 Knobloch, A.F. and P.Komarek[1]: Cumulative impact of innovations. In: Tokamak concept innovations, Vienna 1986, IAEA-TECDOC-373, 593-596.

87 Knobloch, A.F. and P.Komarek[1]: High field superconductors for central solenoid application. In: INTOR Phase IIA-3rd Part, Intor-related specialist's meeting, CEC, Brussels 1986, EURFUBRU/XII-52/86/EDV1, Vol.II, E 4.5.

88 Knobloch, A.F. and P.Komarek[1]: High field superconductors for central solenoid application. In: Tokamak concept innovations, Vienna 1986, IAEA-TECDOC-373, 266-269.

89 Knobloch, A.F. and P.Komarek[1]: Joints in superconducting coils. In: INTOR Phase IIA-3rd Part, Intor-related specialist's meeting, CEC, Brussesl 1986, EURFUBRU/XII-52/86/EDV1, Vol. II, E 4.6.

90 Knobloch, A.F. and P.Komarek[1]: Joints in superconducting coils. In: Tokamak concept innovations, Vienna 1986, IAEA-TECDOC-373, 270-273.

91 Knobloch, A.F., C.A.Flanagan[1], H.Iida[1], S.Itoh[1], B.N.Kolbasov[1] and K.Tomabechi [1]: Technical benefit of partitioning INTOR component design and fabrication. In: International Tokamak Reactor Phase Two A Part II, Report of INTOR Workshop, Vienna 1984/1985, IAEA 1986, STI/PUB/714, 397-451.

92 Knobloch, A.F.: Balanced selection of alternative enhanced INTOR parameters. In: INTOR Phase IIA-3rd Part, Critical issues, Europ. Contrib. to the 13th Workshop Meeting, Vienna 1986, CEC, Brussels 1986, Physics Groups, App.3, EURFUBRU/XII-52/86/EDV10.

93 Knobloch, A.F.: Cumulative impact of innovations. In: INTOR Phase IIA-3rd Part, Intor-related specialist's meeting, CEC, Brussels 1986, EURFUBRU/XII-52/86/EDV1, Vol.II, G 9.8.

94 Köppendörfer, W., M.Blaumoser. K.Ennen, J.Gruber, O.Jandl, M.Kaufmann, H.Kollotzek, H.Kotzlowski, E.Lackner, K.Lackner. T.v.Larcher. J.M.Noterdaeme, M.Pillsticker, R.Pöhlchen, H.Preis, H.Schneider, U.Seidel, B.Sombach, E.Speth, B.Streibl, H.Vernickel, F.Werner, F.Wesner and A.Wieczorek: The ASDEX Upgrade toroidal field magnet and poloidal divertor field coil system adapted to reactor requirements. Nucl. Eng. and Design/Fusion 3, 265-272 (1986).

95 Kornherr, M., A.Eberhagen, J.Gernhardt, O.Klüber, F.Wagner, G.Becker, H.S.Bosch, H.Brocken, G.Fussmann, O.Gehre, G.v.Gierke, E.Glock, O.Gruber, G.Haas, J.Hofmann, A.Izvozchikov[1], G.Janeschitz, F.Karger, M.Keilhacker, M.Kornherr, K.Lackner, M.Lenoci, G.Lisitano, F.Mast, H.M.Mayer, K.McCormick, D.Meisel, V.Mertens, E.R.Müller, H.Murmann, H.Niedermeyer, J.-M.Noterdaeme, A.Pietrzyk[1], W.Poschenrieder, H.Rapp, H.Riedler, H.Röhr, J.Roth, F.Ryter[1], F.Schneider, C.Setzensack, G.Siller, P.Smeulders[1], F.X.Söldner, E.Speth, K.Steinmetz, K.-H.Steuer, O.Vollmer, F.Wesner and D.Zasche: MHD-effects with NI and ICRF heating on ASDEX. In: Proc. 13th Europ. Conf. on Contr. Fusion and Plasma Heating, Eds. G. Briffod, M. Kaufmann, EPS, Schliersee 1986, 10 C, Part I, 140-143.

96 Kotzlowski, H.: Actively cooled graphite limiters. In: Proc. 11th Intern. Plansee Seminar, Eds. H.Bildstein, H.M.Ortner, 1986, 3, 307-312.

97 Lackner, K., R.Chodura, J.Neuhauser and W.Schneider:

Plasma boundary phenomena in toroidal devices: I. In: Basic Physical Processes in Toroidal Fusion Plasmas, 1986, 2, CEC Bruxelles/Belgium, 633-657.

98 Lagin, L.[1], U.Schneider, N.Arnold[1], R.Fonck[1], K.Jaehnig[1], P.Roney[1], W.Davis[1] and G.Christianson[1]: CHERS software system - a microVAX-based diagnostic. In: Proc. 6th Topical Conf. on High Temperture Plasma Diagnostics, South Carolina, USA. Rev. Scientific Instruments 57, No 8, Part II, 1889-1891 (1986).

99 Lallia, P.P. and JET-Team (from IPP: J.Ehrenberg, H.Jäckel, S.Kissel, U.Küphnapfel, R.Müller, A.Stäbler and A.Weller): Plasma heating in JET. Plasma Phys. Contr. Fus. 28, 1211 (1986).

100 Lengyel, L.L.: Ignition and fueling scenario calculations for neutral-beam-heated tokamak reactors based on pellet injection. Fusion Technology 3, 354-363 (1986).

101 Lenoci, M., G.Haas, G.Becker, H.S.Bosch, H.Brocken, A.Eberhagen, D.Eckhartt, G.Fussmann, O.Gehre, J.Gernhardt, G.v.Gierke, E.Glock, O.Gruber, J.Hofmann, A.Izvozchikov[1], G.Janeschitz, F.Karger, M.Keilhacker, O.Klüber, M.Kornherr, K.Lackner, F.Leuterer, G.Lisitano, F.Mast, H.M.Mayer, K.McCormick, D.Meisel, V.Mertens, E.R.Müller, H.Murmann, H.Niedermeyer, A.Pietrzyk[1], W.Poschenrieder, H.Rapp, H.Röhr, J.Roth, F.Ryter[1], F.Schneider, C.Setzensack, G.Siller, P.Smeulders[1], F.X.Söldner, K.-H.Steuer, N.N.Tsois[1], F.Wagner and D.Zasche: Probe measurements of plasma inhomogeneities in the scrape-off layer of ASDEX during LH. In: Proc. 13th European Conf. on Contr. Fusion and Plasma Heating, Eds. G. Briffod, M. Kaufmann, EPS, Schliersee 1986, 10 C, Part II, 397-400.

102 Leuterer, F., D.Eckhartt, F.Söldner, R.Bartiromo[1], G.Becker, K.Bernhardi, H.S.Bosch, M.Brambilla, H.Brocken, H.Derfler, A.Eberhagen, G.Fußmann, O.Gehre, J.Gernhardt, G.v.Gierke, A.Giuliana[1], E.Glock, O.Gruber, G.Haas, M.Hesse[1], G.Janeschitz, F.Karger, M.Keilhacker, O.Klüber, M.Kornherr P.B.Kotzé[1], A.Kislyakov[1], M.Lenoci[1], G.Lisitano, H.M.Mayer, K.McCormickk, D.Meisel, V.Mertens, E.R.Müller, M.Münich, H.Murmann, H.Niedermeyer, W.Poschenrieder, H.Rapp, F.Ryter[1], K.H.Schmitter, F.Schneider, G.Siller, P.Smeulders, K.-H.Steuer, T.Vien, G.Vlases[1], F.Wagner, F.v.Woyna and M.Zouhar: Lower hybrid current drive and recharging of the ohmic heating transformer in ASDEX. In: Tokamak Start-Up, Problems and Scenarios related to the Transient Phases of a Thermonuclear Fusion Reactor, Ed. H. Knöpfel, Plenum Press, New York 1986, 26, 191-201.

103 Leuterer, F., D.Eckhartt, F.X.Söldner, R.Bartiromo[1], G.Becker, K.Bernhardi, H.S.Bosch, M.Brambilla, H.Brocken, H.Derfler, A.Eberhagen, G.Fußmann, O.Gehre, J.Gernhardt, G.v.Gierke, A.Giuliana[1], E.Glock, O.Gruber, G.Haas, M.Hesse[1], G.Janeschitz, F.Karger, M.Keilhacker, O.Klüber, M.Kornherr P.B.Kotzé[1], A.Kislyakov[1], M.Lenoci[1], G.Lisitano, H.M.Mayer, K.McCormick, D.Meisel, V.Mertens, E.R.Müller, M.Münich, H.Murmann, H.Niedermeyer, W.Poschenrieder, H.Rapp, F.Ryter[1], K.H.Schmitter, F.Schneider, G.Siller, P.Smeulders, K.-H.Steuer, T.Vien, G.Vlases[1], F.Wagner, F.v.Woyna and M.Zouhar: Lower hybrid current drive and recharging of the ohmic heating transformer in ASDEX. (Invited Lecture). Proc. Course and Workshop on Applications of RF Waves to Tokamak Plasmas, Varenna 1985, Eds. S. Barnabei, V. Gasparino, E. Sindoni, EUR 10333, EN II, 633-642.

104 Leuterer, F., LH-Group[9] and ASDEX-Team[2]: Influence of the $N_{\parallel}$-spectrum on lower hybrid current drive in ASDEX. In: Proc. 13th Europ.Conf. on Contr.Fus. and Plasma Heating, Eds. G.Briffod, M.Kaufmann, EPS, Schliersee 1986, 10C, Part II, 409-412.

105 Liebl, H. and H.Weiss: Ion optics of submicron ion beams. Scanning Electr. Microscopy III, 793-798 (1986).

106 Lotz, W.: Monte Carlo simulation of loss rates in stellarators and tokamaks. In: Proc. 8th Europhys. Conf. on Comp. Physics, Ed. J.Nührenberg, EPS, Eibsee 1986, ECA 10D, 105-108 (1986).

107 Mathis, R. and J.Sapper: Structural analysis of magnetic coils. In: Proc. 3rd Int. Conf. on Computational Methods and Experimental Measurements, Eds. G.A. Keramidos, C.A.Brebbia, Porto Carras, Greece, 1986. Springer-Verlag Berlin, 1986, 419-429.

108 McCormick, K., F.X.Söldner, F.Leuterer, H.Murmann, D.Eckhartt, G.Becker, H.S.Bosch, H.Brocken, A.Eberhagen, G.Fussmann, O.Gehre, J.Gernhardt, G.v.Gierke, E.Glock, O.Gruber, G.Haas, J.Hofmann, A.Izvozchikov[1], G.Janeschitz, F.Karger, M.Keilhacker, O.Klüber, M.Kornherr, K.Lackner, M.Lenoci, G.Lisitano, F.Mast, H.M.Mayer, D.Meisel, V.Mertens, E.R.Müller, H.Niedermeyer, A.Pietrzyk[1], W.Poschenrieder, H.Rapp, H.Röhr, J.Roth, F.Ryter[1], F.Schneider, C.Setzensack, G.Siller, P.Smeulders[1], K.-H.Steuer, F.Wagner and D.Zasche: Influence of the lower hybrid wave spectrum on the current distribution in ASDEX. In: Proc. 13th Europ. Conf. on Contr. Fusion and Plasma Heating, Eds. G. Briffod, M. Kaufmann, EPS, Schliersee 1986, 10 C, Part II, 323-326.

109 Meisel, D., H.Murmann, H.Röhr, K.-H.Steuer, G.Becker, H.S.Bosch, H.Brocken, A.Eberhagen, G.Fussmann, O.Gehre, J.Gernhardt, G.v.Gierke, E.Glock, O.Gruber, G.Haas, J.Hofmann, A.Izvozchikov[1], G.Janeschitz, F.Karger, M.Keilhacker, O.Klüber, M.Kornherr, K.Lackner, M.Lenoci, G.Lisitano, F.Mast, H.M.Mayer, K.McCormick, V.Mertens, E.R.Müller, H.Niedermeyer, A.Pietrzyk[1], W.Poschenrieder, H.Rapp, J.Roth, F.Ryter[1], F.Schneider, C.Setzensack, G.Siller, P.Smeulders[1], F.X.Söldner, F.Wagner and D.Zasche : Periodic Thomson scattering diagnostic with 16 spatial channels on ASDEX. In: Proc. 13th Europ. Conf. on Contr. Fusion and Plasma Heating, Eds. G. Briffod, M. Kaufmann, EPS, Schliersee 1986, 10 C, Part I, 97-100.

110 Merkel, P., J.Nührenberg and R.Zille: Finite ß and vacuum field studies for the Helias stellarator. In: Proc. 13th Europ. Conf. on Contr. Fusion and Plasma Heating, Eds. G. Briffod, M. Kaufmann, EPS, Schliersee 1986, 10C, Part I, 283-286.

111 Merkel, P.: An integral equation technique for the exterior and interior Neumann problem in toroidal regions. J.Comput.Physics 66, 83-98 (1986).

112 Möller, W.: A computer study of the collisional mixing of Pt in Si. Nucl. Instr. & Meth. in Phys. Res. B15, 688-691 (1986).

113 Morsi, H.W. and W.Reicher[1]: A new 32 GHz radio continuum receiving system for the Effelsberg 100-m telescope. Astron. Astrophys. 163, 313-320 (1986).

114 Müller, E.R., G.Janeschitz, P.Smeulders[1], G.Fussmann, M.Kornherr, F.Mast, G.Becker, H.S.Bosch, H.Brocken, A.Eberhagen, O.Gehre, J.Gernhardt, G.v.Gierke, E.Glock, O.Gruber, G.Haas, J.Hofmann, A.Izvozchikov[1], F.Karger, M.Keilhacker, O.Klüber, K.Lackner, M.Lenoci, G.Lisitano, H.M.Mayer, K.McCormick, D.Meisel, V.Mertens, H.Murmann, H.Niedermeyer, A.Pietrzyk[1], W.Poschenrieder, H.Rapp, H.Riedler, H.Röhr, J.Roth, F.Ryter[1], F.Schneider, C.Setzensack, G.Siller, F.X.Söldner, E.Speth, K.-H.Steuer, O.Vollmer, F.Wagner and D. Zasche: Evolution of radiation power profiles in ASDEX H-mode discharges. In: Proc. 13th Europ. Conf. on Contr. Fusion and Plasma Heating, Eds. G. Briffod, M. Kaufmann, EPS, Schliersee Schliersee 1986, 10 C, Part I, 172-175.

115 Murmann, H., F.Wagner, G.Becker, H.S.Bosch, H.Brocken, A.Eberhagen, G.Fussmann, O.Gehre, J.Gernhardt, G.v.Gierke, E.Glock, O.Gruber, O.Gruber, G.Haas, J.Hofmann, A.Izvozchikov[1], G.Janeschitz, F.Karger, M.Keilhacker, O.Klüber, M.Kornherr, K.Lackner, M.Lenoci, G.Lisitano, F.Mast, H.M.Mayer, K.McCormick, D.Meisel, V.Mertens, E.R.Müller, H.Niedermeyer, A.Pietrzyk[1], W.Poschenrieder, H.Rapp, H.Röhr, J.Roth, F.Ryter[1], F.Schneider, C.Setzensack, G.Siller, P.Smeulders[1], F.X.Söldner, K.-H.Steuer and D.Zasche: Analysis of the invariance property of the electron temperature during auxiliary heating in ASDEX. In: Proc. 13th Europ. Conf. on Contr. Fusion and Plasma Heating, Eds. G. Briffod, M. Kaufmann, EPS, Schliersee 1986, 10 C, Part I, 216-219.

116 Neuhauser, J., W.Schneider and R.Wunderlich: Thermal instabilities and poloidal asymmetries in the tokamak edge plasma. Nucl. Fusion 26, 1679-1692 (1986).

117 Niedermeyer, H., K.Büchl, M.Kaufmann, R.Lang, V.Mertens, W.Sandmann, G.Vlases[1], G.Becker, H.S.Bosch, H.Brocken, A.Eberhagen, G.Fussmann, O.Gehre, J.Gernhardt, G.v.Gierke, E.Glock, O.Gruber, G.Haas, J.Hofmann, A.Izvozchikov[1], G.Janeschitz, F.Karger, M.Keilhacker, O.Klüber, M.Kornherr, K.Lackner, M.Lenoci, G.Lisitano, F.Mast, H.M. Mayer, K.McCormick, D.Meisel, E.R. Müller, H.Murmann, A.Pietrzyk[1], W.Poschenrieder, H.Rapp, H.Riedler, H.Röhr, J.Roth, F.Ryter[1], F.Schneider, C.Setzensack, G.Siller, P.Smeulders[1], F.X.Söldner, E.Speth, K.-H. Steuer, O.Vollmer, F.Wagner and D.Zasche: Increase of the density limit in ASDEX by repetitive pellet injection. In: Proc. 13th Europ. Conf. on Contr. Fusion and Plasma Heating, Eds. G. Briffod, M. Kaufmann, EPS, Schliersee 1986, 10 C, Part I, 168-171.

118 Noterdaeme J.-M., F.Ryter, M.Söll, ICRH-Team[8], ASDEX-Team[2] and NI-Team (ASDEX)[4]: The role of the Faraday screen in ICRF antennae: comparison of an optically open and optically closed screen in ASDEX. In: Proc. 13th Europ.Conf. on Contr.Fus. and Plasma Heating, Eds. G.Briffod, M.Kaufmann, EPS, Schliersee 1986, 10C, Part II, 137-140.

119 Nührenberg, J. and R.Zille: Stable stellarators with medium ß and aspect ratio. Phys. Letters 114A, 129-132 (1986).

120 Onsgaard, J.[1], W.Huang[1] and E.Taglauer: On the use of the quartz crystal microbalance for surface analysis in combination with surface sensitive spectroscopies. Surface and Interface Analysis 9, 119-123 (1986).

121 Pfirsch D. and P.Gräff: Stochastic runaway of dynamical systems. Physica 136A, 393-416 (1986).

122 Poschenrieder, W. and ASDEX-Team[2]:
Wall carbonization in ASDEX: A collation of characteristic results. In: Proc. 13th Europ. Conf. on Contr. Fusion and Plasma Heating, Eds. G.Brifford, M. Kaufmann, EPS, Schliersee 1986, Part I, 10C, 196-199.

123 Preis, H.:
Die Berechnung von Wirbelströmen und magnetischen Kräften in Kernfusions-Experimenten. Archiv für Elektrotechnik 69, 359-365 (1986).

124 Rau, F., M.A.Abdou[1], E.Bertolini[1], R.Hancox[1], W.J.Hogan[1], A.I.Kostenko[1], G.L.Kulcinski[1], R.L.Miller[1], V.V.Orlov[1], I.N.Sviatoslavsky[1] and J.Kupitz[1]:
Fusion Reactor Design IV.
Report on the 4th IAEA Technical Committee and Workshop on Fusion Reactor Design and Technology, Yalta, USSR. Nucl. Fus. 26, No. 10, 1377-1428 (1986).

125 Renner, H., W VII-A Team[3], ECRH Group (IPF Stuttgart)[7] and NI-Team[5]:
Influence of shear, ι t/t on the confinement in the W VII-A stellarator. Proc. 13th Europ. Conf. on Contr. Fus. and Plasma Heating, Eds. G.Brifford, M.Kaufmann, EPS, Schliersee, 1986, 10 C, Part I, 287-290.

126 Renner, H.:
Stellarator experiments at Garching. In: Proc. Workshop on Basic Physical Processes of Toroidal Fusion Plasmas, Varenna 1985, Eds. S.Bernabei, V.Gasparino, E.Sindoni, EUR 10418, Brüssel 1986, II, 479-507.

127 Riedler, J.M., G.H.Miley and M.Heindler:
Coulomb Scattering between Maxwellian plasma and monoenergetic beam. Phys.Fluids 29, 1049, 1986.

128 Riyopoulos, S.[1], T.Tajima[1], T.Hatori[1] and D.Pfirsch:
Diffusion induced by cyclotron resonance heating. Nucl.Fusion 26, 627-632 (1986).

129 Rogozik, J. and V.Dose:
The role of the 2 π level in CO chemisorption on metals surfaces. Surf. Sci. 176, L847-L851 (1986).

130 Röhr, H., K.-H.Steuer, D.Meisel, H.Murmann, G.Becker, H.S.Bosch, H.Brocken, A.Eberhagen, G.Fussmann, O.Gehre, J.Gernhardt, G.v.Gierke, E.Glock, O.Gruber, G.Haas, J.Hofmann, A.Izvozchikov[1], G.Janeschitz, F.Karger, M.Keilhacker, O.Klüber, M.Kornherr, K.Lackner, M.Lenoci, G.Lisitano, F.Mast, H.M.Mayer, K.McCormick, V.Mertens, E.R.Müller, H.Niedermeyer, A.Pietrzyk[1], W.Poschenrieder, H.Rapp, J.Roth, F.Ryter[1], F.Schneider, C.Setzensack, G.Siller, P.Smeulders[1], F.X.Söldner, F.Wagner and D.Zasche:
Measurement of plasma emission profiles in the range from 800-1000 nm for Z_{eff}-analysis in ASDEX. In: Proc. 13th Europ. Conf. on Contr.Fusion and Plasma Heating, Eds. G. Briffod, M. Kaufmann, EPS, Schliersee 1986, 10 C, Part I, 93-96.

131 Roth, J., W.Möller, D.B.Poker[1] and K.Wittmaack[1]:
Ion induced self diffusion of carbon. Nucl. Instr. & Meth. in Phys. Res. B13, 409-415 (1986).

132 Ryter, F., ASDEX-Team[2] und LH-Group[9]:
Study of fast ions during lower hybrid experiments on ASDEX. In: Proc. of Varenna Workshop, Eds. S.Bernabei, V.Gasparino, E.Sindoni, 1985, II, 746-751.

133 Ryter, F., H.Brocken, A.Izvozchikov[1], F.Leuterer, H.Maaßberg, H.M.Mayer, F.X.Söldner, K.Steinmetz, G.Becker, H.S.Bosch, A.Eberhagen, D.Eckhartt, G.Fussmann, O.Gehre, J.Gernhardt, G.v.Gierke, E.Glock, O.Gruber, G.Haas, J.Hofmann, G.Janeschitz, F.Karger, M.Keilhacker, O.Klüber, M.Kornherr, K.Lackner, M.Lenoci, G.Lisitano, F.Mast, K.McCormick, D.Meisel, V.Mertens, E.R.Müller, H.Murmann, H.Niedermeyer, J.-M.Noterdaeme, A.Pietrzyk[1], W.Poschenrieder, H.Rapp, H.Riedler, H.Röhr, J.Roth, F.Schneider, C.Setzensack, G.Siller, P.Smeulders[1], E.Speth, K.-H. Steuer, O.Vollmer, F.Wagner, F.Wesner and D.Zasche:
Comparison of ICRH and LH accelerated hydrogen ions in NI heated ASDEX plasmas. In: Proc. 13th Europ. Conf. on Contr. Fusion and Plasma Heating, Eds. G. Briffod, M. Kaufmann, EPS, Schliersee 1986, 10 C, Part I, 101-104.

134 Sawicka, B.D.[1], J.A.Sawicki[1], F.E.Wagner, W.Möller, P.Børgesen and R.Wordel[1]:
Mössbauer study of the modification of iron during bombardment with deuterium at low temperature. Hyperfine Interact. 29, 1205 (1986).

135 Scherzer, B.M.U.:
Bubbles, blisters and exfoliation. In: Erosion and Growth of Solids Stimulated by Atom and Ion Beams. Eds. G.Kiriakidis, G.Carter, J.L.Whitton, Martinus Nijhoff Publishers, Dordrecht, Boston, Lancaster, NATO ASI Series E. Appl. Sciences 112, 1986, 222-246.

136 Schlüter, A.:
Die Chancen des Fusionsreaktors. Atomwirtschaft, Atomtechnik 31/1, 34-37 (1986).

137 Schlüter, A:
Remarks on MHD stability of general toroidal confinement systems. In: Proc. Course and Workshop on Basic Physical Processes of Toroidal Fusion Plasmas, Varenna 1985, EUR10418EN, 251-257 (1986).

138 Schmitter, K.H.:
Fusionstechnologie. Atomwirtschaft, 31 (8-9), 455-456, (1986).

139 Schumacher, U.:
Considerations for alpha particle diagnostics. Physica Scripta 34, 560-564 (1986).

140 Schumacher, U.:
Measurements of crystal properties for versatile double crystal monochromators in fusion plasma spectroscopy. Nucl. Instr. Meth. in Phys. Research A251, 564-573 (1986).

141 Schwenn, U.:
Computation on nonlinear nonlocal ideal MHD modes. In: Proc. 8th Europhys. Conf. on Comp. Physics, Ed. J.Nührenberg, Eibsee 1986, 10D, 149-152 (1986).

142 Seidel, U., K.Lackner, G.Lappus[1], H.Preis and H.Woyke[1]:
Plasma position control in ASDEX Upgrade. In: Tokamak Start-up, Problems and Scenarios Related to the Transient Phases of a Thermonuclear Fusion Reactor, Ed. H.Knoepfel, Plenum Press, New York 1986, 325-336.

143 Smeulders, P.:
Tomography of quasi-static deformations of constant-emission surfaces of high-beta pasmas in ASDEX. Nucl. Fusion, 26, 267 (1986).

144 Söldner, F.X., D.Eckhartt, F.Leuterer, K.McCormick, G.Becker, H.S.Bosch, H.Brocken, H.Derfler, A.Eberhagen, G.Fussmann, O.Gehre, J.Gernhardt, G.v.Gierke, E.Glock, O.Gruber, G.Haas, J.Hofmann, A.Izvozchikov[1], G.Janeschitz, F.Karger, M.Keilhacker, O.Klüber, M.Kornherr, K.Lackner, M.Lenoci, G.Lisitano, F.Mast, H.M.Mayer, D.Meisel, V.Mertens, E.R.Müller, M.Münich, H.Murmann, H.Niedermeyer, A.Pietrzyk[1], W.Poschenrieder, H.Rapp, H.Riedler, H.Röhr, J.Roth, F.Ryter[1], F.Schneider, C.Setzensack, G.Siller, F.Smeulders[1], E.Speth, K.-H.Steuer, T.Vien, O.Vollmer, F.Wagner, D.Zasche and M.Zouhar:
Stabilization of sawtooth oscillations by lower hybrid waves in ASDEX. In: Proc. 13th Europ. Conf. on Contr. Fusion and Plasma Heating, Eds. G. Briffod, M. Kaufmann, EPS, Schliersee 1986, 10 C, Part II, 319-322.

145 Söldner, F.X., K.McCormick, D.Eckhartt, M.Kornherr, F.Leuterer, R.Bartiromo, G.Becker, H.S.Bosch, H.Brocken, H.Derfler, A.Eberhagen, G.Fussmann, O.Gehre, J.Gernhardt, G.v.Gierke, A.Giuliana, E.Glock, O.Gruber, G.Haas, M.Hesse, J.Hofmann, A.Izvozchikov[1], G.Janeschitz, F.Karger, M.Keilhacker, O.Klüber, K.Lackner, M.Lenoci, G.Lisitano, F.Mast, H.M.Mayer, D.Meisel, V.Mertens, E.R.Müller, M.Münich, H.Murmann, H.Niedermeyer, A.Pietrzyk[1], W.Poschenrieder, H.Rapp, H.Riedler, H.Röhr, F.Ryter[1], K.H.Schmitter, F.Schneider, C.Setzensack, G.Siller, P.Smeulders[1], E.Speth, K.-H.Steuer, T.Vien, O.Vollmer, F.Wagner, F.v.Woyna and D.Zasche:
Suppression of sawtooth oscillations by lower-hybrid current drive in the ASDEX tokamak. Phys. Rev. Lett. 57, 1137-1140 (1986).

146 Söldner, F.X., M.Brambilla, D.Eckhartt, A.Giuliana[1], F.Leuterer, V.Mertens, H.Murmann, F.Ryter[1], R.Bartiromo[1], G.Becker, H.S.Bosch, H.Brocken, R.Burhenn, H.Derfler, A.Eberhagen, G.Fußmann, O.Gehre, J.Gernhardt, G.v.Gierke, E.Glock, O.Gruber, H.Haas, M.Hesse[1], G.Janeschitz, F.Karger, M.Keilhacker, A.J.Kislyakov[1], O.Klüber, M.Kornherr, P.B.Kotzé[1], M.Lenoci[1], G.Lisitano, H.M.Mayer, K.McCormick, D.Meisel, E.R.Müller, M.Münich, H.Niedermeyer, W.Poschenrieder, H.Rapp, H.Röhr, N.Ruhs, K.H.Schmitter, F.Schneider, G.Siller, P.Smeulders, K.-H.Steuer, T.Vien, G.Vlases[1], F.Wagner, F.v.Woyna and M.Zouhar:
Electron and ion heating by lower hybrid waves in ASDEX. In: Proc. Varenna Workshop, Eds. S.Bernabei, V.Gasparino, E.Sindoni, 1985, II, 740-745.

147 Speth, E., O.Gruber, G.Janeschitz, H.Murmann, H.Niedermeyer, F.Wagner, O.Vollmer and ASDEX-Team[2]:
Neutral beam deposition experiments at elevated densities in ASDEX. In: Proc. 13th Europ.Conf. on Contr.Fus. and Plasma Heating, Eds.: G.Briffod, M.Kaufmann, EPS, Schliersee 1986, 10C, Part II, 281-284.

148 Steinmetz, K., F.Wagner, F.Wesner, A.Izvozchikov, J.-M.Noterdaeme, F.Ryter, ICRH-Team[8], ASDEX-Team[2] and NI-Team (ASDEX)[4]:
ICRF H-mode and $2\Omega_{CH}/D(H)$-minority heating on ASDEX. In: Proc. 13th Europ.Conf. on Controlled Fusion and Plasma Heating, Eds. G.Briffod, M.Kaufmann, Schliersee 1986, 10C, Part II, 21-24 (1986).

149 Steinmetz, K., F.Wesner, H.Niedermeyer, ICRH-Team[8], ASDEX-Team[2] and NI-Team (ASDEX)[4]:
Ion cyclotron resonance heating in the divertor tokamak ASDEX. Journ. Vac. Sci. Technol. A, 4 (3), 1088 (1986).

150 Steinmetz, K., G.Fussmann, O.Gruber, H.Niedermeyer, E.R.Müller, F.Ryter, F.Wagner, F.Wesner, ICRH-Team[8], ASDEX-Team[2] and NI-Team (ASDEX)[4]:
High power ICRF heating on the divertor tokamak ASDEX. Plasma Physics and Controlled Fusion, 28 (1A) 235 (1986).

151 Stredulinsky, E.[1], R.Meyer-Spasche and D.Lortz:
Asymptotic behavior of solutions of certain parabolic problems with space and

time dependent coefficients. Comm.Pure Appl.Math. 39, 233-266 (1986).

152 Streibl, B., S.B.Mukherjee, R.Pöhlchen, R.Carezzano[1], P.L.Cimbrico[1], M.Danese[1], P.Gagliardi[1], A.Laurenti[1], G.Prini[1] and G.Varni[1]:
Method of manufacturing the ASDEX Upgrade toroidal field (TF) coils. In: Proc. 9th Int. Conf. on Magnet Techn.(MT-9), Eds. C.Marinucci, P.Weymuth, Zürich/Switzerland 1986, 46-49.

153 Taglauer, E. and J.Onsgaard[1]:
Angular distribution of sputtered particles measured by quartz crystal microbalances and Auger electron spectroscopy. Appl. Phys. Lett. 48,(9), 575-582 (1986).

154 Taglauer, E., N.Tolk[1], R.Riedel[1], E.Colavita[1], G.Margaritondo[1], N.Gershenfeld[1], N.Stoffel[1], J.A.Kelber[1], G.Loubriel[1], A.S.Bommanavar[1], M. Bakshi[1] and Z.Huric[1]:
Temperature dependence of photon stimulated desorption of ground state and excited state Na from NaCl. Surf. Sci. 169, 267-274 (1986).

155 Taglauer, E., P.Varga[1] and K.Ertl:
Analysis of TiC and TiN coatings exposed to fusion plasmas. Vacuum 36, No 1-3, 23-25 (1986).

156 Taglauer, E.:
Atomic collision processes during plasma-wall interaction in fusion devices. Nucl. Instr. Meth. B13, 218-224 (1986).

157 Tasso, H.:
Lyapunov stability and attractors of some system of nonlinear oscillators. Z. Naturforsch. 41a, 987-988 (1986).

158 Tasso, H.:
On phase space and statistics of continua. Z. Naturforsch. 41a, 1258-1259 (1986).

159 Thomsen, K. et al. (from IPP: H.Krause, F.Mast and A.Stäbler):
Energy transport in JET with ohmic and auxiliary heating. In: Proc. 13th Europ. Conf. on Contr.Fus. and Plasma Heating, Eds. G.Briffod, M.Kaufmann, Schliersee 1986, 10C, Part I, 29-32.

160 Tutter, M. and W VII-A Team[3]:
Calculation of the influence of suprathermal electron radiation on ECE spectra, with oblique direction of observation. Proc. 13th Europ. Conf. on Contr. Fus. and Plasma Heating, Eds. G.Brifford, M.Kaufmann, EPS, Schliersee, 1986, 10 C, Part I, 311-314.

161 Verbeek, H.:
A low-energy neutral particle analyzer for plasma experiments. J.Phys. E: Sci. Instrum. 19, 964-970 (1986).

162 Vernickel, H.:
Choice of materials for the first-wall of magnetic confinement fusion devices. High Temperatures - High Pressures 18, 119-126 (1986).

163 Wagner, F. et al.:
An experimental study of the principles governing tokamak transport. Phys. Review Lett. 56, 2187 (1986).

164 Wagner, F. et al.:
Combined application of neutral injection, lower hybrid, and ion cyclotron resonance heating in ASDEX and synergetic effects. 13th Europ. Conf. on Controlled Fusion and Plasma Heating, Schliersee, April 1986 (Invited Paper). In: Plasma Phys. and Contr. Fus. 9A, 1225-1239 (1986).

165 Wagner, F., ASDEX-Team[2] and NI-Team (ASDEX)[4]:
The H-regime of ASDEX. In: Proc. Workshop on Basic Physical Processes of Toroidal Fusion Plasmas. Varenna 1985, Eds. S.Bernabei, V.Gasparino, E.Sindoni, EUR 10418, Brüssel 1986, II, 65-86.

166 Wagner, F.:
The H-mode of ASDEX, a favourable operational regime of tokamak plasmas at near-ignition Conditions. Europhys. News 17, 4, 48 (1986).

167 Wandelt, K.[1], W.Jacob, N.Memmel and V.Dose:
Inverse Photoemission of adsorbed xenon multilayers on Ru(001): Refutation of final state screening effects. Phys. Rev. Lett. 57, 1643 (1986).

168 Wesner, F., F.Braun, J.Wyss[1] und W.Schminke[1]:
HF-Anordnung zur Aufheizung von Plasmen im Bereich der Ionenzyklotronfrequenz. Atomwirtschaft, 31, 38-41, (1986).

169 Wesner, F., J.-M.Noterdaeme, J.Bäumler, F.Braun, F.Hofmeister und H.Wedler:
ICRF Heating for the ASDEX-Upgrade Tokamak. In: Proc. 13th Europ.Conf. on Contr.Fus. and Plasma Heating, Eds. G.Briffod, M.Kaufmann, EPS, Schliersee 1986, 10C, Part II, 173-176.

170 Winter, J.[1], H.G.Esser[1], P.Wienhold[1], V.Philipps[1], E.Vietzke[1], E.H.Besocke[1], W.Möller and B.Emmoth[1]:
Properties of carbonisation layers relevant to plasma surface interaction. Nucl. Instr. Meth B, 415-421 (1986).

171 Wobig, H. and W VII-A Team[3]:
A transport model of ECR-heated plasmas in W VII-A. Proc. 13th Europ. Conf. on Contr. Fus. and Plasma Heating, Eds. G.Brifford, M.Kaufmann, EPS, Schliersee, 1986, 10 C, Part I, 291-294.

172 Wobig, H.:
A dissipative model of plasma equilibrium in toroidal systems. Zeitung für Naturforschung 41a, 1101-1110 (1986).

173 Wobig, H.:
Magnetic surfaces and localized perturbations in the stellarator Wendelstein VII-A. Proc. 8th Europhys. Conf. on Comp. Phys. Ed. J. Nührenberg, EPS, Eibsee 1986, 10D, 161.

174 Zehrfeld, H.P. and H.Bruhns:
Magnetohydrodynamic compact flow equilibria. In: Proc. 8th Europhys. Conf. on Comp. Phys., Ed. J.Nührenberg, EPS, Eibsee 1986, 10D, 19-22.

175 Zehrfeld, H.P.:
Free boundary flow equilibria for ASDEX and ASDEX Upgrade. In: Proc. 13th Europ. Conf. on Contr. Fus. and Plasma Heating, Eds. G.Briffod, M.Kaufmann, EPS, Schliersee 1986, 10C, Part I, 57-60.

176 Zimmermann, D.:
A local area network in the ASDEX data acquisition system. In: Proc. 11th Symp. on Fus. Engineering, Austin, Texas 1985, I, 297-300.

177 Zouhar, M., T.Vien, F.Leuterer, M.Münich, M.Brambilla, H.Derfler, D.Eckhartt, F.v.Woyna and ASDEX-Team[2]:
Coupling of lower hybrid waves to the ASDEX Plasma. In: Proc. 13th Europ.Conf. on Contr.Fus. and Plasma Heating, Eds. G.Briffod, M.Kaufmann, EPS, Schliersee 1986, 10C, Part II, 378-381.

DOCTORAL THESES

178 Bosch, H.S.:
Diagnostik geladener Fusionsreaktorprodukte an ASDEX. Technische Universität München 1986.

179 Braams, B.J.:
Computational studies in tokamak equilibrium and transport. University of Utrecht, The Netherlands, 1986.

180 Engelmann, G.:
Einfluß der Oberflächentemperatur auf die Streuung von niederenergetischen Ionen (ISS) an einer Cu(110)-Oberfläche. Technische Universität München, 1986.

181 Kardaun, O.:
On Statistical Survival Analysis. University of Groningen, 1986.

182 Rogozik, J.:
Bremsstrahlungs-Spektroskopie an adsorbierten Molekülen. Universität Würzburg, 1986.

DIPLOMA THESES

183 Dürr, H.:
Neutralisation und Ionisation von Edelgasionen an Metalloberflächen. Universität Würzburg, 1986.

184 Hartwig, D.:
Ionenstreuexperimente an reinen und adsorbatbedeckten Metalloberflächen. Universität Würzburg, 1986.

185 Memmel, N.:
Inverse Photoemissionsstudie der Adsorption von Kohlenmonoxid sowie der Koadsorption von Kohlenmonoxid und Kalium auf einer Ruthenium-Oberfläche. Universität Würzburg, 1986.

186 Rudyj, A.:
Untersuchung der Randschichtfluktuation am Divertor-Tokamak ASDEX. Technische Universität München, 1986

187 Senftinger, B.:
Winkelselektiver Photonennachweis bei der inversen Photoemission. Universität Würzburg, August 1986.

PATENTS

188 Derfler, H., J.Perchermeier und H.Spitzer:
Verhinderung von Störungen durch Sekundärelektronenemission. (11383); Europa 0113907 (D, B, F, I, Lux, NL, S, A, CH, GB); erteilt: 16.04.1986

189 Frischmuth, H., J.Perchermeier, A.Stimmelmayr und H.Weichselgartner:
Gaschromatographie-Wasserstoff-Isotopentrennung. (11307); Europa 0113049 (D, GB, F, I, S, CH); erteilt: 04.06.1986; Kanada 1,201,390; erteilt: 04.03.1986

190 Haas, G.:
Heißkathoden-Ionisationsmanometer. (12031); Deutschland P 36 28 847.0; angemeldet: 25.08.1986; Deutschland Gbm 86 22 773.4; angemeldet: 25.08.1986; eingetragen: 04.12.1986

191 Kasparek, W.[1] und G.Müller[1]:
Wellenzahl-Spektrometer für überdimensionierte Mikrowellenhohlleiter. (11811); Europa 86108332.7 (D, F, GB, NL, I, CH); angemeldet: 19.06.1986

192 Kotzlowski, H.*:
Aktiv gekühlte Einrichtung. (11571); Europa 181385 (D, B, F, GB, I, Lux, NL, A, CH); erteilt: 21.05.1986

193 Kotzlowski, H.:
Hitzeschild. (11015); USA 4,619,807; erteilt: 28.10.1986

* In cooperation with a company.

194 Kotzlowski, H.:
Verfahren und Vorrichtung zum Bolzenschweißen. (11042); Europa 82107065.3 (GB, F, I); erteilt: 30.12.1986

195 Liebl, H.:
Kombinierte elektrostatische Objektiv- und Emissionslinse. (11299); Großbritannien 2,128,396; erteilt: 03.04.1986

196 Müller, G.[1] und R.Wilhelm[1]:
Mikrowellenfenster. (11951); Deutschland P 36 17 779.2; angemeldet: 27.05.1986

197 Schneider, F.:
Synchronisierter Meßverstärker. (12032); Deutschland P 36 27 610.3; angemeldet: 14.08.1986

198 Schüller, P.[1] und R.Wilhelm[1]:
Feststoffabsorber. (11952); Deutschland Gbm 86 10 138.2; angemeldet: 14.04.1986; eingetragen: 13.11.1986

199 Schüller, P.[1] und R.Wilhelm[1]:
Mikrowellenkalorimeter. (11953); Deutschland Gbm 86 10 137.4; angemeldet: 14.04.1986; eingetragen: 13.11.1986

200 Spensberger, W.:
Hohlleiterelement für Mikrowellen. (11635); Deutschland P 34 27 283.6; offengelegt: 30.01.1986

201 Weichselgartner, H.:
Tritiumrückhaltesystem für mehrere Arbeitsräume. (11754); Deutschland P 35 11 320; erteilt: 09.10.1986; Europa 86100009.9 (D, B, F, GB, I, Lux, NL, A, S, CH); angemeldet: 02.01.1986; offengelegt:15.10.1986; Japan 61/65035; angemeldet: 25.03.1986; USA 826,138; angemeldet: 04.02.1986

202 Weichselgartner, H.:
Verfahren und Einrichtung zum Entfernen von Tritium. (10802); Deutschland P 30 25 494; erteilt: 16.01.1986

203 Weichselgartner, H.:
Verfahren zum Dekontaminieren der Oberfläche eines Gegenstandes. (11654); Deutschland P 34 46 931; offengelegt: 03.07.1986; Europa 0185393 (D, B, F, GB, I, NL, A, S, CH); offengelegt: 25.06.1986

LECTURES

204 Altmann, W., K.Desinger, V.Dose, H.Eschenbacher[1] und T.Fauster:
Ein Spektrometer für inverse Photoemission mit variabler Photonenenergie. Verhandl. DPG (VI) 21, 1409 (1986).

205 Andelfinger, C., E.Buchelt, M.Ulrich and G.Weber:
Device for varying pellet size in a centrifuge pellet injector. 14th SOFT, Avignon 1986, Comm. EC, EP40.

206 Baretzky, B., W.Möller and E.Taglauer:
Collisional processes in preferential sputtering of tantalum oxide. Internat. Conf.on Sputtering of Solids, (SOS) Spitz, Österreich, June 1986.

207 Behringer, K. et al. (from IPP: G.Fussmann):
Impurity production mechanisms and behaviour during additional heating in JET. 11th Int. Conf. on Plasma Phys. and Contr. Nucl. Fusion Res., Kyoto 1986.

208 Behrisch, R., J.Ehrenberg, A.P.Martinelli, P.E.Stott[1], G.M.McCracken[1], J.P.Coad[1] and L.de Kock[1]:
Änderung der Oberflächenschichten des Limiters von JET in verschiedenen Experimentierphasen. Verhandl. DPG (VI) 21, 112 (1986).

209 Behrisch, R., J.Ehrenberg, H.Bergsaker[1], J.P.Coad[1], L.de Kock[1], B.Emmoth[1], H.Kukral, A.P.Martinelli, G.M.McCracken[1] and J.W.Partridge[1]:
Contamination of the JET limiters with metals during the different operational phases. 7th Int. Conf. on Plasma Surface Interactions in Controlled Fusion Devices, Princeton, USA, May 1986.

210 Behrisch, R., J.Ehrenberg, M.Wielunski, A.P.Martinelli, H.Bergsaker[1], B.Emmoth[1], L.de Kock[1] and J.P.Coad[1]:
Hydrogen and deuterium retention in wall samples of JET. 7th Int. Conf. on Plasma Surface Interactions in Controlled Fusion Devices, Princeton, USA, May 1986.

211 Behrisch, R.:
Sputtering in fusion devices. (Invited talk). Int. Conf. on Sputtering of Solids (SOS), Spitz, Österreich, May 1986.

212 Behrisch, R.:
Surface layer modifications at the solid walls in high temperature plasma experiments. (Invited talk). Int. Conf. on Ion Beam Material Modifications, Catania, Italien, June 1986.

213 Behrisch, R.:
Die Plasma-Festkörper-Wechselwirkung. (Invited talk). Physikalisches Kolloquium, Universität Gießen, November 1986.

214 Bergsaker, H.[1], R.Behrisch, J.P.Coad[1], J.Ehrenberg, B.Emmoth[1], S.K.Erents[1], G.M.McCracken[1], A.P.Martinelli and J.W.Partrigde[1]:
Hydrogen isotope retention at the JET limiters. 7th Int. Conf. on Plasma Surface Interactions in Controlled Fusion Devices, Princeton, USA, May 1986.

215 Biskamp, D., D.Pfirsch and F.Pohl:
Variational principles for tokamak profiles. 11th Int. Conf. on Plasma Physics and Contr. Nucl. Fus. Res., Kyoto 1986, IAEA-CN-47/I-I-5.

216 Biskamp, D.:
Numerical simulation of drift wave turbulence. Int. Workshop on Small Scale Turbulence and Anomalous Transport, Cargése, Corsica, July 1986.

217 Biskamp, D.:
On the theory of the sawtooth disruption. 11th Int. Conf. on Plasma Physics and Contr. Nucl. Fus. Res., Kyoto 1986, IAEA-CN-47/E-I-1-2.

218 Blaumoser, M., D.Dorst, A.Wieczorek, F.Feilcke[1] and W.Weigand[1]:
ASDEX Upgrade - OH circuit. 14th SOFT, Avignon 1986, Comm. EC, CP52.

219 Blaumoser, M., M.Kottmair, A.Wieczorek and O.Gruber:
ASDEX Upgrade - Power supply systems. 14th SOFT, Avignon 1986, Comm. EC, CP51.

220 Bohdansky, J. and J.Roth:
Temperature dependence of sputtering behaviour of Cu-Li alloys. 7th Int. Conf. on Plasma Surface Interactions in Controlled Fusion Devices, Princeton, USA, May 1986.

221 Bohdansky, J., A.Croessmann[1], J.Linke[1], J.M.McDonald[1], D.M.Morse[1], A.E.Pontau[1], R.D.Watson[1], J.B.Whitley[1], D.M.Goebel[1], Y.Hirooka[1], O.Leung[1], R.W.Conn[1], J.Roth, W.Ottenberger and H.Kotzlowski:
Behaviour of graphite under heat load and in contact with a hydrogen plasma. 7th Int. Conf. on Plasma Surface Interactions in Controlled Fusion Devices, Princeton, USA, May 1986.

222 Bosch, H.-S., U.Schumacher and ASDEX-Team[2]:
Measurements of charged fusion products in ASDEX. Proc. 3rd JET Workshop on Neutron and Charged Particle Diagnostics, Culham 1986, JET-IR(86)04, 135.

223 Bosch, H.S., U.Schumacher und ASDEX-Team[2]:
Plasmadiagnostik mit Fusionsprotonen und -tritonen in ASDEX. Verhandl. DPG (VI) 21, 59 (1986).

224 Bosch, H.S.:
Plasma diagnostics with charged fusion products from the D-D reactions in ASDEX Course and Workshop on Application of RF Waves to Tokamak Plasmas, Varenna 1986 (to be published).

225 Brambilla, M. and T.Krücken:
1-d Modell für Wellenausbreitung in der Nähe der Ionenzyklotronenresonanz in Tokamak Plasmen. Verhandl. DPG (VI) 21, 59 (1986).

226 Brambilla, M.:
A critical review of global modelling of HF waves at ion cyclotron frequencies in tokamaks. Europ. Theory Meeting, Wepion/Belgium, June 1986.

227 Cattanei, G., W VII-A Team[3] and ICRH-Team[8]:
ICRH in the WENDELSTEIN VII-A Stellarator. Verhandl. DPG (VI) 21, 64 (1986).

228 Cheetham, A.D.[1], A.Gondhalekar[1], K.Büchl, M.Bures[1], D.Campbell[1], A.Edwards[1], R.Cranetz[1], N.Gottardi[1], F.Hendriks[1], P.D.Morgan[1], J.O'Rourke[1], F.Schüller[1], M.Watkins[1] and A.Weller:
Results of pellet injection experiments in JET. Course and Workshop on Basic and Advanced Fusion Plasma Diagnostic Techniques. Int. School of Plasma Physics Varenna, September 1986.

229 Cordey, J.G. et al. (from IPP: H.Jäckel and A.Stäbler):
Energy confinement with ohmic and strong auxiliary heating in JET. 11th Int.Conf. Plasma Phys. and Conf.Nucl.Fus.Res., Kyoto 1986 (to be publ.).

230 Desinger, K., V.Dose und R.Drube:
Unbesetzte Zustände an schwefelbedeckten Nickeloberflächen. Verhandl. DPG (VI) 21, 1381 (1986).

231 Donath, M., V.Dose, M.Glöbl[1] und B.Senftinger:
Messung von Symmetrien unbesetzter elektronischer Zustände. Verhandl. DPG (VI) 21, 1413 (1986).

232 Dorst, D., G.Grieger, R.Mathis and J. Sapper:
The Wendelstein VII-AS experiment. (Invited Paper) 14th SOFT, Avignon 1986, EI.01.

233 Dose, V.:
Adsorbate induced empty electronic states. (Invited talk). Université de Haute Alsace, Mühlhausen, France, October 1986.

234 Dose, V.:
Adsorbate induced unoccupied electronic states. (Invited talk). Proc. 8th Int. Conf. on Vacuum Ultraviolet Radiation Physics (VUV), Göteborg, Sweden, August 1986.

235 Dose, V.:
Electron structure of metals and semiconductors. (Invited talk). 10th Internat. Vac. Congress, 6th Int. Conf. of Solid Surfaces, 33th Nat.Symp. of the Am. Vac. Soc., Baltimore, Maryland, USA, October 1986. In: Proc. Am. Vac. Soc., 1986, 163.

236 Dose, V.:
Image potential surface states. (Invited talk). Adriatico Conf., Symp. on Dynamical Screening and Spectroscopy of Surfaces, Trieste, Italy, June 1986.

237 Dose, V.:
Instrumentation in Inverse Photoemission. (Invited talk). Lectures on Surface Sci., Eds. Castro, M. Cardona, Caracas, Venezuela, August 1986.

238 Dose, V.:
Wo stehen wir in der Oberflächenphysik? (Invited talk). Kolloquium, Fritz-Haber-Institut Berlin, BESSY Mai 1986.

239 Duesing, G., P.Lomas, A.Stäbler, P.Thomas and E.Thompson:
First neutral beam heating experiments on JET. Royal Society Discussion Meeting on the JET Project and the Pospects for Controlled Nuclear Fusion, London, March 1986; (to be published in: Phil.Trans.Roy.Soc. (Series A))

240 Dürr, H., D.Hartwig und T.Fauster:
Anregung und Neutralisation von niederenergetischen Ne-Ionen an Nickel-Oberflächen. Verhandl. DPG (VI) 21, 1423 (1986).

241 Eckstein, W.:
Atomare Prozesse in der Plasma-Wand-Wechselwirkung. Verhandl. DPG (VI), 21, 62 (1986).

242 Eckstein, W.:
Direct recoil sputtering and secondary ion production. (Invited talk). IISC-6, Argonne Nat. Lab., IL, USA, Aug. 1986.

243 Eckstein, W.:
Low energy sputtering model. (Invited talk). Topical Symp. on Sputtering, Baltimore, Maryland, USA, Oct. 1986.

244 Eckstein, W.:
Recoil spectroscopy. (Invited talk). Oak Ridge Nat. Lab, TN, USA, July 1986.

245 Eckstein, W.:
Spektroskopie von Recoil-Atomen. (Invited talk). Universität Gießen, Dezember, 1986.

246 Eckstein, W.:
Zerstäubung und Rückstreuung mit Computer-Simulation. (Invited talk). Universität Linz, Österreich, November 1986.

247 Ehrenberg, J., R.Behrisch, J.P. Coad[1], L.de Kock[1], D.H.J.Goodall[1], G.M.McCracken[1] and A.P.Martinelli:
The redistribution of metals on the JET vessel wall. 7th Int. Conf. on Plasma Surface Interactions in Controlled Fusion Devices, Princeton, USA, May, 1986.

248 Ehrenberg, J.:
Modelling of isotope exchange experiments. 7th Int. Conf. on Plasma Surface Interactions in Controlled Fusion Devices, Princeton, USA, May 1986.

249 Elsner, A.:
Interdependence of surface tension, vapor pressure and fluid density of saturated fluids. 6th Cryogenics Intersociety Symp., Annual AIChE Meeting 1986.

250 Engelmann, G. und E.Taglauer:
Neutralisationseffekte bei der Streuung von Ne^+ und Na^+ an Cu(110). Verhandl. DPG (VI) 21, 1423 (1986).

251 Erckmann, V., R.Wilhelm[1], O.Janzen[1], W.Kasparek[1], G.Müller[1], E.Räuchle[1], P.G.Schüller[1], K.Schwörer[1], M.Thumm[1] und W VII-A Team[3]:
Elektronen-Zyklotron Heizung am Stellarator W VII-A. Verhandl. DPG (VI) 21, 56 (1986).

252 Erckmann, V., W VII-A Team[3] and ECRH Group (IPF Stuttgart)[7]:
ECRH experiments in the W VII-A stellarator with O- and X-Mode. Proc. Int. Stellarator/Heliotron Workshop, Kyoto, Japan 1986.

253 Erckmann, V., W VII-A Team[3], ECRH Group (IPF Stuttgart)[7] und NI-Team (W VII-A)[5]:
Plasmaverhalten im W VII-A Stellarator mit ECRH. IPF-Kolloquium Universität Stuttgart, 1986.

254 Erckmann, V., W.Kasparek[1], G.A.Müller[1], P.G.Schütter[1], M.Thumm[1] and R.Wilhelm[1]:
The 70 GHz/1MW long pulse ECRH-system on the advanced stellarator W VII-AS. 14th SOFT, Avignon 1986, paper CP 25.

255 Erckmann, V., W.Kasparek[1], H.Kumric[1], G.A.Müller[1], P.G.Schüller[1], M.Thumm[1] and R. Wilhelm[1]:
Components for transmission of very high power mm-waves (200 kW at 28, 70 and 140 GHz) in overmoded circular waveguides). Contribution to MIOP 1986, Wiesbaden.

256 Erckmann, V.:
ECRH on the W VII-A stellarator with 28 and 70 GHz. Workshop, KfK Karlsruhe, Dec. 86, (to be publ. in Proc. 4th Gyrotron Development).

257 Evans, T.E. et al. (from IPP: G.Haas): Analysis of TEXT intra-island limiter experiments. Bull. Am. Phys. Soc. 31, 9, 1572 (1986).

258 Fauster, T., H.Dürr and D.Hartwig: Determination of the geometry of sulphur on nickel surfaces by low energy ion scattering. 8th European Conf. on Surf. Science, (ECOSS), KFA Jülich, April 1986.

259 Fauster, T., H.Dürr and D.Hartwig: Determination of the positions of adsobarte atoms by low-energy ion scattering. (Invited talk). University of Texas, USA, July 1986.

260 Fauster, T.: Die Bestimmung der Position von Oberflächenatomen durch Ionenstreuung. (Invited talk). Kolloquium Universität Würzburg, Mai 1986.

261 Feist, J.-H., S.Götz, and J.Sielanko: Calculations and measurements: Ion removal system in the ASDEX/W VII-AS long-pulse neutral-injection beam line. 14th SOFT, Avignon 1986 (to be publ.).

262 Feist, J.-H., W.Kraus, E.Speth, J.Freisinger[1], and M.Kaufmann[1]: Test of an rf-ion source with a large scale extraction system. 14th SOFT, Avignon 1986 (to be publ.).

263 Freund, H.-J.[1], J.Rogozik and V.Dose: Combined photoelectron and Brems-strahlungs-Isochromat, spectroscopic study of the system CO/Ni(110): Strong inter-molecular interaction. Verhandl. DPG (VI) 21, 1385 (1986).

264 Fussmann, G., J.Hofmann, G.Janeschitz et al.: Impurity production and plasma performance in ASDEX discharges with ohmic and auxiliary heating. 7th Conf. on Plasma Surface Inter-action, Princeton 1986, (to be published in J.Nucl.Mater.).

265 Fussmann, G.: Charge exchange recombination radiation of Na and Li-like ions in ASDEX. QUACS-Meeting, St. Hilda's College, Oxford, Sept. 1986.

266 Fussmann, G.: Spektroskopie an Fusionsplasmen. Verhandl. DPG (VI) 21, 18 (1986).

267 Gehre, O.: Measurements of electron density profiles on ASDEX by means of HCN-laser interferometry. Course and Workshop on Application of RF waves to Tokamak Plasmas, Varenna 1986 (to be published).

268 Goede, A.P.H., C.Challis, T.T.C.Jones, A.Stäbler, D.Storck and E.Thompson: Performance of the first JET neutral beam injector. 14th SOFT, Avignon 1986 (to be publ.).

269 Goldston, R.J. et al. (from IPP: F.Wagner): Energy confinement and profile consistency in TFTR. 11th Int. Conf. on Plasma Phys. and Contr. Nucl. Fusion Res., Kyoto 1986.

270 Grassie, K., G.Becker, O.Gruber, O.Klüber, K.Lackner and H.P.Zehrfeld: Stability analysis of ASDEX discharges. Int. Workshop on Small Scale Turbulence and Anomalous Transport in Magnetised Plasmas, Cargese/Corsica, July 1986.

271 Grieger, G. and INTOR Group[11]: Heating and current drive for INTOR. Proc. 11th Int. Conf. on Plasma Physics and Contr. Nucl. Fus. Res., Kyoto, Japan 1986 (IAEA-CN-47, paper G.I-5, to be publ. in Nuclear Fus., Supplement, IAEA Vienna, 1987).

272 Grieger, G. and INTOR Group[11]: Impurity control studies for INTOR. Proc. 11th Int. Conf. on Plasma Physics and Contr. Nucl. Fus. Res., Kyoto, Japan 1986 (IAEA-CN-47, paper G.I-3, to be publ. in Nuclear Fus., Suppl., IAEA Vienna, 1987).

273 Grieger, G. and INTOR Group[11]: INTOR: Operational limits and confinement. Proc. 11th Int. Conf. on Plasma Physics and Contr. Nucl. Fus. Res., Kyoto, Japan 1986 (IAEA-CN-47, paper G.I-4, to be publ. in Nuclear Fus., Suppl., IAEA Vienna, 1987).

274 Grieger, G. and INTOR Group[11]: Overview of INTOR Workshop (presented by G. Grieger). Proc. 11th Int. Conf. on Plasma Physics and Contr. Nucl. Fus. Res., Kyoto, Japan 1986 (IAEA-CN-47, paper G.I-1 to be publ. in Nuclear Fusion, Supplement, IAEA Vienna, 1987).

275 Grieger, G., J.Kißlinger, E.Harmeyer, F.Rau and H.Wobig: Advanced stellarator and burner studies. Proc. 4th Technical Committee Meeting and Workshop on Fusion Reactor Design, Yalta, USSR, 1986 (to be publ. by IAEA, Vienna).

276 Grieger, G.: Tokamak concept innovations. Proc. 4th Technical Committee Meeting and Workshop on Fusion Reactor Design, Yalta, USSR, 1986 (to be publ. by IAEA, Vienna).

277 Gruber, O., ASDEX-Team[2], NI-Team (ASDEX)[4], ICRH-Team[8], LH-Group[9] and Pellet-Team[10]: Observation of profile consistency in ASDEX. Europ. Tokamak Physics Workshop, Toledo/Spain, December 1986.

278 Gruber, O., G.Becker, G.v.Gierke, O.Klüber, K.Lackner, J.K.Lee[1], H.P.Zehrfeld, H.S.Bosch, H.Brocken, A.Eberhagen, G.Fussmann, O.Gehre, J.Gernhardt, E.Glock, G.Haas, J.Hofmann, A.Izvozchikov[1], G.Janeschitz, F.Karger, M.Keilhacker, M.Kornherr, M.Lenoci,

G.Lisitano, F.Mast, H.M.Mayer, K.McCormick, D.Meisel, V.Mertens, E.R.Müller, H.Murmann, H.Niedermeyer, W.Poschenrieder, H.Rapp, H.Riedler, H.Röhr, J.Roth, F.Ryter, F.Schneider, C.Setzensack, G.Siller, P.Smeulders, F.X.Söldner, E.Speth, K.-H.Steuer, O.Vollmer, F.Wagner and D.Zasche:
Energy confinement and MHD stability in ASDEX near the ß limit. IAEA (INTOR-related) Specialists' Meeting on Confinement in Tokamaks with Intense Heating, Kyoto/Japan, November 1986.

279 Gruber, O., G.Becker, G.v.Gierke, O.Klüber, K.Lackner, J.K.Lee[1], H.P.Zehrfeld, H.S.Bosch, H.Brocken, A.Eberhagen, G.Fussmann, O.Gehre, J.Gernhardt, E.Glock, G.Haas, J.Hofmann, A.Izvozchikov[1], G.Janeschitz, F.Karger, M.Keilhacker, M.Kornherr, M.Lenoci, G.Lisitano, F.Mast, H.M.Mayer, K.McCormick, D.Meisel, V.Mertens, E.R.Müller, H.Murmann, H.Niedermeyer, W.Poschenrieder, H.Rapp, H.Riedler, H.Röhr, J.Roth, F.Ryter, F.Schneider, C.Setzensack, G.Siller, P.Smeulders, F.X.Söldner, E.Speth, K.-H.Steuer, O.Vollmer, F.Wagner and D.Zasche:
MHD stability and transport of beam-heated ASDEX discharges in the vicinity of the beta limit. Proc. 11th Int. Conf. on Plasma Phys. and Contr. Nucl. Fusion Res., Kyoto 1986, IAEA-CN-47/A-VI-2.

280 Gruber, O., W.Jilge, V.Mertens, ASDEX-Team[2] und Pellet-Team[10]:
Energie und Teilchentransport bei Pelletinjektion an ASDEX. Verhandl. DPG (VI) 21 (1986).

281 Gruber, O.:
Energieeinschluß in ASDEX - Analyse mit dem TRANSP-Code. Plasmaphysik-Seminar der KFA-Jülich, Dezember 1986.

282 Gruber, O.:
Energieeinschluß in ASDEX: Analyse, Skalierung und Interpretation. Verhandl. DPG (VI) 21, 79 (1986).

283 Haas, G. et al.:
Recycling studies in the ASDEX-divertor with pellet or gas puff refuelling. 7th Conf. on Plasma Surface Interaction, Princeton 1986 (to be published in J. Nucl. Mater.).

284 Hanatani, K., F.-P. Penningsfeld, and H.Wobig:
Confining mechanism of perpendicular injected fast ions in the W VII A stellarator with radial electric field. Int. Stellarator/Heliotron Workshop, Kyoto, Japan, Nov. 1986.

285 Harmeyer E., J.Kißlinger, F.Rau and H.Wobig:
Mechanical behaviour of medium sized modular stellarator coil configurations. 14th SOFT, Avignon 1986, paper HP.05.

286 Harmeyer, E., F.Herrnegger, J.Kisslinger, F.Rau and H.Wobig:
Magnetic field studies for advanced stellarator reactors. Proc. 4th Technical Committee Meeting and Workshop on Fusion Reactor Design, Yalta, USSR, 1986 (to be publ. by IAEA, Vienna).

287 Harmeyer, E., J.Kisslinger, F.Rau and H.Wobig:
Engineering Considerations of Modular Coils for ASRA6C, an advanced stellarator reactor. Proc. 4th Technical Committee Meeting and Workshop on Fusion Reactor Design, Yalta, USSR 1986 (to be publ. by IAEA, Vienna).

288 Harmeyer, E., J.Kisslinger, F.Rau and H.Wobig:
Heating and burn scenarios for ASR and ASB. Proc. 4th Technical Committee Meeting and Workshop on Fusion Reactor Design, Yalta, USSR 1986 (to be publ. by IAEA, Vienna).

289 Hartfuß, H.J., H.Maaßberg, M.Tutter, W VII-A Team[3] und ECRH Group (IPF Stuttgart)[7]:
Methoden zur experimentellen Bestimmung der Elektronenwärmeleitung im Stellarator W VII-A bei Elektronen-Zyklotron-Resonanz-Heizung. Verhandl. DPG (VI) 21, 57 (1986).

290 Hartfuß, H.J., M.Tutter, W VII-A Team[3], ECRH Group (IPF Stuttgart)[7] und NI-Team (W VII-A)[5]:
Elektronenzyklotronemissionsspektren bei Anwesenheit nichtthermischer Elektronen im WENDELSTEIN VII-A. Verhandl. DPG (VI) 21, 105 (1986).

291 Hartwig, D., H.Dürr und T.Fauster:
Bestimmung der Struktur von Schwefel auf Nickeloberflächen durch niederenergetische Ionenstreuung. Verhandl. DPG (VI) 21, 1422 (1986).

292 Hawryluk, R.J.[1] et al. (from IPP: F.Wagner):
TFTR plasma regimes. 11th Int. Conf. on Plasma Phys. and Contr. Nucl. Fusion Res., Kyoto 1986.

293 Hill, K.W. et al. (from IPP: F.Wagner):
Impurity and particle transport and control in TFTR. 11th Int. Conf. on Plasma Phys. and Contr. Nucl. Fusion Res., Kyoto 1986.

294 Hofmann, J., G.Fussmann, G.Janeschitz, ASDEX- Team[2] and NI-Team (ASDEX)[4]:
Beobachtung von Ladungsaustausch- Rekombinationslinien vollständig ionisierter Atome in ASDEX. Verhandl. DPG (VI) 21, 107, (1986.)

295 Jacob, W., K.Desinger, V.Dose und H.Scheidt[1]:
Dispersion unbesetzter, sauerstoffinduzierter Energiebänder auf Kupfer-Einkristall-Oberflächen. Verhandl. DPG (VI) 21, 1380 (1986).

296 Janeschitz, G. and F.Wagner:
The H-regime on ASDEX. Boston, CIT-Workshop, May 1986.

297 Janeschitz, G., G.Fussmann, ASDEX-Team[2], NI-Team (ASDEX)[4] und ICRF-Team (ASDEX)[8]:
Verunreinigungsproduktion bei ICRH geheizten ASDEX Plasmen. Verhandl. DPG (VI) 21, 52 (1986.)

298 Karger, F.:
Demonstration of particle flux diversion in a resonant helical divertor in TEXT. Introduction to the evening session on "Resonant Helical Divertors - Recent Results and Future Plans". 11th Int. Conf. Plasma Phys., Contr. Nucl. Fus. Res., Kyoto 1986.

299 Karger, F.:
Recent results in resonant helical divertor research. IAEA Technical Committee Meeting on Research Using Small Tokamaks, Nagoya, Japan November 1986.

300 Karger, F.:
The principle of the resonant helical divertor and its influence on particle flux in TEXT. IREQ, Varennes, Canada, July 1986.

301 Kato, S.[1], W.Englert und E.Taglauer:
Prozeß der Adsorption und Desorption von Wasser an Edelstahloberflächen. 27. Vakuum-Symp. der Japan Vacuum Society, Osaka, Dec. 1986.

302 Kerner, W.:
Generalized eigenvalue solver for non-symmetric banded matrices. Centre de Calcul - Ecole Polytechnique Fédérale de Lausanne, Lausanne, 25.8.1986.

303 Kerner, W.:
Kerner/Weitzner model of collision particle transport. ASDEX Upgrade - Ringberg-Seminar, 22.-25.9.1986.

304 Kick, M., A.Weller, F.Sardei, H.Ringler, W VII-A Team[3], ECRH Group (IPF Stuttgart)[7] und NI-Team (W VII-A)[5]:
Spektroskopische Bestimmung des zeitlichen Verlaufs von O^{8+} und O^{7+} im W VII-A Stellarator und dessen Vergleich mit einem numerischen Transportmodell. Verhandl. DPG (VI) 21, 106 (1986).

305 Kisslinger, J. und H.Wobig:
Plasmagleichgewicht im WENDELSTEIN VII-AS. Verhandl. DPG (VI) 21, 60 (1986).

306 Köppendörfer, W. and ASDEX Upgrade Team (M.Blaumoser, K.Ennen, J.Gernhardt, J.Gruber, O.Gruber, D.Jacobi, W.Jakobus, M.Kaufmann, H.Kollotzek, E.Lackner, K.Lackner, T.v.Larcher, R.Mathis, S.B.Mukherjee, J.M.Noterdaeme, J.Neuhauser, M.Pillsticker, H.Preis, W.H.Reese, H.Schneider, S.Schweizer, U.Seidel, B.Sombach, E.Speth, M.Troppmann, G.Venus, H.Vernickel, F.Wesner and A.Wieczorek):
Progress report on ASDEX Upgrade. 14th SOFT, Avignon 1986, Comm. EC, EI03.

307 Kornherr, M., ASDEX-Team[2], NI-Team (ASDEX)[4] und ICRF-Team (ASDEX)[8]:
MHD-Aktivitäten in zusatzgeheizten ASDEX-Plasmen. Verhandl. DPG (VI) 21, 80 (1986).

308 Kotzlowski, H.E., B.Sombach, U.Blumer[1], P.Lüthi[1] and F.König[1]:
Concept, calculation and design of the insulation gap in the vacuum vessel of ASDEX Upgrade. 14th SOFT, Avignon 1986, Comm. EC, BP18.

309 Kühner, G. und W VII-A Team[3]:
Absoluteichung von Ge-Bolometern. Verhandl. DPG (VI) 21, 105 (1986).

310 Kühner, G., W VII-A Team[3], ECRH Group (IPF Stuttgart)[7] and NI-Team (W VII-A)[5]:
Bolometrie als Neutralteilchendiagnostik im Stellarator W VII-A. Verhandl. DPG (VI) 21, 58 (1986).

311 Lackner, K.:
Summary on magnetic confinement theory. 11th IAEA Conf. on Plasma Phys. and Contr. Nucl. Fusion Res., Kyoto/Japan 1986, November 1986.

312 Lackner, K.:
Theoretisches Verständnis von Plasmaheizung und Energieeinschluß, Aspekte der Kernfusionsforschung. Wien, April 1986.

313 Lang, R.S. K.Büchl, M.Kaufmann, H.Niedermeyer, W.Sandmann. O.Gehre, D.Meisel, H.Murmann, H.Röhr, K.-H.Steuer, ASDEX-Team[2] and NI-Team (ASDEX)[4]:
Erzeugung von Plasmen hoher Dichte in ASDEX durch quasistationäre Injektion von D_2-Pellets mittels Zentrifuge. Verhandl. DPG (VI) 21, 91 (1986).

314 Lee, J-K.[1], L.Lao[1], R.D.Stambough[1], E.J.Strait[1], K.Grassi, O.Gruber, O.Klüber, K.Lackner and H.P.Zehrfeld:
Tearing and kind stability for ASDEX and DIII discharges. Bull. Am. Phys. Soc. 31, 1593 (1986).

315 Lenoci, M., G.Haas, ASDEX-Team[2] and LH-Group[9]:
Floating potential measurements in the scrape-off layer of ASDEX during LH. Verhandl. DPG (VI) 21, 102 (1986).

316 Leuterer, F., LH-Group[9] und ASDEX-Team[2]:
Lower Hybrid Stromtrieb-Experimente in ASDEX. Verhandl. DPG, (VI), 21, 55 (1986).

317 Leuterer, F.:
Lower hybrid current drive on ASDEX: experiments and modelling. IAEA INTOR-Related Specialists Meeting on Noninductive Current Drive, Garching, Sept. 1986.

318 Liebl, H.:
A compact double-focusing mass spectrometer. 2nd Int. Conf. on charged particle optics, Albuquerque, N.M., USA, May, 1986.

319 Liebl, H.:
Ion optics of submicron ion beams. (Invited talk). Int. Conf. on Scanning Electron Microsopy, New Orleans, LA, USA, May 1986.

320 Liebl, H.:
On a combined electrostatic objective and emission lens for charged particles of opposite or equal polarity. ISEOB-Conf., Beijing, People's Republic of China, September 1986.

321 Lisitano, G.:
Schlieren diagnostic of particle density perturbation in additionally heated plasmas. Course and Workshop on Application of RF Waves to Tokamak Plasmas, Varenna 1986 (to be publ.).

322 Lortz, D.:
Introduction to fluid dynamics. Lecture at Munich University, May 1986 - July 1986.

323 Lortz, D.:
Introduction to plasma physics. Lecture at Munich University, May 1986 - July 1986.

324 Lortz, D.:
Theory of elasticity. Lecture at Munich University, Nov. 1985 - Febr. 1985.

325 Maassberg, H. and W VII-A Team[3]:
Ion cyclotron instabilities driven by the nearly perpendicular neutral beam injection in the Wendelstein VII-A stellarator. Proc. Int. Stellarator/ Heliotron Workshop, IAEA Technical Committee Meeting, Kyoto, Japan, 1986.

326 Maassberg, H. und W VII-A Team[3]:
Neoklassischer Ionentransport im W VII-A Stellarator. Verhandl. DPG (VI) 21, 60 (1986).

327 Maassberg, H.:
Radial electric fields and confinement in W VII-A. Proc. Int. Stellarator/Heliotron Workshop, IAEA Technical Committee Meeting, Kyoto, Japan, 1986.

328 Mahn, C., G.Müller, W VII-A Team[3], ECRH Group (IPF Stuttgart)[7] and NI-Team (W VII-A)[5]:
Messungen von Plasmafluktuationen im W VII-A Stellarator. Verhandl. DPG (VI) 21, 106 (1986).

329 Margraf, R., J. Leyrer[1], H.Knözinger[1] und E.Taglauer:
Ionenstreuung an Aluminiumoxid-Trägerkatalysatoren. Verhandl. DPG (VI) 21, 1422 (1986).

330 Martinelli, A.P., R.Behrisch, H.Hammer[1] and J.Hackmann[1]:
Surface composition of the Be limiters and the stainless steel torus wall after operation in UNITOR. 7th Int. Conf. on Plasma Surface Interactions in Controlled Fusion Devices, Princeton, USA, May 1986.

331 Massmann, P., E.Deksnis, H.D.Falter, R.S.Hemsworth, R.Shaw and A.Stäbler:
Carbon protection files for JET. 14th SOFT, Avignon 1986 (to be publ.).

332 McCarthy, P.J. and B.J.Braams[1]:
The use of function parameterisation for fast data analysis on ASDEX and ASDEX Upgrade. Bull. Am. Phys. Soc. 31, 1543 (1986).

333 McCormick, K. et al.:
Parametric investigation of the density profile in the scrape-off layer of ASDEX. 7th Conf. on Plasma Surface Interaction, Princeton 1986 (to be publ. in J. Nucl. Mater.)

334 McCormick, K.:
Lithium beam diagnostics on ASDEX. DFG-Kolloquium, Garching, November 1986.

335 McCormick, K.:
Current density measurements on ASDEX during OH and LHCD. Princeton/USA, May 1986.

336 McCormick, K.:
Measurement of the poloidal field distribution in a tokamak plasma via neutral lithium beam spectroscopy. Course and Workshop on Application of RF Waves to Tokamak Plasmas, Varenna 1986 (to be publ.)

337 McCormick, K.:
Q-Profile measurements on ASDEX during OH and LHCD. Workshop on the stabilization of Internal Modes via Lower Hybrid Current Drive, Frascati/Italy, January 1986.

338 McCormick, K.:
Q-profile measurements on ASDEX via Li-beam spectroscopy. 5th European Tokamak Program Workshop, Toledo/Spain, December 86

339 McCracken, G.M.[1], J.Ehrenberg, P.E.Stott[1], R.Behrisch and L.de Kock[1]:
Recycling of impurities at the JET limiters. 7th Int. Conf. on Plasma Wall Interactions in Controlled Fusion Devices, Princeton, USA, May 1986.

340 McGuire K. et al. (from IPP: F. Wagner):
Coherent and turbulent fluctuations in TFTR. 11th Int. Conf. on Plasma Phys. and Contr. Nucl. Fusion Res., Kyoto 1986.,

341 Memmel, N., J.Rogozik, W.Jacob, V.Dose und A.M.Bradshaw[1]:
Koadsorption von CO und K auf Pt(111). Verhandl. DPG (VI) 21, 1395 (1986).

342 Meyer-Spasche, R.:
A parameter dependent nonlinear eigenvalue problem. Tagung über Eigenwertaufgaben in den Ingenieurwissenschaften und ihre numerische Behandlung. Math. Forschungsinstitut Oberwolfach, Nov./Dez. 1986.

343 Meyer-Spasche, R.:
Numerical Mathematics II. Lecture at Freie Universität Berlin, April 1986 - July 1986.

344 Meyer-Spasche, R.:
Numerical study of taylor vortex flows. Int. Congress on Computational and Applied Mathematics, University of Leuven, Belgium, July 1986.

345 Meyer-Spasche, R.:
Numerical treatment of bifurcation problems. Seminarvortrag, Freie Universität Berlin, May 1986.

346 Meyer-Spasche, R.:
Numerische Approximation von axialsymmetrischen Taylorwirbelströmungen. Kolloqiumvortrag, Freie Universität Berlin, 9.12.1986.

347 Meyer-Spasche, R.:
On the approximation of steady axisymmetric Taylor vortex flows. Tagung über Numerische Methoden der approximationstheorie. Math. Forschungsinstitut Oberwolfach , Sept./Okt. 1986.

348 Meyer-Spasche, R.:
Steady axisymmetric Taylor vortex flows with free stagnation points of the poliodal flow. Int. Meeting on Bifurcation: Analysis-Algorithms-Applications, Universität Dortmund, August 1986.

349 Meyer-Spasche, R.:
The basic (n, 2n)-fold of steady axisymmetric Taylor vortex flows. Int. Symp. on the Physics of Structure Formation: Theory and Simulation. Universität Tübingen, Oct. 1986

350 Möller, W., P.Bøgesen and B.M.U. Scherzer:
Thermal and ion-induced release of hydrogen atoms implanted into graphite. Ion Beam Modification of Materials Conf., Catania, Italy, June 1986.

351 Möller, W.:
Hochenergiestreuverfahren zur Bestimmung des Wasserstoffgehalts in a-c:H-Schichten. Workshop über amorphe wasserstoffhaltige Kohlenstoffschichten. Bad Honnef, 1986.

352 Morris, R.N., S.P.Hirshman, G.H.Neilson and P.Merkel:
Simulation of magnetic loop diagnostic signal for ATF. Bull.Am.Phys.Soc. 31, 1543 (1986).

353 Murmann, H., D.Meisel, H.Röhr, K.-H.Steuer, ASDEX- Team[2], NI-Team (ASDEX)[4], ICRH-Team (ASDEX)[8] und Pellet-Team[10]:
Temperatur- und Dichteprofile in ASDEX bei Heizung und Nachfüllung. Verhandl. DPG (VI) 21, 61 (1986).

354 Murmann, H.:
A periodically operating multichannel Thomson scattering system on the Tokamak ASDEX. Course and Workshop on application of RF waves to Tokamak Plasmas, Varenna 1986 (to be published).

355 Närmann, A.[1], W.Heiland[1], K.Snowdon[1] und E.Mühling:
Die Neutralisation von Wasserstoff an Aluminium: Ein Beitrag zur Theorie des Ladungsaustausches zwischen Ionen und Oberflächen. Verhandl. DPG (VI) 21, 1323 (1986).

356 Neuhauser, J. and R.Wunderlich:
A radially continuous two-chamber model for the high-recycling divertor edge layer. 7th Int. Conf. on Plasma-Surface Interactions in Controlled Fusion Devices, Princeton, USA, May 1986.

357 NI-Group[6], presented by J.H.Feist:
Long-pulse neutral injection for ASDEX, ASDEX-Upgrade, and Wendelstein VII-AS: Design, development and systems performance. 14th SOFT, Avignon 1986 (to be publ.).

358 Niedermeyer, H., ASDEX-Team[2], NI-Team (ASDEX)[4], und Pellet-Team[10]:
Untersuchungen zum Dichtelimit an ASDEX. Verhandl. DPG, (VI) 21, 90 (1986)

359 Niedermeyer, H., F.Wagner, G.Becker, K.Büchl, A.Eberhagen, G.Fussmann, O.Gehre, G.v.Gierke, O.Gruber, G.Janeschitz, M.Kaufmann, K.Lackner, R.Lang, V.Mertens, H.Murmann, W.Sandmann, E.Speth, K.Steinmetz, G.Vlases[1], H.S.Bosch, H.Brocken, J.Gernhardt, E.Glock, G.Haas, J.Hofmann, A.Izvozchikov[1], F.Karger, M. Keilhacker, O.Klüber, M.Kornherr, M.Lenoci, G.Lisitano, F.Mast, H.M.Mayer, K.McCormick, D.Meisel, E.R.Müller, A.Pietrzyk[1], W.Poschenrieder, H.Rapp, H.Riedler, H.Röhr, J.Roth, F.Ryter[1], F.Schneider, C.Setzensack, G.Siller, P.Smeulders[1], F.X.Söldner, K.-H.Steuer, O.Vollmer and D. Zasche:
The achievement of regimes with high density, low q_a and good confinement on ASDEX. Proc. 11th Int. Conf. on Plasma Phys. and Contr. Nucl. Fusion Res., Kyoto 1986., IAEA-CN-47/A- II-5.

360 Niedermeyer, H., K.Büchl, M.Kaufmann, R.Lang, V.Mertens, W.Sandmann, G.Vlases[1], ASDEX- Team[2] and NI-Team (ASDEX)[4]:
High density discharges in ASDEX with pellet injection and at very low q-values. JET-Kolloquium, 4.7.1986.

361 Niedermeyer, H., K.Büchl, M.Kaufmann, R.Lang, V.Mertens, W.Sandmann, G.Vlases[1], ASDEX- Team[2], und NI-Team (ASDEX)[4] :
Dichte- und q-Grenze an ASDEX. IPP-Kolloquium, 14.7.1986.

362 Niedermeyer, H., K.Steinmetz, ASDEX-Team[2], ICRH- Team[8], LH-Group[9], NI-Team (ASDEX)[4], Pellet-Team[10] und PWW-Team: ASDEX- Experimente - Eine Übersicht. DFG- Kolloquium, Garching, 5.11.1986.

363 Niedermeyer, H., K.Steinmetz, ASDEX-Team[2], ICRH- Team[8], NI-Team (ASDEX)[4], Pellet-Team[10] und PWW-Team: Aktuelle Experimente an ASDEX. IPF-Kolloquium,Universität Stuttgart, 4.12.1986.

364 Noterdaeme, J.-M., F.Ryter[1], M.Söll, J.Bäumler, F.Braun, R.Fritsch, F.Hofmeister, E.Mark, S.Puri, K.Steinmetz, H.Wedler, F.Wesner, ASDEX-Team[2] und NI-Team (ASDEX)[4]: Änderung in Faradayschirm-Konfigurationen von ICRH-Antennen und ihr Einfluß auf das Plasma. Verhandl. DPG, (VI), 21, 52 (1986).

365 Noterdaeme, J.-M., M.Söll, F.Wesner, F.Braun, R.Fritsch, F.Hofmeister, H.-J.Kutsch, J.Perchermeier, E.Trcka, W.Radtke[1], M.Eckert[1], L.Kaiser[1], R.Löw[1], A.Mühlratzer[1] J.-G.Ströhle[1], and D.J.Hoffmann[1]: The ASDEX ICRF antennae in their uncooled and cooled versions. 14th SOFT, Avignon 1986 (to be published).

366 Noterdaeme, J.-M.: Antennae for W VII AS. Notes on the W VII-A and W VII-AS Stellarators, Ringberg, Jan. 1986.

367 Noterdaeme, J.-M.: ASDEX-Upgrade plans and ICRF Heating in Garching. JAERI, Tokai-Mura, Japan, Dec. 1986.

368 Noterdaeme, J.-M.: ICRH Experimente in Garching. Kolloquiumsvortrag, FOM-Instituut voor Plasmafysica, The Netherlands. Juni 1986.

369 Ohlendorf, W.: Recent results of the Garching Asdex tokamak and of the Wendelstein VII-A stellarator. XIII Yugoslav Summer School and Intern. Symp. on Physics of Ionized Gases, Sibenik, 1986.

370 Ohlendorf, W.: Spectroscopy in high-temperature (keV)-plasmas, such as encountered in fusion research. XIII Yugoslav Summer School and International Symposium on Physics of Ionized Gases, Sibenik, 1986.

371 Pfirsch, D.: Einführung in die Theoretische Plasmaphysik 1 (Kinetische Theorie). Lecture at Technische Universität München, Nov. 1986 - Febr. 1987.

372 Pfirsch, D.: Einführung in die Theoretische Plasmaphysik 2 (Makroskopische Theorie). Lecture at Technische Universität München, May 1986 - July 1986.

373 Pöffel, W.[1], K.-H.Schartner[1], G.Fussmann and G.Janeschitz: Radiation losses from C- and O-plasma impurities in the spectral range of the VUV. Conf. on the Physics of Multiply Charges Ions, Gröning, October 1986. (to be published in Nucl. Instr. and Methods).

374 Poschenrieder, W.: Mass spectrometric gas analysis as a versatile diagnostic on plasma experiments in fusion research. (Invited talk). 10th Int. Vacuum Congress, 6th Int.. Conf. on Solid Surfaces, 33rd Nat. Symp. of the Am.Vac. Soc. Baltimore, USA, October 1986. Proc. Am. Vac. Soc., 1986, 251.

375 Preis, H.: Numerical analysis of the Eddy currents and magnetic forces in the vacuum vessel of ASDEX Upgrade. 14th SOFT, Avignon 1986, Comm. EC, BP04.

376 Rapp, H., H.Niedermeyer, M.Kornherr, ASDEX- Team[2], NI-Team (ASDEX)[4] and ICRH-Team[8]: Experiences with the ASDEX neutralizer plates and construction of water-cooled plates for long-pulse heating. 14th SOFT, Avignon, September 1986 (to be published).

377 Rapp, H.: Design, technical features and experimental results of ASDEX. Plasma Physics Programme, Ahmedabad, February 1986.

378 Rapp, H.: Neutron diagnostics in ASDEX. Plasma Physics Programme. Ahmedabad, February 1986.

379 Rau, F.: Advanced stellarator reactor studies. Proc. Int. Stellarator/Heliotron Workshop, IAEA Technical Committee Meeting, Kyoto, Japan, 1986.

380 Rebut, P.H. and JET-Team (from IPP: J.Ehrenberg, H.Jäckel, S.Kissel, U.Küphnapfel, R.Müller, A.Stäbler and A.Weller): The impact of first JET results on the development of fusion, 14th SOFT, Avignon 1986 (to be publ.).

381 Renner, H., W VII-A Team[3] and ECRH Group (IPF Stuttgart)[7]: Experimental results with W VII-A in the torsatron mode of operation. Proc. Int. Stellarator/Heliotron Workshop, IAEA Technical Committee Meeting, Kyoto, Japan, 1986.

382 Renner, H., W VII-A Team[3], ECRH Group (IPF Stuttgart)[7], NI-Team (W VII-A)[5] and ICRH-Team[8]: Die Bedeutung der Verscherung $\iota/\iota = 0$. Verhandl. DPG (VI) 21, 59 (1986).

383 Renner, H., W VII-A Team[3], ECRH-Group (IPF Stuttgart)[7], NI-Team (W VII-A)[5] und ICRH-Team[8]:
W VII-A Stellarator 10 Jahre. Verhandl. DPG (VI) 21, 79 (1986).

384 Renner, H., W VII-A Team[3], NI-Team (W VII-A)[5], ICRH-Team [8], Pellet Group (K.Büchl, R.Lang) and ECRH Group (IPF Stuttgart)[7]:
Status of the Wendelstein VII-AS advanced stellarator. Proc. Int. Stellarator/ Heliotron Workshop, IAEA Technical Committee Meeting, Kyoto, Japan, 1986.

385 Renner, H., W VII-A Team[3], NI-Team (W VII-A)[5], ICRH-Team[8], ECRH Group (IPF Stuttgart)[7]:
Overview on recent W VII-A experimental results. Proc. Int. Stellarator/Heliotron Workshop, IAEA Technical Committee Meeting, Kyoto, Japan, 1986.

386 Riedler, J.M.:
Computation of neutral energy spectra at detector position. Technische Universität Graz, August 1986.

387 Ringler, H., F.Sardei, A.Weller, W VII-A Team[3], ECRH Group (IPF Stuttgart)[7] and NI-Team (W VII-A)[5]:
Impurity behaviour in the Wendelstein VII-A stellarator. Proc. 11th Int. Conf. on Plasma Physics and Contr. Nucl. Fus. Res., Kyoto, Japan, 1986, (IAEA-CN-47, paper D.V-1, to be publ. in Nuclear Fus., Suppl., 1987).

388 Ringler, H., W VII-A Team[3] and NI-Team (W VII-A)[5]:
Measurement of orbit losses during NI in W VII-A and a quantitative comparison with code calculations. Proc. Int. Stellarator/ Heliotron Workshop, IAEA Technical Committee Meeting, Kyoto, Japan, 1986.

389 Ringler, H.:
Impurity behaviour during NI and ECF. Proc. Int. Stellarator/Heliotron Workshop, IAEA Technical Committee Meeting, Kyoto, Japan, 1986.

390 Röhr, H., K.-H.Steuer, D.Meisel, H.Murmann und ASDEX-Team[2]:
Ortsaufgelöste Messung der Plasmastrahlung an ASDEX im Bereich von 800-1000nm zur Bestimmung von Z_{eff}. Verhandl. DPG (VI) 21, 107, 1986.

391 Roth, J. and J.Bohdansky:
Sputtering of graphite with light ions at energies between 20 and 1000 eV. 7th Int. Conf. on Plasma Surface Interactions in Controlled Fusion Devices, Princeton, USA, May 1986.

392 Roth, J., G.Fussmann and ASDEX-Team[2]:
Untersuchung der Verunreinigungsquellen in He^{++} und D^{+}-Entladungen an ASDEX. (Invited talk). Verhandl. DPG (VI) 21, 94 (1986).

393 Roth, J., J.Ehrenberg, K.Wittmaack[1], P.Coad[1] and J.B.Roberto[1]:
Erosion of long-term wall samples in JET. 7th Int. Conf. on Plasma Surface Interactions in Controlled Fusion Devices, Princeton, USA, May 1986.

394 Roth, J.:
Erosion and impurity production of C and Be: A comparison. (Invited talk). 7th Int. Conf. on Plasma Surface Interactions in Controlled Fusion Devices, Princeton, USA, May 1986.

395 Roth, J.:
Leichtionenzerstäubung. (Invited talk). Kolloquium Universität Braunschweig, Oktober 1986.

396 Roth, J.:
Oberflächenprobleme in der Plasmaphysik. (Invited talk). Kolloquium Universität Würzburg, May, 1986.

397 Santaniello, A., J.Appelt, J.Bohdansky and J.Roth:
Sputtering and ion-induced mixing of thin Fe layers on graphite. Ion Beam Modification of Materials Conf., Catania, Italy, June 1986.

398 Santaniello, A., J.Appelt, J.Bohdansky und J.Roth:
Zerstäubung und ioneninduzierte Mischung dünner Fe-Schichten auf Graphit. Verhandl. DPG (VI) 21, 976, (1986).

399 Sardei, F., A.Weller, H.Hacker und W VII-A Team[3]:
Verunreinigungstransportstudien bei Al-Ablation im W VII-A Stellarator. Verhandl. DPG (VI) 21, 106 (1986).

400 Scherzer, B.M.U.:
Swelling, blistering and flaking. (Invited talk). Workshop on Helium Bubbles in Metals, Orsay, France, Sept. 1986.

401 Schneider, F., H.Czich, F.Gresser and K.Stockinger:
Electronics for data preparation and diagnostics control in ASDEX. 14th SOFT, Avignon, September 1986 (to be published).

402 Schumacher, U. and H.Röhr:
Optimierung der Kristall-Reflexionseigenschaften für große Doppelkristall-Monochromatoren. Verhandl. DPG (VI) 21, 92 (1986).

403 Schumacher, U.:
Considerations for alpha particle diagnostics. Symposium Lecture, Göteborg/Sweden, June 1986.

404 Schumacher, U.:
Kernfusion mit magnetischem Plasmaeinschluß unter Berücksichtigung internationaler Forschung. Hanns-Seidel-Stiftung, Wildbad Kreuth, September 1986.

405 Schumacher, U.:
Kontrollierte Kernverschmelzung. MPG-Hauptversammlung, Aachen, Juni 1986.

406 Schumacher, U.:
Neuere Entwicklung der Diagnostik heißer Plasmen. Kolloquiumsvortrag an der Technischen Hochschule Darmstadt, Januar 1986.

407 Setzensack, C., G.Fussmann, R.Isler, H.Niedermeyer, G.Janeschitz und ASDEX-Team[2]:
Zunahme der Einschlußzeit von Verunreinigungen an der Hochdichtegrenze. Verhandl. DPG (VI) 21, 91 (1986)

408 Söder, B., J.Roth and W.Möller:
The influence of molybdenum atoms on the radiation enhanced selfdiffusion of pyrolytic graphite. Ion Beam modification of Materials Conf., Catania, Italy, June 1986.

409 Söder, B., J.Roth und W.Möller:
Der Einfluß von Molybdän-Verunreinigungen auf die strahleninduzierte Diffusion in pyrolytischem Graphit.
Verhandl. DPG (VI) 21, 985, (1986).

410 Söldner, F.X., LH-Group[9] und ASDEX Team[2]:
Optimierung des Stromtriebs im Tokamak durch Kombination von induktivem und HF-Stromtrieb. Verhandl. DPG (VI) 21, 56 (1986).

411 Söldner, F.X.:
Sawtooth stabilisation by lower hybrid waves in ASDEX. JET, Culham, 8.4.1986.

412 Söldner, F.X.:
Efficiency of voltsecond saving in combined OH/LH-current drive. IAEA Meeting, Garching, 16.9.1986.

413 Söldner, F.X.:
Energieeinschluß bei Lower-Hybrid-Heizung und -Stromtrieb. ASDEX-Workshop in Ringberg, 29.7.1986.

414 Söldner, F.X.:
Lower hybrid experiments on ASDEX. IREQ, Varennes, Canada, September 1986.

415 Söldner, F.X.:
Lower hybrid on ASDEX. Ad hoc group meeting, IPP Garching, 25.9.1986.

416 Söldner, F.X.:
Lower Hybrid Wellen - Aktuelle Anwendungen in Fusionsexperimenten.
Kolloquiumsvortrag, IPP Garching, 21.1.1986.

417 Söldner, F.X.:
Profile consistency and profile control with lower hybrid waves. European Program Workshop, Toledo, Dec. 1986.

418 Söldner, F.X.:
Results from lower hybrid experiments. JAERI, Japan, 26.11.1986.

419 Söldner, F.X.:
Review on lower hybrid experiments on ASDEX. Kolloquiumsvortrag in Frascati, 22.5.1986.

420 Söldner, F.X.:
Sawtooth stabilisation by lower hybrid waves in OH and NBI-heated plasmas on ASDEX. PPL Princeton, 11.6.1986.

421 Söldner, F.X.:
Sawtooth stabilisation by lower hybrid waves on ASDEX. Kolloquiumsvortrag MIT, Cambridge, 13.6.1986.

422 Söldner, F.X.:
Skalierungsuntersuchungen zur Lower-Hybrid-Heizung bei Ohmscher und Neutralinjektions- Vorheizung. Verhandl. DPG, (VI) 21, 56 (1986).

423 Söldner, F.X.:
Suppression of sawteeth by lower hybrid waves on ASDEX. Workshop on Internal Mode Stabilisation, Frascati, January 1986.

424 Söldner, F.X.:
Suprathermal electron production and profile control with lower hybrid waves, a conceptual study for JET. Workshop on Profile Control on JET, Culham, 14.5.1986.

425 Söldner, F.X.:
Suprathermal electron production and scaling studies on current drive with lower hybrid waves on ASDEX. PPL Princeton, 30.5.1986.

426 Sombach, B.:
Concept, calculation and design of the insulation gap in the vacuum vessel of ASDEX Upgrade. 14th SOFT, Avignon, Sept. 1986.

427 St.John, H.[1], L.Lao[1], W.Howl[1], K.H.Burrel[1], K.Lackner, P.J.McCarthy[1], T.S.Taylor[1] and R.D.Stambaugh[1]:
Principal component analysis of a simulated DIII-D database. Bull. Am. Phys. Soc. 31, 1535 (1986).

428 Staudenmaier, G. and W.R.Wampler[1]:
Metal impurity release in diverted tokamak discharges. 7th Int. Conf. on Plasma Surface Interactions in Controlled Fusion Devices, Princeton, USA, May 1986.

429 Staudenmaier, G.:
Lokaler Verunreinigungstransport im Divertor-Tokamak ASDEX. Verhandl. DPG (VI), 21 1424 (1986).

430 Steinmetz, K., F.X.Söldner, D.Eckhartt, G.Janeschitz, F.Leuterer, F.Mast, K.McCormick, J.-M.Noterdaeme, C.Setzensack, F.Wagner, F.Wesner, ICRH-Team[8], LH-Group[9], ASDEX-Team[2] and NI-Team (ASDEX)[4]:

Ion cyclotron resonance heating and lower hybrid experiments on ASDEX. 11th Int. Conf. on Plasma Physics and Controlled Nucl. Fusion Research, Kyoto, Japan 1986 (to be publ.).

431 Steinmetz, K., ICRH-Team[8], ASDEX-Team[2] and NI-Team (ASDEX)[4]:
Eigenschaften von ICRF geheizten Tokamak-Plasmen in ASDEX. Verhandl. DPG (VI) 21, 51 (1986).

432 Steinmetz, K.:
ICRH am Tokamak ASDEX: Heizung von Fusionsplasmen mittels Ionenzyklotron-wellen. Kolloquiumsvortrag, Universität Heidelberg, Mai 1986.

433 Steinmetz, K.:
Ionenzyklotronresonanzheizung an ASDEX. Kolloquiumsvortrag, IPP Garching, Juli 1986.

434 Steuer, K.-H.:
Anwendung der Laser in der Plasma-diagnostik. Ferienkurs Plasmaphysik, IPP Garching, 10.10.1986.

435 Steuer, K.-H.:
Fusionsreaktoren, Schnelle Brüter und Sonnenkraftwerke - Chancen und Probleme bei der Erschließung neuer Energiequellen. Schulvortrag, MPG Hauptversammlung, Aachen 1986.

436 Steuer, K.-H.:
Z_{eff}-Profilmessung. ASDEX Upgrade Workshop, Ringberg, 25.9.1986.

437 Stimpfle, C.J. und J.Rogozik:
Elastische Reflexion und Transmission niederenergetischer Elektronen an reinen und adsorbatbedeckten Einkristalloberflächen. Verhandl. DPG (VI) 21, 1424 (1986).

438 Storck, D., T.T.C.Jones, A.Burt, D.Cooper, J.F.Davies, D.T.Ewers, J.G.Krom, P.McCullen, J.P.Nijman, A.Stäbler, K.D.Starley, D.Young and I.D.Young:
Overview and operation of the control, safety and interlock on the JET neutral beam injector. 14th SOFT, Avignon 1986 (to be publ.).

439 Streibl, B., E.A.Maier, J.Perchermeier, P.L.Cimbrico[1], G.Varni[1], D.Pisani[1], R.Deska[1] and J.Endreat[1]:
Shear strength of the ASDEX Upgrade TF-coil insulation: rupture fatigue and creep behaviour. 14th SOFT, Avignon 1986, Comm. EC, HP01.

440 Taglauer, E., A.P. Martinelli, K.Ertl, B.M.U.Scherzer and ASDEX-Team[2]:
Impurity flux measuremens with a collector probe in the ASDEX divertor. 7th Int. Conf. on Plasma Surface Interactions in Controlled Fusion Devices, Princeton, USA, May 1986.

441 Taglauer, E., J.Onsgaard[1] und W.Huang[1]:
Untersuchung der Zerstäubung dünner Schichten mit Quarz-Mikrowaagen und Oberflächenspektroskopien. Verhandl. DPG (VI) 21, 978 (1986).

442 Taglauer, E.:
Atomkernverschmelzung - die Energie der Zukunft? (Invited talk). Symp. on Sputtering, (SOS), Spitz, Österreich, 1986.

443 Taglauer, E.:
Ionenstreuung und Oberflächenstruktur. (Invited talk). WEH-Seminar, Bad Honnef, 1986.

444 Taglauer, E.:
Surface analysis in fusion devices. (Invited talk).10th Int. Vacuum Congress, 6th Int. Conf. on Solid Surfaces, 33rd Nat. Symp. of the Am. Phys. Soc., Baltimore, Maryland, USA, Oktober 1986. In: Proc. Am. Vac. Soc., 1986, 291.

445 Taglauer, E.:
Surface investigations using low energy ion scattering. (Invited talk). University of Dayton, USA, 1986.

446 Verbeek, H. und ASDEX-Team[2]:
Neutralteilchenflüsse auf die Wand von ASDEX bei He- und Deuteriumentladungen. Verhandl. DPG (VI) 21, 94 (1986).

447 Vollmer, O., R.-C.Kunze, H.Lohnert, E.Speth, A.Stäbler, and K.Wittenbecher:
Achievements with the ASDEX neutral beam system during operation. 14th SOFT, Avignon 1986 (to be publ.).

448 Wagner, F., ASDEX-Team[2] and NI-Team (ASDEX)[4]:
Experimental evidence from ASDEX of a transport mechanism which affects simultaneously energy and particle transport. Workshop on Particle and Impurity Transport, Austin, USA, Febr. 1986.

449 Wagner, F., ASDEX-Team[2] und NI-Team (ASDEX)[4]:
Zur Physik der Einschlußverschlechterung bei Neutralinjektion in ASDEX. Verhandl. DPG, (VI) 21, 80 (1986).

450 Wagner, F.:
Confinement results of ASDEX. IAEA (Intor-Related) Specialists' Meeting on Confinement in Tokamaks with Intense Heating, Kyoto, 22.11.1986.

451 Wagner, F.:
Confinement studies in ohmically and auxiliary heated ASDEX plasmas. Kolloquiumsvortrag, ENEA, Frascati, 30.5.1986.

452 Wagner, F.:
Confinement studies on ASDEX. Kolloquium, MIT, Boston, 5.12.1986.

453 Wagner, F.:
Confinement studies on ASDEX. Kolloquium, ORNL, Oak Ridge, 12.12.1986.

454 Wagner, F.:
Confinement studies on ASDEX. Kolloquiumsvortrag PPPL, Princeton, 17.9.1986.

455 Wagner, F.:
Recent results from ASDEX. DOE Washington, 3.9.1986.

456 Wagner, F.:
The divertor diagnostic of ASDEX. Vortrag beim Alcator-Team, Boston, 4.12.1986.

457 Wandelt, K.[1], W.Jacob, N.Memmel und V.Dose:
Inverse Photoemission von adsorbiertem Xenon (IPAX) auf Ru(001). Verhandl. DPG (VI) 21, 1406 (1986).

458 Wedler, H., F.Wesner, M.Söll[1], E.van Mark, F.Braun, R.Fritsch and F.X.Pitschi[1]:
Development and testing of components for the ASDEX and W VII AS ICRF long-pulse heating. 14th SOFT, Avignon 1986 (to be publ.).

459 Weichselgartner, H., H.Frischmuth, A.Stücheli[1] and D.Ulrich[1]:
Progress in tritium technology in the IPP-T-Laboratory: scale-up of gas chromatograph system; removal of tritium from secondary containments. 14th SOFT, Avignon 1986, Comm. EC GP54.

460 Weichselgartner, H.:
Large-scale gas chromatography for tritium processing in the fuel cycle of fusion experiments. Int. Symp. of Fus. Reactor Blanket and Fuel Cycle Techn., Tokai-mura/Japan, Oct. 1986.

461 Weichselgartner, H.:
Tritium removal from secondary containments by means of organic getters. Int. Symp. of Fus. Reactor Blanket and Fuel Cycle Techn., Tokai-mura, Japan, Oct. 1986.

462 Weller, A., K.Behringer, A.Edwards[1], H.U.Fahrbach, G.Fussmann, R.D.Gill[1], R.Granetz[1], D.Pasini[1] and D.Zasche:
Soft x-radation losses during additional heating in JET. Bull.Am.Phys.Soc. 31, 1590 (1986).

463 Werner, F., M.Pillsticker, H.Brandl[1] and A.Jäckle[1]:
ASDEX Upgrade poloidal field coils - concept, manufacturing, test. 14th SOFT, Avignon 1986, Comm. EC, HP24.

464 Wesner, F.:
ICRH results and technological limitations. 14th SOFT, Avignon 1986 (to be publ.).

465 Winter, J.[1], H.G.Esser[1], P.Wienhold[1], K.Besocke[1], G.Flentje[1], V.Phillips[1], W.Möller und B.Emmoth[1]:
Eigenschaften von karbonisierten Oberflächen im Hinblick auf die Plasma-Wand-Wechselwirkung. Verhandl. DPG (VI) 21, 65 (1986).

466 Wobig, H., H.Maassberg, H.Renner, W VII-A Team[3], NI-Team (W VII-A)[5] and ECRH Group (IPF Stuttgart)[7]:
Plasma confinement in the W VII-A stellarator. Proc. 11th Int. Conf. on Plasma Physics and Contr. Nucl. Fus. Res., Kyoto, Japan, 1986 (IAEA-CN-47, paper D.I-2, to be publ. in Nuclear Fus., Suppl., 1987).

467 Wobig, H.:
A dissipative model of plasma equilibrium in toroidal systems. Fusion Theory Meeting, Wépion, Belgium, 1986.

468 Wobig, H.:
Destruction of magnetic surfaces in stellarators. Proc. Int. Stellarator/Heliotron Workshop, IAEA Technical Committee Meeting, Kyoto, Japan, 1986.

469 Wobig, H.:
Dissipatives Modell des Plasmagleichgewichts in toroidalen Systemen. Verhandl. DPG (VI) 21, 85 (1986).

470 Wobig, H.:
Status report of the W VII-X stellarator project. Proc. Int. Stellarator/Heliotron Workshop, IAEA Technical Committee Meeting, Kyoto, Japan, 1986.

471 Zehrfeld, H.P., H.Bruhns, J.Steiger[1] und L.Schugmann[1]:
Kompakte Doppeltoroide: numerische Gleichgewichte und Experiment. Verhandl. DPG (VI) 21, 64 (1986).

472 Zouhar, M., T.Vien, F.Leuterer, M.Brambilla, H.Derfler, D.Eckhartt, M.Münich und F.v.Woyna:
Ankopplung von Lower Hybrid-Wellen an das ASDEX-Plasma. Verhandl. DGP, (VI), 21, 63 (1986).

LABORATORY REPORTS

IPP 1/229 Preis, H.: Calculation of the Electromagnetic Forces on the ASDEX Upgrade Vacuum Vessel on Disruption of the Plasma Current. (1986)

IPP 1/238 Büchl, K., W VII-A Team[2)]: Pellet Ablation in the Stellarator W VII-A. (1986)

IPP 2/281 Maassberg, H.: Monte Carlo Simulation of Neutral Beam Injection in the Wendelstein VII-A Stellarator. (1986)

IPP 2/283 Wobig, H.: Magnetic Surfaces and Localized Perturbations in the Wendelstein VII-A Stellarator. (1986)

IPP III/108 Fussmann, G.: Spektroskopie als Schwerpunktsprogramm an ASDEX - eine Diskussionsstudie. (1986)

IPP III/109 Becker, G.: Anomalous Transport in Tokamaks with Ohmic and Auxiliary Heating. (1986)

IPP III/110 ASDEX-Team[2)]: ASDEX Papers at the 13th European Conference on Controlled Fusion and Plasma Physics. (1986)

IPP III/111 Söldner, F.X.: Study of Profile Control and Suprathermal Electron Production with Lower Hybrid Waves. (1986)

IPP III/112 Müller, E.R.: Evolution of Radiation Power Profiles in ASDEX H-Mode Discharges. (1986)

IPP III/113 Lenoci, M., Haas, G.: Investigation of the Parameters in the Boundary Plasma of ASDEX by Means of a Langmuir Probe. (1986)

IPP III/114 Bernhardi, K.: Bestimmung der Verteilung suprathermischer Elektronen aus ihrer Bremsstrahlung. (1986)

IPP 4/224 Knobloch, A.F.: INTOR rescaling for non-indented plasma shape applying preliminary scalings for energy confinement and density limit. (1986)

IPP 4/227 Puri, S.: Comments on The Alfvén Wave Spectrum as Measured on the TCA Tokamak. (1986)

IPP 4/228 Puri, S.: Antenna Optimization For Alfvén Wave Heating. (1986)

IPP 4/229 Penningsfeld, F.P.: Computation of the Density Distribution of Injected Neutral Beam Particles by the Program NEUDEN. (1986)

IPP 4/230 Puri, S.: Role of Plasma Equilibrium Current in Alfven Wave Antenna Optimization. (1986)

IPP 4/231 Riedler, H.M.: Wechselwirkung des Neutralstrahls mit dem Plasma. (1986)

IPP 5/9 Krücken, T.: 1-d Model for Propagation and Adsorption of HF Waves Near Ion Cyclotron Resonances in Large Tokamak Plasmas. (1986)

IPP 5/10 Brambilla, M.: A Model for the Numerical simulation of Ion Cyclotron Heating in Tokamak Plasmas. (1986)

IPP 5/11 Brambilla, M.: Numerical Simulation of Reflectometry Density Measurements in a Reversed Field Pinch. (1986)

Laboratory Reports

IPP 5/12 McCarthy, P.J., Sexton, M.C.: Plasma Profile Recovery by Function Parameterisation.(1986)

IPP 6/257 Salat, A.: Integrable and Nonintegrable Non-KAM Hamiltonias and Magnetic Field Topology. (1986)

IPP 6/258 Biskamp, D.: Natural Current Profiles in Tokamaks. (1986)

IPP 6/259 Tasso, H.: Lyapunov Stability and Attractors of Some Systems of Nonlinear Oscillators. (1986)

IPP 6/260 Tasso, H.: An Integrable System of two Nonlinear Oscillators as Attractor. (1986)

IPP 6/261 Pohl, F.: Solution of a Fokker Planck Equation for Turbulent Diffusion. (1986)

IPP 6/262 Lortz, D.: Magnetohydrodynamik. (1986)

IPP 6/263 Pfirsch, D., Pohl, F.: Entropy Principle for Tokamak Profiles. (1986)

IPP 6/264 Tasso, H.: On Phase Space and Statistics of Continua. (1986)

IPP 9/56 Mühling, E.: Charge state fractions of backscattered, desorbed and sputtered particles. (1986)

IPP 9/57 Børgesen, P., Svendsen, L.G.[1)], Ehrenberg, J.: Routine ion beam analysis of impurities collected on solid probes during plasma experiments. (1986)

IPP 9/58 Barth, H.J., Mühling, E., Eckstein, W.: Investigation of a Copper-lithium alloy as possible first wall and limiter material in fusion devices. (1986).

IPP 9/59 Eckstein, W., Heifetz, D.B.[1)]: Data sets for hydrogen reflection and their use in neutral transport calculations. (1986)

IPP 9/60 Martinelli, A.P., R.Behrisch, H.Hammer[1)], J.Hackmann[1)]: Surface composition of the Be limiters and the stainless-steel torus wall after operation in UNITOR. (1986).

IPP-JET REPORTS

Nr. 32 Scherzer, B.M.U., Børgesen, P., Möller, W.: Reemission Tapping and Desorption of Implanted Deuterium from JET samples. (1986)

EXTERNAL LABORATORY REPORTS

IPF 86-2 Erckmann, V., Thumm, M.[1)], Kasparek, W.[1)], Kumric, H.[1)], Müller, G.A.[1)], Schüller, P.G.[1)], Wilhelm, R.[1)]: Components for transmission of very high power mm-waves (200 kW at 28, 70 and 140 GHz) in overmoded circular waveguides. Institut für Plasmaforschung, Universität Stuttgart (1986).

JET-R(86)07 Feneberg, W., Mast, F.K., Gottardi, N.[1)], Martin, P.: Neoclassical Impurity Transport and Observation of Poloidal Asymmetries in JET. (1986)

PPPL 2346 Heidbrink, W.W.[1)], Milora, S.L.[1)], Schmidt, G.L.[1)], Schneider, W.[1)], Ramsey, A.[1)]: Neutron and Hard X-Ray Measurements During Pellet Deposition in TFTR. Princeton Plasma Physics Lab., USA, UC20-F (1986)

PPPL 2361 Schneider, W., Bateman, G.[1]: Mapping from Rectangular to Harmonic Representation. Princeton Plasma Physics Lab., USA, UC20-G (1986)

LA-UR-86-4011 Wurden, G.A.[1], Weber, P.G.[1],, Watt, R.G.[1],, Munson, C.P.[1], Ingraham, J.C.[1], Howell, R.B.[1], Cayton, T.E.[1], Büchl, K., Nilles, E.J.[1]: Pellet Refuelling of the ZT-40M Reversed Field Pinch. Los Alamos National Lab., USA (1986)

PPLK R-12 Morimoto, S., W VII-A Team[2], ECRH Group (IPF Stuttgart)[7]: On the second harmonic ECRH-plasmas in Wendelstein VII-A. Research Report, Plasma Physics Laboratory, Kyoto University, Japan (1986)

IPPJ - 793 Eckhartt, D.: On the Evaluation of Currents in a Tokamak Plasma During Combined Ohmic and RF Current Drive. Nagoya University, Japan. (1986)

1) No Member of Max-Planck-Institut für Plasmaphysik

2) **ASDEX-Team:** Becker, G., Bosch, H.S., Brocken, H., Eberhagen, A., Fussmann, G., Gehre, O., Gernhardt, J., Gierke, G.v., Giuliana, A., Glock, E., Gruber, O., Janeschitz, G., Karger, F., Keilhacker, M., Klüber, O., Kornherr, M., Lackner, K., Lenoci, M., Lisitano, G., Mayer, H.M., McCormick, K., Meisel, D., Mertens, V., Müller, E.R., Murmann, H., Niedermeyer, H., Poschenrieder, W., Rapp, H., Ryter, F., Siller, G., Smeulders, P., Söldner, F., Steuer, K.-H., Wagner, F.,

3) **W VII-A Team:** Cattanei, G., Dorst, D., Elsner, A., Engelhardt, K., Erckmann, V., Fowler, R., Gasparino, U., Grieger, G., Grigull, P., Hacker, H., Hartfuß, H.J., Jäckel, H., Jaenicke, R., Junker, J., Kick, M., Kroiss, H., Kuehner, G., Maaßberg, H., Mahn, C., Mathis, R., Müller, G., Münch, H., Ohlendorf, W., Rau, F., Renner, H., Ringler, H., Sapper, J., Sardei, F., Schoenewolf, I., Tutter, M., Weller, A., Wobig, H., Würsching, E., Zippe, M.,

4) **NI-Team (ASDEX):** Riedler, H., Speth, E., Stäbler, A., Vollmer, O.,

5) **NI-Team (W VII-A):** Freudenberger, K., Ott, W., Penningsfeld, F.-P., Speth

6) **NI-Group:** Feist, J.H., Freudenberger, K., Götz, S., Kolos, J., Kunze, R.C., Lohnert, H., Melkus, W., Ott, W., Penningsfeld, F.P., Riedler, H., Sielanko, J., Speth, E., Stäbler, A., Vollmer, O., Wittenbecher, K., Wulff, G.

7) **ECRH Group (IPF Stuttgart):** Barkley, H., Kasparek, W., Kumrić, H., Müller, G.A., Räuchle, E., Schüller, P.G., Schwörer, K., Thumm, M., Wilhelm, R.

8) **ICRH-Team:** Bäumler, J., Becker, W., Braun, F., Fritsch, R., Hofmeister, F., Noterdaeme, J.-M., Mark, E.v., Puri, S., Steinmetz, K., Wedler, H., Wesner, F.

9) **LH-Group:** E., Brambilla, M., Derfler, H., Eckhartt, D., Leuterer, F., Münich, M., Schmitter, K.H., Vien, T., Zouhar, M.

10) **Pellet-Team:** Büchl, K., Lang, R., Sandmann, W., Vlases, G.

11) **INTOR Group:**
EC: Grieger, G., Chazalon, M., Engelmann, F., Farfaletti-Casali, F., Harrison, M.F.A., Knobloch, A.F., Leger, D., Salpietro, E., Schiller, P.

Japan: Mori, S., Fujisawa, N., Honda, T., Iida, H., Kasai, M., Seki, M., Sugihara, M., Tomabechi, K.

USA: Stacey, W.M., Baker, C.C., Colestock, P.L., Flanagan, C.A., Mattas, R.F., Peng, Y.-K.M., Post, D.E., Spampinato, P.T., Thome, R.J.

USSR: Kadomtsev, B.B., Kolbasov, B.N., Kostenko, A.I., Kukushkin, A.S., Litunosvkij, R.N., Pistunovich, V.I., Serebrennikov, D.V., Shatalov, G.E.

AUTHOR INDEX

Abdou , M.A., 124
Albridge, R.G., 55
Altmann, W., 1,204
Amenda, W., 2
Andelfinger, C., 205
Appelt, J., 397,398
Arnold, N., 98

Abdou , M.A., 124
Albridge, R.G., 55
Altmann, W., 1,204
Amenda, W., 2
Andelfinger, C., 205
Appelt, J., 397,398
Arnold, N., 98

Baker, C.C., 72,271,272,273,274
Bakshi , M. , 154
Baretzky, B., 3,206
Barkley, H., 41,51,58,59,60,61,84,125,252,253,289, 290,304,310,328,381,382,383,384,385,387,466, Rep.PPLK R-12
Barth, H.J., 4,33, IPP-Rep. 9/58
Bartiromo, R., 5,6,76,79,102,103,146,145
Bartlett, D.V., 48
Bateman, G., Rep.PPPL 2361
Battiston, L., 7
Bäumler, J., 118,148,149,150,227,277,297,307,353,362, 363,376,382,383,384,385,431,169,364,430
Becker, G., 5,6,8,9,10,17,43,46,47,53,75, 76,79,85,95,101,102,103,104,108,109,114, 115,117,118,122,130,132,133,144,145,146,147, 148,149,165,177,222,223,270,277,278,279,280, 297,307,313,315,316,358,359,362,363,364,390, 392,430,431,446,448,449, 7,294,353,360,361,376,407,410,440, IPP-Rep. III/109,III/110
Becker, W., 118,148,149,150,227,277,297,307,353,362, 363,376,382,383,384,385,431,430
Behringer, K., 11,207,462
Behrisch, R., 12,13,36,37,208,209,210,211,212,213, 214,247, 330,339, IPP-Rep.9/60
Bergsaker, H., 209,210,214
Bernhardi, K., 102,103,IPP-Rep. III/114
Bertolini , E., 124
Besocke , E.H., 170,465
Biersack, J.P., 31,32
Biskamp, D., 14,15,215,216,217,IPP-Rep. 6/258
Blaumoser, M., 54,94,218,219,306
Blumer , U., 308
Børgesen, P., 16,134,350,IPP-Rep. 9/57, IPP-JET-Rep.32
Bohdansky, J., 220,221,391,397,398
Bommanavar , A.S., 154
Bosch, H.S., 5,6,17,43,46,47,52,53,75,76,79, 85,95,101,102,103,104,108,109,114,115,117,118, 122,130,132,133,144,145,146,147,148,149,165, 177,178,222,223,224,277,278,279,280,297,307, 313,315,316,358,359,362,363,364,390,392,430, 431,446,448,449, 7,294,353,360,361,376,407,410,440, IPP-Rep. III/110
Braams, B.J., 18,179,332
Bracco, G., 48
Bradshaw , A.M., 341
Brambilla, M., 5,6,19,20,102,103,104,132,146,177, 225, 226,277,315,316,362,410,430,472, IPP-Rep 5/10,5/11
Brandl , H., 463
Braun, F., 118,148,149,150,227,277,297,307,353, 362,363,376,382,383,384,385,431,168,169,364, 365,430,458
Brocken, H., 5,6,17,43,46,47,52,53,75,85,95, 101,102,103,104,108,109,114,115,117,118,122, 130,132,133,144,145,146,147,148,149,165,177, 222,223,277,278,279,280,297,307,313,315,316, 358,359,362,363,364,390,392,430,431,446,448, 449, 7,294,353,360,361,376,407,410,410, IPP-Rep. III/110
Bruhns, H., 174,471
Buchelt, E., 205
Büchl, K., 47,51,53,117,228,277,280,313,353,359, 360,361,362,363 IPP-Rep.1/238, Rep.LA-UR-86-4011
Buende, R., 50
Bures , M., 228
Burhenn, R., 5,6,146
Burrel, K.H., 427
Burt, A., 438

Campbell, D.J., 34,48,228
Canobbio, E., 25
Carezzano , R., 152
Cattanei, G., 40,41,51,58,59,60,61, 84,125,160,171,227,251,252,253,289,290,304, 309,310,325,326,328,381,382,383,384,385,387, 388,399,466,IPP-Rep. 1/238, Rep.PPLK R-12
Cayton, T.E., Rep.LA-UR-86-4011
Challis, C., 268
Chazalon, M., 72,271,272,273,274
Cheetham, A.D., 228
Cherry, D.W., 55
Chodura, R., 21,22,97
Christianson , G., 98
Cimbrico, P.L., 152,439
Coad , J.P., 36,37208,209,210,214,247,393
Colavita , E., 154
Cole, R.K., 55
Colestock, P.L., 72,271,272,273,274
Conn , R.W., 221
Cooper, D., 438
Cordey, J.G., 229
Correa-Restrepo, D., 23,24
Corti, S., 48
Costley, A.E., 48
Cranetz , R., 228
Croci, R., 25
Croessmann , A., 221
Czich, H., 401

Danese , M., 152
Davies, J.F., 438
Davis , W., 98
Deksnis, E., 331
Derfler, H., 5,6,102,103,104,132,144,145,146, 177,188,277, 315,316,362,410,430,472
Deschamps, G.H., 62
Desinger, K., 204,230,295

Deska , R., 439
Dommaschk, W., 26
Donath, M., 27,231
Dorst, D., 40,41,51,58,59,60,61,84,125,160,171,
218,227,232,251,252,253,289,290,304,309,310,
325,326,328,381,382,383,384,385,387,388,399,
466, IPP-Rep. 1/238, Rep.PPLK R-12
Dose, V., 1,28,29,44,73,74,129,167,204,230,231,
233,234,235,236,237,238,263,295,341,457
Drube, R., 28,230
Duesing, G., 30,239
Dürr, H., 183,240,258,259,291

Eberhagen, A., 5,6,17,43,46,47,52,53,75,76,79,
85,95,101,102,103,104,108,109,114,115,117,118,
122,130,132,133,144,145,146,147,148,149,165,
177,222,223,277,278,279,280,297,307,313,315,
316,358,359,362,363,364,390,392,430,431,446,
448,449,
7,294,353,360,361,376,407,410,440,
IPP-Rep. III/110
Eckert , M., 365
Eckhartt, D., 5,6,17,47,79,101, 102,103,104,
108,132,133,144,145,146,177,277,315,316,362,
410,430,472, Rep.IPPJ - 793
Eckstein, W., 4,31,32,33,71,241,242,243,244,245,
246,IPP-Rep. 9/58,9/59
Edwards, A.W., 11,34,35,48,228,462
Ehrenberg, J., 30,36,37,38,99,208,209,210,214,247,
248,339,380,393,IPP-Rep. 9/57
Elsner, A., 40,41,51,58,59,60,61,84,125,160,171,
227,249,251,252,253,289,290,304,309,310,325,
326,328,381,382,383,384,385,387,388,399,466,
IPP-Rep. 1/238, Rep.PPLK R-12
Emmoth , B., 170,209,210,214,465
Endreat , J., 439
Engelhardt, K., 40,41,51,58,59,60,61,84,125,160,
171,227,251,252,253,289,290,304,309,310,325,
326,328,381,382,383,384,385,387,388,399,466,
IPP-Rep. 1/238, Rep.PPLK R-12
Engelhardt, W., 34,38,48
Engelmann, F., 72,271,272,273,274
Engelmann, G., 39,180,250
Englert, W., 301
Ennen, K., 54,94,306
Erckmann, V., 40,41,42,51,58,59,60,61,84,
125,160,171,227,251,252,253,254,255,256,289,
290,304,309,310,325,326,328,381,382,383,384,
385,387,388,399,466, IPP-Rep. 1/238, Rep.PPLK
R-12, Rep.IPF 86-2
Erents , S.K., 214
Ertl, K., 43,155,440
Eschenbacher , H., 204
Esser , H.G., 170,465
Evans, T.E., 257
Ewers, D.T., 438

Fahrbach, H.U., 11,34,35,48,462
Falter, H.D., 62,331
Farfaletti-Casali, F., 72,271,272,273,274
Fauster, T., 29,74,204,240,258,259,260,291
Feilcke , F., 218
Feist, J.-H., 261,262,357
Feneberg, W., Rep.JET-R(86)07
Flanagan, C.A., 72,91,271,272,273,274
Flentje , G., 465
Fonck ,, R., 98
Fowler, R., 40,41,51,58,59,60,61,84,125,160,171,227,
251,252,253,289,290,304,309,310,325,326,328,
381,382,383,384,385,387,388,399,466, IPP-Rep.
1/238, Rep.PPLK R-12
Freisinger , J., 262
Freudenberger, K., 41,51,84,125,290,304,310,328,357,
382,383,384,385,387,388,466
Freund, H.-J., 44,263
Frischmuth, H., 189,459
Fritsch, R., 118,148,149,150,227,277,297,307,353,362,
363,376,382,383,384,385,431, 364,365,430,458
Fujisawa, N., 72,271,272,273,274
Fussmann, G., 5,5,6,17,43,45,46,47,52,53,75,76,79,
85,95,101,102,103,104,108,109,114,115,117,118,
122,130,132,133,144,145,146,147,148,149,150,
165,177,207,222,223,264,265,266,277,278,279,
280,294,297,307,313,315,316,358,359,362,363,
364,373,390,392,407,430,431,440,446,448,449,46
2,
7,353,360,361,376,410,IPP-Rep.III/108,III/110

Gagliardi , P., 152
Gambier, D.J., 48
Gasparino, U., 40,41,51,58,59,60,61,84,125,160,
171,227,251,252,253,289,290,304,309,310,325,
326,328,381, 382,383,384,385,387,388,399,466,
IPP-Rep. 1/238, Rep.PPLK R-12
Gehre, O., 5,6,17,43,46,47,52,53,75,76,79,85,
95,101,102,103,104,108,109,114,115,117,118,
122,130,132,133,144,145,146,147,148,149,165,
177,222,223,267,277,278,279,280,297,307,313,
315,316,358,359,362,363,364,390,392,430,431,
440,446,448,449,
7,294,353,360,361,376,407,410, IPP-Rep.
III/110
Gernhardt, J., 5,6,17,43,46,47,52,53,75,76,
79,85,95,101,102,103,104,108,109,114,115,117,
118,122,130,132,133,144,145,146,147,148,149,
165,177,222,223,277,278,279,280,297,306,307,
313,315,316,358,359,362,363,364,390,392,430,
431,440,446,448,449,
7,294,353,360,361,376,407,410, IPP-Rep.
III/110
Gershenfeld , N., 154
Gierke, G.v., 5,6,17,43,46,47,52,53,75,76,79,85,95,
101,102,103,104,108,109,114,115,117,118,122,
130,132,133,144,145,146,147,148,149,165,177,
222,223,277,278,279,280,297,307,313,315,316,
358,359,362,363,364,390,392,430,431,446,448,
449,
7,294,353,360,361,376,407,410,440,
IPP-Rep. III/110
Gill, R.D., 11,34,35,48,462
Giuliana, A., 5,6,43,53,79,102,103,146,104,
118,122,132,145,147,148,149,165,177,222,223,
277,280,297,307,313,315,316,358,362,363,364,
390,392,430,431,440,446,448,449,
7,294,353,360,361,376,407,410, IPP-Rep.
III/110
Glöbl, M., 27,231
Glock, E., 5,6,17,43,46,47,52,53,75,76,79,85,95,
101,102,103,104,108,109,114,115,117,118,122,
130,132,133,144,145,146,147,148,149,165,177,
222,223,277,278,279,280,297,307,313,315,316,
358,359,362,363,364,390,392,430,431,446,448,
449,
7,294,353,360,361,376,407,410,440,
IPP-Rep.III/110
Goebel , D.M., 221
Goede, A.P.H., 62,268
Goldmann, A., 1,73,74
Goldston, R.J., 269
Gondhalekar , A., 228
Goodall , D.H.J., 247
Gottardi, N., 11,228, Rep.JET-R(86)07
Götz,, S., 261,357
Gowers, C.W., 48
Gräff, P., 121

Granetz, R.S., 11,34,35,48,462
Grassie, K., 85,270,314
Gresser, F., 401
Grieger, G., 40,41,49,50,51,51,58,59,60,61,72,84, 125,160,171,227,232,251,252,253,271,272,273, 274,275,276,289,290,304,309,310,325,326,328, 381,382,383,384,385,387,388,399,466, IPP-Rep. 1/238, Rep.PPLK R-12
Grigull, P., 40,41,51,58,59,60,61,84,125,160, 171,227,251,252,253,289,290,304,309,310,325, 326,328,381,382,383,384,385,387,388,399,466, IPP-Rep. 1/238, Rep.PPLK R-12
Grohnheit, P.E., 50
Gruber, J., 54,94,306
Gruber, O., 5,6,17,43,46,47,52,53,53,54,75,76, 79,85,95,101,102,103,104,108,109,114,115,117, 118,122,130,132,133,144,145,146,147,148,149, 150,165,177,219,222,223,270,277,278,279,280, 281,282,297,306,307,313,314,315,316,358,359, 362,363,364,390,392,430,431,440,446,448,449, 7,294,353,360,361,376,407,410, IPP-Rep.III/110
Gulden, W., 50

Haas, G., 5,6,17,43,46,47,52,53,75,76,79, 85,95,101,102,103,104,108,109,114,115,117,118, 122, 130,132,133,144,145,146,147,148,149,165, 177,190,222,223,257,277,278,279,280,283,297, 307,313,315,316,358,359,362,363,364,390,392, 430,431,446,448,449, IPP-Rep. III/110,III/113
Hacker, H., 40,41,51,58,59,60,61,84,125,160,171, 227,251,252,253,289,290,304,309,310,325,326, 328,381,382,383,384,385,387,388,399,466, IPP-Rep. 1/238, Rep.PPLK R-12
Hackmann , J., 330, IPP-Rep. 9/60
Haglund, R.F., 55
Hammer , H., 330, IPP-Rep. 9/60
Hanatani, K., 284
Hancox , R., 124
Harmeyer, E., 56,275,285,286,287,288
Harned, D.S., 57
Harries, D.R., 12
Harrison, M.F.A., 72,271,272,273,274
Hartfuß, H.J., 40,41,51,58,59,59,60,61,84, 125,160,171,227,251,252,253,289,290,304,309, 310,325,326,328,381,382,383,384,385,387,388, 399,466, IPP-Rep. 1/238, Rep.PPLK R-12
Härtl, A., 28
Hartwig, D., 184,240,258,259,291
Hatori , T., 128
Hawryluk, R.J., 292
Heidbrink, W.W., Rep.PPPL 2346
Heifetz, D.B., IPP-Rep. 9/59
Heiland , W., 355
Heindler, M., 127
Hemsworth, R.S., 62,331
Hendriks , F., 228
Herrnegger, F., 63,64,65,66,286
Hertweck, F.R., 67,68
Hesse, M., 5,6,102,103,145,146
Hill, K.W., 293
Hirooka , Y., 221
Hirshman, S.P., 69,70,352
Hoffmann , D.J., 365
Hofmann, J., 6,17,46,47,52,75,85,95,101,108,109, 114,115,117,130,133,144,145,264,278,279,294, 359
Hofmeister, F., 118,148,149,150,227,277,297,307, 353,362,363,376,382,383,384,385,431,169,364, 365,430
Hogan , W.J., 124
Honda, T., 72,271,272,273,274
Hou, M., 71
Howell, R.B., Rep.LA-UR-86-4011
Howl, W., 427
Huang , W., 120,441
Hubbard, A., 48
Huric , Z., 154

Iida, H., 72,91,271,272,273,274
Ingraham, J.C., Rep.LA-UR-86-4011
Isler, R., 407
Itoh, S., 91
Izvozchikov, A., 6,17,46,47,52,75,85,95,101,108, 109,114,115,117,130,133,144,145,148278,279,359

Jäckel, H., 11,30,38,40,41,51,58,59,60,61,84,99,125, 160,171,227,229,251,252,253,289,290,304,309, 310,325,326,328,380,381,382,383,384,385,387, 388,399,466, IPP-Rep. 1/238, Rep.PPLK R-12
Jäckle , A., 463
Jackson, D.P., 39
Jacob, W., 73,74,167,295,341,457
Jacobi, D., 306
Jaehnig , K., 98
Jaenicke, R., 40,41,51,58,59,60,61,84, 125,160,171,227,251,252,253,289,290,304,309, 310,325,326,328,381,382,383,384,385,387,388, 399,466, IPP-Rep. 1/238, Rep.PPLK R-12
Jakobus, W., 306
Jakoby, A., 80
Jandl, O., 94
Janeschitz, G., 5,6,17,43,46,47,52,53,75,76, 79,85,95,101,102,103,104,108,109,114,115,117, 118,122,130,132,133,144,145,146,147,148,149, 165,177,222,223,264,277,278,279,280,294,296, 297,307,313,315,316,358,359,362,363,364,373, 390,392,407,430,431,440,446,448,449, 7,353,360,361,376,410, IPP-Rep. III/110
Janzen, G., 40,251
Jilge, W., 18,52,53,280
Johnson, J.L., 64
Jones, T.T.C., 268,438
Junker, J., 40,41,51,58,59,60,61,84, 125,160,171,227,251,252,253,289,290,304,309, 310,325,326,328,381,382,383,384,385,387,388, 399,466, 1/238, Rep.PPLK R-12
Jüttner, B., 43

Kadomtsev, B.B., 72,271,272,273,274
Kaiser , L., 365
Kardaun, O., 181
Karger, F., 5,6,17,43,46,47,52,53,75,76, 79,85,95,101,102,103,104,108,109,114,115,117, 118,122,130,132,133,144,145,146,147,148,149, 165,177,222,223,277,278,279,280,297,298,299, 300,307,313,315,316,358,359,362,363,364,390, 392,430,431,440,446,448,449, 7,294,353,360,361,376,407,410, IPP-Rep. III/110
Kasai, M., 72,271,272,273,274
Kasparek, W., 41,51,58,59,60,61,84,125,252,253,289, 290,304,310,328,381,382,383,384,385,387,466, 40,42,191,251,254,255, Rep.IPF 86-2, Rep.PPLK R-12
Kato, S., 301
Kaufmann, M., 262
Kaufmann, M., 47,54,77,78,94,117,306,313, 359,360,361
Keilhacker, M., 5,6,17,43,46,47,52,53,75, 76,79,85,95,101,102,103,104,108,109,114,115, 117,118,122,130,132,133,144,145,146,147,148, 149,165,177,222,223,277,278,279,280,297,307,

313,315,316,358,359,362,363,364,390,392,430,
431,440,446,448,449,
7,294,353,360,361,376,407,410, IPP-Rep.
III/110
Kelber , J.A., 154
Kerner, W., 57,80,81,82,83,302,303
Kessler, G., 50
Kißlinger, J., 56,275,285
Kick, M., 40,41,51,58,59,60,61,84,84,125,160,
171,227,251,252,253,289,290,304,309,310,325,
326,328,381,382,383,384,385,387,388,399,466,
1/238, Rep.PPLK R-12
Kislyakov , A., 76,102,103,146
Kissel, S., 30,38,48,99,380
Kisslinger, J., 286,287,288,305
Klippel, H., 50
Klüber, O., 5,6,17,43,46,47,52,53,75,76,79,
85,95,101,102,103,104,108,109,114,115,117,118,
122,130,132,133,144,145,146,147,148,149,165,
177,222,223,270,277,278,279,280,297,307,313,
314,315,316,358,359,362,363,364,390,392,430,
431,440,446,448,449,
7,294,353,360,361,376,407,410, IPP-Rep.
III/110
Knobloch, A.F., 72,86,87,88,89,90,91,92,93,271,
272,273,274, IPP-Rep. 4/224
Knözinger , H., 329
Kock , L.de , 36,37,208,209,210,247,339
Kolac, U., 74
Kolbasov, B.N., 72,91,271,272,273,274
Kollotzek, H., 54,94,306
Kolos, J., 357
Komarek, P., 86,87,88,89,90
König , F., 308
Köppendörfer, W., 54,94,306
Kornherr, M., 5,6,17,43,46,47,52,53,75,76,
79,85,95,101,102,103,104,108,109,114,115,117,
118,122,130,132,133,144,145,146,147,148,149,
165,177,222,223,277,278,279,280,297,307,313,
315,316,358,359,362,363,364,376,390,392,430,
431,440,446,448,449,
7,294,353,360,361,376,407,410, IPP-Rep.
III/110
Kostenko, A.I., 72,124,271,272,273,274
Kottmair, M., 219
Kotzé , P.B., 76,102,103,146
Kotzlowski, H., 54,94,96,192,193,194,221,308
Kraus, W., 262
Krause, H., 159
Kroiss, H., 40,41,51,58,59,60,61,84,125,160,
171,227,251,252,253,289,290,304,309,310,325,
326,328,381,382,383,384,385,387,388, 399,466,
1/238, Rep.PPLK R-12
Krom, J.G., 438
Krücken, T., 19,225, IPP-Rep. 5/9
Kuehner, G., 40,41,51,58,59,60,61, 84,125,160,
171,227,251,252,253,289,290,304,309,310,325,
326,328,381,382,383,384,385,387,388, 399,466,
1/238, Rep.PPLK R-12
Kukral, H., 209
Kukushkin, A.S., 72,271,272,273,274
Kulcinski , G.L., 124
Kumrić , H., 41,51,58,59,60,61,84,125,252,253,289,
290,304,310,328,381,382,383,384,385,387,466,
42,255, Rep.IPF 86-2, Rep.PPLK R-12
Kunze, R.-C., 357,447
Küphnapfel, U., 30,38,99,380
Kupitz , J., 124
Kutsch, H.-J., 365

Lackner, E., 54,94,306
Lackner, K., 5,17,18,43,46,47,52,53,54,77,
79,85,94,95,97,101,104,108,109,114,115,117,
118,122,130,132,133,142,144,145,147,148,149,
165,177,222,223,270,277,278,279,280,297,306,
307,311,312,313,314,315,316,358,359,362,363,
364,390,392,427,430,431,440,446,448,449,
7,294,353,360,361,376,407,410, IPP-Rep.
III/110
Lagin, L., 98
Lallia, P.P., 99
Lang, R.,
2,47,51,53,117,277,280,353,362,363,313,359,
360,361
Lao, L., 314,427
Lappus , G., 142
Larcher, T.v., 54,94,306
Laurenti , A., 152
Lee , J.K., 278,279,314
Leger, D., 72,271,272,273,274
Lengyel, L.L., 77,100
Lenoci, M., 5,6,17,43,46,47,52,53,75,76,
79,85,95,101,104,108,109,114,115,117,118,
122,130,132,133,144,145,147,148,149,165,177,
222,223,277,278,279,280,297,307,313,315,316,
358,359,362,363,364,390,392,430,431,440,446,
448, 449, 102,103,146,
7,294,353,360,361,376,407,410, IPP-Rep.
III/110,III/113
Lerbinger, K., 80,82
Leung , O., 221
Leuterer, F., 5,6,17,47,79,101,102,103,104,108,
132,133,144,145,146,177,277,315,316,317,362,
410,430,472
Leyrer , J. , 329
Liebl, H., 105,195,318,319,320
Linke , J., 221
Lisitano, G., 5,6,17,43,46,47,52,53,75,76,
79,85,95,101,102,103,104,108,109,114,115,117,
118,122,130,132,133,144,145,146,147,148,149,
165,177,222,223,277,278,279,280,297,307,313,
315,316,321,358,359,362,363,364,390,392,430,
431,440,446,448,449,
7,294,353,360,361,376,407,410, IPP-Rep.
III/110
Litunosvkij, R.N., 72,271,272,273,274
Lohnert, H., 357,447
Lomas, P., 239
Lopes-Cardozoy, N., 48
Lortz, D., 151,322,323,324, IPP-Rep. 6/262
Lotz, W., 106
Loubriel , G., 154
Löw , R., 365
Lüthi , P., 308

Maaßberg, H., 40,41,51,58,59,60,60,61,84,125,133,
160,171,227,251,252,253,289,290,304,309,310,
325,326,327,328,381,382,383,384,385,387,388,
399,466, IPP-Rep. 2/281, 1/238, Rep.PPLK R-12
Magyar, G., 48
Mahdavi, A., 76
Mahn, C., 40,41,51,58,59,60,61,84,125,160,
171,227,251,252,253,289,290,304,309,310,325,
326,328,381,382,383,384,385,387,388,399,466,
IPP-Rep.1/238, Rep.PPLK R-12
Maier, E.A., 439
Maier, J., 68
Margaritondo, G., 55,154
Margraf, R., 329
Mark, E.v., 118,148,149,150,227,277,297,307,353,362,
363,376,382,383,384,385,431, 364,430,458
Martin, P., Rep.JET-R(86)07

Martinelli, A.P., 208,209,210,214,247,330,440, IPP-Rep. 9/60
Massmann, P., 62,331
Mast, F., 6,17,46,47,52,75,85,95,101,108,109,114, 115,117,130,133,144,145,159,278,279,359,430, Rep.JET-R(86)07
Mathis, R., 40,41,51,58,59,60,61,84,107,125, 160,171,227,232,251,252,253,289,290,304,306, 309,310,325,326,328,381,382,383,384,385,387, 388,399,466, IPP-Rep.1/238, Rep.PPLK R-12
Mattas, R.F., 72,271,272,273,274
Mayar, G., 11
Mayer, H.M., 5,6,17,43,46,47,52,53,75,76, 79,85,95,101,102,103,104,108,109,114,115,117, 118,122,130,132,133,144,145,146,147,148,149, 165,177,222,223,277,278,279,280,297,307,313, 315,316,358,359,362,363,364,390,392,430,431, 440,446,448,449, 7,294,353,360,361,376,407,410, IPP-Rep. III/110
McCarthy, P.J., 332,427, IPP-Rep. 5/12
McCormick, K., 5,6,17,43,46,47,52,53,75,76,79, 85,95,101,102,103,104,108,109,114,115,117,118, 122,130,132,133,144,145,146,147,148,149,165, 177,222,223,277,278,279,280,297,307,313,315, 316,333,334, 335,336,337,338,358,359,362,363, 364,390,392,430, 431,440,446,448,449, 7,294,353,360,361,376,407,410, IPP-Rep. III/110
McCracken , G.M., 36,37,208,209,214,247,339
McCullen, P., 438
McDonald , J.M., 221
McGuire K., 340
Meisel, D., 5,6,17,43,46,47,52,53,75,76,79, 85,95,101,102,103,104,108,109,114,115,117,118, 122,130,132,133,144,145,146,147,148,149,165, 177,222,223,277,278,279,280,297,307,313,315, 316,353,358,359,362,363,364,390,392,430,431, 440,446,448,449, 7,294,360,361,376,407,410, IPP-Rep. III/110
Melkus, W., 357
Memmel, N., 167,185,341,457
Mendenhall, M.H., 55
Merkel, P., 64,70,110,111,352
Mertens, V., 5,6,17,43,46,47,52,53,53,75,76,79, 85,95,101,102,103,104,108,109,114,115,117,118, 122, 130,132,133,144,145,146,147,148,149,165, 177,222,223,277,278,279,280,297,307,313,315, 316,358,359,360,361,362,363,364,390,392,430, 431,440,446,448,449, 7,294,353,360,361,376,407,410, IPP-Rep. III/110
Meyer-Spasche, R., 151,342,343,344,345,346,347,348,349
Miley, G.H., 127
Miller , R.L., 124
Milora, S.L., Rep.PPPL 2346
Möller, W., 16,112,131,134,170,206,350,351,408, 409,465, IPP-JET-Rep.32
Morgan , P.D., 228
Mori, S., 72,271,272,273,274
Morimoto, S., Rep.PPLK R-12
Morris, R.N., 352
Morse , D.M., 221
Morsi, H.W., 113
Mühling, E., 4,33,355, IPP-Rep. 9/56,9/58
Mühlratzer , A., 365
Mukherjee, S.B., 152,306
Müller, E.R., 5,6,11,17,30,38,43,46,47,52,53,75,76, 79,85,95,99,101,102,103,104,108,109,114,115, 117,118,122,130,132,133,144,145,146,147,148, 149,165,177,222,223,277,278,279,280,297,307, 313,315,316,358,359,362,363,364,380,390,392, 430,431,440,446,448,449, 7,294,353,360,361,376,407,410, IPP-Rep. III/110,III/112
Müller, G., 40,41,51,58,59,60,61,84,125,160, 171,196,227,251,252,253,289,290,304,309,310, 325,326,328,381,382,383,384,385,387,388,399, 466, IPP-Rep.1/238, Rep.PPLK R-12
Müller , G., 191,251
Müller, G.A., 41,51,58,59,60,61,84,125,252,253,289,290 304,310,328,381,382,383,384,385,387,466,40,422 54,255,Rep.IPF 86-2, Rep.PPLK R-12
Münch, H., 40,41,51,58,59,60,61,84,125,160, 171,227,251,252,253,289,290,304,309,310,325, 326,328,381,382,383,384,385,387,388,399,466, IPP-Rep.1/238, Rep.PPLK R-12
Münich, M., 5,6,79,102,103,104,132,144,145,146, 177,277, 315,316,,362,410,430, 472
Munson, C.P., Rep.LA-UR-86-4011
Murmann, H., 5,5,6,17,43,46,47,52,53,75,76,79,85, 95,101,102,103,104,108,109,114,115,117,118, 122,130,132,133,144,145,146,147,148,149,165, 177,222,223,277,278,279,280,297,307,313,315, 316,353,354,358,359,362,363,364,390,392,430, 431,440,446,448,449, 7,294,360,361,376,407,410, IPP-Rep. III/110

Närmann, A., 355
Neilson, G.H., 352
Neuhauser, J., 54,97,116,306,356
Neumann, M., 44
Niedermeyer, H., 5,6,17,43,46,47,52,53,75,76,79, 85,95,101,102,103,104,108,109,114,115,117,118, 122, 130,132,133,144,145,146,147,148,149,150, 165,177,222,223,277,278,279,280,297,307,313, 315,316,358,359,360,361,362,363,364,376,390, 392,407,430,431,440,446,448,449, 7,294,353,410, IPP-Rep. III/110
Nijman, J.P., 438
Niles, D., 55
Nilles, E.J., Rep.LA-UR-86-4011
Noterdaeme, J.-M., 17,47,75,94,95,118,133,148,169, 306,364,365,366,367,368,430,149,150,227,277, 297,307,353,362,363,382,383,384,385,431,
Nührenberg, J., 69,110,119

O'Rourke, J., 48,228
Ohlendorf, W., 40,41,51,58,59,60,61,84,125,160, 171,227,251,252,253,289,290,304,309,310,325, 326,328,369,370,381,382,383,384,385,387,388, 399,466, IPP-Rep.1/238, Rep.PPLK R-12
Onsgaard, J., 120,153,441
Oord, E., 35,48
Orlov , V.V., 124
Ott, W., 41,51,84,125,290,304,310,357,328,382,383, 384,385,387,388,466
Ottenberger, W., 221

Partrigde , J.W., 209,214
Pasini , D., 462
Peatman, W.C.B., 55
Peng, Y.-K.M., 72,271,272,273,274
Penningsfeld, F.P., 41,51,84,125,284,290,304,310, 328,357, 382,383,384,385,387,388,466, IPP-Rep. 4/229
Perchermeier, J., 188,189,365,439
Pericart, J., 50
Pfirsch, D. , 23,215,371,372,121,128, IPP-Rep. 6/263
Phillips , V., 170,465

Pietrzyk , A., 6,17,46,47,85,95,359,101,108,109,114, 115,117,130,133,144,145
Pillsticker, M., 54,94,306,463
Pisani , D., 439
Pistunovich, V.I., 72,271,272,273,274
Pitschi , F.X., 458
Pöffel, W., 373
Pohl, F., 215, IPP-Rep. 6/261,6/263
Pöhlchen, R., 54,94,152
Poker , D.B., 131
Pontau , A.E., 221
Poschenrieder, W., 5,6,17,43,46,47,52,53,75,76,79, 85,95,101,102,103,104,108,109,114,115,117,118, 122, 130,132,133,144,145,146,147,148,149,165, 177, 222,223,277,278,279,280,297,307,313,315, 316, 358,359,362,363,364,374,390,392,430,431, 446, 448,449, 7,294,353,360,361, 376,407,410, 440, IPP-Rep. III/110
Post, D.E., 72,271,272,273,274
Preis, H., 54,94,123,142,306,375, IPP-Rep. 1/229
Prini , G., 152
Puri, S., 118,148,149,150,227,277,297,307, 353,362,363,376,382,383,384,385,431,364,430, IPP-Rep. 4/227,4/228,4/230

Radtke , W., 365
Ramsey, A., Rep.PPPL 2346
Rapp, H., 5,6,17,43,46,47,52,53,75,76,79, 85,95,102,103,104,108,109,114,115,117,118,122, 130, 132,133,144,145,146,147,148,149,165,177, 222,223,277,278,279,280,297,307,313,315,316, 358,359,362,363,364,376,377,378,390,392,430, 431,440,446,448,449, 7,294,353,360,361,407,410, IPP-Rep. III/110
Rau, F., 40,41,51,56,58,59,60,61,63,84,124,125,160, 171,227,251,252,253,275,285,286,287,288,289, 290,304,309,310,325,326,328,379,381,382,383, 384,385,387,388,399,466, IPP-Rep.1/238, Rep.PPLK R-12
Räuchle , E., 41,51,58,59,60,61,84,125,251, 252,253, 289,290,304,310,328,381,382, 383,384,385,387,466, Rep.PPLK R-12
Rebut, P.H., 380
Reese, W.H., 306
Reicher , W., 113
Renner, H., 40,41,51,58,59,60,61,84,125,126,160, 171,227,251,252,253,289,290,304,309,310,325, 326,328,381,382,383,384,385,387,388,399,466, IPP-Rep.1/238, Rep.PPLK R-12
Riedel , R., 154
Riedel, K., 82
Riedler, H., 17,47,52,85,95,114,117,133,144,145,278, 279,294,353,359,360,361, 118,148,149,150,165, 277,297,307,313,357,358,362,363,364,376,430, 431,448,449, IPP-Rep. 4/231
Riedler, J.M., 127,386
Rij, W.I. van, 70
Ringler, H., 40,41,51,58,59,60,61,84,84,125,160, 171,227,251,252,253,289,290,304,309,310,325, 326,328,381,382,383,384,385,387,388,389,399, 466, IPP-Rep.1/238, Rep.PPLK R-12
Riyopoulos, S., 128
Roberto , J.B., 393
Rocco, P., 50
Rogozik, J., 44,129,182,263,341,437
Röhr, H., 6,17,46,47,52,75,85,95,108,109,114,115, 117,130,133,144,145,146,278,279,353,359,390, 402
Roney , P., 98
Roth, J., 17,46,47,52,76,85,95,108,109,114,115, 117,130,131,133,144,220,221,278,279,359,391, 392,393,394,395,396,397,398,408,409
Rouyer, J.L., 50
Rudyj, A., 186
Ruhs, N., 6,146
Ryter, F., 5,6,17,43,46,47,52,53,75,76,79, 85,95, 104,118,122,132,133,147,148,149,165,177,222, 223,277,278,279,280,297,307,313,315,316,358, 359,362, 363,364,390,392,430,431,446, 448, 449,102,103, 108,109,114,115,117,130,144,145, 146,364, 7,294,353,360,361,376,407,410,440, IPP-Rep. III/110

Salat, A., IPP-Rep. 6/257
Salpietro, E., 72,271,272,273,274
Sandmann, W., 47,53,117,277,280,313,353,359,360, 361,362,363,Santaniello, A., 397,398
Sapper, J., 40,41,51,58,59,60,61,84,107,125,160, 171,227,232,251,252,253,289,290,304,309,310, 325,326,328,381,382,383,384,385,387,388,399, 466, IPP-Rep.1/238, Rep.PPLK R-12
Sardei, F., 40,41,51,58,59,60,61,84,84,125, 160,171,227,251,252,253,289,290,304,309,310, 325,326,328,381,382,383,384,385,387,388,399, 466, IPP-Rep.1/238, Rep.PPLK R-12
Sawicka, B.D., 134
Sawicki , J.A., 134
Schartner , K.-H., 373
Scheidt , H., 295
Scherzer, B.M.U., 16,135,350,400,440, IPP-JET-Rep.32
Schiller, P. 72,271,272,273,274
Schlüter, A., 136,137
Schmidt, G.L., Rep.PPPL 2346
Schminke , W., 168
Schmitter, K.H., 5,102,103,104,132,138,145,146, 277,315,316,362,410,430
Schneider, F., 17,46,47,52,75,76,79,85,95,102,103, 108,109,114,115,117,130,133,144,145,146,197, 278,279,359,401
Schneider, H., 54,94,306
Schneider, R., 29
Schneider, U., 98
Schneider, W., 77,97,116, Rep.PPPL 2346,PPPL 2361
Schoenewolf, I., 40,41,51,58,59,60,61,84,125,160, 171,227,251,252,253,289,290,304,309,310,325, 326,328,381,382,383,384,385,387,388,399,466, IPP-Rep.1/238, Rep.PPLK R-12
Schramm, G., 35
Schugmann , L., 471
Schüller , F., 228
Schüller , P.G., 40,41,42,51,58,59,60,61,84, 125,198,199,251,252,253,254,255,289,290,304,310, 328,381,382,383,384,385,387,466 Rep.IPF 86-2, Rep.PPLK R-12
Schumacher, U., 17,139,140,222,223,402,403, 404,405,406
Schwarz, E., 81
Schweizer, S., 306
Schwenn, U., 141
Schwörer , K., 41,51,58,59,60,61,84,125,251,252, 253,289,290,304,310,328,381,382,383,384,385, 387,466, Rep.PPLK R-12
Seidel, U., 54,94,142,306
Seki, M., 72,271,272,273,274
Senftinger, B., 27,187,231
Serebrennikov, D.V., 72,271,272,273,274
Setzensack, C., 17,46,47,52,75,85,95,108,109,114, 115, 117,130,133,144,145,278,279,359,407,430
Sexton, M.C., IPP-Rep. 5/12
Shatalov, G.E.72,271,272,273,274
Shaw, R., 331
Sielanko, J., 261,357

Siller, G., 5,17,43,46,47,52,53,75,76,79,
85,95,102, 103,104,108,109,114,115,117,118,
122,130,132,133, 144,145,146,147,148,149,165,
177, 222,223, 277,278, 279,280,297,307, 313,
315, 316,358,359,362,363,364, 390, 392,430,
431,446,448, 449, 7,294,353,360,361,376,407,
410,440,IPP-Rep. III/110
Smeulders, P., 5,17,43,46,47,52,53,75,76,79,
85,95,102,103,104,108,109,114,1115,117,118,
122,130,132,133,143,144,145,146,147,148,149,
165,177,222,223,277,278,279,280,297,307,313,
315,316,358,359,362,363,364,390,392,430,431,
446,448,449,
7,294,353,360,361,376,407,410,440,
IPP-Rep. III/110
Snowdon , K., 355
Söder, B., 408,409
Söldner, F.X., 5,6,17,43,46,47,52,53,75,76,79,85,
95,102,103,104,108,109,114,115,117,118,122,
130,132,133,144,145,146,147,148,149,165,177,
222,223,277,278,279,280,297,307,313,315,316,
358,359,362,363,364,390,392,410,411,412,413,
414,415,416,417,418,419,420,421,422,423,424,
425,430,431,446,448, 449,
7,294,353,360,361,376,407,440,
IPP-Rep. III/110, III/111
Söll, M., 118,364,365,458
Sombach, B., 54,94,306,308,426
Spampinato, P.T., 72,271,272,273,274
Spears, W.R., 50
Spensberger, W., 200
Speth, E., 17,47,52,75,76,79,85,94,95,114,117,133,
144,145,147,262,278,279,294,306,353,359,360,
361,376,447,
41,51,84,118,125,148,149,150,165,277,290,297,
304, 307,310,313,328,357,358,362,363, 364,383,
384,385, 387,388,430,431,448,449,466
Spitzer, H., 188
St.John, H., 427
Stäbler, A., 30,38,62,99,159,229,239,268,294,
331,353,360,361,376,380,438,447,
118,148,149, 150,165,277,297,307,313,357,
358,362,363,364, 376,430,431,448,449
Stacey, W.M., 72,271,272,273,274
Stambaugh, R.D., 85,314,427
Starley, K.D., 438
Staudenmaier, G., 428,429
Steiger , J., 471
Steinmetz, K., 17,47,75,76,79,95,118,133,148,149,
150,227,277,297,307,353,359,362,363,364,376,
382,383,384,385,430,430,431,432,433
Steuer, K.-H., 5,17,43,46,47,52,53,75,76,79,
85,95,102,103,104,108,109,114,115,118,117,122,
130, 132,133,144,145,146,147,148,149,165,177,
222,223,277,278,279,280,297,307,313,315,316,
353,358,359,362,363,364,390,392,430,431,434,
435,436,440,446,448,449,
7,294,360,361,376,407,410, IPP-Rep. III/110
Steuerwald, J., 81
Stimmelmayr, A., 189
Stimpfle, C.J., 437
Stockinger, K., 401
Stoffel, N.G., 55,154
Storck, D., 268,438
Stott , P.E., 36,37,208,339
Strait , E.J., 314
Stredulinsky, E., 151
Streibl, B., 54,94,152,439
Ströhle, J.-G., 365
Stücheli , A., 459
Sugihara, M., 72,271,272,273,274
Svendsen, L.G., IPP-Rep. 9/57
Sviatoslavsky , I.N., 124

Taglauer, E., 3,39,55,76,120,153,154,155,156,206,250,
301,329,440,441,442,443,444,445
Tajima , T., 128
Tasso, H., 157,158, IPP-Rep. 6/264,6/260,6/259
Taylor, T.S., 427
Thomas, P., 239
Thome, R.J.72,271,272,273,274
Thompson, E., 239,268
Thomsen, K., 159
Thumm , M., 40,41,42,51,58,59,60,61,84,125,251,
252,253,254,255,289,290,304,310,328,381,382,
383,384,385,387,466, Rep.IPF 86-2,
Rep.PPLK R-12
Tolk, N.H., 55,154
Tomabechi, K.72,91,271,272,273,274
Trcka, E., 365
Troppmann, M., 306
Tsuji, S., 34,35
Tubbing, B.J.D., 34
Tutter, M., 40,41,51,58,58,59,59,60,60,
61,61,84,125,160,171,227,251,252,253,289,
290,304,309,310,325,326, 328,381,382,383,384,
385,387,388,399,466, IPP-Rep.1/238, Rep.PPLK
R-12

Ugniewski, S., 75
Ulrich , D., 459
Ulrich, M., 205
Varga , P., 155
Varni , G., 152,439
Venus, G., 306
Verbeek, H., 161,446
Vernickel, H., 94,162,306
Vien, T., 5,6,102,103,104,132,144,145,146,177,
277,315,316,362,410,430,472
Vietzke , E., 170
Vlases , G., 46,53,102,103,117,146,277,280,353,
359,360,361,362,363,
Vollmer, O., 17,47,52,75,76,79,85,95,114,117,133,144,
145,147,278,279,294,353,359,360,361,376,447,
118,148,149,150,165,277,297,307,313,357,358,
362,363,364,376,430,431,448,449

Wagner, F., 5,6,17,43,46,47,52,53,75,76,79,
85,95,102,103,104,108,109,114,115,117,118,122,
130,
132,133,144,145,146,147,148,149,163,164,165,
166, 177, 222,223,269,277,278,279,280,292,293,
296,297, 307,313,315,316,340,358,359,362,363,
364,390,392, 430,431,446,448,449,450,451, 452,
453,454,455,456,
7,294,353,360,361,376,407,410,440,
IPP-Rep. III/110
Wagner, F.E., 134
Wampler, W.R., 428
Wandelt, K., 167,457
Watkins , M., 228
Watson , R.D., 221
Watt, R.G., Rep.LA-UR-86-4011
Weber, G., 205
Weber, P.G., Rep.LA-UR-86-4011
Wedler, H., 118,148,149,150,169,227,277,297,307,
353, 362,363,364,376,382,383,384,385,430,431,
458
Weichselgartner, H., 189,201,202,203,459,460,461
Weigand , W., 218
Weiss, H., 105

Weller, A., 11,30,34,35,38,40,41,51,58,59,60,
61,84,84,99,125, 160,171,227,228,251, 252,
253,289,290,304,309, 310,325,326,328,380,381,
382,383,384,385,387, 388,399,462,466, IPP-
Rep.1/238, Rep.PPLK R-12
Werner, F., 54,94,463
Wesner, F., 17,47,75,76,79,94,95,118,133,148,149,
150,168,169,227,277,297,306,307,353,362,363,
364,365,376,382,383,384,385,430,431,458,464
Wesson, J.A., 34,48
Whitley , J.B., 221
Wieczorek, A., 54,94,218,219,306
Wielunski, M., 210
Wienhold , P., 170,465
Wilhelm , R., 40,41,42,51,58,59,60,61,84,125,196,
198,199,251,252,253,254,255,289,290,304,310,
328,381,382,383,384,385,387,466, IPP-Rep.
III/110, Rep.PPLK R-12
Wimmel, H.K., 23
Winter, J., 170,465
Wittenbecher, K., 357,447
Wittmaack , K., 131,393
Wobig, H., 40,41,49,51,56,58,59,60,61,
84,125,160, 171,172,173,227,251,252,253, 275,
284,285,286, 287,288,289,290,304,305,309,310,
325,326,328, 381,382,383,384,385,387,388,399,
466,467,468, 469,470, IPP-Rep. 2/283, IPP-
Rep.1/238, Rep.PPLK R-12
Wordel , R., 134
Woyke , H., 142
Woyna, F.v., 6,102,103,145,146,177,472
Wulff, G., 357
Wunderlich, R., 116,356
Wurden, G.A., Rep.LA-UR-86-4011
Würsching, E., 40,41,51,58,59,60,61,
84,125,160, 171,227,251,252,253,289,290,304,
309,310,325, 326,328,381,382,383,384,385,387,
388,399,466, IPP-Rep.1/238, Rep.PPLK R-12
Wyss , J., 168

Young, D., 438
Young, I.D., 438

Zanza, V., 48
Zasche, D., 6,11,17,34,35,46,47,48,75,79,85,95,108,
109,114,115,117,130,133,144,145,278,279,359,
462
Zehrfeld, H.P., 85,174,175,270,278,279,314,471
Zille, R., 69,110,119
Zimmermann, D., 176
Zippe, M., 40,41,51,58,59,60,61,84,125,160,
171,227,251,252,253,289,290,304,309,310,325,
326,328,381,382,383,384,385,387,388,399,466,
IPP-Rep.1/238, Rep.PPLK R-12
Zouhar, M., 5,6,102,103,104,132,144,146,177,277,
315,316,362,410,430,472

University Contributions to IPP Programme

INSTITUT FÜR PLASMAFORSCHUNG (IPF)
DER UNIVERSITÄT STUTTGART
(Prof. Dr. H. Zwicker*)
(Prof. Dr. R. Wilhelm**)

In 1986 the IPP-IPF cooperation in the field of fusion related research and development has been successfully continued.

The ECRH project as the largest activity is concentrated on the completion of the 1 MW/70 GHz long-pulse ECRH-system for the W VII-AS stellarator. The components tests promise optimum technical and -hopefully- physical results.
Theoretical investigations mainly concern ray propagation and time dependent transport calculations for stellarators at ECRH conditions.
A first successful experimental demonstration of the LIDAR scattering concept on JET was a rather encouraging progress for the laser diagnostic group. Besides this project the FIR scattering was continued on ASDEX with measurements of the k-spectra of the low frequency fluctuations during the various kinds of plasma heating.
On the WEGA stellarator a programme of flux surface mesurements with electron beams has been started. A meanwhile improved detection method will be applied - in cooperation with the Wendelstein team - at the coming W VII-AS stellarator.
In the last year the plasma focus experiment POSEIDON achieved successful operation at full bank energy.

*) until October 1986
**) from October 1986

1. ELECTRON CYCLOTRON RESONANCE HEATING (ECRH)

(R. Wilhelm, H. Barkley, V. Erckmann +,
W. Kasparek, H. Kumric, G.A. Müller,
P.G. Schüller, M. Thumm)

The work of the ECRH-group in 1986 was mainly concentrated on the assembly and further completion of the 70 GHz/1MW long-pulse system for the coming W VII-AS stellarator. This includes the development and manufacture of the transmission line components (bends, tapers, filters, mode transformers, microwave diagnostic components) and the electrotechnical equipment (modulators, protection- and control units) at the IPF Stuttgart and a successful operational test of the first two long-pulse gyrotrons at the IPP Garching.

Besides the work for the 70 GHz system, the developments for a planned 140 GHz ECRH experiment (cooperation between IPF Stuttgart, IPP Garching and KfK Karlsruhe) have proceeded at the IPF.

+ IPP Garching

1.1 Development and First Tests of the 70 GHz 1 MW ECRH System for W VII-AS

1.1.1 Microwave generator system

The microwave generator system consists of five modules each comprising a 70 GHz, 200 kW gyrotron together with the cooling systems and the electrical power supply. The first module containing a 100 ms-pulse gyrotron was tested as a prototype during 10 000 pulses on W VII-A in 1985. Based on these experimental results the electrical supply for the electron gun of the gyrotron and the tube protection system was redesigned by the IPF. Five of such new units were manufactured and delivered to the IPP in 1986.

The new electron gun supply ensures high stability as well as a modulation capability with arbitrary functions of cathode heater power and gun anode voltage. For long pulse operation (3s) heater power has to be time dependent for counteracting emission cooling. Microwave output power is controlled by the gun anode voltage which enables stabilisation or programming of power via an external feedback loop. Monitoring of tube currents is done with specially designed constant flux transformers usable for long pulse operation.

The tube protection systems consist of sensors for overcurrents and overvoltages, of light detectors for arcs at the gyrotron output window and a microwave power monitor for forward and reflected power (see 1.1.3.1). In a fault condition these sensors trigger a fast switch-off of the gyrotron input power.

During 1986 module no. 2 and 3 were completed with gyrotrons VARIAN VGE-8007 and tested in long-pulse operation (70 GHz, 200 kW, 3s).

1.1.2 ECRH transmission line system

The transmission line between one of the long-pulse gyrotrons and W VII-AS is shown schematically in Fig. 1. The Table I gives an overview of the basic waveguide components and summarizes their features and purpose. The indicated losses were determined experimentally for the individual components in specific low-power tests. All experimental values were found to be in good agreement with the theoretical calculations. The transmission lines include several mode converters to transform the circular symmetric gyrotron output mode mixture (mainly TE02) to the almost perfectly linearly polarized HE11 hybrid mode through the conversion sequence ΣTEOn→TE01→TE11→HE11. This conversion scheme has the advantage that the converters can all be made without bends allowing an arbitrary choice and fast change of the polarization plane by simply rotating the serpentine TE01-to-TE11 converter around its axis. The intermediate TE01 wave is appropriate for weakly attenuated long-distance propagation through highly oversized smooth-wall circular waveguides. Close to the access port to the experiment this mode is transfered into the quasi-optical Gaussian-like HE11 mode (propagates in corrugated waveguide) which has nearly no cross polarization and low sidelobe levels.

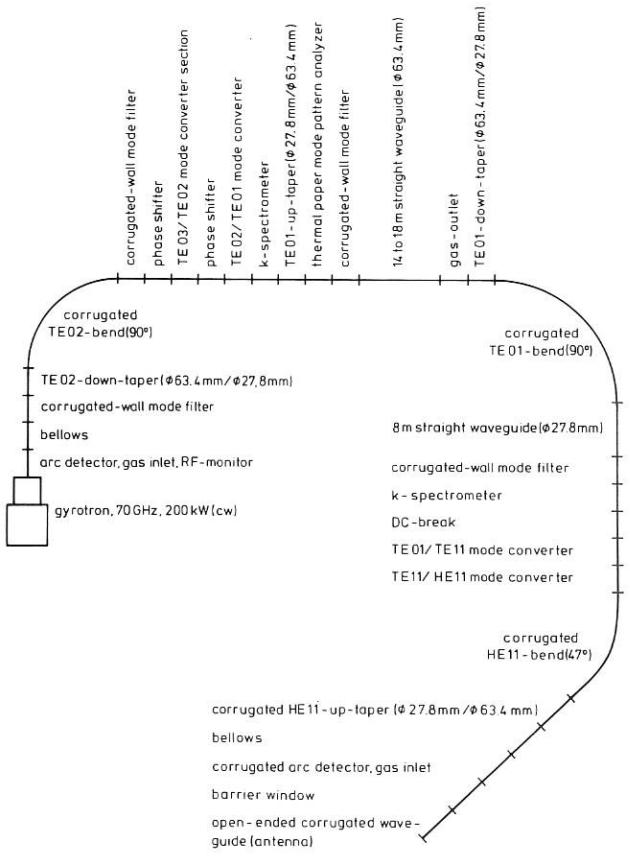

Fig. 1: Setup of a 70 GHz ECRH transmission line for W VII-AS.

The mode purity in the transmission lines is conserved by using waveguide diameter tapers with optimized non-linear profiles and circumferentially corrugated, gradual waveguide bends with tapered curvature variation and matched corrugation. Highly efficient corrugated-wall mode filters (selective for asymmetric modes) decouple the different waveguide sections and the gyrotrons from the plasma load and avoid trapped-mode resonances. The structures of wall perturbations in the advanced rippled-wall mode converters (ΣTEOn→TE01 and TE01→TE11), the curvature distributions, lengths and corrugations of the gradual bends, and the non-linear contours of the diameter tapers were optimized by numerically integrating the corresponding coupled mode differential equations. Computer-aided designs of the corrugated TE11→HE11 mode converter and of the corrugated-wall mode filters were obtained with a scattering matrix code. The overall efficiency in the desired HE11 mode of a complete transmission line was calculated to be 87%, the total transmission efficiency is expected to be approximately 91% of the initial ΣTEOn gyrotron mode content.

The four long-pulse gyrotrons feed two pairs of corrugated antennas mounted at two adjacent tan-

gential injection ports of W VII-AS, launching Gaussian-like microwave beams into the plasma. At the poloidal position of these injection ports the plasma exhibits an upright, elongated D-shaped contour and the magnetic field has the usual 1/R-decay (launching from the low-field side, gradient length ≈ 1.2 m). The microwave beams are deflected and focussedby ellipsoidal stainless steel reflectors. The features of the beams are: plane phase-fronts at the edge of the plasma, focal diameter $(1/e^2)$ = 6 cm, and power density ≦ 6 kW/cm^2. Fig. 2 shows a low-power measurement of the field pattern in the beam waist after reflection. The mirrors are tiltable around the horizontal and vertical axis and thus allow different heating scenarios (see stellarator part of this annual report).

component	waveguide mode	purpose and features	typical losses
gyrotron	≈ 95% TE02	200 kW millimeter-wave power source	(≈ 5%)
corrugated mode filter	TE02	attenuation of high-order asymmetric modes of the gyrotron	< 0.1%
down-taper	TE02	non-linear reduction of gyrotron waveguide diameter from 63.5 to 27.8mm, length 0.71m	< 0.1%
corrugated bend	TE02	gradual 90°-bend with sinusoidal curvature, corrug. depth 0.3·(λ/4), arc length 1.74m	≦ 1.5%
mode converter	TE02 → TE01 (TE03)	transformation into low-loss fundamental circular electric mode, periodic radius perturbations,8 geometrical periods, 0.87m	0.4%
corrugated mode filter	TE01	attenuation of spurious TEmn (m≠0) and TMmn modes by 90-99%, length 1.2m	≦ 1%
up-taper	TE01	non-linear enlargement of waveguide diameter from 27.8 to 63.4mm, length 0.71m	< 0.1%
straight waveguide	TE01	14-18 m transmission line with D=63.4 mm	0.13%
down-taper	TE01	non-linear reduction of waveguide diameter from 63.4 to 27.8mm, length 0.71m	< 0.1%
corrugated bend	TE01	gradual 90°-bend with triangular curvature, corrug. depth 0.2·(λ/4), arc length 2.40m	≦ 1.5%
straight waveguide	TE01	8 m transmission line with D=27.8 mm	0.8%
corrugated mode filter	TE01	attenuation of spurious TEmn (m≠0) and TMmn modes by 90-99%, length 1.2m	≦ 1%
mode converter	TE01 → TE11	transformation into almost linearly pol. mode, periodic curvature perturbations 8 geometrical periods, length 2.53m	2.7%
corrugated mode converter	TE11 → HE11	transformation into optimum linearly pol. mode, non-linear variation of corrugation depth from λ/2 to λ/4, length 0.37m	1.5%
corrugated bend	HE11	gradual 47°-bend with sin²-curvature, corrug. depth λ/4, arc length 1.50m	≦ 1.5%
corrugated up-taper	HE11	non-linear enlargement of waveguide diameter from 27.8 to 63.5mm, length 0.70m	≦ 0.2%
barrier window	HE11	corrug. waveguide, sapphire, FC75-cooled	
antenna waveguide	HE11	corrugated stainless steel waveguide for HE11 launching	< 0.1%
focusing mirror	HE11	ellipsoidal stainless steel reflector for perpendicular HE11 launching	1%

TABLE I: Waveguide mode, purpose, features and typical losses of the basic components in the 70 GHz ECRH transmission lines on W VII-AS.

The power of the 100 ms-pulse gyrotron will be transmitted through a transmission line similar to the described ones and will be launched into the poloidal plane of W VII-AS where the plasma cross section has a triangular shape. At this location the magnetic field gradient is reversed showing a rather weak gradient (gradient length ≈ 10 m). This peculiarity allows irradiation of the plasma from the high-field side, which is in this case the torus outside (see stellarator part of this annual report).

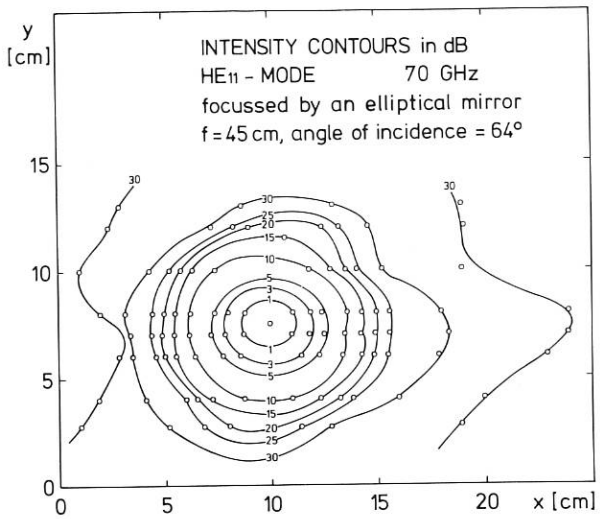

Fig. 2: Measured intensity contours of the 70 GHz HE11 mode radiated from an open-ended corrugated waveguide (D=63.4 mm) and focused by an ellipsoidal mirror (f=45 cm).

1.1.3 Microwave diagnostics

1.1.3.1 Wavenumber spectrometers

During the last year the wavenumber spectrometer was upgraded in several points. Two types of receiver antennas were developed to increase the resolution of the instrument. The prime focus parabolic reflector antenna measures the full range of evaluation angles (6° - 174°) with a resolution (FWHM) of 2°, while the other antenna consisting of a tiltable spherical reflector and a receiver horn gives access to angles between 0° and 20° with a resolution of approx. 1°. The suppression of sidelobes and cross-polarization is better than 30 dB. A precise antenna drive with an angle encoder controls the elevation of the antenna with an accuracy of 0.1°. Bearings with rotable flanges allow the measurement of the polarization direction for asymmetric modes.

Besides the test of the many components for the transmission lines (see 1.1.2), the instrument was used to measure the mode content of the VARIAN gyrotrons which are foreseen for the ECRH system on W VII-AS.

The mode purity of the 100 ms-pulse gyrotron was determined using two different wavenumber spectrometers with internal diameter D = 63.4 mm and D = 27.8 mm, respectively. Fig. 3 shows the $\underline{E} \perp \underline{k}$ and $\underline{E} \parallel \underline{k}$ spectra measured with the smaller diameter spectrometer. Besides the main mode TE02, major impurities in the TE03 mode (3.5%) and the TE13 mode (6%) as well as spurious TM11 and TM12 modes (<1%) were detected. The unwanted TE03 contribution might result from nonideal waveguide tapering and the asymmetric modes from a small tilt within

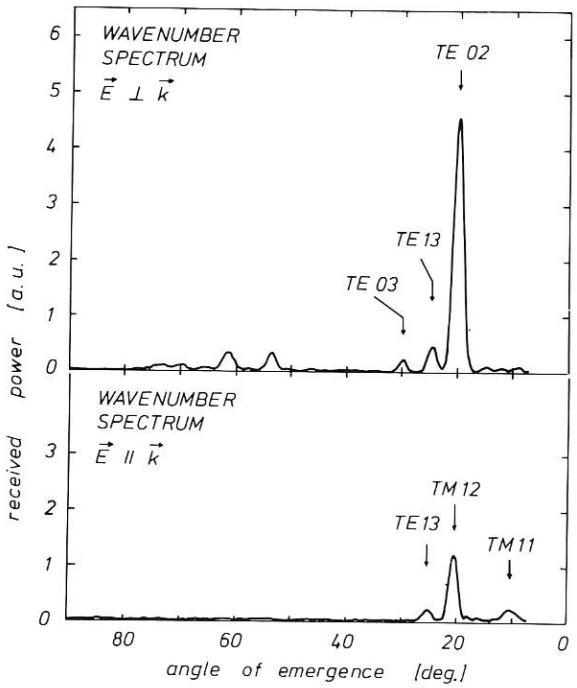

Fig. 3: $\underline{E} \perp \underline{k}$ and $\underline{E} \parallel \underline{k}$ spectra of the radiation of a 100 ms VARIAN 70 GHz gyrotron (VGE-8070) measured with a k-spectrometer (D= 27.8 mm).

the gyrotron. Measurements with the larger diameter spectrometer reveal some amount of additional spurious high-order asymmetric modes which are in the smaller waveguide diameter under cutoff conditions. Mode purity measurements on two long-pulse gyrotrons (VARIAN VGE-8007) reveal a remarkably reduced level of asymmetric modes compared to the pulsed tube. Only a small amount of less than 1% in the modes TM11, ..., TM14 is observed, which may be excited either by asymmetries in the tube (e.g. pumping channels) or by slightly deformed bellows between gyrotron and spectrometer. The main portion of the parasitic modes are TE0n modes which probably are excited from the TE02-mode in the taper section as the up and down taper of these gyrotrons are assembled from different conical parts and thus have not the ideal contour. The power contribution of these modes (TE01, TE03, ..., TE08) is in total 5%, so that the mode purity of the cw-gyrotron is around 94%.

1.1.3.2 Matched loads for linearly polarized waves

The development of matched loads for absorption and calibrated power measurements of high-power millimeter waves has been carried on. A new type of load was built which is applicable to measurements of linearly polarized modes (e.g. TE11 or HE11). The principle of construction is shown in Fig. 4 which gives a schematic view of a fire-clay load as dummy load for high-power microwaves. The power is absorbed in a flat absorber chamber containing the absorbing medium either fire-clay or octanol which is separated from the load cavity by a thin planar dielectric window, e.g. alumina or PTFE. The absorber chamber is mounted in an oblique position so that its normal forms an angle α with the microwave beam. This angle α corresponds to the Brewster angle, so that matched linearly polarized radiation enters the absorber chamber without reflection. In the calorimeter load with octanol as absorbing medium a polarizing filter which is penetrable only to linearly polarized radiation can be installed in front of the oblique chamber. Thus an exact determination of the power of the linearly polarized fraction of the incoming beam is possible.

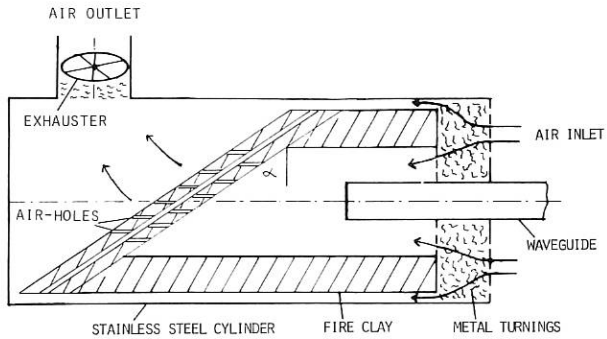

Fig. 4: Schematic view of the fire-clay load for linearly polarized radiation (TE11/HE11).

1.2 Overmoded Waveguide Components for ECRH at 140 or 150 GHz

1.2.1 Improved TE03-to-TE01 mode converters

Two-step high-power TE03-to-TE01 mode transducers (TE02 is the intermediate mode) were designed to transform the TE03 output mode of the first 150 GHz KfK gyrotron into the fundamental circular symmetric TE01 mode for low-loss propagation and further conversion into the linearly polarized quasi-optical HE11 mode. The advanced perturbation structures of the rippled-wall mode converters (with input- and output-diameter D = 27.8 mm) were optimized by numerically solving the proper coupled-wave differential equations.

The overall TE03-to-TE01 conversion efficiency was calculated to be 99.1% for long converters (total length L = 2.67 m) and 97.8% for short converters (L = 1.07 m); ohmic attenuation is included. In the special case of TE02-to-TE01 transformation an efficiency of 99.5% can be achieved with merely 2 geometrical periods because the generated TE01 mode is the lowest order circular symmetric mode. The computed normalized power in each mode and the total transmitted power P_{TOT} as a function of z along this short TE02-to-TE01 mode transducer is plotted in Fig.5.

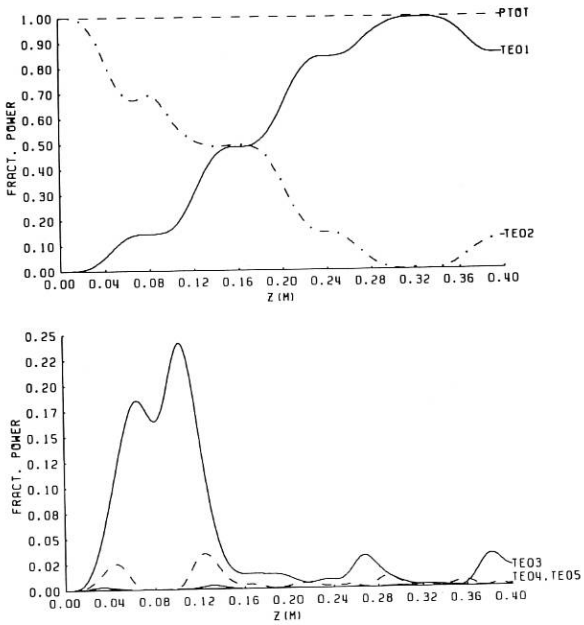

Fig. 5: Calculated fractional power in desired (upper part) and unwanted (lower part) modes and total transmitted power (P_{TOT}) as a function of z along the improved short 150 GHz TE02-to-TE01 mode converter (2 geometrical periods, input- and output radius a = 13.9 mm, total length L = 322 mm, theoretical conversion efficiency at 150 GHz η_o = 99.5%).

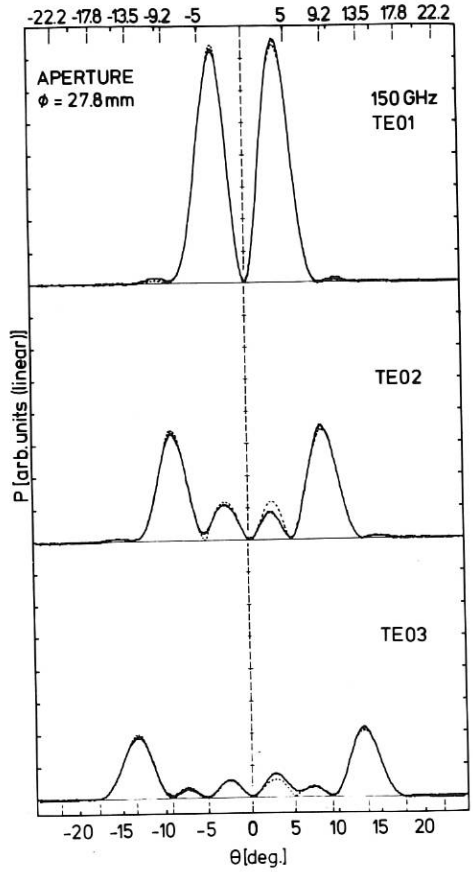

Fig. 6: Measured far-field radiation pattern (low-power measurements, linear scale) of the TE02 and TE03 modes successively generated by the improved short 150 GHz mode converters from a TE01 input mode (uppermost trace). The theoretical patterns are superimposed (dashed curves).

The numerically optimized mode converters were manufactured in the workshop of the IPF Stuttgart by direct machining on a numerically controlled lathe and assembled from individual sections. They were tested at low power levels by means of far-field radiation pattern measurements and by determination of insertion losses through back-to-back converters using frequency sweeping and phase shifting techniques. Fig. 6 shows the measured far-field radiation patterns (150 GHz, linear scale) of the TE02 and TE03 modes successively produced from the TE01 input mode (uppermost trace) by the short converters. The agreement between these patterns and the theoretical ones (dashed curves) is good and consistent with the calculated efficiencies. The overall TE03-to-TE01 conversion efficiency at 150 GHz was measured to be (99±1)% for the long converters and (98.5±1.5)% for the short converters. Measured conversion efficiencies versus frequency for the long and the short TE03-to-TE02-to-TE01 mode transformers are shown in Figs. 7 and 8, respectively. The theoretical graphs are superimposed (solid curves). In both cases calculated and measured frequency dependence is in agreement within the experimental uncertainties. The bandwidth for an efficiency ≥ 95% is ±1.4 GHz for the long converter and ±2 GHz for the short converter.

1.2.2 Corrugated TM11-to-HE11 mode converter

At very high frequencies, the mode conversion scheme TE01-to-TM11-to-HE11 for generating the linearly polarized, quasi-optical HE11 hybrid mode is more suitable than the TE01-to-TE11-to-HE11 conversion sequence because efficient TE01-to-TM11 transducers (bent smooth-wall circular waveguide; see annual report 1985) can be made considerably shorter than serpentine TE01-to-TE11 mode transducers.

Adiabatic TM11-to-HE11 conversion is obtained in a straight, circumferentially corrugated waveguide section by non-linearly tapering the corrugation depth from 0 to nominally λ/4. This transducer has to be long enough (L = 0.84 m for a_o = 13.9 mm at 140 GHz; slot width = tooth width = λ/6) in order to suppress mode hopping to the TE11-EH11 surface mode branch as well as to the TE12-HE12 mode branch. Computer-aided optimizations of converter

length, shape of corrugations and slot depth profile along the converter also have been studied with the scattering matrix code (MAC). The theoretical conversion efficiency is around 98.5%. The slot depth increases most slowly at the converter input where coupling to both unwanted mode branches is strongest.

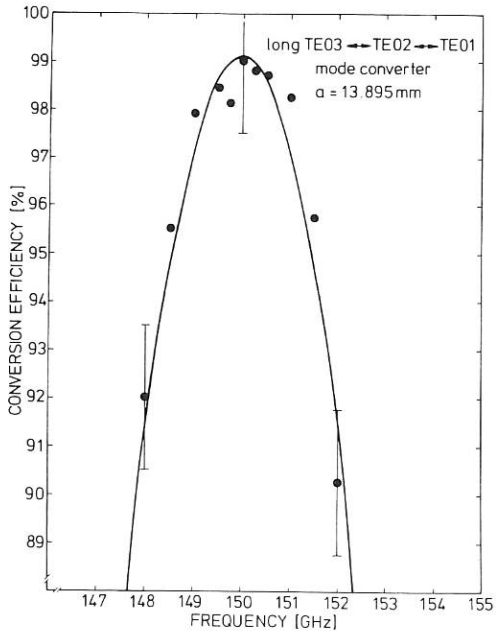

Fig. 7: Measured conversion efficiency versus frequency for the long TE03→TE02→TE01 mode transducer. The theoretical graph is superimposed (solid curve).

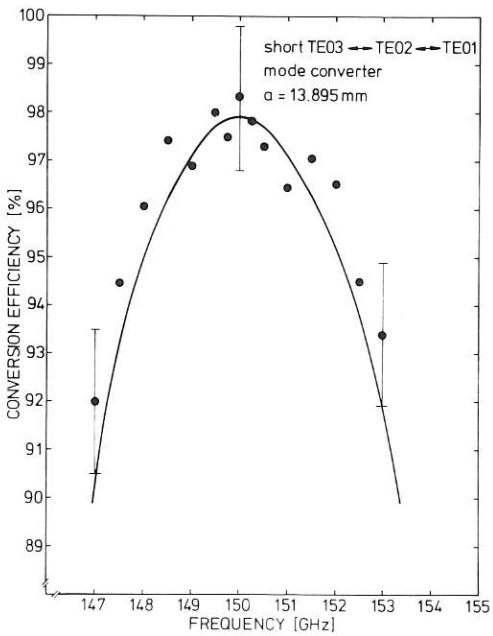

Fig. 8: Measured conversion efficiency versus frequency for the short TE03→TE02→TE01 mode transducer. The theoretical graph is superimposed (solid curve).

A first prototype of the optimum 140 GHz TM11-to-HE11 mode transducer was fabricated by direct machining on a numerically controlled lathe and assembled from 12 elements (aluminium waveguide, gold plated). Fig. 9 shows the measured H- and E-plane radiation patterns of the generated HE11 mode, radiated from the converter output aperture. The theoretical HE11 mode pattern is superimposed. The input to the TM11-to-HE11 converter was fed from the TE01-to-TM11 transformer. Within the experimental uncertainties the measured H-plane pattern is identical to the E-plane pattern, as expected theoretically.

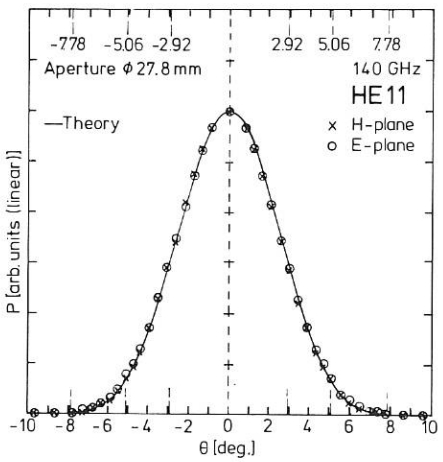

Fig. 9: Measured H- and E-plane radiation patterns (low power measurements) at the output of optimum 140 GHz TM11-to-HE11 mode converter (indicated by points 'x' and 'o', respectively; linear scale) superimposed on ideal HE11 pattern ($D = 2a_o = 27.8$ mm).

1.2.3 Waveguide bends

Unintentional mode conversion losses in circumferentially corrugated TE0n bends scale with $a_o^3 f^2 / k_{on}$, where a_o is the waveguide radius, f is the frequency, and k_{on} is the n-th zero of the Bessel function J_1. Therefore, bends can be made shorter if they propagate higher TE0n modes ($n \geq 3$ at 140 GHz). The properties of a corrugated 140 GHz TE03-mode bend ($\theta = 90°$, $a_o = 13.9$ mm) were optimized using numerical integation of the coupled-mode equations for the six coupled modes: TE03, HE13, EH13, EH14, HE23 and EH23. Optimum electrical slot depths appear at values of $(0.3\text{-}0.4)\cdot\lambda/4$. Unwanted conversion to spurious modes can be reduced by changing the curvature continuously instead of abruptly. Fig. 10 shows the power P_L in unwanted modes at the output of a bend with sinusoidal curvature distribution as a function of arc length L.

TE01- and HE11-bends with low mode conversion at 140 GHz can be realized as quasi-optical mitre-bends. The transmission efficiency of a 90° TE01-bend ($D = 2a_o = 63.4$ mm) was measured to be $(99.2 \pm 0.3)\%$.

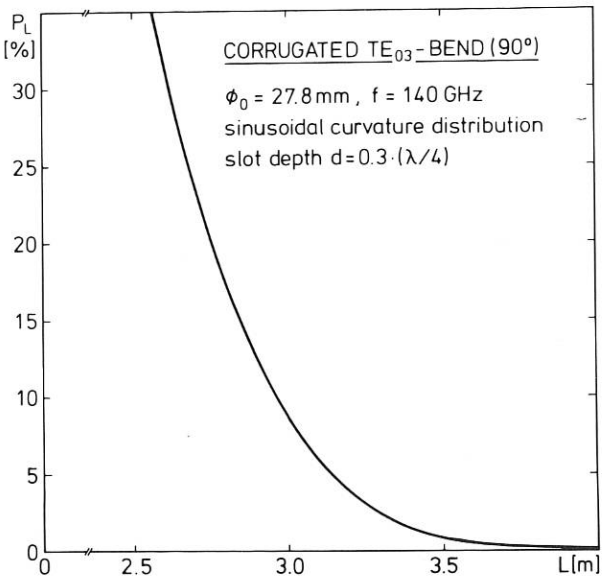

Fig. 10: Mode conversion as a function of arc length L for TE03 propagation in a 90-degree corrugated bend with sinusoidal curvature distribution (a_o = 13.9 mm, f = 140 GHz, effective (electrical) corrugation depth = $0.3 \cdot \lambda/4$).

1.2.4 Reflector beam waveguide

The transmission characteristics of reflector beam waveguides consisting of a HE11 hybrid mode feed (oversized, corrugated circular waveguide antenna) and up to 10 ellipsoidal mirrors have been investigated at 70 and 140 GHz. The measured transmission losses which include coupling losses from the HE11 waveguide mode to the free-space fundamental Gaussian beam mode and diffraction losses as well as ohmic attenuation on the reflector surfaces are in good agreement with the calculated values. The experiments demonstrate the practicability of reflector beam waveguides for millimeter-wave power transmission. They should be capable of transmitting enormous amounts of microwave power in a nearly loss-less, efficient fashion. Recent advances in the design of megawatt gyrotron cavities suggest that the source problems are solvable. Therefore, the windows appear to be the most difficult components of the overall system.

1.2.5 Quasi-optical mode converters

The development of megawatt gyrotrons particularly at 140 GHz will necessitate the use of higher order cavity modes, such as the so called whispering gallery modes. Thus the study of quasi-optical techniques which can convert these higher order modes directly to Gaussian output beams is of particular importance.

Initial measurements of the far-field patterns of Vlasov type converters (without parabolic mirror) show that diffraction effects significantly alter the far-field patterns from those predicted by the simple Brillouin wave theory. This can be clearly seen in the measured pattern of a circularly symmetric TE01 mode using a conventional stepped-cut Vlasov converter, as shown in Fig. 11. In order for these devices to be used extensively as mode converters or launching antennae, their efficiencies would need to be improved from the presently obtained 80 - 85%. Further investigations of these converters will be able to determine whether the maximum possible efficiency obtainable can be increased so as to compare with the greater than 95% efficiency achieved with conventional, wall-perturbation, waveguide mode-converters.

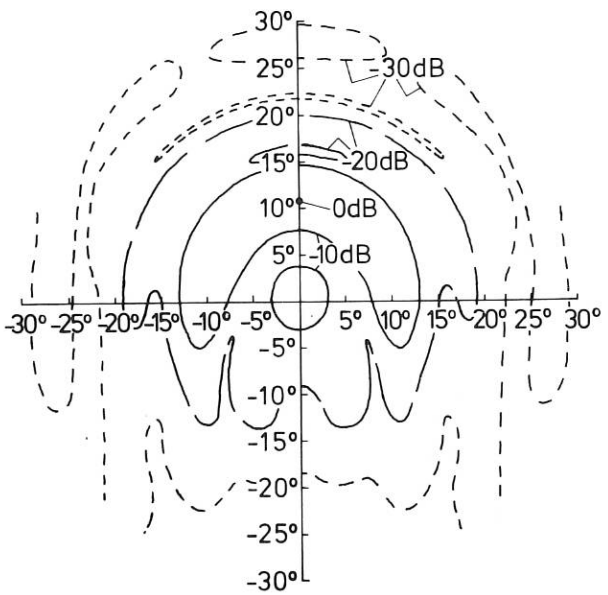

Fig. 11: The far-field pattern of a circular TE01 mode from a stepped-cut Vlasov converter, without a parabolic mirror.

2. P L A S M A - T H E O R Y

(E. R ä u c h l e, U. Erz, F. Moser, J. Mayer-Stöhr)

2.1 Ray Tracing and Transport Calculations.

The ray tracing technique is applied to electron cyclotron heating. The deposition profile of the absorbed power is calculated numerically for typical tokamak and stellarator (W VII-A, W VII-AS) geometries. Transport theory is applied to calculate the temporal development of the radial distribution of electron and ion temperature for prescribed and for self consistently calculated deposition profiles. In Fig. 12 the radial electron temperature distribution is shown as a function of time for both constant and time modulated electron cyclotron heating. An application of these results to experiments allows the determination of transport coefficients.

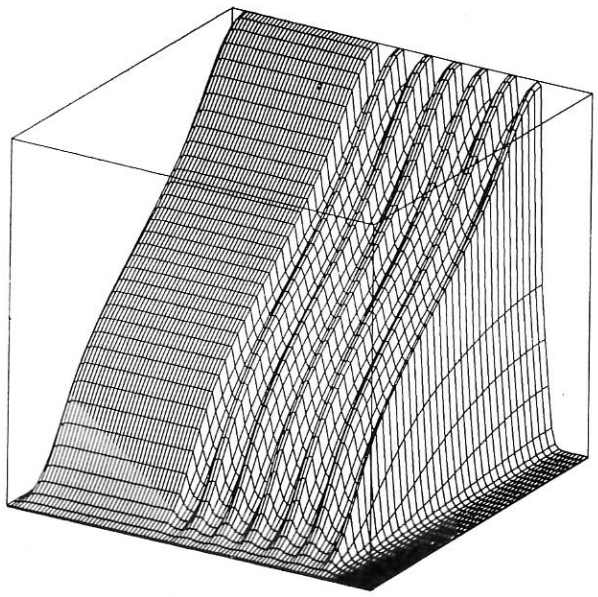

Fig. 12: Radial profile of the electron temperature as a function of time.

2.2 Numerical Plasma Simulation

The temporal evolution of the distribution function in phase space under the influence of an external electrostatic wave is calculated numerically. It is shown that ponderomotive effects exist and that chaotic processes can be expected for this system.

2.3 Electromagnetic Waves in Inhomogeneous Plasmas.

The influence of drift motions on the dispersion relations is investigated theoretically. In the derivation of the dielectric tensor, relativistic effects and anisotropic temperatures are considered. Dispersion, absorption and polarization of electromagnetic waves are calculated for electron-cyclotron resonance conditions.

3. L A S E R D I A G N O S T I C S

(H. S a l z m a n n, G. Dodel, K. Hirsch, E. Holzhauer, M. Köchel[1], G. Merkle[2], J. Singethan[2])

The work of this group deals with the development of laser diagnostics for fusion devices and the application of such diagnostics to tokamaks and stellarators.

3.1 LIDAR-Thomson Scattering for Measuring Spatial n_e, T_e-Profiles in Large Fusion Devices.

At the IPF, the preparations for the LIDAR scattering experiment on JET were completed in September: The spectrometer was set up and tested. The six spectral channels showed high average transmission (about 70%) and rejection of ruby laser stray light by a factor greater than 10^5. This performance is achieved with a filter polychromator in which the incident light is shone onto a stack of short wave pass interference edge filters with decreasing cut-on wavelengths, the filters being tilted against each other. The transmission bandwidth of a spectral channel observed in reflection from this filter stack is defined by the cut-on wavelengths of two adjacent filters of the stack. Additional interference short wave pass edge filters in front of each detector improve further the rejection of ruby laser stray lights. The collection optics rather than the scattering volume is imaged onto the filter stack, since this is illuminated homogeneously by scattered light during the passage of the laser pulse through the plasma. This avoids the problem of any slight variation of the cut-on wavelength across the surface of the 200 mm diameter edge filters causing a variation in calibration when the scattering volume moves through the plasma. In the course of the first measurements, only four spectral channels were used. Their transmission bands were 658 nm - 628 nm, 639 nm - 602 nm, 598 - 533 nm and 540 - 480 nm, respectively.

[1]) Diplomand
[2]) Doktorand

Since the detection electronics developed at Risø were also ready, a preliminary scattering arrangement was set up at JET using the ruby laser at reduced energy level (2.5 J instead of 5 J) and using provisional laser input optics. This set-up became operative during the last two weeks of JET operation before the shutdown in December 1986. The campaign was successful: stray light signals were sufficiently suppressed and Thomson scattering signals of a level expected for the given experimental conditions were obtained. Signals from about 50 JET discharges were down loaded into the JET data acquisition system for later analysis. The initial evaluation of these results is very encouraging, yielding temperature profiles over a wide range of plasma conditions which are consistent with temperature profile measurements (made on the outer plasma radius) by ECE diagnostics.

3.2 Far Infrared Collective Scattering on ASDEX

A 119 µm cw laser scattering experiment was run on ASDEX to investigate the low frequency (100 kHz < f < 2 MHz) density turbulence. The results are given in the chapter "ASDEX Project", Section 1.3.4 "Fluctuation measurements".

3.3 Pumping of far Infrared Laser Transitions with a CW Waveguide CO_2 Laser.

In recent years waveguide (wg) CO_2 lasers have turned out to be a very useful tool for pumping far infrared (FIR) molecular gas lasers. High pump frequency tunability due to pressure broadening effects in wg lasers up to their free spectral range (FSR) allows resonant FIR laser pumping in the regime of about ± 150 MHz from CO_2 laser line centers with sufficient power (several Watts). To close the frequency spectrum gap between two neighboured CO_2 emission lines (about 2 GHz), where quite a lot of FIR laser absorption transitions are expected, large efforts have been made to expand the CO_2 laser frequency tuning range.

We already have reported mode selection techniques to suppress longitudinal mode jumping at frequencies of half the FSR. A radio frequency (rf) excited wg CO_2 laser with a gain length of about 80 cm and a resonator length of 1 m (FSR=150 MHz) delivers now with a FOX-SMITH mode selector on the strong CO_2 laser lines a frequency tunability within 5 times its FSR at a CW power at line center of about 5 W. This expanded tuning range makes accessible several thousand new transitions in FIR molecular gas lasers. The stable frequency behaviour of this CW laser also allows the study of the gain characteristics of FIR lasers at defined pump frequency offsets around absorption resonance. Of special interest is the experimental investigation of the NH_3 SR(5,0) transition which is pumped resonantly at -180 MHz and as a Raman-line at -30 MHz from CO_2 9R(30) center. Being able to pump both transitions we would result in a 180 MHz frequency tunable FIR laser at a wavelength of 67.2 µm.

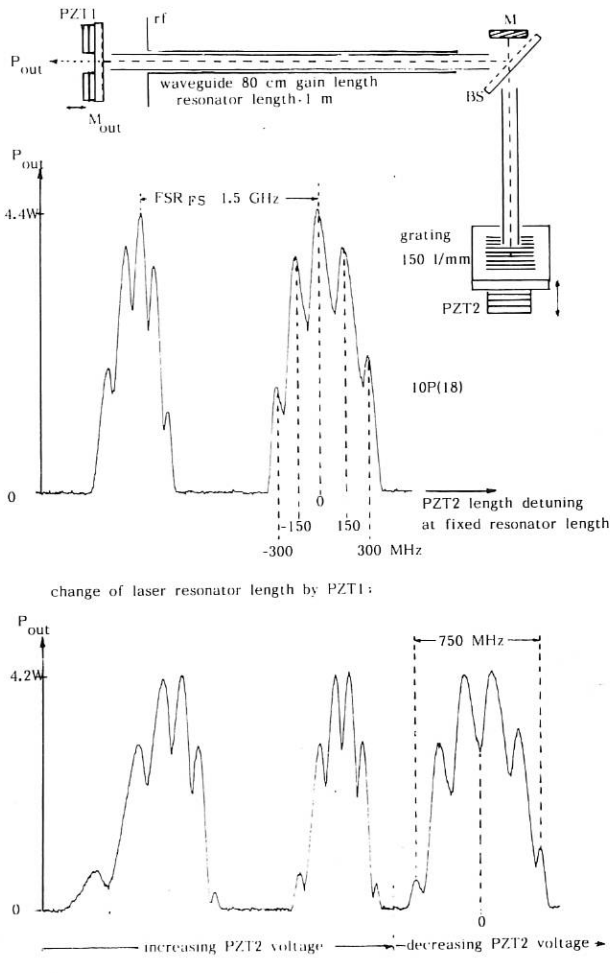

Fig. 13: Experimental set up of the rf excited CO_2 waveguide laser with FOX-SMITH mode selector (FS) and longitudinal mode scans of the line 10P(18) for two different resonator lengths. The position of the modes within the pressure broadened gain profile (180 mbar) has been measured by a slow increase or decrease of the FS length by PZT2. The waveguides of the laser and the FS are 3 mm inner diam. quartz tubes. M_{out}: ZnSe mirror R = 95%, M: flat gold mirror, BS: ZnSe beam splitter R = 60%.

3.4 Laser Spectroscopy

Doppler-free spectroscopy offers the potential to measure plasma parameters such as electric and magnetic fields, ion temperature, and electron density.

The possibilities of the Doppler-free polarization spectroscopy are investigated in a hydrogen discharge using a tunable single mode dye-laser.

The tests of the detection optics and electronics were completed. To achieve the extinction ratio specified for the polarizer/analyzer pair in the

experimental arrangement, which includes the windows and the external magnetic field, the magneto-optic and birefringent effects had to be compensated. First Doppler-free spectra of the H_α-line were recorded over a scan range of 3.6 GHz.

4. PLASMA FOCUS

(H. Herold, W. Hesselmaier[1], U. Jäger[2], H.J. Kaeppeler, H. Schmidt, R. Schmidt[2], A. Schumacher[1], M. Shakhatre, A. Wieder[1], Thein Win[3], C.S. Wong[4])

4.1 Poseidon Plasma Focus

The evaluation of measurements concerning fast ion and neutron production was continued and concluded. The main activity was still directed to the understanding of saturation effects of the neutron yield in the operating range of the device above 300 kJ. For this purpose the dynamics and the structure of the current sheath were further investigated using magnetic probes, high speed photographic and interferometric methods as well as optical spectroscopy. Furthermore the investigation of the anode-directed fast electron beam was continued.

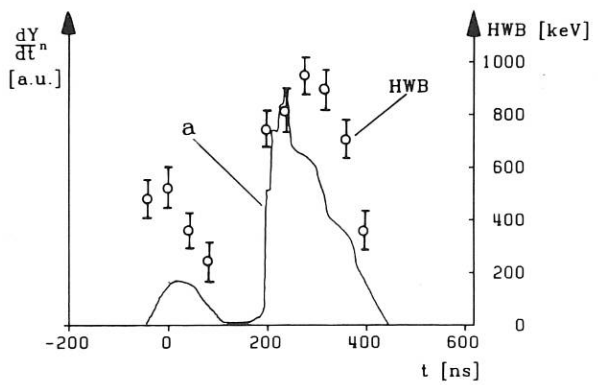

Fig. 14 Neutron flux (a) and FWHM (HWB) of the neutron spectra as a function of time (t = 0 at maximum compression), measured during shot No. 7522.

[1]) Diplomand
[2]) Doktorand
[3]) Univ. of Rangoon, Birma, DAAD-Stipendiat
[4]) Univ. of Malaysia, Kuala Lumpur, Humboldt Stipendiat

*) Annual Report 1985

1) From the evaluation of the time-of-flight measurements of the neutrons*) it was found, that different mechanisms of deuteron acceleration are essential for the beam target fusion reactions in the focus. In Fig. 14 the measured FWHM of the neutron spectra and the corresponding neutron flux are plotted as a function of time for a typical discharge (70 kV, 380 kJ, 8 mbar D_2).

Under the assumption, that the FWHM corresponds to a quasi temperature T_i* in the fast deuteron distribution function this quasi temperature T_i* amounts to 15 keV to 80 keV in the first neutron pulse. Deuteron acceleration starts 100 ns to 50 ns before the maximum compression and may be caused by ion reflection at the radially collapsing plasma sheath and/or by inductively generated electric fields.

Deuteron acceleration resulting in the second neutron pulse can be described in three consecutive phases a) to c):

a) First, the onset of the m = 0 instability. The deuterons are accelerated in this phase up to 70 keV to 120 keV in electric fields generated inductively or by anomalous resistivity.

b) Second, 30 ns to 100 ns after the onset of the m = 0 instabilities. In this phase the neutron flux decreases but the deuteron energy increases to 100 to 250 keV. Consecutive m = 0 constrictions, as observed in Schlieren framing pictures and neutron pinhole measurements, may be efficient in this phase. An explanation for the high deuteron energies would be a tandem acceleration in the constrictions.

c) Third, the final phase of the second neutron pulse occurs 100 ns to 200 ns after the onset of the m = 0 instabilities. The observed deuteron energy is reduced to 15 keV to 70 keV. The decrease of the neutron flux in the interval 50 ns to 200 ns after the onset of the m = 0 instability can be explained by relaxation of the fast deuterons (beam properties) and decrease of the plasma density (target properties). The observed neutron flux up to 200 ns after the onset of the m = 0 instability, however, cannot be explained by confinement of fast deuterons during 100 ns to 200 ns in the turbulent plasma phase. A third acceleration process has to occur, whose origin may be found in fast decaying magnetic fields of plasma structures.

2) Measurements of the sheath structure were carried out with magnetic probes and with framing pictures. In the run down phase, the sheath current I_s and the total current I_t increase with the charging voltage (I_s from 2.7 MA at 60 kV to 3.4 MA at 80 kV). The current diversion I_s/I_t even improves with the voltage reaching ≈ 90%. There is not much difference in sheath parameters of the run down phase for shots with strongly reduced neutron yield, besides a small decrease (≤ 5%) in the sheath current. So very likely the malfunction of the focus at high energy densities may predominantly have to do with the radial compression. Measurements with magnetic probes in the top surface of the anode are in progress, but encounter serious technical difficulties.

Measurements of the impurity level in the plasma sheath and the investigation of its influence on the discharge are continuing using two monochromator/photomultiplier channels.

3) The investigation of the anode-directed, fast electron beam by means of a magnetic spectrometer and Faraday-cups was concluded this year. There are three main results: a) The electron emission depends strongly on the discharge parameters such as electrode geometry, charging voltage, and filling pressure. b) Electrons are emitted in 3 main pulses consisting of many bursts during a relatively long period of up to more than 650 ns. c) The first pulse occurs shortly before (20 ns) the maximum compression, the second pulse coincides roughly with the m = 0 instability , whereas a third pulse may have to do with ion and electron acceleration processes in plasma islands, which may occur in a later phase of the discharge. Comparing the fast electron flux with the neutron flux, it is found, that generally during the third electron pulse no neutron emission can be detected. The main reason for this may be that the plasma density has decreased in this phase to such a low level, that the accelerated deuterons cannot efficiently interact with a target.

4.2 DPF 78 and Minifocus

The main objectives of investigations with the plasma focus device DPF 78 (50 kJ, 80 kV) - which was reactivated in the end of 1985 - were phenomena of sheath formation in the ignition phase and plasma dynamics and x-ray emission in the compression and pinch phase.

1) It was found that UV-preionization of the discharge volume (around $3 \cdot 10^{11}$ photons/cm^2 at the insulator surface, 250 nm $\leq \lambda \leq$ 350 nm) by means of a discharge along the surface of an outer glass cylinder inside the discharge vessel did not influence the focus operation in a positive way.

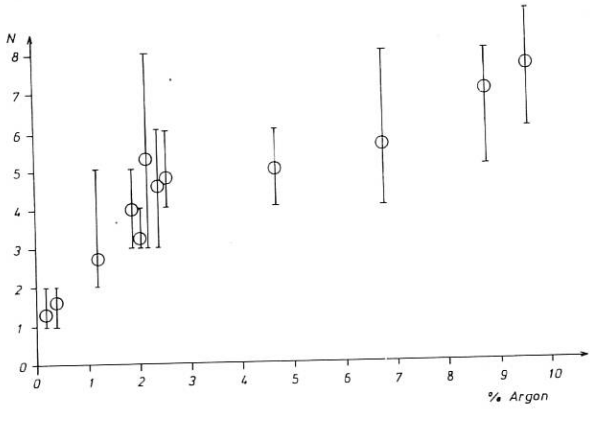

Fig. 15: Number of hot spots N as a function of Argon (percent of volume) admixture to deuterium. Shots at 60 kV, 28 kJ, ϕ_i = 5 cm, ℓ_i = 13.3 cm, 8 mbar D_2 without admixture. The total filling was chosen in such a way, that the gas density remained constant.

2) The observation of the plasma sheath during the compression phase using Schlieren optical methods sheath and strong decrease of the neutron yield. From streak pictures it was found that for normal discharges with high neutron yields ($1.5 \cdot 10^{10}$), the sheath velocity increases considerably during the compression phase ($1 \cdot 10^5$m/s → $2 \cdot 10^5$m/s), but it remains nearly constant for discharges with reduced neutron yield (< 10^9).

For the investigation of the soft x-ray emission two pinhole-cameras and four scintillator/photomultiplier detectors equipped with metal absorption filters were used simultaneously. The spatial and temporal distribution of the x-ray emission was measured for discharges in pure deuterium gas as well as with admixtures of noble gases such as Neon, Argon and Xenon. As in vacuum sparks one finds so called "hot spots" (= small regions of high radiation) in the plasma focus under certain conditions. The occurence of these hot spots depends strongly on the type and the amount of noble gas admixture. Hot spots could only be found regularly with admixtures of Argon and Xenon. In Fig. 15the number of hot spots is plotted as a function of Argon admixture to deuterium. From the measurements it was found that the dimensions of the hot spots are < 50 µm, the densities in them are at least of the order of $n_e \approx 10^{21}$ cm^{-3}, and their lifetimes are < 8 ns. In Fig. 16 an example of hot spot emission with Xe gas admixture, as seen in an x-ray pinhole picture, is shown. The investigation of these spots, which are characterized by very high density and strong pulsed emission of x-radiation, is being continued.

Experiments with pulsed gas filling in the ignition region, which were performed at the Minifocus device (18 kV, 10 kJ, ϕ_i = 25 mm, ℓ_i = 265 mm) did not show any improvement in the neutron yield.

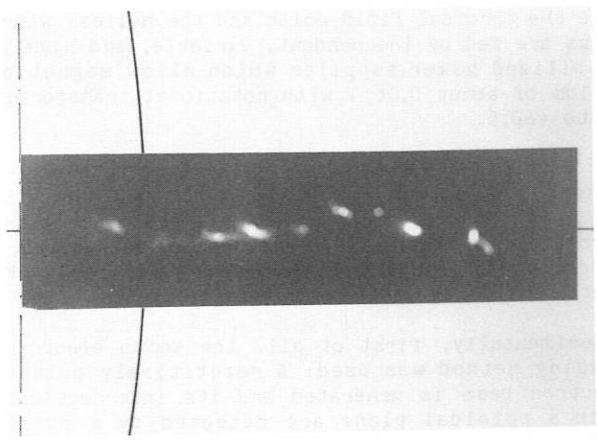

Fig. 16: X-ray pinhole picture through 21 µm Ti-filter of discharge No. 803 (60 kV, 3.8 mbar D_2 + 0.9% Xe).

4.3 Plasma Focus Theory

The problem of the development of filamentary structures in the plasma focus and their connection with neutron production during the pinch phase with high currents (> 500 kA) was studied theoretically. Contrary to earlier assumptions that $m \geq 2$ instabilities cause the filaments, the possibility of current filamentation was studied. For this purpose, the theory of beam filamentation was applied to the late compression phase in a model theory. The resulting electric field due to filament decay and particle acceleration was calculated. The mean particle energy and number of accelerated particles agree with experimental observations.

5. STELLARATOR EXPERIMENT WEGA

(H. Zwicker, H. Hailer, J. Massig, F. Schuler, K. Schwörer)

The toroidal experiment WEGA, transferred from the CEN Grenoble to the IPF Stuttgart, was reassembled in the stellarator configuration. In 1986 this assembling was completed, and the cooling system was installed. Since the repair of the vacuum pumps a pressure of 2×10^{-7} mbar can be obtained.

The WEGA stellarator has $\ell = 2$, $m = 5$ helical windings. The major and minor radii of the vessel are $R = 0{,}72$ m and $r = 0{,}19$ m respectively.

As first experimental program the magnetic field configuration is being investigated. For that purpose the toroidal field coils and the helical windings are fed by independent, variable, and highly stabilized power supplies which allow magnetic fields of about 0,06 T with rotational transforms up to $\iota \geq 0{,}5$.

The magnetic field geometry is studied both experimentally and theoretically to examine the effects of constructive inaccuracies and other perturbations on the flux surfaces of the vacuum magnetic field, and to try a compensation of such perturbations by additional magnetic coils.

Experimentally, first of all, the known electron tracing method was used: A repetitively pulsed electron beam is generated and its intersections with a poloidal plane are detected by a point probe. When the rotational transform is not close to a rational value, such as 1/2 or 1/3, the measurements show the expected nearly elliptic shape of the flux surface cross setions, and the rotational transform can easily be determined from the positions of the intersection points.

If, however, the currents in the magnetic field coils are chosen such that ι on the magnetic axis is very near to 1/2 two magnetic islands appear (Fig. 17). These are predominantly caused by a horizontal displacement of about 1 mm between the axes of the toroidal field coil arrangement and of the vessel supporting the helix. It was not attempted to correct this displacement in order to study its effects and the possibility of a compensation by additional magnetic coils. Tests of compensation coils are currently being performed.

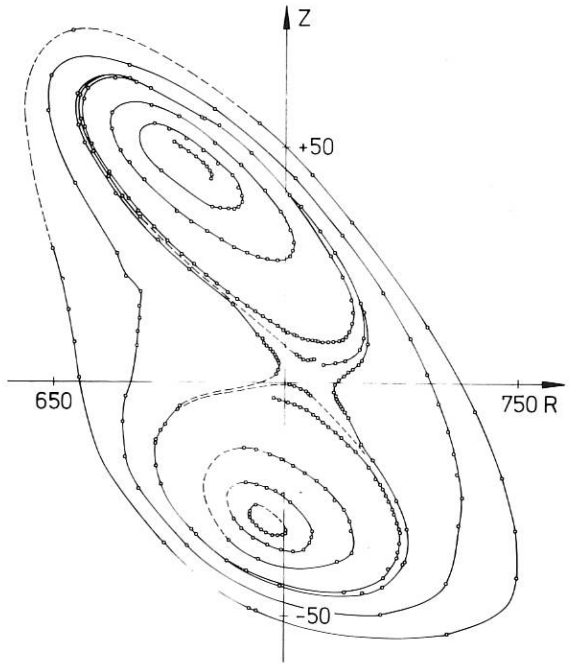

Fig. 17: Measured electron drift surfaces at $\iota = 1/2$

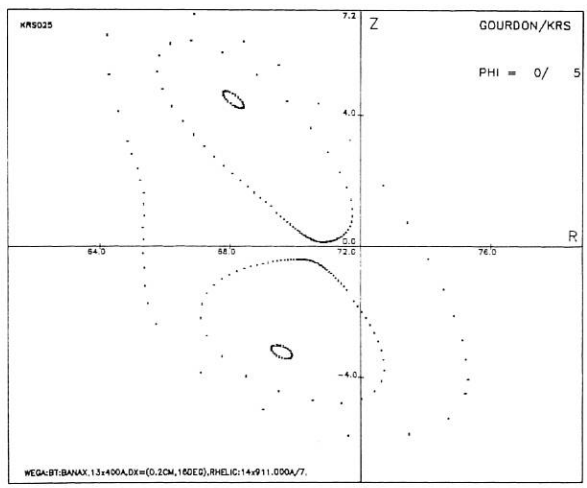

Fig. 18: Calculated electron drift surfaces at $\iota = 1/2$.

Since the measurement of the flux surface cross sections by detecting the intersection points of the electron beam by means of a point probe is very time consuming faster detection methods are being prepared. Meshes or movable wires coated with a fluorescent material are used to make visible the electron beam drift surfaces. Lateron the best of the tested methods will be used for similar investigations on the stellarator W VII-AS at the IPP Garching.

Calculations of the magnetic field lines and the electron guiding center trajectories in WEGA are done using the GOURDON code. Thereby the most serious poblem was to get a sufficiently realistic description of the helix windings. The assumption of an ideal winding law $d\vartheta/d\phi = m/\ell$ for all helix conductors resulted in too large values of the rotational transform. Much better results were obtained assuming the conductors within each helix bundle having constant orthogonal spacing. The latter assumption conformed well with the design values for the positions of the right hand boundaries of the helix bundles. But any inaccurate placing of the helix conductors on the vessel cannot be accounted for because they are no longer accessible.

At low non-rational values of the rotational transform ($\iota \approx 0{,}1 \ldots 0{,}2$) very good agreement between calculated and measured results was achieved. At ι near 1/2 at least a good qualitative agreement resulted, which could be improved by variation of the relevant parameters. Parameter variations at ι near 1/2 showed extremely sensitive dependencies of the size and position of the islands on the relevant parameters. For example, the magnitude and the effective radius of the helix current must be known with a precision of about 10^{-3} or better.

Figure 18 shows calculated drift surface cross sections at $\iota \approx 1/2$ with island formation due to the torus displacement which compare favourably with the measured contours of Fig. 17 In such cases the numerical results assisted the measurement by providing ideas on the forms and positions of the flux surfaces and by giving hints for a favourable positioning of the electron gun.

PUBLICATIONS AND CONFERENCE REPORTS

Janzen, G.:
"Technische Plasmen" appeared in Taschenbuch der Hochfrequenztechnik (Meinke, Gundlach), Springer Verlag, Berlin, 4. Auflage (1986).

Grieger, G., W VII-A Team, NI-Team, ECRH Group (W. Kasparek, G. Müller, P.G. Schüller, K. Schwörer, M. Thumm, R. Wilhelm), Pellet Injection Group:
Confinement of stellarator plasmas with neutral beam and RF heating in W VII-A, Plasma Phys. and Contr. Fusion 28, 43 (1986).

Erckmann, V., W VII-A Team, NI-Team, ECRH Group (W. Kasparek, G.A. Müller, E. Räuchle, P.G. Schüller, M. Thumm, R. Wilhelm):
Electron cyclotron resonance heating in the Wendelstein VII-A Stellarator, Plasma Phys. and Contr. Fusion 28, 1277 (1986).

Wagner, F. et al.:
Experimental study of the principles governing tokamak transport, Phys. Rev. Letters 56, 2187 (1986).

Laguarta, F., G. Merkle, J. Heppner, R. Corbalon and R. Vilaseca:
Standing-wave forward-backward gain asymmetry in optically pumped gas lasers, Phys. Rev. Lett. 57, 7 (1986).

Hartfuß, H.J., H. Maaßberg, M. Tutter, W VII-A Team, ECRH Group (W. Kasparek, G. Müller, K. Schwörer, M. Thumm, R. Wilhelm):
Evaluation of the local heat conductivity coefficient by power-modulated electron cyclotron heating in the Wendelstein VII-A stellarator, Nuclear Fusion 26, 678 (1986).

Kumrić, H., M. Thumm:
Optimized overmoded TE01-to-TM11 mode converters for high-power millimeter wave applications at 70 and 140 GHz, Int. J. Infrared and Millimeter Waves 7, 1439 (1986).

Thumm, M., V. Erckmann, W. Kasparek, H. Kumrić, G.A. Müller, P.G. Schüller, R. Wilhelm:
Very high power mm-wave components in oversized waveguides, Microwave Journal 29, 103 (1986).

Wilhelm, R., W. Kasparek, H. Kumrić, G.A. Müller, P.G. Schüller, M. Thumm:
Components for high power millimeter wave applications using pulsed or cw gyrotrons, Mikrowellen Magazin 12, 607 (1986).

Thumm, M.:
High power mode conversion for linearly polarized HE11 hybrid mode output, Int. J. Electronics 61, 1135 (1986).

11th Int. Conf. on Plasma Physics and Controlled Nuclear Fusion Research, Kyoto, 1986.

Wobig, H., H. Maaßberg, H. Renner, W VII-A Team, ECRH Group (W. Kasparek, G.A. Müller, P.G. Schüller, M. Thumm, R. Wilhelm) , NI Group:
Plasma confinement in the Wendelstein VII-A Stellarator, IAEA-CN-47/D-I-2.

Ringler, H., F. Sardei, A. Weller, W VII-A Team, ECRH Group (W. Kasparek, G.A. Müller, P.G. Schüller, M. Thumm, R. Wilhelm), NI Group:
Impurity behaviour in the Wendelstein VII-A Stellarator, IAEA-CN-47/D-V-1.

13th European Conf. on Contr. Fusion and Plasma Heating, Schliersee, 1986.

Renner, H., W VII-A Team, ECRH Group (W. Kasparek, G.A. Müller, P.G. Schüller, K. Schwörer, M. Thumm, R. Wilhelm), NI Team:
Influence of shear, $\Delta\iota/\iota$, on the confinement in the W VII-A stellarator, Proc., Contributed papers, Part I, p. 287.

Hartfuß, H.J., H. Maaßberg, M. Tutter, W VII-A Team, ECRH Group (W. Kasparek, G.A. Müller, P.G. Schüller, K. Schwörer, M. Thumm, R. Wilhelm):
Experimental determination of the local heat conductivity coefficient $\chi_e(r)$ in the W VII-A stellarator, Proc., Contributed papers, Part I, p. 315.

Kick, M., H. Ringler, F. Sardei, A. Weller, W VII-A Team, NI-Team, ECRH Group (W. Kasparek, G.A. Müller, P.G. Schüller, K. Schwörer, M. Thumm, R. Wilhelm):
CX-recombination spectroscopy during NBI heating of ECRH target plasmas in the W VII-A stellarator and comparison with a transport model, Proc., Contributed papers, Part I, p. 319.

Wilhelm, R., V. Erckmann, G. Janzen, W. Kasparek, G.A. Müller, P.G. Schüller, M. Thumm, W VII-A Team:
Performance of the 70 GHz ECRH System on W VII-A, Proc., Contributed papers, Part II, p. 211.

14th Symposium on Fusion Technology (SOFT), Avignon, 1986.

Kasparek, W., G.A. Müller, P.G. Schüller, M. Thumm, R. Wilhelm, V. Erckmann:
The 70 GHz/1 MW long-pulse ECRH system on the advanced stellarator W VII-AS, Paper CP25.

11th Int. Conf. on Infrared and Millimeter Waves, Tirrenia, Pisa, 1986.

Kasparek, W., M. Thumm:
Experimental studies on beam waveguides for use with high-power gyrotrons, Proc., p. 212.

Thumm, M., H. Kumrić, H. Stickel:
TE03-to-TE01 mode converter for use with a 150 GHz gyrotron, Proc., p. 215.

Dodel, G., E. Holzhauer, J. Massig, T. Vogel, P. Ignacz, ASDEX-, ICRH-, LH-, NI-, Pellet-Teams:
Collective Scattering at 119 µm from lower hybrid waves and low frequency density fluctuations in the ASDEX tokamak, Proc., p. 399.

Merkle, G., J. Heppner:
Waveguide CO_2 Laser with mode selector for cw pumping of FIR lasers, Proc., p. 463.

Frühjahrstagung der Deutschen Physikalischen Gesellschaft, Stuttgart, 1986.

Hirsch, K., M. Köchel und H. Salzmann:
Eigenschaften eines gepulsten MCP-Photomultipliers, Verhandl. DPG (VI) 21, 34 (1986).

Moser, F.:
Ausbreitung elektromagnetischer Wellen in inhomogenen Plasmen mit Driften, Verhandl. DPG (VI), 21, 53 (1986).

Wilhelm, R., V. Erckmann, G. Janzen, W. Kasparek, G. Müller, E. Räuchle, P.G. Schüller, K. Schwörer, M. Thumm, W VII-A Team:
Elektron-Zyklotron Heizung am Stellarator W VII-A, Verhandl. DPG (VI) 21, 56 (1986).

W VII-A Team, ECRH Gruppe (W. Kasparek, G. Müller, P.G. Schüller, K. Schwörer, M. Thumm, R. Wilhelm), H. Maaßberg, M. Tutter, H.J. Hartfuß:
Methode zur experimentellen Bestimmung der Elektronenwärmeleitung im Stellarator W VII-A bei Elektronen-Zyklotron-Resonanz-Heizung, Verhandl. DPG (VI) 21, 59 (1986).

Hirsch, K., H. Salzmann, C. Gowers, M. Gadeberg, P. Nilson and G. Schröter:
Lidar-Thomsonstreuung an JET, Verhandl. DPG (VI) 21, 58 (1986).

W VII-A Team, ECRH Gruppe (W. Kasparek, G. Müller, P.G. Schüller, K. Schwörer, M. Thumm, R. Wilhelm), NI-Team, G. Kühner:
Bolometrie als Neutralteilchendiagnostik im Stellarator W VII-A, Verhandl. DPG (VI) 21, 58 (1986).

W VII-A Team, ECRH Gruppe (W. Kasparek, G. Müller, P.G. Schüller, K. Schwörer, M. Thumm, R. Wilhelm), NI-Team, H. Renner:
Bedeutung der Verscherung $\Delta\iota/\iota \neq 0$, Verhandl. DPG (VI) 21, 59 (1986).

Schmidt, R. und U. Jäger:
Zeitaufgelöste Neutronenspektroskopie an POSEIDON, Verhandl. DPG (VI), 21, 75 (1986).

Jäger, U. und H. Herold:
Untersuchungen zur Kinetik der Fusionsreaktionen im Plasmafokus, Verhandl. DPG (VI), 21, 75 (1986).

Maurer, M., A. Hayd, W. Satzger und H.J. Kaeppeler:
Erweiterung der quasianalytischen Methode (QAM) zur Lösung nichtlinearer Differentialgleichungen für turbulente inhomogene und berandete Systeme, Verhandl. DPG (VI), 21, 78 (1986).

W VII-A Team, ECRH Gruppe (W. Kasparek, G. Müller, P.G. Schüller, K. Schwörer, M. Thumm, R. Wilhelm), ICRH Team, H. Renner:
W VII-A Stellarator 10 Jahre, Verhandl. DPG (VI), 21, 79 (1986).

Holzhauer, E., W. Kasparek und F. Schuler:
Messung der Magnetfeldrichtung in einem Plasma mittels hochauflösender Laserlichtstreuung, Verhandl. DPG (VI), 21, 84 (1986).

E. Räuchle:
Beispiele für deterministische Stochastizität. Verhandl. DPG (VI), 21, 88 (1986)

Biermayer, W., H. Herold, B. Hesselmaier, H. Schmidt und R. Schmidt:
Strommessungen und Untersuchung der Plasmadynamik am Plasmafokus POSEIDON, Verhandl. DPG (VI), 21, 96 (1986).

W VII-A Team, ECRH Gruppe (W. Kasparek, G. Müller, P.G. Schüller, K. Schwörer, M. Thumm, R. Wilhelm), NI-Team, H.J. Hartfuß, M. Tutter:
Elektronzyklotronemissionsspektren bei Anwesenheit nichtthermischer Elektronen im Wendelstein VII-A, Verhandl. DPG (VI) 21, 105 (1986).

W VII-A Team, ECRH Gruppe (W. Kasparek, G. Müller, P.G. Schüller, K. Schwörer, M. Thumm, R. Wilhelm), NI-Team, M. Kick, A. Weller, F. Sardei, H. Ringler:
Spektroskopische Bestimmung des zeitlichen Verlaufs von O^{8+} und O^{7+} im W VII-A Stellarator und dessen Vergleich mit einem numerischen Transportmodell, Verhandl. DPG (VI), 21, 106 (1986).

W VII-A Team, ECRH Gruppe (W. Kasparek, G. Müller, P.G. Schüller, K. Schwörer, M. Thumm, R. Wilhelm), NI-Team, C. Mahn, G. Müller:
Messungen von Plasmafluktuationen im W VII-A Stellarator, Verhandl. DPG (VI) 21, 106 (1986).

Holzhauer, E.:
Fluktuationsmessungen, Verhandl. DPG (VI) 21, 144 (1986).

Frühjahrstagung der Deutschen Physikalischen Gesellschaft, Heidelberg 1986.

Laguarta, F., G. Merkle, J. Heppner:
Neue Mehrphotonenresonanzen in optisch gepumpten Ferninfrarot-Lasern, Verhandl. DPG (VI) 21, 715 (1986).

Vogel, T., G. Dodel and H. Salzmann:
Schalten von Ferninfrarot (FIR)-Strahlung durch UV-Bestrahlung von Silizium-Wafern: Vergleich von Experiment und Theorie, Verhandl. DPG (VI) 21, 732 (1986).

IAEA INTOR-Related Specialists' Meeting on Non Inductive Current Drive, Garching, 1986.

Wilhelm, R.:
Electron cyclotron current drive in the W VII-A Stellarator, Proc. (NET-PM-86-003), p. 512.

International Stellarator/Heliotron Workshop (IAEA Technical Committee Meeting) Kyoto, 1986.

Erckmann, V., W VII-A Team ECRH-Group (W. Kasparek, G.A. Müller, P.G. Schüller, M. Thumm, R. Wilhelm):
ECRH experiments in the W VII-A stellarator with O-and X-mode, Proc., to be published by IAEA Vienna.

Renner, H., W VII-A Team, NBI Group, ICF Group, Pellet Group, ECRH Group:
Status of the Wendelstein VII-AS Advanced Stellarator, Ibid.

Renner, H., W VII-A Team, ECRH Group:
Experimental results with W VII-A in the torsatron mode of operation, Ibid.

Renner, H., W VII-A Team, NBI Group, ICF Group, ECRH Group:
Overview on recent W VII-A experimental results, Ibid.

4th KfK Gyrotron Development Workshop, Karlsruhe, 1986.

Kasparek, W., H. Barkley, H. Kumrić, G.A. Müller, P.G. Schüller, M. Thumm, R. Wilhelm, V. Erckmann: Mode analysis with the wavenumber spectrometer at 70 GHz.

Kumrić, H., M. Thumm, R. Wilhelm: Optimization of mode converters for generating the fundamental TE01 mode from TE06 gyrotron output at 140 GHz.

MIOP'86, Mikrowellentechnologie und Optoelektronik, Wiesbaden, 1986.

Thumm, M., V. Erckmann, W. Kasparek, H. Kumrić G.A. Müller, P.G. Schüller, R. Wilhelm:
Components for transmission of very high power mm-waves (200 kw at 28, 70 and 140 GHz) in overmoded circular waveguide, Proc., Vol. 2.

1. Bundesdeutsche Fachtagung Plasmatechnologie, Stuttgart, 1986.

H. Bauch, J. Mentges, V. Paquet, W. Siefert, Schott-Glaswerke, Mainz.
G. Janzen, E. Räuchle, R. Wilhelm, Institut für Plasmaforschung, Univ. Stuttgart:
PICVD-Verfahren zur Herstellung von Lichtwellenleitern.

DIPLOMA THESES

Hesselmaier, B.:
Untersuchungen zur Elektronenemission des Plasmafokus.

Schumacher, A.:
Untersuchung der Dynamik und Feinstruktur des Plasmafokus.

Köchel, M.:
Rausch- und Verstärkungseigenschaften des Circular-Cage Photomultipliers.

DISSERTATIONS

Jäger, U.:
Über die Reaktionsmechanismen im Plasmafokus - Untersuchungen an beschleunigten Deuteronen und Reaktionsprotonen.

Vogel, T:
Schnelles Schalten von Ferninfrarot-Strahlung durch Brechungsindexänderung in Halbleitern über Photoionisation.

LABORATORY REPORTS

IPF-86-2
Thumm. M., V. Erckmann, W. Kasparek, H. Kumrić, G.A. Müller, P.G. Schüller, R. Wilhelm:
Components for transmission of very high power mm-waves (200 kW at 28, 70 and 140 GHz) in overmoded circular waveguides.

PPLK-R-12
Morimoto, S., W VII-A Team, ECRH Group (IPF Stuttgart):
On the second harmonic ECRH plasmas in Wendelstein VII-A, Research Report, Plasma Physics Laboratory, Kyoto University, 1986.

INVITED TALKS

Dodel, G.,
Collective scattering at 119 µm from lower hybrid waves and low frequency density fluctuations in the ASDEX Tokamak, Euratom ENEA, Frascati, 27. oct. 1986.

Holzhauer, E.:
FIR laser scattering from density fluctuations in the ASDEX tokamak, JET, England, June 24 1986.

Holzhauer, E.:
Laserlichtstreuung an thermischen Elektronendichtefluktuationen in einem Wasserstoffplasma, Universität Heidelberg, May 26, 1986.

G. Janzen:
"Plasmadiagnostik mit Mikrowellen"
Frühjahrssitzung des Arbeitskreises "Plasmawärmebehandlung und Plasmabeschichtung",
Dortmund, 14.5.1986.

Kasparek, W.:
Wellenzahl-Spektrometer zur Modenanalyse in überdimensionierten Hohlleitern,
Seminarvortrag, Kernforschungszentrum Karlsruhe (KfK), Karlsruhe, 1986.

Räuchle, E.:
Plasmatechnik, Kolloquiumsvortrag, Universität Bochum, 8.6.1986.

Wilhelm, R.:
Plasmatechnologie, Kolloquiumsvortrag, Max-Planck Institut für Plasmaphysik (IPP), Garching, 1986.

Wilhelm, R.:
Plasmatechnologie, Kolloquiumsvortrag, Siemens AG, Erlangen, 1986.

Wilhelm, R.:
Elektronen-Zyklotron-Resonanz-Heizung,
Kolloquiumsvortrag,Kernforschungsanlage Jülich (KfA), Jülich, 1986.

Wilhelm, R.:
Mikrowellenplasmen, Kolloquiumsvortrag, Universität Heidelberg, 1986.

ISOTOPE SEPARATOR LABORATORY OF THE PHYSIKDEPARTMENT AT THE TECHNICAL UNIVERSITY MUNICH

(Dr. E. Hechtl)

Radiation-enhanced sublimation of graphite bombarded with C^+ was measured. Furthermore, various graphite samples were prepared with a tracer either by implantation or by building up layers of ^{13}C for transport investigations.

Sputtering of Solid Surfaces with Heavy Ions

(E. Hechtl, U. Mayerhofer)

Measurements of radiation-enhanced sublimation of graphite were made with Papyex strips irradiated with C^+ ions. The samples were ohmically heated by applying a voltage to the sample holder clamps. Temperatures of 2000 K were reached. The bombarding energies so far were between 1 keV and 3 keV. Further measurements will be extended to lower energies. The sputtering yields show a steep increase at temperatures exceeding 1000 K. This enhanced sputtering yield is called enhanced sublimation. Measurements of J. Roth et al. (IPP AR 1985) show a similar yield increase with the temperature for a variety of other ion species. So far only a qualitative interpretation of this phenomenon can be given. Since this effect occurs with every ion species studied it cannot be a chemical effect. Energetic ions hitting the surface of a solid material create interstitials and vacancies, so-called Frenkel pairs. The interstitials diffuse with a high mobility to the surface and then desorb very readily at temperatures of above 1000 K. For a better insight into this mechanism of diffusion and sublimation a lot of graphite samples were marked with the carbon isotope ^{13}C. This was done either by implanting ^{13}C into the graphite lattice with energies of 10 keV or by building up layers of ^{13}C on the surface of graphite samples using ion beams of 200 eV.

Sample preparations were also done for various other purposes, such as for PIXE calibration measurements. Implantations with sulphur and chlorine were made in, for example, graphite samples with an energy of 20 keV and fluences of 10^{17} atoms/cm^2. All these samples were turned over to IPP for further investigations there or at JET.

The investigation of graphite sputtering with oxygen was brought to an end. Strong chemical effects are observed in this ion-target combination: there is evidence of the production of volatile oxides. Nevertheless no temperature effect could be detected between room temperature and 1000 K since mainly carbon monoxide is formed in this temperature range. This can be seen in Fig. 1, where the yield versus the target temperature is plotted for differently cut pyrolytic graphite.

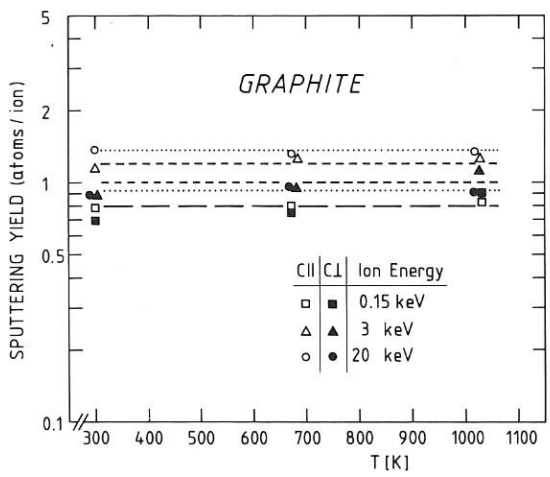

Fig. 1: Oxygen sputtering yield of pyrolytic graphite versus temperature. Open symbols: samples cut parallel to the net plane; solid symbols: samples cut perpendicularly. Long-dashed lines are drawn for the ion energy of 0.15 keV, short-dashed lines for the energy of 3 keV, and dotted lines for the energy of 20 keV.

Publication and Conference Contributions

Hechtl, E. and Bohdansky, J.:
Sputtering of Pyrolytic Graphite with Oxygen Ions at Various Target Temperatures, J. Nucl. Mater. 141-143, 139 (1986).

Bohdansky, J., Lindner, H., Hechtl, E., Martinelli, A.P. and Roth, J.:
Sputtering Yield of Cu and Ag at Target Temperatures Close to the Melting Point, Symposium on Sputtering, Spitz a.d. Donau, Vienna, Austria, June 2-6, 1986.

Hechtl, E.:
Low-Energy Ion Beam Work for the Preparation of Various Delicate Isotopic Samples as well as for Sputtering and Implantation Tasks, 11th Int. Conf. on Electromagnetic Isotope Separators and Techniques Related to their Applications, Los Alamos, New Mexico, U.S.A., Aug. 18-21, 1986.

Diploma Thesis
Mayerhofer, U.:
Untersuchung zur strahlungsinduzierten Sublimation von Graphit, Lehrstuhl E 18, Institut für Kernphysik und nukleare Festkörperphysik, Technische Universität München.

INSTITUT FÜR ANGEWANDTE PHYSIK II
DER UNIVERSITÄT HEIDELBERG
(Prof. Dr. Klaus Hübner)

In 1986 our cooperation with IPP in the field of neutron diagnostics was continued. It concerns neutron measurements at ASDEX and their interpretation as well as automated scanning of nuclear emulsions.

Automatic searching for tracks

(H. Hinsch, F. Stadler)

With the algorithm described in /1/ we could not reach reasonable execution times. Three new methods of automatic searching for tracks were therefore developed and tested. As before, a few binary pictures (256 x 256 pixels) each with a distance of 2 µm in the z-direction are added. In the first new method this picture is reduced by generating run length codes. Small pixel areas of the background are eliminated by setting a minimum value of the pixel area. For the remaining objects the quotient of the moment of inertia and the square of the area size is calculated, which is significant for tracks with a length-to-thickness ratio larger than 6. The second method uses the Hough transformation, which is made sensitive on elongated objects by an appropriate choice of the parameter space. As the Hough transformation is rather time-consuming if applied to the whole picture, a special algorithm is used beforehand which divides the whole picture into smaller areas and eliminates those not containing track-like objects. The result of the Hough transformation applied to an area with a track (Fig. 1) is shown in Fig. 2. The maximum represents the track of Fig. 1. The main idea of the third algorithm is to connect rows of the picture by the AND function. This method is able to find tracks with a length of above 12 µm and within an angle area of 45° and yields the shortest execution time.

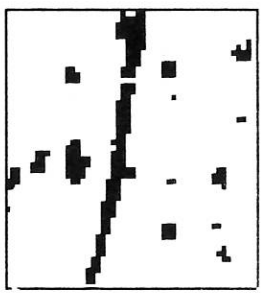

Fig. 1: Binary figure of a track.

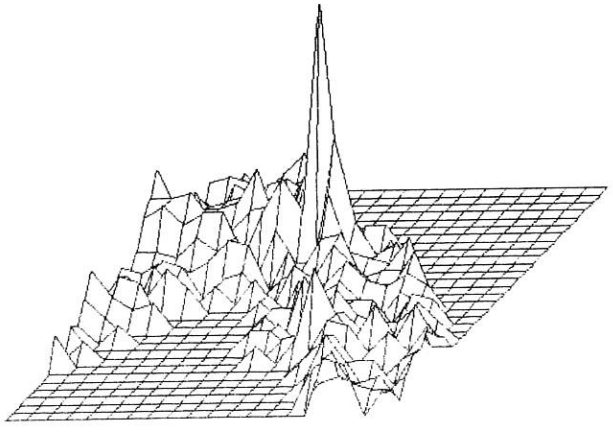

Fig. 2: Parameter space of the Hough transformation of the track in Fig. 1.

All programs are running on a VME system with the 16-bit microprocessor MC68000 with a clock rate of 8 MHz and are written in C. Tests on real pictures yielded execution times of 200 to 400 ms. An essential acceleration of the scanning procedure will be reached by running the scanning algorithm on a multiprocessor system with about four MC68000 with 16 MHz which will work in parallel and be synchronized by a master processor.

Automatic measurement of tracks
(A. Diehl, H. Hinsch)

The automatic scanning will give the x-y coordinates of a point on a track. The measuring procedure therefore only has to investigate the part of the whole picture containing the track. By stepwise variation of the focused plane in the z-direction 32 pictures of 128 x 128 pixels are stored in an image memory with a resolution of 6 bits/pixel. The 32 pictures correspond to a total z-scan of 16 μm, which is the maximum z-length of tracks which are of interest. No further mechanical movements are thus necessary. The automatic tracking is mainly done by calculating the centre of mass of areas around the track and extensively testing the occurrence of special cases, e.g. tracks of nuclear reactions, crossing tracks, disrupted tracks. Tests on real tracks yielded execution times of about 10 to 20 s.

Numerical simulation of the nuclear emulsion
(K. Hübner, L. Ingrosso, M. Roos)

The response function of the nuclear emulsion is determined by proton scattering in the emulsion and errors in track measurement but it is also broadened by off-line incidence of neutrons caused by the large extent of the neutron source in a tokamak. It is impossible to investigate these effects experimentally in detail and, therefore, we started development of appropriate software to study the effects on the response function.
Our NEP software analytically calculates the proton energy spectrum and the apparent neutron energy spectrum for given energy and direction of incoming neutrons. In order to demonstrate the effects, Fig. 3 shows for a monoenergetic neutron flux of 2.45 MeV the resulting neutron spectrum for different angles α of incidence. The broadening of the line and the consequent reduction in amplitude is already essential for a few degrees of off-line incidence.
Our NEPMC software, which is a Monte Carlo code, also accounts for range straggling of protons and measuring errors. Furthermore it allows studies of the statistical errors in the spectra caused by the limited number of tracks available. The numerical results are to be compared with measurements on both accelerators and tokamaks and we expect that they will be very helpful in the interpretation of our ASDEX measurements.

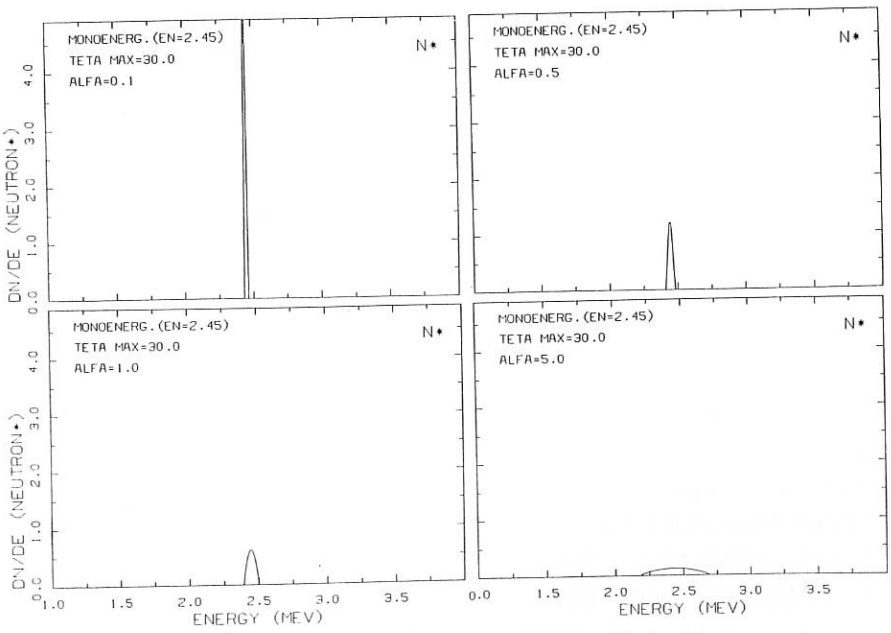

Fig. 3: Apparent neutron spectra for different angles α of incidence with respect to the axis of the emulsion.

/1/ Annual Report 1985, p. 242, MPI für Plasmaphysik, Garching

INSTITUT FÜR KERNPHYSIK; STRAHLENZENTRUM
JUSTUS-LIEBIG-UNIVERSITÄT GIESSEN
(Prof. Dr. E. Salzborn)

The Electron-Cyclotron-Resonance (ECR) ion source for the production of intense beams of highly charged ions has been tested in 1986. The experimental set-up in our laboratory has been completely rearranged to allow new experiments with the ions extracted from this source.

An ECR Ion Source for Atomic Collision Studies

(G. Mank, M. Liehr and E. Salzborn)

Tests and improvements

In extensive test runs with different working gases the Giessen ECR ion source has successfully produced intense beams of highly charged ions. The ion source always provided an easy and stable operation; so far we did not encounter lifetime problems.

Several tests were made to improve the magnetic field and to change the mirror ratio of the axial field. Most successful with respect to the production of increased ion currents and higher charge states was the admixture of a gas with a lower atomic number to the main working gas. A new system for the gas supply allows to admix even smallest amounts of a second gas species. Although gas mixing is widely and successfully applied in the use of ECR ion sources the underlying mechanisms are not yet understood. The emittance of a q x 10 keV nitrogen ion beam was measured to $\varepsilon_{90\%} = 95\ \pi$ mm mrad. This result is in agreement with previous measurements at the Jülich ECR source PRE-ISIS II which was the prototype of the Giessen ion source.

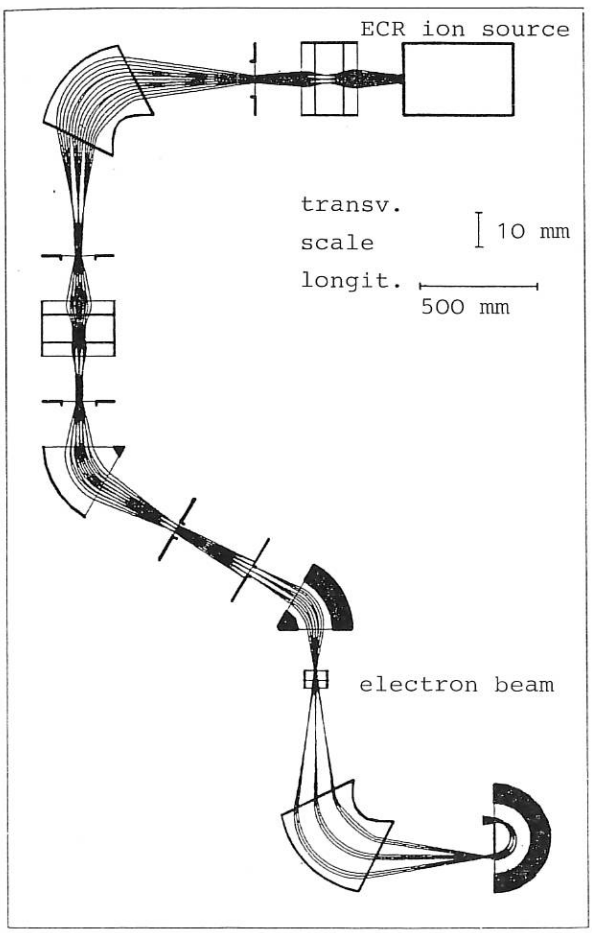

Fig. 1: Beam transport system for the electron impact ionization experiment.

Set-up of a beam transport system

In order to extend our investigations of electron impact ionization of multiply charged ions we have installed a new beam transport system based on computer calculations using the GIOS[1] code (Fig. 1).

Ion beam extraction from the ECR source is realized by an 'accel-decel' two-element electrode system. The extraction system can be remotely positioned with respect to the 8 mm diameter extraction hole. An einzel lens focusses the beam onto the entrance slits of a double-focussing 90° magnet with a ρ = 25.8 cm radius of curvature. Faraday cups in front and behind this magnet serve for measuring the total extracted ion current and the intensities of the charge-state-analyzed beam components, respectively. Fig. 2 shows for example a part of the charge state spectrum of xenon ions accelerated with U_{acc} = 10 kV. The charge states below q = 5 have been omitted.

By means of an electrostatic quadrupole triplet one selected charge component is transported to an electrostatic 60° spherical beam switcher which directs the ions into the beam line of the electron impact ionization experiment. The ion beam is cleaned, shortly before intersection with the electron beam, by electrostatic deflection from particles in other charge states which result from charge changing collisions in the residual gas. Downstream from the electron-ion interaction region the collision products are separated from the parent ions by a second 90° double-focussing magnet. The ions selected by this analyzer have to pass subsequently an electrostatic 180° hemispherical deflector before being counted individually by a channeltron detector.

Xenon (with N_2-Gasmixture)

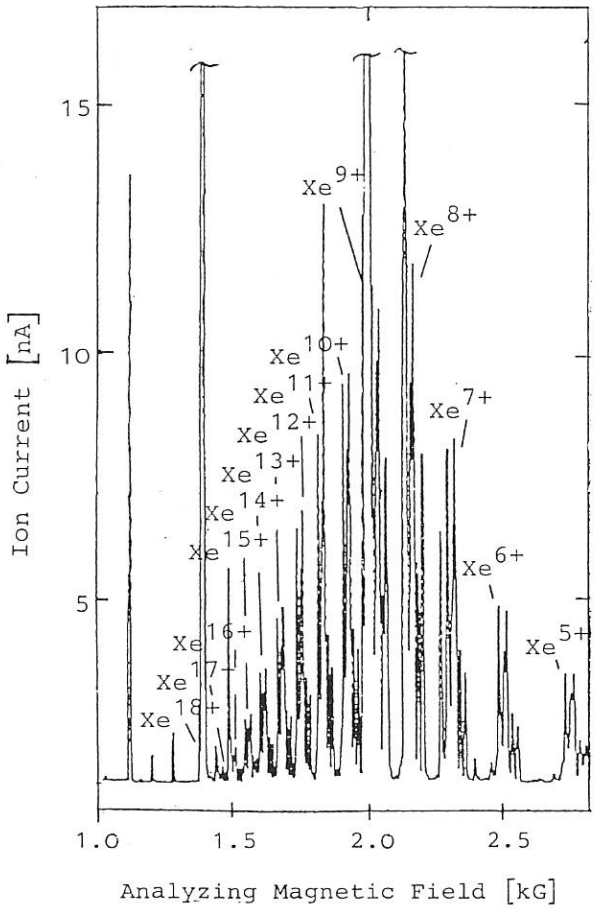

Fig. 2: Measured charge state spectrum of qx10keV Xe^{q+} ions ($q \geq 5$) obtained with 1 mm x 1 mm slits in front and behind the double-focussing 90° analyzing magnet.

1) H.P.Wollnik, J.Brezina, M.Berz and W.Wendel, Proc.AMCO 7, Darmstadt 1984, 679

Conference Contributions

"Aufbau einer Elektron-Zyklotron-Resonanz Ionenquelle für atomphysikalische Experimente mit langsamen hochgeladenen Ionen"
G. Mank, M. Liehr und E. Salzborn
Arbeitsbericht "Energiereiche atomare Stöße" EAS-7 (1986), S. 188

"Status of the Giessen ECR-Source"
G. Mank, M. Liehr und E. Salzborn
7th Workshop on ECR-Ion-Sources
Jülich, 22.-23.Mai 1986, p. 203

"Aufbau einer EZR-Ionenquelle für atomphysikalische Experimente mit langsamen hochgeladenen Ionen"
G. Mank, M. Liehr und E. Salzborn
Verhandl. DPG (VI) 21, 364 (1986)

Universität Osnabrück

SURFACE SCIENCE GROUP AT THE UNIVERSITY OF OSNABRÜCK

(Prof. Dr. W. Heiland)

As results from the project "Light emission from Ion-Surface Interaction" we report results from the scattering of molecular ions from surfaces, a comparison of secondary ion mass spectrometry (SIMS) and ion produced photons (IPP) and further results from the theory of charge exchange between ions and solids.

A direct comparison of the scattering of N_2^+ and O_2^+ from a clean Ni(111) and a Cs covered Ni(111) surface (Fig.1) lead to surprising results. In contrast to previous results for H_2^+ (B.Willerding et al,Phys.Rev.Letters 53(1984)2031) we find no evidence for O_2 formation from the interaction of O_2^+ with Ni(111) or Ni(111) + Cs. For N_2^+ the yield of N_2 increases for the cesiated surfaces compared to the clean surface. For all particles and surfaces studied we could not detect any evidence for excited state formation by using the optical monochromator. The results can partly be understood by rules of symmetry conservation, i.e. the non bonding state of N_2 is $^5\Sigma^+$, whereas the equivalent states of O_2 have Π character. The neutral ground states are N_2 $X^1\Sigma_g^+$ and $O_2X^3\Sigma_g^-$ resp. Therefore, considering the initial ionic states $N_2^+X^2\Sigma_g$ and O_2^+ $X^2\Pi_g$ and the possible orientations of the molecules to the surface normal, electron capture into the O_2 ground state may be rather unlikely, if the electrons from the surface have a momentum vector predominantly perpendicular to the surface (S. Schubert, J. Neumann, U. Imke, K. J. Snowdon and P. Varga).

Fig. 2 shows a direct comparison of SIMS and IPP from Nb using a primary ion beam of Ar^+ at 12 KeV. The optical spectrum contains only a part of the total spectrum which has been measured from 300 nm to 700 nm. Since we are presently using a simple lens to collect the light from the emitted neutrals the detection sensitivity could be improved by a suitable optic. (A. Klekamp, H. Koschmieder and K. J. Snowdon).

The theoretical studies of the charge exchange processes between ions and surfaces have been continued. Based on a parameter - free perturbation theory Auger transition probabilities for the neutralisation of light

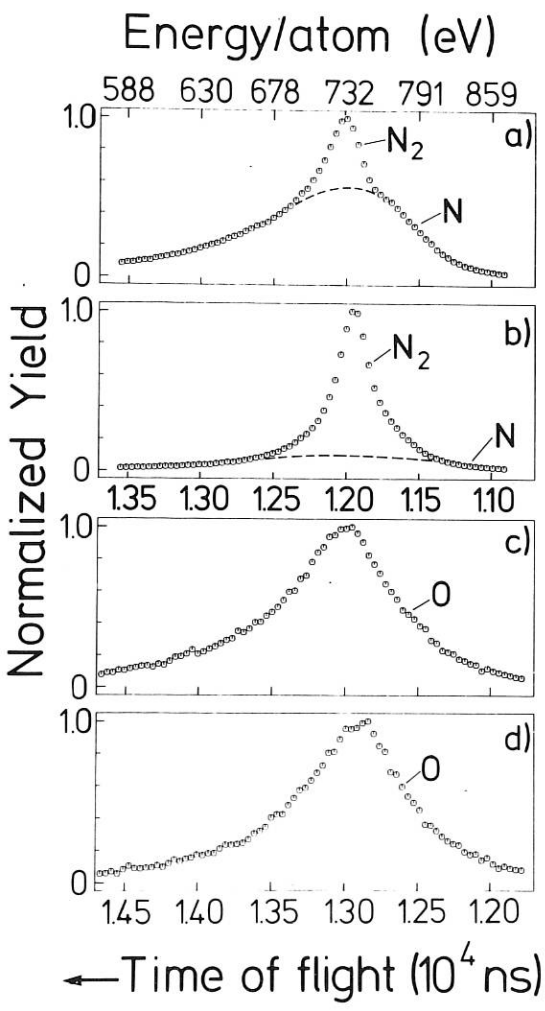

Fig. 1:
Time of flight spectra of neutral products from the interaction of 1.5 KeV N_2^+ and O^+ with clean Ni (a and c) and cesiated Ni (b and d).

ions on Au and Al are calculated. The dependence of the transition probability on various parameters, i.e. details of surface electronic properties, is rather large. Further work will concentrate especially on the influence and the realistic modelling of the surface electron density profile. (K. J. Snowdon, R. Hentschke, A. Närmann).

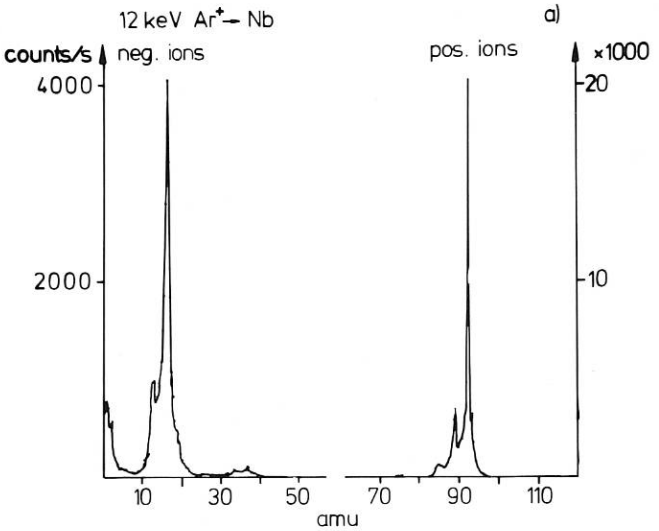

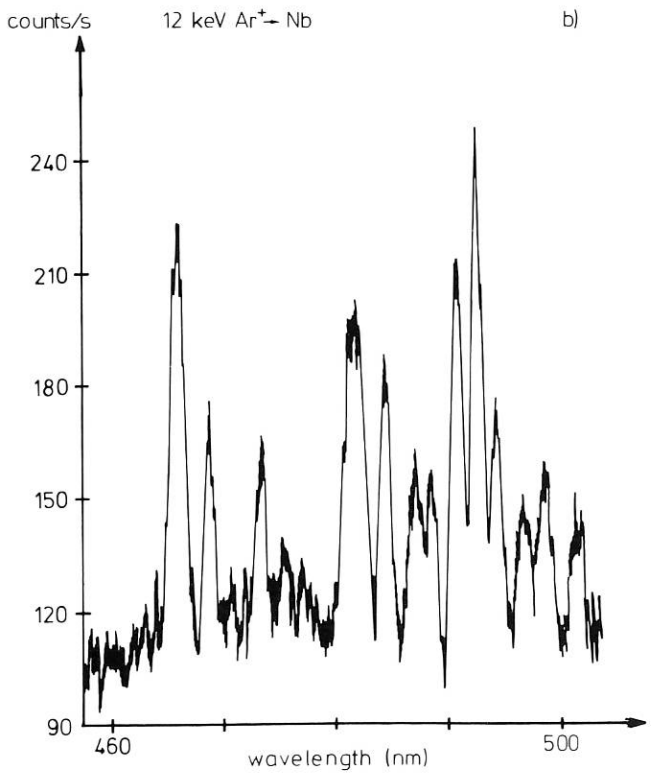

Fig. 2:
'Positive' and 'negative' SIMS (a) and IPP (b) from Nb under 12 KeV Ar^+ bombardment.

Publications:

S. Schubert, J. Neumann, U. Imke, K. J. Snowdon, P. Varga and W. Heiland: Neutralization and Dissociative Attachment in Molecular Ion-Surface Interaction: Scattering of N_2^+ and O_2^+ from Ni(111). Surf. Sci. 171 (1986) L 375.

K. J. Snowdon, B. Willerding and W. Heiland: Molecular Excitation in Sputtering, Scattering and Electron or Photon Induced Desorption. Nucl. Instr. Math. B 14 (1986) 467.

R. Hentschke, K. J. Snowdon, P. Hertel and W. Heiland: Matrix Element and Transition Rate for Auger Neutralization of Low Energy Ions Near Metal Surfaces. Surf. Sci. 173 (1986) 565.

K. J. Snowdon, R. Hentschke, A. Närmann and W. Heiland: Auger and Resonant Neutralization of Low Energy Ions Near Metal Surfaces. Surf.Sci.173(1986)581.

Conference Contributions:

Joint USA-Mexico Workshop on Two Electron Phenomena, Cocoyoc, Mexico 1986.
K. J. Snowdon: Two and One Electron Processes in Energetic Positive Ion-Metal Surface Collisions (inv.).
March Meeting of the American Physical Society, Las Vegas, 1986
K. J. Snowdon: Surface Neutralization of Low Energy Molecular Ions. (inv.)
6th Int. Workshop on Inelastic Ion-Surface Collisions Argonne, 1986.
W. Heiland: The Interaction of Swift Molecular Ions with Surfaces. (inv.)

SITE PLAN OF MAX-PLANCK-INSTITUT FÜR PLASMAPHYSIK

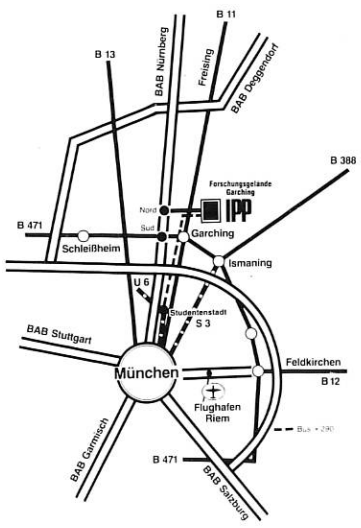

D1	Theory Division 2
W2, L4, D3	Plasma-Wall Interaction Division
L3, L3M, L7, L7A, I1	Experimental Plasma Physics Division 2 (Stellarators)
D2, D2A	Theory Division 1
D2, D2A	Computer Science Division
D2, D2A	Computer Centre Garching
L6, L5	Experimental Plasma Physics Division 3 (ASDEX)
D1, D1A, L1, W1 L2, L6, L5	Experimental Plasma Physics Division 1
T1, D1, D1A	NET Study Group
I1	Technology Division
ZW1, ZW2, I1	Central Technical Services
EZ, EZ2, L5E	Power Plants
B3, B6	Equipment Pool
H1	Directorate, Administration
B1, B2	Building Administration
C	Cafeteria
P	Main Entrance
F1, F2	Motor Pool
HZ	Heating Plant
A	Staff Quarters, Guest Accomodation
X1-X4, Y	Max-Planck-Institut für Physik und Astrophysik (Institut für Extraterrestrische Physik, Institut für Astrophysik)
Z	European Southern Observatory (ESO)

ANNUAL REPORT 1986

Max-Planck-Institut für Plasmaphysik (IPP) 8046 Garching bei München
Telephone (0 89) 32 99-1, Telex 05 215 808

Editing and Layout: Dr. Irmtraud Kramer and Isabella Milch
Printing: Graphis-Druck, München

Printed in Germany

This work was performed under the terms of the agreement between Max-Planck-Institut für Plasmaphysik and the European Atomic Energy Community to conduct joint research in the field of plasma physics.

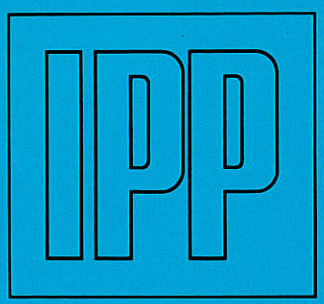
IPP